AUTOMATED DIESEL ENGINE CONDITION & PERFORMANCE MONITORING & THE APPLICATION OF NEURAL NETWORKS TO FAULT DIAGNOSIS

by

CHRISTOPHER LLOYD OWEN

A thesis submitted to the University Of Plymouth
in partial fulfilment for the degree of

DOCTOR OF PHILOSOPHY

School of Manufacturing, Materials & Mechanical Engineering

In collaboration with
The Ministry Of Defence

May 1998

AUTOMATED DIESEL ENGINE CONDITION & PERFORMANCE MONITORING & THE APPLICATION OF NEURAL NETWORKS TO FAULT DIAGNOSIS

by

CHRISTOPHER LLOYD OWEN

ABSTRACT

The overall aim of this research was to design, configure and validate a system which was capable of on-line performance monitoring and fault diagnosis of a diesel engine. This thesis details the development and evaluation of a comprehensive engine test facility and automated engine performance monitoring package. Results of a diesel engine fault study were used to ascertain commonly occurring faults and their realistic severities are discussed. The research shows how computer simulation and rig testing can be applied to validate the effects of faults on engine performance and quantify fault severities. A substantial amount of engine test work has been conducted to investigate the effects of various faults on high speed diesel engine performance. A detailed analysis of the engine test data has led to the development of explicit fault-symptom relationships and the identification of key sensors that may be fitted to a diesel engine for diagnostic purposes. The application of a neural network based approach to diesel engine fault diagnosis has been investigated. This work has included an assessment of neural network performance at engine torques and speeds where it was not trained, noisy engine data, faulty sensor data, varying fault severities and *novel faults* which were similar to those which the network had been trained on. The work has shown that diagnosis using raw neural network outputs under operational conditions would be inadequate. To overcome these inadequacies a new technique using an on-line diagnostic database incorporating 'weight adjusting' and 'confidence factor' algorithms has been developed and validated. The results show a neural network combined with an on-line diagnostic database can be successfully used for practical diesel engine fault diagnosis to offer a realistic alternative to current fault diagnosis techniques.

CONTENTS

LIST OF TABLES

LIST OF FIGURES

NOMENCLATURE

A	Area
A_e	Effective flow area
A_p	Piston area
C	Gas velocity at throat
C_p	Specific heat at constant pressure
C_{piston}	Mean piston speed
C_v	Specific heat at constant volume
d_n	Nozzle hole diameter
Δp	Pressure drop
γ	Specific heat ratio
h	Specific enthalpy
η	Efficiency
η_{ct}	Compressor isentropic efficiency
h_e	Enthalpy of exhaust
h_{for}	Specific enthalpy of formation of fuel w.r.t absolute zero
h_i	Enthalpy of inlet air
η_{ic}	Intercooler effectiveness
η_{tt}	Turbine isentropic efficiency
η_{vol}	Volumetric efficiency
K	Arbitrary constant
λ	Air/Fuel ratio
L	Stroke
m	Mass
M	Mach number
m_e	Exhaust mass flow
m_f	Mass of fuel
m_i	Inlet air mass flow
N	Rotational speed [revs/min]
N_{ct}	Compressor rotational speed [revs/min]
N_t	Turbine rotational speed [revs/min]
n	Rotational speed [revs/sec]
N_c	Number of firing cylinders per engine revolution
p	Pressure
P_b	Brake power
P_i	Indicated power
p_{cin}	Pressure at compressor inlet
p_{cout}	Pressure at compressor outlet
p_{max}	Maximum cylinder pressure
p_{tin}	Pressure at turbine inlet
p_{tout}	Pressure at turbine outlet
p_t	Throat gas pressure
p_u	Upstream pressure
Q	Heat transfer
Q_a	Inlet air volume flow rate
Q_c	Fuel calorific value

Q_f	Heat release by fuel
Q_w	Heat loss through cylinder walls
R	Gas constant
ρ_g	Gas density
ρ_l	Liquid density
s	Specific entropy
S	Spray penetration
T	Temperature
t	Time
T_{a0}	Air temperature inlet into charge cooler
T_{a1}	Air temperature out of charge cooler
T_b	Brake torque
T_{cin}	Temperature at compressor inlet
T_{cout}	Temperature at compressor outlet
T_g	Gas temperature
T_{tin}	Temperature at turbine inlet
T_{tout}	Temperature at turbine outlet
T_u	Upstream temperature
T_w	Combustion chamber wall temperature
T_{w0}	Water temperature inlet to charge cooler
u	Specific internal energy
V	Volume or Volts
V_{sw}	Cylinder swept volume
W	Work
X	Cumulative average
Y	Database output
Z	Cumulative product

ACKNOWLEDGEMENTS

The author wishes to express his gratitude to all those individuals who have provided assistance and encouragement during the research and preparation of this thesis.

My sincerest thanks goes to **Prof. Tom Ruxton**, Dean Of Engineering, University of Stafford, in his role as director of studies. He has offered guidance and support throughout the research and preparation of this thesis. Sincere thanks also goes to **Dr. Murray Bell**, Principle Lecturer, University Of Plymouth, in his role as supervisor, who has given me guidance and encouragement throughout the research and preparation of this thesis.

Thanks is also due to **Lt. Cdr. D. Adcock, Lt. Cdr. J. Forrest** and **Lt. Cdr. C. Barnes** who have all been members of the supervision team but unfortunately could not provide support for the duration of this work due to the de-commissioning of H.M.S Thunderer, The Royal Naval Engineering College.

A special thank you to my friends and colleagues of the Thermal Power Group, RNEC. **Mr. R.C. Vickers, Mr A. Ray, Mr. R. Donaldson, Cdr. M.J. Kitchin & Dr. J.G. Hawley**, for your encouragement, support and hard work which has allowed the successful completion of this research.

Thanks to **Mr. Jeff Ecob**, ABB Propulsion, Derby, for his assistance during the fault study conducted as part of this research.

Thanks to **Mr. J.B. Gibson**, Quality Engineering Manager, Perkins Engines, for his encouragement and support during the preparation of this thesis.

Finally, thanks to my parents Bruce & Margaret, to whom this thesis is dedicated, for their continuous encouragement throughout the research and preparation of this thesis.

AUTHORS DECLARATION

At no time during the registration for the degree of Doctor of Philosophy has the author been registered for any other University award.

This study was financed by The Ministry Of Defence and was conducted at HMS Thunderer, The Royal Naval Engineering College, Manadon.

Relevant scientific seminars were attended at which work was occasionally presented.

Publications & Presentations:

The Application Of Neural Networks To Fault Diagnosis, Journal Of Naval Engineering, Vol 34, December 1993, pp 587

Instrumentation, Data Acquisition And Data Processing Applied To Diesel Engine Performance Monitoring. I Mar E CPD Seminar, 6th October 1994.

An Experimental Investigation Into Condition Monitoring & Fault Diagnosis Of A Marinised Diesel Engine. Society Of Underwater Technology Research Seminar. 12th October 1995, Aberdeen

Diesel Engine Condition Monitoring & Fault Diagnosis. University Of Plymouth Research Seminar. October 1993

Signed.....

Christopher Lloyd Owen
May 1998

CHAPTER 1

INTRODUCTION

1.0 Diesel Engine Condition & Performance Monitoring

The application of condition monitoring and fault diagnosis strategies to diesel engines is a well recognised method of increasing operational efficiency [1,2]. The term 'condition monitoring' covers the application of a multiplicity of approaches and methods to many different systems. Condition monitoring can be defined as "an assessment on a continuous or periodic basis of the mechanical condition of machinery, equipment and systems from observations and/or measurements of selected parameters" [3]. In essence, condition monitoring is any technique which is capable of assessing a system's physical condition under operational conditions. Condition monitoring offers significant advantages over more traditional 'hours run' or 'calendar based' maintenance strategies. The primary benefits are summarised below.

- Only equipment which requires attention is dismantled for assessment. This minimises wastage of labour, replacement consumables such as gaskets and seals and engine operating time. Often engine manufacturers will err on the side of caution and include an 'abuse margin' when specifying hours run to maintenance.
- Only components or assemblies which are defective are replaced. The philosophy of replacing components because the engine is dismantled is exceedingly common and creates higher replacement parts costs.

- Effective prediction and planning of maintenance operations. Down-time can be planned and used much more effectively since the nature of the fault is known in advance and spares and labour can be planned during the increased lead time.
- The rate of development of a fault can be monitored and informed decisions can be made as to when corrective action should take place. This increases reliability, minimises unplanned down-time and allows a fault to develop until maintenance is forced by safety considerations, catastrophic failure or long term engine damage.
- Improved decision making ability when selecting optimum engine operating conditions.
- More effective negotiations with manufacturers or sub-contracted engineers, backed up by systematic measurements of engine condition.
- Measurements of the engine parameters from new, at the end of the guarantee/warranty period and after overhaul gives useful comparative data.
- Good clear accurate records of engine performance are easy to obtain and therefore this data can be utilised in future diesel engine design.

The main methods applied to diesel engine health assessment can be classified into three distinct categories, these are discussed below;

- Lubricating oil and wear debris analysis. A broad survey of mechanical breakdowns suggest that well over half of all failures are linked to tribology, that is to implicate the working faces of mechanical contact [4] . Bearings, pistons, cylinders, gears and other lubricated components account for most mechanical

troubles. Damage at the contacts takes the forms described as mechanical wear, abrasion, scoring, pitting, deposit formation, corrosion, overheating, seizure etc.; each may be attributed to lubrication failure. The vast majority of problems of this nature are initiated by small amounts of wear but are quickly accelerated to problems of larger magnitude. Each problem gives rise to particles of foreign material in the lubricating oil. These particles may be of metal, metal oxides or traces of corrosion products. The particles have characteristic composition, shape, size and concentration. These properties indicate which component is failing, the failure mode and how serious the fault is. Generally detailed lubricating oil analysis is conducted under laboratory conditions and is therefore not regarded as an on-line technique.

- Noise and vibration assessment. These techniques are based upon the measurement and interpretation of engine or component vibration signatures. In reality engines are built to tolerances, and therefore, will always exhibit a vibration characteristic. The extent of vibration is due to two factors, the quality of engine build and the condition of components. If vibration analysis is undertaken on a new engine the signature is attributable to build quality only and could be termed the 'baseline signature'. Any subsequent analysis can be compared to the baseline signature and differences can be attributed to engine damage or deterioration.
- Thermodynamic performance monitoring. This is the most favoured approach to condition monitoring since the data generated not only indicates the health of the machinery but also enables engine efficiency to be monitored and optimised

simultaneously. This is achieved through the measurement of physical properties like temperatures, pressures and flow rates The primary objectives of performance monitoring are;

(a) To monitor specific fuel consumption data and ensure that the engine is running efficiently and economically.

(b) Analysis of fuel injection and combustion data to ensure fuelling levels, timing and combustion is optimal. This is increasingly important due to gaseous and particulate emissions regulations.

(c) To generate trends in engine performance data over an extended duration which can reflect degradations in performance.

(d) The examination of engine performance trends to allow fault diagnosis.

1.1 Overview Of Diesel Engine Condition Monitoring & Fault Diagnosis Systems

To date, several commercial diesel engine condition monitoring and fault diagnosis systems have been developed. The following sections give an overview of the techniques which have been applied to commercial systems.

1.1.1 Diesel Engine Expert Diagnostic System 'DEEDS'

This system was jointly developed by The University Of Newcastle and Lloyds Register [5,6] . The system was designed to work on a four stroke, turbocharged, direct injection, medium speed marine diesel engine. DEEDS consisted of two separate modules, signal conditioning and condition assessment. The signal

conditioning element performed the data acquisition, assessment of engine stability for steady state operating conditions and the calculation of data variability. A mathematical model was used to derive the normalised values for the sensor readings under healthy operating conditions. The readings from the sensors were compared to the model outputs and deviations outside a tolerance band invoked the condition assessment system. The condition assessment system was essentially a knowledge based system with an embedded rule structure. The results from the signal conditioning system were fed to the knowledge based rule structure which performed the fault diagnosis.

1.1.2 Fault Avoidance Knowledge System 'FAKS'

FAKS has been developed by Wartsilla Diesels[7] . The system uses approximately 10 transducers per cylinder which are mainly temperatures and pressures. These are read every 15 minutes and are passed for diagnostic analysis. Diagnosis based on the sensor data is performed by three operations. Firstly, data normalisation is applied to take account of varying engine operating conditions. The normalised data is condition checked to assign qualitative expressions like high or low to a parameter. Finally, these expressions are then operated on by a knowledge base rule structure to determine the diagnosis.

1.1.3 MODIS-Geadit

This system was developed by MAN B & W and AEG electronics in 1989[8] and embraced both condition and performance monitoring. It was based around an expert system which was developed using many years of diesel engine experience.

The philosophy of the system was to embed the knowledge of the manufacturers into a system and make it available to it's customers. The system targeted the combustion, fuel injection, turbocharger and load bearing components. The engine's condition and performance was assessed using thermodynamic performance parameters including exhaust temperatures, cylinder pressures, manifold pressures and fuel flow rate. Subsequent diagnosis was achieved by applying an expert system rule base to the recorded data.

1.1.4 Diesel Engine Intelligent Monitoring System 'DIEMOS'

This system was developed by Ricardo [9] as part of the government's programme for intelligent information systems. The system consisted of several separate information systems which were linked by a supervisory system. The engine data was gathered by an on-line data acquisition system and compared to database information and simulation results. This gave rise to performance deviations which were analysed by feature finding and pattern recognition techniques.

1.1.5 Compuchek

Compuchek was designed and developed by Cummins Diesels [10] as a comprehensive service centre tool and is widely used in North America. It examined induction temperature & pressure, lubricating oil temperature and pressure and cooling water system temperature and pressure, blowby, fuel vacuum pressure, air filter pressure drop, engine speed and cranking parameters. These physical measurements were operated on by simple causal logic statements to provide a diagnosis and information on specific service operations.

1.1.6 Cylinder Pressure Monitoring For Diesel & Gas Engines 'CYLDET'

This Asea Brown Boveri [11] developed system concentrated primarily on cylinder pressure and fuel injection system data measurement and analysis. From the raw data the system calculated ignition delay, P_{max} , mean indicated pressure, start of combustion, indicated power etc. All of the calculated data was monitored against operator set limits and made available in trend format. In addition to this, heuristic logic was applied to the data to provide diagnostic and corrective action information.

1.1.7 Diesel Engine Unit Condition Evaluator 'DEUCE'

Developed jointly by Cummins, Caterpillar and GEC in early 1992 [12] this system differs significantly from those described above since it relies heavily on vibration analysis. The system employed sophisticated signal processing techniques to refine vibration signals which originate from the engine internal mechanisms but are measured on the external surfaces of the block. After a baseline signal had been established for a particular engine, comparisons were made with subsequent vibration data. The system used the vibration signal to perform a heuristic operation which subsequently lead to a closer analysis of engine subsystems and a diagnosis. For example, if the vibration signature identified that cylinder combustion pressure was low for a particular cylinder the system automatically checked the fuel injection system performance, and so on.

1.1.8 Computer Aided Maintenance Of Diesel Engines 'CAMODE'

CAMODE is a system which was developed at the University of Adelaide. It is essentially a knowledge based expert system which required the manual input of data. Work by Autor in 1994 [13] looked at developing a new front end for CAMODE which would facilitate automated data collection, post processing and interface with the expert system. The sensor configuration included vibration monitoring, oil temperatures and pressures, crankcase pressures, exhaust gas temperature and pressure, exhaust emissions, inlet manifold conditions and fuel delivery. The data acquisition system managed the collection of the data and the application software also acted as a data reduction tool. Processed data was fed to a database where it resided until the expert system was activated. When a diagnosis was performed healthy data sets were compared with current data sets. Differences in these two data sets were analysed by the expert system rule structure. Any abnormalities were reported and actions required were recommended.

1.2 Overview Of Fault Diagnosis Techniques

The performance of a condition monitoring system can be greatly enhanced if the data it generates can be operated on by a decision making tool as described above. This enables the system to inform the engineer or maintenance personnel of exactly what is required to return the engine to a healthy state. The application of a diagnostic tool has the following advantages.

- It reduces the dependency on experienced personnel and allows manning levels and overhead costs to be reduced.

- It can easily analyse large amounts of data and draw conclusions based on multi-dimensional relationships.
- It can repeatably diagnose faults of a safety critical nature which could otherwise be vulnerable to human error.
- Experienced personnel may not be available. The equipment may be new or its location inaccessible which is particularly applicable to marine installations.
- Decision making is faster and trend analysis to determine the rate of fault development is easier.

Diesel engine fault diagnosis has been performed by the comparison of data when the engine is operating in both healthy and faulty modes. Operation of a system in a faulty mode may give rise to a deviation of sensor data from the expected healthy running mode. In the examples discussed above, comparative data has been generated by computer simulation, experimental engine testing and traditional mathematical modelling (parameter identification). This information has been stored in complex look-up tables, databases or knowledge bases for comparative purposes.

Parameter identification techniques involve the generation of a mathematical model of a system to map the inputs onto the outputs. If a system is highly non-linear this process is often very difficult and time consuming. The real outputs for a set of given inputs are then compared to the model and a difference or residual is generated, using Kalman filtering for example, characterising the fault. One great disadvantage of this approach is that the mathematical model must fit the process very closely otherwise residuals are generated during healthy operation giving rise to incorrect diagnosis. Development of the mathematical model is often very time consuming and requires an

understanding of the physical relationships between the inputs and the outputs. An example of this can be seen in work by Kouremenos et al. in 1996 [14] which characterised a set of constants relating to specific engine or sub-system processes and used changes in these constants to perform diagnoses.

The knowledge based system approach, commonly called the expert system approach, has found widespread application in the field of fault diagnosis as described in Sections 1.1.1 to 1.1.8. The knowledge base contains a series of IF...THEN and AND statements in an attempt to capture an experts knowledge and experience. This rule structure may then be applied to a problem in the hope that it will emulate the experts decision making process and arrive at the correct conclusions. Despite the vast success of this style of approach to practical fault diagnosis its serious limitations became evident in the early eighties. These limitations are discussed in detail later in Section 1.4.

More recent advances in the field of artificial intelligence and computer technology have brought new techniques to light. One such technique is the neural network. Since fault diagnosis is essentially a problem of pattern classification it is now widely realised that artificial neural networks offer a potential alternative to traditional mathematical models or knowledge based systems.

1.3 An Introduction To Neural Networks

The advent of neural networks can be dated back to the 1940's. Early pattern classification research was conducted throughout the 60's and 70's the results,

however, had few practical connotations and little attention was paid to real world applications [15] . Since then, rapid developments in the field of microcomputer technology have allowed neural networks to be applied in practical situations such as system dynamics modelling, speech, vision, robotics and fault diagnosis.

1.3.1 Artificial Neural Network Principles

Artificial neural networks aim to mimic the structure of the brain on a very simple level. The microcomputer is a high speed serial machine whereas the brain runs at a much lower speed but is a massively parallel system. This parallel system is capable of representing and storing knowledge in an accessible way so that it may be applied to problem solving. Perhaps one of the most important features of the brain is its ability to learn by example and reapply the newly acquired knowledge. To enable a microcomputer to behave like the brain it is necessary to analyse the brains basic structure and then model this on the microcomputer.

The brain's structure is highly complex and is generally poorly understood. It consists of about ten thousand million basic units, called neurons, as shown in Figure 1. The soma forms the body of the biological neuron and the dendrites form the connection through which all the inputs to the neuron arrive. The output from each neuron is known as the axon, these in turn maybe coupled to other dendrites via a synapse. The synapse is a chemical connection which effectively governs the weighting of the inputs into the dendrite. Each dendrite is capable of summing its inputs and transmitting the result to the soma. When the potential in the soma rises above a

certain critical level the axon produces a voltage pulse known as an action potential, as shown in Figure 2.

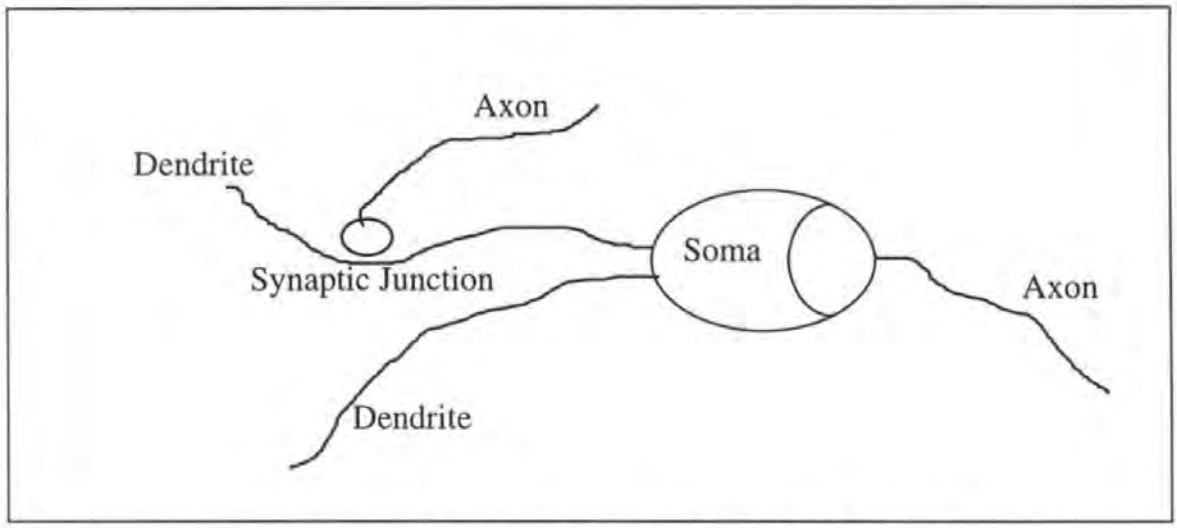

Figure 1 Basic Components Of A Biological Neuron

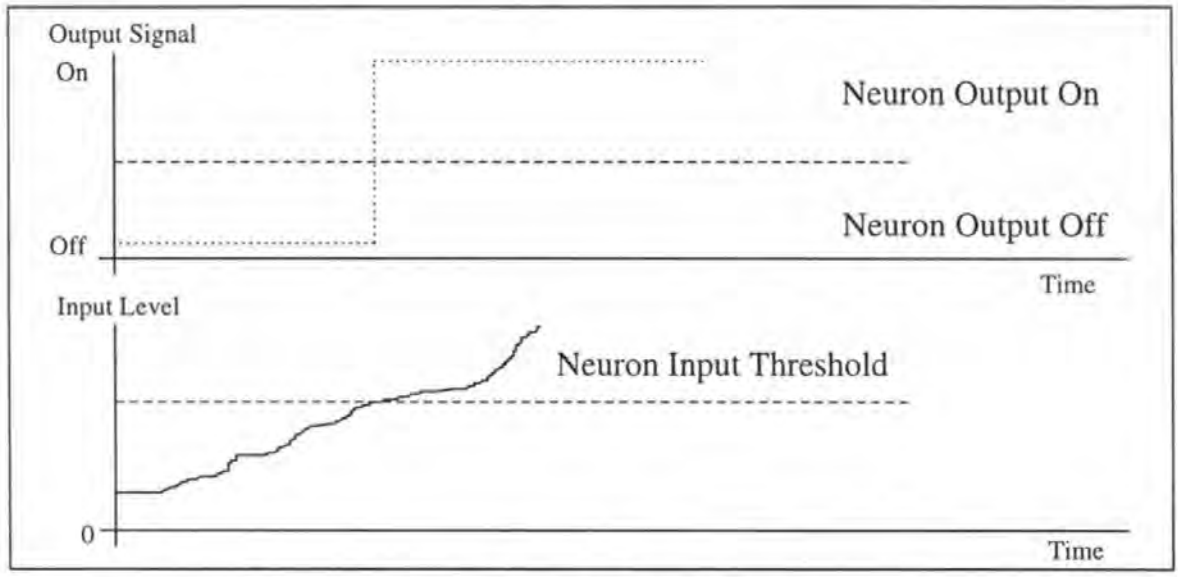

Figure 2 Neuron Input & Output Relationship

This basic understanding of how the neuron functions allows the design of a microcomputer model. Figure 3 outlines the basic model of the neuron. A number of inputs are applied to the neuron via links, each link has an associated weighting. Each input is multiplied by its weighting and the neuron sums the weighted inputs and applies a transfer function to determine the neuron output.

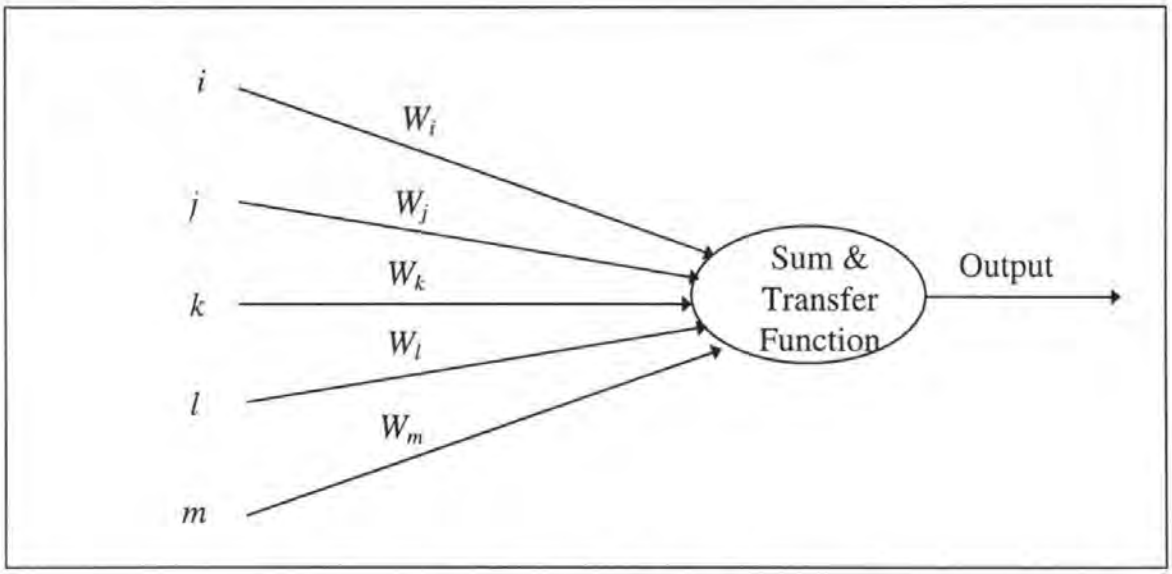

Figure 3 Computer Model Of A Neuron

Many of these neurons or nodes may now be linked together to form a network. Figure 4 shows a multi-layer feed forward network. It consists of three layers of neurons, the input layer, the hidden layer of which there maybe one or more, and the output layer.

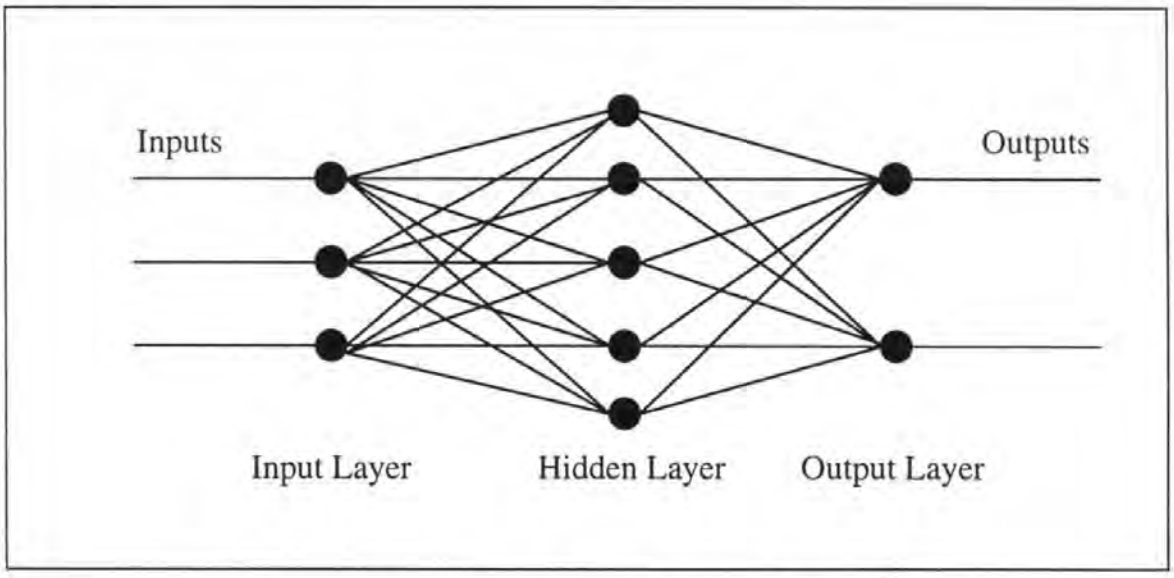

Figure 4 Multi-layer Feed Forward Network

1.3.2 Learning In Artificial Neural Networks

Probably the most important attribute of the neural network is its ability to learn by example and progressively improve its performance. The learning process can be categorised into two basic classes: unsupervised learning and supervised learning.

1.3.3 Supervised Learning

For a network to undergo supervised learning it must be presented with pairs of training data, in the form of inputs and desired outputs. During training the features extracted from the example data will be entered into the input layer of neurons. The consequent results will feed through the network until they reach the output layer. The results will then be compared to the desired output. Through the implementation of a training algorithm, back propagation for example, the weights in the network maybe manipulated so as to reduce the error between the output from the network and the desired output. This process is repeated until the output from the network matches the desired output within a particular tolerance level. Each forward pass is known as an 'epoch'.

1.3.4 Unsupervised Learning

Unlike supervised learning only input training data is required by the network. Implementation of the training algorithm will again adjust the weights in the network but this time the network is trained to produce the same output for similar inputs. This process allows the network to group or cluster inputs which exhibit similar properties. This technique proves most useful in the realms of fault diagnosis since the network does not need to be trained to recognise every possible fault. Providing the network

has been given a sufficient variety of training data it is possible for the network to classify a novel fault simply by virtue of the fact that it does not closely match any of the clusters derived during training.

1.3.5 Neural Networks Applied To Fault Diagnosis

The aim of this section is to give an over view of research in the field of neural networks applied to fault diagnosis. This area of work began in the late 1980's and is currently one of the fastest expanding research topics. Research work conducted to date on both process plant [16-21]and machinery [22-36] has produced several systems which are in commercial operation today [18-22] . Other programmes of research which are not yet technically mature are, however, producing some very promising results.

1.3.6 The Application Of Neural Networks To Process Plant Fault Diagnosis

By far the most popular research field has been chemical process plants. The relatively new approach of neural networks stems from earlier work by Venkatasubramanian and Chan [16] 1989 and Watanabe et al. [18] .

Work by Venkatasubramanian and Chan [16] 1989 demonstrated how a neural network approach maybe substituted for an expert system approach. It showed how a fault tree maybe utilised by a neural network to diagnose process faults. The work also investigated the effects of network training and hidden layer architecture by evaluating the accuracy of diagnosis. This work was extended further to analyse how the neural network would perform on multiple faults, noisy data and novel faults. The research revealed that the neural networks diagnosis of trained single faults was nearly

perfect at 98%. It was also discovered that multiple faults comprising of single trained faults could be diagnosed successfully whilst diagnosis of totally novel single faults was poor. It was concluded that the network performed well under novel conditions that were similar to those encountered in training but network performance deteriorated under totally novel conditions. The work also proved that neural networks have the ability to function successfully even in the presence of noisy input data. These findings are also reinforced by research work carried by Hoskins [17] et al. 1991.

Research by Watanabe [18] et al. 1989 investigated the training and testing of a 3 layer neural network using the back propagation algorithm on 5 process faults. The eventual approach used a cascade of two networks. One to recognise the 5 faults and 5 further separate networks to diagnose the faults. The results showed that the two tier structure of networks proved very successful and could not just diagnose a particular fault but could also class the degree of severity of the fault.

Later work by Venkatasubramanian [19] et al. 1990 investigates the implementation of a neural network on a more complex chemical process plant. The main difference between this and previous work was that the faults to be investigated affect almost all of the network inputs making the derivation of fault-symptom relationships a difficult task. The work completed on noisy input data was taken further to include faulty sensor data. Again it was found that diagnosis of single trained faults and multiple faults was successful. The network also demonstrated its robustness in the presence of both noisy and faulty sensor data.

1.3.7 The Application Of Neural Networks To Machinery Fault Diagnosis

The application of neural networks to machinery fault diagnosis generated a great deal of interest from industry and educational establishments in the early 1990's. Research work has included EDS Scicon [22], Lloyds Register [23,24] and T & EE Pyestock .

A study by Ray [25] showed how a two layer neural network may be interrogated with a knowledge based system. This off-line approach interrogated the user in order to determine what symptoms were present on the machinery. The user would classify whether the symptoms were present, likely present, unknown, likely absent, or absent. These five classes represented numbers between +1 and -1, present and absent respectively. These numbers were fed to the neural network input layer and the outputs were analysed. The outputs represented a number of weighted causes. The magnitude of the weighting inferred the probability of the fault presence. Although this system gave a correct diagnosis 75% of the time it was found that some symptoms generated too many causes with similar weightings. Another good example of how neural networks have been integrated with other techniques is the work by Healey et al.[26] . This demonstrated how system identification and Kalman filtering could produce inputs to a neural network for the diagnosis of underwater machinery.

Chow and Yee [27] investigated the use of neural networks to detect incipient faults in squirrel cage motors. Healthy and faulty motor data was generated through computer simulation and used to create a two level network. The first network acted as a data filter to remove noisy data and the second performed the diagnosis. The results

showed that the two tier network had the ability of identifying and diagnosing faults in 95 to 99% of instances.

Dietz [28] examined real time diagnosis of jet and rocket engine faults using neural networks. The work used a three layer feed forward network trained by the back propagation algorithm. The network was tested on data representing various fault severities, duration's of fault presence and noisy data on two faults. The results showed that the network could easily classify the two faults and give an indication of severity.

Kirkman and Elliot [29] undertook feasibility studies in the application of neural networks to diesel engine viscous damper condition, reconstruction of direct cylinder pressure from load cell washers and health monitoring of gas turbines. The work concluded that the neural network approach had the following limitations;

- The nature of the problem to be solved should be fully understood before neural networks are applied.
- Effective development of a neural network requires vast quantities of 'real life' data.
- Neural network input data will usually require some form of pre-processing.

Similar work by Gu et al.[30] investigated the use of a non-parametric Radial Basis Function (RBF) neural network to model the relationship between instantaneous crankshaft velocity and cylinder pressure. The work demonstrated that the neural network could be trained to model the relationship between crankshaft velocity and

cylinder pressure and hence could predict in-cylinder pressure. Although cylinder pressure can be reconstructed this research did not prove the validity of the technique for the identification of diesel engine faults. In some instances the occurrence of a diesel engine fault will only give rise to very small sensor deviations hence demanding that any reconstructed data matches the measured data very accurately.

Work by Leonhardt et. al. [31, 32] and Ludwig [33] has also investigated the use of neural networks and cylinder pressure to supervise a diesel engine fuel injection system. The research has focused on the relationship between fuel injection timing and delivery and cylinder pressure data. The research examined features of the cylinder pressure trace and used a Radial Basis Function (RBF) neural network to draw relationships between these cylinder pressure data features and fuel delivery and injection timing. By measuring cylinder pressure it was possible to reconstruct both fuel delivery and injection timing using the neural network. These reconstructed values could then be compared to the desired fuel delivery and injection timing. Any discrepancies **could** lead to the display of specific messages like 'injection timing too advanced' or 'fuel delivery too low'. The fault diagnosis capability was not substantiated using real engine data taken under realistic fault conditions. This research also relies on the inclusion of cylinder pressure measurement on the engine. Whilst the work has shown some of the operational problems of using in-cylinder pressure transducers can be overcome, fitting of expensive, intrusive transducers should be avoided for practical fault diagnosis.

Scaife et al. [34] showed how computer simulation results could be applied to neural network training for both a CHP plant and a diesel engine. The research investigated the computer simulation and subsequent training of a neural network on the following diesel engine faults;

- Exhaust restriction
- Exhaust manifold leak
- Inlet manifold leak
- Exhaust valve leak
- Intercooler fault

The research concluded that neural network techniques showed potential for further investigation but before neural networks could be confirmed as a commercially viable tool, the following areas of concern would need to be addressed.

- Degree of network training
- The effects of different training algorithms
- A more detailed analysis of engine instrumentation and inputs into the neural network
- The effect of different network architectures

Ayoubi [35] and Ludwig [36] have investigated the use of a dynamic neural network to diagnose a diesel engine turbocharger waste gate fault. In this approach a Dynamic Multi Layer Perceptron (DMLP) was used to model the turbine performance. Exhaust temperature and pressure upstream and downstream were used as network inputs,

turbine speed was used as the output. This work showed that an accurate model of the turbine could be developed. Further to this, the model could be used to identify a leaky waste gate by comparing the actual measured turbine speed with the neural network predicted turbine speed. Whilst promising, the work has concentrated on one specific fault which has not necessarily been introduced at a realistic fault severity. In addition to this, it has used a number of very specific transducers to identify one fault which could prove disadvantageous for practical application.

1.4 Conclusions Drawn From The Review Of Previous Diesel Engine Condition Monitoring & Fault Diagnosis Experience

By far the most intensively researched areas are expert systems/ knowledge based approaches and traditional mathematical models. Previous experience has shown that systems developed using these approaches have the following disadvantages.

- Building a knowledge base system is both costly, time consuming and relies heavily on consultation with one or more experts in a particular domain.
- Because of the often very specific structure of the knowledge base modifications to account for physical changes in the plant or novel faults are very difficult.
- The occurrence of novel faults or noisy or corrupted data often results in a severe degradation in the performance of a knowledge based system.
- If a system is highly non-linear mathematical modelling is often very difficult and time consuming.
- The mathematical model must fit the process very closely otherwise residuals are generated during healthy operation giving rise to incorrect diagnosis.

- Development of a mathematical model requires an understanding of the physical relationships between the inputs and the outputs.

Research into the application of neural networks to fault diagnosis in both process plant and machinery has shown that neural networks have the potential to be very competent diagnostic tools whilst eliminating many of the problems identified above. The following conclusions can be drawn from the research.

- Neural networks offer a realistic alternative to knowledge based systems and traditional mathematical models.
- Computer simulation of the process and its faults can provide invaluable information for the development of a neural network approach.
- Network topology and training is critical to the performance of the network, in terms of training times and accuracy of diagnosis.
- The most widely used training method is the back propagation algorithm.
- Most process faults can be diagnosed with either one or two hidden layers.
- Diagnosis of faults which the network has been trained on is very successful.
- Neural networks can generalise and diagnose multiple faults which comprise single faults on which the network has been trained.
- Neural networks prove to be very robust classifiers in the presence of both noisy and faulty sensor data.
- Neural networks offer no user transparency making the insight into the problem solving process impossible.

- Unlike knowledge based systems, neural networks suffer a progressive degradation in performance when faced with incomplete data sets.

Although neural networks have found widespread use as diagnostic tools, the amount of experience in applying them to diesel engine fault diagnosis, particularly at a practical level, is very limited. Current knowledge in this area of work is non-existent or deficient in the following areas;

- The training and testing of neural networks on real engine test data representing realistic fault conditions.
- Trend determination and identification of fault-symptom relationships.
- The analysis of neural network diagnostic ability on authentic diesel engine faults at genuine levels of fault severity.
- A detailed analysis of the most effective diagnostic sensors on high speed diesel engines for a variety of faults in various engine sub-systems.
- Training and testing of neural networks on direct fault-symptom relationships using various training algorithms.
- Training and testing neural networks to obtain an optimal degree of learning.
- The effect of neural network architecture on diesel engine fault diagnosis.
- Neural network diagnostic performance on a wide range of diesel engine faults including fuel injection equipment.
- Neural network performance under noisy and faulty diesel engine sensor data.
- Neural network performance on new diesel engine faults which it has not been trained on.

- The diagnostic performance of a neural network at different torques and speeds which it has not been trained at.

The following overall research aim and objectives were identified as a suitable vehicle for investigating these areas of weakness in current knowledge.

1.5 Aims And Objectives Of This Research

The overall aim of the research was to design, configure and validate a system which would perform on-line condition monitoring and fault diagnosis of a marine diesel engine. In order to achieve this the following objectives were identified.

1. Design and configure a sensor & hardware platform to gather engine data under both healthy and faulty modes of engine operation.
2. Develop & validate an on-line diesel engine performance monitoring system which will facilitate on-line fault diagnosis using a neural network approach.
3. Identify faults/fault groups which could be analysed by an advanced condition monitoring and fault diagnosis system of limited scope.
4. Assess engine fault conditions using computer simulation modelling and rig testing.
5. Compile operating maps of the engine's performance under both healthy and faulty modes of operation by the use of a diesel engine test bed facility.
6. Configure a neural network based system that will perform on-line condition monitoring and fault diagnosis based on the data generated from the performance monitoring system.

1.6 Major Achievements Of This Research

By satisfying the research objectives outlined above the work has led to several major achievements. These are summarised in the following points.

- The development of a comprehensive, fully automated, PC based system to monitor engine performance using largely 'off the shelf' software and hardware.
- A detailed analysis of high speed diesel engine instrumentation repeatability and the effects of data sampling and averaging.
- A comprehensive study of commonly occurring high speed diesel engine faults, reasons for their occurrence and quantification of fault severities experienced on real in-service engines.
- As a result of **engine testing genuine faults of realistic severity**, explicit fault-symptom relationships were developed and key diagnostic sensors for a high speed diesel engine were identified.
- The **training and testing** of a neural network based diagnostic system on real engine data including fuel injection system faults.
- An assessment of several neural network training algorithms and neuron configurations to give optimum diagnostic performance when applied to diesel engine diagnostics.
- The **development of a new technique** which greatly enhances the diagnostic ability of neural networks through the use of an on-line diagnostic database.
- The **development of 'weight adjusting' and 'confidence factor' algorithms** which operate on raw neural network outputs to ensure a correct, reliable and repeatable diagnosis can be achieved under operational conditions.

- The development of a neural network diagnostic sensor filter to demonstrate that sensor failures can also be detected by neural networks.
- Neural network testing on engine faults which the network was not trained on and torques and speeds which the network had not been trained on. And an assessment of neural network performance on noisy and faulty engine test data.

CHAPTER 2

THE DIESEL ENGINE TEST CELL FACILITY

2.0 Introduction

This chapter describes the diesel engine test cell developed in the Thermal Power Group test cells at RNEC Manadon. The engine used for all testing in this research was a 6 cylinder Perkins T6.354(M) diesel engine. The engine was fully refurbished before installation to check that components were within manufacturers tolerances and that performance was to specification. This minimised the possibility of the engine developing an unknown fault, detrimentally affecting the validity of the data representing both healthy and faulty test conditions. The engine was run in for several hundred hours to ensure stable engine performance and to minimise the effects of initial component run in before experimental results were taken.

Load was applied using an eddy current dynamometer. Both engine and dynamometer were housed in an enclosed and sound proofed test cell as shown in Figure 5.

Cooling water and fuel was supplied to the test cell from external tanks, air was supplied through the cell ventilation system. The engine was controlled externally from the test cell console, which also served as a focal point for data collection and is shown in Figure 6.

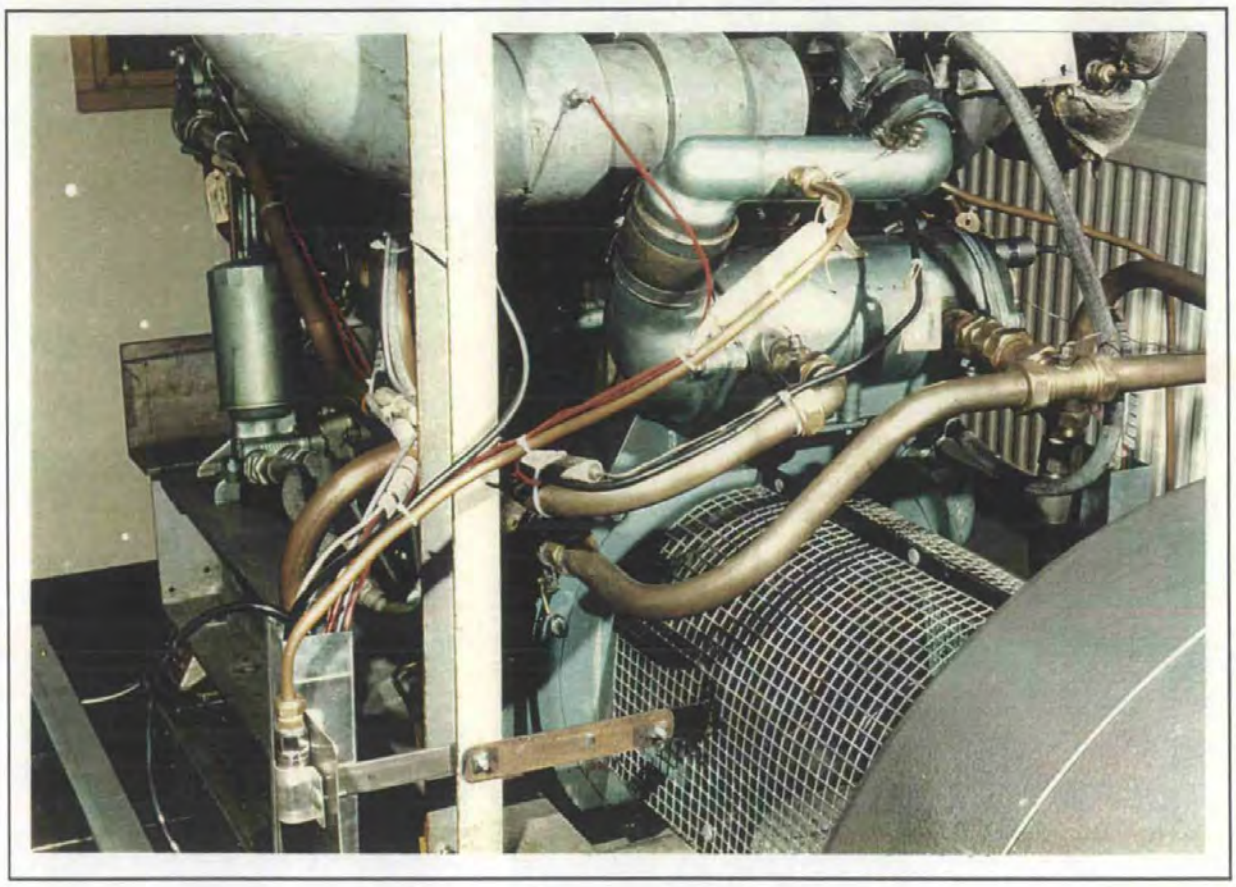

Figure 5 Engine & Dynamometer

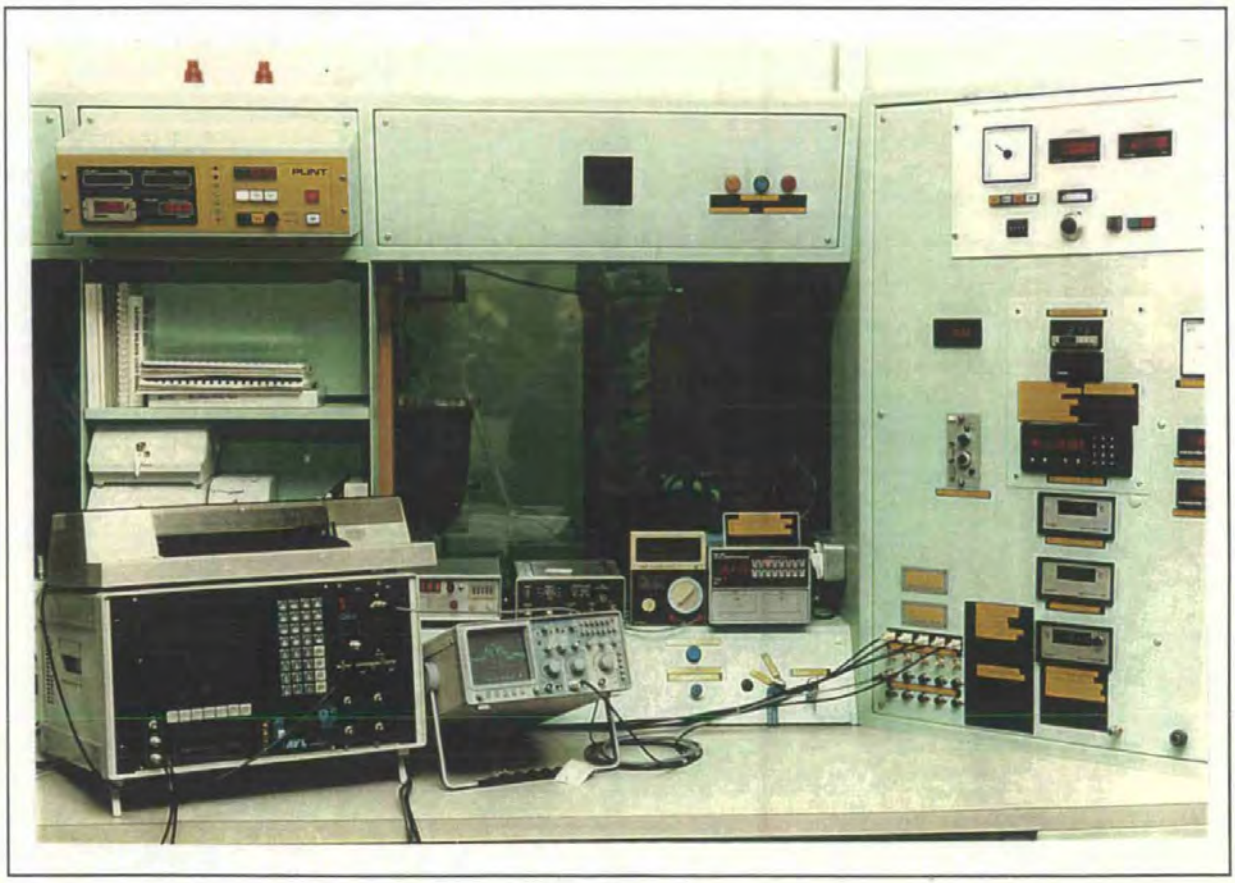

Figure 6 The Test Cell Console

Engine data could be recorded manually using the panel meters and an AVL 647 Indiskop or automatically using the engine performance monitoring package developed as part of this research . All data collected for the purposes of this research used the latter method. The panel meters and the AVL 647 Indiskop were, however, initially used to cross check results recorded by the automated engine performance monitoring system.

2.1 The Perkins T6.354(M) Diesel Engine

The Perkins T6.354(M) diesel engine has two core applications within the Royal Navy. It is used for the main propulsion of small craft such as LVCP's, launches and patrol vessels and on warships as a generating set engine.

Since the engine is employed in propulsive and gen-set applications this enabled the research to realistically target two main areas of diesel engine operation. Some of the most salient features of the engine specification are listed below, a full specification can be found in Appendix 'A'.

Type:	4 stroke, DI, CI, marinised
Number of cylinders:	6
Rated speed	2250 revs.min^{-1}
Brake power at full load rated speed	90 kW
Nominal cylinder bore:	98.4 mm
Stroke:	127 mm
Connecting rod length:	219.07 mm
Swept volume:	5.8 litres

Nominal compression ratio:	16:1
Firing order:	1-5-3-6-2-4
Manifold groupings:	Inlet: single
	Exhaust: Twin (1,2,3 & 4,5,6)
Fuel injection pump:	Lucas CAV mechanical DPA
Turbocharger:	Holset 3LD Mk.I (Appendix 'A')

2.2 Engine Instrumentation

The ability to generate accurate and repeatable engine test data is fundamental to the application of diesel engine condition monitoring and fault diagnosis techniques. Since any diagnosis or assessment of engine performance is solely dependent on engine data, the engine instrumentation must be seen as the most important component in any condition monitoring or diagnostic system. The viability of any condition monitoring or diagnostic system is largely dictated by the number, location and type of sensors required to derive an accurate assessment of engine health. Ideally, the sensor configuration chosen for condition monitoring and diagnostic type applications should meet the following criteria;

- Sensors should give accurate, and more importantly, repeatable data.
- Instrumentation should be non intrusive.
- Sensor installation should require minimal engine modification.
- Sensors should have a reliability much greater than the engine itself.
- Instrumentation should be robust.
- Instrumentation cost should be low.
- A degree of sensor redundancy should be incorporated.

The Perkins T6.354(M) diesel engine was comprehensively instrumented allowing a thorough evaluation of engine performance and the processes leading to the development of the fault-symptom relationships. The adoption of this strategy meant that the instrumentation system was initially complex, but allowed the potential of all sensors as diagnostic aids to be investigated fully, with sensor minimisation only being applied after fault-symptom relationship development.

2.3 General Instrumentation

The most commonly measured parameters were temperature and pressure of the charge air and exhaust gas. In all instances temperature was measured using 'K' type thermocouples and pressure was measured using resistive strain gauge transducers.

2.3.1 Temperature measurement

Several types of temperature measuring devises were considered including in-glass thermometry, resistance thermometry and themocouples. The eventual use of the data acquisition system ruled out the use of in-glass techniques. Resistance thermometry, although accurate, was rejected on the grounds of the signal conditioning required and the cost. It was concluded that the thermocouple offered a cheap, simple, reliable and versatile form of temperature measurement which could be easily interfaced with the data acquisition hardware.

The 'K' type thermocouple junction was composed of two base metal alloys, nickel-chromium and chromium-aluminium. This type of junction had an operating range

of 73 K to 1673 K and produces approximately 42 microvolts per K. The relationship between temperature and EMF was not linear particularly in the range 323 K to 473 K and the measuring junction required a reference cold junction. Linearisation and cold junction referencing could be performed by either a 'K' type thermocouple panel meter or a suitable data acquisition card. Because the EMF produced was a function of the composition of the metal in the junction, thermocouple accuracy often varied from batch to batch. The only means of quantifying this variation was through calibration, this is discussed more fully in Chapter 4. Temperature measurement of flowing streams of gas was made difficult because the velocity of the gas and the orientation of the thermocouple junction to the direction of flow both affect the indicated temperature reading[37] . Exhaust gas temperature measurement was also subject to further inaccuracies due to radiation effects from the manifold walls, especially at higher temperatures[37] .

2.3.2 Pressure Measurement

The strain gauge pressure transducer features a diaphragm which was exposed to the pressure to be measured. The diaphragm deformed under the pressure of the fluid and this deflection was passed through a push rod mechanism to a bending beam which had strain gauges mounted on its surface. By using a wheatstone bridge principle, beam deflection and hence diaphragm pressure could be gauged by output voltage. Typically these transducers had a natural frequency of 15 kHz. This low natural frequency made them more suitable for indicating average pressures in turbulent or pulsating fluid flows, than piezo electric or piezo resistive transducers

with a higher natural frequency. All pressure tappings were drilled perpendicular to the direction of fluid flow thus recording static pressure[38] .

2.4 Instrumentation Specification

For ease of presentation the engine instrumentation is best divided into the following sub systems.

- Atmospheric conditions
- Charge air system
- Exhaust system
- Combustion monitoring
- Fuelling & power
- Lubricating oil and cooling water

2.4.1 Atmospheric Conditions

Ambient conditions were monitored at regular intervals inside the test cell for the duration of all engine tests. Table 1 gives a brief description of the instruments used.

Code	Instrument Description	Instrument Type
H1	Atmospheric humidity	Capacitive relative humidity sensor
P1	Barometric pressure	Aneroid barometer
T1	Ambient temperature	'K' Type thermocouple

Table 1 Instrumentation To Measure Atmospheric Conditions

2.4.2 Charge Air System Instrumentation

This set of instrumentation covered the charge air path from the intake filter to the inlet valves including the turbocharger compressor and intercooler. Table 2

summarises the instrumentation system. Figure 7 shows a schematic diagram of instrumentation arrangement

Code	Instrument Description	Instrument Type
Q1	Inlet air volumetric flow rate	Scheme IPL Vortex frequency sensor
T2	Air temperature before compressor	'K' Type thermocouple
P2	Air pressure before compressor	Strain gauge pressure transducer
T3	Air temperature after compressor	'K' Type thermocouple
P3	Air pressure after compressor	Strain gauge pressure transducer
T4	Inlet manifold temperature	'K' Type thermocouple
P4	Inlet manifold Pressure	Strain gauge pressure transducer
S1	Turbocharger rotational speed	Inductance pick-up

Table 2 Charge Air Instrumentation Summary

The following describes the function of the charge air instrumentation with regard to performance monitoring and fault diagnosis.

- **Charge air filter condition**

The difference between atmospheric pressure and the pressures downstream of the filter coupled with the air mass flow rate gave an indication of the amount of filter fouling.

- **Compressor performance**

Pressure and temperature both upstream and downstream of the compressor combined with measurements of air flow rate and turbocharger rotational speed allowed compressor operating points to be plotted on the compressor map. Plotting the data in this format would identify any deterioration in compressor performance.

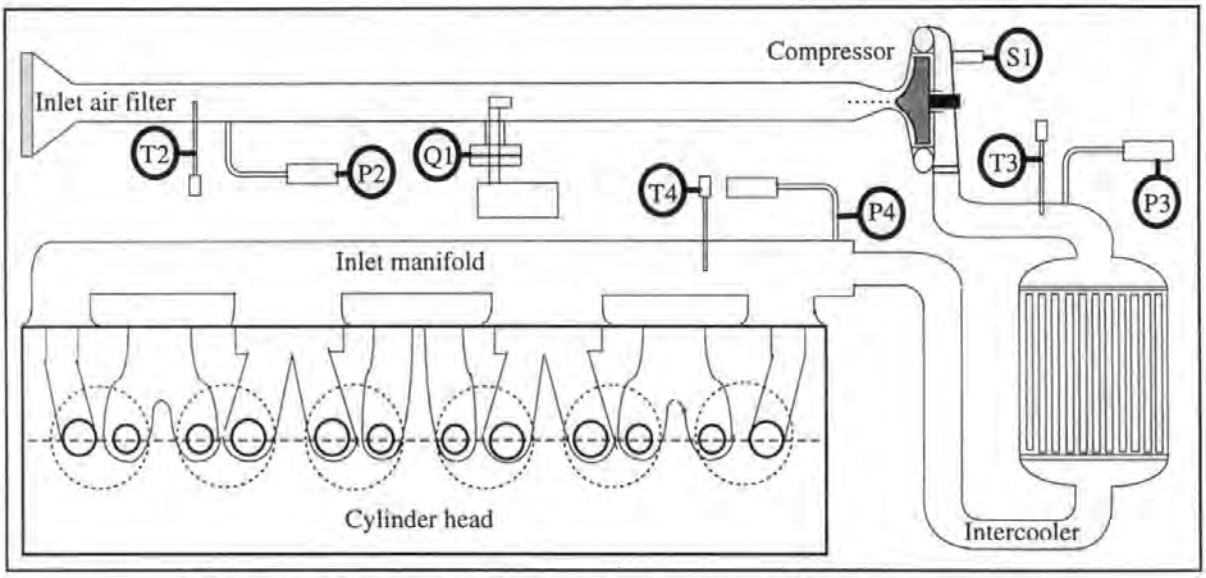

Figure 7 Charge Air System Instrumentation Arrangement

- **Intercooler performance**

Measurement of temperature and pressure upstream and downstream of the intercooler and a knowledge of the air mass flow rate and cooling water temperature differential allowed the intercooler effectiveness to be quantified. Intercooler fouling, corrosion or cross mixing of fluids would lead to a reduction in effectiveness.

- **Inlet manifold conditions**

Manifold pressure and temperature were measured since they would be effected, to some extent, by both charge air system performance and valve faults. Manifold conditions also directly affect combustion and therefore overall engine performance.

2.4.3 Exhaust System Instrumentation

The exhaust system instrumentation followed the gas path from the exhaust valves along the exhaust manifold through to the turbine discharge. Table 3 summarises the instrumentation system.

Code	Instrument Description	Instrument Type
T5	Exhaust port temperatures 1 & 2 cylinders	'K' Type thermocouple
T6	Exhaust port temperature 3 cylinder	'K' Type thermocouple
T7	Exhaust port temperature 4 cylinder	'K' Type thermocouple
T8	Exhaust port temperatures 5 & 6 cylinders	'K' Type thermocouple
T9	Collective exhaust manifold temperature	'K' Type thermocouple
P5	Collective exhaust manifold pressure	Strain gauge pressure transducer
T10	Turbine exit temperature	'K' Type thermocouple
P6	Turbine exit pressure	Strain gauge pressure transducer
S1	Turbocharger rotational speed	Inductance pick-up

Table 3 Exhaust System Instrumentation

The exhaust system consisted of two separate manifolds combined in one water cooled casting. One manifold served cylinders 1,2 & 3 the other served cylinders 4, 5 & 6. The two exhaust gas streams mixed in a separate casting just upstream of the turbine entrance. The collective manifold instruments, T9 and P5, were located in this casting. The cross sectional area of the casting reduced towards the turbine entrance increasing the kinetic energy of the exhaust gas. The pressure was measured at the largest cross sectional area of the casting which was of a similar size to the manifold exit ensuring that a representative measure of collective manifold pressure was obtained. The exhaust manifold cooling water jacket made collective manifold temperature and pressure difficult to measure in any other way.

Only four exhaust port thermocouples served the six cylinders, this was due to the nature of the head casting. Gas paths for cylinders 1 & 2 and 5 & 6 were common whereas cylinders 3 and 4 had individual exhaust gas paths. Some of the injection faults, discussed later in this thesis, were introduced on to number six cylinder only, due to the location of the combustion and injection instrumentation. The thermocouple serving cylinders 5 & 6 was positioned with the junction close to

number six cylinder valve. This minimised the risk of exhaust gas flow from number five cylinder diluting any changes in number six cylinder exhaust temperature due to faults introduced. Similarly the thermocouple serving cylinders 1 and 2 had its junction located close to number one cylinder exhaust valve as a comparitor for the number six cylinder thermocouple.

The exhaust manifold is a harsh environment for most instrumentation. To withstand this environment sheathed thermocouples were used. The subsequent increase in thermocouple diameter reduced the thermocouple response time. Since exhaust gas temperature was being monitored as a steady state parameter and not on an in-cycle variation basis, this loss in response rate was accepted. Figure 8 shows the general arrangement of the exhaust system instrumentation.

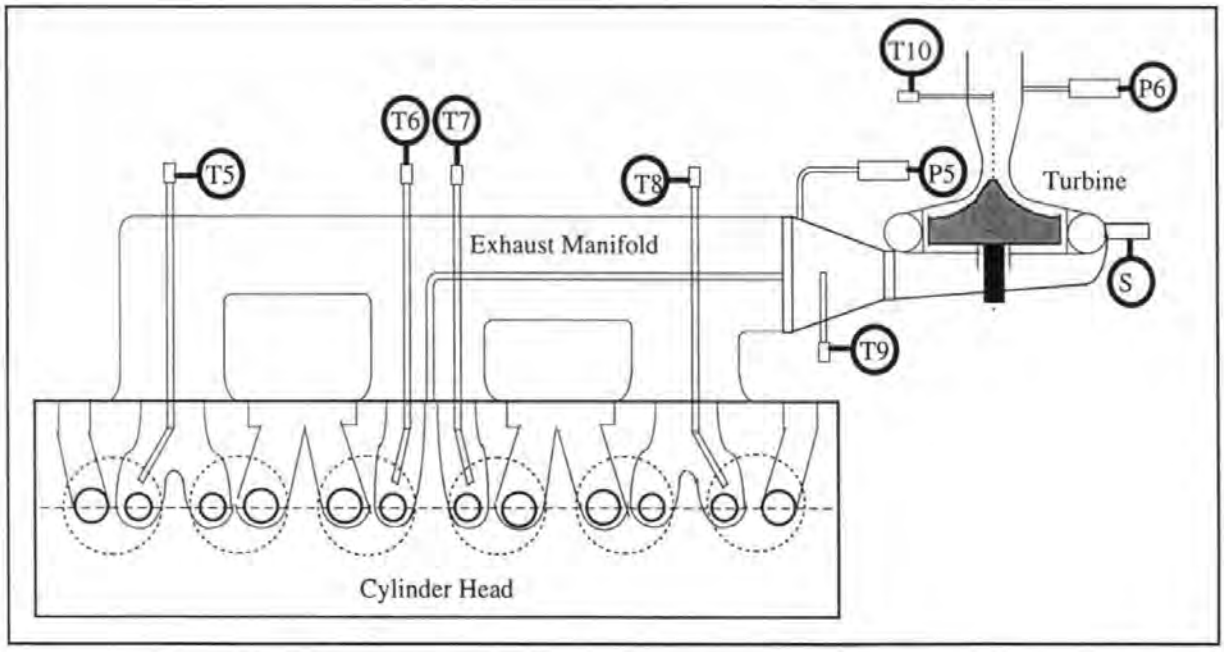

Figure 8 Exhaust System Instrumentation

The following comments outline the purpose of the exhaust system instrumentation.

- **Exhaust gas temperature measurement**

Exhaust gas temperature measurement could provide a wealth of diagnostic information since it bore a direct relationship to in-cylinder combustion. This in turn meant that a knowledge of the charge air system and fuel injection equipment performance could be gained. The close proximity of the thermocouple junctions to the exhaust valves also maximised the chances of detecting exhaust valve faults.

- **Turbine performance**

Measurement of temperature and pressure upstream and downstream of the turbine combined with turbine speed and exhaust gas mass flow rate allowed operating points to be plotted directly on the turbine map. Any deterioration in turbine performance due to fouling or mechanical failure could be identified by the position of the operating point on the map.

2.4.4 Combustion Monitoring

The combustion is the single most important process when determining the performance of a diesel engine. Poor combustion leads to excessive fuel consumption, high gaseous emissions & particulates and abnormally high wear rates and fouling of cylinder components. Four pieces of instrumentation were dedicated to combustion monitoring, these are shown in Table 4.

In-cylinder conditions vary from cylinder to cylinder, however, due to the high cost and problematic installation of these instruments only one cylinder was monitored.

All combustion data was taken from number six cylinder and was considered representative of the performance of the other five cylinders.

Code	Instrument Description	Instrument Type
CA	Crank angle encoder	AVL 364 Optical shaft encoder & signal conditioners
CP	Cylinder pressure	AVL QC32C-E Water cooled piezo electric pressure transducer
NL	Injector needle lift	Wolff controls Hall effect adjustable length sensor
FL	Fuel line pressure	AVL KG6 Piezo electric fuel line pressure transducer

Table 4 Combustion Monitoring Instrumentation

Cylinder pressure, needle lift and fuel line pressure were all recorded with respect to crank angle position. The optical shaft encoder, mounted on the crank nose as shown in Figure 9, allowed these parameters to be sampled at 0.5° crank angle increments and also indicated TDC of the monitored cylinder.

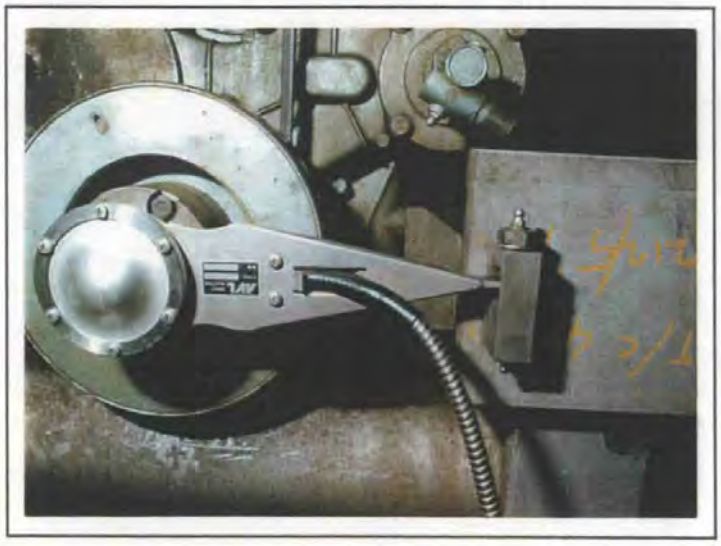

Figure 9 Crank Angle Measurement

2.4.5 Cylinder Pressure Measurement

The piezo electric transducer was fitted vertically down through the cylinder head avoiding the valves and the injector and was exposed to the edge of the cylinder

bore. Research has shown that the in cylinder position of the transducer can effect the pressure reading due to a phenomena known as 'squish'. Squish effects are due to the flow across the piston crown at and around TDC as the compressed mixture migrates from the cylinder walls towards the piston bowl. Due to the geometry of the cylinder head and transducer, fitting is limited to the position described above making it susceptible to squish effects. For the purposes of this research squish effects were ignored since precision was considered more critical than absolute accuracy.

The transducer was connected directly to a Kistler 5007 charge amplifier which gave an output voltage proportional to input charge. This linear analogue voltage was then scaled to engineering units to indicate cylinder pressure. Direct measurement of cylinder pressure is key to determining the thermodynamic performance of a diesel engine. When measured with respect to crank angle, cylinder pressure data gave rise to the following performance parameters which identified any abnormal combustion characteristics and in cylinder conditions.

- Maximum cylinder pressure (P_{max}) and its position with respect to TDC. Abnormally high P_{max}· are caused by well developed fuel premixing and atomisation leading to a rapid and uncontrolled first phase of combustion. High P_{max}· are usually associated with advanced injection timing or long ignition delay periods.
- Indicated Mean Effective Pressure (IMEP). Since IMEP equates to the indicated work done per cylinder per cycle it gives a general indication of the combustion

efficiency. Once the IMEP has been determined, Friction Mean Effective Pressure (FMEP), indicated thermal efficiency and mechanical efficiency can be calculated.

- Pumping Mean Effective Pressure (PMEP). Faults in the charge air system, inlet or exhaust valve faults leading to poor engine breathing would manifest themselves in an abnormally shaped pumping loop, leading to a change in the PMEP value. PMEP's determined through the use of piezo electric pressure transducers should be treated with some scepticism since the transducer is rapidly cooled during the pumping loop and the effect of cyclic thermal shock can lead to large percentage errors in these relatively small pressure readings.
- Approximate rate of heat release. Heat release diagrams derived from cylinder pressure will usually rely on empirical relationships to estimate change of species and heat transfer during combustion. Despite this, heat release diagrams give valuable information on premixing, atomisation, injection timing and determination of phases of combustion. Long combustion periods can often destroy the cylinder liner lubrication film because the liner is exposed to flame for a greater period of time, leading to accelerated wear of cylinder components.
- Ignition delay . Ignition delay is defined as the time period between the point of injection and the point when heat release becomes positive. The delay period is a function of premixing ,atomisation, injection timing, cylinder pressure and charge temperature.

2.4.6 Dynamic Injection Timing Measurement

Point of injection, ignition delay and duration of injection are all determined from injector needle lift. Needle lift was detected using the Hall effect principle. A magnetic cap was mounted on the injector spindle and a fixed probe held a semi-conducting slice in close proximity to the magnetic cap. When high pressure fuel entered the injector nozzle the needle and spindle moved upward against the injector spring. As the magnetic cap moved closer to the semi-conducting slice an EMF was produced proportional to needle lift. Needle lift traces can provide valuable diagnostic information on the injection pump and injector performance.

2.4.7 Fuel Line Pressure Measurement

Fuel line pressure was measured by a cheap, simple, non-intrusive and robust piezo electric device which was designed to give a qualitative rather than quantitative indication of fuel line pressure. The transducer clipped on to the high pressure injection pipes running between the injection pump and the injector. The high pressure fuel pulse generated by the injection pump instantaneously deformed the fuel pipe. The sensor used this deformation to produce a charge which was then conditioned by a Kistler 5007 charge amplifier to produce a 0 - 10 volt analogue voltage signal. Fuel line pressure data provides diagnostic data on fuel pump and injector performance. Figure 10 shows the cylinder pressure, needle lift and fuel line pressure transducers.

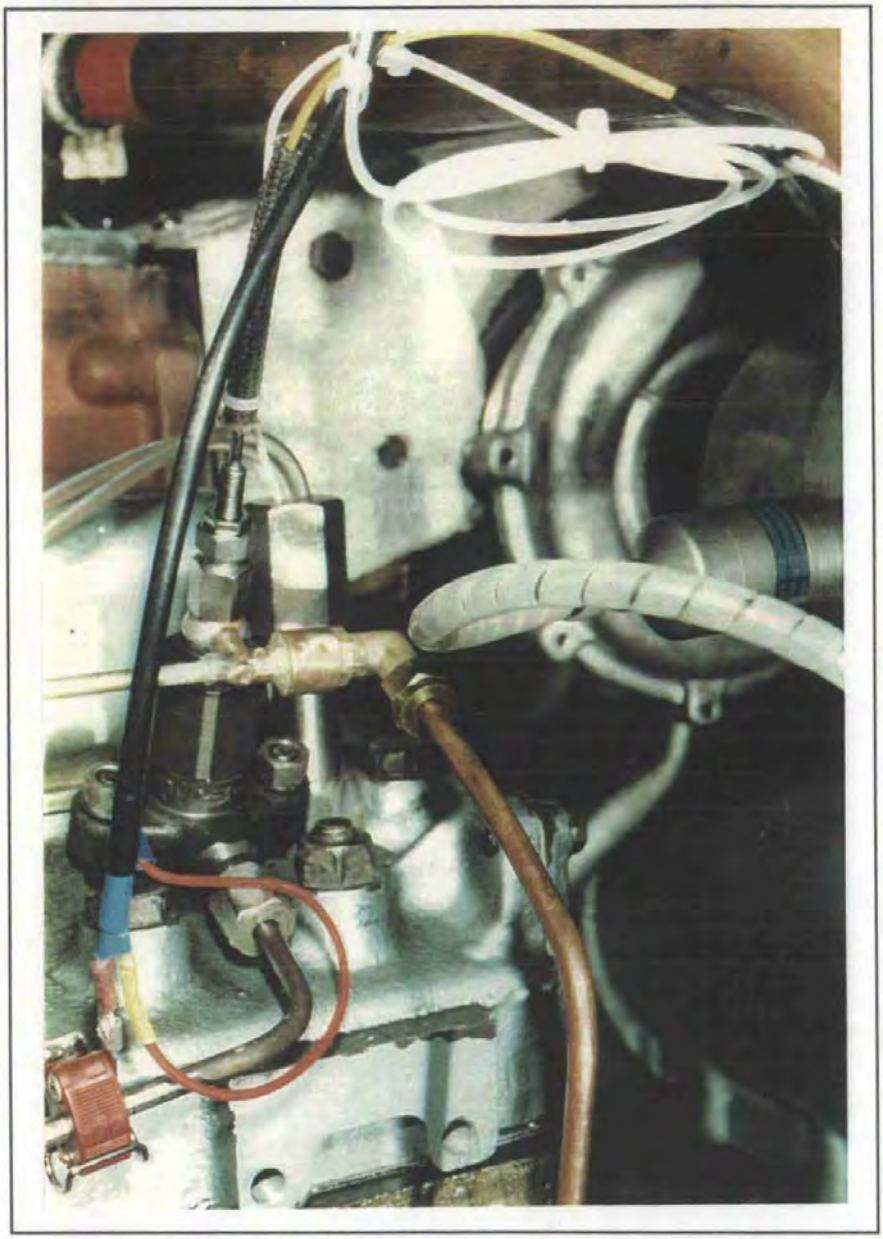

Figure 10 Cylinder Pressure, Needle Lift & Fuel Line Pressure Transducers

2.4.8 Fuelling & Power

Fuel consumption measurement and brake power are the two most important parameters when assessing overall engine performance. Engine load was applied using a Froude AG250 Eddy Current Dynamometer and controlled by a Froude Consine Texcel 50 dynamometer controller. The Texcel 50 Dynamometer controller had four modes of operation, constant speed, constant torque, power law and open loop control. Fuel consumption was measured in volumetric terms. Table 5 outlines

all instrumentation associated with fuelling and power measurement. A schematic diagram of the instrumentation layout is shown in Figure 11.

Code	Instrument Description	Instrument Type
S2	Dynamometer rotational speed	Inductance pick - up
Z1	Engine torque	Maywood U4000 Load cell
S3	Engine rotational speed	Inductance pick - up
F1	No. 1 Fuel flow rate meter	Plint fuel meter
T11	Fuel temperature in fuel flask	'K' Type thermocouple
F2	No. 2 Fuel flow rate meter	Hydrotechnic GFM 01 geared flow meter
T12	Fuel temperature at meter	'K' Type thermocouple
X1	Fuel Rack Position	Potentiometer
T13	Fuel temperature at injection pump supply	'K' Type thermocouple

Table 5 Fuelling & Power Instrumentation

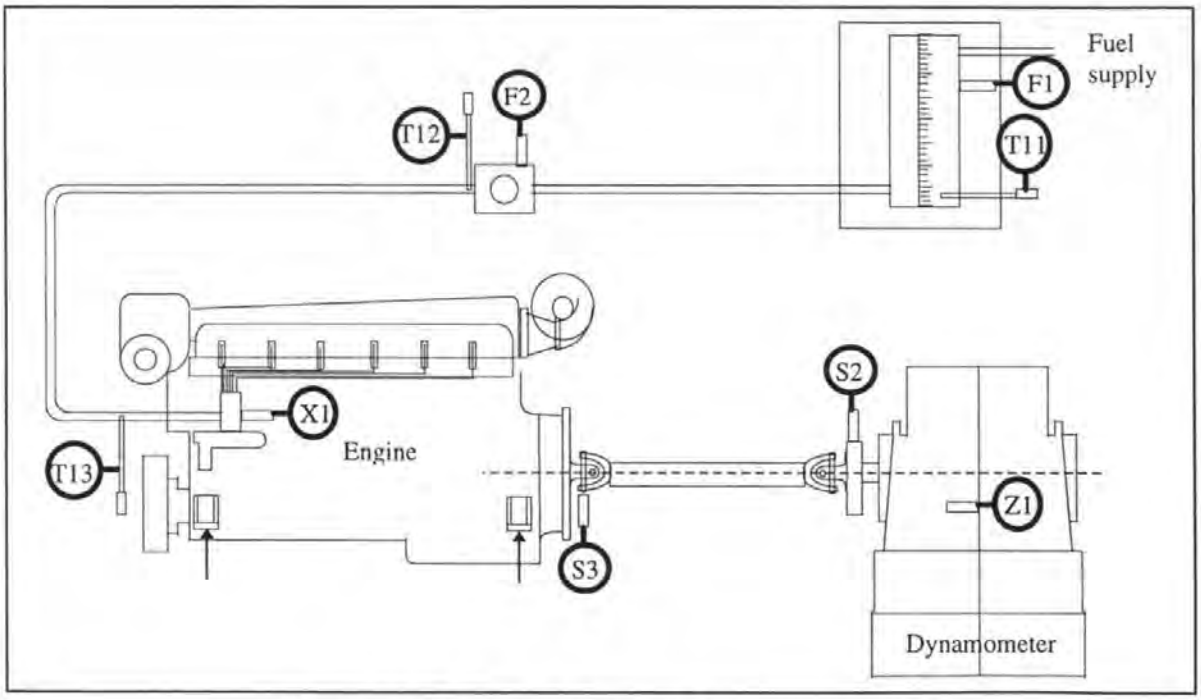

Figure 11 Fuelling & Power Instrumentation

Engine fuel consumption was measured by two independent instruments. F1 recorded the time period and number of engine revolutions required for the engine

to use a specified volume of fuel, usually 200 ml. F2 was a very accurate geared flow meter which measured the volumetric flow rate in litres per second. Both instruments included temperature measurement and fuel specific gravity was measured periodically for volume flow rate to mass flow rate conversion. Engine speed was measured by two individual sensors. S2 was linked to the Texcel 50 dynamometer controller and S3 was connected to the Plint fuel measuring system.

2.4.9 Lubricating Oil & Cooling Water System Instrumentation

Lubricating oil temperature was monitored by a 'K' type thermocouple at one point on the main oil gallery in the block. Lubricating oil pressure was also measured at this point using a strain gauge pressure transducer. The cooling water system was monitored by 'K' type thermocouples placed in the following locations.

- Cooling water inlet
- Intercooler inlet
- Engine discharge
- Intercooler discharge
- Engine thermostat housing

Abnormal intercooler cooling water temperature differentials could identify if fouling or corrosion existed in the intercooler, particularly if these trends could also be linked to data obtained from the charge air instrumentation. The remainder of cooling water instrumentation could give a measure of the cooling systems effectiveness and identify abnormal heat transfer processes.

2.5 Summary

This chapter has detailed the overall test facility layout, engine and instrumentation specification which was used to undertake this research. This comprehensive test facility was developed from the base test engine over a 9 month period. This chapter has also discussed the rationale applied to instrumentation selection and installation and some of the difficulties experienced during fitting and commissioning of engine test instrumentation. In addition to this, the measuring principles of the instrumentation have been discussed. Completion of this work satisfied research objective 1 detailed in Chapter 1 and formed the foundation for the development of an automated performance monitoring system.

CHAPTER 3

AUTOMATED ENGINE PERFORMANCE MONITORING

3.0 Introduction

This chapter details the development of an automated diesel engine performance monitoring package. One of the objectives of this research was to perform on-line diagnosis which necessitated automated data capture and post-processing. Initially the test cell used panel meters to display all parameters except the fuel injection and combustion data which was recorded by an AVL 647 Indiskop. This was then superseded by an IBM compatible PC based data acquisition system to facilitate automatic data collection. The following sections outline the instrument signal processing, data acquisition hardware and software and the development of the automated diesel engine performance monitoring package.

3.1 Instrument Signal Processing

Many of the instruments outlined in Chapter 2 required some form of signal conditioning before they could be connected to the data acquisition cards. In general the data acquisition cards accepted various analogue voltage ranges. Table 6 details the instrument type, signal conditioning applied, card input signals and the subsequent engineering units and range of each parameter as defined in the data acquisition software.

No.	Instrument Description	Instrument Type	Sensor OP	Signal Conditioning	Card IP	Engineering Units
1	Atmospheric Humidity	Hygrometer	0 - 10 V	none	0 - 10 V	10 - 90 % [RH]
2	Atmospheric Pressure	Aneroid Barometer	manual	none	none	0 - 1500 [m Bar]
3	Atmospheric Temperature	K Type Thermocouple	µV	TC16H Card	µV	273 - 1600 [K]
4	Inlet Air Flow Rate	Vortex Frequency Flow Meter	Frequency	VFM588 Panel Meter	2 - 10 V	9 - 540 [cubic m]
5	Air Temperature Before Compressor	K Type Thermocouple	µV	TC16H Card	µV	273 - 1100 [K]
6	Air Pressure Before Compressor	Strain Gauge Pressure Transducer	0 - 25 mV	none	0 -25 mV	0 - 2 [Bar A]
7	Air Temperature After Compressor	K Type Thermocouple	µV	TC16H Card	µV	273 - 1600 [K]
8	Air Pressure After Compressor	Strain Gauge Pressure Transducer	0 -100 mV	none	0 - 100 mV	0 - 2 [Bar G]
9	Inlet Manifold Temperature	K Type Thermocouple	µV	TC16H Card	µV	273 - 1100 [K]
10	Inlet Manifold Pressure	Strain Gauge Pressure Transducer	0 -25 mV	none	0 - 25 mV	0 - 2 [Bar A]
11	Turbocharger Rotational Speed	Inductance Pick up	Frequency	Fylde F-V converter	0 -10 V	0 - 100000 revs/min
12	Exhaust Port Temperatures 1 & 2 Cylinders	K Type Thermocouple	µV	TC16H Card	µV	273 - 1600 [K]
13	Exhaust Port Temperature 3 Cylinder	K Type Thermocouple	µV	TC16H Card	µV	273 - 1600 [K]
14	Exhaust Port Temperature 4 Cylinder	K Type Thermocouple	µV	TC16H Card	µV	273 - 1600 [K]
15	Exhaust Port Temperatures 5 & 6 Cylinders	K Type Thermocouple	µV	TC16H Card	µV	273 - 1600 [K]
16	Collective Exhaust Manifold Temperature	K Type Thermocouple	µV	TC16H Card	µV	273 - 1600[K]
17	Collective Exhaust Manifold Pressure	Strain Gauge Pressure Transducer	0 - 100 mV	none	0 - 100 mV	0 - 5 [Bar G]
18	Turbine Exit Temperature	K Type Thermocouple	µV	TC16H Card	µV	273 - 1100 K
19	Turbine Exit Pressure	Strain Gauge Pressure Transducer	0 - 100 mV	none	0 - 100 mV	0 - 100
20	Crank Angle Encoder	AVL Optical Shaft Encoder	Frequency	AVL 3064A02 Unit	clean TTL	0 - 360° (0.5° res.)
21	No. 6 Cylinder Pressure	AVL QC32C - E Transducer	Pc (charge)	Kistler 5007 Charge Amp	0 - 10 V	0 - 150 [Bar A]
22	No. 6 Cylinder Injector Needle Lift	Wolf Controls Hall Effect Sensor	0 - 3.6 V	none	0 - 3.6 V	0 - 0.3 mm
23	No. 6 Cylinder Fuel Line Pressure	AVL Piezo Electric Transducer	Pc (charge)	Kistler 5007 Charge Amp	0 - 10 V	0 - 1000 [Bar G]
24	No.1 Fuel Flow Rate	Plint Fuel Metering Unit	TTL	none	none	none
25	No. 2 Fuel Flow Rate	Geared Flow Meter	Frequency	PRA1 F-V converter	0 - 10 V	0.005 - 1.000 [l/sec]
26	Fuel Temperature	K Type Thermocouple	µV	TC16H Card	µV	273 - 1600 [K]
27	Fuel Rack Position	Potentiometer Circuit	0 - 3.8 V	none	0 - 3.8 V	0 - 50 [mm]
28	Engine Torque	Maywood U4000 Load Transducer	0 - 5 V	Froude Texcel 50	0 - 10 V	0 - 1000 [Nm]
29	Engine Speed	Inductance Pick-Up	Frequency	Froude Texcel 50	0 - 10 V	0 - 2500 [revs/min]
30	Lubricating Oil Temperature	K Type Thermocouple	µV	TC16H Card	µV	273 - 1600 [K]
31	Lubricating Oil Pressure	Strain Gauge Pressure Transducer	0 - 100 mV	none	0 - 100 mV	0 - 5 [Bar G]
32	Cooling Water Inlet Temperature	K Type Thermocouple	µV	TC16H Card	µV	273 - 1600 [K]
33	Intercooler Cooling Water Inlet Temperature	K Type Thermocouple	µV	TC16H Card	µV	273 - 1600 [K]
34	Cooling Water Temp. At Engine Dischg.	K Type Thermocouple	µV	TC16H Card	µV	273 - 1600 [K]
35	Cooling water Temp. At Intercooler Dischg	K Type Thermocouple	µV	TC16H Card	µV	273 - 1600 [K]
36	Engine Thermostat Cooling Water Temperature	K Type Thermocouple	µV	TC16H Card	µV	273 - 1600 [K]

Table 6 Instrumentation Signal Conditioning

3.2 Data Acquisition Hardware And Software

Engine data was gathered using two separate data acquisition devices linked to a 486 DX2 50 MHz IBM compatible PC. Instruments which read steady state parameters such as temperatures, pressures, speeds and flows were connected to an external Microlink 3000 rack which contained a number of data acquisition cards. High speed instruments such as the fuel line pressure transducer, needle lift transducer and cylinder pressure transducer were connected to a Microlink 570 high speed data acquisition card.

3.2.1 Steady State Parameter Data Acquisition

The Microlink 3000 data acquisition rack was linked to the PC using a GPIB (IEE 488) link. Communication and data transfer between the PC and the data acquisition rack was controlled by 2 cards, one inserted into the data acquisition rack and the other installed into a vacant AT expansion slot on the PC motherboard. The data acquisition rack comprised the following cards;

- **Power Module Card:** Provided a stabilised power supply to all the cards in the rack.
- **GPIB Control Card:** Managed the communication between the cards in the rack and an interface card inserted into one of the AT expansion slots on the PC motherboard.
- **12 Bit Analogue To Digital Buffered Card:** Performed all A to D conversion to 12 bit accuracy (1 in 4096 steps). It also contained some buffer for short term data storage.

- **16 Channel IO Analogue Voltage Card :** This card read all of the slow speed analogue voltage signals as shown in Table 6 except the thermocouples.
- **2 off 16 Channel Thermocouple Cards :** All thermocouples were connected to these cards via an isothermal box, which performed cold junction referencing electronically. The thermocouple cards linearised and amplified the thermocouple signal.

All of the hardware located in the data acquisition rack was controlled through Windows environment software called Windmill. Four applications in the Windmill program group were used to configure the data acquisition system and acquire the raw data, these are as follows.

- **Conf IML**: Used to set addresses and device numbers of the hardware and configure the channels.
- **Setup IML**: Used to set channel specification through assignment of name, signal type, input voltage range and a scaling and offset factor to calibrate into engineering units.
- **Windmill Logger**: Used to select channels and sampling rates and log the data in a table type format. The data was simultaneously displayed on-screen and saved to the hard drive in a logger file on-line. The channel and sampling details were saved as a logger set-up file to avoid unnecessary repetition in specifying the logger parameters.
- **Windmill Chart:** Used to simulate a paper and pen chart recorder and display data in a graphical format on-screen. Up to 8 channels could be logged

simultaneously, sampling frequency and parameter ranges could also be specified. This application was particularly useful when a generalised picture of transient behaviour was needed. Figure 12 gives a diagrammatic representation of the slow speed data acquisition system.

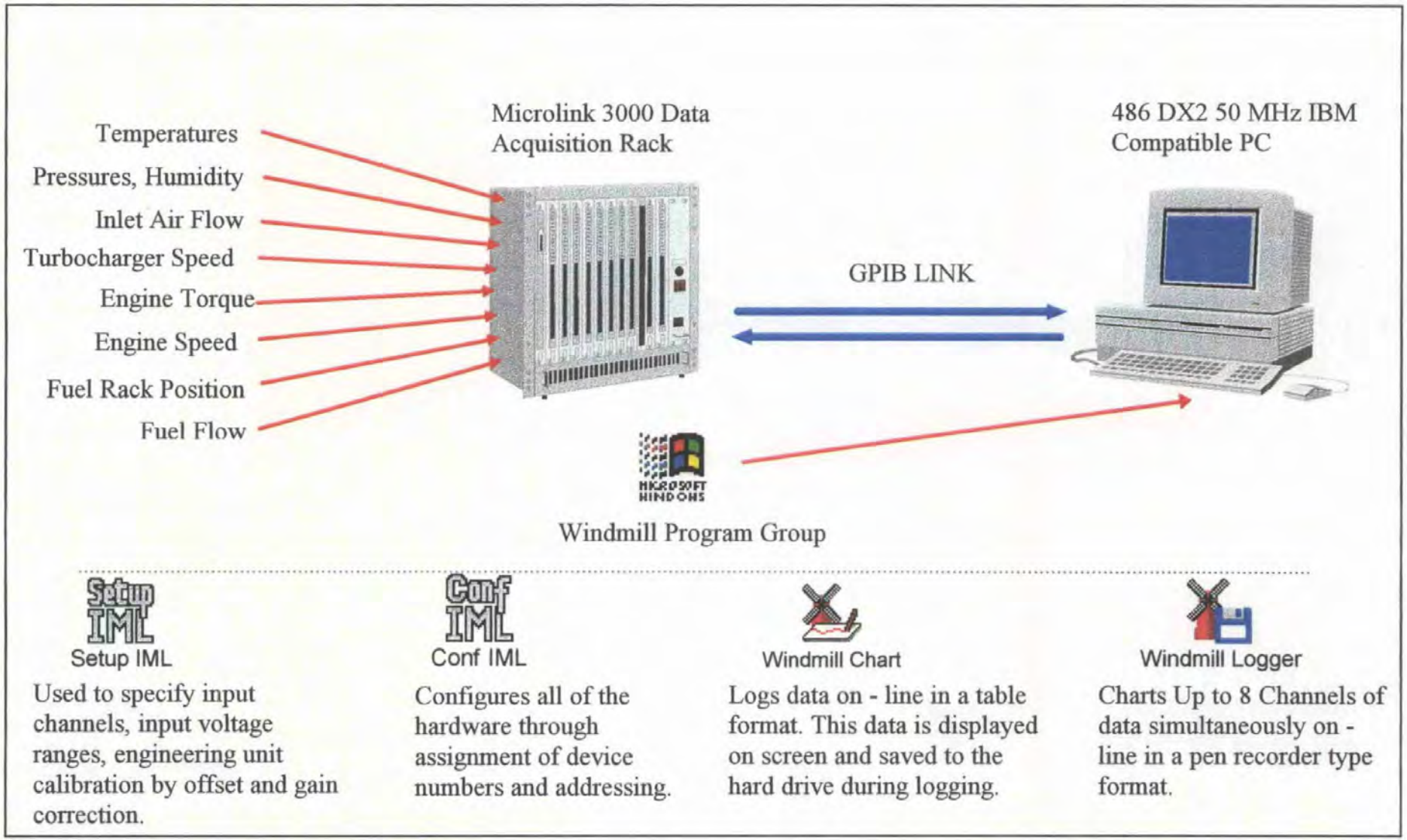

Figure 12 Slow Speed Data Acquisition System

3.2.2 High Speed Data Acquisition

All of the fuel injection and combustion instrumentation was logged by a 16 channel Microlink 570 100 kHz high speed data acquisition card. It was capable of reading the conditioned analogue voltage signals from by the fuel line pressure transducer, cylinder pressure transducer and the needle lift transducer as detailed in Table 6. The card had on-board 12 bit analogue to digital conversion and 512 K bytes of buffer. This enabled large high speed streams of data to be read instantaneously and then written to the hard drive after sampling.

Cylinder pressure, fuel line pressure and needle lift were sampled with respect to crank angle. The AVL 364 Optical Crank Angle Encoder generated 720 TTL pulses per revolution and a single TTL pulse per revolution which was phased with TDC of the instrumented cylinder. The Microlink 570 card used the once per revolution pulse as a trigger to phase the three channels of data with TDC and the 720 pulses per revolution as the clock signal to sample all three channels at 0.5^{o} crank angle increments. The Microlink 570 card was controlled by Windows environment software called Windspeed. Four applications in the Windspeed program group were used to configure the data acquisition system and acquire the raw data.

- **Conf IML**: Used to set addresses and device numbers of the hardware and configure the channels.
- **Setup IML**: Used to set channel specification through assignment of name, signal type, input voltage range and a scaling and offset factor to calibrate into engineering units.

- **Streamer**: Allowed channel selection and specification of sampling details. In this instance sampling was triggered at TDC and subsequent readings of cylinder pressure, fuel line pressure and needle lift occurred at 0.5° CA increments. Streamer initialised the card and controlled the rapid collection of data in one continuous 'stream'. This data was collected far too rapidly to be written to the hard drive during sampling so the data was stored in the on-card buffer. Sampling was terminated when the specified number of samples had been gathered. When sampling had finished the data was written to the hard drive.

  IMX To XL: Converted streamed files to an ASCII format which could be read by a number of applications, including Microsoft Excel.

Figure 13 shows a diagrammatic representation of the high speed data acquisition system.

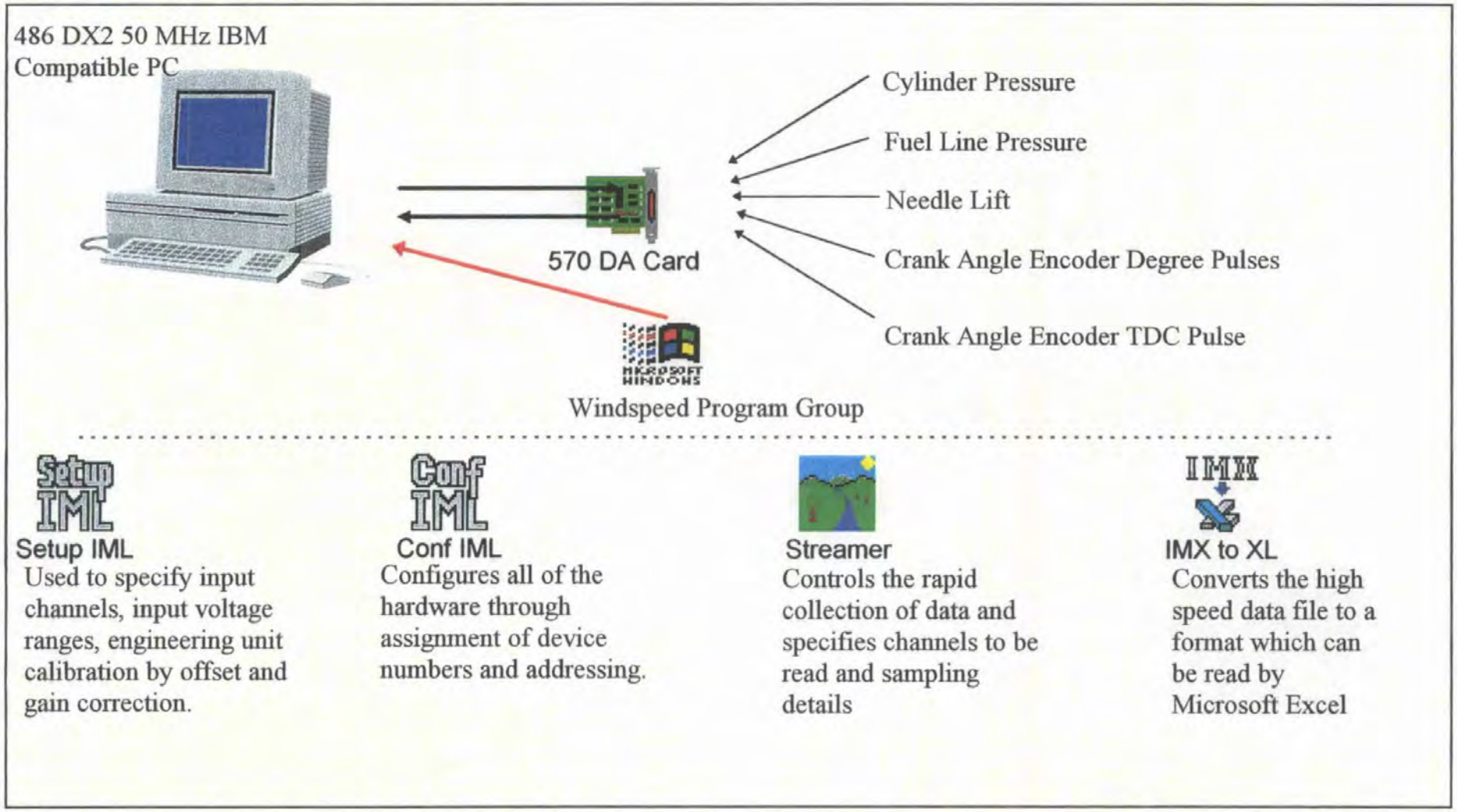

Figure 13 High Speed Data Acquisition

3.3 Automated Engine Performance Monitoring

The final stage in the development of the performance monitoring system was to automate the entire instrumentation, collection and post processing of data. The aim was to create a package which would automatically generate a single performance file characterising every aspect of the engine's performance. A Windows 3.1 environment was chosen as the operating system platform because it;

- Supports Dynamic Data Exchange (DDE) and Dynamic Link Libraries (DLL's) which allows software operating in a windows environment to share and manipulate data without the need for writing lengthy programs to ensure data compatibility.
- Is a multi tasking environment allowing several processing operations to be performed simultaneously.
- Is a cheap, well supported and readily available piece of software which will operate on most modern IBM compatible PC's
- Is an object orientated environment allows the rapid development of custom applications.
- Uses, and allows, the development of highly intuitive Man Machine Interfaces (MMI's).
- Supported the data acquisition software.
- Supports Microsoft Excel which can be used for a large proportion of the data post processing.

The final package developed, called Performance Monitor, consisted of 6 Microsoft Excel command macros, 1 Turbo C program and a number of Excel worksheets to manipulate the data. Essentially Performance Monitor was made up of a central command macro which controlled all of the other programs and applications. The central command macro controlled when data acquisition started and finished. It also controlled the movement of data from one application or worksheet to another and initiated each stage of data processing. Performance Monitor performed three major functions, firstly the collection and processing of the high speed data, secondly the collection and processing of the slow speed data and thirdly, the compilation of the performance file. Figure 14 shows a diagrammatic representation of Performance Monitor's structure. Hard copies of the programs and macros can be found in Appendix 'B'.

3.3.1 High Speed Data Collection & Processing

Once the RUN command had been selected from Performance Monitor's initial user screen, shown in Figure 15, the central command macro sent a series of commands to WINDSPEED, the Microlink 570 high speed data acquisition software. WINDSPEED initialised the card and selected and calibrated the channels. The central command macro then ran STREAMER which controlled the data acquisition, read cylinder pressure, needle lift and fuel line pressure and stored the data on the 570 card buffer. Performance monitor moved the streamed data into IMX To XL where the data was converted into a ASCII file format. This ASCII file was then read by the Turbo C program which divided the data into 720° crank angle blocks from TDC to TDC.

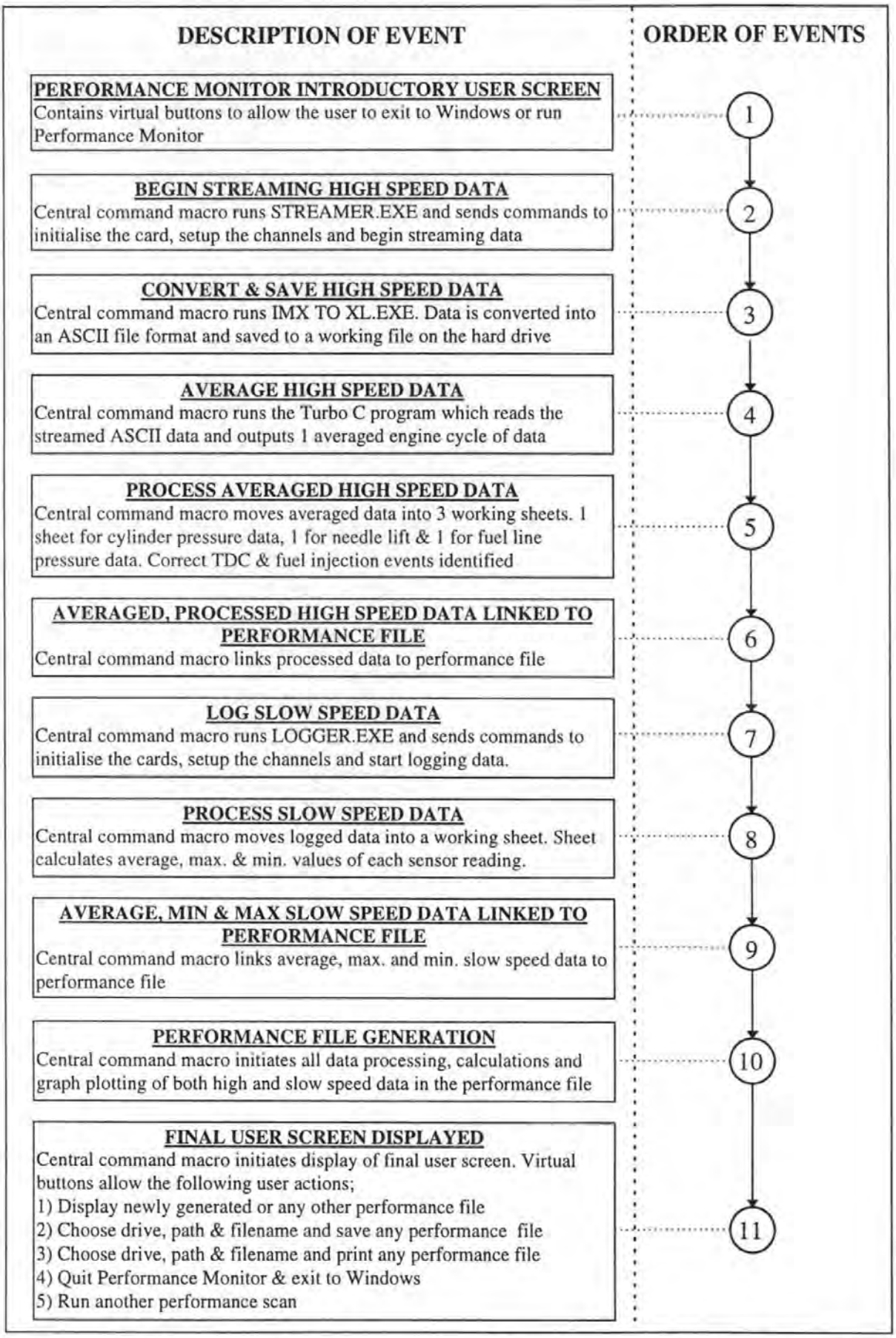

Figure 14 Diagrammatic Representation Of Performance Monitors Structure

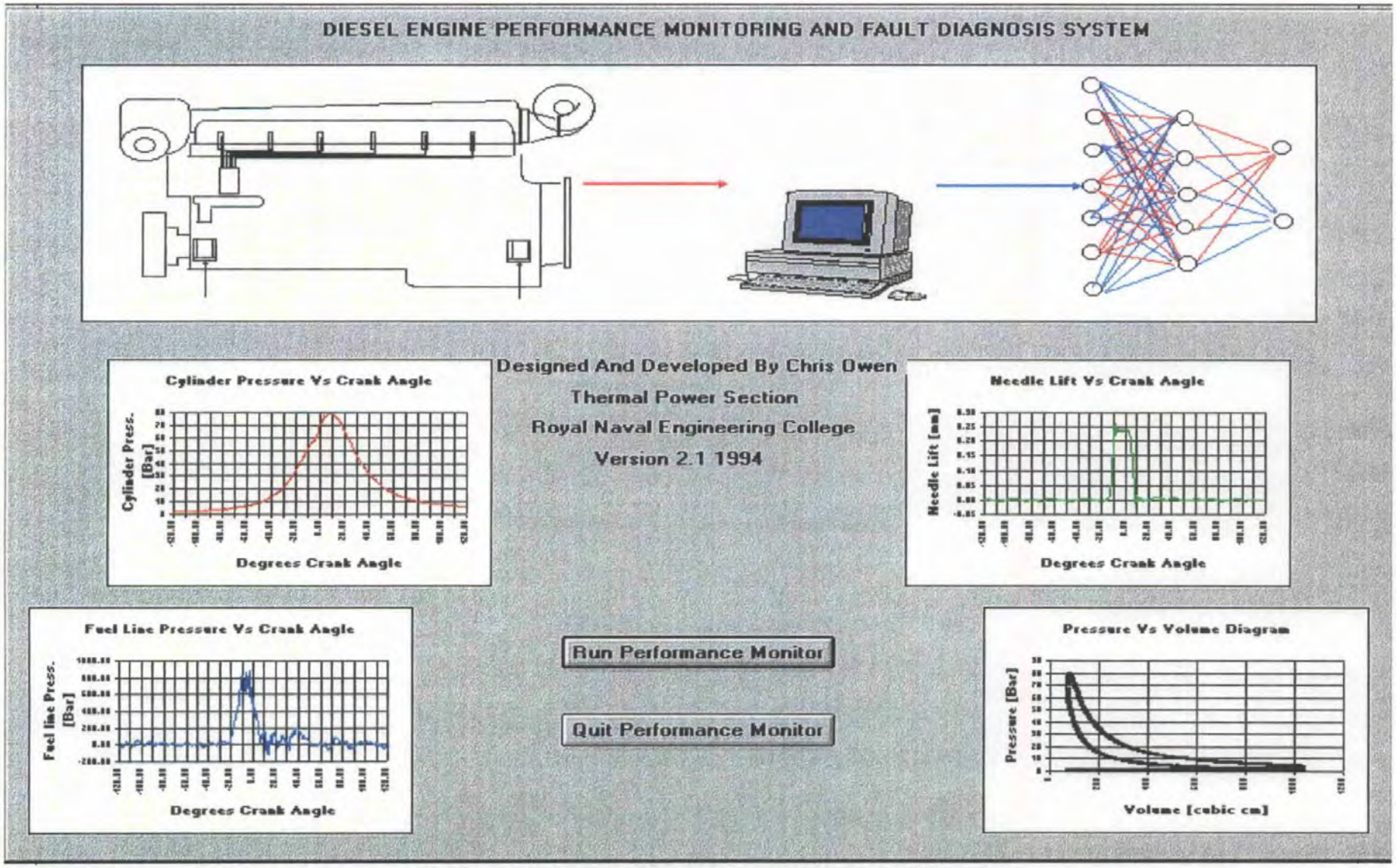

Figure 15 Performance Monitor Initial User Screen

The 720° blocks were then averaged by the Turbo C program to give a single 720° average cycle of cylinder pressure, needle lift and fuel line pressure. The central command macro then moved the cylinder pressure data from the averaged file created by the Turbo C program into an Excel worksheet for processing. The crank angle encoder gave two TDC pulses per engine cycle (720°). The data acquisition equipment could not distinguish between these two pulses resulting in cylinder pressure, fuel line pressure and needle lift data being collected in two formats, 360° out of phase. This is illustrated in Figure 16

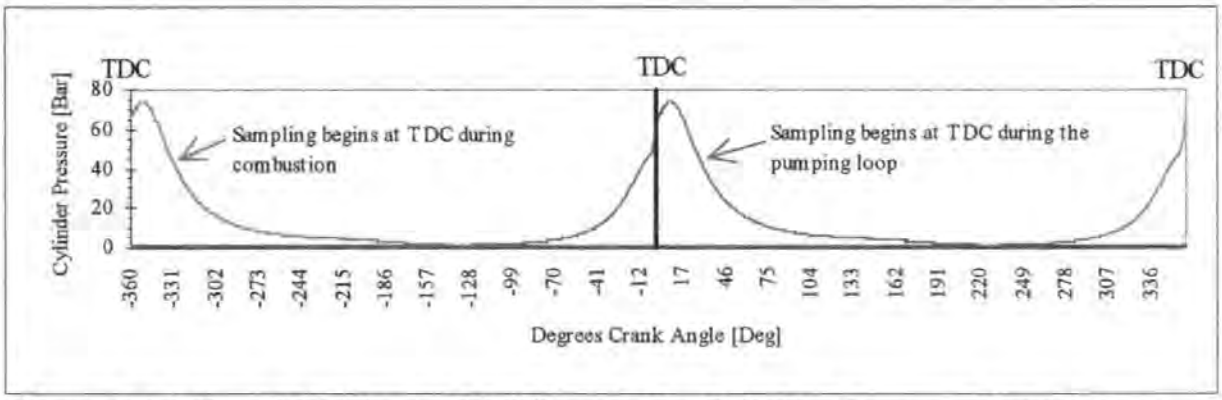

Figure 16 Affect Of Different TDC Signals On Cylinder Pressure Data Format

To perform calculations on the high speed data it needed to be recorded or rearranged into a consistent format. This was done by an Excel macro which looked at the first value of cylinder pressure in the data stream. If the value was greater than 5 [Bar] the macro identified that the card had been triggered during combustion (red curve) and rearranged the cylinder pressure data to resemble that collected on a pumping loop TDC (blue trace). If rearrangement of cylinder pressure data was necessary needle lift and fuel line pressure data were also rearranged accordingly in separate worksheets. If the first cylinder pressure value was less than 5 [Bar] no rearrangement of data was required. Following the checking and, if necessary, rearrangement, the cylinder pressure data was linked to the Performance File.

After checking the format of the needle lift data an Excel macro determined the point of injection and duration of injection. The macro identified these points by searching through the averaged needle lift data and finding the points where the value of needle lift exceeded 5% of the peak needle lift. The macro counted the number of samples it needed to find the 5% values and knew that the first piece of data checked related to TDC and that all subsequent samples occurred at 0.5° increments. This allowed the macro to convert the number of samples counted to degrees crank angle from TDC. The first piece of data to exceed the 5% threshold was identified as the point of injection and the next value to fall below the 5% threshold was the end of injection. The difference between these two points is the duration of injection.

The 5% threshold was selected as it prevented the macro from mistaking signal noise for a genuine needle lift yet identified the point of injection accurately. A decrease in the threshold value meant that random points were being identified as the point of injection. Conversely, an increase in the threshold value resulted in the macro giving a retarded value for the point of injection and an advanced value for the end of injection. Once the macro had identified the point and duration of injection the values together with all of the averaged needle lift data were transferred to the Performance File.

Start and duration of fuel pump discharge were determined from the fuel line pressure data using the same search and count method described above. Because the fuel line pressure trace was more erratic than the needle lift trace the threshold value

was raised to 7%, however, this had little effect on the results because the rate of change of line pressure rise and decay was so great. Once point and duration of pump discharge had been ascertained this data together with the averaged fuel line pressure data was transferred to the Performance File.

3.3.2 Slow Speed Data Collection & Processing

As with the high speed data collection and processing the central command macro controlled this part of the Performance Monitoring Package. The process of slow speed data collection and processing is shown in Figure 14.

The central command macro sent a series of instructions to Windmill, the data acquisition software, this initialised the rack and selected and calibrated all of the channels before data logging began. The central command macro then started the data logging. Data was displayed on the screen in a table type format and was also written to a hard disk file simultaneously. Logging was terminated by the central command macro and the data was linked to an Excel worksheet. The worksheet automatically identified the maximum, minimum and mean values for each channel and transferred this data to the Performance File.

3.3.3 The Performance File

Once the averaged high speed and slow speed data reached the Excel worksheet called the 'performance file', the majority of the performance parameters could be calculated. This file showed all of the numerical data and plotted all of the performance curves on autoscaled axes. The final user screen , shown in Figure 17,

allowed the performance files to be viewed on screen or as hard copies. They could also be written to the PC hard drive, 3.5" floppy or the preferred storage media, 128 MB magneto optical floppy disk. Part of an example performance file can be seen in Figures 18 & 19, each file contained the following subsections of data.

- File description, date, time, file name etc.
- Atmospheric conditions.
- General performance parameters.
- Charge air system performance parameters.
- Exhaust gas system performance parameters.
- Fuel injection and combustion parameters.
- Maximum, minimum and mean slow speed instrumentation data.
- Average high speed data for cylinder pressure, needle lift and fuel line pressure for 720° Crank angle.
- Plots of cylinder pressure, needle lift & fuel line pressure against crank angle.
- Approximate heat release diagram.
- Cylinder Pressure Vs Cylinder Volume plot.
- Log Cylinder Pressure Vs Log Cylinder Volume plot.

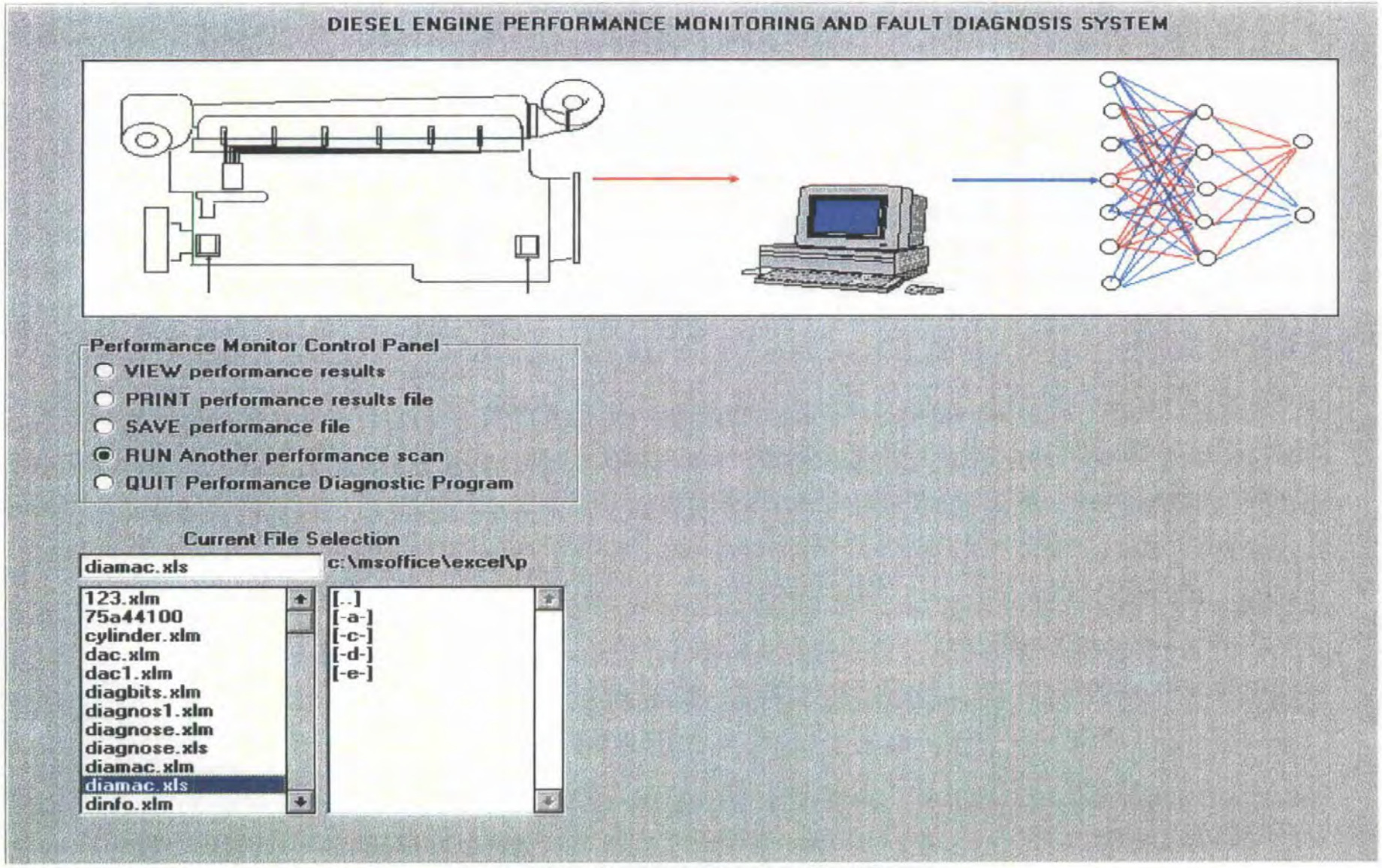

Figure 17 Performance Monitor Final Screen

PERKINS T6.354(M) PERFORMANCE FILE	
File Name	XB0308
File Date & Time	17-2-95 [15:32]
Atmospheric Pressure [kPa]	99.62
Atmospheric Temperature [K]	300.89
Humidity [%]	34.3
Seawater Inlet Temp [K]	298.24
GENERAL PERFORMANCE PARAMETERS	**Average Parameter Value**
Engine Torque [Nm]	354.58
Engine Speed [Revs/min]	2008.57
Brake Power [kW]	74.58218583
Indicated Power [kW]	88.28243345
BMEP [Bar]	7.689540363
PMEP [Bar]	0.506448725
IMEP [Bar]	9.102057385
FMEP [Bar]	1.412517022
BSFC [kg/kW.Hr]	0.253529496
ISFC [kg/kW.Hr]	0.214185125
Brake Thermal Efficiency [%]	33.1259964
Indicated Thermal Efficiency [%]	39.21101989
Mechanical Efficiency [%]	84.48134348
CHARGE AIR SYSTEM	
Inlet Air Mass Flow Rate [kg/s]	0.12249539
Inlet Air Mass Flow Rate Parameter	2.132858937
Compressor Pressure Ratio	1.394892466
Compressor Speed Parameter	3323.939569
Compressor Isentropic Efficiency [%]	56.84423333
Intercooler Air Temperature Gradient [K]	29.68
Intercooler Air Pressure Gradient [kPa]	1.06
Intercooler Water Temperature Gradient [K]	3.05
Intercooler Effectiveness [%]	53.51914224
Volumetric Efficiency [%]	85.48016764
EXHAUST GAS SYSTEM	
Exhaust Gas Mass Flow Rate [kg/s]	0.12774783
Exhaust Gas Mass Flow Rate Parameter	2.511175379
Turbine Expansion Ratio	1.449209802
Turbine Speed Parameter	1989.212126
Turbine Isentropic Efficiency [%]	77.49244287
FUEL INJECTION & COMBUSTION PARAMETERS	
Mass Flow Rate Fuel [kg/s]	0.00525244
Max Fuel Line Pressure [Bar]	812.5867985
Degrees CA Max Fuel Line Pressure [Degrees]	-10.5
Degrees CA Estimated Fuel Pump Discharge Point [Degrees]	-18.5
Degrees CA Estimated Fuel Pump Discharge Termination [Degrees]	5
Degrees CA Pump Discharge Period [Degrees]	23.5
Point Of Injection [Degrees]	-12
End Of injection [Degrees]	6.5
Duration Of Injection [Degrees]	18.5
Max Needle Lift [mm]	0.25
Degrees CA Max Needle Lift [Degrees]	-9
Pmax Cylinder [Bar]	75.15110126
Degrees CA Pmax Cylinder [Degrees]	9
IMEP [Bar]	9.102057385
Overall Air/Fuel Ratio	23.32161617
Point Of Ignition [Degrees]	1
Ignition Delay [Degrees]	13

Figure 18 Summary Of Numeric Data As Displayed In A Performance File

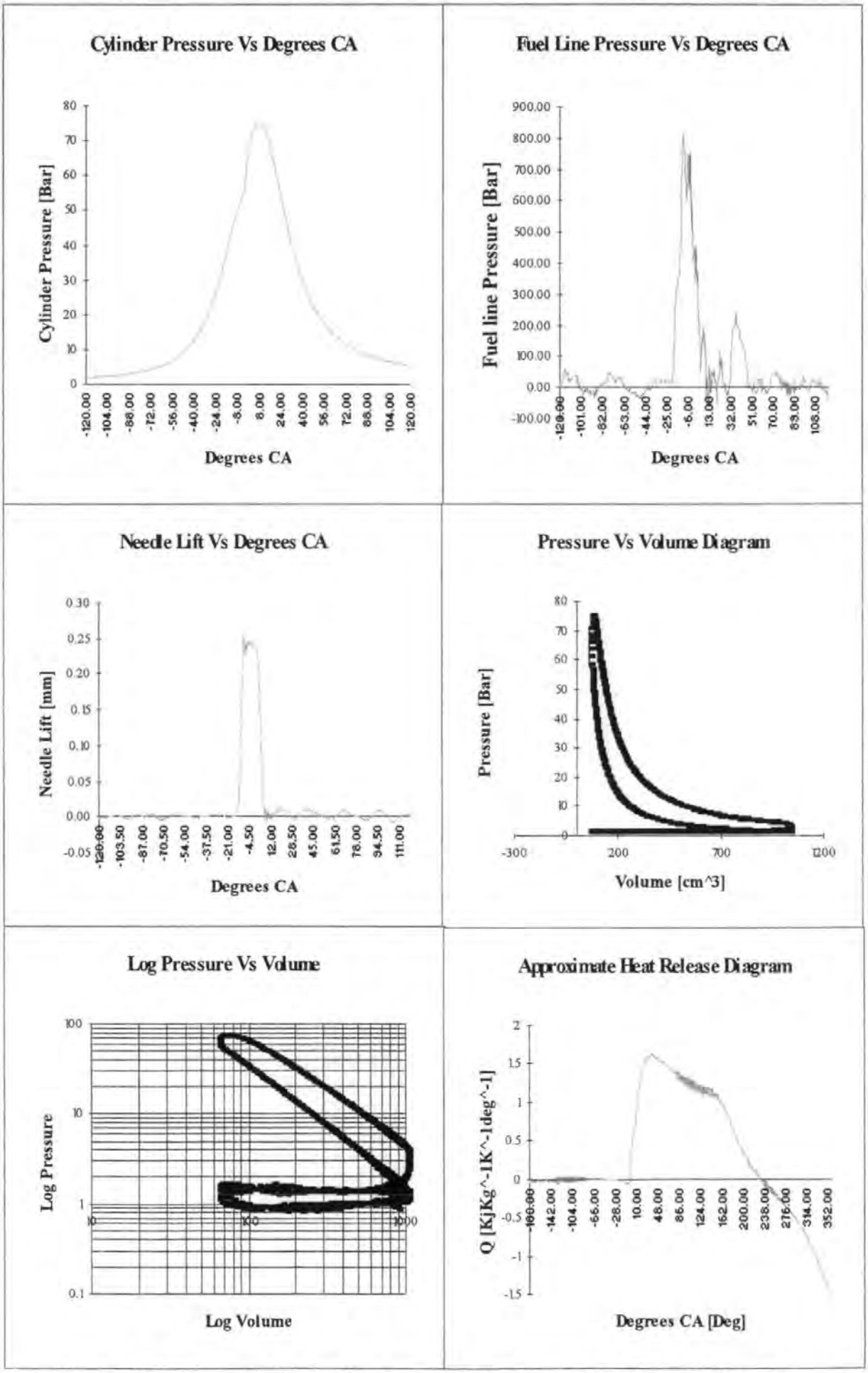

Figure 19 Automatic Plots Displayed In Performance Monitor Format

3.3.4 Performance Monitor Calculations

Some of the parameters which feature under the headings of general performance parameters, charge air system performance parameters, exhaust gas system performance parameters and fuel injection and combustion parameters were averaged sensor readings. However, the majority of performance parameters needed to be calculated from the averaged sensor data. Cylinder pressure calculations are discussed below. Full details of all the calculations used in Performance Monitor can be found in Appendix 'B'.

Indicated Mean Effective Pressure IMEP [Bar]

The indicated mean effective pressure was determined from the cylinder pressure data. IMEP is defined as the indicated work output per cylinder per mechanical cycle divided by the swept volume per cycle. The gross work done per cylinder per cycle is the area enclosed between the compression and expansion lines on the pressure Vs volume diagram. For the purpose of IMEP calculation Performance Monitor treated the compression and expansion lines as two separate curves between BDC and TDC. Performance Monitor then calculated the cylinder volume at each 0.5° of crank angle for the compression and expansion strokes. Using the trapezoidal rule at each 0.5° increment the area under each curve was calculated. The difference between these two areas is the area enclosed between the two curves, the gross work done per cylinder per cycle. The gross work done divided by the cylinder swept volume gives the IMEP value.

Pumping Mean Effective Pressure

Pumping mean effective pressure was calculated in exactly the same way as IMEP but used the area between the induction and exhaust strokes instead of the compression and expansion strokes.

Approximate Heat Release, Point Of Ignition & Ignition Delay

Approximate heat release data was generated from the cylinder pressure measurements. If the compression and expansion strokes of a motored cylinder are assumed to be an adiabatic process the resulting temperature T_2 due to a compression from V_1 to V_2 is given by;

$$T_2 = T_1\left(\frac{V_1}{V_2}\right)^{\gamma - 1} \qquad \text{Equation 1}$$

Therefore T_2 can be calculated for 0.5° crank angle increments. If a similar incremental calculation is carried out on the experimental cylinder pressure data it is possible to calculate T_2 for a pressure rise from p_1 to p_2;

$$T_2 = T_1\left(\frac{p_2}{p_1}\right)^{\frac{\gamma - 1}{\gamma}} \qquad \text{Equation 2}$$

If the T_2 values from both methods are compared at each 0.5° increment it can be seen that T_2 calculated from the experimental cylinder pressure data during combustion will appear higher than the T_2 value calculated from the volumetric data. This difference can be attributed to the heat released by the combustion process. Coupling this temperature differential with a knowledge of the trapped mass, from the inlet manifold conditions, it was possible to compute the heat

released by the combustion. Plotting the value of heat released against degrees crank angle gave an approximate rate of heat release diagram.

These calculations were made more difficult because the value of the specific heats and hence γ change as the charge temperature increases. This was largely due to the dramatic change of C_p for CO_2 with temperature. To allow Performance Monitor to calculate the heat release data it also needed to calculate C_p, C_v and γ at each 0.5° crank angle increment using the JANAF table thermodynamic data [39] and a 4th order polynomial. The rate of heat release diagram generated by performance monitor was only approximate for the following reasons;

- The motored compression & expansion were assumed to be adiabatic.
- Calculation of the specific heats was made very difficult due to the change of species during combustion
- Specific heats were not calculated for the exhaust gas species
- Heat transfer to the cylinder walls was neglected, generally around 20%
- Temperature and specific heats were assumed to remain constant for each 0.5° crank angle increment

The point of ignition is defined as the point at which heat release becomes positive. An Excel macro similar to that used for determination of point of injection was used to determine the point of ignition and the result was read into the Performance File. Ignition delay is defined as the time interval between the point of injection and the

start of combustion. Since both of these pieces of information were already held in the performance file computation of ignition delay was straight forward.

3.4 Summary

This chapter has detailed the design and development of an automated performance monitoring system for a high speed marine diesel engine. It has described the original approach of developing and configuring a comprehensive, fully automated, PC based system. This was achieved using largely 'off the shelf' hardware, software and instrumentation. The system combined high speed fuel injection and combustion data with other physical measurements and performance parameters. By combining all of these individual elements in an effective way the system could generate a single 'performance file' characterising engine performance under both healthy and faulty modes of operation. This allowed the performance and condition of the diesel engine to be continuously monitored. The information could be easily managed, compared and trended using a readily available PC based spreadsheet package. Ultimately the data could be accessed and used by a neural network based diagnostic tool. Completion of this work partially satisfied research objective 2, outlined in Chapter 1.

CHAPTER 4

CALIBRATION, EXPERIMENTAL PROCEDURE & ERROR ANALYSIS

4.0 Introduction

Prior to the experimental phase of the research beginning it was considered necessary to validate the test facility and the data it generated. This chapter concentrates on the methods used to check the quality of the data obtained from the performance monitoring system. It also outlines the experimental procedure applied to all testing conducted during the research. Finally, sources of error are identified and discussed.

Calibration of all the instrumentation used in this research was traceable to National Standards. This was either performed by instrument manufacturers, calibration houses or in the test cell using certified calibrators. The slow speed instrumentation was calibrated statically. The high speed instrumentation was calibrated both statically and dynamically.

4.1 Slow Speed Instrumentation Calibration

The slow speed instrumentation consists of thermocouples, pressure transducers, flow meters, inductive pick - ups, a load cell and a hygrometer. The calibration of these instruments is briefly discussed below.

4.1.1 Thermocouple Calibration

The calibration rig consisted of a drilled brass block fitted with two thermocouple glands, a high temperature furnace, a domestic freezer and a calibrated 'K' type thermocouple and panel meter. Between 7 and 10 calibration test points were selected around the normal operating temperature of each thermocouple. The thermocouple to be tested and the calibrated thermocouple were inserted into the brass block ensuring uniform temperature. For thermocouples operating in a cool environment the brass block was initially chilled in a freezer allowing the calibration range to start at sub zero temperatures. For thermocouples consistently operating at a high temperature the block chilling was omitted.

The brass block temperature was slowly raised using the furnace through the desired test points until the maximum test temperature was reached. The temperatures from the thermocouple under test were read from the PC screen and compared to those read from the calibrated thermocouple meter. This procedure was repeated three times for each thermocouple to give an average reading. Although thermocouple calibration could not be changed through the software because a default calibration value was used, it was important to reference against the National Standard in case any thermocouple needed replacing part way through testing.

4.1.2 Pressure Transducer Calibration

Calibration was performed by selecting approximately 9 points around the operating range of the individual transducers. A calibrated aneroid barometer was used to determine barometric pressure before and after each calibration run. Calibration was

performed on each transducer by a Druck DPI601/S which allowed pressures to be applied and measured traceable to National Standards. The results from each transducer were read from the PC screen and compared to the calibrator reading at each of the test points. Each calibration run was performed three times to give averaged values. If necessary, the span and zero variables in the data acquisition software were altered until the pressure transducer reading agreed with the calibrator.

4.1.3 Air Flow Meter & Geared Fuel Flow Meter Calibration

Both of these instruments were calibrated by the manufacturer. The tabulated calibration results from the manufacturer showed a range of flow rates and the respective instrument analogue output voltages. The data acquisition channels were calibrated by applying a range of known voltages to the channel, simulating the instrument outputs. The results were read from the PC screen and compared to the calibration certificate. If necessary, the span and zero values in the data acquisition software were changed until the screen and calibration certificate were in agreement.

4.1.4 Engine Speed Pick - Up Calibration

Only the speed signal from the Texcel 50 Dynamometer controller was fed to the data acquisition system. The signal was an analogue voltage from the controller back panel calibrated by the controller manufacturers. The signal was connected to the data acquisition equipment and the engine speed was read from the PC screen and compared to the readout on the dynamometer controller panel. The span and

zero values in the data acquisition software were adjusted until the PC screen and the dynamometer controller panel were in agreement.

4.1.5 Load Cell Calibration

The load cell was calibrated using static calibration arms supplied by the dynamometer manufacturers. The arms were connected to the dynamometer and weights were suspended from the end. This simulates a torque reaction through the dynamometer casing and load cell. The applied torque was calculated from the length of arm, mass suspended and acceleration due to gravity. The torque signal was taken from the dynamometer controller back panel and connected to the data acquisition card. The calculated torque values were compared to the torque readings on the PC screen and, if necessary, the zero and span values in the data acquisition software were adjusted until the calculated torque values were in agreement with the PC screen values.

4.1.6 Turbocharger Rotational Speed Pick - Up Calibration

As shown in Table 6, Chapter 3, the turbocharger speed pick up is connected to a Frequency to Voltage, F-V, converter . The nominal output of the F-V converter was 10V for an input frequency of 100 kHz. The data acquisition software span and offset values were set to reflect this nominal range and display a revs/min value on screen. The analogue voltage output from this unit was connected to the data acquisition card and a range of frequencies were applied to the unit's frequency input using an oscilloscope and a signal generator. The applied input frequencies were compared to the on screen values of revs/min. If necessary, the span and offset

values were adjusted in the data acquisition software until the revs/min value displayed on the PC screen agreed with the corresponding input frequency values. This procedure ensured the data acquisition equipment and F-V converter were both calibrated.

The pick - up signal was connected to the F-V converter and the inlet trunking was removed from the compressor inlet to give a clear view of the compressor vanes. A strobe was shot into the compressor inlet and the engine was run at several torques and speeds. The strobe frequency was varied until the compressor vanes appeared stationary and the on screen revs/min reading was recorded. The strobe frequencies were then compared with the on screen values of turbocharger revs/min. This is not a calibration but does give some confidence that the pick-up is generating frequencies which equate to the turbocharger rotational speed.

4.1.7 Hygrometer Calibration

The hygrometer only required a two point calibration. Two calibration capsules were used, one to represent dry conditions (11% Rh) and the other to represent a wet condition (73% Rh). Each capsule was placed on the instrument and the instrument output was connected to the data acquisition card. The on screen values were observed and compared to the 11 and 73 % values and, if necessary, the span and offset values in the data acquisition software were changed until the screen values agreed with the 11 and 73% values.

4.1.8 Fuel Rack Position Calibration

The fuel pump throttle lever was moved to the low idle position and a dial test indicator accurate to 0.01 mm was fitted and the potentiometer voltage reading was noted. The throttle lever was moved in small increments towards the full throttle position, the travel and potentiometer voltage were noted. These values were plotted and a straight line graph was produced. The intersection and gradient of the line were entered into the data acquisition software as the offset and span values respectively. The fuel pump throttle lever was moved back and forth and the on screen values were compared to the dial test indicator reading. If necessary the offset and span values in the data acquisition software were adjusted until both readings agreed.

4.2 High Speed Instrumentation Calibration

The cylinder pressure transducer was the only high speed instrument which could be calibrated both statically and dynamically. The needle lift and fuel line pressure transducers could only be dynamically calibrated. After transducer calibration all three readings must be phased with the crank angle encoder both statically and dynamically.

4.2.1 Cylinder Pressure Transducer Calibration

The piezo electric transducer was connected to a Kistler 5007 Charge Amplifier which gave an output voltage proportional to input charge. Prior to calibration the transducer, cables and connectors were thoroughly cleaned. Having let the charge amplifier, set to long time constant, warm up and stabilise for a period of at least 1

hour the transducer was subject to pressures from atmospheric to 120 [Bar] in 10 [Bar] increments using a Budenburg dead weight tester, calibrated to National Standards. The transducer sensitivity was set on the charge amplifier and the correct scaling factor was entered into the data acquisition software. The transducer was pressurised and 1000 samples of data were collected using the Microlink 570 Card over a 2 second period at each pressure station. The 1000 samples were then averaged to give the average pressure recorded by the data acquisition during the 2 second period. This procedure was repeated three times at each pressure to obtain average values. Unfortunately, the scaling factor entered in the data acquisition software needed to be adjusted before accurate results could be achieved.

Experimental trials showed that the data recorded during in-cylinder operation suffered problems that were not apparent during static Budenburg calibration. When Performance Monitor began to produce Cylinder Pressure Vs Cylinder Volume plots the pumping loop consistently appeared at a pressure several bars below atmospheric. Checking the raw cylinder pressure data confirmed this to be true. To remedy this the cylinder pressure reading at BDC after the induction stroke was mathematically corrected to equal zero, all other cylinder pressure readings were subsequently corrected by the same amount. Theoretically, at this point in the cycle the cylinder pressure transducer reading should equal the inlet manifold pressure since the exhaust valve is closed, the effective flow area of the inlet valve is minimal having taken in a complete fresh charge and the piston is stationary. Once the cylinder pressure readings had been corrected to zero the reading from the inlet manifold pressure transducer was added to all of the cylinder pressure readings

ensuring the BDC value equalled inlet manifold pressure. Piezo electric cylinder pressure transducers are well known for the number of operational problems they suffer, some of these are identified below;

- The need for complete cleanliness of associated cables, plugs and sockets in a dirty environment.
- The location of the transducer in the cylinder head can affect the pressure reading.
- Setting of a reference pressure, illustrated by the problems outlined above
- Build up of carbon deposits on the transducer diaphragm can effect the pressure reading.
- Thermal shock through high temperatures encountered in the combustion chamber.
- Correct phasing of the pressure signal with engine TDC, discussed later.

4.2.2 Needle Lift Transducer Calibration

The needle lift transducer gave an analogue voltage output directly proportional to needle displacement. Lucas CAV advised that the maximum needle lift was 0.26mm. A recently tested injector was fitted and the engine was run at peak torque to achieve maximum lift for several degrees of crank angle. Offset and span values were entered into the data acquisition software so that the needle lift during the injection was recorded as 0.26mm.

4.2.3 Fuel Line Pressure Transducer Calibration

The transducer outputs a charge signal and suffers from many of the same problems as the cylinder pressure transducer. The signal is conditioned by a Kistler 5007 Charge Amplifier to produce the analogue voltage required by the data acquisition card. The transducer produces a charge proportional to the rate of change of fuel line pressure. This makes static calibration impossible and as a result calibration could only take place when the engine was running.

The injector was fitted with a needle lift transducer and the opening pressure was set at 210 [Bar] as recommended by Lucas CAV. Having let the charge amplifier warm up and stabilise for a minimum of 1 hour the engine was run at peak torque. The needle lift and fuel line pressure channels were sampled by the data acquisition card. The needle lift trace identified when lifting occurred, and the fuel line pressure transducer offset and span values in the data acquisition software were adjusted so that a pressure of 210 [Bar] registered when the needle lifted. The low level of accuracy of this method was accepted since the fuel line pressure transducer is primarily a qualitative rather than quantitative device.

4.2.4 High Speed Data Dynamic Phasing

All of the high speed instrumentation was sampled with respect to crank angle. Phasing the high speed data channels with the crank angle encoder is critical to ensure that Performance Monitor can accurately determine the following;

- IMEP and mechanical efficiency
- Point of injection

- Point of fuel pump discharge
- Point of ignition.

To ensure correct phasing, the crank angle encoder was initially phased with TDC statically. This was achieved by removing the injector and placing a long throw dial test indicator on the piston crown. The engine was slowly rotated by hand until the dial test indicator reaches a maximum reading and piston movement became negligible. This only set TDC approximately because of the very small change in piston position with crank rotation. To set TDC more accurately statically the engine was rotated to approximately 60 degrees past TDC. The engine was then rotated back to 40 degrees after TDC, as indicated by the flywheel markings and a dial test indicator reading was taken. The engine was then rotated to 60 degrees before TDC and then moved back towards TDC until the dial test indicator reading equalled the previous reading and the flywheel was marked. TDC was then identified as the midpoint between the 40 degree after TDC point and the marked point approximately 40 degrees before TDC. The engine was then rotated to this mid point and the crank angle encoder TDC marker pulse position was re-adjusted. This procedure was repeated until no further adjustment was required.

Static calibration alone is not accurate enough to ensure that the high speed data is correctly phased with crank position. In a dynamic situation the TDC apparently shifts and leads to the generation of inaccurate data. The reasons for this shift have not been investigated in this research but are thought to be a combination of mechanical variations and signal processing lags. TDC was dynamically set using a method developed by Lancaster [40] et al.. This paper showed how correct phasing

of the cylinder pressure signal with crank angle position could be determined through the shape of a Log Cylinder Pressure Vs Log Cylinder Volume plot.

The engine was run at constant torque and speed and cylinder pressure was recorded with respect to crank angle. The results were then plotted on a Log Cylinder Pressure Vs Log Cylinder Volume graph. The crank angle encoder TDC marker pulse was adjusted until the desired graph shape was achieved. Copies of these graphs can be found in Appendix 'C'. IMEP and consequently mechanical efficiency are both very sensitive to changes in phasing as shown in Table 7.

Degrees Crank Angle Shift From True TDC	Mechanical Efficiency [%]
-3	105.61
-2	95.49
-1	87.87
0	81.41
+1	75.87
+2	71.04
+3	66.82

Table 7 Sensitivity Of Mechanical Efficiency Value To Phasing

4.3 Performance Monitoring System Validation

After Performance monitor had been calibrated it was run through a series of tests to validate its performance. These are identified below;

- Averaging trials to determine data repeatability.
- Comparison of Performance Monitor data with test cell panel meters and the AVL 364 Indiskop.
- Willans Line test comparison

4.3.1 Data Averaging & Repeatability Trials

These trials were conducted to ascertain how the number of samples recorded and averaged affected the repeatability of the data in the Performance File. The engine was run at a nominal speed of 1800 [revs/min] and torque of 300 Nm as this represented a mid range operating point. The fuel rack position and speed were held constant for the duration of the trial and the engine was allowed a 1 hour stabilisation period before any data was taken. The central command macro in Performance Monitor was edited so that it recorded varying numbers of high and slow speed data samples as shown in Table 8. Ten separate performance scans were taken with each combination of sampling conditions.

Test No.	Number Of Slow Speed Samples Averaged	Number of Engine Cycles Averaged	Number Of Repetitions
1	10	10	10
2	30	50	10
3	60	100	10
4	120	200	10

Table 8 Numbers Of Samples Taken By Performance Monitor

Slow speed samples were logged at an interval of 1 second, high speed samples were logged at 0.5° crank angle increments. After the data had been logged the ten runs in each test were compared to ascertain the repeatability. For both high speed and slow speed data the repeatability of the data generated by Performance Monitor improved with number of samples averaged. Tables 9 and 10 show the percentage variation of the slow speed and high sensor readings as a function of number of samples averaged.

Instrument Description	% Variation 10 Samples Average	% Variation 30 Samples Average	% Variation 60 Samples Averaged	% Variation 120 Samples Averaged
Air Flow [m^3/Hr]	1.424338146	0.87583371	0.907390991	0.77985007
Compressor Discharge Pressure [kPa]	2.897713302	1.488675411	1.671756722	0.729802641
Compressor Discharge Temperature [K]	0.580998984	0.238582276	0.606541402	0.144421593
Compressor Inlet Pressure [kPa]	1.533895772	1.126636587	1.340830327	1.276281667
Compressor Inlet Temperature [K]	0.577345534	0.231838418	0.494322076	0.087068058
Cylinder 1&2 Port Temperatures [K]	0.708219066	0.45078671	1.909508149	0.940792302
Cylinder 3 Port Temperature [K]	0.682592866	0.495906274	1.634771317	0.791289013
Cylinder 4 Port Temperature [K]	1.087654277	1.158851074	2.042019043	0.826651432
Cylinder 5&6 Port Temperatures [K]	0.710749262	0.475465336	1.277512048	0.688102921
Engine Cooling water Discharge Temperature [K]	0.385390194	0.56822783	0.536253101	0.39955657
Engine Water Temperature [K]	0.394113647	0.279168089	0.272079244	0.195939651
Engine Speed [Revs/Min]	0.265145421	0.284393355	0.282048698	0.033897087
Exhaust Manifold Pressure [kPa]	23.42756731	23.09772093	9.887961504	4.56623711
Exhaust Manifold Temperature [[K]	0.996566222	0.593267326	1.568763428	0.604834242
Fuel Rack Position [mm]	0.218811575	0.087332551	1.528847663	0.060667027
Fuel Temperature [K]	0.487356823	0.170147851	0.289373244	0.382762959
Intercooler Cooling water Discharge Temperature [K]	0.519918789	0.569236448	0.513851864	0.463735005
Inlet Manifold Pressure [kPa]	3.922277196	2.145412336	2.310386176	2.037809623
Inlet Manifold Temperature [K]	0.495444533	0.364286511	0.437982922	0.267460757
Lubricating Oil Temperature [K]	0.840233639	0.132573599	0.233782866	0.096412258
Engine Torque [Nm]	1.697283556	0.909252793	3.884648856	1.173187891
Turbine Discharge Temperature [K]	0.553366854	0.366643082	1.338673631	0.373282542
Turbine Discharge Pressure [kPa]	1.101065587	1.198237528	0.753052003	0.52536983
Turbocharger Speed [Revs/min]	3.361749487	7.225733916	5.853865776	1.942743116
Cooling Water Supply Temperature [K]	0.508957807	0.515452211	0.555413964	0.486593811
Fuel Mass Flow Rate [Kg/s]	10.76207574	8.127403278	6.920350134	2.896244976

Table 9 Slow Speed Data Repeatability As A Function Of Number Of Samples Averaged

Measurement Description	% Variation 10 Samples Average	% Variation 50 Samples Average	% Variation 100 Samples Average	% Variation 200 Samples Average
Mass Flow Rate Fuel [Kg/s]	10.73162383	8.127403278	6.920350134	2.896244976
Max Fuel Line Pressure [Bar]	6.207417399	2.623299266	5.273639579	4.768760459
Degrees CA Max Fuel Line Pressure [Degrees]	0.5	0	0	0.5
Degrees CA Estimated Fuel Pump Discharge Point [Degrees]	1	0	0	0.5
Degrees CA Estimated Fuel Pump Discharge Termination [Degrees]	0.5	0.5	0.5	0.5
Degrees CA Pump Discharge Period [Degrees]	0.5	0.5	0.5	0.5
Point Of Injection [Degrees]	0	0	0	0.5
End Of injection [Degrees]	0.5	0.5	1	0.5
Duration Of Injection [Degrees]	0.5	0.5	1	0.5
Max Needle Lift [mm]	5.44595937	2.364213817	2.661649608	4.11796474
Degrees CA Max Needle Lift [Degrees]	7	0	0.5	0.5
Pmax Cylinder [Bar]	2.359750417	2.27817199	1.490273172	1.279927448
Degrees CA Pmax Cylinder [Degrees]	1.5	2.5	2	0.5
IMEP [Bar]	1.747889741	1.515564831	3.460721978	2.271190842

Table 10 High Speed Data Repeatability As A Function Of Number Of Samples Averaged

Note: % Variation figures quoted do not apply to those measurements made in degrees crank angle. Crank angle variations are in degrees.

After analysing the results from the repeatability trials the number of slow speed and high speed samples were set to 120 and 200 respectively. All further testing was conducted using these settings. These readings were compared to the test cell panel meters to highlight any gross errors that may have been introduced through wiring or programming mistakes. The comparison confirmed that Performance Monitor's results were in close agreement with the panel meters.

The ability to measure or calculate performance parameters with precision is a very important feature of a diagnostic system. The level of precision of the system will directly affect it's sensitivity and hence it's ability to diagnose faults. A diagnostic system with a high level of precision will have the ability of diagnosing faults which may only cause a marginal change in sensor readings and identify faults at a much lower level of severity. An imprecise system relies heavily on the fault causing large changes in sensor readings since the deviation in the sensor reading must exceed the relatively large tolerance band experienced during normal engine operation before it can positively diagnose. Since the calculation of performance parameters often requires several sensor readings to be combined together the repeatability of calculated parameters becomes slightly more complex. Figures 20 & 21 show the repeatability of the sensor data recorded at one torque and speed. The repeatability of a reading is a function of the engine stability at a particular operating point, the precision of the instrumentation and data acquisition and the variation in ambient conditions. Figures 22 & 23 show the repeatability of calculated parameters.

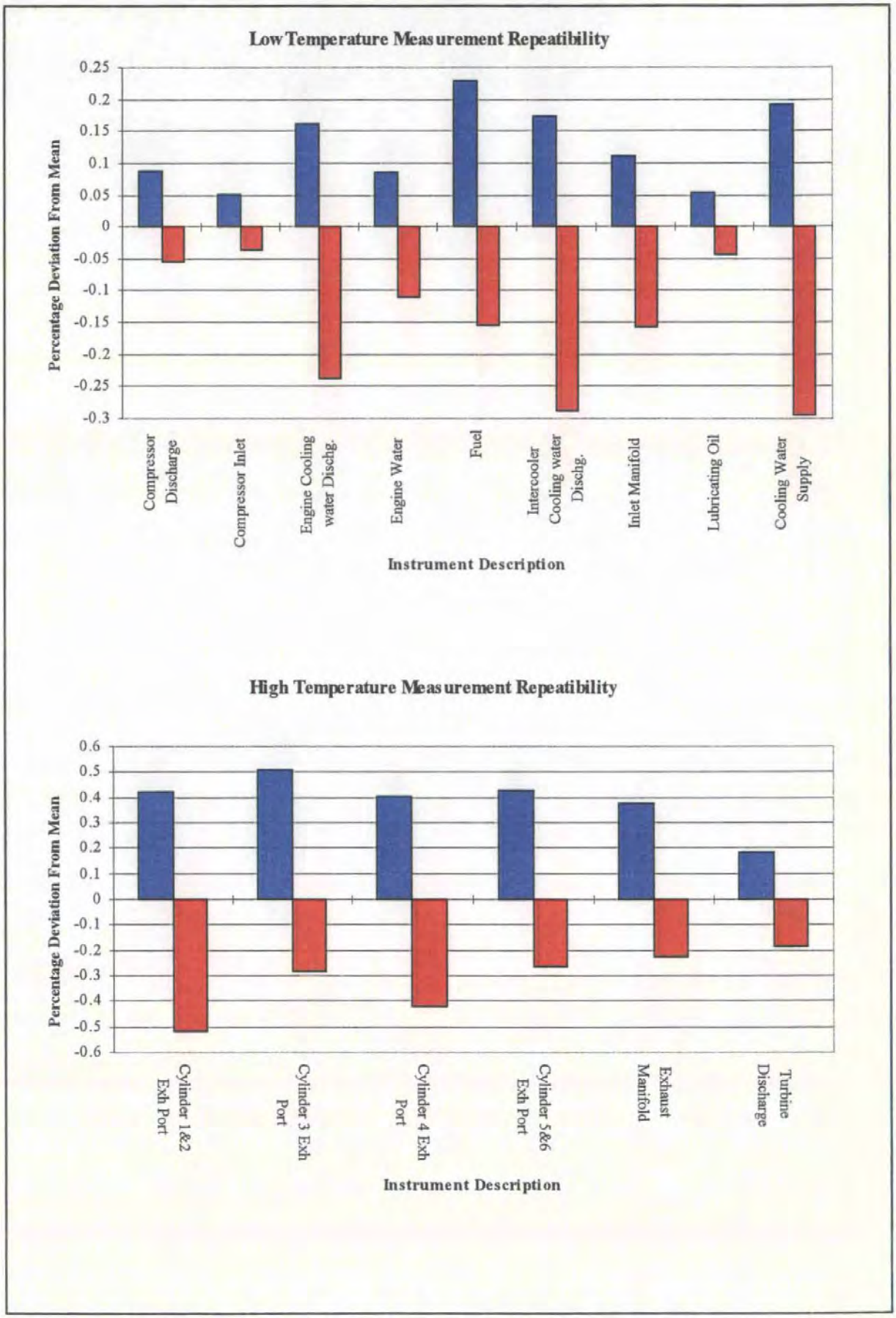

Figure 20 Temperature Measurement Repeatability

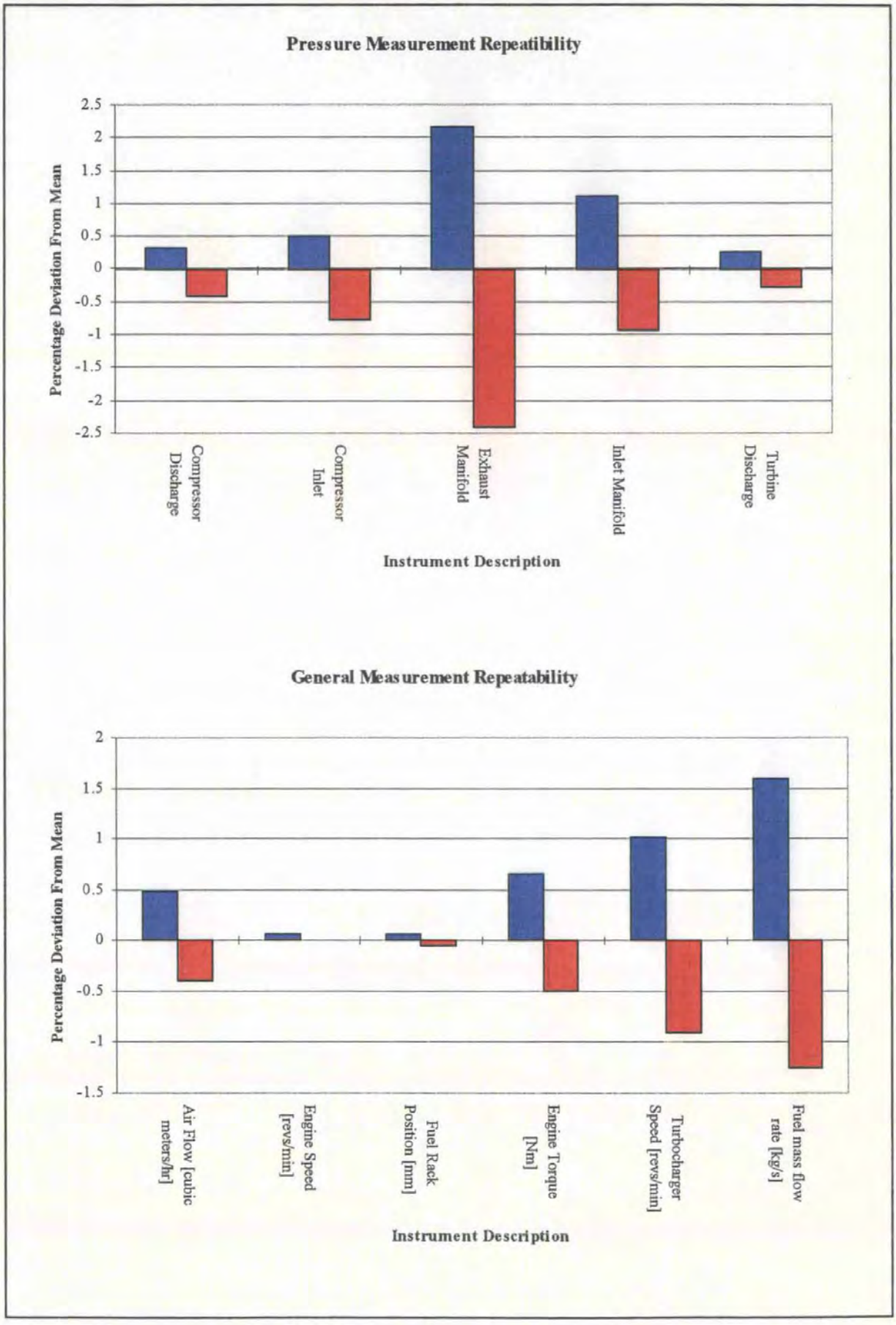

Figure 21 Pressure, Flow, Speed And Position Measurement Repeatability

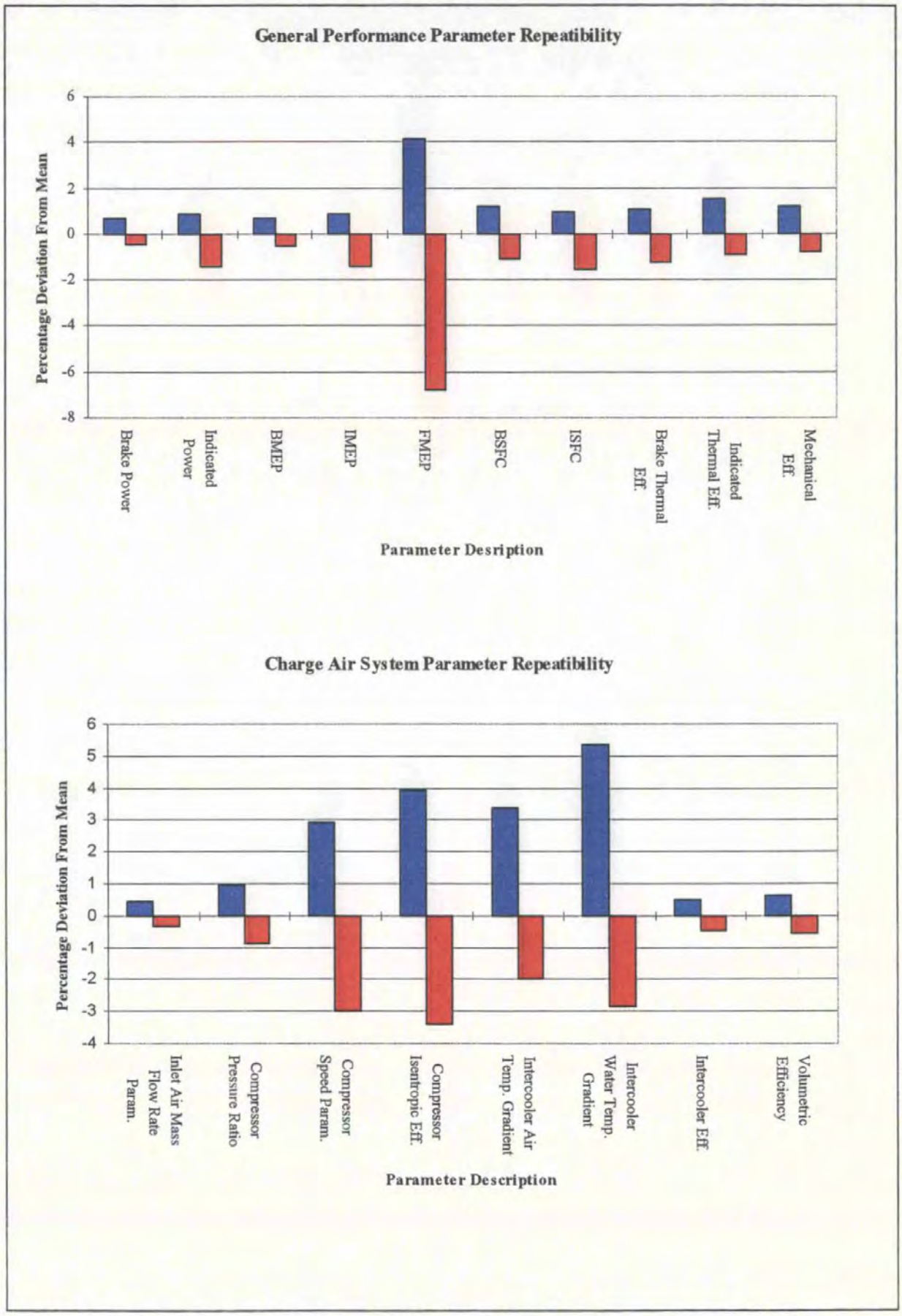

Figure 22 General Performance & Charge Air System Parameter Repeatability

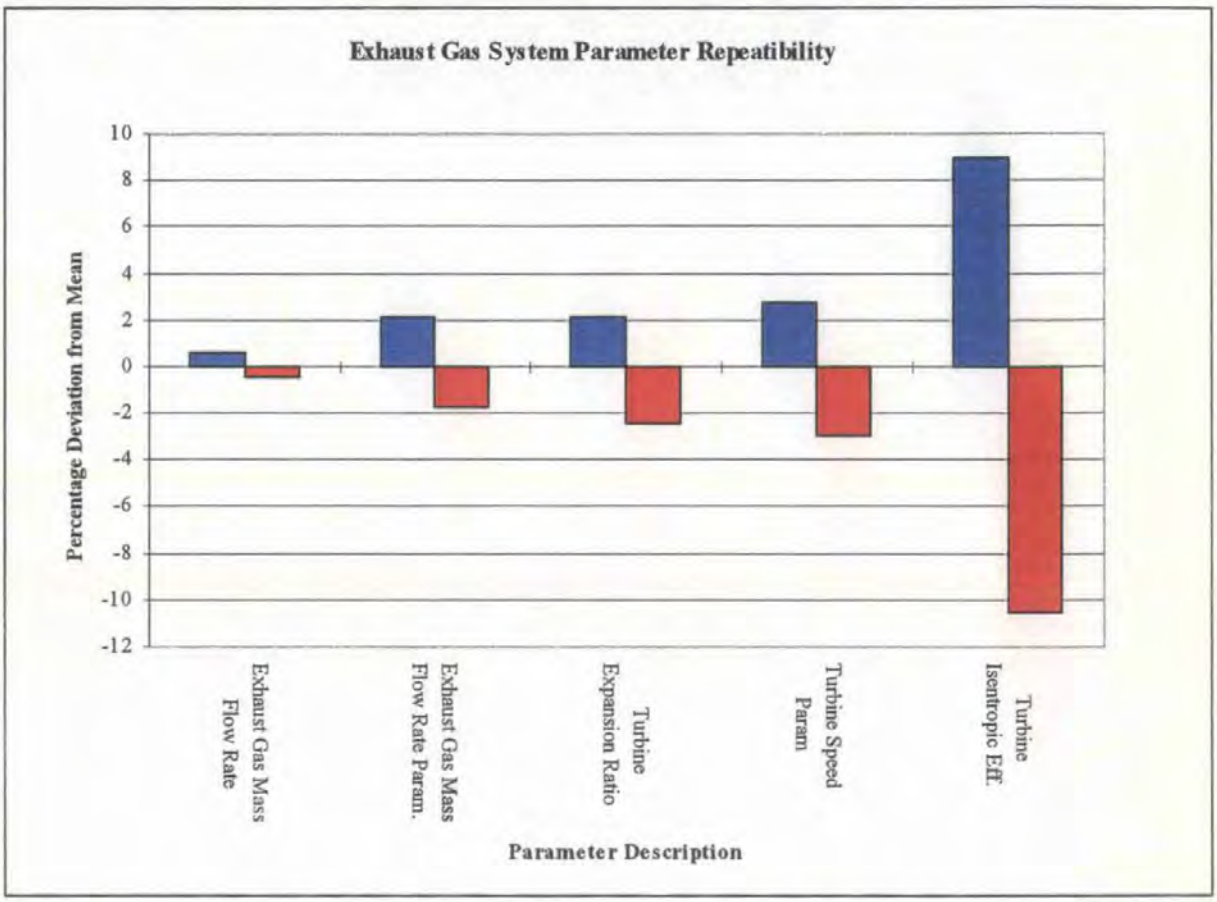

Figure 23 Exhaust Gas System Parameter Repeatability

'K' Type thermocouple temperature measurement is shown to be very repeatable. This is partly due to the thermocouples having a response time far greater than the process temperature variation frequency, which gives a temperature reading damping effect. Pressure measurements are slightly less repeatable particularly in the inlet & exhaust manifolds. The strain gauge pressure transducers used for these measurements had a natural frequency in the order of 15 kHz. Despite the low natural frequency of these transducers the complex pressure wave phenomena in the manifolds caused the transducer to have an erratic output. By introducing a section of pipe work and averaging the samples taken every second these pressure variations were reduced to less than +/- 2.5 % as shown in Figure 21. Ideally, the pressure transducer should have been sampled at more than twice the frequency of the pressure waves to avoid aliasing. This was not possible due to data acquisition

sampling speed limitations. Once the exhaust gas had passed through the turbine the pressure pulsations were further damped and the variation in exhaust gas pressure measurement was reduced to less than +/- 0.5 %.

Turbocharger speed showed an approximate variation of less than +/- 1%. This was deemed acceptable because of it's extreme sensitivity to engine torque which could only be controlled to +/- 0.5 %.

Fuel flow measurement repeatability was approximately +/- 1.5 %. The flow meter was mounted upstream of the lift pump which was a positive displacement reciprocating device driven from the camshaft. Due to the nature of the pump the flow rate reading taken at each sample was dependant upon where the pump was in it's stroke at that instant. The flow meter was mounted as far as practically possible upstream of the lift pump and a large number of samples were averaged to minimise the variation in the fuel flow readings as shown in Table 9. Fuel flow was also measured by a timed fixed volume device as shown in Chapter 2.0, Table 5 and Figure 11, to give added confidence in fuel flow measurement.

Figures 22 & 23 show that calculated parameters using two or more measured variables are susceptible to a lower degree of repeatability. This is because tolerance band of each variable contributes to the repeatability of the overall result. If, for the purpose of this example, if it is assumed that pressure and temperature are independent variables during the turbine expansion process the 'worst case'

repeatability of turbine isentropic efficiency can be calculated from the repeatability trial results.

Variable	Max Value	Min Value	+ve % Deviation From mean	-ve % Deviation From Mean	Total % Variation
Exhaust Manifold Pressure [kPa]	135.64	129.58	2.16	2.41	4.57
Exhaust Manifold Temp [K]	769.22	764.58	0.377	0.227	0.60
Turbine Discharge Pressure [kPa]	104.46	103.91	0.248	0.277	0.525
Turbine Discharge Temp. [K]	723.82	721.13	0.185	0.187	0.372

Table 11 Repeatability Of Variables Used To Calculate Turbine Isentropic Efficiency

Table 11 shows the variables used to calculate turbine isentropic efficiency and their respective repeatability's. The maximum and minimum values shown are the maximum and minimum values encountered throughout the whole testing programme and therefore did not necessarily occur together during any single test run. If these values are substituted into the isentropic efficiency equation the maximum and minimum efficiency values can be obtained as follows.

Turbine Isentropic Eff. $= (1 - (T_{tout}/T_{tin})) / (1 - [(p_{tout} / p_{tin})^{(\gamma-1)/\gamma}])$ Equation 3

Min Turbine Isentropic Eff. $= (1-(723.82/764.58))/(1-[(103.91/135.64)^{0.2587}]$

Min Turbine Isentropic Eff. $= 0.800$

Max. Turbine Isentropic Eff. $= (1-(721.13/769.22))/(1-[(104.46/129.58)^{0.2587}])$

Max. Turbine Isentropic Eff. $= 1.153$

% Deviation From The Mean $= (((0.800+1.153)/2) - 0.800)/((0.800+1.153)/2)*100$

% Deviation From The Mean **= +/- 18 %**

Figure 23 shows that in practice, turbine isentropic efficiency variation from + 8.94 /- 10.53 % as oppose to the calculated +/- 18%. This smaller practical variation

suggests that although sensor repeatability contributed to the efficiency variations, the above set of wide maximum and minimum conditions used in the calculation did not occur in the experimental environment. This could be because either not enough data sets were taken and therefore the maximum repeatability range was not found or the physical relationship between temperature and pressure variations across the turbine are such that these max and min conditions could not occur simultaneously in practice.

4.3.2 AVL 647 Indiskop Comparison

To give added confidence in the high speed data generated by Performance Monitor a comparison was made to the AVL 647 Indiskop. The Indiskop was the only other piece of equipment capable of accurately determining the point and duration of injection & position of maximum cylinder pressure. The engine was run at a series of torques and speed and a comparison was made at each. Figure 24 summarise the results taken at 1600 [revs/min] and 236 [Nm].

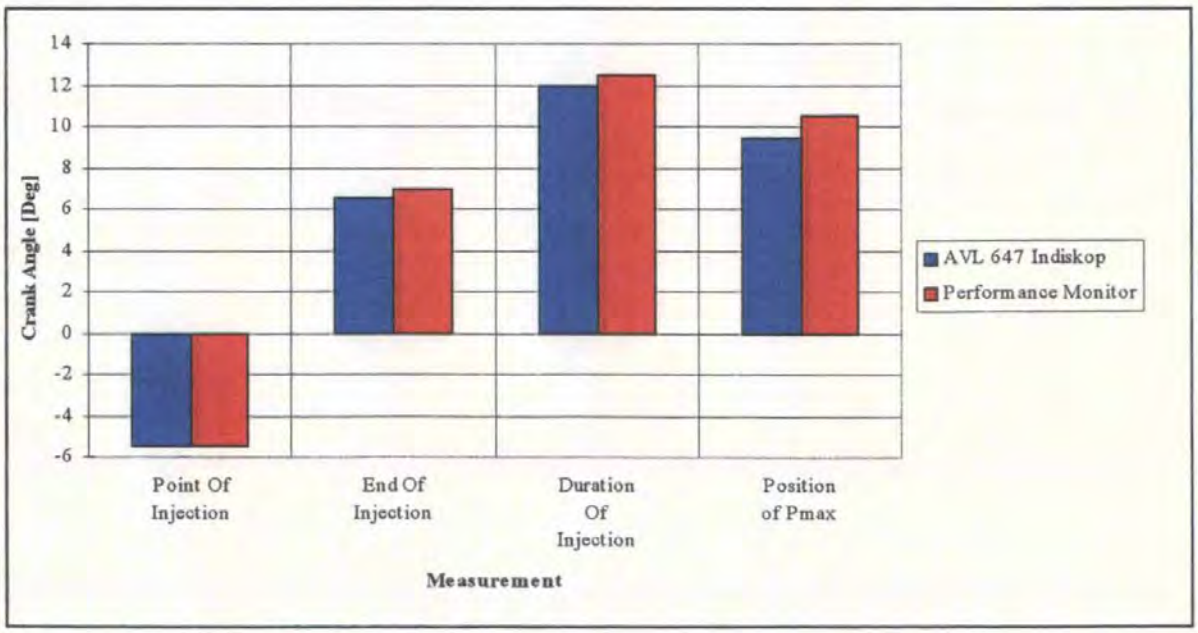

Figure 24 AVL 647 Indiskop & Performance Monitor Comparison

Throughout the torque and speed range the AVL 647 Indiskop and Performance Monitor agreed within 3° on all crank angle position measurements. For medium and high torque conditions the two systems agreed within 1° crank angle, the greater variations only occurred under light torque conditions. This can be attributed to the more erratic fuel pump behaviour at light torques. AVL647 Indiskop values for peak cylinder pressure, position of peak cylinder pressure and fuel line pressure measurements were also in close agreement with the Performance Monitor data. Based on these results the high speed data generated by Performance Monitor was deemed acceptable.

4.3.3 Validation Of IMEP & Mechanical Efficiency Data

Performance Monitor IMEP values were checked against values obtained from the AVL 647 Indiskop and the Willans Line method . The results for an engine speed of 1500 [revs/min] are summarised below in Figure 25.

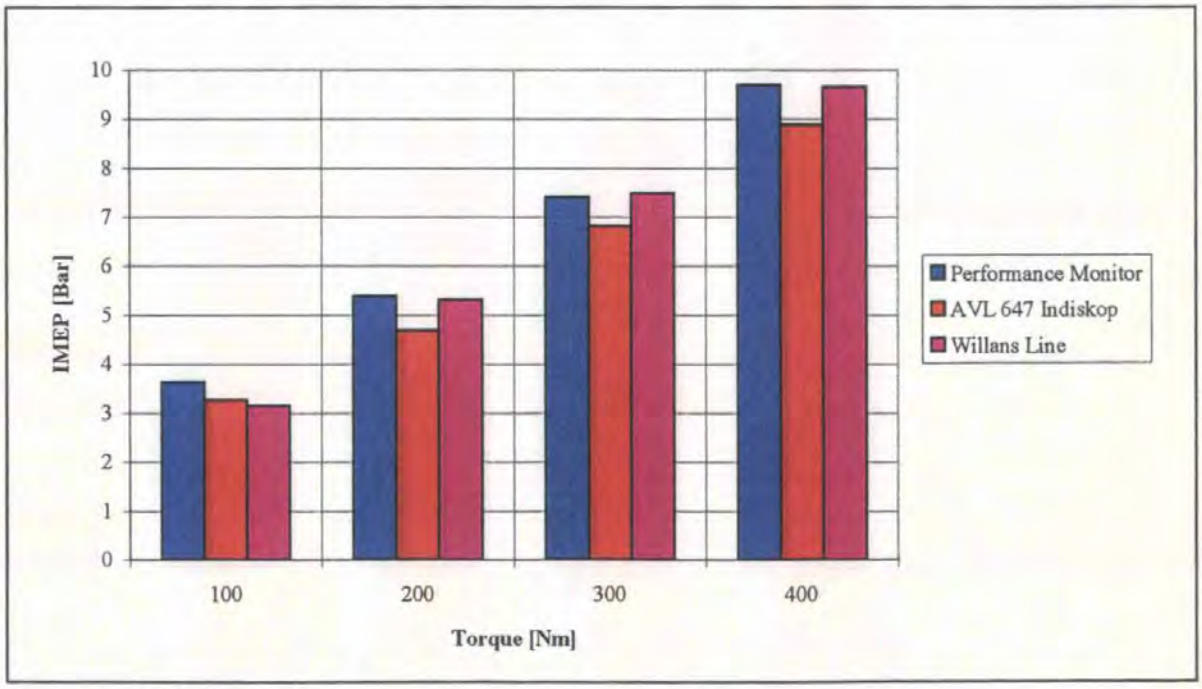

Figure 25 Comparison Of IMEP Values

The IMEP values obtained from all three methods were in close agreement throughout the torque and speed range. However, the AVL 647 Indiskop gave lower IMEP values than the other two methods at most torques. These lower IMEP values gave abnormally high mechanical efficiencies in the 89 to 98 % band. Similar calculations using the Willans Line and Performance Monitor IMEP values gave mechanical efficiencies ranging from 58 to 89%.

Based on the mechanical efficiency values Performance Monitor's IMEP calculation was accepted. Although it recorded consistently higher IMEP's than the AVL 647 Indiskop the Indiskop mechanical efficiencies were unrealistic. The close agreement between the Willans Line method and Performance Monitor gave added confidence that the Performance Monitor IMEP values were correct.

4.4 Experimental Procedure

The following sections outline how the testing strategy was developed. This involved selecting the most suitable speeds and torques and then arranging the most efficient way to collect data at these conditions. This necessitated an understanding of the engines performance envelope and warm up behaviour.

4.4.1 Selection Of Torque-Speed Operating Points

When selecting operating points three main factors were considered;

- They are evenly spaced throughout the engines operating range
- They are representative of real applications, either propeller law or gen-set.

- They are practically possible, avoiding problems of overheating, vibration and max. intermittent powers.

For generating set application 1500 [revs/min] is favoured because of the electrical frequency implications. Four torques were picked 100, 200, 300, and 430 [Nm] to simulate varying current being drawn from the gen-set. The propeller law points were selected using Perkins Engine Ltd. power curves. The curve showed that the max continuous rating was 91 kW at 2150 [revs/min]. Using a propeller law index of 2.8 the constant K could be found, thus;

$P_b = KN^{2.8}$ Equation 4

$91000 = K.\ 2150^{2.8}$

$K = 4.25\ E^{-5}$

Subsequent torque-speed points were found by substituting in speed values ranging from 1400 [revs/min] to 2150 [revs/min] in 200 [revs/min] increments. Table 12 shows both propeller law [P] and gen-set [G] operating points. Figure 26 Shows the power and torque curves for the engine and propeller law points.

No.	Engine Speed [revs/min]	Engine Torque [Nm]	Brake Power [kW]	Gen-set = G Prop Law = P
1	1500	100	15.71	G
2	1400	186.6	27.36	P
3	1500	200	31.42	G
4	1600	237.3	39.77	P
5	1500	300	47.12	G
6	1800	293.2	55.27	P
7	1500	Full (430 Nm)	67.53	G
8	2000	354.6	74.28	P
9	2150	Full (404 Nm)	91.00	P

Table 12 Engine Torque-Speed Operating Points

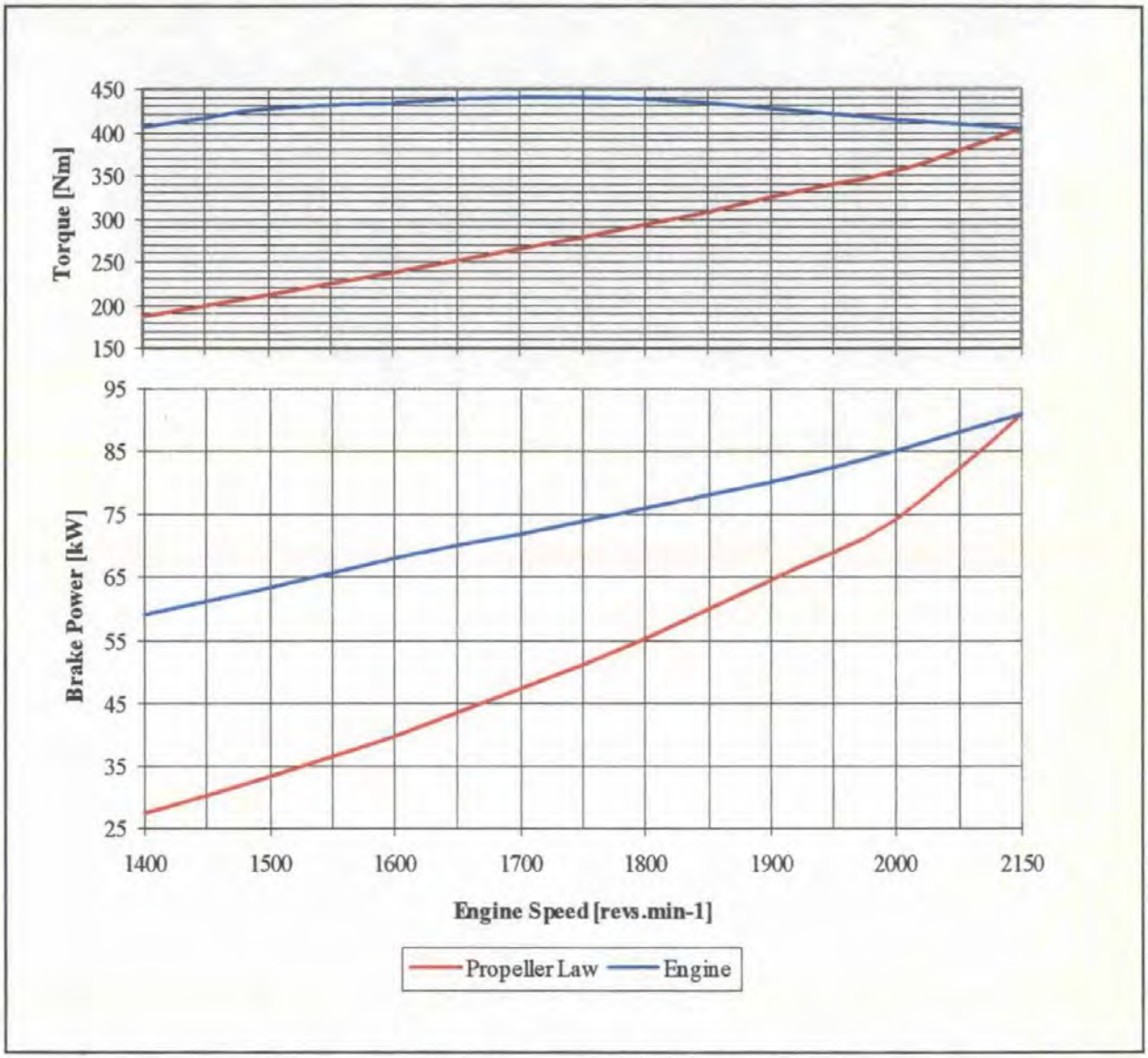

Figure 26 Engine Speed Vs Power & Torque

4.4.2 Determination Of Steady State Conditions

To ensure that the engine had reached steady state conditions before data was sampled a warm up trial was conducted. The engine was started from cold and run through the sequence of torques and speeds shown in Table 12. Initially the 1500 [revs/min] full torque condition was run between the 2000 [revs/min] and 2150 [revs/min] operating points. This however, showed that temperatures took a downward trend during the 1500 [revs/min] full torque condition and that the sequence needed to be arranged as displayed in Table 12 to maintain a temperature rise throughout a test run. After start up the engine was set to run at low idle for 10

minutes before moving to the first torque-speed station. Subsequent changes in torque and speed were made when every channel had held a constant reading for a minimum of 5 minutes. Each channel of slow speed data was logged at 5 second intervals for the duration of the test.

The results showed that the parameter with the longest time constant of 17 minutes (63% value) was lubricating oil temperature. Based on the results from this test all subsequent engine runs started with a warm through period of 1 hour at the first torque-speed station. The remaining eight torque-speed stations were given a 20 minute stabilisation period before data collection. An example plot of some of the temperatures monitored during the stabilisation trial can be seen in Figure 27. Copies of all of the stabilisation plots can be found in Appendix 'C'.

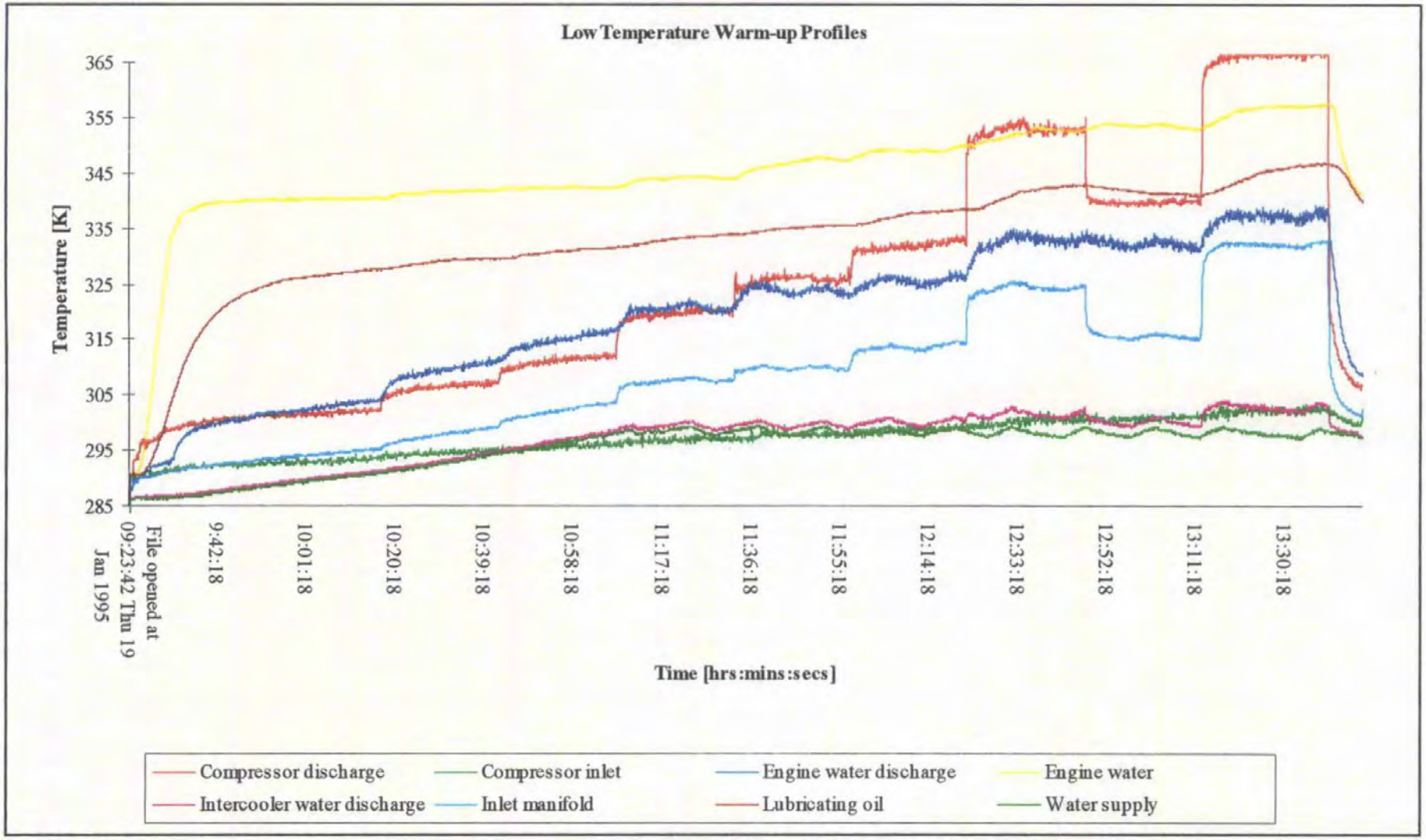

Figure 27 Engine Warm-up Trial Low Temperature Profiles

4.5 Summary

This chapter has described the techniques and testing used to validate the quality of engine test data generated by Performance Monitor. This included the calibration of each individual transducer and its associated signal conditioning. The affects of data averaging for both high and low speed instrumentation have been investigated to establish an optimum sampling duration. An indication of repeatability for each sensor reading and calculated parameter has been determined. Where practically possible instrumentation repeatability was improved by a number of methods. Reasons for the larger repeatability variations have been discussed. The trials have shown that calculated performance parameters which use two or more sensor readings generally have poorer repeatabilities than directly measured parameters. In all cases the data from the high and slow speed instrumentation was compared to data generated from panel meters, the AVL 647 Indiskop and other methods.

Finally, the experimental testing procedure was developed through the selection of appropriate test speeds and torques and an assessment of engine behaviour to ensure performance was stable before test data was recorded. Completion of this phase of the research satisfied research objective 2 and confirmed that the developed test facility and performance monitoring package were acceptable. The research could now focus on the analysis of diesel engine fault conditions.

CHAPTER 5

DIESEL ENGINE FAULT INVESTIGATION & COMPONENT FAILURE MECHANISMS

5.0 Introduction

This chapter discusses the results of a detailed study into Perkins T6.354(M) diesel engine faults and details some of the mechanisms responsible for their occurrence. The results of this study allowed realistic faults to be targeted for experimental investigation. Engine testing of unrealistic faults, either those which do not happen in practice or those who's severity is inappropriate, ultimately meant that the experimental data would have been unrepresentative and subsequent conclusions drawn about the performance of the neural network would be invalid.

5.1 Fault Study Results

Data was gathered from various maintainers and refitters who had an interest in Perkins T6.354(M) diesel engines of the same build list as the test engine. Information was collected through direct discussion with the engineers and fitters, questionnaire forms, refitters/maintainers records and photography. All of the data gathered was specific to Perkins T6.354(M) diesel engines and related to 25 individual engines refitted over a 3 year period. Table 13 and Figure 28 summarise the results of the study. It should be noted that the majority of these faults were discovered as a result of routine maintenance, not due to a noticeable change in engine operating characteristics. Most of these would however, have had an effect on rated power, fuel economy, or long term engine health.

No.	Description Of Fault	No. Of Engines	% of Engines
1	12 Valve Guides worn Over Limits	23	92
2	6 Cylinder Liners Over Limits	20	80
3	Intercooler Element Corroded Or Blocked	20	80
4	12 Valve Seats Worn Or Pitted	19	76
5	6 Exhaust Valves Pitted	16	64
6	6 Pistons Damaged	16	64
7	Fuel Pipes Corroded	16	64
8	Idler Timing Gear Bushes Worn	16	64
9	6 Inlet Valves Pitted	15	60
10	Crank Shaft Cracked	14	56
11	6 Exhaust Valves Worn On Stems	13	52
12	Camshaft Followers Worn	13	52
13	Rocker Shaft Worn Over Limits	13	52
14	6 Inlet Valves Worn On Stems	11	44
15	Exhaust Manifold Cracked Or Corroded	11	44
16	Turbocharger Heat Shield Corroded	6	24
17	Damper Unit Faulty	5	20
18	Camshaft Worn Over Limits	5	20
19	Pushrods Bent	5	20
20	Aux Drive Bushes Worn	5	20
21	Spill Rail Corroded	5	20
22	12 Rocker Arms Worn	4	16
23	Some Rocker Arms Worn	4	16
24	Camshaft Gear Teeth Worn	3	12
25	Injector Nozzle Protrusion Over Limits	3	12
26	Rocker Shaft Oil Feed Pipe Damaged	1	4
27	Injectors Corroded	1	4
28	Fuel Pump Housing Seal Broken	1	4
29	Some Exhaust Valves Pitted	1	4
30	Valve Springs Faulty	1	4

Table 13 Results Of Perkins T6.354(M) Diesel Engine Fault Study

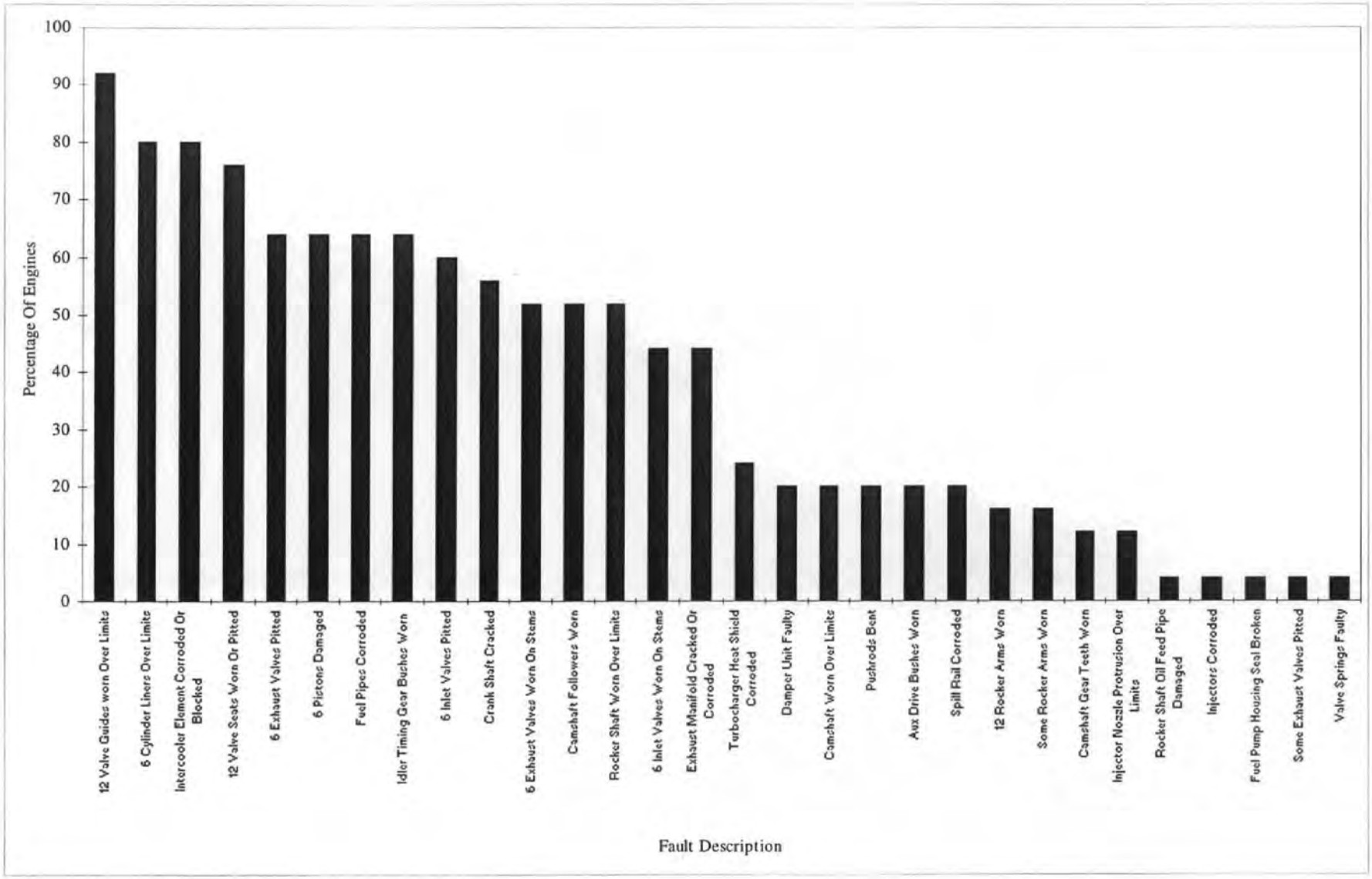

Figure 28 Perkins T6.354(M) Fault Data Frequency Distribution

Fault data specific to the Perkins T6.354(M) fuel injection system and turbocharger was relatively scarce since refurbishment of these pieces of equipment is specialist task often undertaken by the respective manufacturers. Similarly data on fuel and charge air filter blockages were not specifically recorded as faults since filter replacement was a mandatory function during refurbishment. Examination of a number of filters, however, revealed these were also commonly occurring due to poor maintenance routines.

To increase confidence in the results obtained from the fault study and review a more global picture of diesel engine faults, statistics from the Diesel And Gas Turbine Engineers Working Cost And Annual Report[41] years 1983 to 1993 were analysed. The results of their findings are summarised below in Figure 29

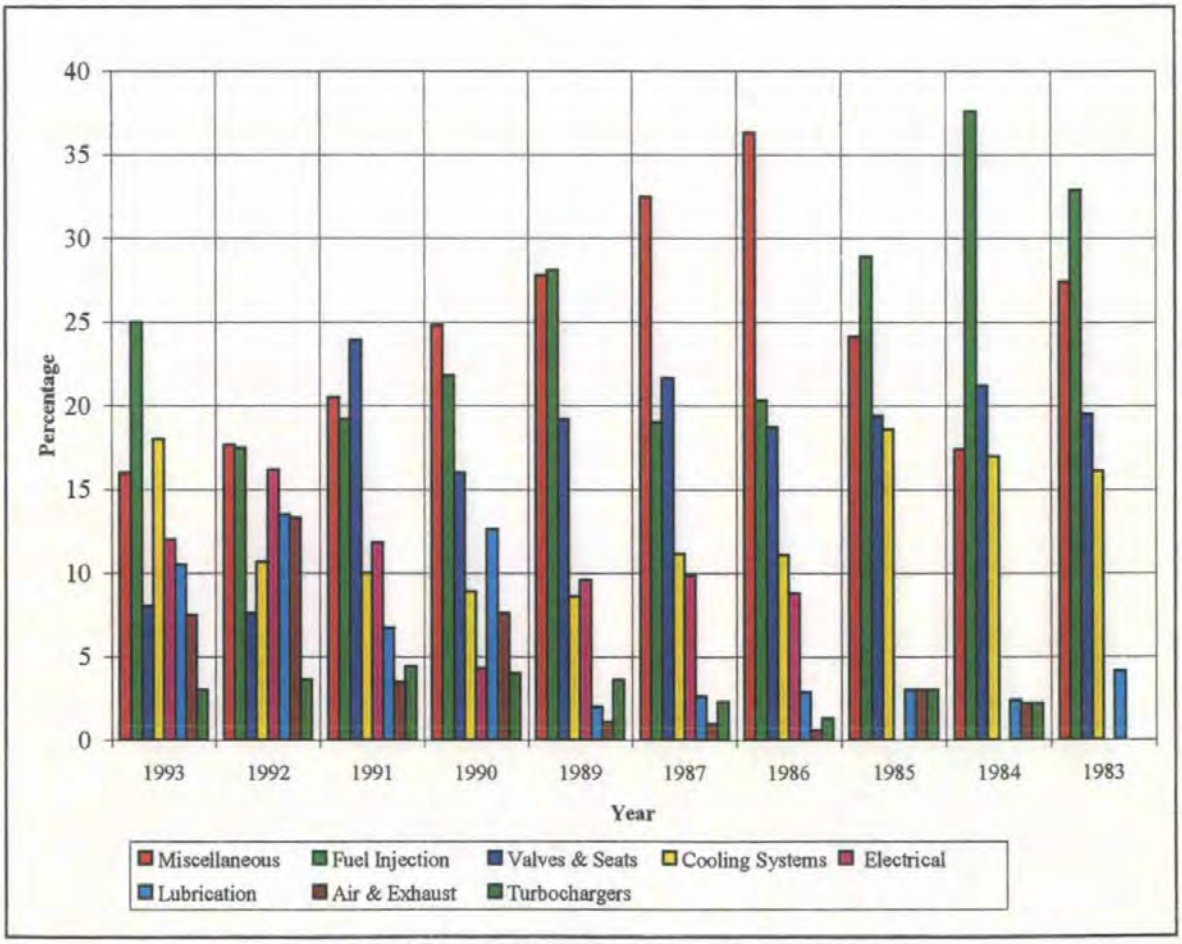

Figure 29 Causes Of Diesel Engine Stoppages

5.2 Conclusions Of Fault Study

Table 13 & Figure 28 show that the most commonly occurring faults lie in the following areas;

- Valves, valve guides & seats
- Cylinder bores & pistons
- Intercooler
- High pressure fuel injection pipe corrosion

Figure 29 shows a good correlation with Table 13 & Figure 28 also identifying valves and seats and cooling systems to be problematic. It also shows that fuel injection system faults are consistently high. Through the combination of both sets of statistics and knowledge gained during the investigation the following areas were short-listed as possible candidates for further investigation.

- Valves and valve seats
- Fuel injection equipment
- Intercooling
- Filter blockages
- Cylinder bores & pistons

It was decided due to the practical implications and time-scale allocated to the testing program that cylinder bores, rings & pistons could not be properly investigated. Further to this, they have been the subject of previous research. The faults finally identified as suitable for investigation fall in to three categories, charge air, valve, and fuel injection.

5.3 Charge Air System Faults

Two charge air system faults were selected for experimental investigation, these were, a fouled charge air filter and a defective intercooler. These were selected since they were relatively easy to introduce and represented genuine faults that were being experienced in practice.

5.3.1 Fouled Charge Air Filter

Inspection of a large number of Perkins T6.354(M) diesel engines that had been returned for refurbishment revealed that regular cleaning of the air filter was being omitted despite the manufacturers recommendation of cleaning every 250 hours or every 4 months, whichever occurs first. It was not uncommon to find filters which had 80% of the flow area blocked, a typical example of fouling is shown in Figure 30.

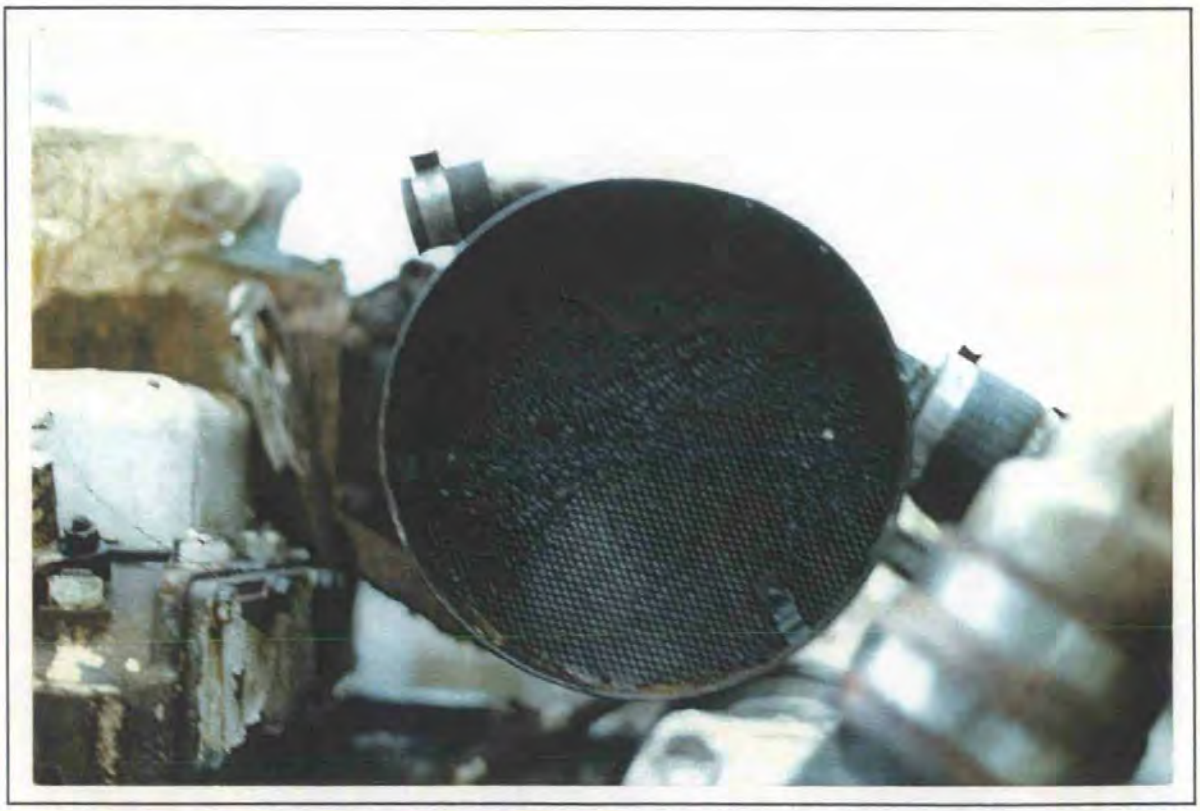

Figure 30 Typical Fouled Perkins T6.354(M) Charge Air Filter

Charge air filters foul because of the presence of oil mist and exhaust particles in the engine space. The Perkins T6.354(M)'s filter consists of a truncated conical section and a removable gauze filter.

Airborne oil mist settles on the gauze and behaves like an adhesive allowing small particles to stick. Gradually the fouling builds up between the holes in the gauze until complete blockage of a hole occurs. Work conducted by Newcastle University[42] suggests that air filters have a significant factor of over-design to accommodate for inadequate maintenance schedules. As a result, a substantial blockage may be required before any deterioration in engine performance is observed. The work conducted by Newcastle University concluded that 80% filter fouling remained almost undetectable.

5.3.2 Faulty Intercooler

Table 13 showed that fouled or corroded intercoolers were found on 80 % of the engines which were inspected. After close examination of the intercooler's water side fouling appeared to be more severe than air side fouling.

Many of today's diesel engines are highly turbocharged giving higher power densities than their naturally aspirated counterparts. As a result there is an inevitable increase in the mechanical and thermal loading of components. Mechanical stresses can be overcome by the use of suitable materials and appropriate design. The increase in thermal loading must be overcome through efficient engine and charge air cooling[43]. Inefficient charge cooling leads to higher exhaust gas temperatures,

increased thermal stress on combustion chamber components, poorer specific fuel consumption and a reduction in rated power.[44]

Intercoolers are often over designed to accommodate for various operating environments. The worst case being tropical climates where air and water temperatures are high. This results in fouling going undetected when the engine is operating in cooler climates and gives scope for both corrosion and fouling to take place. Intercooler effectiveness can be reduced through several mechanisms; these are discussed below.

(a) Marine Growth

The marine growth problem can occur in both temperate and tropical climates. Primarily it reduces the heat transfer coefficient of the matrix and impedes water flow. This can lead to accelerated localised corrosion and material deposition. The use of biocidal treatments such as electrolysis of sodium hypochloride at the vessels sea strainers and regular physical scrubbing can largely eliminate the biological growth.

(b) Precipitation, Deposition and Sedimentation Of Material

Sea water contains many metallic salts which, at ambient conditions, form a stable solution. Solution stability decreases with temperature and at around 80°C some of the metallic salts begin to precipitate[45] . At higher torque and speed conditions the Perkins T6.354(M)'s compressor discharge temperature is approximately 95°C, making it susceptible to salt precipitation. As salts precipitate and crystallise they

crust on to the matrix reducing heat transfer coefficients and effective flows. Secondary to this process, areas of low flow encourage sedimentation and sediment can become superimposed on the crystallisation. Superimposition of sediment material however, leads to weaker crystalline structures and eventually causes the crystalline structure to fracture and decompose[46] . The deposition and crystallisation of salts is greatly affected by matrix surface finish and temperature. The surface roughness and density of cavities will have their most marked effect during the initiation of the crystalline nucleation and sedimentation processes rather than the continued fouling [46] .

(c) Corrosion Of Matrix Material

If sea water is used as the coolant the intercooler materials become particularly vulnerable to corrosion. Even copper-nickel-iron alloys such as CuNilOFe or $CuNi_3OFe$ generally used for intercooler construction are susceptible to extensive corrosion. Corrosion leads to a degradation in heat transfer and, if well developed, will lead to sea water ingressing into the charge air system. Plastic coatings such as Tegon can be used to halt corrosion with the penalty of a reduced heat transfer[43] .

Figure 31 shows a typical Perkins T6.354(M) intercooler matrix which has suffered salt precipitation and crystallisation, sediment deposition and corrosion.

Figure 31 Typical Defective Perkins T6.354(M) Intercooler Matrix

5.4 Valve Faults

The results of the diesel engine fault investigation discussed earlier in this chapter shows that valve faults are some of the most commonly occurring. This is also reinforced through the statistics compiled by the Diesel & Gas Turbine Engineers & Users Association. Valve guide wear is reported as the most commonly occurring defect on Perkins T6.354(M) diesel engines. Valve and valve seat wear and pitting are also frequently occurring and, to a lesser degree, valve stem wear. Fundamentally all of these phenomena contribute to an insufficiently gas tight seal between the cylinder head seat and valve. Examination of a large number of inlet valves also showed severe fouling on the lower portion of the stem and top head face.

The results discussed earlier in this chapter also show that valve and valve seat wear and pitting occurs fairly uniformly for all valves on a particular engine. It is very rare that isolated valves are pitted or worn. Valve catastrophic failure is rare, even with modern two piece valves. It can generally be attributed to poor valve train design i.e. poor cam profiles or incorrect spring rate matching. Very occasionally catastrophic valve failures occur due to engine over-speeding where valve acceleration and hence seat impact loadings are beyond design levels. This type of failure is generally associated with vehicle applications.

Three valve faults were chosen for examination, these were, fouled inlet valves, leaking inlet valves and leaking exhaust valves.

5.4.1 Fouled Inlet Valves

Investigation by A.T. Colwell[47] showed that valve stem deposits cause approximately 50% of all valve trouble. Valve stem deposits are due to the oxidation and subsequent decomposition of lubricating oil. The decomposed oil eventually forms hard coke like material, time for formation is dependent on oil type and engine operating conditions. Valve stem deposits gradually wear valve guides causing the valves to stick open and quickly burn. Valve guide wear, a frequent problem with Perkins T6.354(M)'s, can only ease the passage of lubricating oil to the valve head. Slight inlet valve stem deposits rarely cause problems unless they become large enough to impede the flow of charge air or hold the inlet valve open.

Visual inspection showed that valve stem deposits were in the order of 3mm thick. Figure 32 shows a typically fouled valve with some of the fouling removed to show the cross sectional thickness.

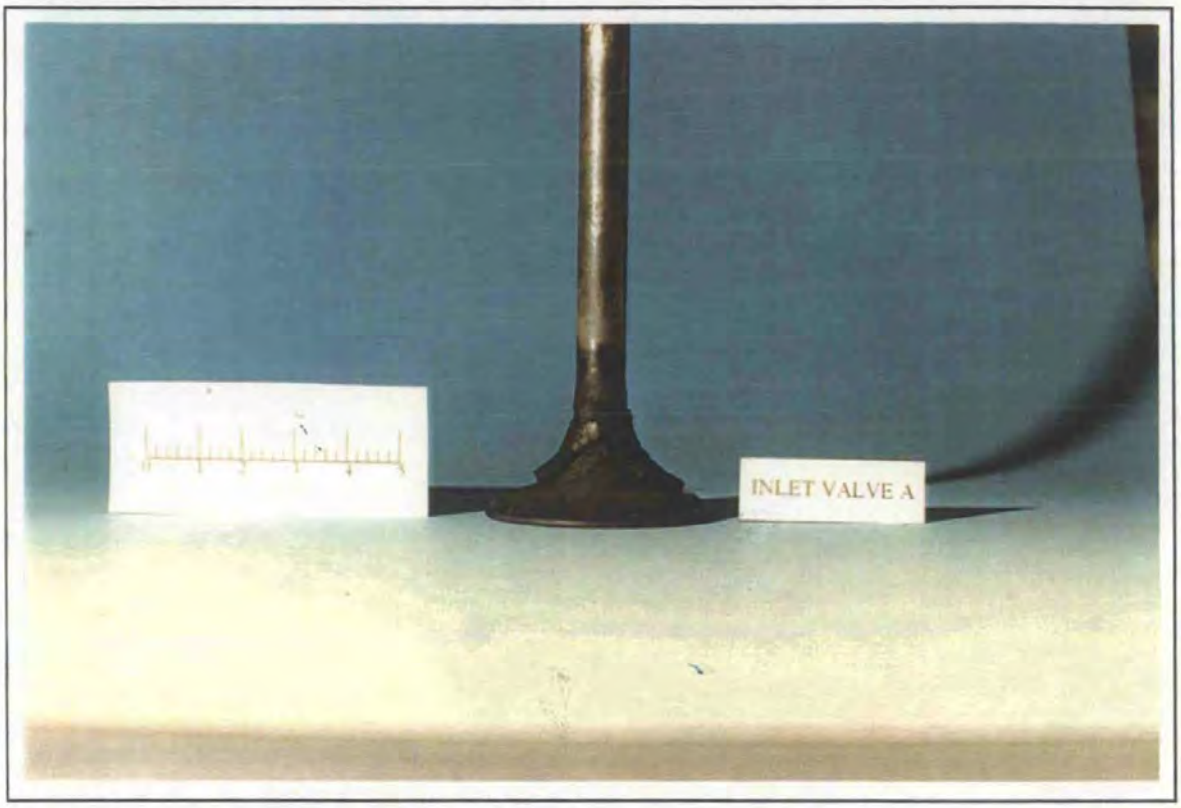

Figure 32 Perkins T6.354(M) Fouled Inlet Valve

5.4.2 Leaking Inlet & Exhaust Valves

Leakage through Inlet and exhaust valves occurs for several reasons, some of these are mentioned below;

- Incorrect setting of tappet clearances
- Weakened valve springs
- Valves sticking open due to valve stem deposits
- Severely pitted valves and seats leading to guttering
- Badly worn valve guides leading to incorrect seating
- Badly worn valves and seats

The fault study discussed earlier in this chapter showed that 76% of T6.354(M) valve seats were beyond regrinding, 64% of exhaust valves and 60% of inlet valves were severely pitted or worn beyond regrinding. Much research has been dedicated to identifying materials and methods of design and production to increase valve life. M.G. Kingston-Jones et al.[48] identified 4 mechanisms of valve damage;

- Deposit formation on the seat which then cracks or flakes.
- Deposit formation that corrodes the valve material.
- Formation of pits which, if densely populated, form gas paths.
- Thermal fatigue of the valve face, leading to cracks in the main seat material.

The formation of deposits is largely due to the oxidation of sulphur, vanadium and sodium which are all constituents of many diesel fuels. The oxidation takes place during the combustion process and oxides such as SO_2, SO_3, V_2O_5 and Na_2O_5 are formed. These oxides readily react with each other and with traces of calcium found in the lubricating oil to form low melting point salts. Many of the salts formed are highly corrosive, particularly the vanadyl species.

The molten salts flow on to the cooler valve seat area and solidify. Umland & Ritzcopf[49] believe that the molten portion of the solid-liquid seat deposit is squeezed out during the valve seating action leaving the solid, brittle deposits behind. These deposits are subsequently impacted through valve action to leave a layered deposit around the valve seat. As the thickness of the deposit increases the temperature of the valve seating face increases due to reduced heat transfer. This rise in temperature results in portions of the deposit flaking off leaving a narrow and

localised gas path. The formation of pits in the valve seating face can be caused by hard particles such as aluminium or silicon oxides, resulting from the combustion process, being pressed into the valve face. Should the pitting become densely populated on the valve face the pits link together to form a gas path, commonly known as a gutter. After gutter formation, blow through occurs throughout the engine cycle and the increased localised temperature and velocity of gas results in accelerated corrosion and rapid removal of valve material[50]. Figure 33 shows a portion of a pitted T6.354(M) exhaust valve sealing face magnified 35 times.

Figure 33 Pitted T6.354(M) Exhaust Valve Seating Face

5.5 Fuel Injection System Faults

Figure 29 shows that the single most problematic engine subsystem is the fuel injection equipment. Faulty fuel injection equipment can have severe secondary affects on other engine components, particularly if the governor action is modified or up-fuelling is used to offset the poorer engine performance caused by the fuel injection equipment fault. Incorrect timing, over-fuelling or poor injection and atomisation will have the following secondary effects.

- Increased combustion temperatures leading to higher thermal stress on rings, pistons liners and valves. Higher combustion temperatures also promote the formation of NO_x which must be controlled due legislative restrictions. Increased combustion temperatures lead to higher exhaust gas temperatures which can cause exhaust manifold fixing torque relaxation and eventual blowing.
- Higher engine temperatures cause a reduction in lubricating oil viscosity and lead to oil oxidation and increased levels of oil soot content.
- Increased mechanical stresses on the combustion chamber components, connecting rod, big end and main bearings and crankshaft.
- Higher levels of noise and vibration due to irregular combustion.
- Increased levels of smoke, particulates, and un-burnt hydrocarbons.
- Accelerated deposition of carbon on valves, rings, piston crowns and lands.
- Breakdown of the bore lubrication film due to fuel impingement and combustion on the liners.

Four fuel injection system faults were selected for further investigation, these were, incorrect fuel pump timing, fouled injector nozzle hole, worn needle and nozzle and incorrect injection pressure.

5.5.1 Incorrect Fuel Pump Timing

Correct fuel pump timing is critical if rated power, fuel consumption and specific emissions and noise targets are to be met. Four mechanisms could be responsible for incorrect fuel pump timing.

- Wear in the timing gears or auxiliary drive. Discussion with engine fitters revealed that excessive wear in the timing gears was relatively rare compared to auxiliary drive wear. In one instance auxiliary drive gear wear was so extensive that the pump could not be re-timed on the engine without replacement parts being refitted.
- Worn suction pump vanes in the hydraulic head. Small carbon vanes which are located in the hydraulic head reciprocate producing a vacuum to suck fuel into the injection pump, the pressure generated is known as the transfer pressure. The Lucas CAV pump fitted to the Perkins T6.354(M) is hydraulically governed by the transfer pressure and any vane wear will cause a shift in the point of injection.
- Pump cam ring or roller wear. Wear in the high pressure pumping components of the Lucas DPA pump would result in an retarded point of injection since contact between the cam ring and rollers will be delayed.
- Incorrect fitting and timing of the pump.

5.5.2 Fouled Injector Nozzle Hole

Injector nozzle fouling can occur through three mechanisms;

(1) Entrapped particles which manage to pass through the fuel filter will eventually deposit in the nozzle sack volume. If these particles are larger than the diameter of the nozzle holes blockage occurs. Smaller suspended solid contaminants may not block the nozzle holes but could damage the injector nozzle, needle valve and barrel as discussed in Section 5.5.3 below.

(2) Particle erosion can liberate material from the internal surface of the high pressure injection pipes[51] and will occur if;

- Low quality material is used for the manufacture of the pipes.
- Pipe connections are over-tightened leading to pipe or olive cracking.
- Excessive vibration is experienced leading to fatigue and crack formation.

If large enough particles are removed from the internal surfaces of the pipes nozzle blocking occurs, small particle debris leads to accelerated needle valve, barrel and nozzle hole wear.

(3) Poor injector cooling, excessive fuel temperatures, incorrect timing or up-fuelling can cause nozzle tip overheating. If temperatures exceed 180 - 200°C there is a high risk of carbon build up in the form of cones extending in the line of spray penetration. If this build up becomes excessive nozzle blockage may occur.

5.5.3 Worn Needle And Barrel With Enlarged Nozzle Holes

Enlarged nozzle holes give poor fuel atomisation and excessive fuel penetration producing some of the undesirable effects discussed in Section 5.5. Nozzle holes enlarge because of the erosion caused by the high pressure fuel and suspended debris which flow through them. This effect is also accelerated by cavitation on needle closure, and gas blow back, which can occur due to incorrect needle lift, a sticky needle or low spring pre tensions. In general needle and barrel wear can be attributed to three mechanisms,

(1) Particle Abrasion: Abrasive particles which pass through the needle valve originate from the two sources discussed above, fuel suspended debris not caught by the filter and material removed from the internal surface of the high pressure pipes. W.J. Gerwiner [52] showed that abrasive wear only occurs if the particle debris is larger than the clearances between the moving surfaces, smaller particles held in suspension pass with no detrimental effect. The same reference also suggests that very small concentrations of large particle contaminants will cause a rapid deterioration in injection system performance. Wear also occurs due to the occasional contact between moving components.

(2) Cavitation Erosion: The cavitation process consists of the formation and collapse of vapour bubbles in a flowing liquid due to large pressure differentials. Vapour bubbles can form in any portion of the nozzle and barrel where the pressure is below the vapour pressure of the fuel at that temperature. When the vapour bubbles are exposed to a higher pressure, generally at the needle valve seat, they collapse generating very high pressures. Constant bombardment of the needle and seat surfaces during collapse erodes the exposed metal. Cavitation erosion is particularly common if the fuel is contaminated by water.

(3) Corrosion: Sodium and sulphurous fuel contaminants in the presence of water will cause corrosive attack on injection system components. Evidence of corrosion is shown by a gradual blackening of components caused by iron oxides which results in a greatly accelerated wear rate of the moving components[53] . Water alone can cause two forms of corrosion. Water corrosion can occur when the fuel

temperature is below the boiling point of water and is identified by a greenish discoloration of the components. Entrained water also causes problems when the surrounding temperatures are in excess of 100°C but the pressure is higher than atmospheric. If the fuel-water mixture leaks from this area of high pressure to an area of lower pressure the water content will flash into steam causing extensive corrosive action.

5.6 Summary

This chapter has presented the results of an 8 month detailed study into Perkins T6.354(M) diesel engine faults, failure and fault mechanisms have also been discussed. This work has satisfied research objective 3 outlined in Chapter 1 and laid the foundation for faults to be evaluated using computer simulation, rig testing and eventually engine test. As a result of the fault study, 9 faults have been clearly identified as worthy of further investigation, these are;

- Fouled Air Inlet Filter, present on the majority of engines examined.
- Faulty Intercooler, occurring on 80% of engines refitted.
- Fouled inlet valves, present on many engines during strip investigation.
- Leaking inlet Valves, present on 60% of field engines.
- Leaking exhaust valves, evident on 64% of engines stripped for rework.
- Incorrect (retarded) fuel pump timing.
- Fouled Injector nozzle holes.
- Worn injector needle and barrel.
- Low Opening pressure injector.

CHAPTER 6

DIESEL ENGINE SIMULATION

6.0 Introduction

This chapter discusses the theory, development and results of a simulation model which was created to validate engine performance due to fault introduction. The simulation approach was adopted because engine test bed time was valuable and the engine modifications required to introduce the faults properly was very time consuming. It was thought that simulation could give **an indication of engine performance trends** when faults were introduced and identify the sensitivity of engine performance to fault severity.

Today's methods of diesel engine thermodynamic cycle simulation are widely recognised as useful tools in assessing engine performance. The developments in simulation are largely due to the rapid increase in the computational ability of computer based systems. There has been many varied approaches to diesel engine simulation. The most common has been the empirical or semi-empirical based models due to their inherent simplicity. Empirical and semi-empirical methods fall into two types, 'emptying and filling' and 'method of characteristics' models.

Emptying and filling models treat the manifolds and cylinders as thermodynamic control volumes in their entirety. The model works on the basis of these volumes 'emptying and filling'. The volumes are linked and filled and emptied via junctions which represent valves, atmosphere or turbomachinery to create a model of the engine. Equations for the conservation of mass and energy are applied to the model

and are solved on a step by step basis assuming quasi-steady processes for each step. Step size will be in the order of 1 degree crank angle or smaller. Within the overall 'filling and emptying' model smaller models for specific processes like heat release, friction, heat transfer and valve flow will be included.

This type of model treats the manifolds as control volumes which have a uniform gas state spatially along their length. This is disadvantageous if the engine is pulse turbocharged since it depends on energy transferred along the manifold in the form of a pressure wave. The degree of error introduced by assuming no spatial differences in gas state will depend on the crank angle displacement required for the pressure wave to travel the length of the manifold. If the crank angle displacement is very small the error will, in turn, be small and vice-versa.

Unsteady compressible flow, as found in diesel engines, can be modelled using hyperbolic partial differential equations. One technique for solving these equations is known as the 'method of characteristics'. Essentially the 'method of characteristics' approach to diesel engine simulation is the same as described for the 'emptying and filling' model with the exception of manifold gas dynamics modelling. The 'method of characteristics' approach solves equations for the modelling of pressure wave and fluid motion in the exhaust manifolds such that each exhaust pipe's flow is modelled. This naturally increases simulation computational complexity and simulation run times.

The aim of this research was to develop a model which could establish performance **trends** due to fault implementation and therefore a simple 'emptying and filling' model was chosen.

The simulation package selected for this work was SPICE (Simulation Program for Internal Combustion Engines). The software was developed by Dr. S. J. Charlton at the School Of Mechanical Engineering, University Of Bath. This package was used because it was a 'filling and emptying' based model which was readily available, user friendly and allowed basic fault models to be developed quickly. Basic models for all of the faults were created with the exception of the injectors. SPICE does not allow spray penetration and atomisation to be directly modelled. Combustion can be modelled through the use of user defined heat release models but this necessitated engine test data which defeated the object of simulation in this instance.

6.1 SPICE Diesel Engine Simulation Theory

The simulation is based on the control volumes being linked by mass or energy transfer and the principles of mass and energy conservation are applied to the inlet manifold, cylinders and exhaust manifold. In summary, the principles of conservation of mass and energy must be applied to the following processes during the cycle

- Mass and therefore energy transfer from the inlet manifold into the cylinders through the inlet valves
- Mass and therefore energy transfer from the cylinders into the exhaust manifold through the exhaust valves

- The addition of a fuel mass into the charge and consequently the heat released by its combustion.
- Heat transfer from the gas to the cylinder walls, cylinder head and piston.
- Work transferred to and from the piston.

These processes are shown below in Figure 34 which is a diagrammatic representation of the cylinder thermodynamic control volume.

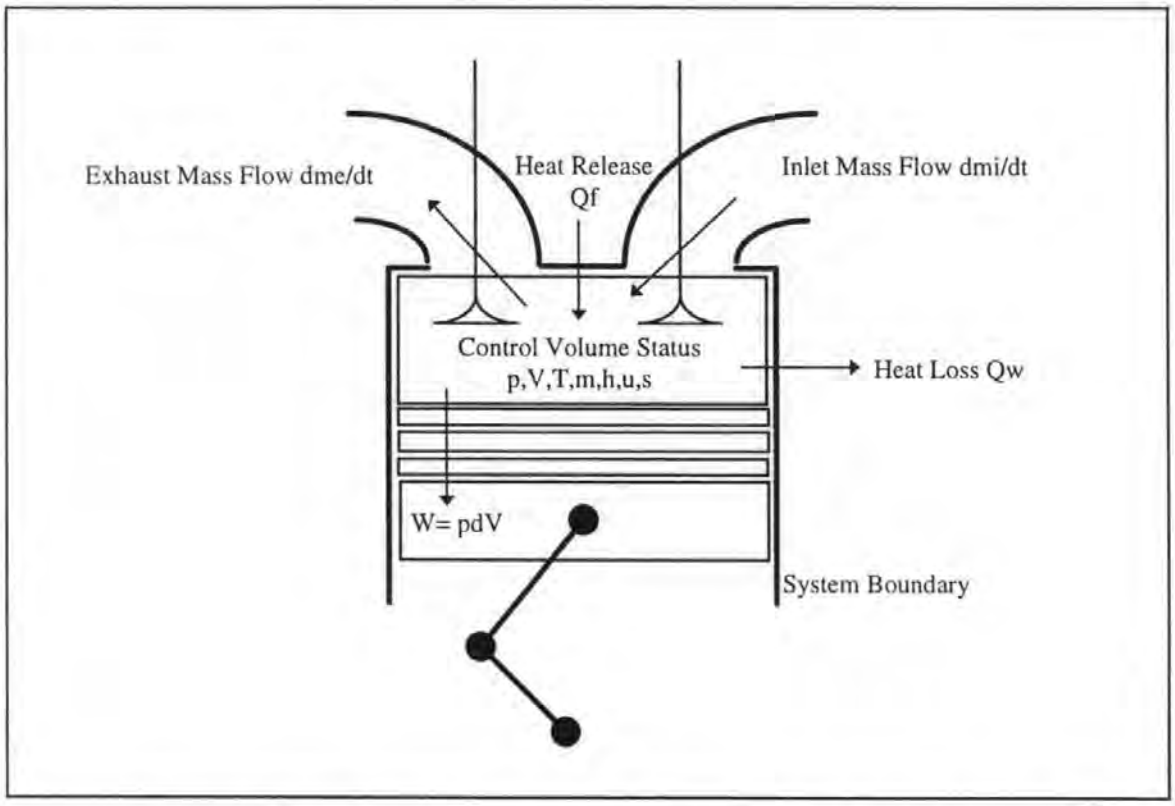

Figure 34 Engine Cylinder Thermodynamic Control Volume [54]

During the simulation it is assumed that all control volumes are in thermodynamic equilibrium and that they follow ideal gas behaviour. It is also assumed that individual control volumes contain homogeneous mixtures of air and products of combustion at every instant and that there is perfect mixing. Property gradients and phenomena such as pressure waves, non equilibrium compositions and fuel evaporation before and during combustion are neglected.

The principles of conservation of mass and energy can be described by three coupled differential equations. These differential equations are solved for each volume using a numerical integration technique on an incremental or step by step basis throughout the 720° cycle.

6.1.1 System Differential Equations

The principles of conservation of mass and energy can be described by three coupled differential equations as shown in equations 5, 6 and 7.

Rate of change of temperature with respect to time

$$\frac{dT}{dt} = \frac{1}{m\frac{\delta u}{\delta T}}\left[\sum \frac{dQw}{dt} + \frac{dQf}{dt} + \sum_i h_i \frac{dm_i}{dt} + h_{for}\frac{dm_f}{dt} - \sum_e h_e \frac{dm_e}{dt} - m\frac{\delta u}{\delta \lambda}\frac{d\lambda}{dt} - \frac{mRT}{V}\frac{dV}{dt} - u\frac{dm}{dt}\right]$$

Equation 5

The total mass flow rate with respect to time

$$\frac{dm}{dt} = \sum_i \frac{dm_i}{dt} + \sum \frac{dm_f}{dt} - \sum_e \frac{dm_e}{dt}$$

Equation 6

Rate of change of air-fuel ratio with respect to time

$$\frac{d\lambda}{dt} = \frac{(1+\lambda)}{m}\left[\frac{dm_f}{dt} + \sum_i \frac{dm_i}{dt}\frac{(\lambda_i - \lambda)}{(1+\lambda_i)}\right]$$

Equation 7

6.1.2 Solution Of The Differential Equations

Section 6.1.1 shows the three first order differential equations, identified as equations 5, 6 & 7. These coupled differential equations describe the general thermodynamic behaviour of a control volume and can be solved using a numerical

integration technique. There are many numerical techniques available for example, modified Euler predictor corrector, Adams-Bashforth and Runge-Kutta. SPICE uses the former and compromises speed of computation and accuracy. Computational difficulties can be experienced, especially during the valve overlap period when the convergence criteria may not be met. This problem can be easily overcome by reducing the step size at the expense of computational speed. The modified Euler predictor method takes the form;

$$y_1 = y_0 + \left\{\frac{dy}{dx}\right\}_0 \Delta x \qquad \text{Predictor} \qquad \text{Equation 8}$$

$$y_1 = y_0 + \left\{\left(\frac{dy}{dx}\right)_0 + \left(\frac{dy}{dx}\right)_1\right\}\frac{\Delta x}{2} \qquad \text{Corrector} \qquad \text{Equation 9}$$

6.2 Development Of A Healthy Perkins T6.354(M) Model

The Perkins T6.354(M) was modelled in the conventional way, by representing the engine as interconnected thermodynamic control volumes and junctions. A diagrammatic representation of the engine model is shown below in Figure 35.

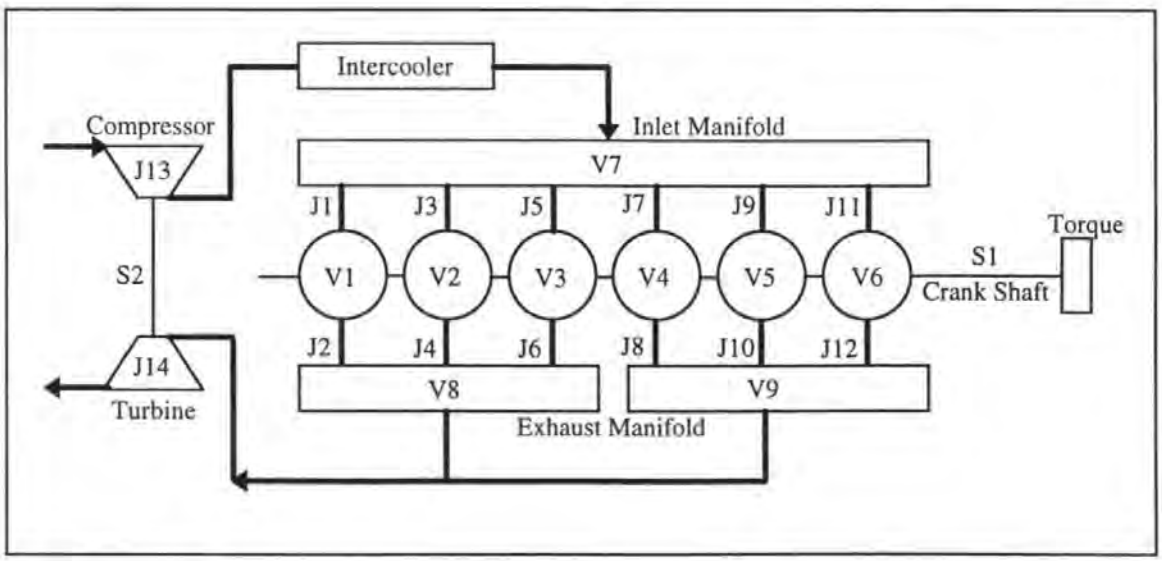

Figure 35 Perkins T6.354(M) Simulation Model

The input data required by the simulation is contained within three files. These are the engine file, compressor file and turbine file. Copies of these files can be found in Appendix 'D' . Besides specifying the configuration, geometric and volumetric data these files contain sub-models used by the simulation. These sub-models are discussed below in more detail.

6.2.1 The Heat Release Model

The heat release model is key to developing an accurate engine simulation model. Much work has been dedicated to developing accurate heat release models which reflect combustion across the engine operating envelope. The heat release model chosen for this simulation was the Dynamic Watson. Amongst others Watson et al.[55] developed a model which was particularly suitable for high speed direct injection engines as used in this research. Watson et. al. attempted to derive a model which matched experimental data closer than previous models throughout a wide range of torque and speed conditions. Watson's model is initiated at the point of injection and the subsequent process can be broken into 4 phases as shown in Figure 36.

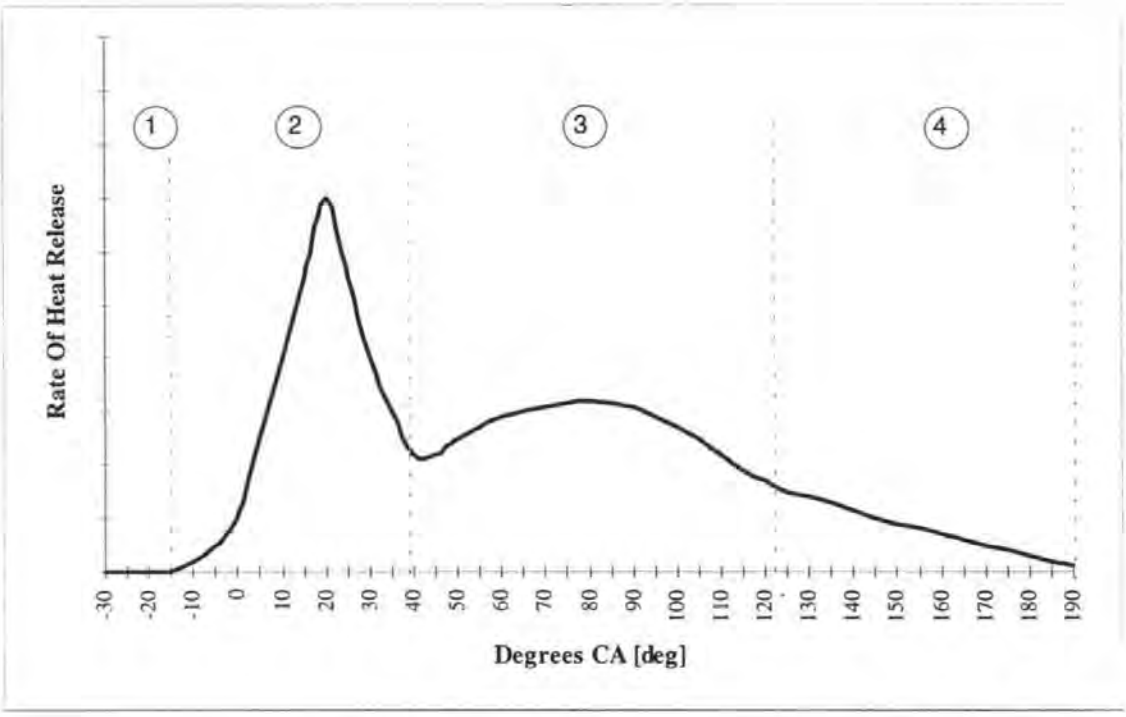

Figure 36 Typical Heat Release Diagram

Phase 1 (ignition delay): The period between the start of fuel injection into the chamber and the start of combustion. Start of combustion is defined as the point at which heat release becomes positive.

Phase 2 (premixed burning): In this phase the fuel already sufficiently mixed with air during the ignition delay period rapidly combusts.

Phase 3 (diffusion burning): The rate of combustion decreases and is a function of rate of atomisation, vaporisation, mixing of fuel vapour with air and pre-flame chemical reactions.

Phase 4 (late combustion phase): Largely due to small residual amounts of fuel burning and the release of heat energy from soot or fuel rich combustion products.

6.2.2 Heat Transfer Model

Determining heat transfer from the hot gases to the combustion chamber walls is a very complex process. As with the heat release models, attempts have been made to

model the heat transfer process. One such model was developed by Woschni[56] and is used in this simulation. The model uses a semi empirical method which considers gas motion due to both piston motion and combustion to determine the instantaneous heat transfer coefficient. The rate of convective heat transfer is calculated from the following equation.

$$\frac{dQ}{dt} = hA\left(T_W - T_g\right) \qquad \text{Equation 10}$$

Where h is the instantaneous heat transfer coefficient, A is the area through which the heat is transferred, T_w is the combustion chamber wall temperature and T_g is the gas temperature outside of the thermal boundary layer. The calculation of heat transfer is made particularly difficult since all of the terms in the above equation are continuously varying. The engine file specifies the fixed surface areas such as piston crown and cylinder head flame face and also assigns mean wall temperatures to these areas. Exposed cylinder liner surface area is computed by the simulation.

6.2.3 The Friction Model

Frictional losses in the engine are calculated using a relationship developed for turbocharged engines by Chen & Flynn[57]. The model expresses the frictional losses as a function of mean piston speed and maximum cylinder pressure. Equating frictional losses to FMEP, their equation takes the form;

$$FMEP = 0.137 + 0.005p_{\max} + 0.162C_{piston} \qquad \text{Equation 11}$$

6.2.4 Valve Flow Mapping

Valves are regarded as junctions which link thermodynamic control volumes. At any instant in time the pressure in each of the volumes can be calculated. The resulting pressure gradient across the junction determines the direction of flow. The mass flow rate through the valve is calculated using the equation which describes one-dimensional compressible flow through an orifice. It is assumed that the static pressure at the throat is equal to the downstream stagnation pressure and that flow upstream of the junction is isentropic.

Velocity at the throat is given by;

$$C = \sqrt{\left\{2C_p T_u \left(1 - \left[\frac{p_t}{p_u}\right]^{\frac{\gamma-1}{\gamma}}\right)\right\}} \qquad \text{Equation 12}$$

The Mach number at the throat may be calculated by;

$$M = \frac{C}{\sqrt{\left\{\gamma R T_u \left[\frac{p_t}{p_u}\right]^{\frac{\gamma-1}{\gamma}}\right\}}} \qquad \text{Equation 13}$$

And the continuity equation states;

$$\frac{dm}{dt} = \rho_t A C \qquad \text{Equation 14}$$

Substituting equation 12 into equation 14 and defining the density term gives;

$$\frac{dm}{dt} = A e \left\{\left[\frac{p_t}{p_u}\right]^{\frac{1}{\gamma}} \frac{p_u}{RT_u} \sqrt{\left\{2C_p T_u \left[1 - \left[\frac{p_t}{p_u}\right]^{\frac{\gamma-1}{\gamma}}\right]\right\}}\right\} \qquad \text{Equation 15}$$

Where $M \geq 1$ then the pressure ratio in equation 15 is substituted hence;

$$\frac{p_t}{p_u} = \left\{\frac{2}{\gamma+1}\right\}^{\frac{\gamma}{\gamma-1}} \qquad \text{Equation 16}$$

For equation 5 to be used to compute valve flow, the effective flow area must be known. The engine file contains two tabulations relating effective valve flow area and crank angle. These tabulations were created by measuring valve lift on engine with a DTI, Dial Test Indicator, with respect to crank angle. Figure 37 shows valve lift vs crank angle for both inlet and exhaust valves.

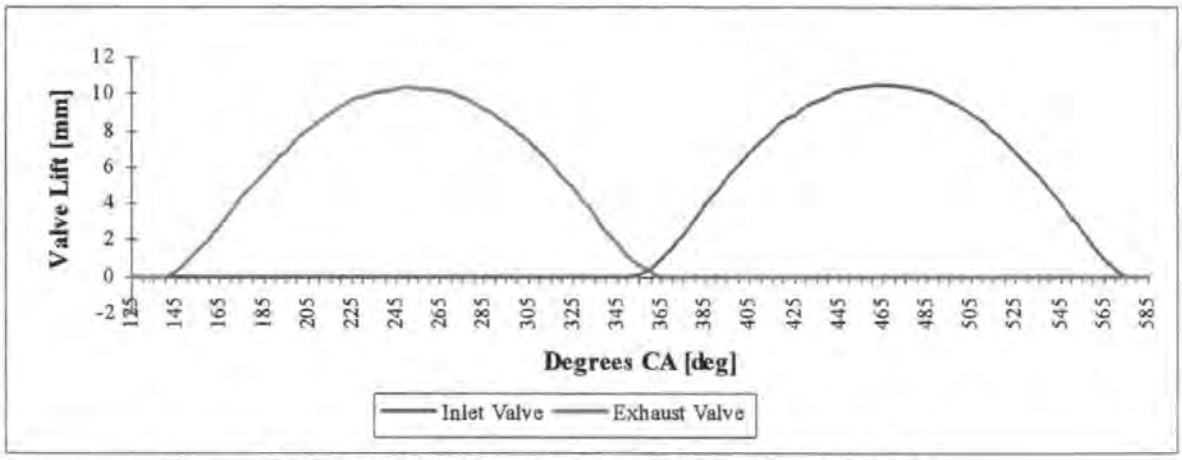

Figure 37 Inlet & Exhaust Valve Lift vs Crank Angle

It was not practically possible to conduct a steady flow test to establish the valve flow discharge coefficients. Instead, the results from work conducted by Annand and Roe[58] into diesel engine gas flows were used. Figure 38 shows how the discharge coefficient varies with non dimensional valve lift for an inlet valve. Three distinct phases of flow regime are evident labelled A, B & C and relate to the three stages of valve lift illustrated.

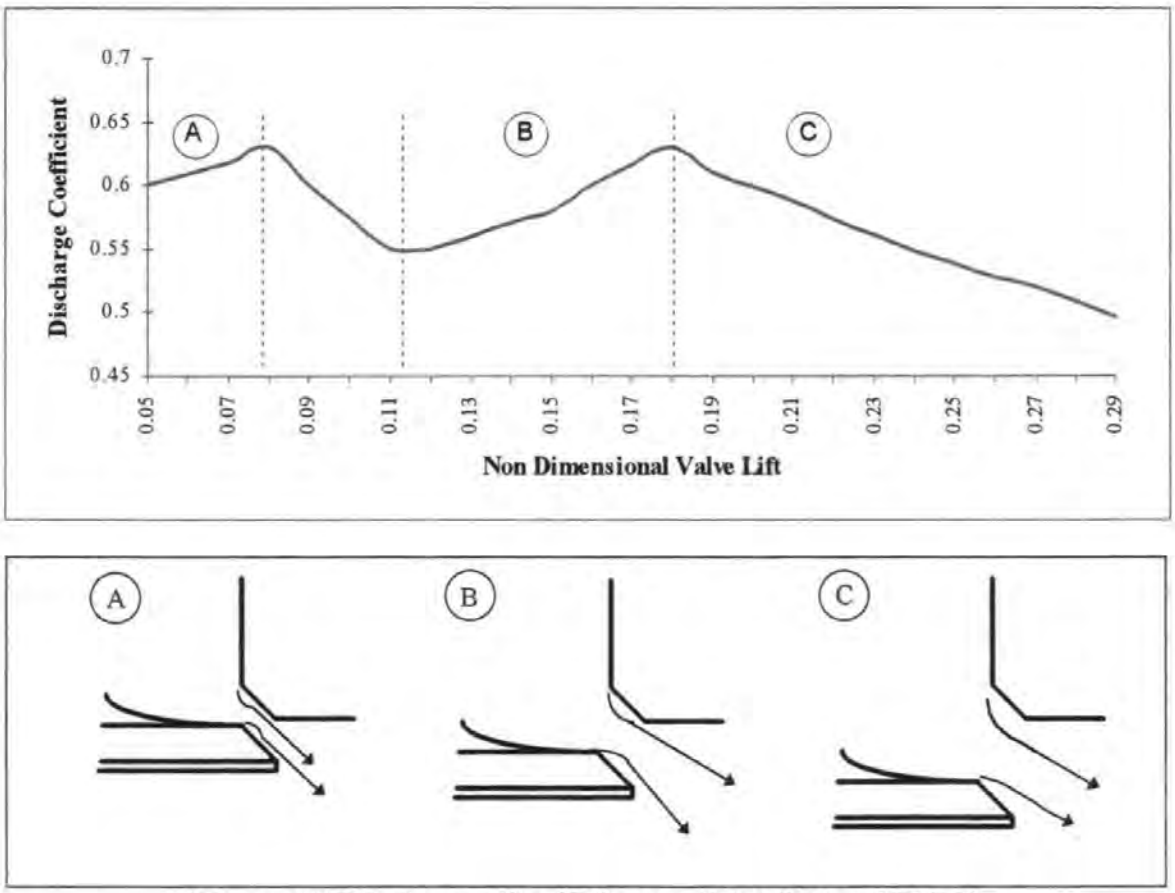

Figure 38 Discharge Coefficient vs Inlet Valve ND Lift

The relationship between discharge coefficient and valve lift for an exhaust valve is shown in Figure 39

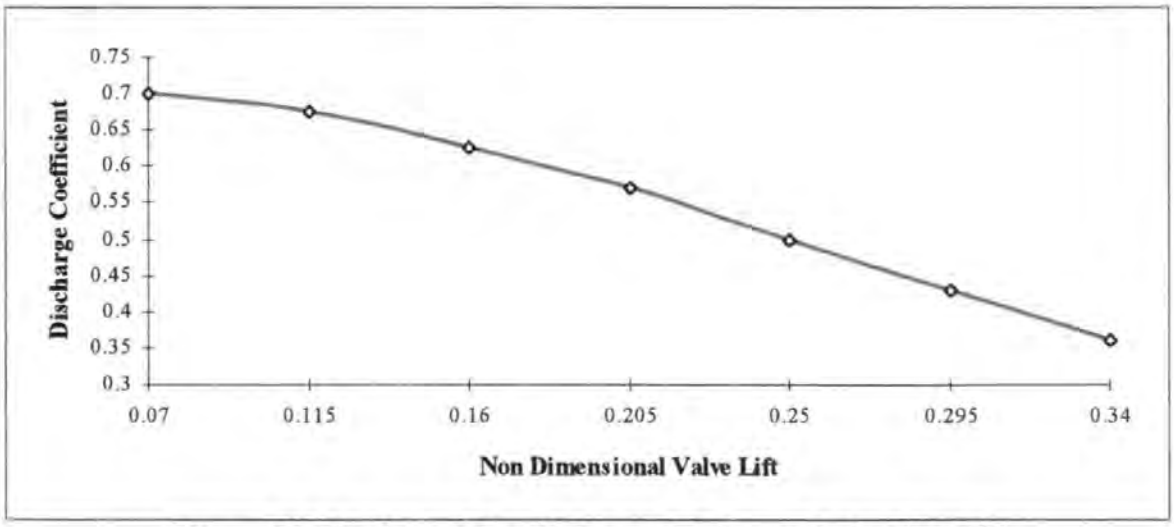

Figure 39 Discharge Coefficient vs Exhaust Valve ND Lift

From the relationships between non-dimensional valve lift and discharge coefficients the effective valve flow areas with respect to crank angle can be derived, and are shown in Figure 40.

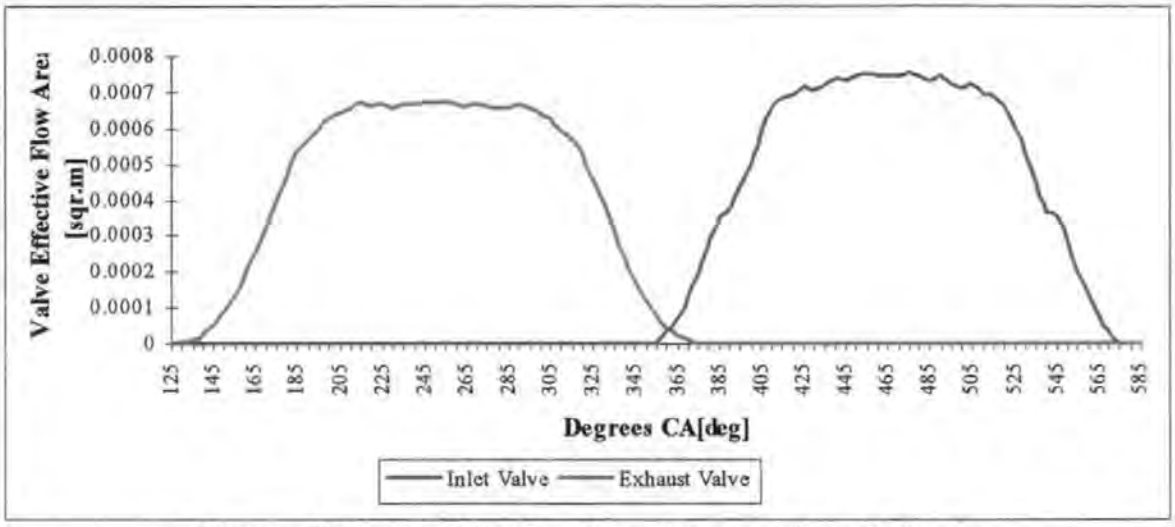

Figure 40 Valve Effective Flow Areas vs Crank Angle

6.2.5 Turbine And Compressor Data

The turbine and compressor are both regarded as junctions as indicated in Figure 35. As with valve flow, compressor and turbine characteristics are represented by tabulated performance maps. The maps provide pressure ratio, mass flow parameter, speed parameter and isentropic efficiency data. At any instant during the simulation the flow through the turbocharger is a function of rotor speed and pressure ratio. The maps are interpolated during the simulation to determine mass flow and isentropic efficiency. The turbocharger is simulated as a fully dynamic system, hence mass flow, efficiency and rotor speed all vary throughout the cycle.

6.3 Validation Of The Engine Simulation

The simulation was set to model engine performance at the experimental operating points determined in Chapter 4 such that a direct comparison could be made between the experimental results and the simulation. Performance Monitor was used to generate the experimental results which reflected healthy engine performance. Performance Monitor generated 15 complete sets of results for each of the 9 operating points, totalling 135 separate engine tests. These tests were conducted

to generate the experimental results which reflected healthy engine performance. Performance Monitor generated 15 complete sets of results for each of the 9 operating points, totalling 135 separate engine tests. These tests were conducted over a 6 month period and therefore allowed for significant changes in ambient conditions such as relative humidity, barometric pressure and temperature. The testing conducted over this period totalled several hundred hours of running and therefore also accounts for variation in engine component bedding, power enhancement and bore condition effects.

6.3.1 Comparison Of Simulation & Experimental Data

The experimental results were averaged at each of the operating points to give a definitive data set which could be compared to the simulation results. A summary of the results are shown in Figures 41 to 45.

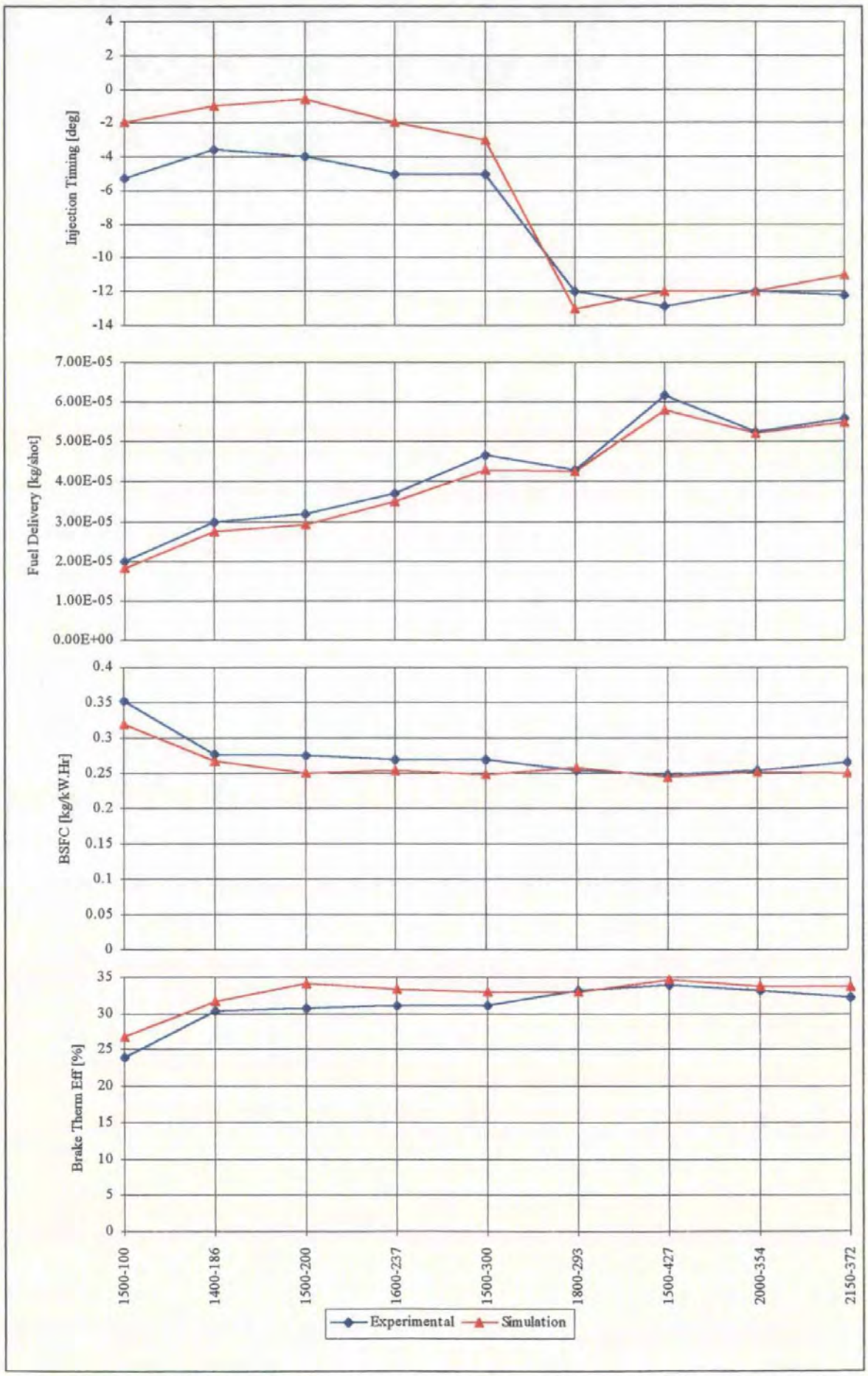

Figure 41 Fuelling and Brake Power Parameters Vs Engine Speed [revs/min] - Torque [Nm] Test Points (simulation & experimental)

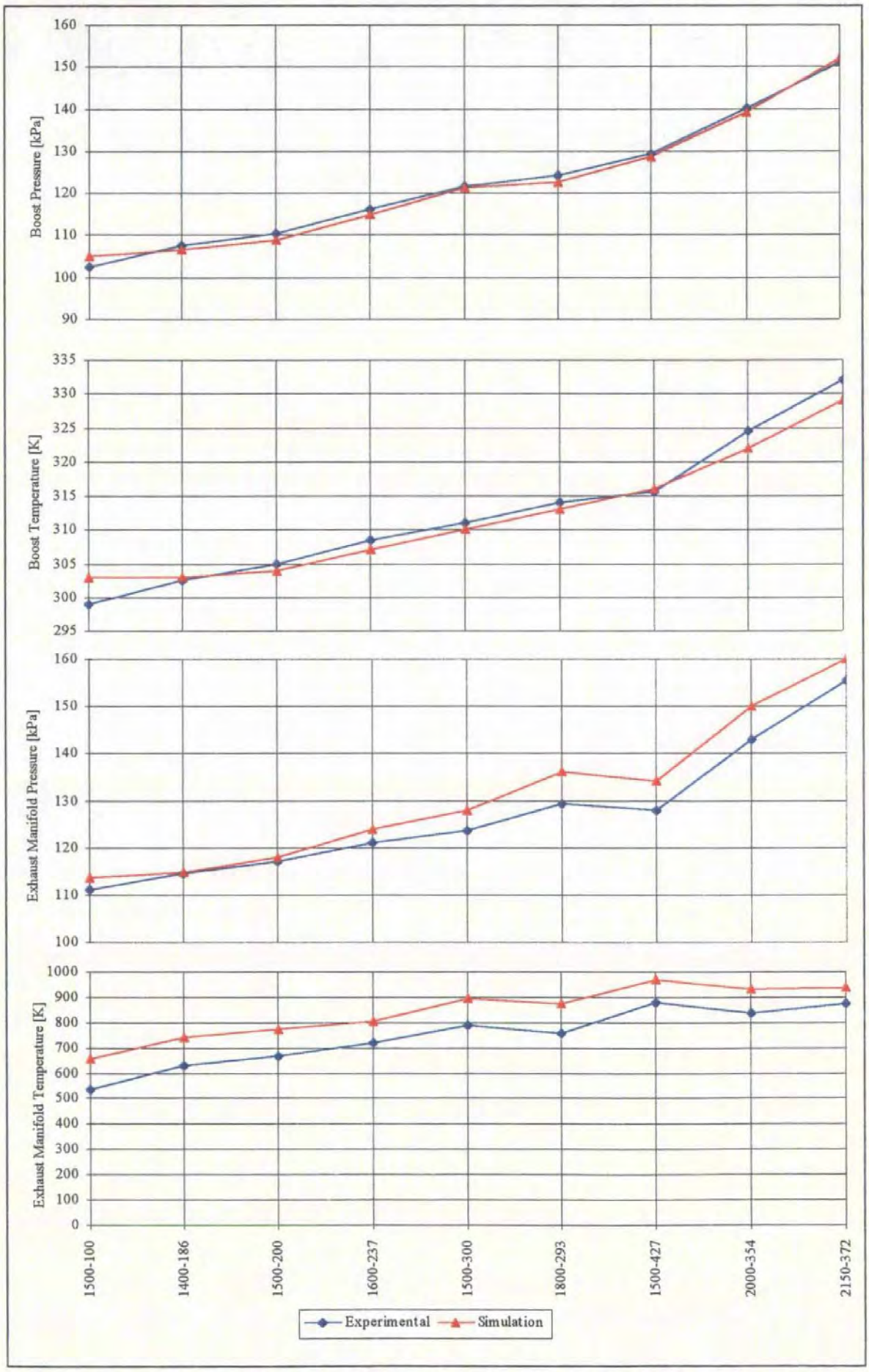

Figure 42 Inlet & Exhaust Manifold Conditions Vs Engine Speed [revs/min] - Torque [Nm] Test Points (simulation & experimental)

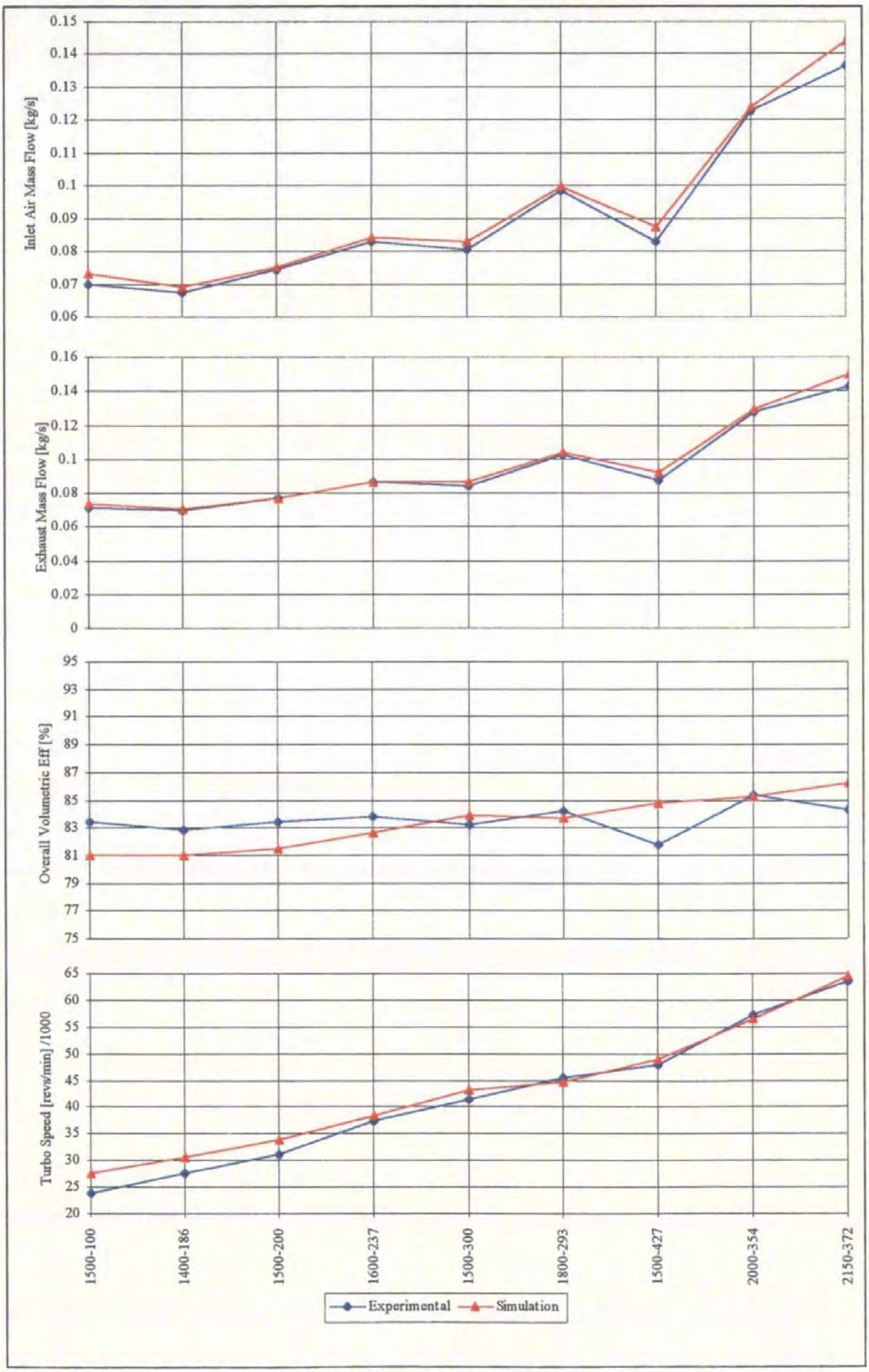

Figure 43 Inlet & Exhaust Flow Parameters & Turbo Speed Vs Engine Speed [revs/min] - Torque [Nm] Test Points (simulation & experimental)

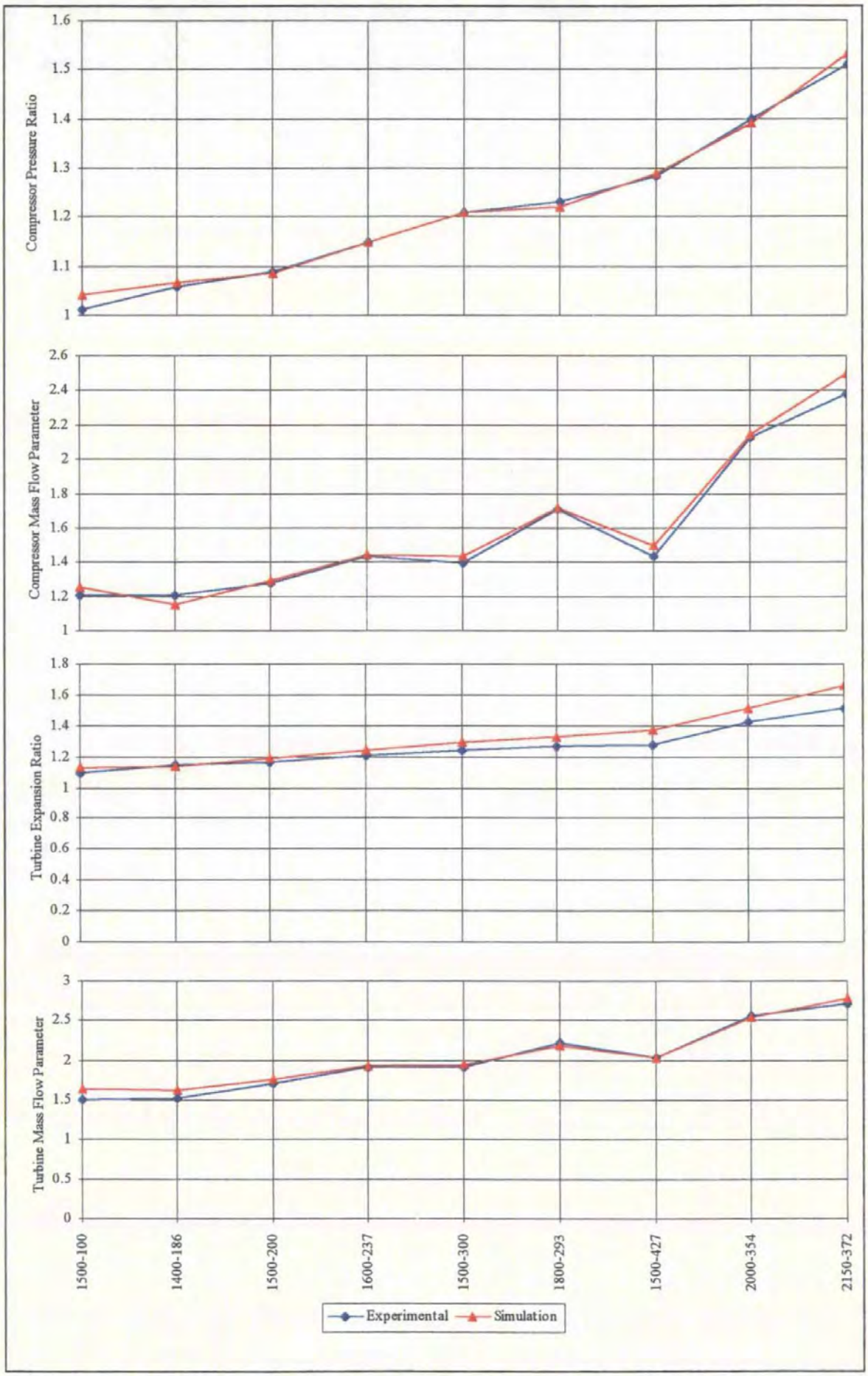

Figure 44 Turbocharger Parameters Vs Engine Speed [revs/min] - Torque [Nm] Test Points (simulation & experimental)

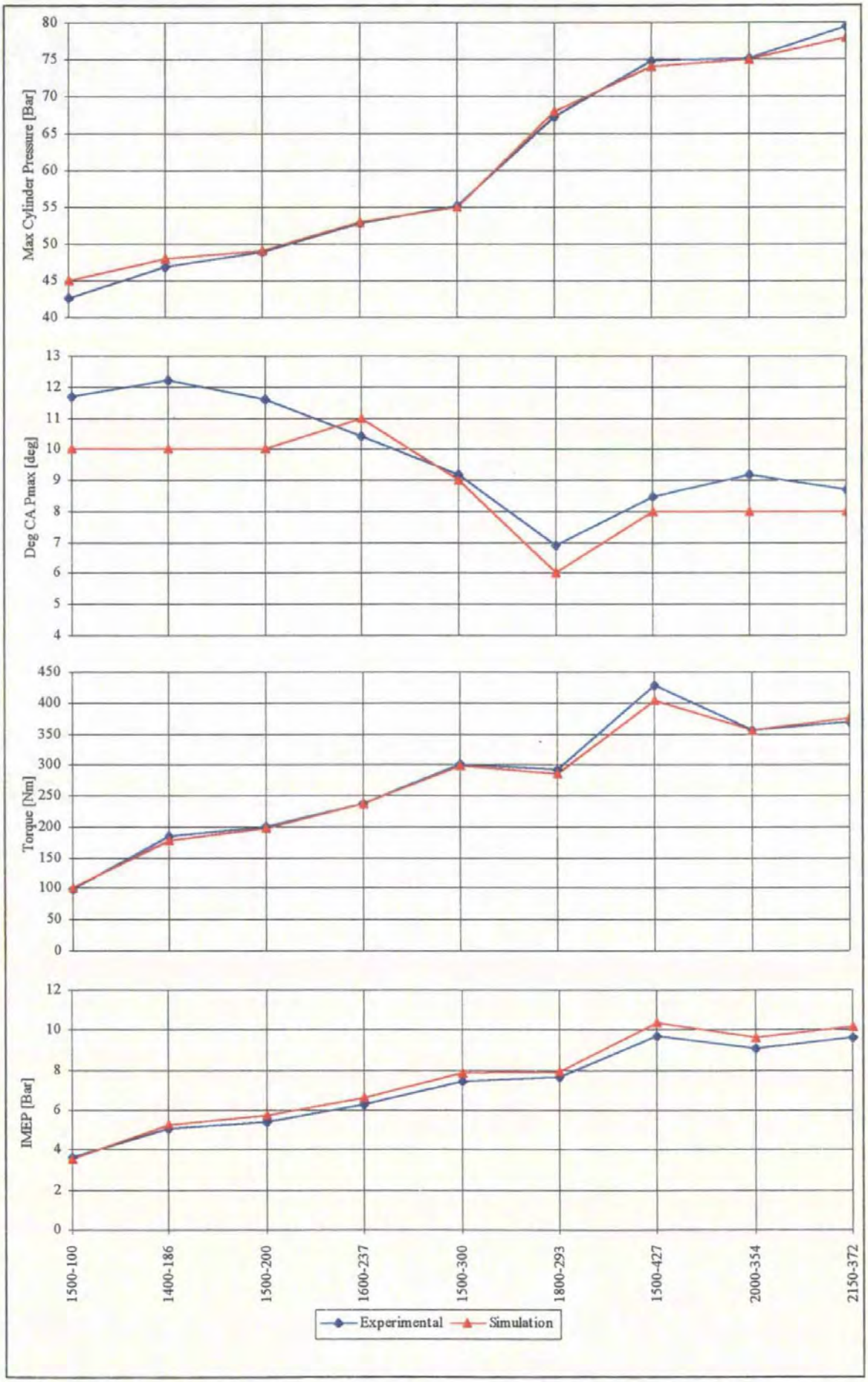

Figure 45 In-Cylinder Parameters Vs Engine Speed [revs/min] - Torque [Nm] Test Points (simulation & experimental)

The results show that the SPICE model simulates the engine performance with a reasonable degree of accuracy. In nearly all cases the trends in performance are matched throughout the torque and speed range. The fact that the general trends are followed is considered more important than the simulation's absolute accuracy. This research used the simulation to predict trends in performance due to fault implementation and not absolute deviations. However, there were some differences between the experimental and simulation results and these are discussed below.

(a) The Charge Air System: All of the charge air system parameters were well modelled, with the exception of low power turbocharger speed. All of the charge air parameters were modelled to within 4.3% throughout the power range. At the lowest power the simulated turbocharger speed was 16.7% higher than the experimental reading. This deviation reduced dramatically to within a few percent by mid range power.

(c) Combustion & Injection: In order that maximum cylinder pressure, angle of maximum cylinder pressure and IMEP could be well modelled the point of injection needed to be retarded from that measured during experimentation for low speed, low torque conditions. Consequently the point of injection specified in the simulation was retarded by a maximum of 3.3° from the experimental results. This deviation is caused by the limitation of the heat release model to accurately predict the ignition delay and pre-mixed burning phases. This problem could have been overcome by specifying heat release through a user defined heat release map but the version of SPICE used for this simulation would not allow user defined heat release modelling. Evidence of the inability of the heat release model to predict the low power conditions is also reflected in the fuel delivery and BSFC data which showed

a maximum deviation of 8%. Again these deviations soon reduced to a few percent at the higher power conditions.

(c) Exhaust System: The exhaust mass flow rate and mass flow rate parameter were well modelled to within a few percent. Exhaust manifold pressure showed a reasonable correlation with a maximum deviation of 5.26%. The low power conditions were well modelled but the discrepancy increased with increasing power. The exhaust manifold is specified in the simulation as a fixed volume reservoir accepting mass flow from the cylinders. The simulation neglects manifold geometry and assumes a uniform gas state spatially along the length of the manifold, neglecting pressure wave effects. Experimentally, exhaust manifold pressure was only measured at one location, close to the turbine inlet. It is thought that this steady trend in discrepancy between the experimental and simulated results was due to a combination of both the pressure wave effects and the location of the transducer. Although absolute exhaust manifold temperatures were poorly modelled the trend throughout the speed and torque range was good. The large temperature difference between the simulation and experimental results can be attributed to a simulation simplification of the exhaust manifold heat transfer characteristics. The engine had a water cooled manifold but the simulation ignored heat transfer processes between the manifold walls and the exhaust gas in an attempt to keep the simulation as simple as possible.

6.4 Summary

This chapter has detailed the development of a simple computer simulation model of a Perkins T6.354(M) diesel engine to evaluate trends in engine performance due to the introduction of faults. The rationale behind program selection and simulation theory have been discussed. The results show that the model gives a good correlation with the experimental data for the majority of parameters. The simulation showed a poorer correlation for some fuelling parameters at low speeds and exhaust manifold temperature and pressure throughout the speed and torque test points. Reasons for this however, are understood and have been explained. Based on the results of the comparison between the experimental and simulated data the SPICE model was regarded as suitable for determining trends in engine performance due to the introduction of faults.

CHAPTER 7

DIESEL ENGINE FAULT VALIDATION & IMPLEMENTATION

7.0 Introduction

The methods used for fault introduction are particularly important. If faults are introduced in an unrealistic fashion the validity of the engine test data and conclusions drawn about the artificial neural network's diagnostic performance are questionable. The majority of faults were introduced using genuinely faulty T6.354(M) components which had been collected during the course of the fault study. These defective components were removed at engine refurbishment and had not been previously identified as being faulty during engine operation. When genuinely faulty components could not be used for engine test, simulated faults were created using a variety of methods which are discussed later in this chapter. Where appropriate, rig testing was used to assess the characteristics of the faulty components prior to engine test. The faults were also assessed using the computer simulation developed in Chapter 6 to estimate their effect on engine performance. The faults were simulated at the five highest power torque - speed stations since these were the most effectively modelled and the faults were expected to be more evident at the higher speeds and torques. Simulation allowed the sensitivity of engine performance to a particular fault to be estimated quickly. The use of simple fault simulation combined with a knowledge of genuine fault characteristics allowed an effective engine testing program to be developed.

A total of nine faults were identified as a result of the fault study which is outlined in Chapter 5. The following sections discuss how each of these faults were validated prior to engine testing. Further to this, methods of introduction of the faults for engine testing are detailed.

7.1 Fouled Charge Air Filter

Work conducted at Newcastle University[42] suggested that significant filter blockages can be tolerated before any degradation in performance can be detected .This is largely due to the degree of over design applied by engine manufacturers. The fault study detailed Chapter 5 revealed that filter blockages of up to 80% were not uncommon on Perkins T6.354(M) engines. Two severities of blockage, 30% and 80%, were simulated using the SPICE model developed in Chapter 6. These were modelled by introducing a fixed volume upstream of the compressor. The additional volume was filled via a variable effective flow area orifice junction which connected between the volume and atmosphere. Where the effective flow area A_e is simply the actual flow cross sectional area multiplied it's discharge coefficient. The junction effective flow area was varied to simulate different severities of fouling. The additional volume was geometrically identical to the filter cone connected to the engine. A copy of the SPICE model file can be seen in Appendix 'D'. The junction effective flow area was derived from the initial engine trials using equation 15. From experimental trials the following conditions were determined for the filter system;

Mass flow rate of air through filter = 0.136 [kg/s]

Temperature of air = 303.4 [K]

Upstream pressure = 100.5 [kPa]

Downstream pressure = 100.4 [kPa]

Assuming $\gamma = 1.39$, $C_p = 1000$ J/kg.K & R = 280 J/kg.K

Substituting values into equation C_p, T, p & γ into equation 12 gives a throat velocity of 15.36 [m/s].

Substituting the calculated velocity into equation 13 gives a Mach number of 0.045, i.e. un-choked flow.

Substituting values of p, T, C_p, R & γ into equation 15 gives an effective flow area of $8.85 * 10^{-3}$ [m^2] for a clean filter.

The effective flow area for the clean filter was entered into the modified SPICE simulation and run through the five highest power torque and speed points to ensure that the addition of the clean filter had not affected the performance. Further simulation runs were conducted, each time reducing the effective flow area until the results began to deviate from the healthy engine simulation data. At an equivalent filter blockage of 80% trends in inlet manifold pressure, inlet air mass flow rate, exhaust temperature and exhaust manifold pressure started to develop. Figure 46 compares data generated from the healthy and 80 % fouled air filter simulation models. To ascertain whether Performance Monitor could detect these predicted changes under engine test conditions, the repeatability of each parameter was plotted against the simulation data in Figure 46. Simulation was not conducted for fouling in excess of 80% because this was considered unrealistic based on the findings of the fault study detailed in Chapter 5. The fact that 80% filter fouling was considered realistic and that the instrumentation, in theory, was capable of

measuring these small performance changes it was decided that this fault was suitable for engine testing. The repeatability study only examined sensor precision under one set of torque and speed conditions. For Figure 46 to be valid it was assumed that sensor repeatability remains constant regardless of the engine operating point and that the engine torque and speed settings can be reproduced. Affects of ambient conditions are also neglected.

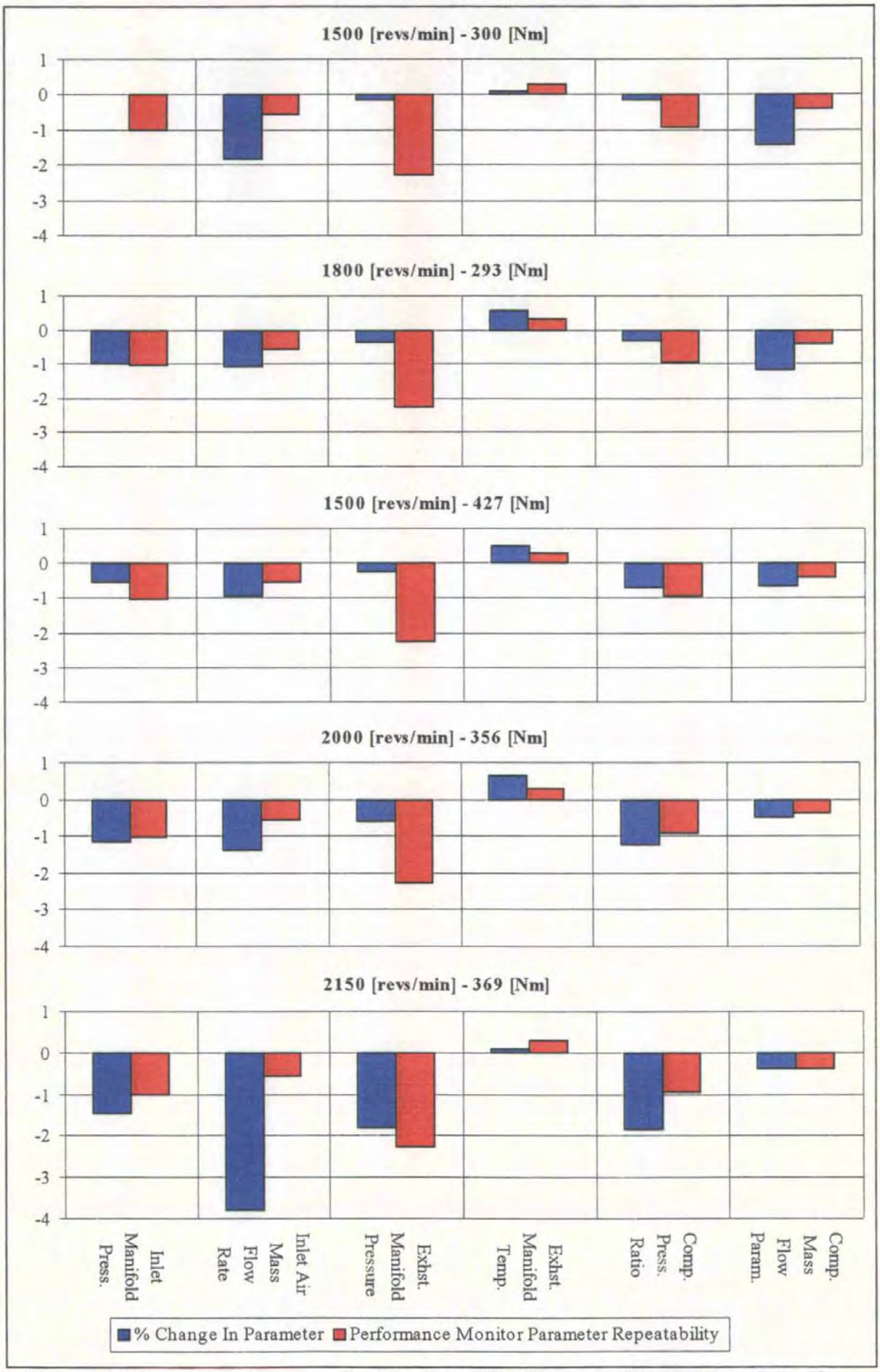

Figure 46 Percentage Change In Simulated Performance Parameters Due To 80% Fouled Air Inlet Filter Compared To Performance Monitors Data Repeatability

In practice air filters foul through the gradual build up material on the filter mesh, effectively blocking each of the mesh holes by a small amount. For this reason it was considered invalid to completely block 80% of the inlet area with a solid membrane. Instead, the fault was created by covering the clean filter with layers of perforated polythene. Since the perforation density and area of each perforation was known the percentage blockage could be calculated.

7.2 Fouled & Corroded Intercooler Matrix

This fault was recorded as the second most popular defect on engines returned for reconditioning. Two genuinely faulty intercooler units were obtained from engines which had been returned to a re-fitters for routine overhaul. Both intercoolers were fitted to the test engine and preliminary trials were conducted to establish their effectiveness. The effectiveness of both intercoolers was found to be almost identical which gave added confidence that the severity of this fault was realistic. Figure 47 compares the effectiveness and air side pressure drop of a new and faulty intercooler.

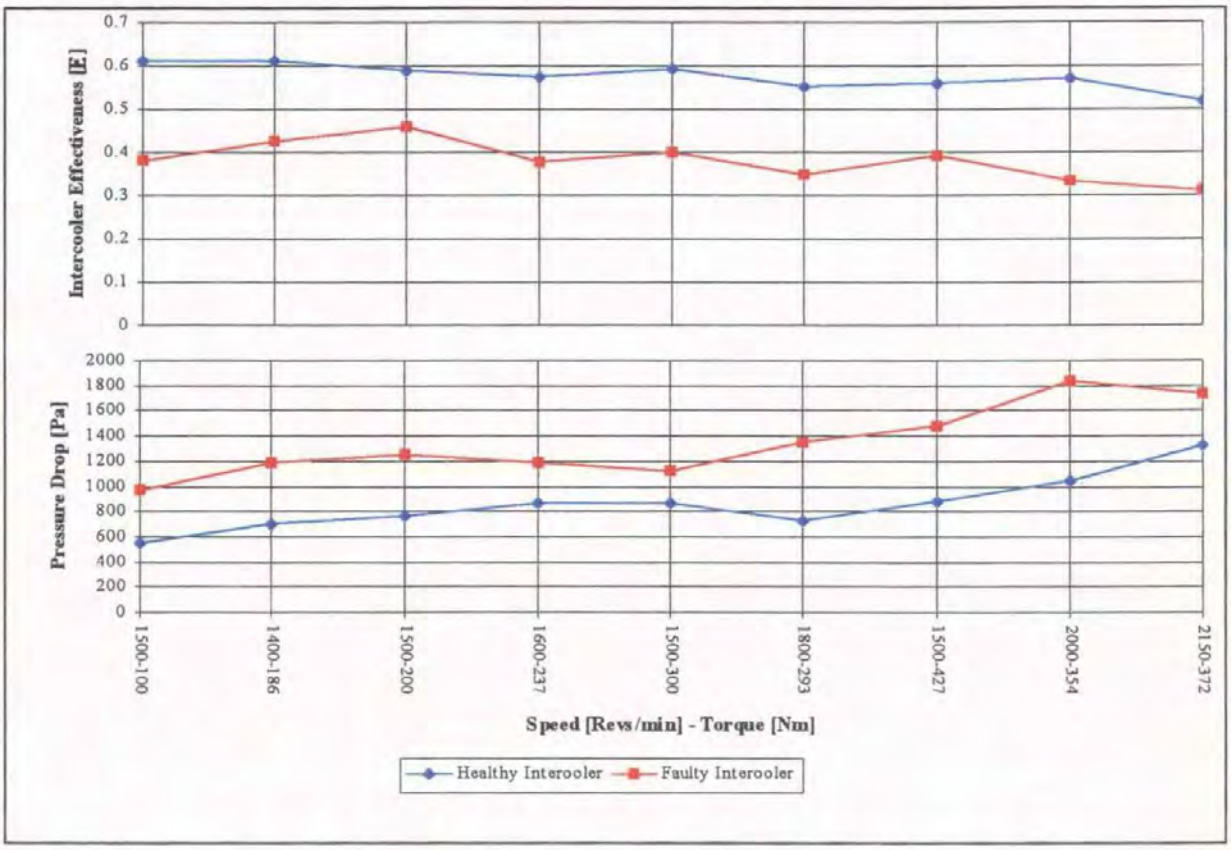

Figure 47 Healthy & Faulty Intercooler Performance Comparison

Figure 47 shows that the returned cooler had a reduced effectiveness and an increased pressure drop on the air side of the matrix due to fouling. From the two intercoolers tested it can be concluded that reduced effectiveness and increased pressure drop will occur simultaneously, since both sides of the matrix are prone to fouling during engine operation. The values of effectiveness and pressure gradient from the intercooler tests were entered into the simulation and set to run at the five highest power torque - speed stations. The results summarised in Figure 48 indicated that a faulty intercooler with a realistic degree of fouling could be detected by Performance Monitor. Based on this prediction it was decided that the intercooler fault warranted further experimental investigation.

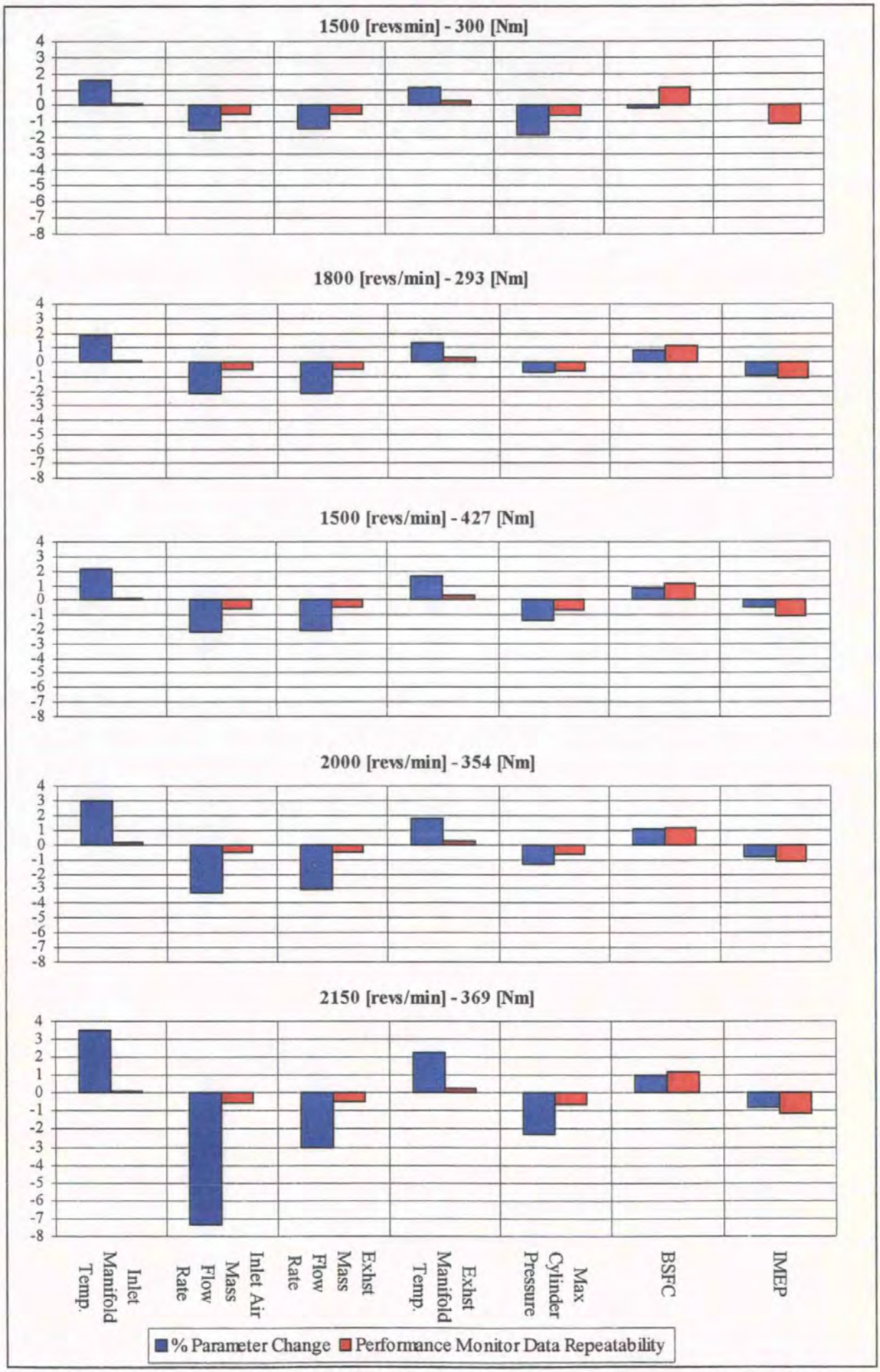

Figure 48 Percentage Change In Simulation Performance Parameters Due To A Faulty Intercooler compared to Performance Monitors Data Repeatability

7.3 Fouled Inlet Valves

The fault study discussed in Chapter 5 showed that inlet valve fouling was a common feature on Perkins T6.354(M) engines. The fouling of the valve, as shown in Chapter 5, Figure 32, changed the shape of the valve head. Relationships between non-dimensional valve lift and discharge coefficient are illustrated in Chapter 6, Figure 38. These relationships do not, however, consider a dramatically changed valve head profile, as was caused by the fouling. For this reason, the flow around a fouled valve was investigated using a Computational Fluid Dynamics, CFD, package known as FIDAP. The work conducted by the thermofluids section at RNEC Manadon concluded that the valve fouling did not reduce the discharge coefficient or mass flow, even when the fouling was increased to a greater level than seen during the fault study. For this reason fouled inlet valves were not investigated any further.

7.4 Leaking Inlet Valves

Four sample inlet valves which had been run in marine applications were acquired from ABB Propulsion Ltd., Derby. They all showed a degree of pitting on the faces and excessive carbon build up on the upper face of the valve head, between the face and stem. Figure 49 depicts a typical valve face which has been magnified 35 times, the pitting is shown quite clearly by the darkened patches.

Figure 49 Typical Pitted Inlet Valve Seating Face

To quantify the leakage between the valve and cylinder head seat a test rig was designed and manufactured, as shown below in Figure 50. This allowed the cylinder head flame face and valves to be subjected to the maximum cylinder pressure experienced in testing, approximately 80 Bar. The pressure chest which butted against the flame face was tapped out to accept a supply of high pressure instrument air and a 200 Bar F.S.R. resistive strain gauge pressure transducer. The transducer was connected to a slow speed data acquisition card and samples were taken at one second intervals to monitor the pressure decay.

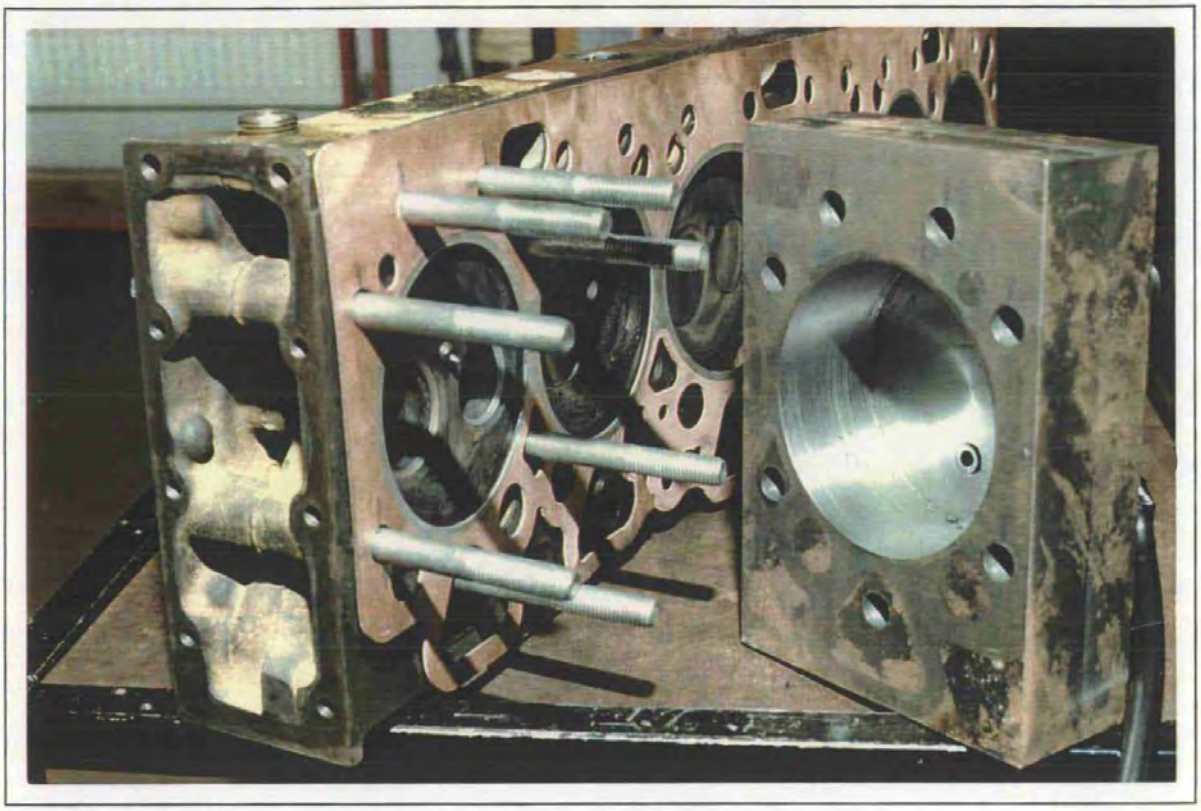

Figure 50 Valve Leakage Test Rig

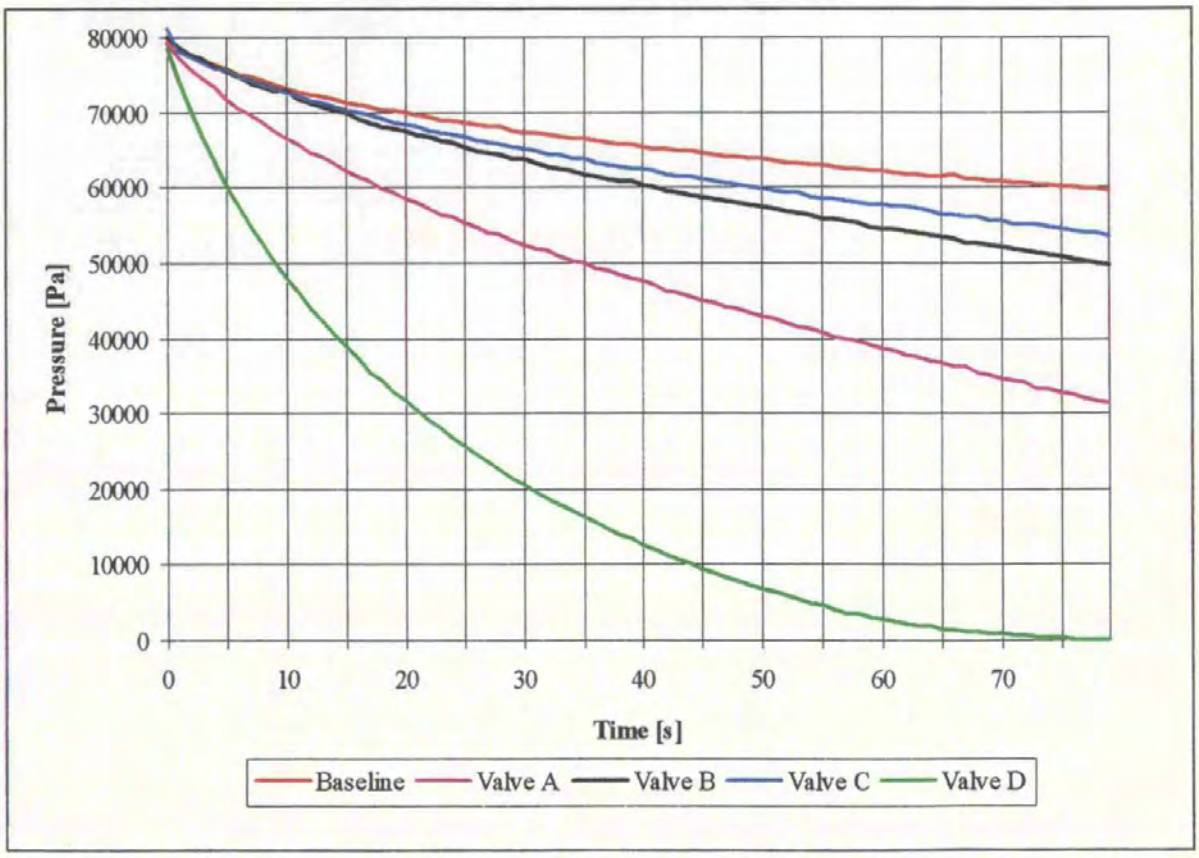

Figure 51 Inlet Valves Leakage Test Results

Figure 51 shows the results of the pressure rig tests. The fault study showed that single valve faults were particularly rare and, in general, catastrophic. For this

reason, it was considered more realistic to investigate a less severe leakage rate but across all inlet valves. Valves B & D were selected for analysis by simulation. The engine simulation model was modified to incorporate flow junctions between the cylinders control volumes and the inlet manifold, copies of the model can be seen in Appendix 'D'. The effective flow area of the junctions were determined from the results of the rig tests and some additional calculation, as detailed below. Where the effective flow area is the product of the hole cross sectional area and the discharge coefficient.

Considering the following conditions;

Nominal pressure in chest, $p_u = 80 * 10^5$ [Pa]

Atmospheric Pressure, $p_t = 1.01 * 10^5$ [Pa]

Temperature of instrument air $T_u = 291$ [K]

$C_p = 1000$ [J/kg.K], $\gamma = 1.39$, $R = 280$ [J/kg.K]

From the pressure rig tests;

Valve B: Pressure at $t_0 = 7991800$ [Pa] and after 1 second $t_1 = 7859400$ [Pa]

Valve D: Pressure at $t_0 = 7842450$ [Pa] and after 1 second $t_1 = 7424860$ [Pa]

From the equation of state;

$$pV = mRT \qquad \text{Equation 17}$$

Valve B mass flow rate = $4.057 * 10^{-4}$ [kg/s]

Valve D mass flow rate = $1.609 * 10^{-3}$ [kg/s]

Substituting the above values into equation 12 and calculating gives C = 506 [m/s].

The Mach number at the throat may be calculated by equation 13, entering C = 506 [m/s] gives a Mach Number of 1.06, hence choked flow. For choked flow, mass flow rate is given by equations 15 & 16.

Substituting in values for mass flow rate, p_u, p_t, R, T_u, γ and C_p the effective flow areas, A_e, for valves B & D can be calculated thus;

A_e Valve B = $2.114 * 10^{-8}$ [m^2]

A_e Valve D = $8.544 * 10^{-8}$ [m^2]

The effective flow areas were entered into the simulation and run at the five highest power torque - speed stations. Figure 52 shows the percentage changes in performance due to the introduction of a leaking inlet valve with an effective flow area of $8.544 * 10^{-8}$ [m^2]. The simulation predicted no change in engine performance when a leaking valve with an effective flow area of $2.114 * 10^{-8}$ [m^2] was introduced. Only four parameters showed a consistent trend which would be measurable in practice. In these four instances the margin between parameter deviation and Performance Monitors repeatability was small. Since this fault could only be engine tested at one severity it was decided to increase the effective leakage area to provoke a more positive response from the engine. Through further simulation it was shown that an effective leakage area of $2.488 * 10^{-7}$ [m^2] would be required for Performance Monitor to detect the fault. This represented a very small increase of 0.159[mm^2] effective flow area, from the genuinely faulty valves tested. It was decided that this increased leakage area was still worthy of engine test since valve face guttering would lead to much greater increases in flow.

To replicate this fault for engine testing new inlet valves were ground into the cylinder head and sent for machining. The effective leakage area was divided by the

discharge coefficient and a groove was machined into the valve face to give the correct leakage area. Figure 53 shows a valve which has been modified to simulate a leak. The machined valve was then pressure tested to verify that the new increased flow area which had been machined still represented a leakage rate which was comparable to the genuinely faulty. The rig test results for the simulated leaking valve are shown in Figure 54.

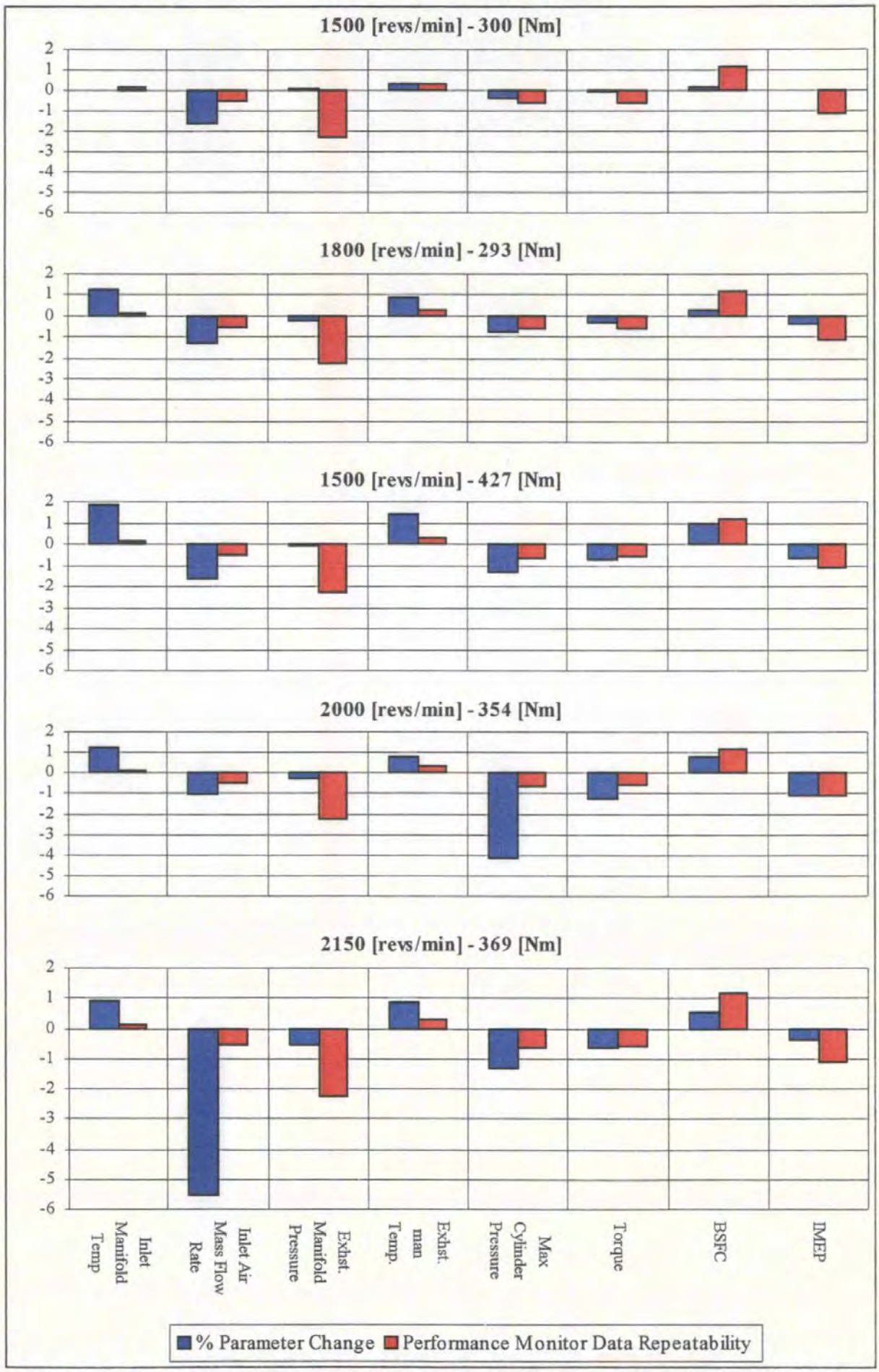

Figure 52 Percentage Change In Simulation Performance Parameters Due To Leaking Inlet Valves Compared To Performance Monitors Data Repeatability

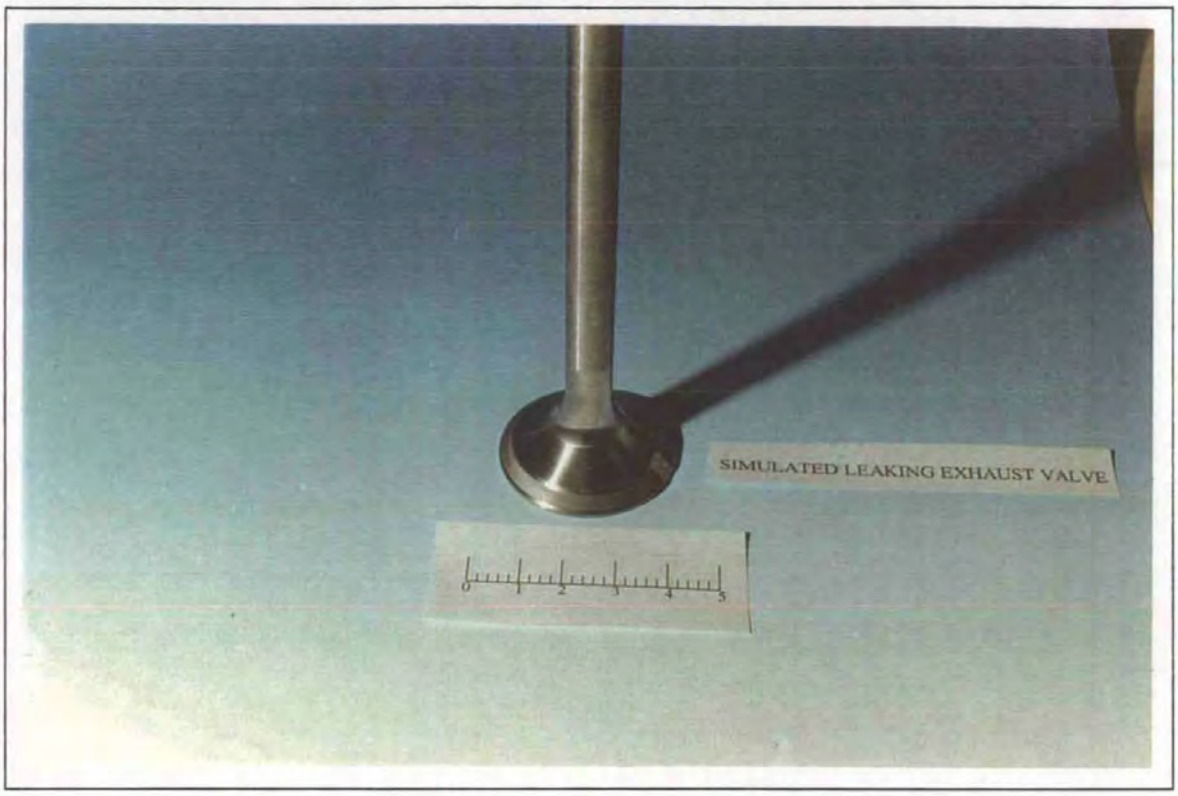

Figure 53 Valve Modification To Simulate Leakage

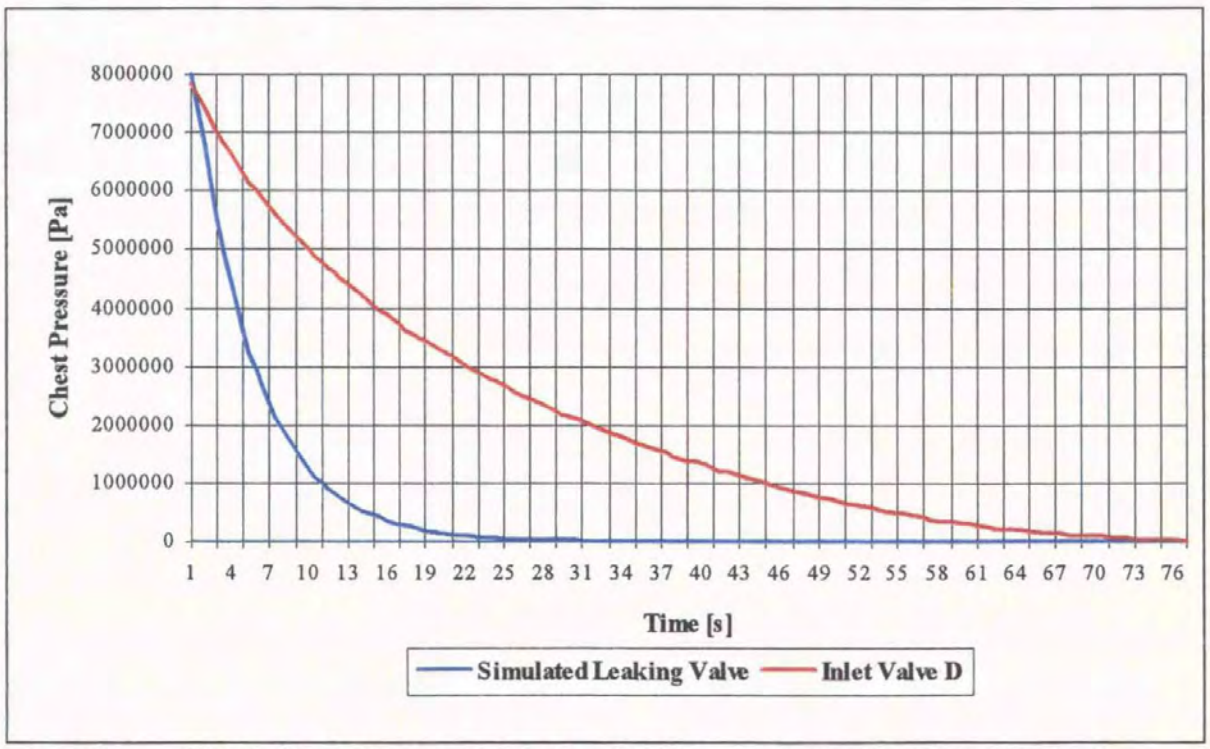

Figure 54 Rig Test Pressure Profiles Of Genuinely Leaky Valve D And A Simulated Leaking Inlet Valve

7.5 Leaking Exhaust Valves

Several genuinely faulty exhaust valves were obtained during the course of the fault study. These were pressure tested using the same rig and test method described above. The results are shown in Figure 55.

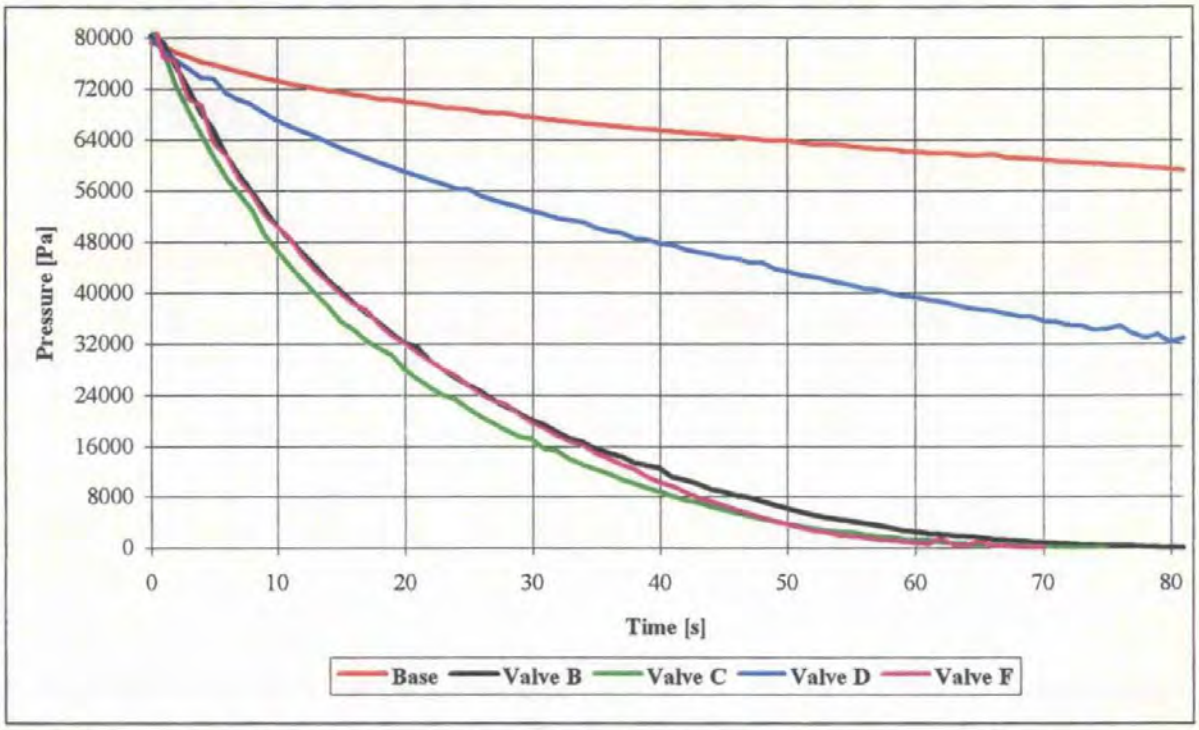

Figure 55 Rig Test Pressure Profiles Of Genuinely Leaky Exhaust Valves

As with the inlet valves, the fault study showed that it was far more realistic to investigate a small leakage area on all exhaust valves, rather than a large leakage, due to a catastrophic failure, on one single valve.

The SPICE simulation model was modified to incorporate flow junctions between the cylinder control volumes and the exhaust manifolds, copies of the simulation model can be found in Appendix 'D'. The effective flow area of the junctions was calculated using the same method as described above for the inlet valves. From the calculations, valves D and C returned effective flow areas of $3.477 * 10^{-8}$ [m^2] and $9.522 * 10^{-8}$ [m^2] respectively. The simulation was run at the five highest power

torque - speed points. The performance parameter deviations predicted by the simulation for valve C are plotted with the respective Performance Monitor data repeatabilities in Figure 56. The simulation model which had leaking exhaust valves with an effective flow area of $3.477 * 10^{-8}$ [m^2] predicted no change in engine performance.

Although the simulation which incorporated an effective leakage area of $9.522 * 10^{-8}$ [m^2] predicted a slight degradation in performance, the deviations generally fell within the repeatability of Performance Monitor. As a result these changes in performance would not be detected during engine test. Through further simulation it was established that an effective leakage flow area of $3.72 * 10^{-7}$ [m^2] would be required before any changes in performance would be detected by Performance Monitor. This represented a very small increase of 0.277[mm^2] effective flow area, from the genuinely faulty valves tested. It was decided that this increased leakage area was still worthy of engine test since valve face guttering would lead to much greater increases in flow. The exhaust valve leakage was reproduced for engine test by the same valve face grooving technique used for the inlet valves.

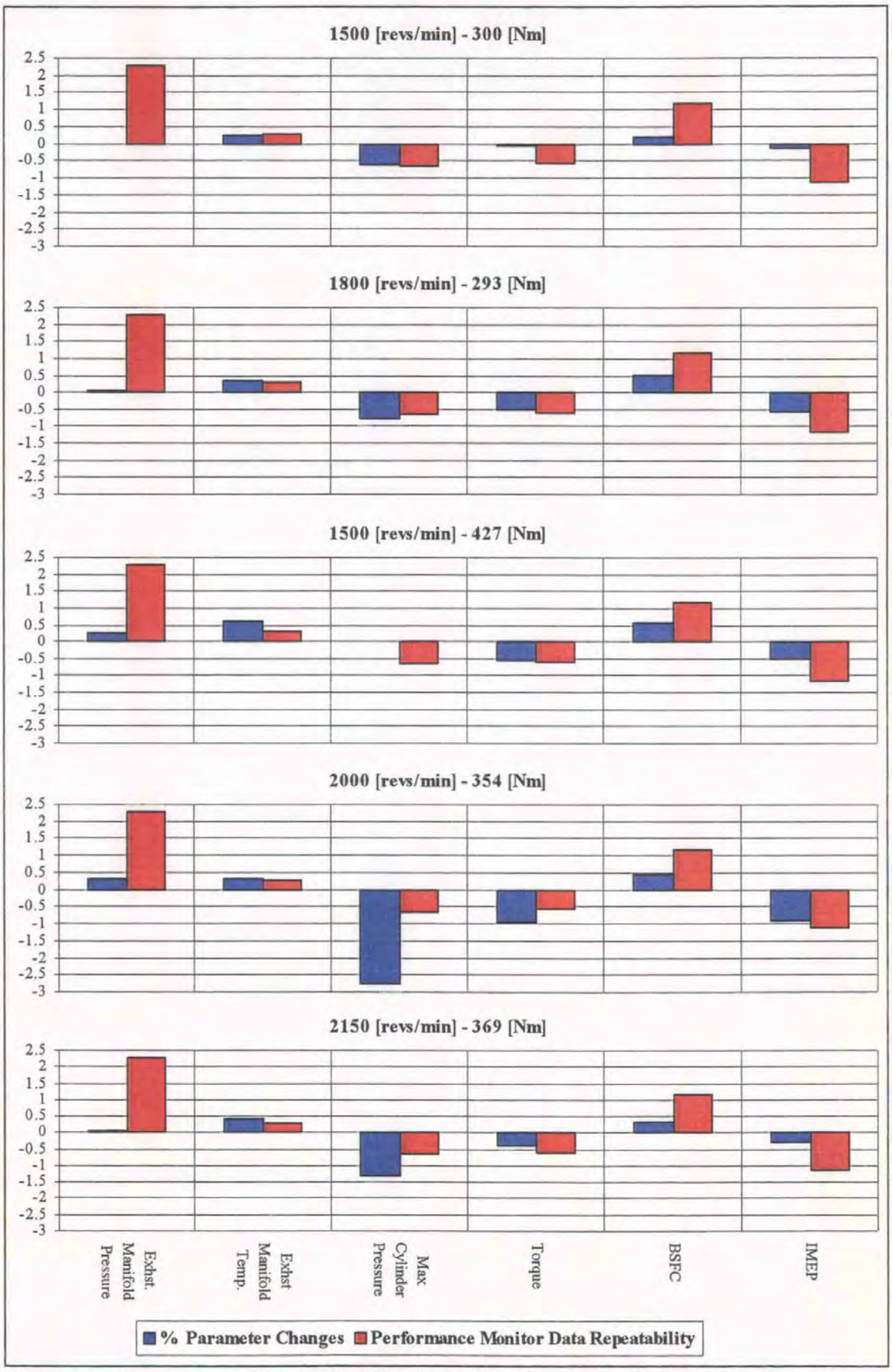

Figure 56 Percentage Change In Simulation Performance Parameters Due To Leaking Exhaust Valves Compared To Performance Monitors Data Repeatability

7.6 Incorrect (retarded) Fuel Pump Timing

No data could be obtained to identify a realistic degree of fuel pump mis-timing. As a result, 1.0° retardation was chosen as a starting point for initial simulation. If the simulation predicted no changes in performance, the degree of retardation would be increased until the changes in performance reached a level which could be detected by Performance Monitor. The SPICE simulation model was modified by retarding the point of injection in heat release data set by 1.0°.

At 3° retarded injection, the simulation model predicted trends in performance which, in theory, could be detected by Performance Monitor. These trends are shown in Figure 57. It was decided that this fault warranted further investigation through engine test. The fault was replicated on the engine by rotating the fuel pump on the auxiliary drive. The amount of rotation was calculated from the pump body diameter, 0.5 mm of arc rotation equated to 1° of crank angle.

7.7 Injector Faults

As a result of the fault study 19 atomisers were acquired from engines in the field and made available for testing. All atomisers were obtained from engines manufactured to the same build list as the test engine. All atomisers were manufactured by Lucas CAV and had identical atomiser & nozzle part numbers as the test engine. Although simulation could not be used to quantify the effect on performance, a substantial amount of rig test work was carried out to assess each atomisers performance.

The rig testing strategy developed allowed the nozzles to be tested statically to assess back-leakage, breaking pressure, spray formation and atomisation during injection. All of the rig testing was conducted on a Hartridge atomiser test rig. Back-leakage and breaking pressure were recorded using the instrumentation on the Hartridge rig. Spray formation and atomisation were recorded using spray pattern tests and high speed photography. The results allowed 3 atomisers from the 19 tested to be selected for engine test, based on the distinct differences between the baseline and faulty atomisers.

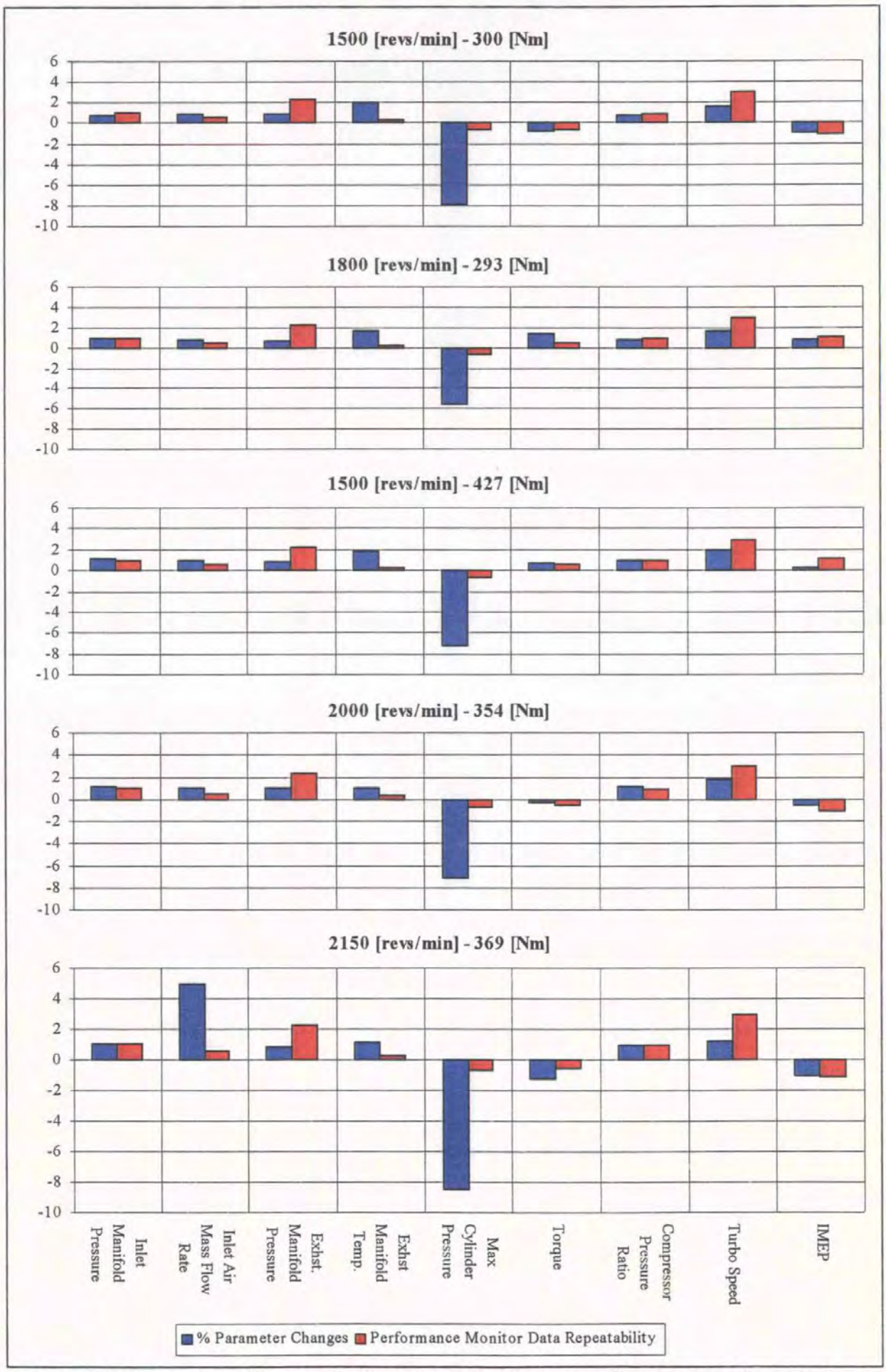

Figure 57 Percentage Change In Simulated Performance Parameters Due To A 3° Retarded Injection Compared To Performance Monitors Data Repeatability

7.7.1 Spray Pattern Tests

The spray pattern tests allowed static comparisons to be made between the baseline and faulty nozzles. The Hartridge rig was adapted to accept a back-plate which would hold sheets of paper to record the spray pattern. Figure 58 shows the modified Hartridge rig. The 4 holes in the nozzle tip were offset to account for the angle of injector mounting in the cylinder head and to achieve the best spray formation across the combustion chamber. The back-plate, however, was mounted perpendicular to the atomiser body. This created a spray pattern which indicated the penetration of the spray from the two holes on the fuel pump side of the engine being much greater than the other two holes, in reality this was not the case. The Hartridge rig operated in the normal way in all other respects. Tests were carried out to identify the ideal back-plate to nozzle tip clearance giving the best clarity results. It was established that 7mm gave the best results. Spray pattern tests were conducted for both the baseline and the returned atomisers.

7.7.2 High Speed Photographic Technique

Since the static tests only gave an indication of spray angle, degree of penetration and to a lesser degree, shape of plume it was decided to use high speed photography. The high speed photography allowed a qualitative assessment of spray penetration, plume shape and degree of atomisation. The camera and film speed was set to 4000 frames per second. The developed photographs were made available in a series of stills which

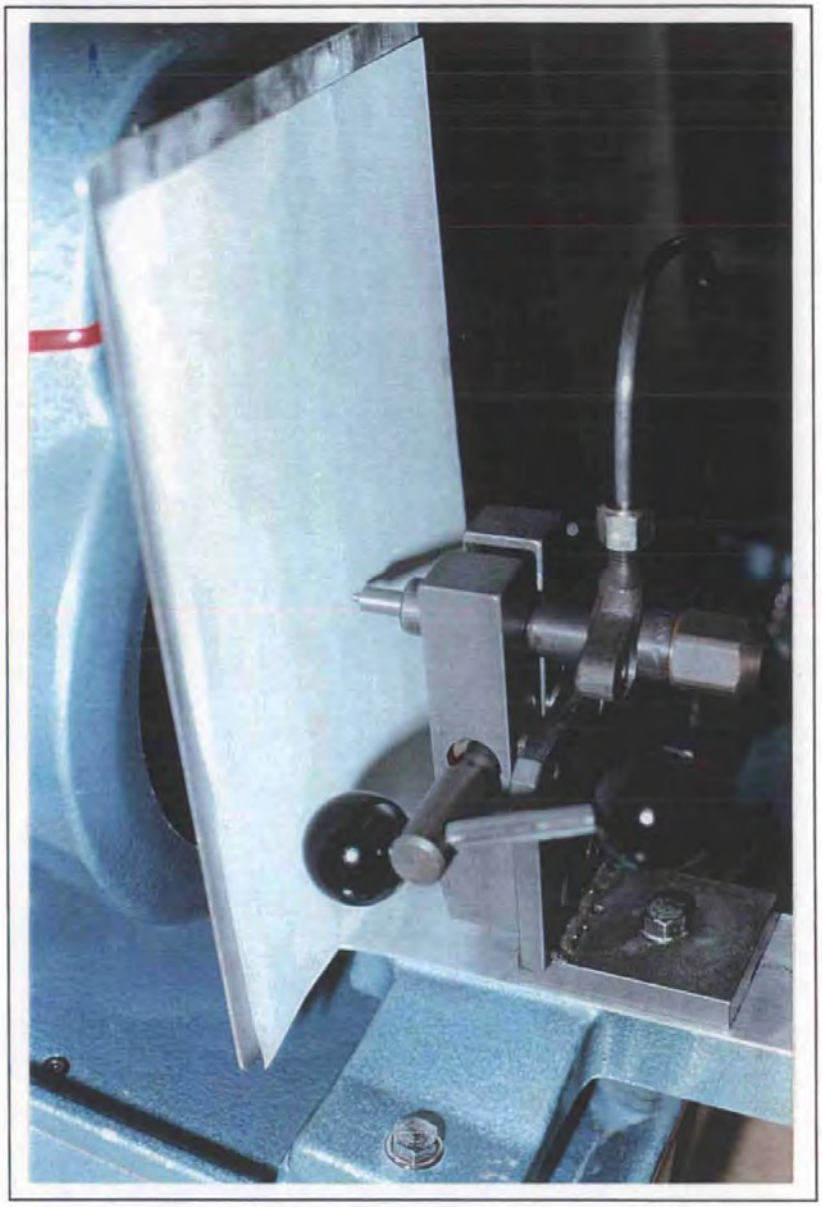

Figure 58 Modified Hartridge Test Rig

shows the progressive formation of the spray in a step by step format and a video showing the dynamic formation. Since it was not possible to apply high speed photographic techniques to all of the returned atomisers 3 were short-listed based on the spray pattern tests.

7.7.3 Baseline Injector Rig Test Results

The baseline injector had been subjected to several hundred hours of engine running prior to rig testing. Despite this, the back leakage time was in excess of 1 minute for

a pressure drop of 50 [Bar] from 150 [Bar],compared to a minimum specified time of six seconds. The breaking pressure was recorded at 203 [Bar], slightly below the recommended level of 205 [Bar]. The characteristic buzzing noise was made during injection.

The spray pattern shown in Figure 59 identified four fairly evenly spread plumes of spray with the right hand side plumes slightly offset from the axis lines, a characteristic present on all nozzles. The spray started to deposited approximately 20mm from the centreline of the nozzle and spread to 80 mm on the lower two nozzle holes and 60 mm on the upper holes. The average spray area was 570 [mm^2] per plume and the maximum plume width was 19[mm].

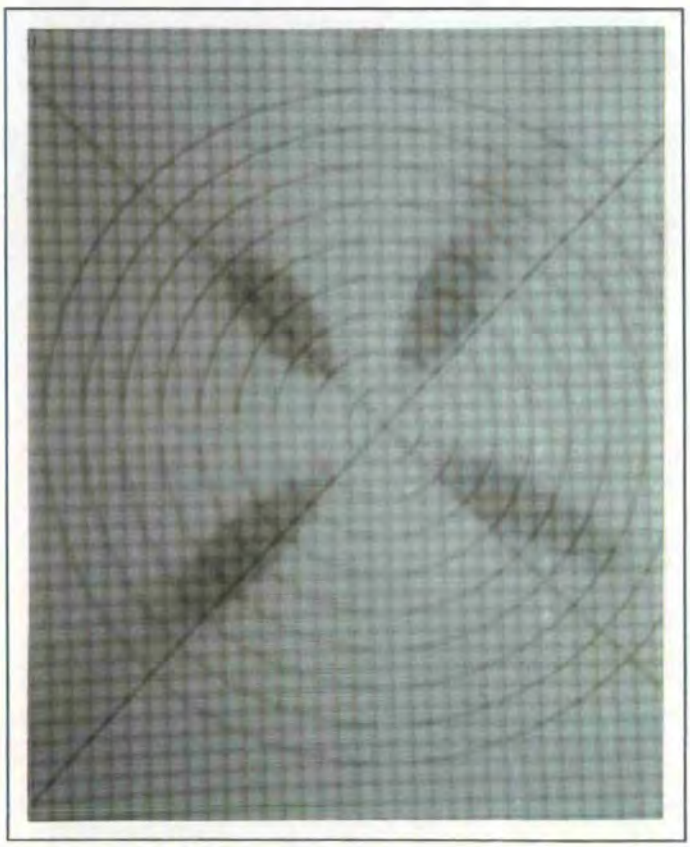

Figure 59 Static Spray Pattern Of The Baseline Injector

The high speed photography results in Figure 60 clearly show the development of four even plumes of spray with a well defined core until the break up distance is reached. The core of each plume is surrounded with an even nebula of finely atomised fuel extending out and showing good penetration.

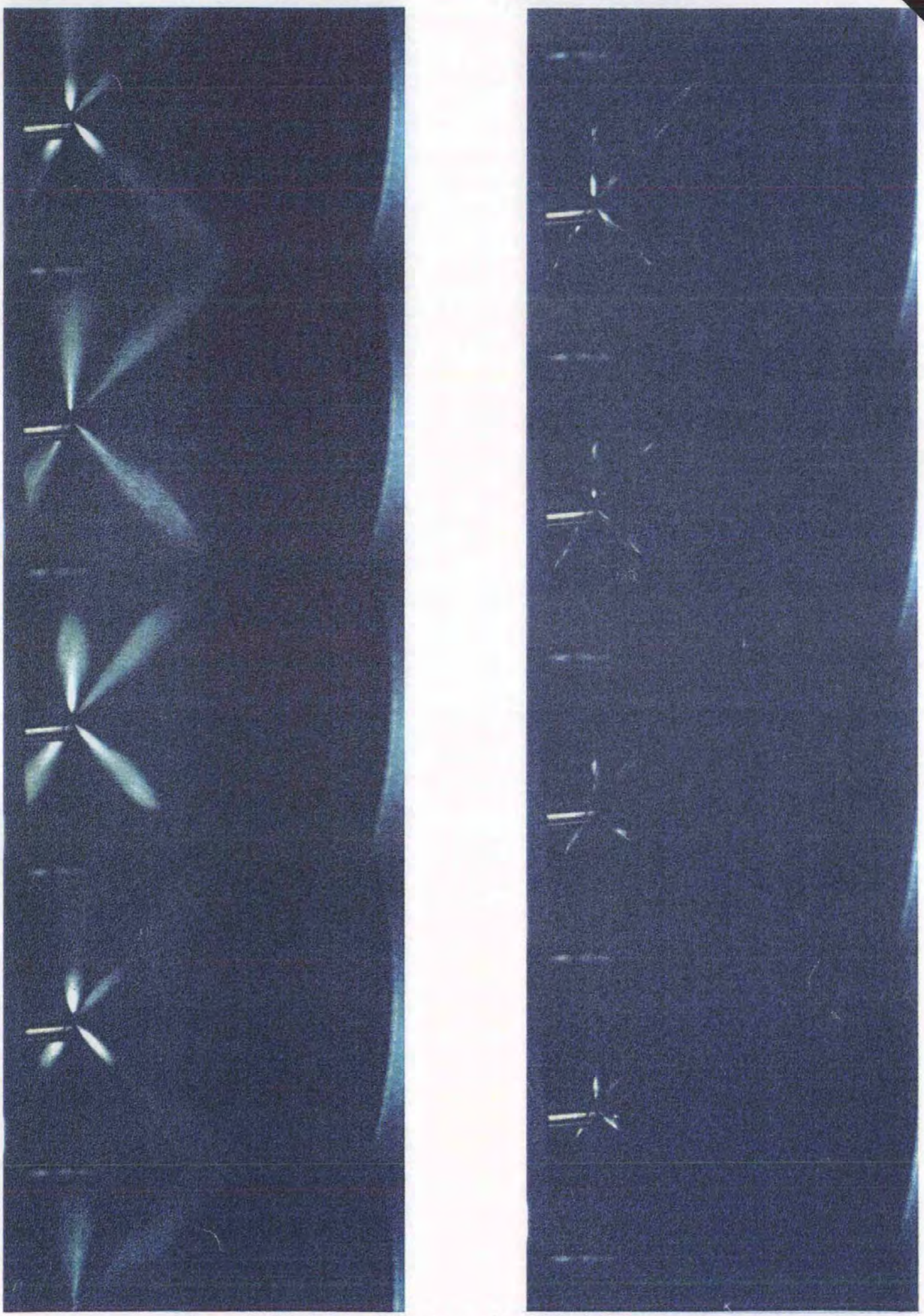

Figure 60 High Speed Photography Stills Of The Baseline Injector Spray

7.7.4 Excessively Worn Needle & Nozzle Rig Test Results

This atomiser gave a back-leakage time of less than 1 second. This atomiser tended to hose fuel and no definitive breaking pressure could be determined, however, fuel started to discharge from the nozzle at approximately 155 [Bar]. Instead of the characteristic buzzing noise made by the baseline nozzle a dead hissing noise was heard. The spray pattern results in Figure 61 showed three heavy patches of spray and one less intense, all in the same angular position as the baseline. Three of the four plumes started to deposit 15 [mm] from the nozzle centre line and extended out to approximately 60 [mm]. The maximum plume width was 24 [mm] and the average spray area per plume was 480 [mm^2].Plume width and spray area were difficult to calculate in this case since the spray laid very densely on the paper and was soon absorbed, spreading the diesel further than originally sprayed.

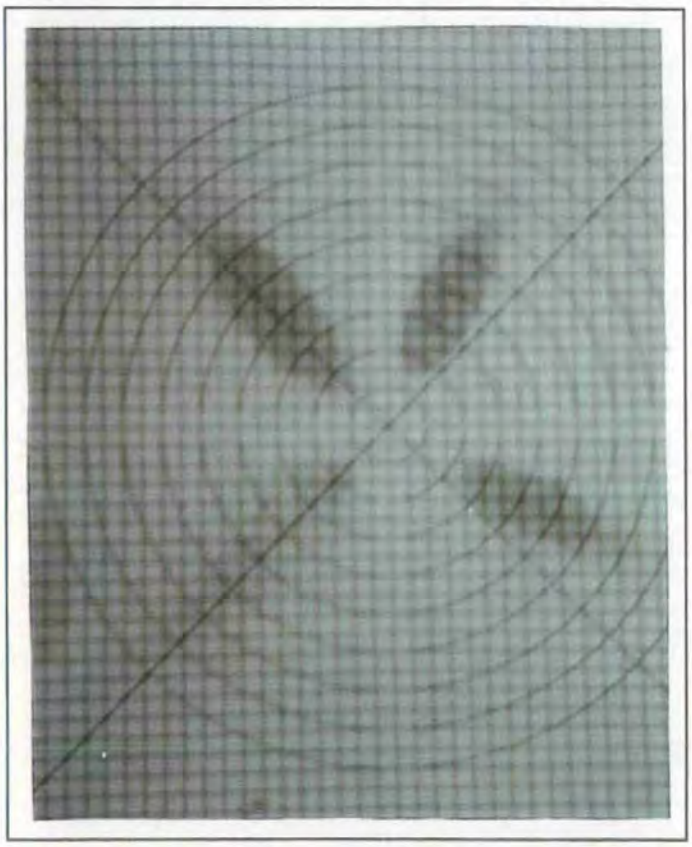

Figure 61 Static Spray Pattern Of The Worn Needle & Nozzle Injector

The high speed photography in Figure 62 clearly shows four streams of un-atomised fuel. Although probably achieving the same degree of penetration as the baseline nozzle, no spray core is formed and little or no atomisation takes place. Figure 63 shows photographs of new nozzle holes and the excessively worn nozzle holes. The excessively worn nozzle holes are not only larger but the exterior edge of the hole is chamfered.

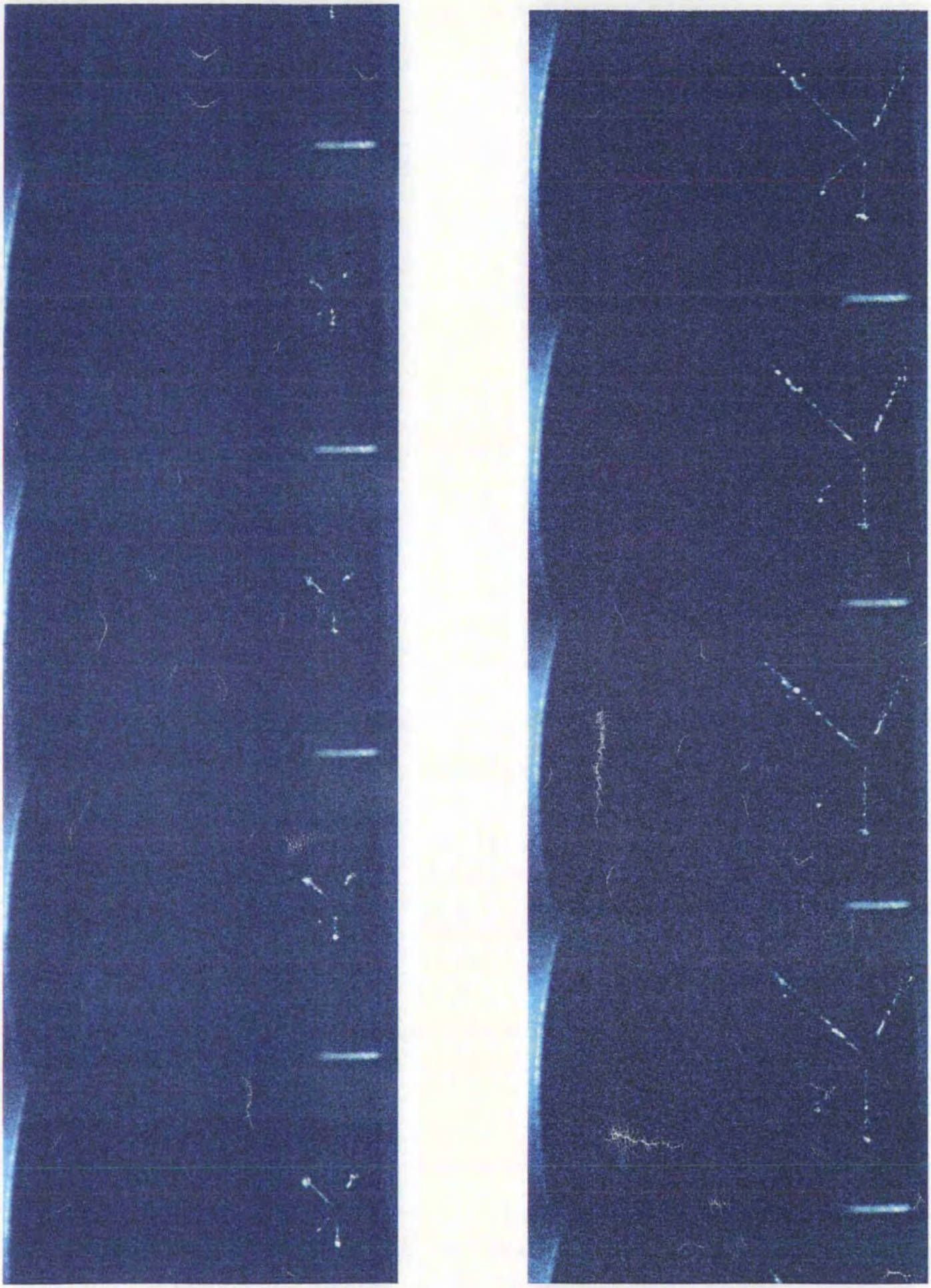

Figure 62 High Speed Photography Stills Of The Worn Needle & Nozzle Injector Spray

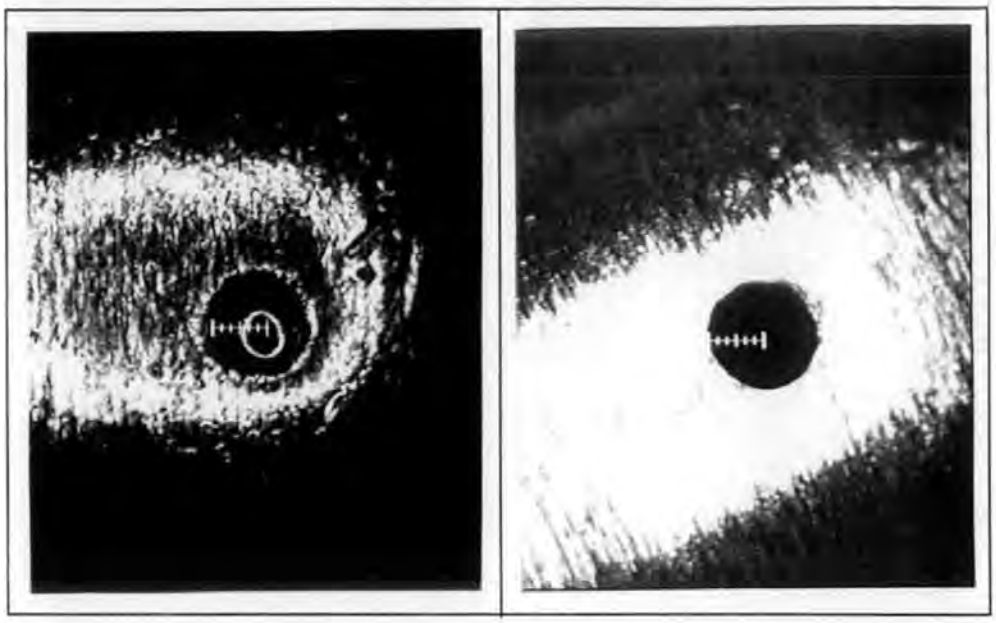

Figure 63 Comparison Of New And Worn Injector Nozzle Holes

This external chamfering will affect both the discharge coefficient of the nozzle hole and its atomising capability. Both spray angle and spray penetration can be related to the diameter of the nozzle holes. For a nozzle which gives a spray in the atomisation regime the spray angle θ follows the relationship;

$$\tan\frac{\theta}{2} = \frac{1}{A} 4\pi \sqrt{\left(\frac{\rho_g}{\rho_l}\right)} \frac{\sqrt{3}}{6} \qquad \text{Equation 19}$$

Where ρ_g and ρ_l are the gas and liquid densities and A is a constant for a fixed nozzle geometry. Based on the high speed photography it is thought that the spray from the worn nozzle does not operate in the atomisation regime. As a consequence this expression can not be applied. It should also be noted that this expression takes no account of hole geometry other than the basic nozzle length - diameter ratio. Spray penetration can be related to nozzle hole diameter from;

$$S = 3.07\left(\frac{\Delta P}{\rho_g}\right)^{\frac{1}{4}}\sqrt{td_n}\left(\frac{294}{T_g}\right)^{\frac{1}{4}} \qquad \text{Equation 20}$$

Where ΔP is the pressure drop across the nozzle, ρ_g & T_g are the density and temperature of the gas respectively, t is time after the point of injection and d_n is the diameter of the nozzle holes. This expression also neglects hole shape effects, it could, however, be argued that any changes in hole shape would change the discharge coefficient and consequently the pressure drop across the nozzle holes.

7.7.5 Blocked Injector Nozzle Hole Rig Test Results

This atomiser gave a back-leakage time of 34 seconds and a breaking pressure of 195 [Bar]. It also emitted the characteristic buzzing noise associated with a good injection. The spray pattern result in Figure 64 shows three plumes of spray as would be expected. Two plumes were not dissimilar to the baseline injector, the third was somewhat more concentrated. Two plumes started to deposit spray 20 [mm] from the nozzle centre line as with the baseline but spread out in excess of 90 [mm], 10 [mm] further than the greatest baseline plume. The remaining plume started at a distance 25 [mm] from the nozzle centreline and spread out to 70 [mm]. The maximum plume width was 22 [mm] and the average spray area per plume was 770 [mm^2]. These results prove that the blocked injector discharges similar width plumes of spray which penetrate further than the baseline, as would be expected. It also suggests that although the injector is blocked the amount of fuel delivered to the combustion chamber will not be dramatically reduced. Equations 19 and 20 also reinforce the spray pattern findings.

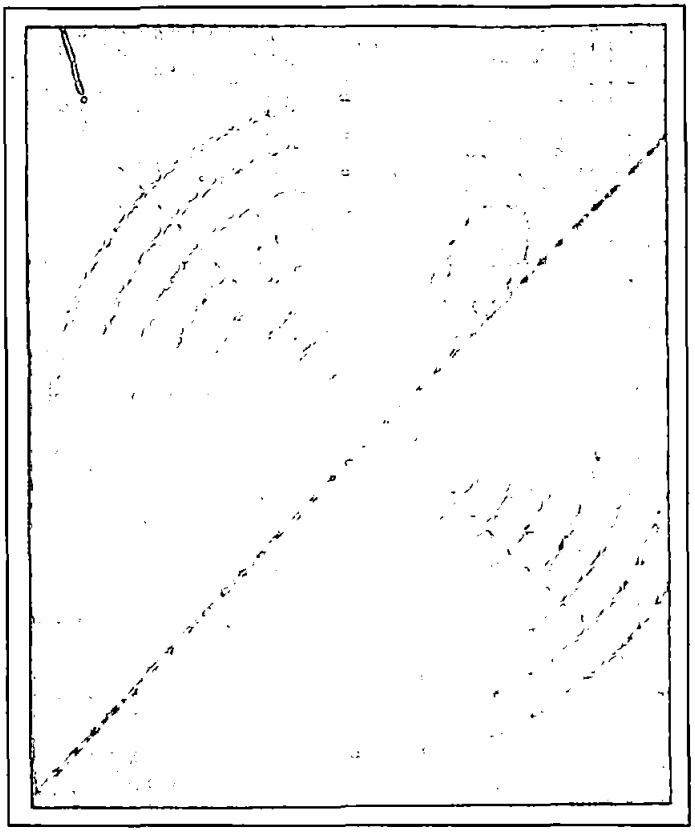

Figure 64 Static Spray Pattern Of The Blocked Nozzle Hole Injector

The high speed photography reinforced this as shown in Figure 65. Two of the plumes show very well defined cores of spray which have an increased break up length. It is interesting to note that the overall spray angle is comparable with the baseline but the core which exists until brake up is wider and shows very little atomised fuel spray along it's flanks. Finely atomised spray readily forms at the tip of plume projecting outwards. The remaining plume never develops a full core, the spray shows penetration and atomisation both less satisfactory than that obtained from the baseline nozzle.

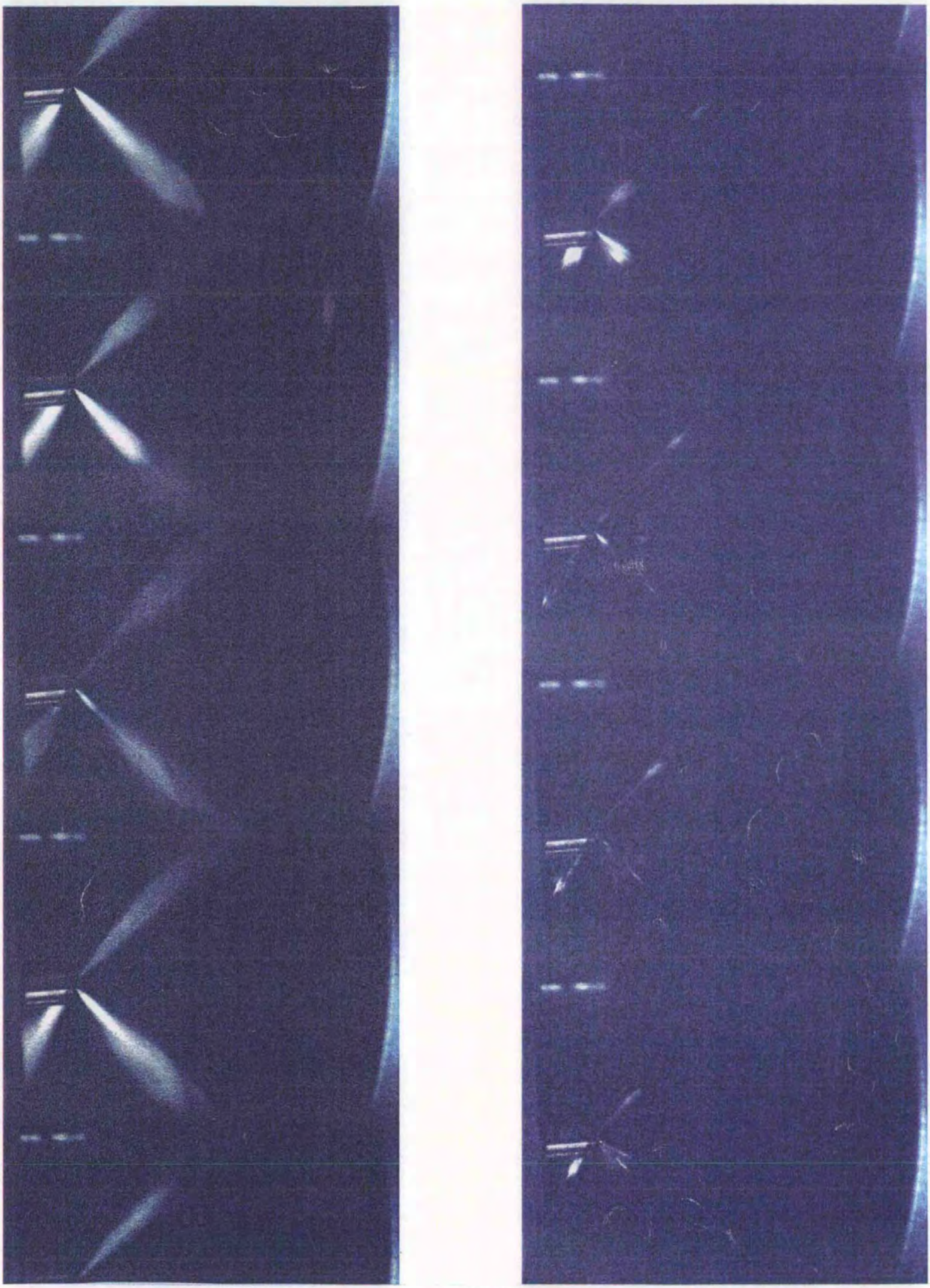

Figure 65 High Speed Photography Stills Of The Blocked Nozzle Hole Injector Spray

7.7.6 Low Breaking Pressure Injector Rig Test Results

This atomiser gave a back-leakage time of 43 seconds and a breaking pressure of 155 [Bar]. The spray pattern test results shown in Figure 66 depicts 4 plumes which started to deposit spray between 10 and 15 [mm] from the nozzle centreline, closer than displayed by the baseline. The spray projected out to 70 [mm], 10 [mm] less than that of the baseline nozzle. The maximum plume width was 28 [mm] and the average spray area per plume was 590 [mm^2]. Occasionally the normal buzzing noise could be heard during injection. The nozzle behaved exactly as expected, wider plumes of spray with less penetration.

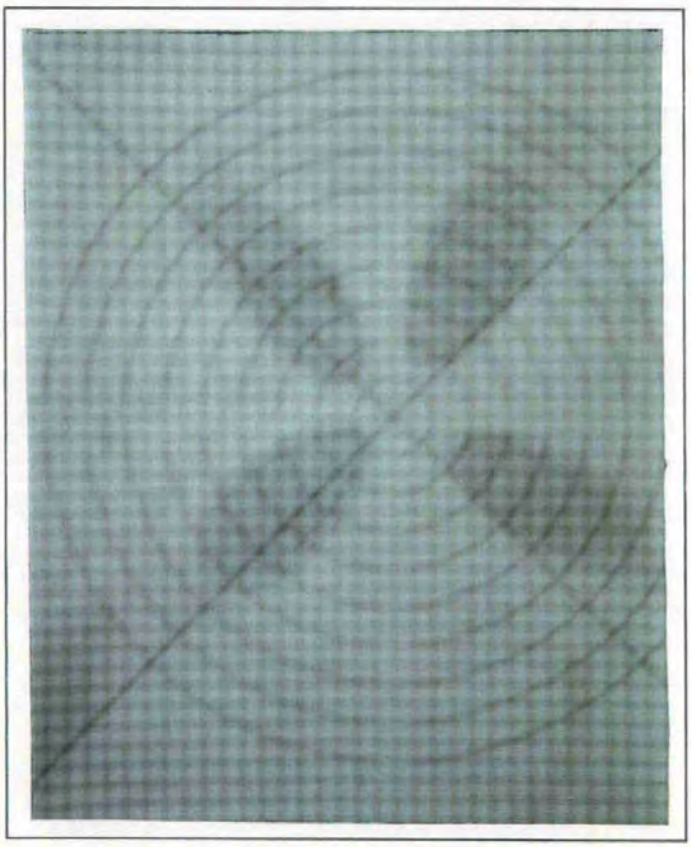

Figure 66 Static Spray Pattern Of The Low Breaking Pressure Injector

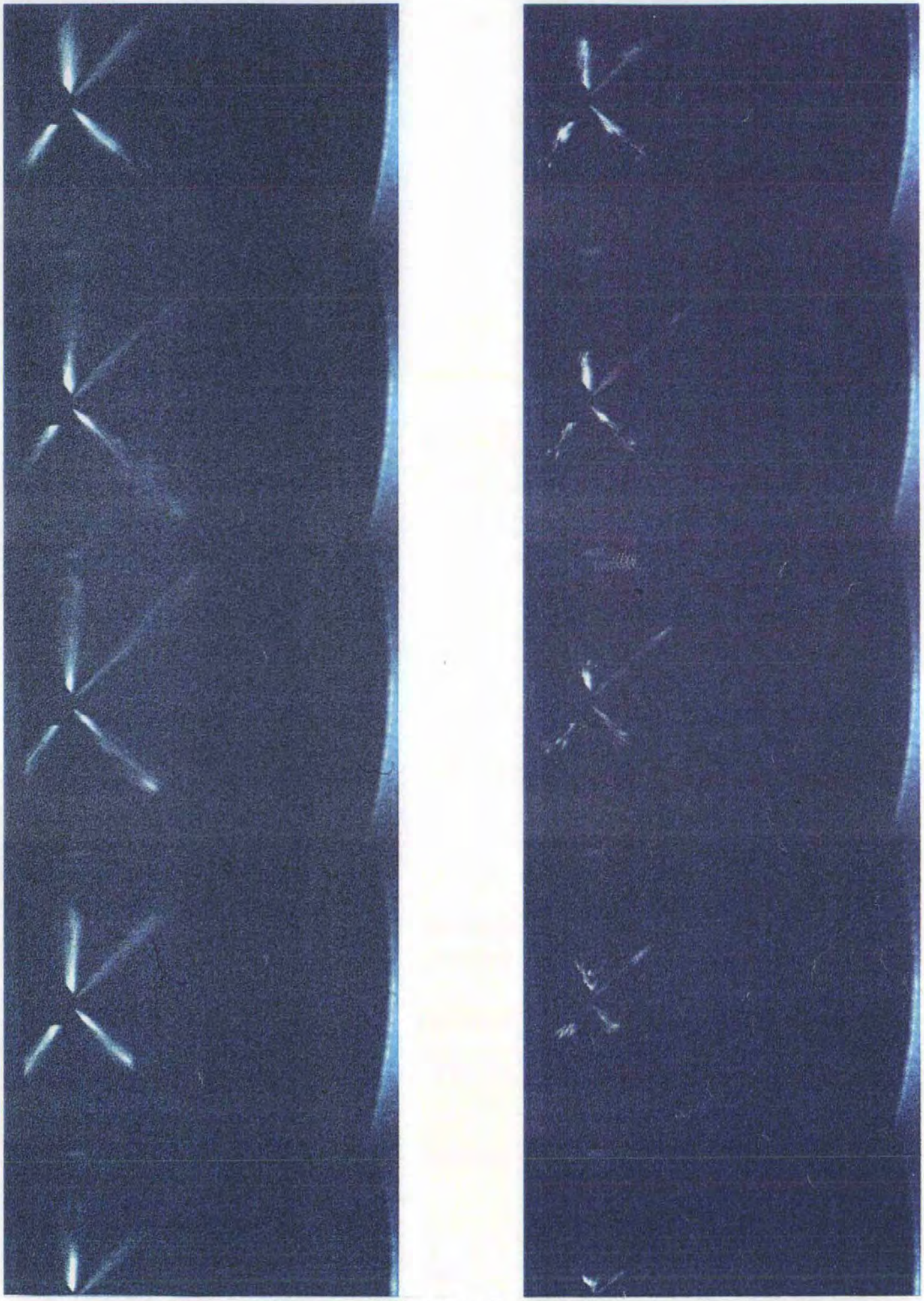

Figure 67 High Speed Photography Stills Of The Low Breaking Pressure Injector Spray

The high speed photography in Figure 67 reinforces these conclusions further. Four even plumes of spray develop, more pointed and all showing a smaller core than the baseline nozzle. The spray surrounding the plume cores consist of a mixture of droplets and spray which is not as finely atomised as the baseline spray. Break-up length and penetration are both slightly reduced when compared to the baseline nozzle.

7.8 Summary

The fault study identified several faults which were worthy of further investigation. This chapter has shown how rig testing and computer simulation techniques can be used to assess genuinely faulty engine components and their effect on engine performance. Each fault has been qualitatively assessed to determine realistic levels of fault severity found in practice. Where possible the faults have been modelled using a simple computer simulation to ascertain their effects on engine performance trends. As a result research objective 4 was satisfied and the following faults were considered suitable for experimental engine test.

1. 80% Fouled air filter
2. 40% Effective genuinely fouled & corroded intercooler
3. Leaking inlet valves with an effective leakage area of 0.248 [mm^2]
4. Leaking exhaust valves with an effective leakage area of 0.372 [mm^2]
5. 3° Crank angle retarded fuel pump timing
6. Excessively worn injector needle & nozzle [genuine faulty component]
7. Blocked injector [genuine faulty component]
8. Low breaking pressure injector [genuinely faulty component]

CHAPTER 8

EXPERIMENTAL RESULTS & DEVELOPMENT OF FAULT SYMPTOM RELATIONSHIPS

8.0 Introduction

This chapter examines the experimental results of the engine testing conducted during this research. The automated performance monitoring package, Performance Monitor, developed as part of this research was used to generate all of the results files for both healthy and faulty modes of operation. This allowed complete results files to be generated and compared in a convenient way. The testing procedure discussed in Chapter 4 was applied to all of the test work undertaken in both healthy and faulty modes of engine operation.

The experimental data was collected over an 11 month period, which allowed for variations in ambient conditions and changes in engine performance. The eight faults discussed in Chapter 7 were investigated under engine test conditions. The engine testing programme began with baseline tests to establish a datum for the healthy engine. Each fault was subsequently introduced, directly followed by another set of baseline testing with the fault removed. This ensured that the introduction and removal of each fault did not affect healthy engine performance. It also acted as a constant check on the performance monitoring system since the results were checked back-to-back with previous baselines.

The severities of fault, determined through the simulation trends and rig testing in Chapter 7, were introduced for engine testing. In some instances, a second series of engine tests were conducted at a different fault severity based on the results of the initial engine test.

The experimental results for each fault were compared against the baseline results and the salient differences were identified, quantified and are discussed in the following sections. These differences were used to create a set of fault symptom relationships which formed the foundation for development of a neural network based diagnostic system. Section 8.1 discusses the baseline data, subsequent sections detailing faulty engine results, show the percentage changes in data due to the introduction of the fault and lead to the development of fault-symptom relationships.

8.1 Baseline Experimental Results

In total 135 separate engine tests were conducted over an eleven month period to establish the healthy performance of the engine. These results were used as the datum with which to compare the engine data taken under faulty condition. The data obtained at each torque and speed for all of the baseline runs was averaged to form a definitive set of baselines. The maximum and minimum values of each parameter recorded during baseline testing were identified to quantify the repeatability demonstrated by each parameter throughout the entire set of baseline tests. The following sections discuss the definitive baseline data sets and the most notable variations in repeatability. For convenience, the analysis and discussion is split into

five sections, sensor data, injection and combustion data, general performance data, charge air system data and exhaust system data.

8.1.1 Analysis Of Baseline Sensor Data

The majority of measurements showed good repeatability to within 5% i.e. +/- 2.5%, and generally speaking, all sensor readings showed an improving percentage repeatability with increasing engine power. Sensors which appeared to give poor repeatability are discussed in more detail below.

- Exhaust manifold pressure showed a maximum variation of 12.79% at 2000 [revs/min] and 354 [Nm], but on average, showed a repeatability of 8.1%. This was expected since the repeatability trials showed that the measurement repeatability was 4.57% neglecting changes in ambient conditions and setting of torque and speed. The poor repeatability of this parameter is largely due to the inherent difficulty of measuring the average pressure of a pulsating gas stream of varying pressure, temperature and velocity as proved by the repeatability trials results.

- Fuel rack position showed a maximum deviation of 10.5% and an average deviation of 7.44%. For engine torque and speed stations where the fuel rack was set to full the deviation was within +/- 1%. This variation in fuel rack position was due to a combination of factors. It was initially thought that the fuel rack position varied due to the inability to set engine torque and speed repeatably. On examination of the data, there was no apparent relationship between variations in torque and speed and fuel rack position. Since the aim was to hold speed and

torque constant all performance deviations caused by ambient conditions would manifest themselves in a varying fuel rack position. In nearly all cases the maximum and minimum fuel rack positions coincided with the minimum and maximum inlet air temperatures respectively. This relationship was further substantiated by the fuel injection and combustion data which is discussed later in this chapter. The linkage between the actuator and the fuel pump rack was checked to confirm that no mechanical play was contributing to this large variation in reading repeatability.

- Turbocharger speed showed a maximum deviation of 8.59% at 1500 [revs/min] and 100 [Nm], but an average repeatability of 4.6% across all torques and speeds. As torque and speed increased through the power range the percentage repeatability improved to 2.6% at 2150 [revs/min] and 354 [Nm] but the actual variation remained fairly constant at approximately 2000 [revs/min]. This was higher than expected based on the repeatability trials result of 1.94%. No relationship between turbocharger speed variation and other parameter variations could be established.

- Mass flow rate of fuel showed a deviation of 10.13% at 1500 [revs/min] and 100 [Nm] which steadily decreased to 1.28% at 2150 [revs/min] and 372 [Nm]. The repeatability trials identified a repeatability of 2.89% neglecting changes in ambient conditions and the ability to consistently set torque and speed. It was thought that a combination of varying ambient conditions and the inability to precisely set engine torque and speed contributed to these large variations. At the

2150 [revs/min] and 372 [Nm] and 1500 [revs/min] and 430 [Nm] test points, fuel throttle position was set at the maximum and effectively became a constant. In these instances fuel mass flow rate repeatability was much improved at 1.28% and 4.34% respectively. This indicates that the variation of fuel throttle position to maintain the set engine torques and speeds was certainly a contributing factor to the variations in fuel mass flow rate readings.

8.1.2 Analysis Of Baseline Fuel Injection & Combustion Data

The repeatability trials showed that all fuel injection and combustion events could be measured to 0.5° crank angle repeatability neglecting variations in ambient conditions and variations in the setting of engine speed and torque. Repeatability of the baseline data was generally good and improved with increasing engine power. The following sections discuss the baseline results in more detail .

- Needle lift data showed a spread in point of injection of 3.5° crank angle. There was no evidence of a direct relationship between point of injection and engine torque and speed as would be expected. Fuel rack position and point of injection could be related and it was thought that since the objective was to hold speed and torque constant that rack position, and consequently the point of injection varied to compensate for changes in ambient conditions. Examination of the ambient conditions revealed that the maximum and minimum values of injection timing and fuel rack position coincided with the maximum and minimum air inlet temperatures. It can be concluded that point of injection is particularly sensitive to inlet air conditions. Duration of injection was very repeatable at all torques and

speeds. Needle lift trace shape was also repeatable with the exception of the lowest power condition at 1500 [revs/min] and 100 [Nm]. The maximum deviation in point of injection also occurred at this torque and speed. It was thought that since the needle never lifts fully and the quantity of fuel injected was relatively small the fuel pumps behaviour was slightly erratic at this low torque, low speed condition.

Fuel line pressure readings showed an excellent correlation with needle lift data. Generally the repeatability was good taking into account the shifts in point of injection discussed above. If fuel line pressure data and needle lift data from two sets of results which both have similar ambient conditions and torque-speed settings the repeatability was excellent as shown in Figure 68. This excellent repeatability was evident at all torques and speeds. The maximum deviation in peak fuel line pressure was 16.3% at the 1500 [revs/min] and 430 [Nm] test point. The average variation in peak fuel line pressure throughout the torque and speed range was 8.2%. Position of maximum fuel line pressure was very repeatable at all torques and speeds except the two highest power test points. Position of maximum fuel line pressure agreed within 0.5° crank angle relative to point of injection. At the two highest power test points the pressure data featured several pressure peaks which only differed from the peak pressure by several bar. Therefore a slight increase or decrease in pressure at any of these peaks resulted in a large change in position of maximum fuel line pressure, even though the overall pressure traces were almost identical.

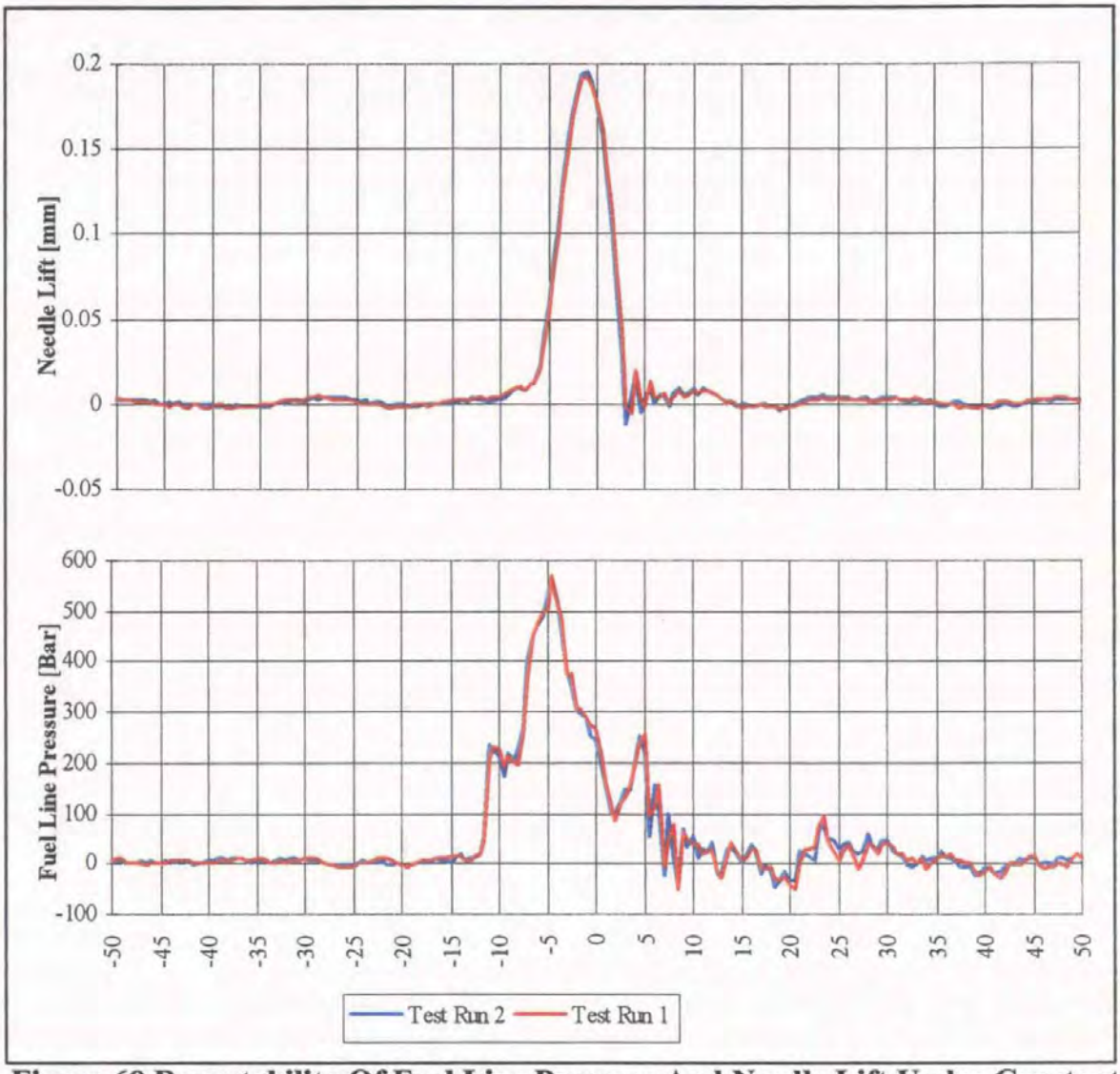

Figure 68 Repeatability Of Fuel Line Pressure And Needle Lift Under Constant Ambient And Engine Torque And Speed Conditions

- The only obvious variations in cylinder pressure were caused by the variation of point of injection. Consequently varying points of injection gave variations in maximum cylinder pressure and it's position relative to crank angle. As with the injection data, maximum cylinder pressure and it's position relative to crank angle showed the greatest variations of 11.2% and 4.5° respectively, at 1500 [revs/min] and 100 [Nm].

8.1.3 Analysis Of Baseline General Performance Data

The majority of these parameters were calculated using slow speed sensor data and cylinder pressure data. Consequently, any variations in cylinder pressure or sensor data had impacts on the repeatability of these performance parameters.

- The variations in cylinder pressure data discussed above caused deviations in IMEP and subsequently any other indicated parameters. In theory, for a given engine speed FMEP should remain constant. Since the objective was to consistently set engine torque and speed, BMEP should also have remained constant. Given this, it was reasonable to assume that IMEP and mechanical efficiency should also have remain constant. In practice this proved not to be the case. The repeatability trials showed that IMEP was repeatable to within 2.3%. The baseline results showed however, that throughout the torque and speed range the average repeatability was 9.9%. It was initially believed that mechanical efficiency may have improved due to running in over the eleven month experimental period. Analysis of the data did not provide conclusive evidence of this. It was therefore concluded that IMEP calculation was susceptible to variations in ambient conditions which may not necessarily have the same impact on BMEP.
- Friction and pumping mean effective pressure showed large percentage deviations throughout the torque and speed range. These high percentage deviations were a result of small pressure deviations relative to the transducer FSR. For example, at 1400 [revs/min] and 186 [Nm] actual pressure deviations of 0.03 [Bar] in PMEP and 0.29 [Bar] in FMEP gave rise to the large percentage

differences of 16.2 and 26.85% respectively. These pressure differences represent 0.02% and 0.19% of the transducer FSR. It was therefore concluded that these deviations were caused by the limitations of transducer sensitivity.

8.1.4 Analysis Of Baseline Charge Air System Data

Some parameters gave very large percentage differences throughout the torque and speed range, these are discussed below;

- Compressor speed parameter showed a maximum variation of 8.9% at 1500 [revs/min] and 100 [Nm]. Throughout the torques and speeds, deviations in compressor speed parameter coincided with variations in turbocharger speed as would be expected. Turbocharger speed variations are discussed in Section 8.1.1.
- Compressor isentropic efficiency variations were caused by pressure instrumentation sensitivity. Maximum and minimum efficiencies coincided with the maximum and minimum compressor discharge pressures and pressure ratios. The maximum and minimum pressure ratios could not be related to either turbocharger rotational speed or mass flow rate parameter maximums and minimums. Although the compressor pressure ratios were generally repeatable giving a maximum deviation of 4.09%, compressor efficiency was very sensitive to pressure ratio particularly when the pressure ratio was small as was the case at the lower engine torques and speeds. This can be illustrated by using the data recorded at 1500 [revs/min] and [100] Nm as an example. If the compressor temperature ratio was held constant and a variation of 0.853% was applied to the pressure ratio there was a significant change in compressor isentropic efficiency as shown below.

Compressor isentropic efficiency is given by;

$$\eta_{ctt} = \frac{(p_2 / p_1)^{\frac{\gamma-1}{\gamma}} - 1}{\left(T_2 / T_1\right) - 1}$$

Applying a constant temperature ratio of 1.0304 and the maximum and minimum pressure ratios of 1.015 and 1.006 gave isentropic efficiencies of 13.51 & 5.42% respectively, representing a percentage change in excess of 100%.

- Intercooler air and water temperature gradients showed maximum variations of 121.2 and 208.251% respectively. These deviations arose because of two reasons. Firstly, the large range of intercooler cooling water inlet temperatures which varied approximately 10[K]. Consequently, the air was cooled significantly more with a cooler water inlet temperature. Secondly, the temperature gradients, particularly for the cooling water, were small, yielding high percentage differences for small absolute temperature changes. This theory is supported by the percentage deviation in intercooler water and air temperature gradients decreasing as engine power and consequently, temperature gradients increase.
- Intercooler air pressure gradient showed a maximum variation of 193.8%. As with the intercooler cooling water temperature gradient, the air pressure gradient was small leading to an enormous percentage variation for small pressure changes. The pressure drop was also particularly small when compared to the FSR of the pressure transducers. The intercooler inlet and discharge pressures, however, show good repeatability to within a couple of percent. It was concluded that the instrumentation sensitivity was certainly a limiting factor when trying to measure such small pressure drops.

8.1.5 Analysis of Exhaust Gas System Data

The largest two variations encountered were turbine speed parameter and turbine isentropic efficiency which showed maximum deviations of 8.11 and 149.9% respectively. The turbine speed parameter displayed a poor repeatability because of the variation in turbocharger rotational speed. Turbine isentropic efficiency was badly affected by the large variations in exhaust manifold pressure in a similar manner to compressor isentropic efficiency discussed above in Section 8.1.4.

8.2 Development Of Fault - Symptom Relationships

The following sections discuss the engine testing conducted and show a summary of the results obtained for each engine fault tested. All results are presented in a tabular format which shows the percentage change in average sensor reading when compared to the average baseline reading. This comparison was performed for every sensor reading and performance parameter contained within the Performance Monitor file. The tables shown only contain the parameters which showed the most consistent trends. Further to this, the magnitude of change due to the fault introduction was compared to the *natural* variation of each parameter recorded during baseline testing. This had the effect of exposing parameters which exhibit a significant change, greater than experimental error or natural variation, due to ambient conditions. Superimposed over the numerical values is a colour coding. Red and blue cells denote positive and negative sensor deviations which exceed the baseline set repeatability. These deviations can therefore almost certainly be attributed to the introduction of the fault. Yellow and green cells identify readings which show positive and negative deviations which fall within the baseline set

repeatability but show a basic trend. Once compiled, these tables represent the fault-symptom relationships used as the foundation for the development of a neural network based diagnostic system.

The salient features of the fuel injection and combustion data, for example point of injection, duration of injection, ignition delay, position of maximum cylinder pressure etc. were also compared and displayed in the fault-symptom tables where appropriate. Plots of average cylinder pressure, fuel line pressure, needle lift and approximate heat release against degrees crank angle for both baseline and faulty conditions are also presented where the introduction of the fault caused the data to change significantly.

8.3 Fouled Charge Air Filter Experimental Results

Ninety separate engine tests were conducted over a five week period to quantify the effect of a fouled charge air filter. Initially forty five tests were conducted at a 80% level of fouling as discussed in Chapter 7. As a result, some clear trends developed in sensor and performance parameter data. Despite previous research and the SPICE simulation model both predicting that 30% fouling would be undetectable, it was decided to engine test at 30% fouling based on the results found at the 80% level of fouling. The two sets of results could subsequently be used to determine the ability of the neural network to correctly diagnose the fault and identify the level of severity. The fouling was introduced by the perforated polythene method described in Chapter 7. The following sections analyse the results obtained at both severities and display the results in the fault-symptom tables.

8.3.1 Analysis Of 80% Fouled Air Filter Sensor Data

Table 14 details the sensor readings which showed a deviation due to the introduction of a 80% fouled air filter. In total, 14 sensor readings showed trends. These are discussed below.

- The reduction in inlet air flow rate was the most positive trend identified, as might be expected. Inlet air volume flow rate showed a maximum decrease of 10.7%. Coupled with the lower flow rate, compressor inlet, discharge and inlet manifold pressures all showed reductions due to the filter fouling. At lower engine powers the pressure decreases fell within the baseline repeatability. As engine power increased the deviation became larger until it exceeded the baseline repeatability showing a strong trend.
- There was a small but consistent trend in reduced turbocharger speed due to the decrease in charge air mass flow and subsequently exhaust gas mass flow. Increased temperatures throughout the exhaust system also gave a clear trend. This was consistent with a fuel rich mixture and later burning during combustion.

Nom. Speed [revs/min]-Torque [Nm]	1500-100	1400-186	1500-200	1600-237	1500-300	1800-293	1500-430	2000-354	2150-372
Inlet Air Volume Flow Rate	-10.2	-9.1	-9.2	-10.7	-10.1	-9.6	-9.6	-9.2	-7.0
Compressor Discharge Pressure	1.6	-0.3	4.9	-0.4	-0.2	-1.6	-1.2	-3.0	-4.4
Compressor Inlet Pressure	1.8	-0.1	-0.8	-0.7	-0.5	-0.7	-0.2	-1.9	-3.2
Inlet Manifold Pressure	1.2	-0.2	4.7	-0.6	-0.7	-1.6	-1.1	-2.9	-4.0
Turbine Discharge Pressure	2.6	1.2	2.1	1.7	1.7	0.6	1.1	1.4	1.1
Turbocharger Speed	-0.1	-0.4	-0.4	-0.6	-0.6	-2.2	-1.0	-1.9	-1.1
Compressor Discharge Temperature	1.1	0.4	2.7	0.4	0.4	0.1	0.2	0.0	0.0
Compressor Inlet Temperature	1.4	0.3	0.6	0.3	0.3	0.3	0.3	0.3	0.2
Cylinder 1&2 Port Temperatures	1.3	0.4	7.1	1.4	0.1	1.0	0.7	1.5	2.2
Cylinder 3 Port Temperature	2.7	1.5	8.7	2.3	3.4	1.2	1.2	3.0	3.1
Cylinder 4 Port Temperature	2.2	0.3	6.7	1.0	0.2	-0.8	1.0	1.1	1.8
Cylinder 5&6 Port Temperatures	3.9	-0.4	7.0	0.8	0.4	0.2	0.7	1.1	2.3
Exhaust Manifold Temperature	2.1	0.6	9.7	1.7	1.6	0.9	0.3	1.6	2.4
Turbine Discharge Temperature	2.1	0.5	8.3	1.5	1.3	1.1	0.6	2.0	2.8

Blue Cells = Negative deviation from baseline average greater than *natural* variation

Red Cells = Positive deviation from baseline average greater than *natural* variation

Green Cells = Negative deviation from baseline average less than *natural* variation

Yellow Cells = Positive deviation from baseline average less than *natural* variation

Table 14 Percentage Changes In Sensor Data From Baseline Due To An 80% Fouled Charge Air Filter

8.3.2 Analysis Of 80% Fouled Air Filter Performance Parameter Data

Twelve performance parameters showed trends due to the 80% fouled air filter as shown in Table 15.

- Volumetric efficiency, inlet and exhaust mass flow parameters and inlet and exhaust mass flow rates used inlet air volume flow in their calculation, consequently they all showed a negative deviation. Compressor speed parameter showed a steady decrease in line with the decrease in turbocharger speed. Turbine speed parameter showed a deviation greater than turbocharger speed decrease due to the increased exhaust temperatures.
- IMEP and PMEP both showed consistent increases which fell within the ranges experienced during baseline testing throughout the speed and torque range. These increases were expected since the cylinder pressure data was corrected using the inlet manifold pressure as described in Chapter 4, Section 4.2.1.
- The intercooler air temperature gradient showed an increase representing greater charge air cooling. It was thought that the rate of heat transfer had remained constant but the mass flow rate of charge air through the intercooler had decreased and it was therefore subjected to greater cooling.

Nom. Speed [revs/min]-Torque [Nm]	1500-100	1400-186	1500-200	1600-237	1500-300	1800-293	1500-430	2000-354	2150-372
Indicated Power	0.0	0.3	0.7	0.3	1.2	0.7	1.8	0.9	1.3
IMEP	0.2	0.3	0.8	0.4	1.3	0.8	1.9	1.0	1.4
Intercooler Effectiveness	1.4	2.6	1.4	0.7	0.1	1.0	0.7	1.0	1.2
Volumetric Efficiency	-8.8	-9.4	-10.7	-10.9	-9.9	-8.9	-8.9	-8.5	-6.6
PMEP	4.0	9.8	3.8	5.0	8.4	2.6	8.1	-0.3	0.2
Inlet Air Mass Flow Rate	-11.2	-9.5	-11.0	-11.6	-10.7	-10.5	-10.0	-11.2	-10.2
Inlet Air Mass Flow Rate Parameter	-10.2	-9.2	-10.4	-10.9	-10.2	-10.0	-9.9	-9.2	-7.1
Compressor Speed Parameter	-0.4	-0.5	-0.5	-0.8	-0.7	-2.3	-1.2	-2.1	-1.2
Intercooler Air Temperature Gradient	7.5	18.3	11.4	7.6	5.3	1.3	2.9	1.0	2.4
Exhaust Gas Mass Flow	-7.6	-9.3	-10.6	-11.2	-10.2	-10.1	-9.4	-10.7	-9.8
Exhaust Gas Mass Flow Parameter	-14.8	-9.1	-9.1	-10.1	-12.6	-8.9	-8.5	-9.9	-7.9
Turbine Speed Parameter	0.1	-0.6	-0.6	-1.4	-1.3	-2.6	-1.2	-2.7	-2.3

Blue Cells = Negative deviation from baseline average greater than *natural* variation

Red Cells = Positive deviation from baseline average greater than *natural* variation

Green Cells = Negative deviation from baseline average less than *natural* variation

Yellow Cells = Positive deviation from baseline average less than *natural* variation

Table 15 Percentage Changes In Performance Parameters From Baseline Due To An 80% Fouled Charge Air Filter

8.3.3 Analysis Of 80% Fouled Air Filter Injection & Combustion Data

There were no detectable trends in the fuel injection data. Similarly the combustion data showed little deviation from the baseline data. A small deviation was present in the cylinder pressure diagram and the approximate heat release profile at 2150 [revs/min] & 372 Nm, these are shown in Figure 69. The cylinder pressure trace shows a decrease in maximum compression pressure as would be expected with a smaller trapped mass. The approximate heat release diagrams show that the introduction of the fault increases the rate of heat release and subsequent burning takes place later in the cycle which lead to the higher exhaust system temperature data shown in Table 14.

8.3.4 Analysis Of 30% Fouled Air Filter Data

With the exception of air flow, all trends in the data had diminished and were undetectable at the 30% level of filter fouling. Table 16 shows the percentage changes in the parameters from the baseline results due to a 30% fouled charge air filter. Air volume flow rate showed a decrease in the order of 2% from the baseline at 30% fouling compared to the 9-10% reduction from the baseline at 80% filter fouling.

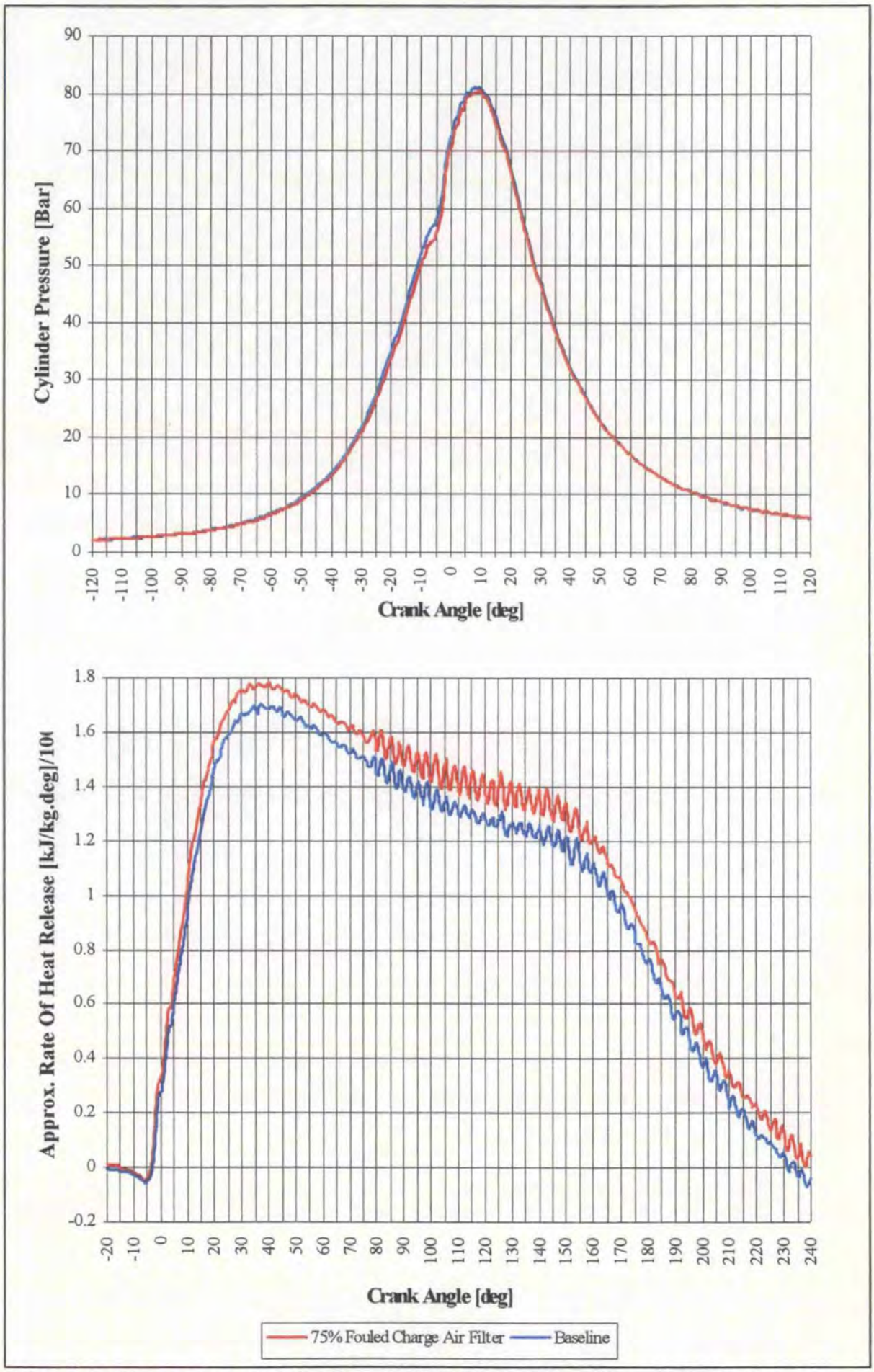

Figure 69 Comparison Of Baseline & 80% Fouled Air Filter Cylinder Pressure & Heat Release Data At 2150 [revs/min] & 372 [Nm]

Nom. Speed [revs/min]-Torque [Nm]	1500-100	1400-186	1500-200	1600-237	1500-300	1800-293	1500-430	2000-354	2150-372
Inlet Air Volume Flow Rate	-2.7	-2.3	-3.0	-2.8	-2.5	-2.0	-2.0	-1.8	0.2
Compressor Inlet Pressure	2.5	0.1	0.1	-0.3	-0.1	0.2	0.4	-4.0	-3.5
Cylinder 3 Port Temperature	2.8	0.7	1.5	1.9	1.3	-0.5	0.5	0.3	-0.1
Inlet Air Mass Flow Rate	-2.5	-2.4	-3.0	-3.2	-2.7	-1.9	-1.7	-5.7	-2.7
Inlet Air Mass Flow Rate Parameter	-2.6	-2.3	-3.0	-3.0	-2.5	-2.3	-2.3	-1.7	0.2
Volumetric Efficiency	-2.2	-3.5	-3.6	-3.8	-3.2	-2.5	-2.4	-6.1	-4.1
Exhaust Gas Mass Flow Rate	0.5	-2.3	-2.8	-3.2	-2.7	-1.9	-1.5	-5.5	-2.6
Exhaust Gas Mass Flow Rate Parameter	-4.5	-4.7	-3.6	-4.4	-2.2	-3.2	3.5	-8.0	-2.6

Blue Cells = Negative deviation from baseline average greater than *natural* variation

Green Cells = Negative deviation from baseline average less than *natural* variation

Yellow Cells = Positive deviation from baseline average less than *natural* variation

Table 16 Percentage Changes In Performance Parameter & Sensor Data Due To A 30% Fouled Air Filter

8.4 Fouled & Corroded Intercooler Matrix Experimental Results

Ninety separate engine tests were conducted over a four week period to assess the affect of a genuinely fouled and corroded intercooler matrix on engine performance. Two genuinely faulty intercoolers were obtained and both underwent preliminary trials as described in Chapter 7. Initially engine testing was performed with one of the genuinely faulty coolers fitted to the engine. The results clearly showed that the introduction of this fault affected engine performance. Further to this, a second series of testing was conducted with a simulated foul condition significantly less than the genuine intercooler. This additional data was collected so that it could be used to determine the neural networks ability to identify not only the fault but also its severity. The following section discusses the results and present the fault-symptom relationship tables.

8.4.1 Analysis Of Genuinely Fouled & Corroded Intercooler Sensor Data

Table 17 shows the percentage changes in average sensor readings from the average baseline results due to the introduction of a genuinely fouled and corroded intercooler. Several sensor readings showed deviations, these are discussed below.

- Charge air temperature in the inlet manifold rose steadily with increasing engine power and maintained a deviation greater than the baseline repeatability for the five highest power test points.
- The increase in charge air temperature caused the exhaust port temperatures, exhaust manifold and turbine discharge temperatures to rise particularly at higher power.

- The inlet manifold pressure increased slightly but never showed a large enough deviation to exceed the baseline repeatability. It was expected that the inlet manifold pressure would decrease because of the greater pressure drop across the intercooler due to air side fouling. Although this may have been evident it was masked by the higher charge air temperature and consequently increased pressure. This was further substantiated by the reduction of inlet air volume flow rate since the higher temperature charge air had a lower density than the cooler baseline charge.
- The intercooler cooling water discharge temperature showed a decrease as was expected with reduced heat transfer across the cooler matrix.
- Turbocharger rotational speed and turbine discharge pressure showed minimal deviations which never exceeded the baseline set repeatability.

8.4.2 Analysis Of Genuinely Fouled & Corroded Intercooler Performance Parameter Data

Table 18 shows the percentage change in performance parameters from the average baseline data due to the introduction of a fouled & corroded intercooler.

- Intercooler air and water temperature gradients and consequently intercooler effectiveness all showed a clear reduction which exceeded the baseline set repeatability.
- Intercooler air pressure gradient increased due to increased air side fouling but did not consistently exceed the baseline set repeatability.

- Inlet air mass flow rate, inlet air mass flow rate parameter and exhaust mass flow rate parameter all showed a reduction which, generally, developed further with increasing engine power due to the reduction of cooling and charge air density.
- Both indicated, and brake specific fuel consumption showed a positive deviation but this trend was particularly weak. The trend for indicated specific fuel consumption and thermal efficiency was stronger than that shown for brake parameters. This was due to the consistent decrease in IMEP and consequently indicated power throughout the power range. PMEP also showed a consistent decrease which strengthened with increasing engine power.
- The trend in increased specific fuel consumptions was matched by a decrease in indicated thermal efficiency.

Nom. Speed [revs/min]-Torque [Nm]	1500-100	1400-186	1500-200	1600-237	1500-300	1800-293	1500-430	2000-354	2150-372
Inlet Air Volume Flow Rate	-0.9	-1.4	-1.8	-1.8	-1.9	-2.1	-2.8	-2.8	-2.1
Cylinder 1&2 Port Temperatures	0.5	0.5	0.3	1.2	0.4	0.6	1.0	0.5	1.1
Cylinder 3 Port Temperature	3.1	0.6	0.4	1.3	2.3	0.9	1.1	1.9	1.8
Cylinder 4 Port Temperature	1.8	1.1	1.0	1.7	1.6	1.4	1.3	2.8	2.6
Cylinder 5&6 Port Temperatures	3.9	0.3	0.2	0.8	1.6	0.9	1.4	1.8	2.2
Exhaust Manifold Temperature	1.1	-0.1	-0.5	1.0	1.4	0.6	0.4	0.8	1.2
Intercooler Cooling water Dischg Temp	2.6	-0.6	-0.4	-0.1	-0.5	-0.1	-0.5	-0.4	-0.9
Inlet Manifold Pressure	1.2	0.1	-0.2	0.4	0.6	0.2	-0.2	1.5	0.6
Inlet Manifold Temperature	2.7	0.4	0.7	1.5	1.7	2.1	2.3	3.3	4.0
Turbine Discharge Temperature	1.3	0.1	-0.1	1	1.4	1.1	0.9	1.3	1.6
Turbine Discharge Pressure	1.3	0.2	0.3	0.6	0.6	0.5	0.5	1.0	0.5
Turbocharger Speed	-0.7	-0.5	-2.1	0.1	0.5	-0.4	-0.4	-0.2	-0.2

Blue Cells = Negative deviation from baseline average greater than *natural* variation

Red Cells = Positive deviation from baseline average greater than *natural* variation

Green Cells = Negative deviation from baseline average less than *natural* variation

Yellow Cells = Positive deviation from baseline average less than *natural* variation

Table 17 Percentage Change In Sensor Readings From Baseline Due To A Genuinely Fouled & Corroded Intercooler

Nom. Speed [revs/min]-Torque [Nm]	1500-100	1400-186	1500-200	1600-237	1500-300	1800-293	1500-430	2000-354	2150-372
Indicated Power	-0.7	-0.5	-1.2	-1.3	-0.3	-0.2	-1.0	-0.1	0.2
PMEP	-3.3	-2.6	-4.2	-6.7	-7.8	-7.2	-14.9	-10.8	-10.9
IMEP	-0.6	-0.5	-1.1	-1.2	-0.2	-0.2	-1.0	-0.1	0.3
BSFC	3.8	0.2	1.2	-0.2	0.2	0.3	-1.1	1.2	-1.0
ISFC	-1.0	0.5	1.3	1.2	0.1	-0.7	1.2	1.7	1.1
Indicated Thermal Efficiency	-1.6	-0.4	-1.3	-1.3	-0.1	-0.2	-0.7	-0.8	0.9
Inlet Air Mass Flow Rate	-1.2	-1.1	-1.5	-1.3	-1.4	-1.4	-2.0	-1.8	-0.9
Inlet Air Mass Flow Rate Parameter	-0.8	-1.4	-1.7	-1.8	-1.9	-2.3	-2.9	-2.6	-2.0
Compressor Speed Parameter	-7.2	-0.4	-2.1	0.1	0.5	-0.4	-0.4	-0.1	-0.2
Intercooler Air Temperature Gradient	-38.1	-20.3	-30.2	-33.5	-28.5	-38.3	-32.3	-37.4	-38.4
Intercooler Air Pressure Gradient	206.0	47.7	61.1	46.1	36.6	68.5	59.7	52.5	19.5
Intercooler Water Temperature Gradient	156.0	-14.8	-33.7	-34.4	-29.2	-39.8	-35.0	-40.5	-40.2
Intercooler Effectiveness	-58.5	-29.7	-30.8	-33.4	-31.8	-36.2	-32.5	-36.6	-38.9
Exhaust Gas Mass Flow Rate	1.8	-1.1	-1.4	-1.3	-1.3	-1.3	-1.9	-1.7	-1.0
Turbine Expansion Ratio	1.8	-2.4	2.3	-1.7	-4.0	-0.7	-3.4	-0.6	-2.9
Turbine Speed Parameter	-7.4	-0.4	-1.9	-0.4	-0.2	-0.7	-0.6	-0.6	-0.8

Blue Cells = Negative deviation from baseline average greater than *natural* variation

Red Cells = Positive deviation from baseline average greater than *natural* variation

Green Cells = Negative deviation from baseline average less than *natural* variation

Yellow Cells = Positive deviation from baseline average less than *natural* variation

Table 18 Percentage Change In Performance Parameters From Baseline Due To A Genuinely Fouled & Corroded Intercooler

8.4.3 Analysis Of Genuinely Fouled & Corroded Intercooler Fuel Injection And Combustion Data

In general, the data showed very small changes which always remained within the baseline repeatability.

- The needle lift data showed no clear trend of either advanced or retarded injection throughout the operating points. At lower powers the point of injection was slightly retarded and became increasingly advanced at higher engine powers with the exception of the full throttle position operating points. This trend was also evident in the fuel line pressure data and combustion data.
- The heat release data showed that the point of ignition is retarded in line with the retarded point of injection. This led to a reduced and retarded maximum cylinder pressure at lower engine powers. There was no evidence of a change in ignition delay at lower engine powers.
- At higher engine powers, the ignition delay decreased and point of injection advanced. These results were expected since the charge air temperature increased significantly and therefore caused combustion to initiate earlier in the cycle. The reduction in ignition delay was, however, small relative to the baseline set repeatability.

8.4.4 Analysis Of Simulated Faulty Intercooler Sensor Data

Table 19 shows the percentage deviation of sensor readings from the baseline average due to the introduction of a simulated faulty intercooler. Eight sensor readings in total showed a reasonably consistent trend, three of these exceeded the

baseline repeatability. All eight sensor readings were previously deviated by the introduction of the genuinely faulty intercooler.

- Inlet air volume flow rate decrease exceeded the baseline set repeatability at all torques and speeds with the exception of the highest power. This was due to the reduced cooling and density of the charge air. Consequently reducing the air volume flow rate at ambient conditions.
- Turbocharger rotational speed showed a fairly consistent decrease throughout the speed and torque range, but never decreased significantly to exceed the baseline set repeatability. It was thought that this was due to reduced exhaust gas mass flow.
- Inlet manifold temperature and exhaust ports 4, 5 & 6 all showed an increase in temperature as with the genuinely faulty intercooler. An increase in turbine discharge, collective exhaust manifold and exhaust ports 1,2 & 3 temperatures was not apparent as with the genuinely faulty intercooler.
- Both inlet manifold and turbine discharge pressures showed a small percentage increase. Inlet manifold pressure never exceeded the baseline set repeatability. Turbine discharge pressure only exceeded the baseline set repeatability at the lowest engine power.

Nom. Speed [revs/min]-Torque [Nm]	1500-100	1400-186	1500-200	1600-237	1500-300	1800-293	1500-430	2000-354	2150-372
Inlet Air Volume Flow Rate	-6.2	-1.8	-1.6	-1.5	-1.3	-1.5	-1.4	-1.6	-0.8
Cylinder 4 Port Temperature	1.9	-0.1	0.1	0.5	0.4	-1.0	0.4	0.3	0.1
Cylinder 5&6 Port Temperatures	4.0	0.5	0.0	0.4	0.9	0.7	0.7	1.3	1.5
Intercooler Cooling Water Dischg Temp	3.5	0.1	0.2	0.4	0.3	0.6	0.6	1.1	1.3
Inlet Manifold Pressure	2.3	0.5	0.4	0.9	0.7	0.1	0.3	0.7	0.7
Inlet Manifold Temperature	2.5	0.1	0.2	0.5	0.6	0.7	0.9	1.3	1.4
Turbine Discharge Pressure	2.1	0.5	0.6	0.7	0.8	0.7	0.7	0.9	0.6
Turbocharger Speed	-0.2	0.3	-1.0	-0.1	-0.1	-1.4	-0.2	-0.9	-0.3

Table 19 Percentage Changes In Sensor Readings From Baseline Data Due To A Simulated Faulty Intercooler

Nom. Speed [revs/min]-Torque [Nm]	1500-100	1400-186	1500-200	1600-237	1500-300	1800-293	1500-430	2000-354	2150-372
PMEP	-1.4	0.5	-1.3	1.3	1.1	-3.4	-1.5	-1.6	-2.5
BSFC	4.0	0.8	0.1	0.9	0.5	-1.0	-1.9	0.7	-0.7
ISFC	1.4	0.1	0.0	1.4	0.1	1.3	0.1	0.2	1.1
Inlet Air Mass Flow Rate	-5.9	-1.4	-1.2	-1.0	-0.7	-0.7	-0.7	-0.8	-0.1
Inlet Air Mass Flow Rate Parameter	-5.9	-1.6	-1.4	-1.4	-1.1	-1.6	-1.4	-1.3	-0.5
Compressor Speed Parameter	-6.6	0.4	-1.3	0.0	0.2	-1.2	-0.1	-0.7	-0.1
Intercooler Air Temperature Gradient	-44.2	-17.9	-22.5	-19.9	-17.4	-21.2	-17.4	-20.1	-18.2
Intercooler Water Temperature Gradient	129.9	122.2	90.7	92.5	103.8	88.7	94.0	91.8	92.6
Intercooler Effectiveness	-14.7	-14.2	-13.6	-15.2	-15.1	-15.8	-14.2	-16.8	-16.1
Volumetric Efficiency	-5.0	-1.7	-1.4	-1.4	-0.8	-0.2	-0.2	-0.5	0.5
Exhaust Gas Mass Flow Rate	-2.6	-1.3	-1.1	-1.0	-0.6	-0.7	-0.6	-0.8	-0.1
Exhaust Gas Mass Flow Rate Parameter	-6.7	-1.2	2.0	-1.6	-1.0	-1.1	-1.2	-1.5	1.2
Turbine Speed Parameter	-7.1	0.2	-1.2	-0.4	-0.4	-1.1	-0.1	-0.8	-0.3

Table 20 Percentage Changes In Performance Parameters From Baseline Data Due To A Simulated Faulty Intercooler

8.4.5 Analysis Of Simulated Faulty Intercooler Performance Parameters

Table 20 shows the percentage deviation in performance parameters from the average baseline due to the introduction of a simulated faulty intercooler. All of the parameters identified also showed a deviation during testing with the genuinely faulty intercooler. Only three parameters showed deviations consistently outside the baseline set repeatability, namely, intercooler effectiveness, air and water temperature gradients. All other parameters generally showed deviations smaller than those experienced with the genuinely faulty intercooler. Several parameters previously showing deviations with the genuine faulty intercooler now ceased to show any trend.

- Both indicated and brake specific fuel consumptions showed an increase. This was consistent with a decreased trapped mass of charge air and poorer combustion.
- Inlet air and exhaust mass flow rates both showed a decrease. This was due to the increased temperature, and therefore, reduced density of the charge air.
- Inlet and exhaust mass flow parameters showed a decrease, largely due to the decrease in inlet air mass flow rate. The deviations for both were generally larger than for the respective mass flow rates. These enhanced deviations were caused by a combination of increased turbine and compressor inlet temperatures and reduced inlet pressures.
- Intercooler effectiveness and air temperature gradient both showed significant decreases as a result of the decreased heat transfer through the cooler matrix.
- Intercooler water temperature gradient increased. The genuine fault showed a marked decrease in water temperature gradient. This conflict was caused by the

method of simulating the faulty intercooler. The simulated fault was introduced by throttling back the water discharge from the intercooler. This in turn caused the cooling water to remain in the matrix for a longer period of time allowing the water to be heated significantly more.

- Volumetric efficiency showed a steady decrease throughout the speed and torque range. This was a direct reflection of the reduction in inlet air volume flow rate.
- Both compressor and turbine speed parameters decreased in line with the decrease in turbocharger rotational speed. This trend was further strengthened when turbine or compressor inlet temperatures increased. This was clearly shown at 1500 [revs/min] and 100 [Nm].

8.4.6 Analysis Of Simulated Faulty Intercooler Injection And Combustion Data

There was no appreciable trends in any of the fuel injection or combustion data. All deviations fell within the baseline set repeatability and fluctuated randomly around the average baseline data.

8.5 Leaking Inlet Valves Experimental Results

A total of forty five separate engine tests were conducted over a three week period to establish the effect of leaking inlet valves on engine performance. The forty five tests consisted of five separate repetitions of the nine speed and torque points identified in Chapter 4. The leaking inlet valves were developed and introduced onto the test engine as described in Chapter 7, Section 7.4.

8.5.1 Analysis Of Leaking Inlet Valve Sensor Data

Table 21 shows the percentage change in average sensor readings from the average baseline readings due to introduction of leaking inlet valves. Sixteen sensor readings showed deviations and approximately twelve of these showed variations which exceeded the baseline set repeatability at more than one engine speed and torque condition.

- Inlet air volume flow rate showed a significant decrease which exceeded the baseline set repeatability at all speeds and torques. The maximum reduction in flow of 6.55 % coincided with the highest engine torque. The reduction in flow was due to the reverse flow of the usually trapped charge past the valve and into the inlet manifold during compression and combustion. This reverse flow replaced charge air normally drawn through the charge air system.
- Compressor inlet and discharge pressures both showed minimal decreases. Despite this, inlet manifold pressure remained unchanged from the baseline test data. It was thought that the reverse flow from the cylinder into the inlet manifold maintained the inlet manifold pressure rather than increasing it, as might be expected. This idea was further substantiated by the consistent decrease in turbocharger rotational speed whilst inlet manifold pressure was similar to that seen in baseline testing.
- Inlet manifold temperature increased significantly and exceeded baseline set repeatability at most torques and speeds. This positively identified that reverse flow from the cylinder into the manifold was occurring, further substantiating the above theory.

- The increased inlet manifold temperature subsequently lead to increased exhaust temperatures at all measuring locations. The exhaust temperature deviations generally exceeded the baseline set repeatability with the exception of the full throttle test points. At these speeds and torques the exhaust temperatures had a tendency to decrease since delivery could not be increased any further. This therefore proves that the increased exhaust temperatures were due to both increased charge temperature and up-fuelling to maintain torque.
- The increased delivery to maintain torque at partial travel rack positions is supported further by both increased rack position and therefore delivery and a subsequent increase in fuel mass flow rate.

8.5.2 Analysis Of Leaking Inlet Valve Performance Parameter Data

Twenty two performance parameters showed deviations due to the introduction of leaking inlet valves. These are shown in Table 22 together with the respective percentage deviations from the baseline data set. Fourteen of the twenty two deviated outside the baseline set repeatability at more than half of the engine test points.

- Engine torque, brake power and BMEP all showed reductions of approximately 8-9 % at the full throttle test points. This was due to the reduced density and quality of charge air, loss of compression pressure and, most importantly, the continued loss of charge through the inlet valve during the combustion and expansion part of the cycle.

Nom. Speed [revs/min]-Torque [Nm]	1500-100	1400-186	1500-200	1600-237	1500-300	1800-293	1500-430	2000-354	2150-372
Inlet Air Volume Flow Rate	-4.3	-5.8	-5.3	-5.9	-6.3	-5.2	-6.5	-4.0	-5.5
Compressor Discharge Pressure	2.1	-0.1	-0.5	-0.5	-0.1	-0.2	-1.2	1.3	-2.7
Compressor Discharge Temperature	2.1	1.2	1.0	1.0	1.1	1.0	0.8	1.6	0.1
Compressor Inlet Pressure	1.2	-1.2	-1.3	-1.3	-1.2	-1.2	-1.0	-1.1	-1.2
Cylinder 1&2 Port Temperatures	3.2	0.6	1.0	1.9	2.7	3.3	-0.2	2.6	-1.6
Cylinder 3 Port Temperature	2.0	1.2	0.5	1.5	3.1	3.5	-0.1	1.2	-0.5
Cylinder 5&6 Port Temperatures	-0.4	0.9	0.7	0.7	1.9	1.6	0.5	0.8	-2.0
Exhaust Manifold Pressure	5.2	-3.0	-0.3	-0.9	-3.5	-0.5	-2.5	0.7	-2.5
Exhaust Manifold Temperature	3.2	1.8	2.1	3.3	5.5	5.4	6.0	6.3	3.0
Fuel Rack Position	0.4	-0.6	0.3	1.8	0.3	2.9	0.2	4.7	-0.1
Intercooler Cooling water Dischg Temp	4.0	0.5	0.30	0.3	0.2	0.4	0.3	0.4	0.2
Inlet Manifold Temperature	3.3	0.8	0.6	0.6	0.6	0.7	0.5	1.0	0.1
Turbine Discharge Temperature	2.5	2.1	2.4	3.3	5.0	5.1	5.1	6.0	3.2
Turbine Discharge Pressure	2.5	1.0	0.9	1.0	1.4	1.3	1.3	1.7	1.1
Turbocharger Speed	-1.1	-1.4	-4.7	-4.0	-2.6	-2.2	-2.9	0.4	-3.3
Fuel Mass Flow Rate	1.8	3.9	2.9	2.9	4.9	7.2	-0.9	8.1	-0.6

Blue Cells = Negative deviation from baseline average greater than *natural* variation

Red Cells = Positive deviation from baseline average greater than *natural* variation

Green Cells = Negative deviation from baseline average less than *natural* variation

Yellow Cells = Positive deviation from baseline average less than *natural* variation

Table 21 Percentage Change In Sensor Readings From Baseline Data Due To Leaking Inlet Valves

Nom. Speed [revs/min]-Torque [Nm]	1500-100	1400-186	1500-200	1600-237	1500-300	1800-293	1500-430	2000-354	2150-372
Engine Torque							-9.0		-8.3
Brake Power							-9.0		-8.3
Indicated Power	-12.6	-0.2	-0.5	-1.5	-0.5	-0.5	-5.2	-2.0	-6.4
BMEP							-9.0		-8.2
PMEP	-17.0	-27.3	-27.3	-31.7	-40.8	-26.1	-49.2	-27.2	-22.1
IMEP	-12.4	-0.1	-0.5	-1.4	-0.4	-0.5	-5.2	-2.1	-6.3
BSFC	2.1	4.6	3.7	4.2	4.9	6.2	8.0	8.9	8.1
ISFC	9.3	4.3	3.6	6.1	5.1	5.6	4.8	10.9	8.1
Brake Thermal Efficiency	-1.4	-4.3	-3.5	-4.1	-4.7	-5.1	-8.1	-7.4	-7.5
Indicated Thermal Efficiency	-13.1	-4.1	-3.5	-5.8	-4.9	-6.1	-4.2	-9.0	-5.6
Inlet Air Mass Flow Rate	-7.2	-8.4	-8.0	-8.5	-8.8	-7.8	-8.9	-6.5	-7.9
Inlet Air Mass Flow Rate Parameter	-5.0	-6.5	-6.0	-6.6	-7.0	-6.2	-7.4	-4.6	-6.1
Compressor Pressure Ratio	1.1	1.2	0.8	0.8	1.1	1.3	-0.2	2.2	-1.4
Compressor Speed Parameter	-8.6	-2.2	-5.5	-4.7	-3.3	-2.9	-3.6	-0.3	-4.0
Compressor Isentropic Efficiency	64.9	36.5	22.9	15.2	11.8	10.7	6.3	7.6	4.7
Intercooler Air Temperature Gradient	17.3	19.2	13.9	10.2	9.8	7.3	4.2	8.7	-0.2
Intercooler Water Temperature Gradient	140.9	28.1	16.2	6.8	9.7	2.2	0.4	4.1	-8.3
Volumetric Efficiency	-5.0	-7.7	-7.2	-7.6	-7.9	-6.9	-7.3	-6.7	-5.2
Exhaust Gas Mass Flow Rate	-3.9	-8.1	-7.5	-8.1	-8.2	-7.2	-8.5	-5.9	-7.6
Exhaust Gas Mass Flow Rate Parameter	-7.1	-4.2	-6.3	-5.7	-2.0	-4.3	-3.4	-3.6	-3.8
Turbine Expansion Ratio	0.5	-4.0	-1.2	-1.9	-4.8	-1.9	-4.1	-1.1	-3.3
Turbine Speed Parameter	-9.0	-2.3	-5.7	-5.5	-5.2	-4.7	-5.7	-2.6	-4.8

Blue/Red Cells = Negative/Positive deviation from baseline average greater than *natural* variation

Green/Yellow Cells = Negative/Positive deviation from baseline average less than *natural* variation

Table 22 Percentage Change In Performance Parameters From Baseline Data Due To Leaking Inlet Valves

- IMEP showed a small deviation throughout the torque and speed range. The largest deviation occurred at the full throttle test points for the same reasons as discussed in the above paragraph.
- The reduction in PMEP throughout the torques and speeds was caused by the significantly lower cylinder pressure at BDC after expansion & combustion and for a reasonable portion of the exhausting stroke. Intake strokes for both baseline and leaking valves were very similar, as expected. This is shown in Figure 70.

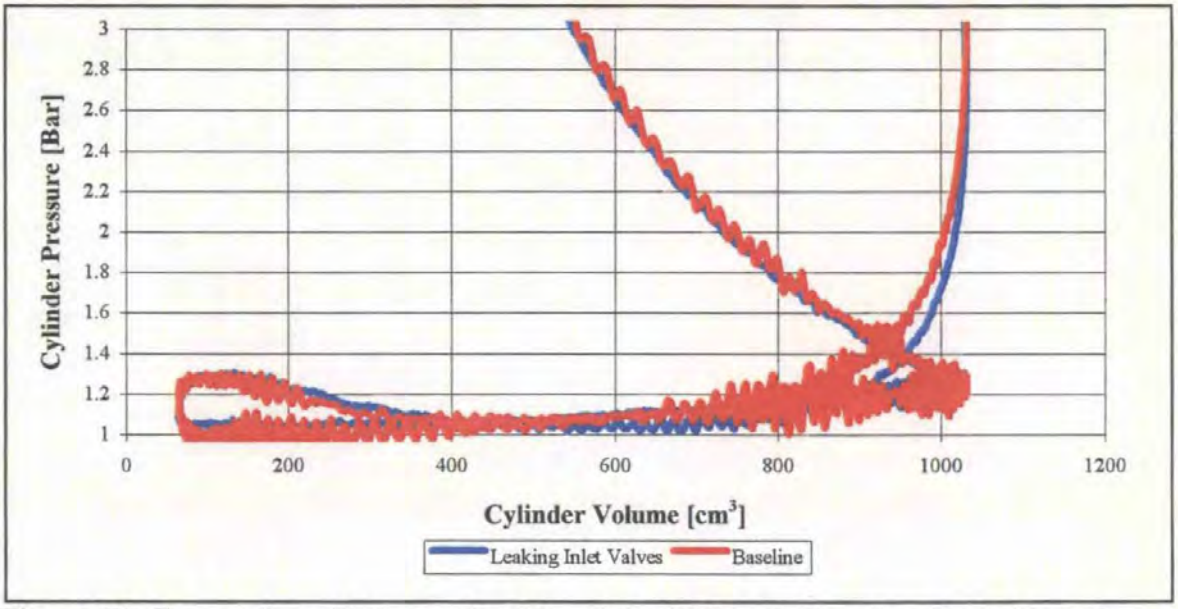

Figure 70 Comparison Between Leaking Inlet Valve & Baseline Data Pumping Loops at 1500 [revs/min] & 430 [Nm]

- Both indicated and brake specific fuel consumption showed strong positive deviations which exceeded the baseline set repeatability significantly. Reasons for this have been discussed in the above sections.
- Indicated and brake thermal efficiencies reduced, again, the deviations were greater than the baseline set repeatability.

- Inlet air mass flow rate reduced beyond the baseline set repeatability. This trend was also evident in the inlet air mass flow rate parameter although to a lesser extent because of the reduced compressor inlet pressure.
- Exhaust gas mass flow rate decreased but not as significantly as the inlet air mass flow because of the increase in fuel mass flow required to maintain engine torque. The exhaust gas mass flow rate parameter also decreased but generally remained within the baseline set repeatability. This was due to the increase in exhaust gas temperature at turbine inlet.
- Compressor pressure ratio, and isentropic efficiency both increased despite a reduction in speed parameter and mass flow parameter. These increases were due to the inlet manifold pressure being maintained by flow from the cylinder into the manifold during compression and combustion rather than increased work being done by the compressor on the charge air.
- Both intercooler air and water temperature gradients showed increases which occasionally exceeded the baseline set repeatability. It was thought that these increases were due to the reverse flow from the cylinder to the manifold. This reverse flow was hotter than the normal charge and occupies volume in the inlet manifold. This has been shown to reduce the volume flow rate of charge air. Consequently the air which passed through the compressor remained in the cooler matrix for a longer period of time allowing greater heat transfer. Further to this, the increased inlet charge air temperature could have transferred heat to the inlet manifold and intercooler castings.
- Turbine mass flow rate parameter and turbine speed parameter both show decreases throughout the speed and torque range. These reductions were

primarily due to the decreases in inlet air mass flow rate and turbocharger rotational speed. Turbine speed parameter shows a stronger trend than turbocharger rotational speed alone. This was due to the increase in turbine inlet temperature. The trend in turbine mass flow rate parameter compared to exhaust mass flow was weakened by the higher exhaust gas temperatures.

8.5.3 Analysis Of Leaking Inlet Valves Fuel Injection & Combustion Data

Figure 71 shows a comparison between leaking inlet valves and baseline needle lift, fuel line pressure, approximate heat release and cylinder pressure data at low speed and low torque. For all but the highest engine speeds and torques the point of injection advanced. The point of injection advanced to maintain a constant point of ignition, despite the reduced compression temperatures and pressures. This is clearly illustrated in Figure 71. At the full throttle travel test points these trends changed as shown in Figure 72. Both point and duration of injection remained unchanged within baseline set repeatability. Heat release always remains retarded due to the fixed point of injection at full throttle. The trend of reduced compression pressure and temperature combined with the fixed point of injection lead to an increased ignition delay. Cylinder compression pressure was reduced at all speeds and torques. The greatest reductions were seen at low speed conditions since the effective time period of leakage was greater.

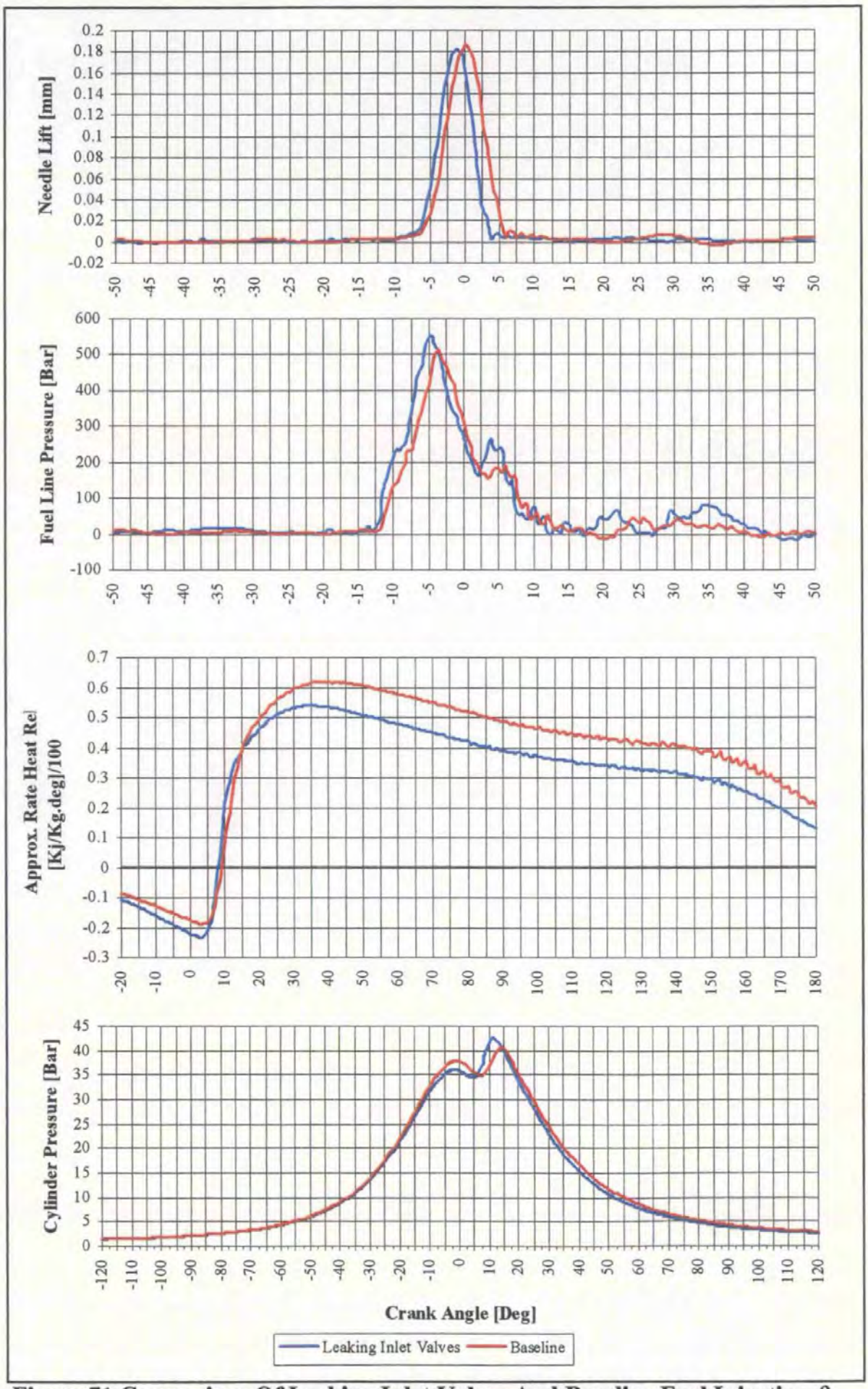

Figure 71 Comparison Of Leaking Inlet Valves And Baseline Fuel Injection & Combustion Data At 1500 [revs/min] And 100 [Nm]

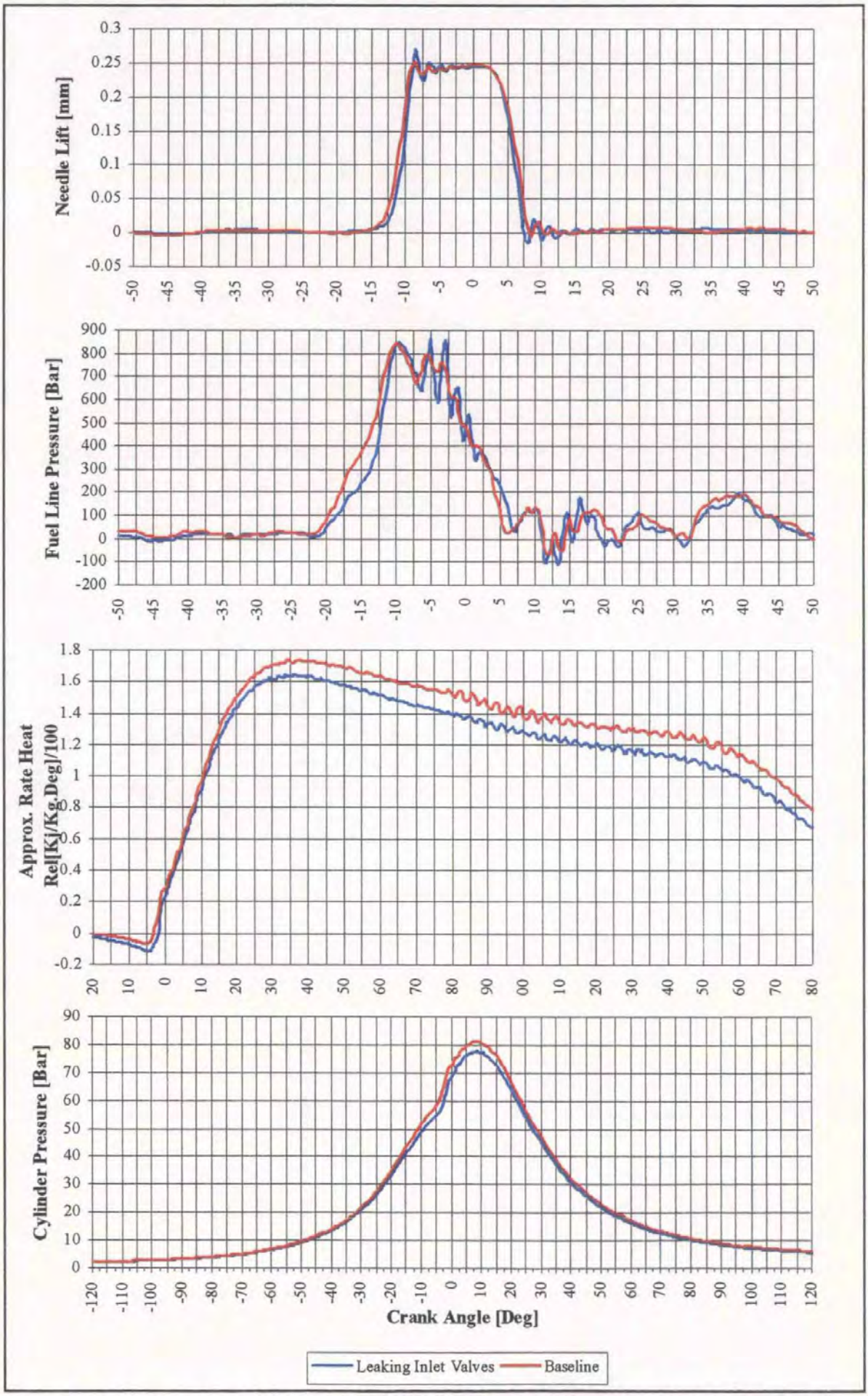

Figure 72 Comparison Of Leaking Inlet Valves And Baseline Fuel Injection & Combustion Data At 2150 [revs/min] And 372 [Nm]

8.6 Leaking Exhaust Valves Experimental Results

Forty five individual engine tests were conducted over a three week period to assess the effect of leaking exhaust valves on engine performance. The testing consisted of five repeated engine runs with data being collected at nine engine speeds and torques, in accordance with the experimental procedure outlined in Chapter 4. The valve faults were introduced onto the test engine as discussed in Chapter 7, Section 7.5.

8.6.1 Analysis Of Leaking Exhaust Valve Sensor Data

Table 23 shows the percentage changes in the sensor readings compared to the average baseline data due to the introduction of leaking exhaust valves. Sixteen sensor readings showed deviations, of these, only two showed negative deviations from the baseline data set.

- Inlet air volume flow rate showed a steadily increasing trend throughout the engine speeds and torques. The maximum deviation of 2.2% occurred at the 2150 [revs/min] and 372 [Nm] position test point. This increased inlet air flow rate was due to the increase in turbocharger speed, boost pressure and, subsequently, charge density.
- Compressor discharge pressure and temperature increased despite the inlet pressure showing a decrease throughout the speed and torque range. These trends are all attributable to the increased turbocharger speed.
- All exhaust temperatures increased with the exception of exhaust port 5 & 6. The majority of these increases exceeded the baseline set repeatability. The positive deviations were partially due to the leakage of trapped charge past the exhaust valves

Nom. Speed [revs/min]-Torque [Nm]	1500-100	1400-186	1500-200	1600-237	1500-300	1800-293	1500-430	2000-354	2150-372
Inlet Air Volume Flow Rate	-3.0	1.5	1.8	1.3	1.3	1.5	1.0	2.2	2.2
Compressor Discharge Pressure	1.5	0.1	0.9	0.5	1.0	0.9	-0.5	2.6	-0.2
Compressor Discharge Temperature	2.2	1.5	1.4	1.4	1.4	1.2	0.5	1.4	0.1
Compressor Inlet Pressure	1.4	-0.7	-0.9	-0.7	-0.8	-0.6	-0.9	-0.6	-0.5
Cylinder 1&2 Port Temperatures	6.2	3.5	3.0	3.6	4.3	4.7	3.1	3.6	-0.1
Cylinder 3 Port Temperature	1.9	2.2	1.3	3.6	6.9	4.2	2.3	2.1	0.0
Cylinder 4 Port Temperature	6.6	1.4	0.3	1.8	0.7	2.0	-0.2	1.3	-2.5
Engine Cooling water Dischg Temp	4.1	0.5	0.5	0.3	0.5	0.6	0.0	0.6	-0.1
Exhaust Manifold Temperature	3.8	2.8	1.8	2.8	4.3	2.9	1.7	3.0	0.4
Intercooler Cooling water Dischg Temp	3.9	0.4	0.4	0.2	0.1	0.2	0.2	0.3	0.1
Inlet Manifold Pressure	1.7	0.1	0.9	0.7	1.1	1.0	-0.5	2.7	-0.2
Inlet Manifold Temperature	3.3	0.8	0.8	0.6	0.7	0.6	0.3	0.8	0.1
Turbine Discharge Temperature	3.2	3.1	2.0	3.0	4.1	2.8	2.0	2.5	0.2
Turbine Discharge Pressure	0.7	-0.7	-0.8	-0.9	-0.7	-1.2	-1.2	-1.3	-1.9
Turbocharger Speed	-0.3	-0.5	2.8	2.2	2.8	1.7	0.1	3.0	-0.4
Fuel Mass Flow Rate	4.9	5.6	3.3	3.5	6.4	6.1	-0.5	7.0	0.0

Blue Cells = Negative % deviation from baseline average greater than *natural* variation

Red Cells = Positive % deviation from baseline average greater than *natural* variation

Green Cells = Negative % deviation from baseline average less than *natural* variation

Yellow Cells = Positive % deviation from baseline average less than *natural* variation

Table 23 Percentage Change In Sensor Readings From Baseline Data Due To Leaking Exhaust Valves

throughout the compression and combustion parts of the cycle. Without doubt, the overriding factor for the increased exhaust temperatures was the up-fuelling required at all partial rack travel test points to maintain engine torque. This was demonstrated by the downward trend of the exhaust port temperatures at the highest power test point which was set at maximum rack travel. The collective exhaust manifold and turbine discharge temperatures also showed a weakened trend at the full throttle travel test points.

- Intercooler cooling water discharge temperature and inlet manifold temperature both showed increases due to the increased compressor discharge temperature.
- Inlet manifold pressure increased but generally the deviation fell within the baseline set repeatability. This increase was due to the increased turbocharger speed and subsequent increase in compressor discharge pressure.
- Turbocharger speed increased through the torque and speed range, except at the 1500 [revs/min] - 430 [Nm] and the 2150 [revs/min] - 372 [Nm] test points. These anomalies were a direct reflection on the combustion process. At these two full throttle travel test points the maximum cylinder pressure and subsequent expansion pressure were reduced. This in turn, reduced the amount of trapped charge escaping passed the exhaust valves. Partial rack travel test points, however, had the ability to be up-fuelled to maintain the combustion and expansion pressures despite the leakage. This gave rise to a higher leakage rate than could be achieved with the fixed rack position test points.
- Fuel mass flow rate showed some large positive deviations in excess of the baseline set repeatability. These increased flows support the theory of up-fuelling required to maintain the specified test torques. This was further substantiated by

the increased exhaust gas temperatures discussed above. Increased fuel mass flow rate was not seen at the two maximum rack travel points since delivery was fixed in these instances.

8.6.2 Analysis Of Leaking Exhaust Valve Performance Parameters

Table 24 summarises the performance parameter deviations from the baseline average due to the introduction of leaking exhaust valves. Seventeen parameters showed deviations, four of these parameters consistently deviated in excess of the baseline set repeatability.

- Engine torque, brake power and BMEP all decreased by approximately 6-7 % at the full throttle travel test points. These reductions were caused by the loss of combustion and expansion pressure because of the leakage of gas into the exhaust manifold.
- IMEP and subsequently indicated power decreased throughout the speed and torque range. The most notable deviations occurred at the maximum rack position test points because of the fixed delivery.
- Brake and indicated specific fuel consumptions showed strong trends. In both cases the trend strengthened with engine power and exceeded the baseline set repeatability at all test points. These trends were consistent with those discussed earlier and highlight that up-fuelling was required to maintain torque at the partial rack travel test points. As already discussed, full throttle travel test points failed to hold the specified test torques despite consuming the same mass flow of fuel.

Nom. Speed [revs/min]-Torque [Nm]	1500-100	1400-186	1500-200	1600-237	1500-300	1800-293	1500-430	2000-354	2150-372
Engine Torque							-6.6		-7.2
Brake Power							-6.5		-7.2
Indicated Power	-10.0	0.7	-0.9	-2.4	-0.9	-5.3	-5.3	-5.4	-9.3
BMEP							-6.6		-7.1
PMEP	-2.5	-1.8	-6.7	-6.6	-5.3	-4.0	1.4	-11.4	-8.0
IMEP	-10.0	0.6	-0.9	-2.5	-1.0	-5.4	-5.4	-5.4	-9.2
BSFC	4.5	4.9	4.1	4.4	5.9	5.7	5.6	8.0	7.4
ISFC	10.1	5.0	4.3	7.6	7.1	10.0	5.5	13.6	12.1
Brake Thermal Efficiency	-4.0	-4.7	-4.0	-4.2	-5.6	-4.7	-6.0	-6.6	-6.9
Indicated Thermal Efficiency	-14.1	-4.7	-4.1	-7.2	-6.7	-9.7	-4.8	-11.2	-9.0
Inlet Air Mass Flow Rate	-5.5	-0.7	-0.4	-0.6	-0.5	-0.2	-0.5	0.8	1.2
Inlet Air Mass Flow Rate Parameter	-3.6	0.8	1.2	0.7	0.8	0.7	0.5	1.9	2.0
Compressor Pressure Ratio	0.3	0.8	1.8	1.2	1.8	1.8	0.3	3.0	0.4
Compressor Isentropic Efficiency	39.3	13.1	19.4	7.0	5.1	5.7	3.9	5.4	3.3
Intercooler Air Temperature Gradient	21.9	32.2	21.3	19.1	14.3	10.4	3.0	8.3	1.1
Volumetric Efficiency	-3.1	-0.2	-0.5	-0.6	-0.9	-0.6	0.1	-1.1	1.4
Exhaust Gas Mass Flow Rate Parameter	-2.4	0.3	2.1	1.5	4.9	0.9	4.6	0.8	2.2

Blue Cells = Negative % deviation from baseline average greater than *natural* variation

Red Cells = Positive % deviation from baseline average greater than *natural* variation

Green Cells = Negative % deviation from baseline average less than *natural* variation

Yellow Cells = Positive % deviation from baseline average less than *natural* variation

Table 24 Percentage Change In Performance Parameters From Baseline Due To Leaking Exhaust Valves

- Brake and indicated specific fuel consumptions increased significantly and showed well defined trends throughout the engine speed and torque range.
- Inlet air mass flow rate, mass flow rate parameter and exhaust gas mass flow rate parameter all decreased despite the volumetric air flow rate increasing. These appeared to conflict but the decreased inlet air pressure and increased temperature reduced the air density sufficiently giving a net reduction in air mass flow.
- Compressor pressure ratio and isentropic efficiency increased due to the increased turbocharger rotational speed discussed earlier in this chapter.
- The intercooler air temperature gradient increased, sometimes exceeding the baseline set repeatability. This increase was due to the higher compressor discharge temperatures caused by the increased compressor inlet temperature and compressor speed. The fact that in nearly all cases the percentage rise in compressor discharge temperature exceeded the percentage rise in inlet manifold temperature lead to the conclusion that more heat must have been rejected during intercooling.

8.6.3 Analysis Of Leaking Exhaust Valve Fuel Injection & Combustion Data

Both needle lift and fuel line pressure traces identified that there was little or no change in point of injection throughout the speeds and torques. Any deviations in timing were directly reflected in the point of ignition meaning no change in ignition delay. At the lower speeds and torques the initial rates of heat release exceeded those experienced during baseline testing. It was suspected that this faster rate of heat release was due to the increased delivery leading to a larger premixed charge and a higher charge air temperature. After a more vigorous phase of premixed

burning the rate of heat release tailed off during the diffusion burning phase. As speed and torque increased the initial heat release phase became almost identical to the baseline data particularly at maximum rack position and fixed delivery test points as shown in Figure 73. Cylinder compression pressure was reduced at all speeds and torques. This reduction was more noticeable at low speeds since the effective time period for leakage was longer.

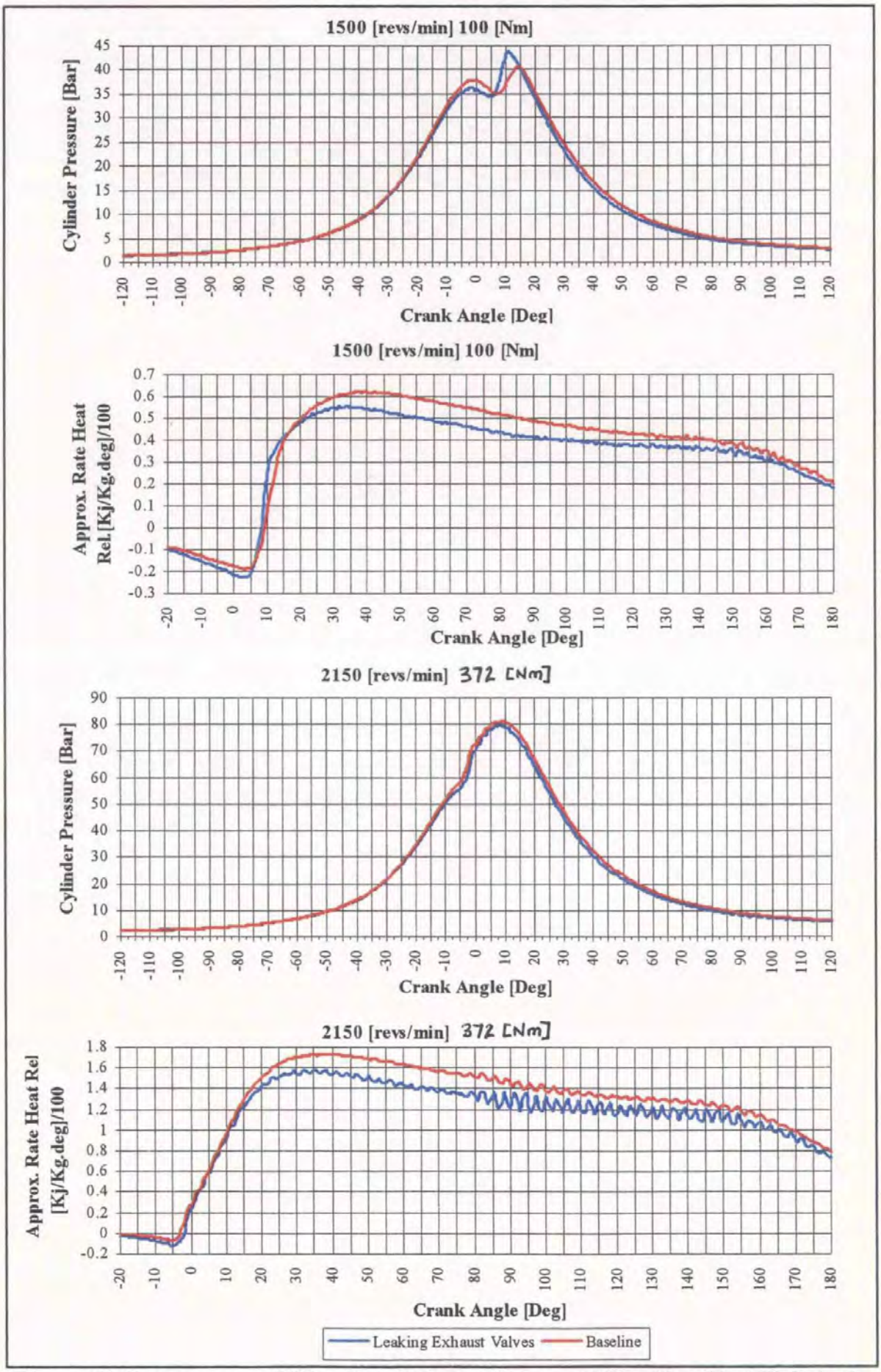

Figure 73 Comparisons Of Leaking Exhaust Valve and Baseline Heat Rel. And Cylinder Press. Data At 1500 [revs/min] 100 [Nm] And 2150 [revs/min] 372 [Nm]

8.7 Incorrect Fuel Pump Timing Experimental Results

Initially fuel pump timing on the test engine was retarded by 3° crank angle as discussed in Chapter 7, Section 7.6. Forty five separate engine tests were conducted over a two week period with the pump retarded by 3° crank angle. The results obtained showed some clear sensor and performance parameter deviations from the baseline data set. Based on these results, the degree of retardation was reduced to 1.5^{o} crank angle and a further forty five engine tests were conducted. These two sets of data of varying severity could then be used to test the neural networks ability to identify fault severity.

8.7.1 Analysis Of 3° Crank Angle Retarded Fuel Pump Timing Sensor Data

Table 25 shows the 16 sensor readings which deviated due to the introduction of the 3° retarded fuel pump timing. All trends showed positive deviations from the baseline set average.

- Inlet air volume flow rate showed a positive deviation although not always exceeding the baseline set repeatability. The maximum deviation occurred at 2150 [revs/min] and 372 [Nm]. The increased volume flow was caused by the higher turbocharger speed.
- The higher turbocharger speed also lead to increases in the compressor discharge and inlet manifold temperatures and pressures.
- All exhaust temperatures showed a strong increase and generally exceeded the baseline set repeatability throughout the torque and speed range.

Nom. Speed [revs/min]-Torque [Nm]	1500-100	1400-186	1500-200	1600-237	1500-300	1800-293	1500-430	2000-354	2150-372
Inlet Air Volume Flow Rate	0.1	0.6	1.1	1.2	1.4	1.0	0.28	1.5	0.2
Compressor Discharge Pressure	2.6	1.6	2.5	2.7	3.2	2.8	1.5	3.7	0.5
Compressor Discharge Temperature	1.0	0.6	0.7	0.9	1.2	0.9	0.5	1.2	0.1
Cylinder 1&2 Port Temperatures	2.3	2.1	2.4	3.0	3.1	2.2	0.6	1.1	-1.0
Cylinder 3 Port Temperature	4.2	3.0	1.9	2.4	2.6	2.3	0.4	2.0	0.6
Cylinder 4 Port Temperature	3.1	2.4	2.2	2.8	2.1	2.1	0.2	2.7	-0.6
Cylinder 5&6 Port Temperatures	5.7	3.6	3.1	3.9	4.2	2.7	1.2	3.7	1.2
Exhaust Manifold Pressure	5.1	-0.2	2.7	2.0	1.4	3.1	-2.0	3.0	1.0
Exhaust Manifold Temperature	2.3	2.5	2.1	3.5	3.7	3.2	1.2	2.2	0.1
Fuel Rack Position	18.9	14.6	13.4	12.6	9.8	9.1	0.1	7.6	0.3
Inlet Manifold Pressure	2.7	1.9	2.8	3.1	3.1	2.8	1.7	3.9	0.5
Inlet Manifold Temperature	2.7	0.2	0.4	0.4	0.6	0.5	0.3	0.6	0.0
Turbine Discharge Temperature	2.3	2.4	1.9	3.0	3.2	2.7	1.2	2.1	0.1
Turbine Discharge Pressure	2.4	1.0	1.2	1.3	1.4	1.2	0.9	1.0	1.0
Turbocharger Speed	2.1	1.4	5.2	4.5	4.7	3.4	1.9	3.3	-0.2
Fuel Mass Flow Rate	2.8	2.6	4.5	3.1	3.7	5.4	0.2	4.0	-2.2

Red Cells = Positive deviation from baseline average greater than *natural* variation

Yellow Cells = Positive deviation from baseline average less than *natural* variation

Table 25 Percentage Change In Sensor Readings From Baseline Due To 3° Crank Angle Retarded Pump Timing

The trend was weakened at both full throttle position test points. These increased temperatures were due to the inlet charge being hotter, up-fuelling to maintain the specified test torques and a delayed point of injection causing combustion to take place later in the cycle.

- Exhaust manifold and turbine discharge pressures showed minor increases which generally failed to exceed the baseline set repeatability. These increases were due to the delayed point of injection causing higher cylinder pressures throughout the expansion stroke and at the point of exhaust valve opening. Trends in combustion data are discussed more fully in Section 8.7.3.
- Turbocharger speed showed a reasonably positive trend which deviated outside the baseline set repeatability on several occasions. The increased speed was caused by the increased exhaust manifold pressure discussed above. This is further substantiated by the turbocharger speed actually reducing below the baseline average at 2150 [revs/min] and 372 [Nm]. This was due to delivery remaining constant at this test point.
- Fuel mass flow rate and rack position both showed healthy increases at all partial rack travel test points. This is consistent with the up-fuelling required to maintain the specified test torques and increased exhaust temperatures.

8.7.2 Analysis Of 3° Crank Angle Retarded Fuel Pump Timing Performance Parameters

Table 26 shows the twenty performance parameters which showed deviations due to 3° crank angle retarded fuel pump timing. No parameter showed a trend which consistently exceeded the baseline set repeatability. The best trends were seen in

Nom. Speed [revs/min]-Torque [Nm]	1500-100	1400-186	1500-200	1600-237	1500-300	1800-293	1500-430	2000-354	2150-372
Engine Torque							-1.9		-7.0
Brake Power							-1.8		-7.0
Indicated Power	-5.0	-0.7	-0.5	-2.1	-2.2	-2.9	-3.4	-0.9	-5.60
BMEP							-1.8		-7.0
IMEP	-4.9	-0.8	-0.6	-2.1	-2.3	-2.9	-3.4	-1.0	-5.6
BSFC	5.9	2.2	4.5	4.9	3.8	4.0	1.2	4.7	4.7
ISFC	3.74	3.5	5.2	6.7	5.7	6.4	4.1	5.4	5.3
Brake Thermal Efficiency	-5.5	-2.2	-4.3	-4.7	-3.7	-3.1	-1.9	-3.6	-4.5
Indicated Thermal Efficiency	-6.6	-3.3	-5.0	-6.6	-5.5	-6.7	-3.5	-4.3	-3.2
Inlet Air Mass Flow Rate	0.5	1.2	1.6	1.7	1.9	1.7	0.8	2.4	0.9
Inlet Air Mass Flow Rate Parameter	0.1	0.5	1.0	1.0	1.2	0.6	0.0	1.6	0.1
Compressor Pressure Ratio	-0.2	0.8	1.8	1.9	2.3	2.1	0.6	2.4	-0.2
Compressor Speed Parameter	-4.5	1.3	5.1	4.3	4.6	3.3	1.7	3.2	-0.3
Compressor Isentropic Efficiency	-3.4	7.2	11.4	5.6	2.7	2.2	0.3	1.5	0.1
Intercooler Air Temperature Gradient	-3.0	16.2	9.4	11.3	11.7	8.2	3.5	7.1	1.0
Volumetric Efficiency	1.1	-0.6	-0.8	-0.9	-0.7	-0.5	-0.6	-0.9	0.2
Exhaust Gas Mass Flow Rate	3.4	1.2	1.8	1.8	2.0	1.9	0.8	2.4	0.7
Exhaust Gas Mass Flow Rate Parameter	0.0	2.9	0.1	1.5	2.4	0.2	3.5	0.5	-0.3
Turbine Expansion Ratio	0.4	-1.2	1.4	0.7	0.1	1.8	-3.2	1.9	0.3
Turbine Speed Parameter	-5.1	0.2	4.2	2.7	2.9	1.8	1.2	2.1	-0.2

Blue/Red Cells = Negative/Positive deviation from baseline average greater than *natural* variation

Green/Yellow Cells = Negative/Positive deviation from baseline average less than *natural* variation

Table 26 Percentage Change In Performance Parameters From Baseline Due To 3° Retarded Fuel Pump Timing

BSFC, brake thermal efficiency, compressor pressure ratio & compressor speed parameter.

- Engine torque, BMEP and brake power all showed a reduction greater than the baseline set repeatability at the maximum engine power test point. The other maximum rack position test point also showed a reduction, but failed to exceed the baseline set repeatability indicating the fault's sensitivity to engine speed.
- IMEP and indicated power both showed a downward trend throughout the test speeds and torques.
- BSFC and ISFC showed strong trends identifying increased specific fuel consumptions. This further reinforces the suspicions of up-fuelling to maintain specified test torques identified from the sensor data in Section 8.7.1.
- Brake and indicated thermal efficiencies decreased in line with the increased specific fuel consumptions, as would be expected.
- Inlet air mass flow rate and mass flow rate parameter both showed small increases from the baseline data. These increases were due to the increased turbocharger speed and subsequent pressure ratio increase. These trends, together with turbocharger rotational speed, weakened at the full throttle position test points.
- Compressor speed parameter, pressure ratio and isentropic efficiency all increased and exceeded the baseline set repeatability occasionally. These increases diminished, as did the trend in turbocharger speed at the full throttle position test points. Turbocharger rotational speed, compressor pressure ratio and speed parameter all showed a negative deviation at 2150 [revs/min] and 372 [Nm].

- Exhaust gas mass flow and mass flow rate parameter showed a small increase for the majority of speeds and torques. This was due to increases in both inlet air and fuel mass flow rates.
- Turbine speed parameter increased but by a smaller margin than turbocharger rotational speed. This was due to the higher exhaust gas temperatures experienced at nearly all speeds and torques.
- The increase in turbine expansion ratio was caused by the increased exhaust manifold pressure. At 1400 [revs/min] and 186 [Nm] and 1500 [revs/min] and 430 [Nm] the expansion ratio fell below the baseline set data. Exhaust manifold pressure also followed this trend. The increased expansion ratio had the effect of increasing the turbocharger rotational speed as discussed above.

8.7.3 Analysis Of 3° Crank Angle Retarded Fuel Pump Timing Fuel Injection & Combustion Data

Table 27 shows the deviations in fuel injection and combustion data due to 3° crank angle retarded pump timing. The needle lift data confirmed that on average the injection was delayed by 3° crank angle. The duration of injection generally exceeded the baseline set repeatability for all partial rack position test points due to the up-fuelling required to maintain the specified test torques. Consequently, end of injection was retarded by more than 3° crank angle. The trends in needle lift data were very closely matched by the fuel line pressure data, which showed excellent repeatability. These trends can be seen in Figures 74, 75 and 76.

Nom. Speed [revs/min]-Torque [Nm]	1500-100	1400-186	1500-200	1600-237	1500-300	1800-293	1500-430	2000-354	2150-372
Pmax Cylinder [% change]	-9.0	-11.2	-9.9	-9.6	-9.7	-6.3	-8.3	-7.1	-10.6
Overall Air/Fuel Ratio [% change]	-0.6	-1.5	-2.9	-3.0	-1.5	-2.3	0.7	-1.1	3.5
Degrees CA Max. Fuel Line Pressure	2.4	2.8	2.7	3.3	3.3	2.1	2.4	2.3	0.8
Degrees CA Est. Pump Dischg. Point	2.4	2.8	2.8	3.6	3.4	2.4	2.1	2.6	3.7
Degrees CA End Of Pump Dischg	2.7	2.9	3.1	3.7	3.5	2.0	1.9	3.6	3.2
Degrees CA Pump Discharge Period	0.3	0.1	0.3	0.2	0.1	-0.4	-0.2	1.0	-0.5
Point Of Injection	2.5	2.7	2.5	3.3	3.3	2.2	2.5	2.7	3.1
End Of injection	2.5	3.0	2.9	3.6	3.4	3.0	2.6	3.4	2.7
Duration Of Injection	0.1	0.3	0.4	0.4	0.1	0.8	0.1	0.7	-0.4
Degrees CA Pmax Cylinder	-13.2	4.0	3.9	3.3	3.3	-0.2	1.4	-0.8	-0.5
Point Of Ignition	4.0	-0.1	2.8	4.0	4.1	1.2	1.2	2.3	3.4

Blue Cells = Negative deviation from baseline average greater than *natural* variation

Red Cells = Positive deviation from baseline average greater than *natural* variation

Green Cells = Negative deviation from baseline average less than *natural* variation

Yellow Cells = Positive deviation from baseline average less than *natural* variation

All measurements in degrees crank angle unless otherwise stated.

Table 27 Deviations In Fuel Injection & Combustion Data From Baseline Due To 3° Retarded Pump Timing

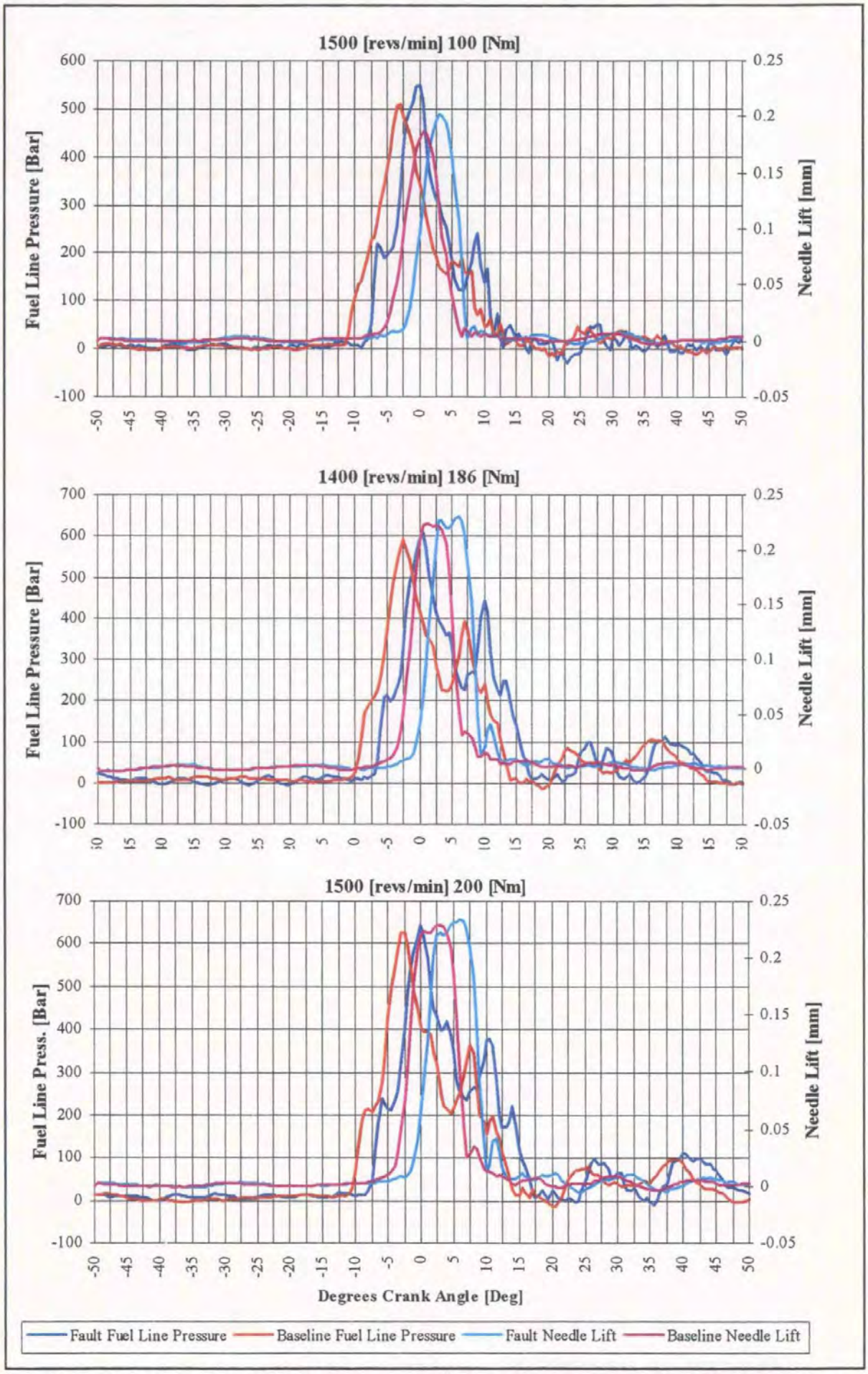

Figure 74 Comparison Of Baseline And 3° Crank Angle Retarded PumpTiming Fuel Line Pressure & Needle Lift Data (Three Lowest Power Test Points)

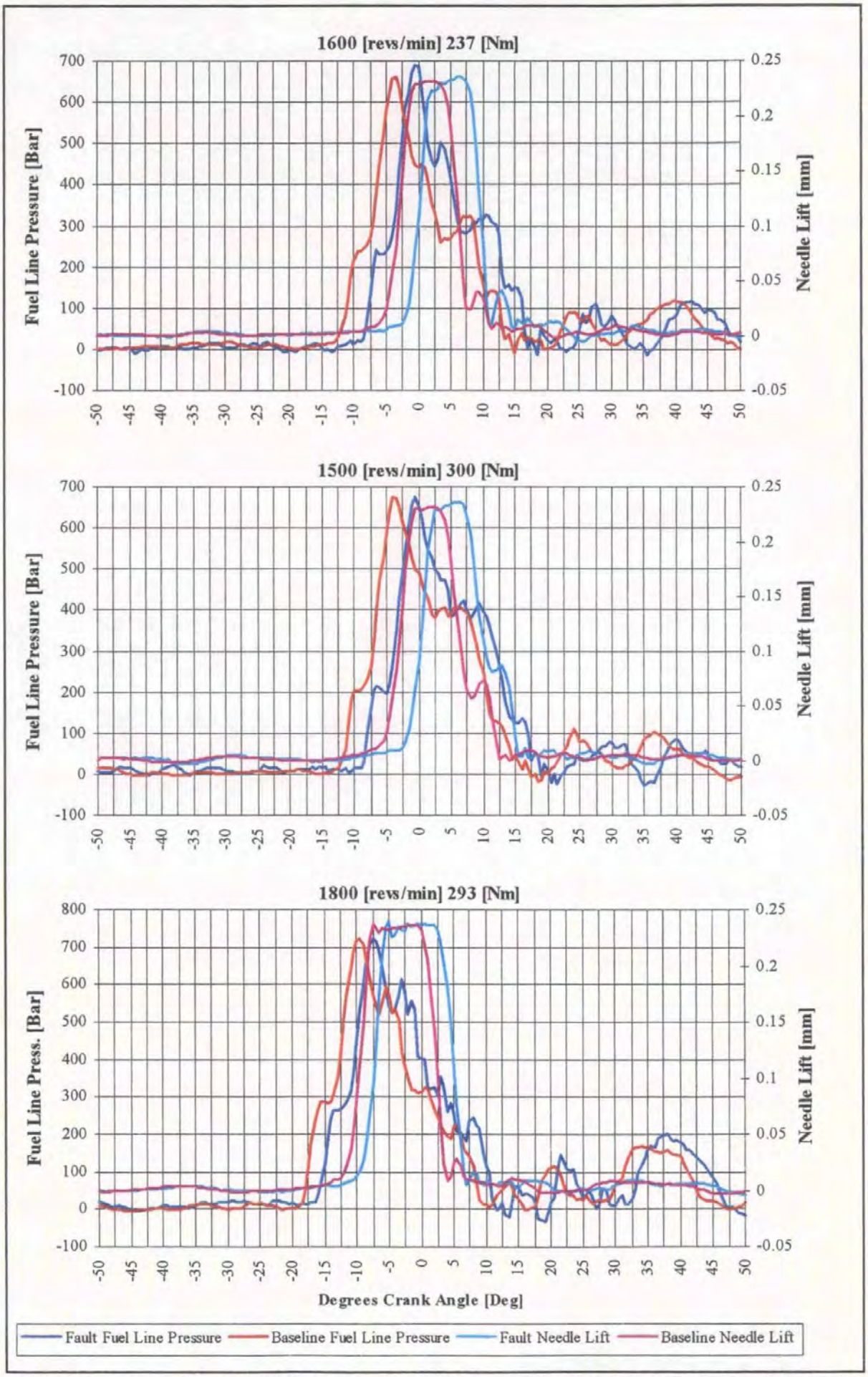

Figure 75 Comparison Of Baseline And 3° Crank Angle Retarded PumpTiming Fuel Line Pressure & Needle Lift Data (Three Medium Power Test Points)

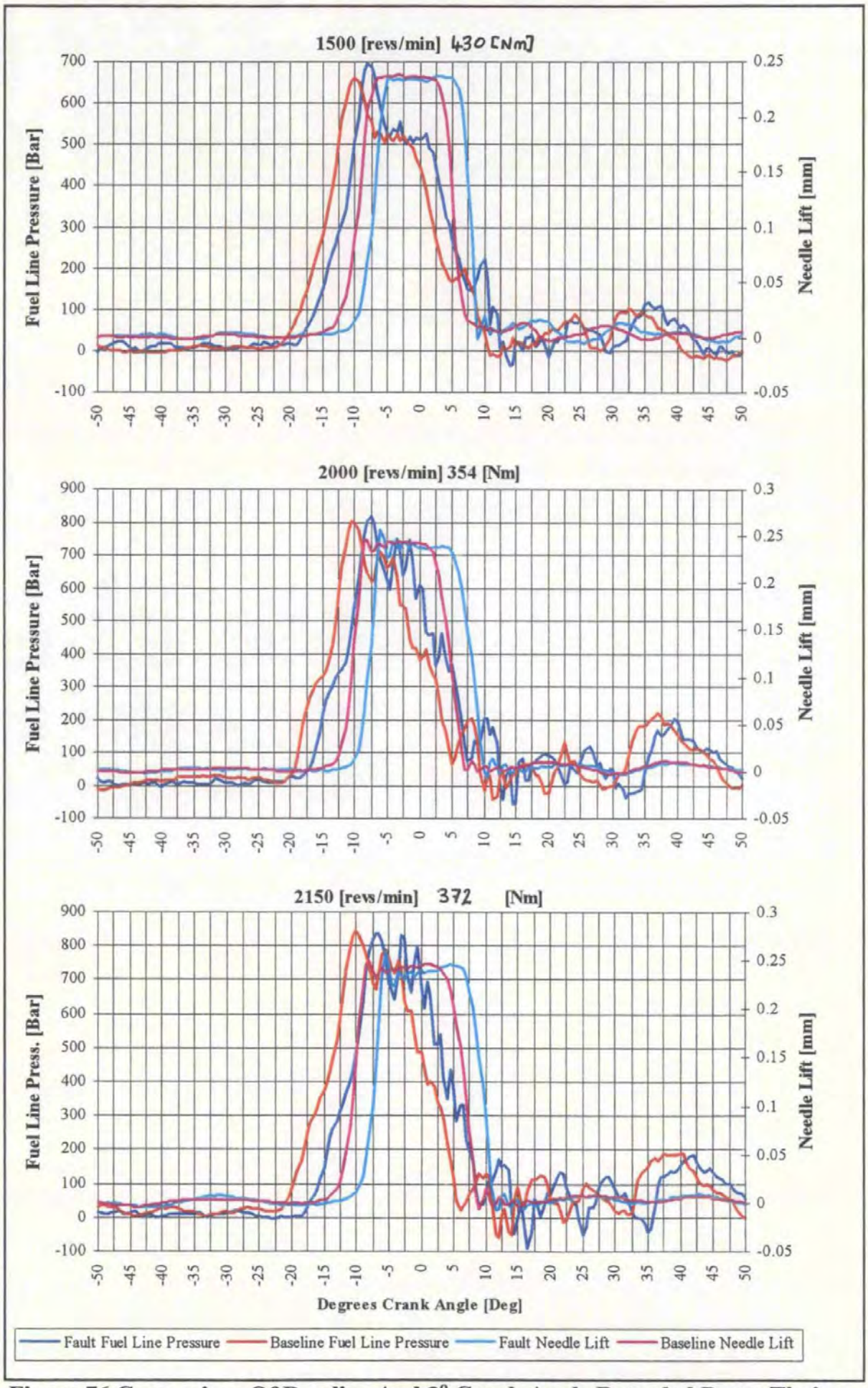

Figure 76 Comparison Of Baseline And 3° Crank Angle Retarded Pump Timing Fuel Line Pressure & Needle Lift Data (Three High Power Test Points)

Due to the retarded injection timing the point of ignition also retarded. This led to consistently lower maximum cylinder pressures which, especially at lower speeds and torques, were also retarded. The reduction in cylinder pressures was due to less premixed charge being available, lower cylinder compression pressures and the increase in crank throw from the crank centre line at the point of ignition.

In addition to the retarded point of ignition, the approximate heat release diagrams also showed a higher sustained heat release during the diffusion burning phase. This is consistent with the up-fuelling identified from the slow speed sensor data, performance parameters and duration of injection data. Figure 77 compares baseline and 3° crank angle retarded pump timing heat release and cylinder pressure data. This data was taken at 1500 [revs/min] and 200 [Nm] and was typical of the trend throughout the speed and torque range.

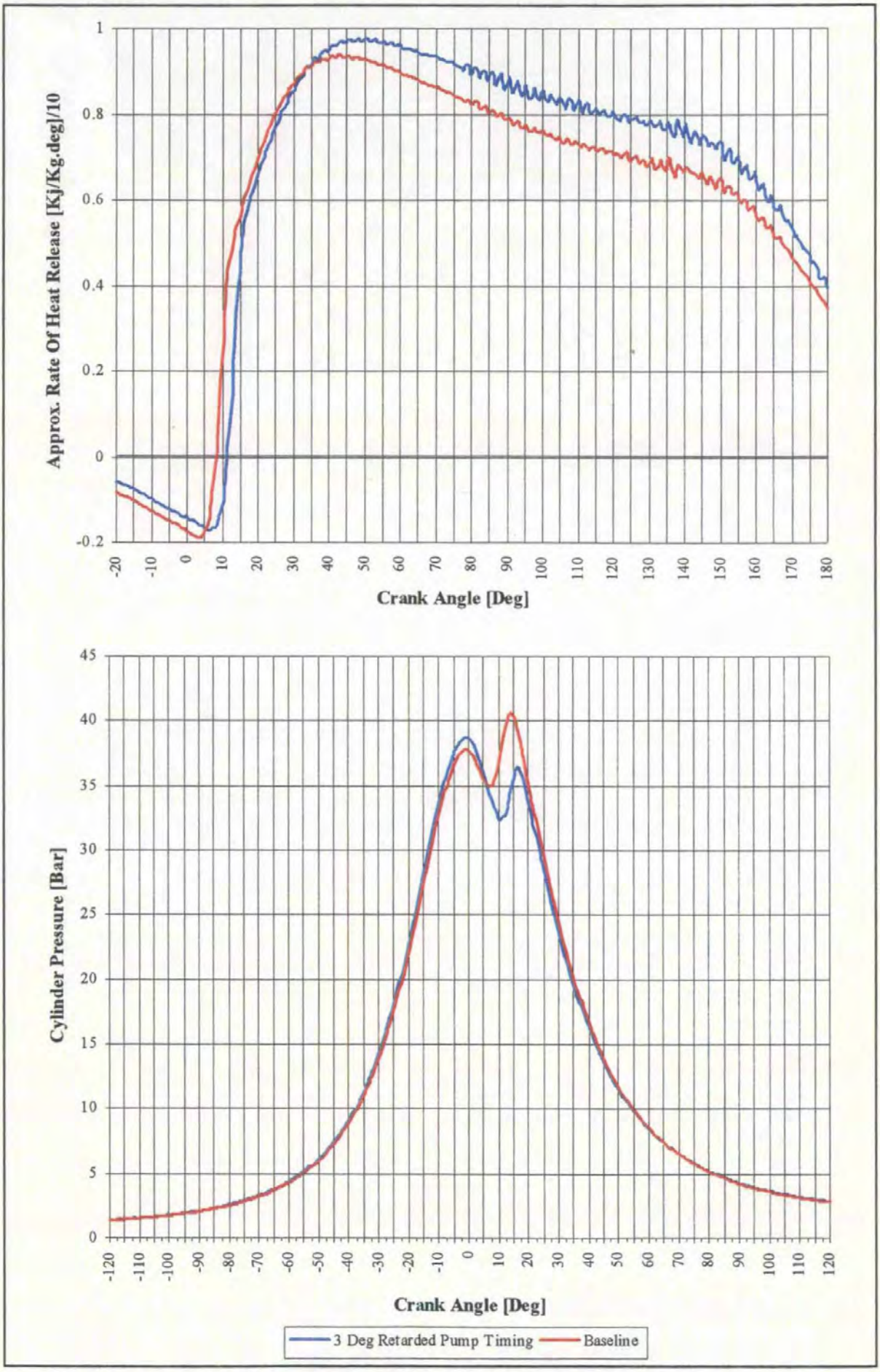

Figure 77 Comparison Of Baseline And 3° Crank Angle Retarded Pump Approximate Heat Release & Cylinder Pressure Data At 1500 [revs/min] 200 [Nm]

8.7.4 Analysis Of 1.5° Crank Angle Retarded Fuel Pump Timing Data

Table 28 shows all of the sensor deviations from the average baseline data due to 1.5° crank angle retarded pump timing. All of the sensor readings which showed a deviation were also identified at 3° crank angle retarded pump timing. Three sensor readings which showed deviations at 3° retarded pump timing failed to show any trend at 1.5° retarded pump timing. These were compressor discharge temperature, inlet manifold temperature and turbine discharge pressure. Those sensors which deviated in both cases generally showed less of a deviation at 1.5° than 3° retarded pump timing. This gives added confidence that any deviations were due to the fault introduction rather than faulty or spurious results. Since the trends in the 1.5° performance parameter data are essentially replications of the 3° retarded pump timing data they will not be discussed in any further detail. Table 29 shows performance parameter data deviations from baseline due to 1.5° retarded pump timing. All of the performance parameters which showed a deviation from the baseline average due to the introduction of the 1.5° retarded pump timing were identified in the original 3° retarded pump timing testing. As with the sensor data the trends in the performance parameters generally showed a weakening at 1.5° retardation, as might be expected. Table 29 shows the performance parameter percentage changes from the baseline set average due to the introduction of 1.5° retarded pump timing. The trends which developed as a result of the 1.5° retarded pump timing will not be discussed in any further detail since they follow the same pattern as those seen in the 3° retarded pump timing data.

Nom. Speed [revs/min]-Torque [Nm]	1500-100	1400-186	1500-200	1600-237	1500-300	1800-293	1500-430	2000-354	2150-372
Air Volume Flow Rate	0.6	1.0	1.3	1.1	1.1	1.1	0.5	1.9	-0.1
Compressor Discharge Pressure	1.9	0.8	1.4	1.8	2.0	1.5	0.8	3.1	-0.8
Cylinder 1&2 Port Temperatures	3.0	1.7	1.9	3.0	2.4	1.9	0.7	1.2	-1.9
Cylinder 3 Port Temperature	4.0	1.5	0.1	1.9	2.6	1.5	-0.2	1.5	-0.7
Cylinder 4 Port Temperature	3.1	1.9	1.7	2.5	1.5	1.9	1.7	2.2	-1.0
Cylinder 5&6 Port Temperatures	6.8	3.6	2.9	4.3	4.0	3.3	1.1	3.1	0.6
Exhaust Manifold Pressure	5.1	-1.0	1.6	0.1	1.9	1.0	1.3	2.5	-0.3
Exhaust Manifold Temperature	3.9	3.0	2.3	3.8	3.8	2.8	1.2	2.1	-0.8
Fuel Rack Position	17.4	11.2	9.4	10.1	7.8	7.1	-0.2	6.7	0.9
Inlet Manifold Pressure	2.2	1.2	2.1	2.1	2.3	1.9	1.2	3.3	-0.5
Turbine Discharge Temperature	3.8	2.9	2.00	3.0	2.9	2.2	0.9	1.5	-0.9
Turbocharger Speed	1.8	5.0	5.8	5.1	4.8	3.6	2.4	3.6	-0.9
Fuel Mass Flow Rate	4.9	3.1	3.0	2.8	2.5	4.3	0.5	3.7	-4.3

Red Cells = Positive deviation from baseline average greater than *natural* variation

Yellow Cells = Positive deviation from baseline average less than *natural* variation

Table 28 Percentage Deviations In Sensor Data From Baseline Due To 1.5° Retarded Pump Timing

Nom. Speed [revs/min]-Torque [Nm]	1500-100	1400-186	1500-200	1600-237	1500-300	1800-293	1500-430	2000-354	2150-372
Engine Torque							-0.6		-8.3
Brake Power							-0.5		-8.2
Indicated Power	-3.0	-1.3	-1.1	1.3	-1.0	-0.7	-2.3	-0.8	-6.2
BMEP							-0.6		-8.3
IMEP	-3.00	-1.4	-1.2	1.2	-1.1	-0.8	-2.4	-1.0	-6.3
BSFC	5.8	3.1	3.7	4.2	2.3	3.0	0.1	4.3	4.00
ISFC	4.0	4.6	4.3	3.3	3.1	3.0	3.1	5.0	3.8
Brake Thermal Efficiency	-5.4	-3.0	-3.5	-4.0	-2.2	-2.1	-0.8	-3.29	-3.8
Indicated Thermal Efficiency	-6.8	-4.4	-4.2	-3.1	-3.1	-3.7	-2.6	-3.9	-1.7
Inlet Air Mass Flow Rate	0.5	1.2	1.5	1.5	1.6	1.7	1.1	2.5	0.9
Inlet Air Mass Flow Rate Parameter	1.1	1.3	1.7	1.5	1.6	1.3	0.8	2.5	0.4
Compressor Pressure Ratio	0.5	1.2	1.9	2.2	2.3	2.0	1.0	3.1	-0.6
Compressor Speed Parameter	-4.3	5.4	6.3	5.5	5.2	4.0	2.8	4.0	-0.4
Compressor Isentropic Efficiency	43.5	10.8	10.8	4.8	1.5	0.1	-0.6	1.9	-1.2
Volumetric Efficiency	0.9	-0.2	-0.7	-0.7	-0.9	-0.2	-0.4	-0.9	0.4
Exhaust Gas Mass Flow Rate	3.5	1.3	1.7	1.5	1.7	1.8	1.0	2.5	0.6
Exhaust Gas Mass Flow Rate Parameter	0.8	3.9	1.1	3.4	1.7	2.1	0.3	1.0	0.5
Turbine Expansion Ratio	2.2	-0.2	2.5	1.2	2.8	1.9	2.0	3.4	1.5
Turbine Speed Parameter	-6.2	3.4	4.7	3.1	2.8	2.1	1.8	2.5	-0.5

Blue/Red Cells = Negative/Positive deviation from baseline average greater than *natural* variation

Red/Yellow Cells = Positive/Negative deviation from baseline average greater than *natural* variation

Table 29 Percentage Deviations In Performance Parameters From Baseline Due To 1.5° Retarded Pump Timing

Table 30 summarises the deviations in fuel injection and combustion data from the baseline average due to 1.5° retarded pump timing. All of the trends were essentially a replication of the 3° retarded pump timing trends except they were generally weaker. The point of injection data shows that the pump was retarded between 1.44° and 2.7° crank angle. The fact that the mean deviation was greater than 1.5° had no detrimental effect on the validity of the data. The mean was substantially less than 3° and therefore remained a valid data set to test the network's ability to distinguish between fault severities.

Examination of the needle lift, fuel line pressure, cylinder pressure and heat release data revealed similar trends to those seen for the 3° retarded pump timing. Figure 78 shows a comparison between baseline and 1.5° retarded pump timing needle lift, fuel line pressure, cylinder pressure and heat release data. These curves show the deviations encountered at 1500 [revs/min] and 200 [Nm] but were typical of the trends seen throughout the speed and torque range.

The trends seen in the 1.5° retarded fuel pump data are not discussed any further since the reasons behind the deviations in the fuel injection and combustion data have been discussed in Section 8.7.3.

Nom. Speed [revs/min]-Torque [Nm]	1500-100	1400-186	1500-200	1600-237	1500-300	1800-293	1500-430	2000-354	2150-372.
Pmax Cylinder [% change]	-8.7	-7.9	-7.9	-6.9	-6.7	-4.2	-3.9	-5.6	-9.7
Overall Air/Fuel Ratio [% change]	-2.7	-1.9	-1.6	-2.9	-0.6	-1.3	0.7	-0.7	5.9
Degrees CA Max Fuel Line Pressure	2.3	2.1	2.1	2.2	2.7	1.3	1.3	2.1	-2.0
Degrees CA Est. Pump Dischg. Point	2.3	2.2	2.3	2.8	2.9	1.7	1.5	2.2	3.4
Degrees CA End Of Pump Dischg	2.6	2.1	2.2	2.9	2.0	1.7	1.6	2.1	2.7
Point Of Injection	2.4	2.1	2.1	2.5	2.7	1.5	1.4	2.2	2.7
End Of injection	2.5	2.1	2.3	2.7	2.1	2.3	1.3	2.9	2.3
Duration Of Injection	0.1	0.1	0.2	0.3	-0.6	0.8	-0.2	0.7	-0.4
Degrees CA Pmax Cylinder	-13.3	2.6	2.7	2.6	2.2	-0.2	0.4	-1.1	-0.2
Point Of Ignition	3.5	0.5	1.8	2.8	3.0	0.5	0.2	1.9	3.2

Blue Cells = Negative deviation from baseline average greater than *natural* variation

Red Cells = Positive deviation from baseline average greater than *natural* variation

Green Cells = Negative deviation from baseline average less than *natural* variation

Yellow Cells = Positive deviation from baseline average less than *natural* variation

All measurements in degrees crank angle unless otherwise stated.

Table 30 Deviations In Fuel Injection & Combustion Data From Baseline Due To 1.5° Retarded Pump Timing

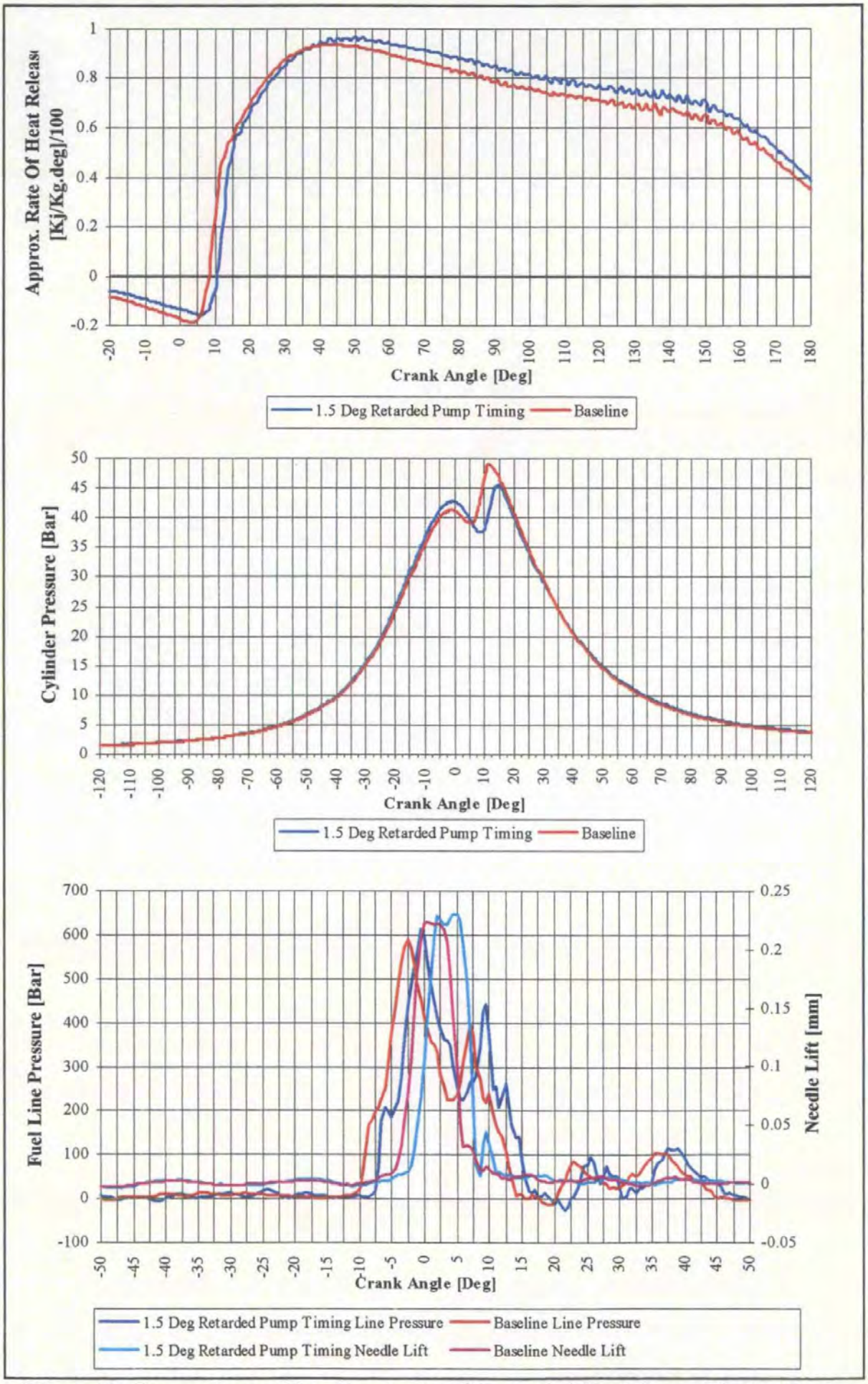

Figure 78 Comparison of Baseline And 1.5° Retarded Fuel Pump Timing Fuel Injection And Combustion Data At 1500 [revs/min] and 200 [Nm]

8.8 Low Opening Pressure Injector Experimental Results

The injector used for engine test was obtained from a marine engine which was to the same build list as the test engine. It had been operating in a marine application but the duration of engine running and time from last service were both unknown. As a result of the rig testing discussed in Chapter 7, Section 7.7, it was identified as having a low opening pressure. The as received condition showed a breaking pressure of 155 [Bar] against a specification of 210 [Bar]. The injector was fitted to No. 6 cylinder of the test engine in the as received condition. Number 6 was the only cylinder which could be monitored by the high speed fuel injection and combustion instrumentation.

Forty five separate engine tests were conducted over a two week period to quantify the effects of a low opening pressure injector on engine performance. The following sections present and discuss the salient differences in results between the average baseline data and the data recorded with the faulty injector fitted.

8.8.1 Analysis Of Low Opening Pressure Injector Sensor & Performance Parameter Data

Table 31 shows that only two performance parameters showed a weak trend. BSFC increased marginally but never deviated sufficiently to exceed the baseline set repeatability. Similarly, brake thermal efficiency showed a small decrease at the majority of test points. It was thought because these trends are based on minimal deviations they could not be used for a positive diagnosis.

Nom. Speed [revs/min]-Torque [Nm]	1500-100	1400-186	1500-200	1600-237	1500-300	1800-293	1500-430	2000-354	2150-372
BSFC	1.3	0.7	0.7	0.7	0.2	0.7	-0.9	1..0	-0.1
Brake Thermal Efficiency	-0.6	-0.7	-0.7	-0.7	-0.2	0.1	0.2	-0.2	0.0
Cylinder 1&2 Port Temperatures	0.2	-2.2	-1.8	-1.3	-0.6	-0.6	-0.2	-1.1	-0.8
Cylinder 3 Port Temperature	1.6	-1.8	-2.3	-2.4	-1.0	-1.5	-1.0	-0.3	-1.2
Cylinder 4 Port Temperature	1.3	-2.6	-2.4	-1.6	-2.6	-1.2	-0.7	2.8	-0.1
Cylinder 5&6 Port Temperatures	3.6	1.6	1.1	0.8	1.5	0.5	0.5	-0.2	0.3
Exhaust Manifold Temperature	0.9	-1.0	-1.0	-0.7	-0.2	-0.9	-0.2	-0.3	-0.6
Turbine Discharge Temperature	1.2	-0.6	-0.7	-0.8	-0.5	-0.7	-0.3	-0.2	-0.7

Blue Cells = Negative % deviation from baseline average greater than *natural* variation

Red Cells = Positive % deviation from baseline average greater than *natural* variation

Green Cells = Negative % deviation from baseline average less than *natural* variation

Yellow Cells = Positive % deviation from baseline average less than *natural* variation

Table 31 Percentage Deviations In Sensor And Performance Data From Baseline Due To A Low Opening Pressure Injector

Cylinder port 5 & 6 exhaust gas temperature showed a marginal increase at the majority of torques and speeds. Despite this increased port temperature, all other exhaust temperatures showed a decrease. This was because the low opening pressure injector fitted to No. 6 cylinder had a detrimental effect on the fuel pump line to line balance causing a de-fuel on cylinders 1 to 5. The net impact of this was a reduction in collective exhaust manifold and turbine discharge temperatures.

8.8.2 Analysis Of Low Opening Pressure Injector Fuel Injection And Combustion Data

Table 32 shows a summary of the deviations in the fuel injection and combustion data due to the introduction of a low opening pressure injector in No. 6 cylinder. The strongest trend was the reduction in maximum fuel line pressure, as might be expected. The point of injection advanced and the duration of injection increased due to the reduced injector spring pre load. This advanced point of injection lead to an advanced position of maximum cylinder pressure and point of ignition in the majority of cases.

By far, the best deviations were found in the fuel line pressure data. Figures 79, 80 and 81 show the deviations between the baseline and low opening pressure injector fuel line pressure and needle lift data.

Nom. Speed [revs/min]-Torque [Nm]	1500-100	1400-186	1500-200	1600-237	1500-300	1800-293	1500-430	2000-354	2150-372
Degrees CA Max Fuel Line Pressure	-15.9	-12.4	-17.4	-12.9	-15.2	-17.2	-9.3	-8.0	-6.8
Point Of Injection	-0.2	-1.0	-0.6	-0.6	-0.1	-1.2	-1.4	0.2	0
Duration Of Injection	0.1	0.9	0.8	0.9	-0.5	1.3	0.7	0.2	1.0
Degrees CA Pmax Cylinder	-1.0	-1.5	-0.3	-0.9	-0.1	0.5	-0.1	-0.7	0.2
Point Of Ignition	-0.3	-3.4	-1.8	-0.7	-0.1	-1.8	-2.3	0.2	0.4

Blue Cells = Negative % deviation from baseline average greater than *natural* variation

Red Cells = Positive % deviation from baseline average greater than *natural* variation

Green Cells = Negative % deviation from baseline average less than *natural* variation

Yellow Cells = Positive % deviation from baseline average less than *natural* variation

All measurements in degrees crank angle unless otherwise stated.

Table 32 Deviations In Fuel Injection & Combustion Data From Baseline Due To A Low Opening Pressure Injector

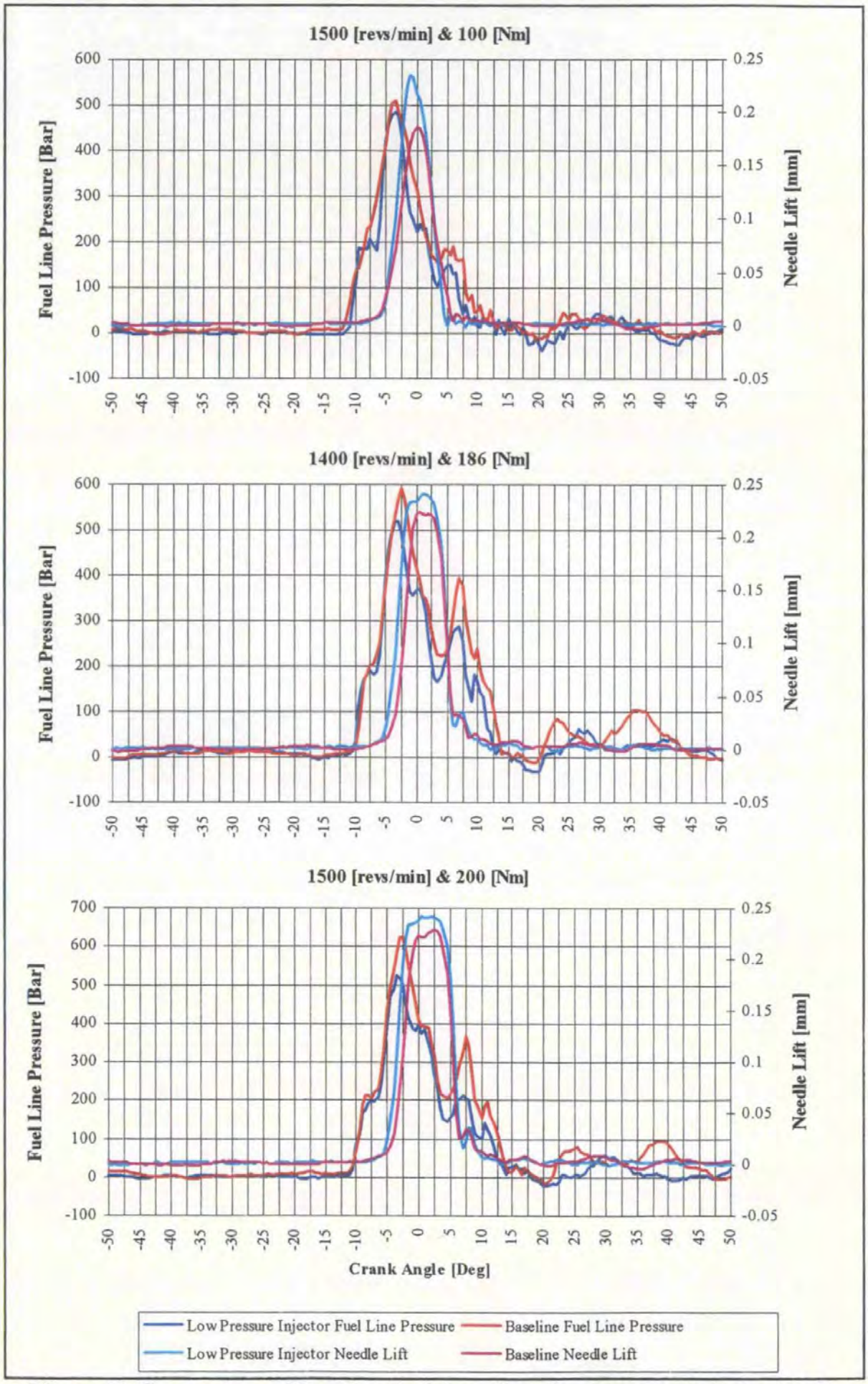

Figure 79 Comparison of Baseline And Low Opening Pressure Injector Fuel Line Pressure And Needle Lift (Low Power Points)

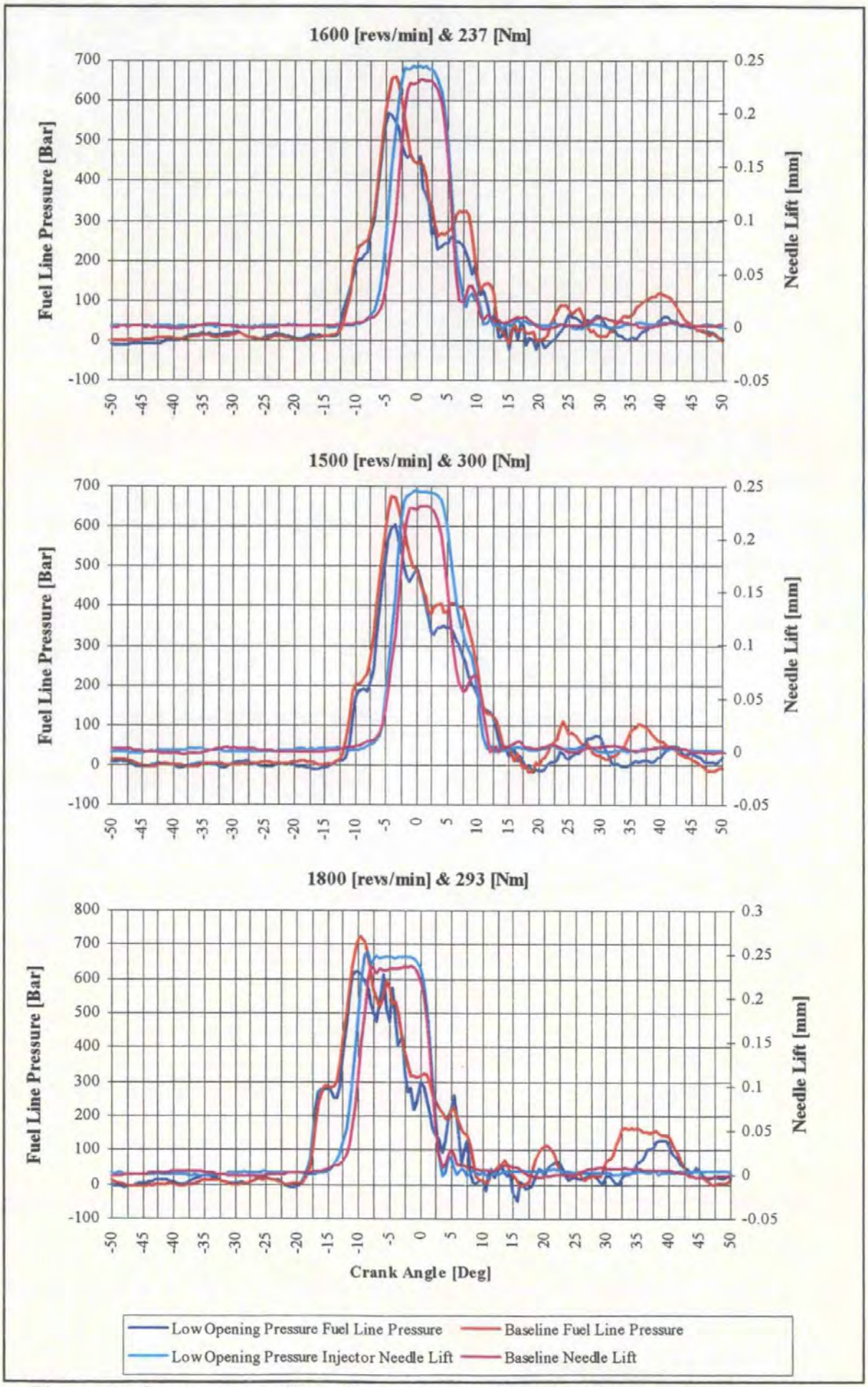

Figure 80 Comparison of Baseline And Low Opening Pressure Injector Fuel Line Pressure And Needle Lift (Medium Power Points)

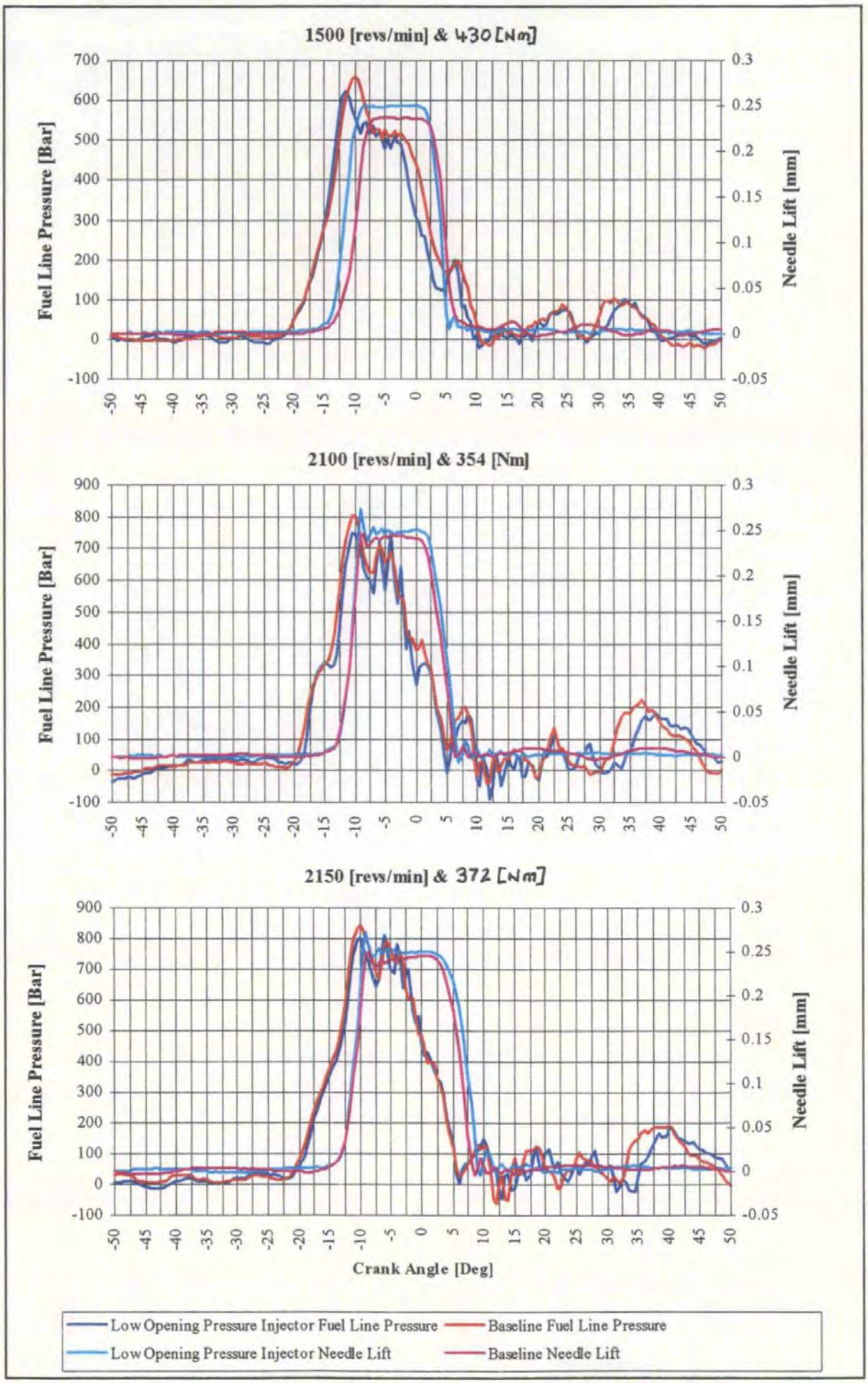

Figure 81 Comparison of Baseline And Low Opening Pressure Injector Fuel Line Pressure And Needle Lift (High Power Points)

At all test points, except those at full throttle, the rising edge of the fuel line pressure trace showed a marked step at the point of injector needle lift. The low opening pressure injector consistently showed a lower fuel line pressure at the rising edge step. In all cases the maximum fuel line pressure and subsequent pressure peaks at the crest of the trace were reduced. At all test points, except maximum power, the falling edge of the trace showed a reduced pressure. This feature was particularly apparent at the point of needle closure. These distinct trends combined with the excellent repeatability of the fuel line pressure data made this data particularly suitable for diagnostics.

Figure 82 shows a comparison between baseline and low opening pressure injector approximate heat release and cylinder pressure data taken at 1500 [revs/min] and 200 [Nm]. The trends seen at this speed and torque were typical of those throughout the speed and torque range. The heat release data showed that the point of ignition is advanced. This was a direct result of the advanced point of injection caused by the lower spring pre-load. The heat release data also showed that the rate of heat release for the low opening pressure injector was reduced in the initial premixed burning phase. This was due to the poorer spray atomisation and penetration identified by the rig testing discussed in Chapter 7, Section 7.7.6. Despite the reduced rate of heat release during premixed burning the rate of heat release remains higher throughout the diffusion burning phase for the low opening pressure injector. This is consistent with the poorer atomisation, longer period of injection, up-fuelling and higher exhaust temperatures for this cylinder.

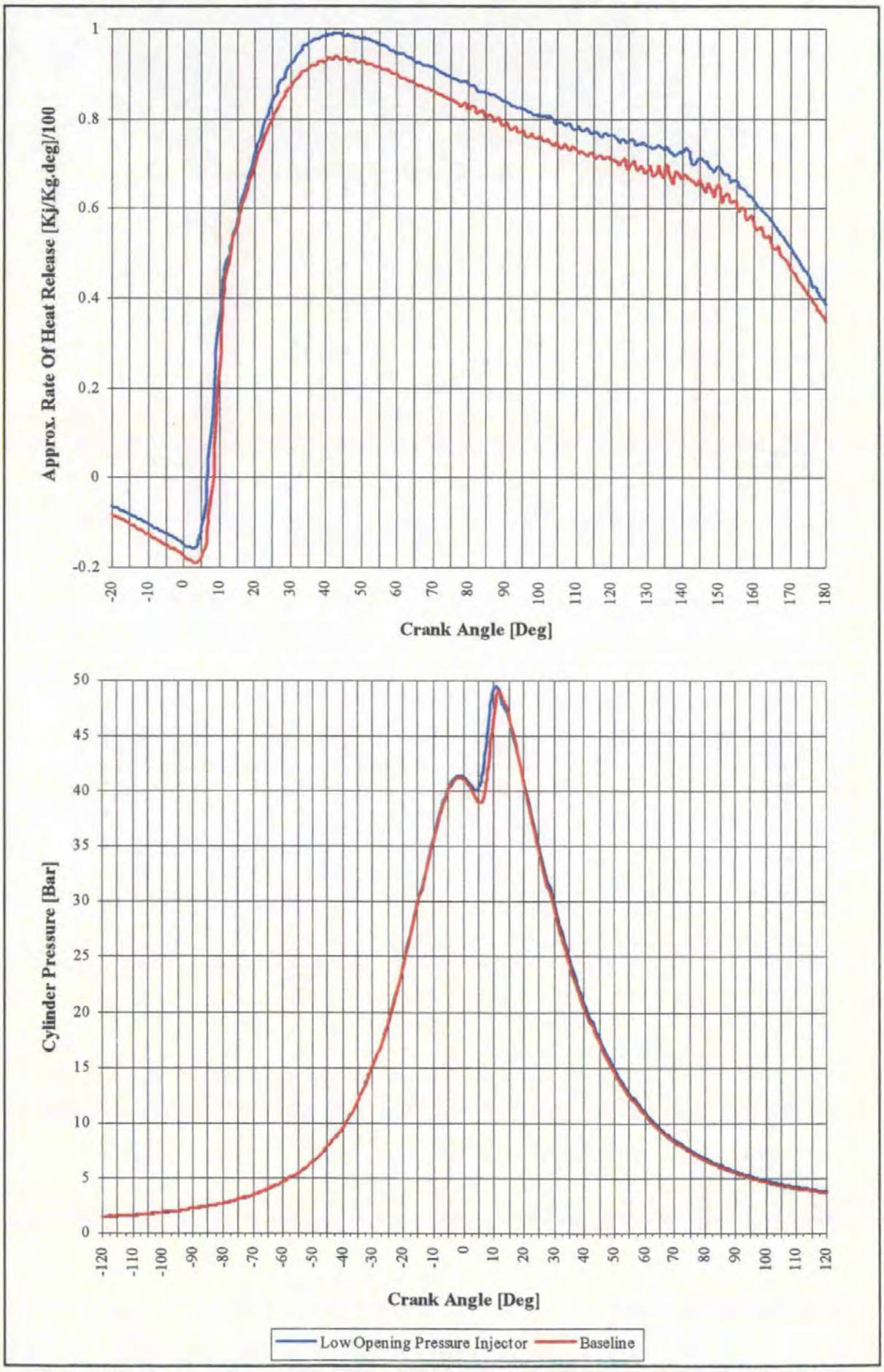

Figure 82 Comparison of Baseline And Low Opening Pressure Injector Fuel Line Pressure Heat Release & Cylinder Pressure Data At 1500 [revs/min] & 200 [Nm]

8.9 Blocked Injector Experimental Results

The injector used for engine testing was obtained from an engine which had been operating in the field. The injector was identified as having one of the four nozzle holes blocked by rig testing as discussed in Chapter 7. On completion of the rig testing the injector was installed into cylinder No. 6 of the test engine in the as received condition. When fitted, forty five separate engine tests were conducted over a four week period.

8.9.1 Analysis Of Blocked Injector Sensor & Performance Parameter Data

Eight performance parameters and three sensor readings deviated from the baseline set due to the introduction of a blocked injector nozzle, as shown in Table 33. Engine torque, brake power and, consequently, BMEP all showed reductions at the full throttle position test points. The baseline set repeatability was only exceeded at the maximum power test point. BSFC and ISFC both showed increases throughout the engine speed and torque range. The trend in BSFC only exceeded the baseline set repeatability at the lowest power test point. ISFC showed a more positive trend because of the lower IMEP values experienced throughout the speed and torque range. Cylinder 5 & 6 exhaust port temperatures showed a decrease despite a small, erratic, trend in increased fuel rack position. In general, sensor and performance parameter deviations were small with the exception of the two highest powers.

Nom. Speed [revs/min]-Torque [Nm]	1500-100	1400-186	1500-200	1600-237	1500-300	1800-293	1500-430	2000-354	2150-372
Engine Torque							-0.0856		-3.3994
Brake Power							0.0766		-3.2487
Indicated Power	-3.6909	-1.7441	-2.7585	-3.9567	-4.1068	-2.8383	-6.6282	-6.9799	-9.3952
BMEP							-0.0414		-3.3511
IMEP	-3.7448	-1.9491	-2.9221	-4.1086	-4.2682	-3.0018	-6.7750	-7.2651	-9.5026
BSFC	1.0234	1.4059	0.8941	0.2016	1.4574	1.4616	0.0890	1.9930	1.7045
ISFC	0.8503	3.5666	3.4169	3.8703	5.5034	2.9931	7.4606	7.9551	9.0515
Brake Thermal Efficiency	-0.3060	-1.4424	-0.8860	-0.2126	-1.4932	-0.6837	-0.8226	-1.1370	-1.7551
Indicated Thermal Efficiency	-3.3670	-3.7195	-3.5155	-4.1511	-5.9229	-3.9526	-7.5944	-7.7114	-7.8009
Cylinder 5&6 Port Temperatures	2.9410	-0.5737	-0.9389	-0.4925	0.6931	0.0802	-2.7947	-1.5834	-2.1712
Fuel Rack Position	5.5490	2.1688	1.3940	2.4659	1.5333	2.0210	-0.0675	4.1828	1.0745

Blue Cells = Negative deviation from baseline average greater than *natural* variation

Red Cells = Positive deviation from baseline average greater than *natural* variation

Green Cells = Negative deviation from baseline average less than *natural* variation

Yellow Cells = Positive deviation from baseline average less than *natural* variation

Table 33 Percentage Deviations In Sensor & Performance Parameter Data From Baseline Due To A Blocked Injector

8.9.2 Analysis Of Blocked Injector Fuel Injection & Combustion Data

Table 34 summarises the fuel injection and combustion results. The point of maximum fuel line pressure advanced as might be expected since the effective flow area of the nozzle was reduced. The point of fuel pump discharge was also shown to be advanced. It was thought, however, that this was not true and the data was misleading. Performance Monitor determined the point of discharge by identifying the point at which the pressure trace exceeds 7.5% of the maximum line pressure. In this instance a fuel line pressure rise of 7.5% was achieved earlier in the cycle due to reduced effective flow area of the nozzle. Duration of injection increased due to the reduced volume flow rate. The reduction in flow caused the line pressure to be sustained above the nozzle opening pressure for a greater period of time.

The fuel line pressure data showed some clear, repeatable, trends which appeared to be engine speed and hence injection rate dependant. At low engine speeds the blocked injector nozzle always showed an increased initial rate of fuel line pressure rise. After maximum fuel line pressure had been achieved there was little difference between the blocked and baseline injector nozzles.

At higher engine speeds the increased initial rate of fuel line pressure rise was still evident. After the point of maximum fuel line pressure, the blocked injector nozzle trace became more erratic and, generally, the line pressure was greater than for the baseline injector.

The needle lift traces generally followed the profile of the fuel line pressure traces. The blocked nozzle injector showed a significantly increased maximum lift over the baseline. It was suspected that this difference was due to the increased wear of the blocked injector spindle and body since this injector was returned from a field engine which had probably run more than several hundred hours. All of the injection data trends can be seen in Figures 83, 84 & 85.

The rig testing conducted in Chapter 7, Section 7.7.5 showed that the degree of spray penetration and atomisation both increased due to the blockage of one nozzle hole. The affect of this on combustion was to reduce the mass of fuel available, but increase atomisation and evaporation for premixed phase combustion. This mechanism is clearly identified in Figure 86, which shows the approximate rate of heat release and cylinder pressure data at 1500 [revs/min] and 200 [Nm].

Nom. Speed [revs/min]-Torque [Nm]	1500-100	1400-186	1500-200	1600-237	1500-300	1800-293	1500-430	2000-354	2150-372
Pmax Cylinder [%]	3.3	0.7	-0.5	-1.1	-3.1	-2.4	0.00	-4.5	-59
Degrees CA Max Fuel Line Pressure	-1.2	-1.0	-0.9	-0.9	-0.2	-0.7	-1.2	2.1	2.6
Degrees CA Point Of Fuel Pump Dischg.	-1.3	-1.0	-0.5	-0.8	-0.4	-0.7	0.5	0.2	1.0
Duration Of Injection	-0.1	0.4	0.3	1.0	-0.4	1.4	0.3	0.7	0.5
Degrees CA Pmax Cylinder	-1.7	-1.6	-1.0	-1.0	-1.0	-0.8	-0.6	-1.8	-1.5
Point Of Ignition	-1.1	-3.3	-1.8	-0.7	-0.3	-1.4	-2.1	0.2	0.8

Blue Cells = Negative deviation from baseline average greater than *natural* variation

Red Cells = Positive deviation from baseline average greater than *natural* variation

Green Cells = Negative deviation from baseline average less than *natural* variation

Yellow Cells = Positive deviation from baseline average less than *natural* variation

All measurements in degrees crank angle unless otherwise stated.

Table 34 Deviations In Fuel Injection & Combustion Data From Baseline Due To A Blocked Injector

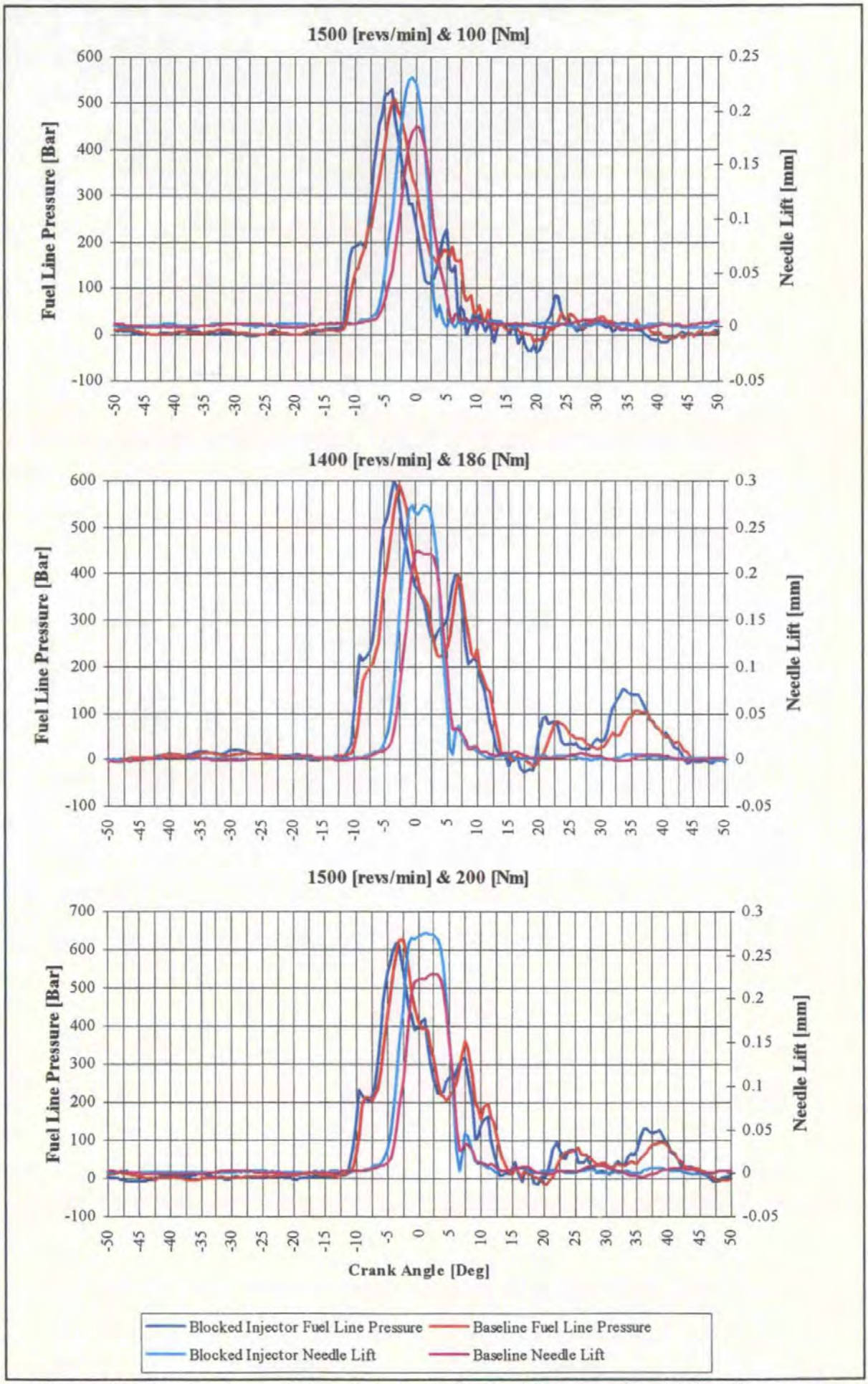

Figure 83 Comparison of Baseline And Blocked Injector Fuel Line Pressure And Needle Lift (Low Power Points)

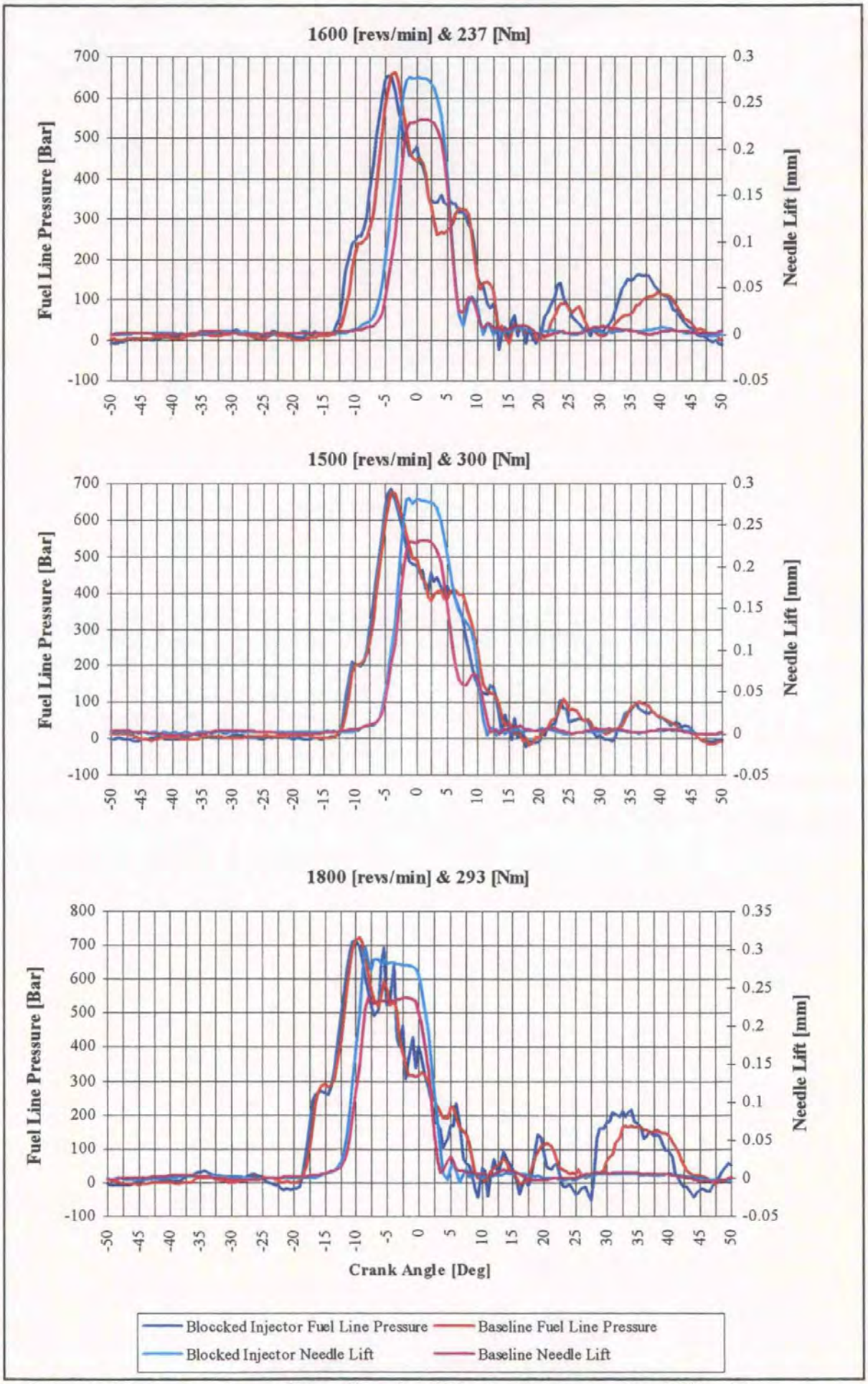

Figure 84 Comparison of Baseline And Blocked Injector Fuel Line Pressure And Needle Lift (Medium Power Points)

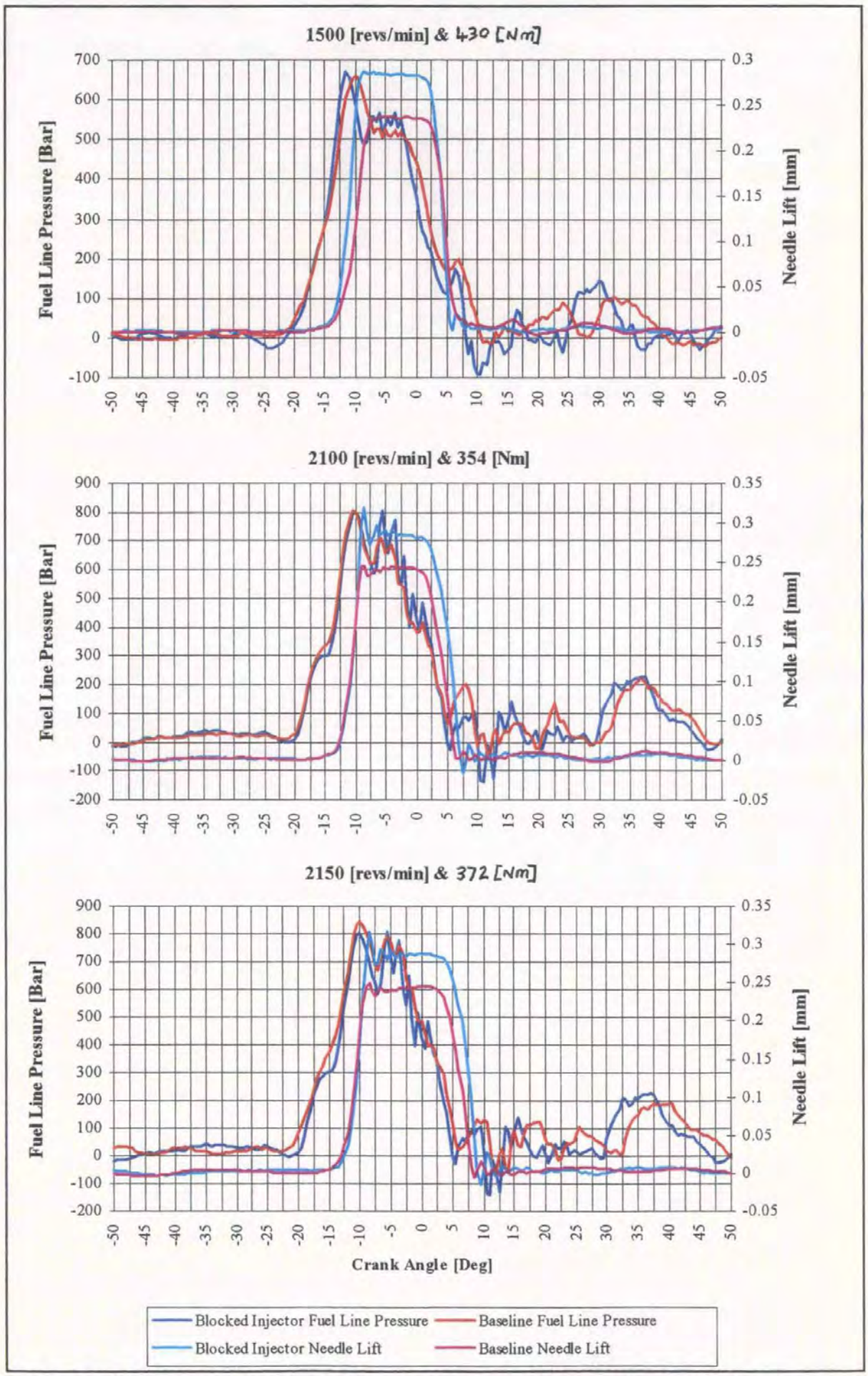

Figure 85 Comparison of Baseline And Blocked Injector Fuel Line Pressure And Needle Lift (High Power Points)

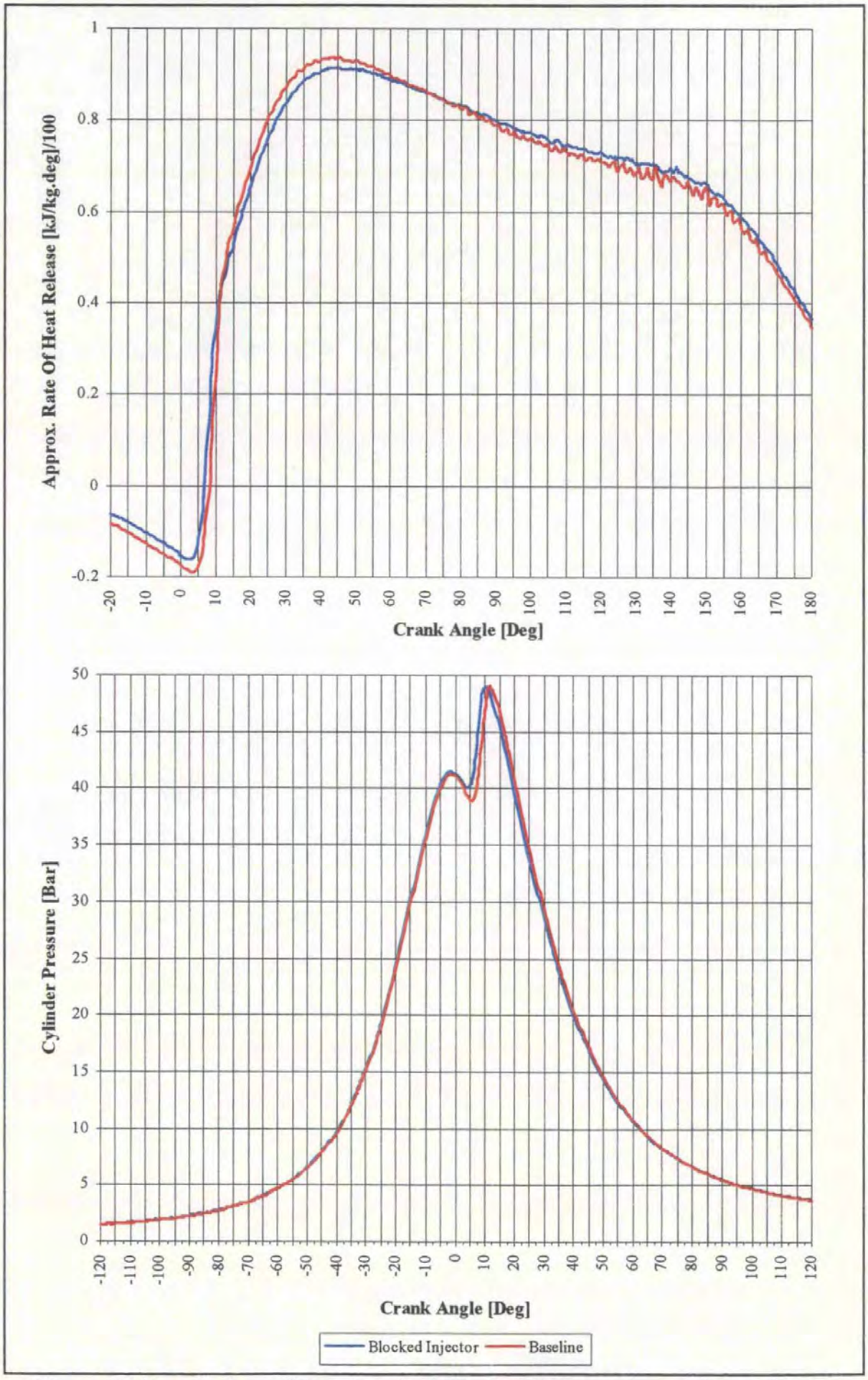

Figure 86 Comparison of Baseline And Blocked Injector Approximate Heat Release And Cylinder Pressure At 1500 [revs/min] & 200 [Nm]

8.10 Worn Injector Experimental Results

As with the previous injector faults, this injector was obtained from an engine which had been running in the field. The duration of hours run since the last service were unknown. The injector was subjected to rig testing to assess its performance before engine test, as detailed in Chapter 7, Section 7.7.4. The injector was fitted to No. 6 cylinder in the as received condition. Forty five engine tests were conducted over a four week period to establish the effect of the worn injector needle and nozzle on engine performance.

8.10.1 Analysis Of Worn Injector Sensor & Performance Parameter Data

Table 35 shows the deviations in both sensor and performance parameter data due to the introduction of a worn injector needle and nozzle. Only two performance parameters showed any marked deviation throughout the speeds and torques, namely, BSFC and brake thermal efficiency. In addition to these changes, three sensor readings showed a positive deviation. The largest deviations were generally experienced at the higher speeds. The increased BSFC and decreased brake thermal efficiency were attributed to the poorer atomisation and spray penetration in No. 6 Cylinder. These trends were further substantiated by the increase in fuel mass flow rate and fuel rack position at partial rack travel test points. Cylinders 5 & 6 port temperature showed a temperature increase consistent with up-fuelling and late burning due to poor atomisation. Analysis of the approximate heat release and combustion data shows why these trends have arisen.

Nom. Speed [revs/min]-Torque [Nm]	1500-100	1400-186	1500-200	1600-237	1500-300	1800-293	1500-430	2000-354	2150-372
BSFC	2.4	0.5	1.2	2.2	-0.3	2.0	-0.6	2.1	1.1
Brake Thermal Efficiency	-1.7	-0.5	-1.2	-2.2	0.3	-1.2	-0.1	-1.3	-1.2
Cylinder 5&6 Port Temperatures	2.9	0.8	0.9	3.1	1.1	3.5	0.1	2.1	1.5
Fuel Rack Position	7.6	2.2	1.1	1.7	0.8	1.9	-0.3	2.9	-0.2
Fuel Mass Flow Rate	3.3	1.2	1.2	1.0	0.1	3.0	1.7	1.5	0.2

Blue Cells = Negative deviation from baseline average greater than *natural* variation

Red Cells = Positive deviation from baseline average greater than *natural* variation

Green Cells = Negative deviation from baseline average less than *natural* variation

Yellow Cells = Positive deviation from baseline average less than *natural* variation

Table 35 Percentage Deviations In Sensor & Performance Param. Data From Baseline Due To Worn Injector Needle & Nozzle

8.10.2 Analysis Of Worn Injector Needle & Nozzle Fuel Injection & Combustion Data

Duration of injection showed a marked decrease through out the speed and torque range. This was due to the inability of the injector to maintain the line pressure because of the excessive leak-off. This theory was further supported by the lower maximum fuel line pressure and the increasing retarded point of injection with speed and torque.

The fuel line pressure data showed some excellent trends and maintained very good repeatability. All worn injector fuel line pressure traces, except the lowest power, showed a marked kink in the rising edge of the trace at the point of needle lift. As power increased the kink became more pronounced showing a clear line pressure decrease at needle lift off. The most noticeable feature of the worn injector fuel line pressure traces was the rapid pressure decay on the falling edge of the trace. Particularly in the portion between maximum fuel line pressure and the secondary peak. In some cases the pressure drop before the secondary peak was so severe it caused the needle to seat and then re-lift for a secondary injection. Needle lift reflected the trends seen in the fuel line pressure trace as might be expected. It was interesting to note that maximum needle lift of the worn injector was 85% greater than the baseline. This was probably due to the faulty injector having run considerably more hours than the baseline causing injector spindle and body wear.

These trends are best seen in Figures 87, 88 and 89 which show the fuel line pressure and needle lift data for both baseline and excessively worn needle and nozzle.

The approximate heat release data, shown in Figure 90, clearly showed a decreased rate of heat release during the premixed phase of burning for the worn needle and nozzle throughout the speed and torque range. This was due to the poorer atomisation and penetration of the worn needle and nozzle discussed in Chapter 7, Section 7.6.4. This trend is also reflected in the lower maximum cylinder pressures shown in Table 36 and Figure 88 . The reduced maximum cylinder pressure near to TDC meant that up-fuelling was required to maintain the specified test torques. The heat release data also shows that the poorer atomisation and up-fuel lead to a greater rate of heat release later in the cycle causing cylinder 5 & 6 port temperatures to rise.

Nom. Speed [revs/min]-Torque [Nm]	1500-100	1400-186	1500-200	1600-237	1500-300	1800-293	1500-430	2000-354	2150-372
Max Fuel Line Pressure [%]	-3.0	-3.2	-5.3	-5.6	-5.4	-7.7	-1.7	-2.5	-2.9
Pmax Cylinder [%]	2.8	0.2	-1.4	-3.6	-5.6	-3.1	0.1	-3.2	-2.9
Degrees CA Start Of Pump Dischg	-0.8	-0.4	0.1	0.2	0.5	0.5	0.7	1.7	1.8
Point Of Injection	-0.7	-0.2	0.0	0.8	1.0	0.7	0.5	1.2	1.6
End Of injection	-1.1	-0.8	-0.6	-0.3	-4.8	-0.2	-0.3	-0.4	-0.5
Duration Of Injection	-0.4	-0.6	-0.6	-1.0	-5.8	-0.9	-0.9	-1.6	-2.0

Blue Cells = Negative deviation from baseline average greater than *natural* variation

Red Cells = Positive deviation from baseline average greater than *natural* variation

Green Cells = Negative deviation from baseline average less than *natural* variation

Yellow Cells = Positive deviation from baseline average less than *natural* variation

All measurements in degrees crank angle unless otherwise stated.

Table 36 Deviations In Fuel Injection & Combustion Data From Baseline Due To A Worn Injector

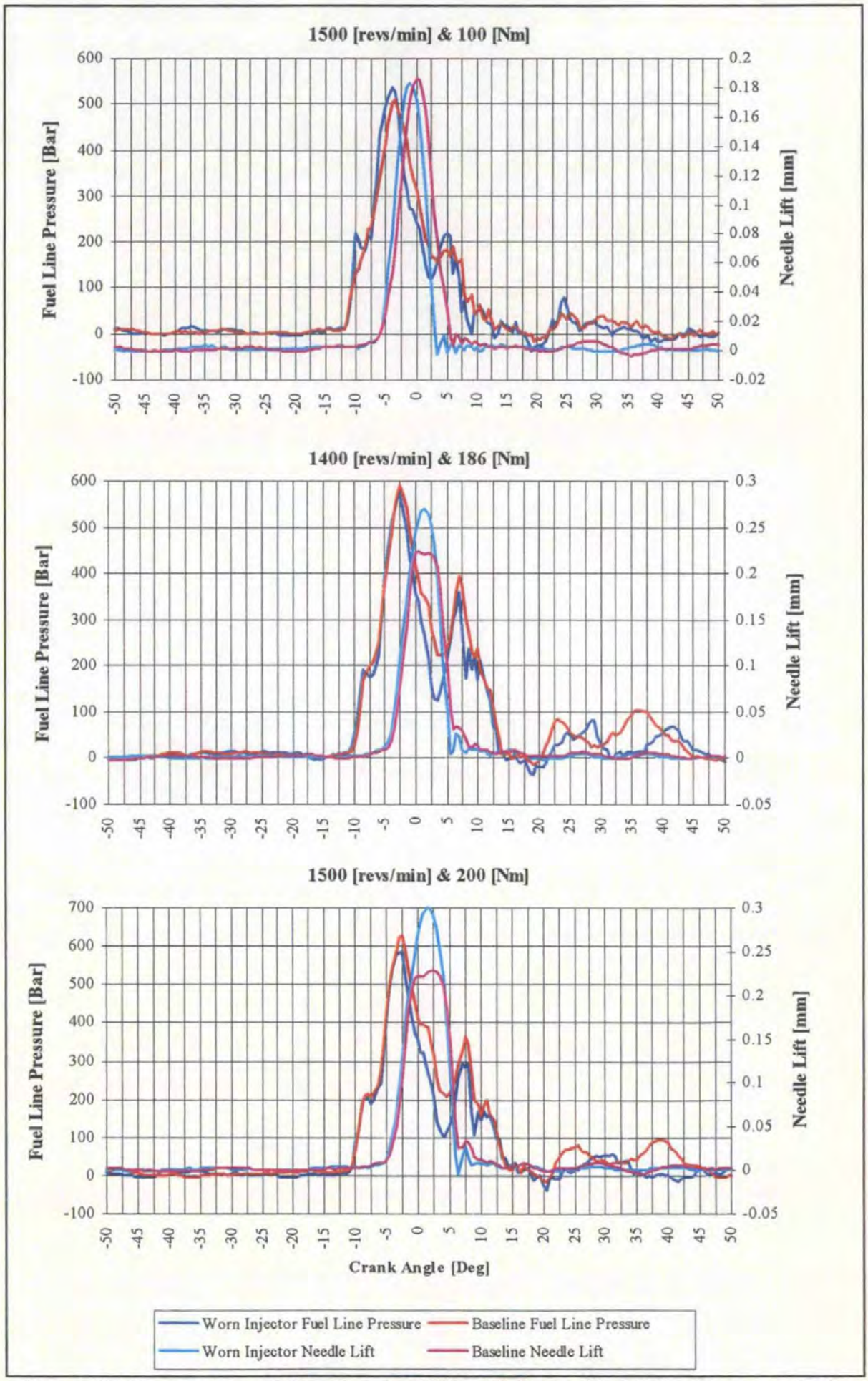

Figure 87 Comparison of Baseline And Worn Injector Fuel Line Pressure And Needle Lift (Low Power Points)

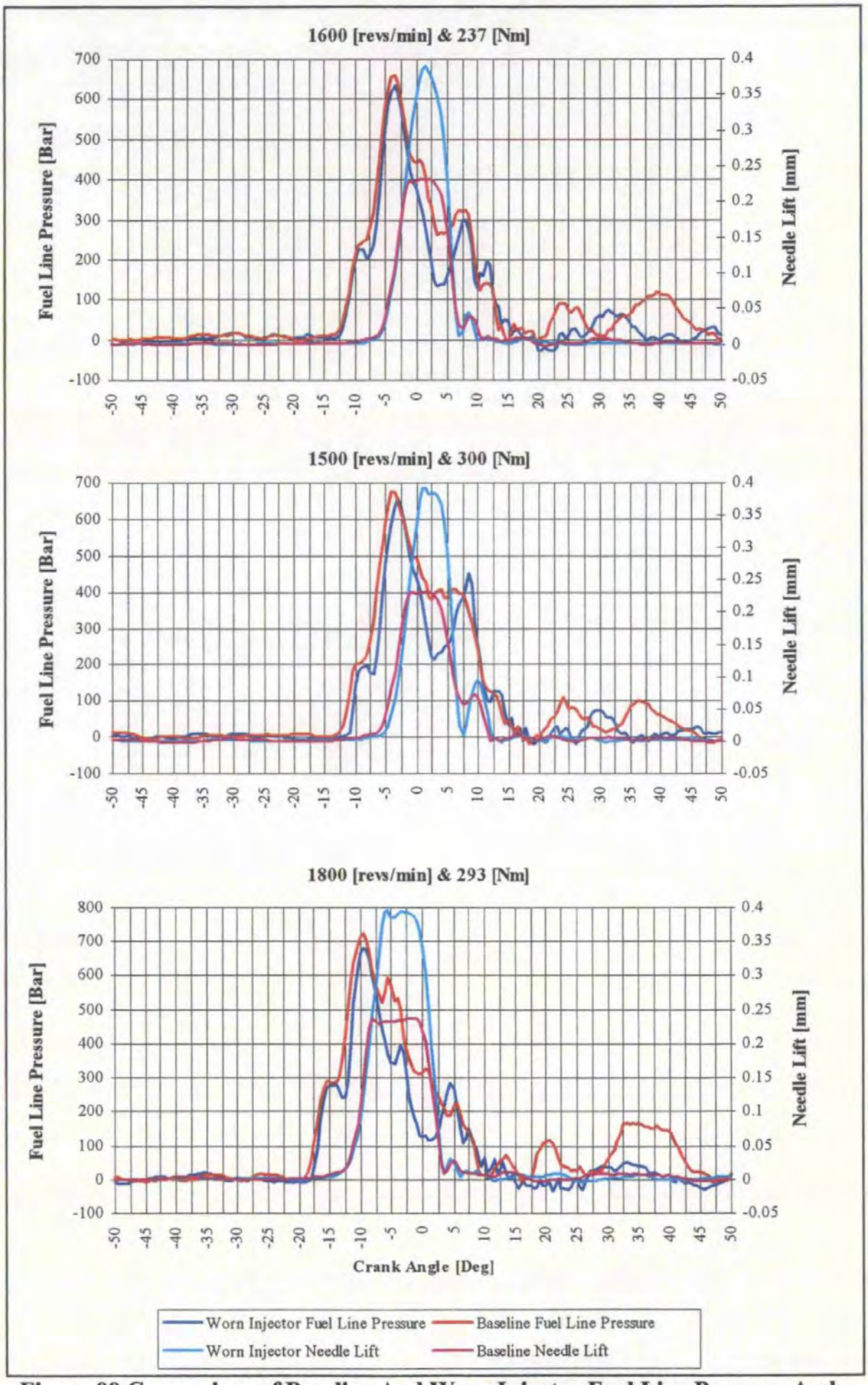

Figure 88 Comparison of Baseline And Worn Injector Fuel Line Pressure And Needle Lift (Medium Power Points)

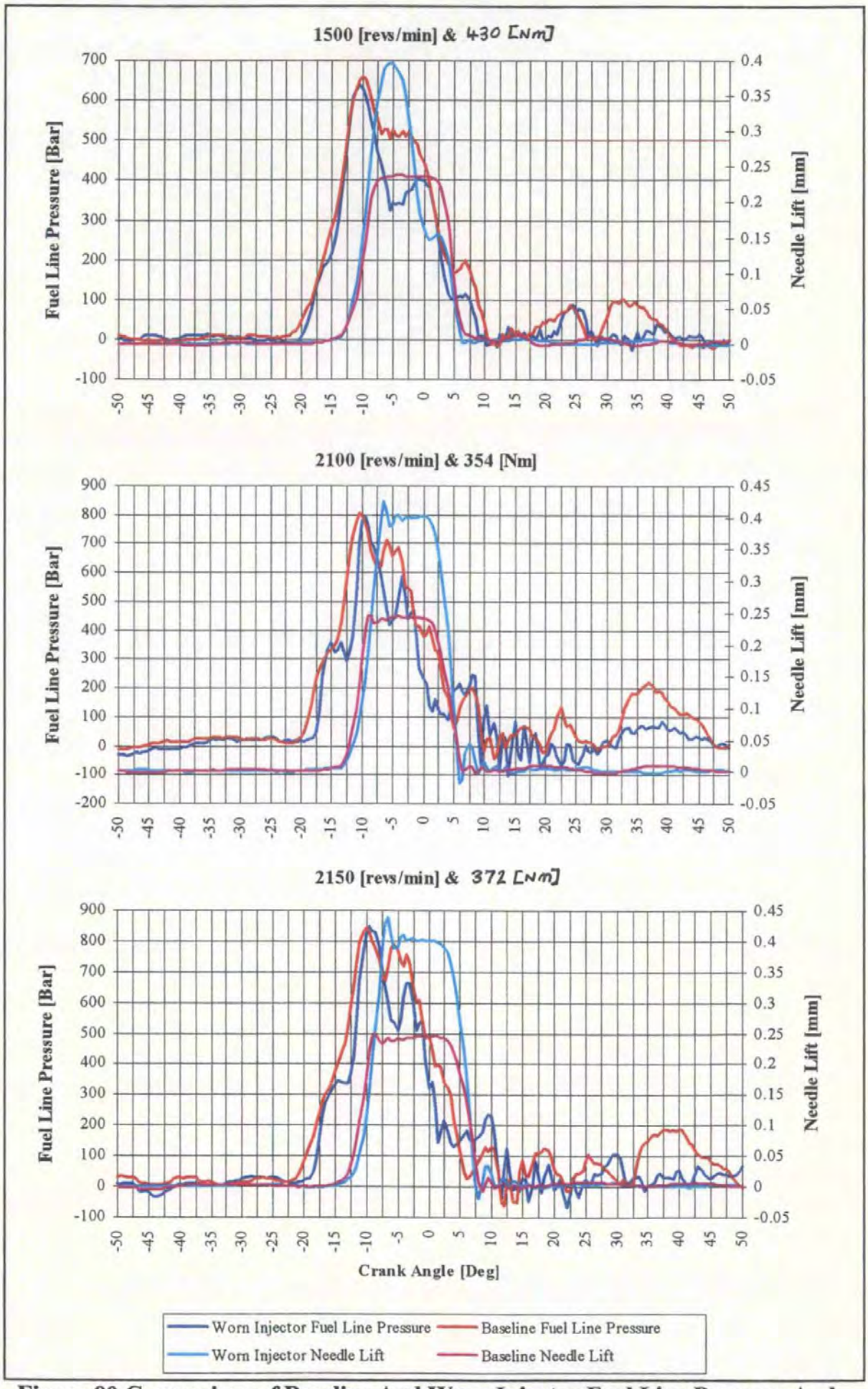

Figure 89 Comparison of Baseline And Worn Injector Fuel Line Pressure And Needle Lift (High Power Points)

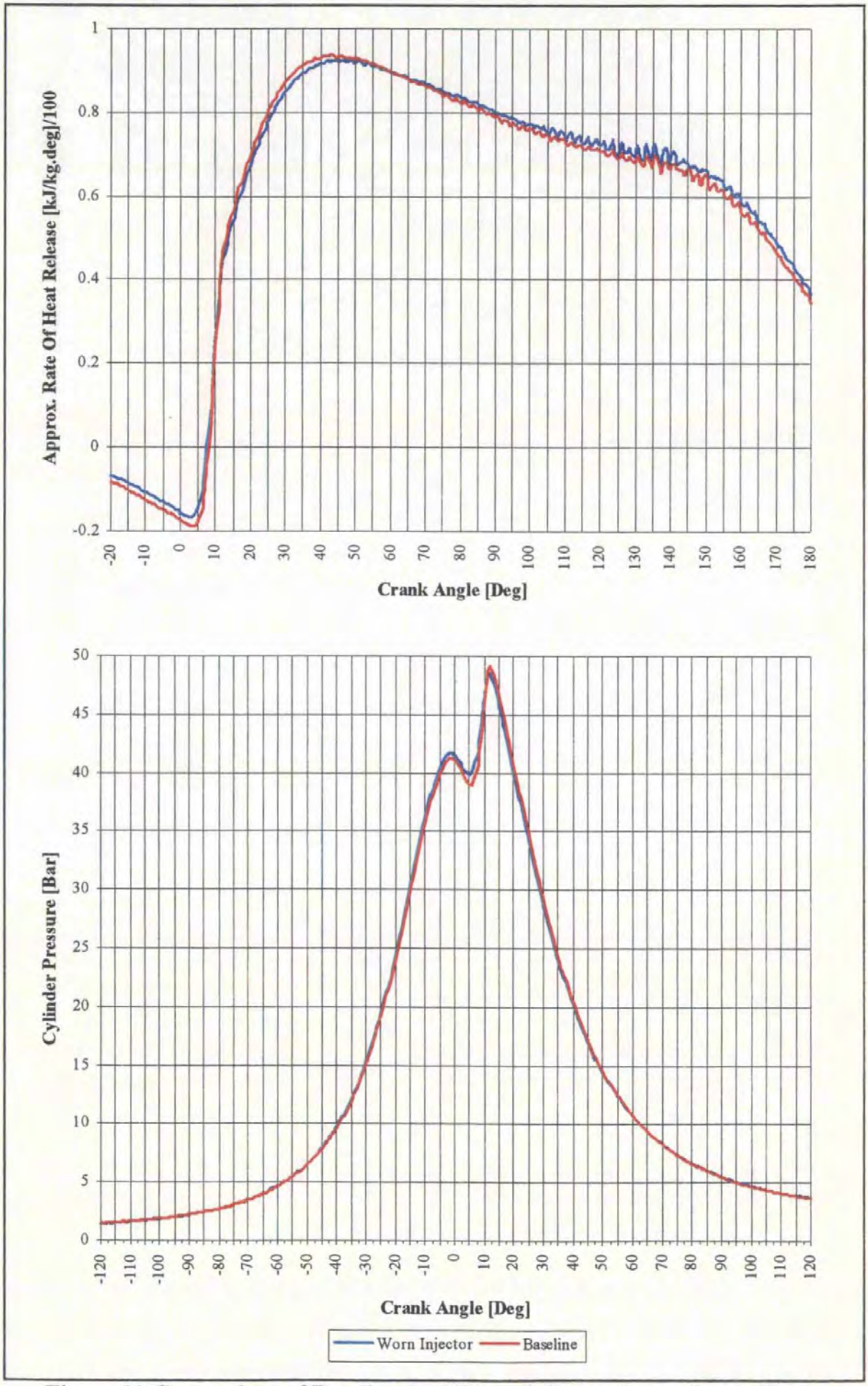

Figure 90 Comparison of Baseline And Worn Injector Approximate Heat Release & Cylinder Pressure Data At 1500 [revs/min] & 200 [Nm]

8.11 Summary

Each of the faults identified in Chapter 7 were the subject of a substantial amount of engine testing. The performance of the engine was assessed during both healthy and faulty modes of operation using the performance monitoring package developed during this research. As a result of a detailed analysis of the test data, explicit and original fault-symptom relationships for each fault have been developed for a high speed marine diesel engine. The sensitivity of engine performance to varying fault severity has also been quantified. In addition to this, variations in engine test data due to instrumentation repeatability and changing ambient conditions have been analysed and combined with the fault-symptom relationship data. This approach has allowed the identification of key diagnostic sensors for each particular fault. The development of fault-symptom relationships and identification of key diagnostic sensors is of primary importance for two reasons. Firstly, if fault detection requires specialist, intrusive, expensive and unreliable instrumentation and signal processing the whole diagnostic system becomes unfeasible for practical application. Secondly, if fault-symptom relationships are indefinable, contradictory or inconsistent it is unlikely that any form of artificial intelligence will perform successfully. There must be a pattern to the data, even if it is complex. The engine test work and subsequent analysis can be summarised by the following comments.

- An 80% fouled charge air filter has a marked effect on high speed diesel engine performance, contrary to indications from similar work[42] on medium speed engines, and simulation. Trends in engine performance were sufficiently well defined at 80% fouling to justify additional engine testing at a much lower

severity of 30% fouling. Performance Monitor was also capable of detecting slight trends at this reduced severity

- Performance Monitor easily detected adverse performance trends due to a genuinely faulty intercooler. Performance Monitor was also capable of detecting similar performance trends when a simulated faulty intercooler of reduced severity was engine tested.
- Performance Monitor could comfortably detect performance trends caused by leaking exhaust and inlet valves. Computer simulation predicted that detection of these faults would be marginal. This demonstrates the distinct advantage of using real engine test data over un-validated simulation data to predict engine performance trends under faulty conditions, as has been the case in previous research[34] . It is regrettable that further engine testing could not be conducted with a smaller leakage area more akin to the valves which were rig tested. In general, research on the effect of leaking valves on engine performance has been inadequate. Engine testing has been conducted [42,45] on single valves with effective leakage areas over 10 times greater than used in this research. Other work [34,59] which has discussed the use of simulation to predict engine performance trends due to leaking valves have not quantified or qualified the effective leakage area used. The size of leakage area is critical when determining a system's ability to detect or diagnose the fault. Until now the effect on engine performance caused by a small degradation in sealing ability across all valves due to valve wear and pitting has not been investigated. The fault study, however, proved this is what happens in practice.

- 3° retarded fuel pump timing can be easily detected by Performance Monitor. Both high and slow speed data were affected significantly. The resulting performance trends were so positive at 3°, further testing was conducted at a lower severity.
- Performance Monitor could detect the presence of all injector faults. The most notable discovery was the excellent quality diagnostic data generated by the simple non-intrusive fuel line pressure transducer.
- Faults were introduced using genuinely faulty components or realistically simulated using a variety of techniques. This work has shown that firstly, engines are operating in service with faults present, detrimentally affecting performance and secondly, Performance Monitor has the ability to detect these faults.

CHAPTER 9

DEVELOPMENT & VALIDATION OF A DIESEL ENGINE DIAGNOSTIC NEURAL NETWORK

9.0 Introduction

The overall aim of this research was to design, develop and validate a system which would perform on-line performance monitoring and fault diagnosis of a diesel engine. This chapter consolidates all of the work conducted during this research and demonstrates how the data captured and post processed by Performance Monitor was used to develop, optimise and validate a diesel engine diagnostic neural network.

Previous research[5,6,7,8,9,10], detailed in Chapter 1, has used complex look-up tables, large knowledge bases or traditional mathematical models to perform diagnosis. In addition to this, sensor readings have often required normalistaion and sophisticated signal processing before diagnosis could be performed. This work shows how a neural network can be developed which eliminates the need for all of the above work and still offers satisfactory performance.

Previous systems discussed in Chapter 1 have often required a significant degree of computing hardware and software. This work also shows how the same relatively low specification PC used to run Performance Monitor can also be used to perform the diagnosis simultaneously.

Until now, neural networks have never been trained and tested on real diesel engine data to perform fault dioagnosis. Neither have they been used to diagnose a wide range of realistic engine faults including fuel injection equipment. Further to this, particular attention has been paid to the development of fault-symptom relationships for high speed diesel engines. This has lead to the identification of key diagnostic sensors which were used as neural network inputs.

Previous work has given little regard to various neural network training methods and network architectures. This work has investigated several algorithms and various network architectures to achieve optimum diagnostic performance. Throughout the development and validation of the neural network diagnostic system, emphasis was put on the practical application of a neural network to diesel engine fault diagnosis. Previous work [34] has given little or no attention to practical application of neural networks to diesel engine fault diagnosis.

To ascertain the neural network based diagnostic system practical limitations the following success criteria were defined. The neural network based system must;

- Be able to be trained on real engine data. This would allow the neural network to be trained simultaneously with endurance, reliability and field trial engine testing which forms part of any engine development programme. This would make the neural network approach more commercially viable than other forms of AI, expert systems for example. Further to this the neural network diagnostic model could train throughout it's service life, continuously improving it's performance.

- Be capable of correctly identifying healthy and faulty conditions repeatably, even when sensor failure occurs. If a system continuously mis-diagnoses it quickly loses credibility.
- Be able to perform an accurate diagnosis with reliable, non-intrusive, cheap instruments.
- Demonstrate that it's diagnostic ability is not severely degraded in the presence of noisy sensor data.
- Have the ability to perform an accurate diagnosis at torques and speeds it was not trained at. If the model needs to be trained on data generated at all speeds and torques, it is not practically viable.
- Be capable of diagnosing faults of varying severity. Ideally, the neural network diagnostic model should be able to detect and diagnose faults of a lesser severity than those it was trained on. This would allow the tracking of faults from infancy and aid effective maintenance planning.
- Demonstrate the ability to make an 'intelligent' diagnosis in the presence of a novel fault which it has not been trained on.

All neural network model development was performed using Neuraldesk V2.11 running on a 100 MHz DX4 IBM compatible PC. This package was chosen since it supported the development of supervised learning, back propagation networks. Previous research has shown that this type of network could be successfully applied to similar diagnostic problems as discussed in Chapter 1. Neuraldesk operated in a windows environment, allowing DDE, and hence, easy interface with Performance Monitor.

9.1 Selection Of Inputs For Neural Network Diagnostic Model Development

Previous work, discussed in Chapter 1, has shown that the choice of input data is critical to the successful development of a neural network. The analysis of the engine test data and subsequent fault-symptom relationship tables shown in Chapter 8 were used to select which sensor readings were key to detecting the presence of a particular fault. It was decided that network development would use key sensors which were cheap, easy to install, non intrusive and reliable.

Generally, the calculated performance parameters showed poorer repeatability than the raw sensor readings, as discussed in Chapter 4. It was decided that neural network development would concentrate on using raw sensor readings. This was beneficial because it allowed raw sensor data to be passed directly to the network, eliminating pre-processing. More importantly, all of the performance parameter deviations were directly caused by sensor deviations. Since the basic principle of the neural network is to create relationships between data it should be capable of using raw sensor data. Similarly, for this reason, engine performance corrections to BS or ISO were not applied. Table 37 shows a summary of the key diagnostic sensors identified from the fault - symptom relationship tables shown in Chapter 8. Although cylinder pressure and needle lift are both key diagnostic sensors they were both omitted from Table 37. They are expensive, intrusive, unreliable and require specialist signal processing. For these reasons they are considered unsuitable for use in any practical application. The following sensors were chosen as practically viable inputs for neural network diagnostic model development.

1. Engine torque
2. Engine speed
3. Compressor inlet pressure
4. Compressor inlet temperature
5. Cylinders 1 & 2 exhaust temperature
6. Cylinder 3 exhaust temperature
7. Cylinder 4 exhaust temperature
8. Cylinder 5 & 6 exhaust temperature
9. Fuel rack position
10. Intercooler cooling water discharge temperature
11. Inlet manifold pressure
12. Inlet manifold temperature
13. Turbine discharge temperature
14. Turbocharger rotational speed
15. Fuel mass flow rate
16. Charge air volume flow rate
17. Cooling water inlet temperature
18. Fuel line pressure (taken at 1° crank angle resolution)

The choice of sensors is of critical importance in the development of any diagnostic system. Sensors should be cheap, non-intrusive, reliable and give repeatable data. In addition to this they should give significant and detectable changes in the presence of a fault. Previous work on the application of Artificial Intelligence, AI, to fault diagnosis has concluded that inputs into the AI should be closely vetted to ensure they do not give contradictory or confusing data but clearly indicate fault-symptom relationships. If this is not possible, the degree of success of the artificial intelligence may well be compromised.

SENSOR DESCRIPTION	FAULT DESCRIPTION							
	Air Filter Blockage	I/ Cooler Blockage	Leaking Inlet valve	Leaking Exh valve	Fuel Pump Timing	Low Press Injector	Blocked Injector	Worn Injector
Air Flow	*	*	*	*	*			
Compressor Discharge Pressure			*		*			
Compressor Discharge Temperature				*	*			
Compressor Inlet Pressure	*							
Compressor Inlet Temperature								
Cylinder 1&2 Port Temperatures	*	*	*	*	*	*		
Cylinder 3 Port Temperature	*	*	*	*	*	*		
Cylinder 4 Port Temperature	*	*	*	*	*	*		
Cylinder 5&6 Port Temperatures	*	*	*		*	*	*	*
Engine Cooling water Discharge Temperature								
Engine Water Temperature								
Engine Speed	*	*	*	*	*	*	*	*
Exhaust Manifold Pressure					*			
Exhaust Manifold Temperature	*	*	*	*	*	*		
Fuel Rack Position			*	*	*		*	*
Fuel Temperature								
Intercooler Cooling water Discharge Temperature		*	*					
Inlet Manifold Pressure	*				*			
Inlet Manifold Temperature		*	*	*	*			
Lubricating Oil Temperature								
Engine Torque	*	*	*	*	*	*	*	*
Turbine Discharge Temperature	*	*	*	*	*	*		
Turbine Discharge Pressure								
Turbocharger Speed	*		*	*	*			
Cooling Water Supply Temperature								
Fuel Line Pressure					*	*	*	*
Fuel Mass Flow Rate			*	*	*	*		*

Table 37 Key Diagnostic Sensors For Neural Network Development

The fuel line pressure sensor has been included since it is cheap, non intrusive and reliable. It also gave excellent diagnostic data relating to the fuel injection equipment faults. Fuel line pressure was sampled with respect to crank angle at 0.5° resolution, as discussed in Chapters 2 and 3. Crank angle was measured using a specialised AVL 364 optical encoder which is both expensive and fragile and is only suitable for research test cell applications. It was thought that fuel line pressure data could only be used if the sampling resolution could be decreased to 1° crank angle. This would allow fuel line pressure to be sampled using a more robust and practical method such as a toothed flywheel and inductive pick-up or a rear end oil seal embedded inductive encoder. The latter are now cheap, reliable, easy to fit and common place in the automotive industry.

All 9 temperature measurements chosen were measured using 'K' type thermocouples, both pressures were measured using simple strain gauge transducers. Both of these forms of instrumentation were cheap, easily fitted and reliable. Turbocharger rotational speed was easily measured using an inductive probe which is a cheap sensor well suited to practical situations.

Fuel flow and air flow sensors are the only 'specialist' pieces of instrumentation listed. The drive for low gaseous and particulate emission engines and increased efficiency has lead to the advent of engine management and electronic fuel injection systems. These systems, in particular automotive based, already use air and fuel flow sensors together with much of the instrumentation specified above.

9.2 Training Of Neural Network Diagnostic Models

The engine test data from the sensors identified in Section 9.1 was divided into two distinct data sets. These were, training input data and validation input data sets. Both data sets contained data taken during healthy and all faulty modes of engine operation at all nine speed and torque test points. The validation input data comprised randomly selected sets of engine test data, the remainder of the engine test data, and by far the majority, formed the training input data. Supervised neural network training requires input data and output data for training. To compliment the training input data a set of neural network outputs were devised to characterise both healthy and faulty modes of engine operation. The output vector was a simple binary code as shown in Table 38.

	Output Layer Neuron Demanded Response							
Fault Description	Neuron 1	Neuron 2	Neuron 3	Neuron 4	Neuron 5	Neuron 6	Neuron 7	Neuron 8
Healthy	0	0	0	0	0	0	0	0
Fouled air filter	1	0	0	0	0	0	0	0
Fouled intercooler	0	1	0	0	0	0	0	0
Leaky inlet valves	0	0	1	0	0	0	0	0
Leaky exhaust valves	0	0	0	1	0	0	0	0
Fuel pump timing	0	0	0	0	1	0	0	0
Low pressure injector	0	0	0	0	0	1	0	0
Blocked injector	0	0	0	0	0	0	1	0
Worn injector	0	0	0	0	0	0	0	1

Table 38 Neural Network Diagnostic Model Outputs

Neuraldesk contained a selection of 4 training algorithms, Stochastic Back Propagation, Skeletonising Back Propagation, Wiegend Weight Eliminator, and Standard Back Propagation. Each of these training algorithms was applied to the training input and output data sets. The networks trained on the Wiegend Weight Eliminator and the Standard Back Propagation Algorithm both failed to train and

converge properly after numerous attempts using varying architectures. The networks trained on the Stochastic and Skeletonising Back Propagation Algorithms both trained and converged successfully. These are discussed in more detail below and will be referred to as model 'A' and model 'B' respectively.

9.2.1 Training Using The Stochastic Back Propagation Algorithm [Model 'A']

The input and output training data sets were entered into Neuraldesk and the input data sets were autoscaled between 0 and 1. The network architecture was set to auto-design and Neuraldesk generated a 3 layer network. The input layer was set to 117 input neurons, 17 inputs were dedicated to the slow speed data inputs, for example, temperature and pressure. The remaining input layer neurons took the digitised fuel line pressure readings taken from -50° BTDC to +50° ATDC at 1° sampling resolution. The output layer contained 8 neurons dictated by the binary outputs shown in Table 38.

The optimal number of hidden layer neurons was established through trial and error. Three separate models were trained with six, seven and eight hidden layer neurons. The first model developed had six hidden neurons which gave high neuron outputs correctly which positively diagnosed the faults but also tended to mis-classify and give high neuron outputs for faults that were not present, giving a confusing diagnosis. Eight hidden layer neurons generally caused neuron outputs to be lower, reducing the confidence of diagnosis and also tended to give low neuron outputs on a large number of other neurons making the diagnosis too 'fuzzy'. Training and testing proved that the optimal number of hidden neurons was seven.

The Stochastic Back Propagation Algorithm was chosen from the algorithm menu and Neuraldesk generated default learning parameters of momentum = 0.9 and Learn rate =0.1. The seven hidden layer network was set to train and the maximum network error and number of epochs was monitored. Figure 91 shows the reduction in maximum network error against number of epochs.

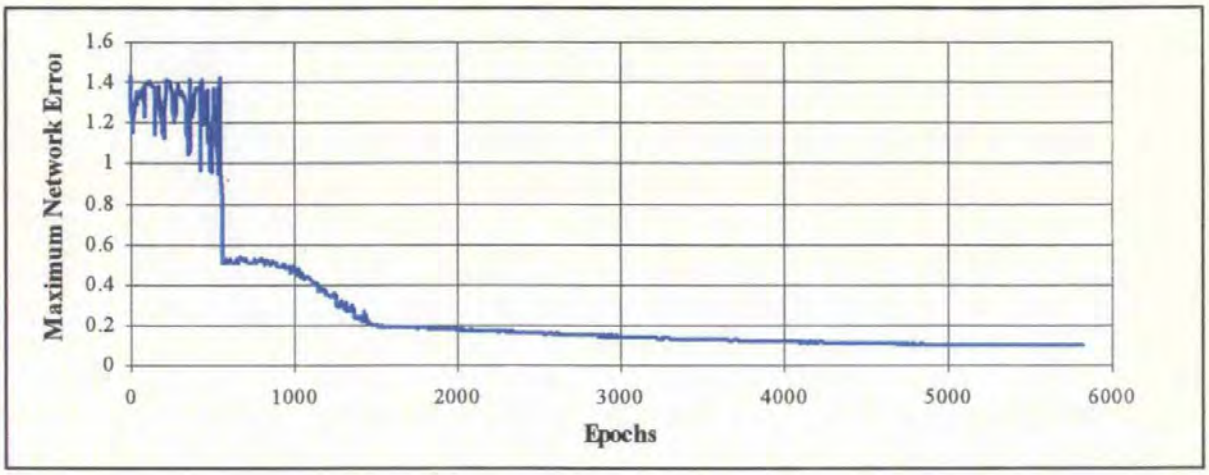

Figure 91 Model 'A' Training Error Reduction With Increasing Epochs

At 540 epochs the learning rate was decreased from 0.1 to 0.01 since the network was failing to converge and the error value showed increasing instability. This had the effect of dramatically reducing the error initially and then learning progressed in a slower but more controlled manner. At 1440 epochs the learning rate was decreased further to 0.001. Again the rate of change of error decreased but the network moved slowly towards convergence. The network was occasionally tested using the validation input data sets until it's performance ceased to improve with further training. After 13 hours and 40 minutes of training the maximum network error had decreased to less than 0.1 and there was no evidence of the network's performance improving. The degree of training did affect network performance. The results showed that reduced network training lead to poorer diagnostic clarity. Correct neuron outputs were reduced in magnitude whilst the other incorrect

neurons started to give small activations. Increased training gave high neuron outputs correctly which positively diagnosed the faults but also tended to mis-classify and give high neuron outputs for faults that were not present, giving a confusing diagnosis

9.2.2 Training Using The Skeletonising Back Propagation Algorithm [Model B]

The Skeletonising Back Propagation Algorithm is similar to the Stochastic Back Propagation Algorithm except it focuses on the most and least important weighted connections in the network. Connections of lower significance are actually removed from the network all together. The procedure for setting the network to train was identical to that used for Model 'A' except the Skeletonising Algorithm was chosen. When the Skeletonising Back Propagation Algorithm was selected values of momentum (alpha) = 0.9, Learn rate = 0.1 and Skel rate = 0.3 were set by software default. The network architecture before training was identical to Model 'A'. The network was set to train and the maximum error and epochs were monitored. Figure 92 shows the reduction in maximum network error with increasing number of epochs. After 370 epochs the learning rate was reduced from 0.1 to 0.01. This steadied learning, and at 1190 epochs the network began to rapidly converge. Training became slightly unstable at 1410 epochs and the learning rate was further reduced to 0.001. The network was periodically tested on the validation data throughout training to ensure optimum diagnostic performance. After 8 hours and 20 minutes of training the maximum

network error was 0.0998 and the network performance was ceasing to improve so training was terminated.

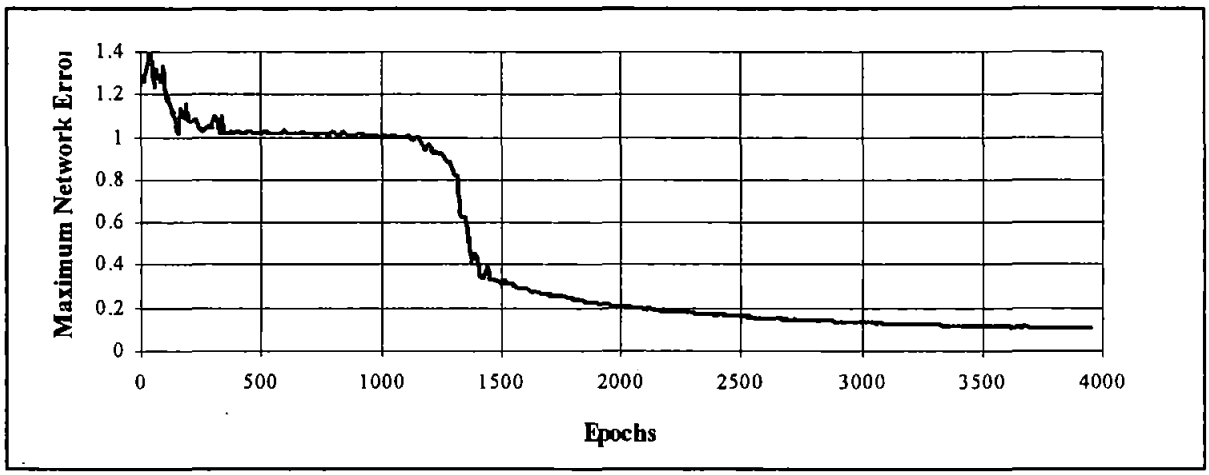

Figure 92 Model 'B' Training Error Reduction With Increasing Epochs

9.3 Validation Of Neural Network Diagnostic Models 'A' & 'B'

Initially the basic diagnostic performance was assessed on normal engine test data which represented both healthy and all faulty conditions at all speeds and torques. Once it was established that the models could successfully train and diagnose on real engine test data a series of tests were performed to assess each models performance against the success criteria outlined in Section 9.0. The following sections detail the validation testing methods and results

9.3.1 Validation Of Neural Network Diagnostic Models 'A' & 'B' - Basic Diagnostic Performance

The models were validated using the previously unseen engine data contained in the validation set. Examples of data taken at all speeds and torques under healthy and all faulty conditions were presented to the network input layer of both Model 'A' and Model 'B'. The models were interrogated and returned output vectors in less than a second. The results are shown in Figures 93 to 100.

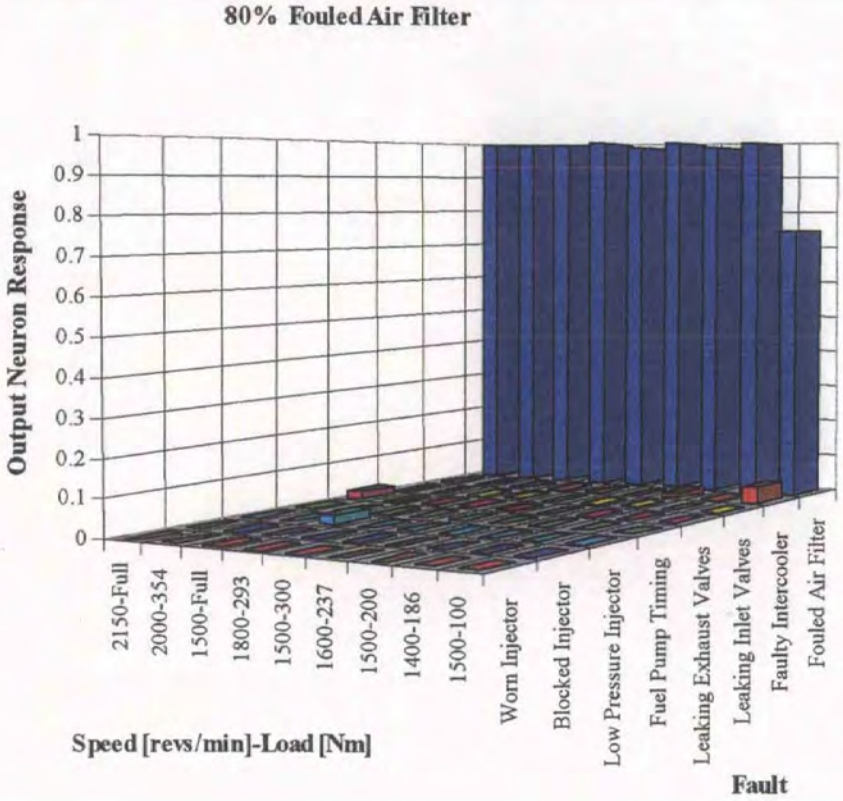

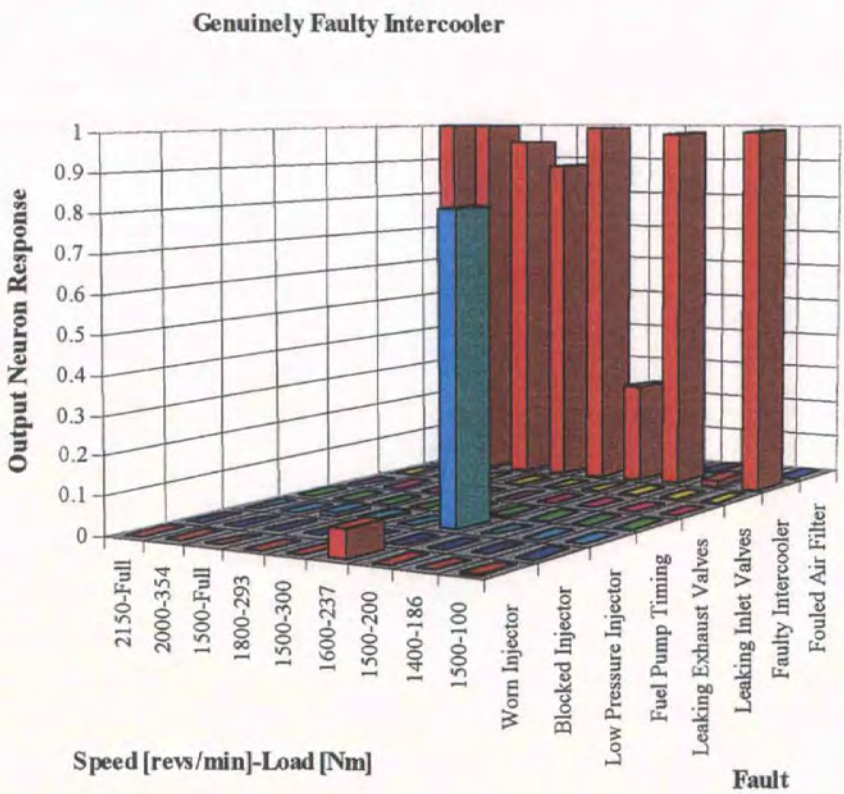

Figure 93 Ability Of Model 'A' To Diagnose Fouled Air Filter & Intercooler Faults When Tested With Previously Unseen Engine Data

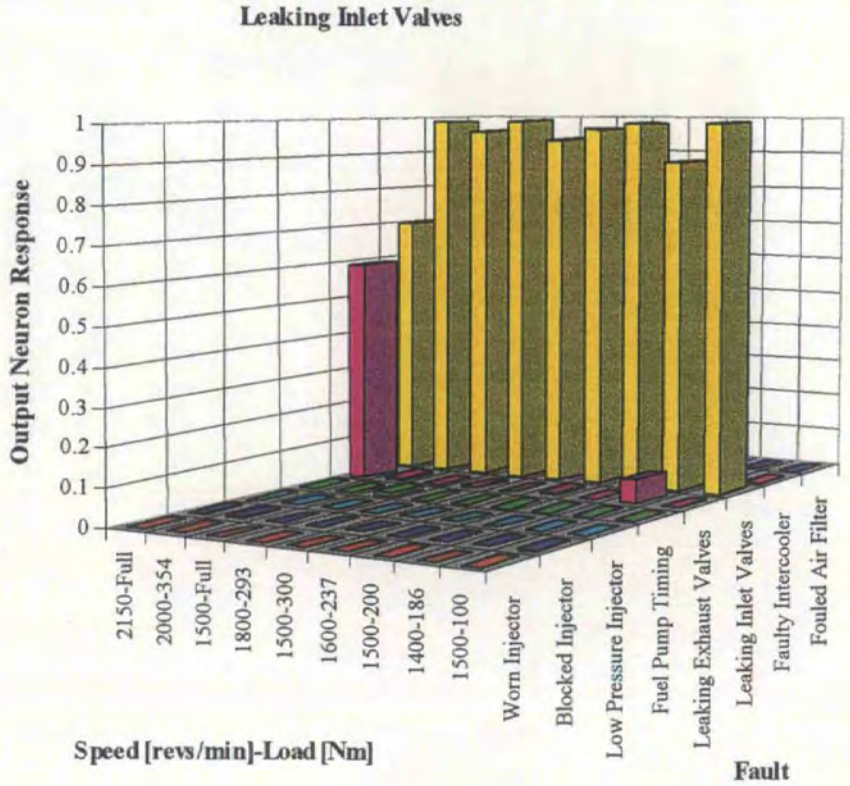

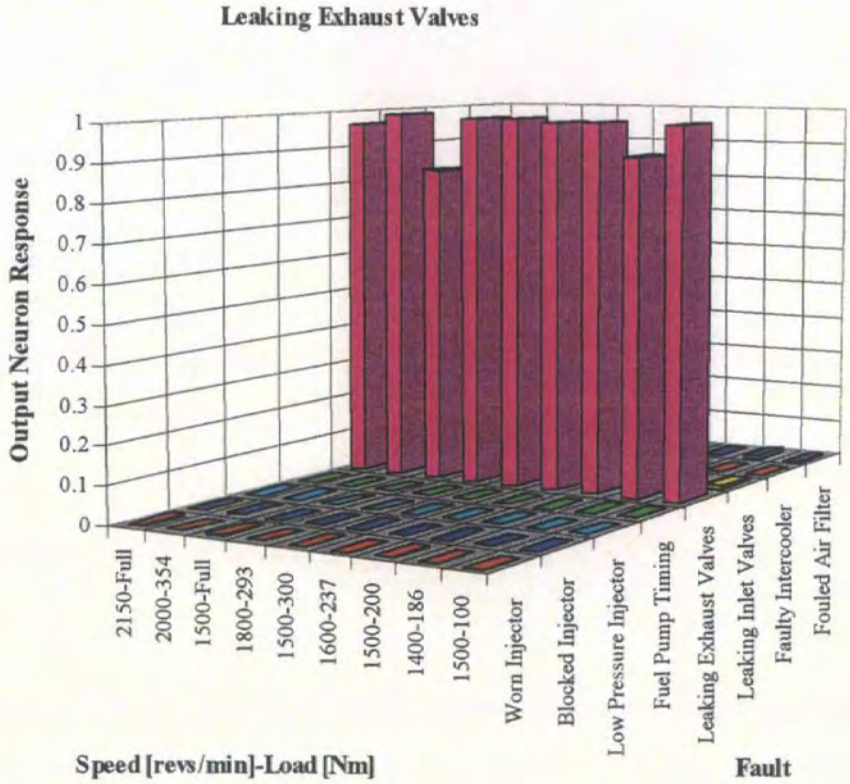

Figure 94 Ability Of Model 'A' To Diagnose Leaking Inlet and Exhaust Valves When Tested With Previously Unseen Engine Data

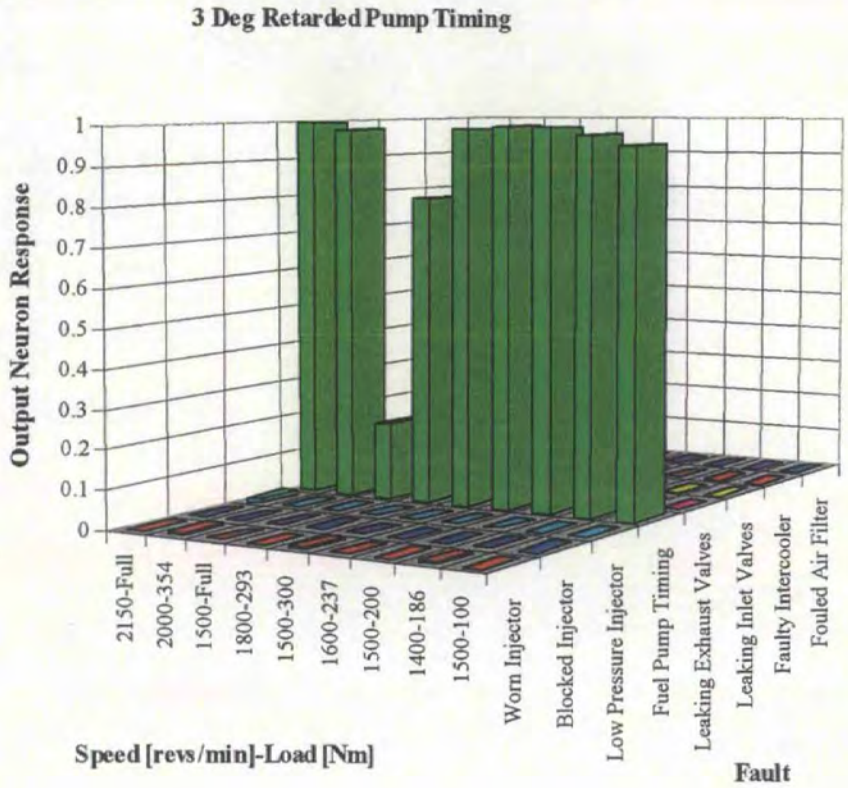

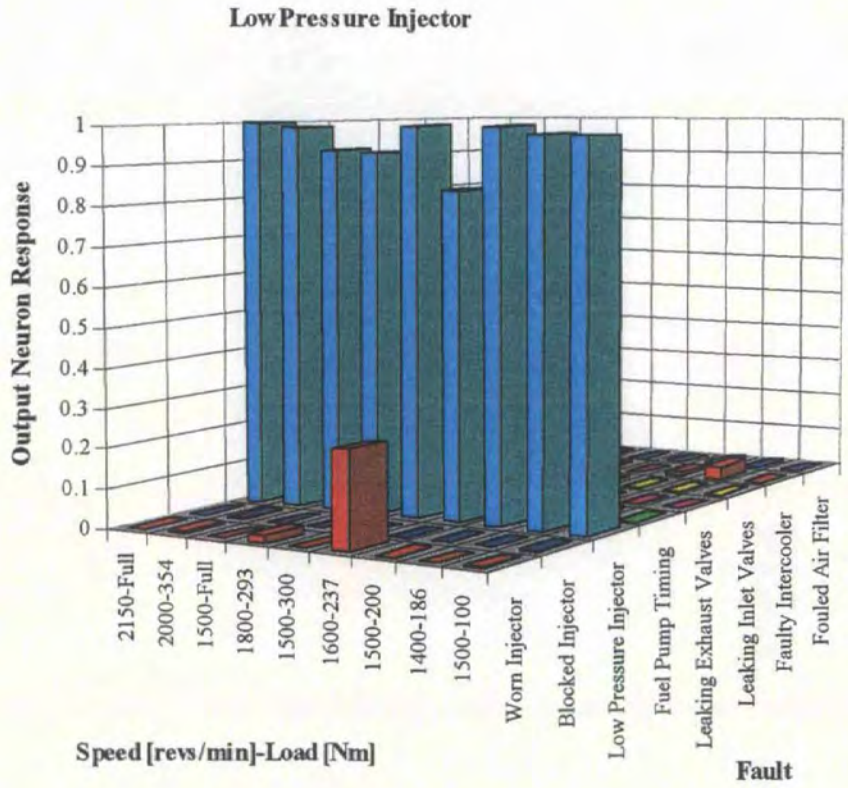

Figure 95 Ability Of Model 'A' To Diagnose Retarded Fuel Pump Timing & A Low Pressure Injector When Tested With Previously Unseen Engine Data

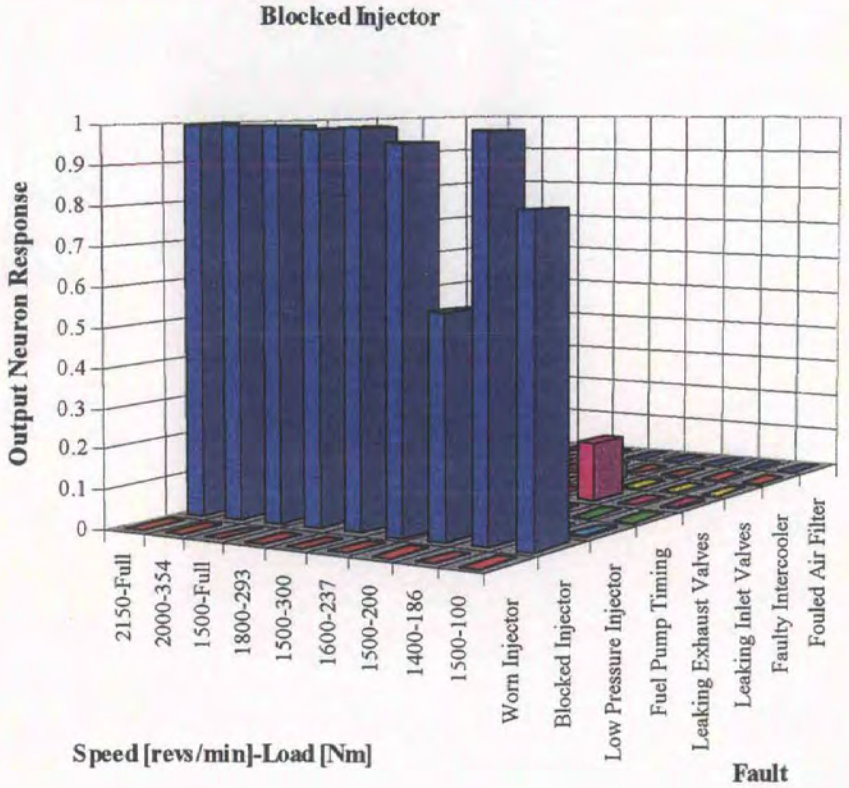

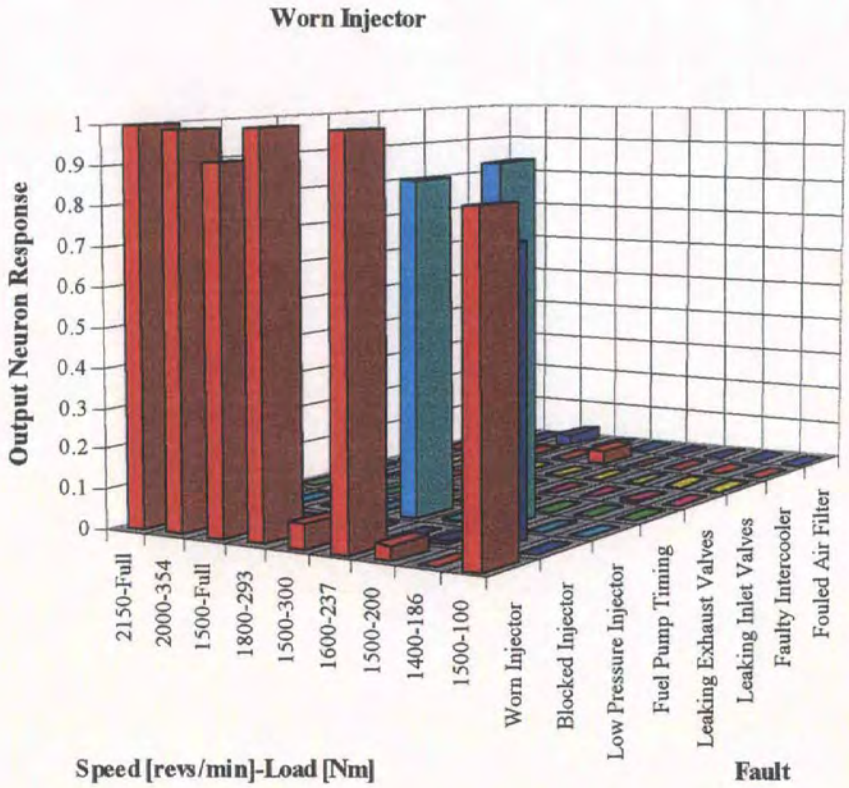

Figure 96 Ability Of Model 'A' To Diagnose A Blocked Injector & A Worn Injector When Tested With Previously Unseen Engine Data

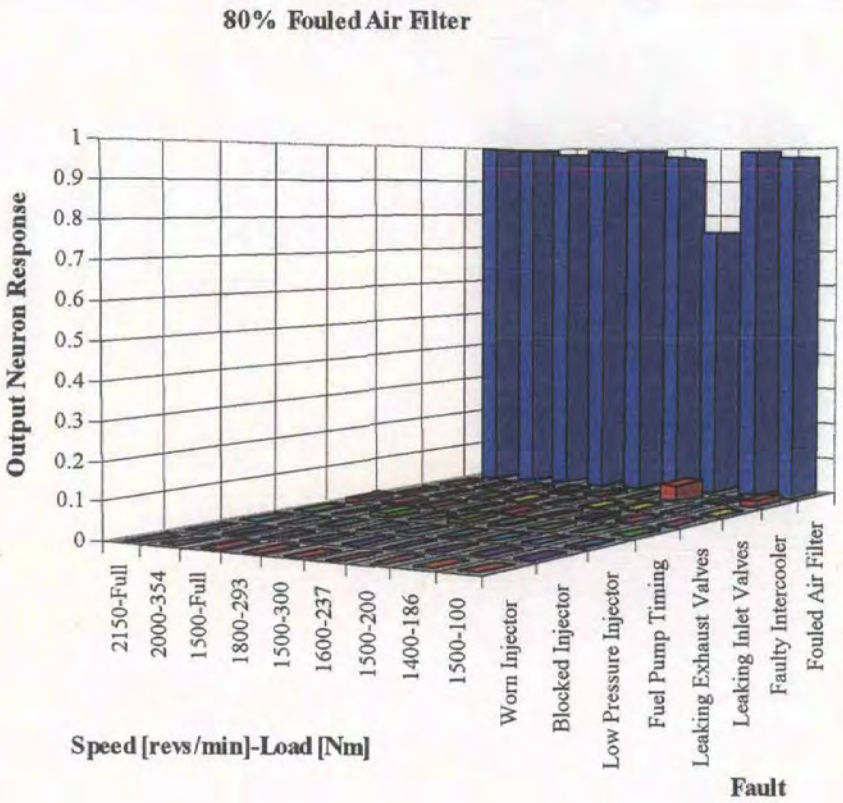

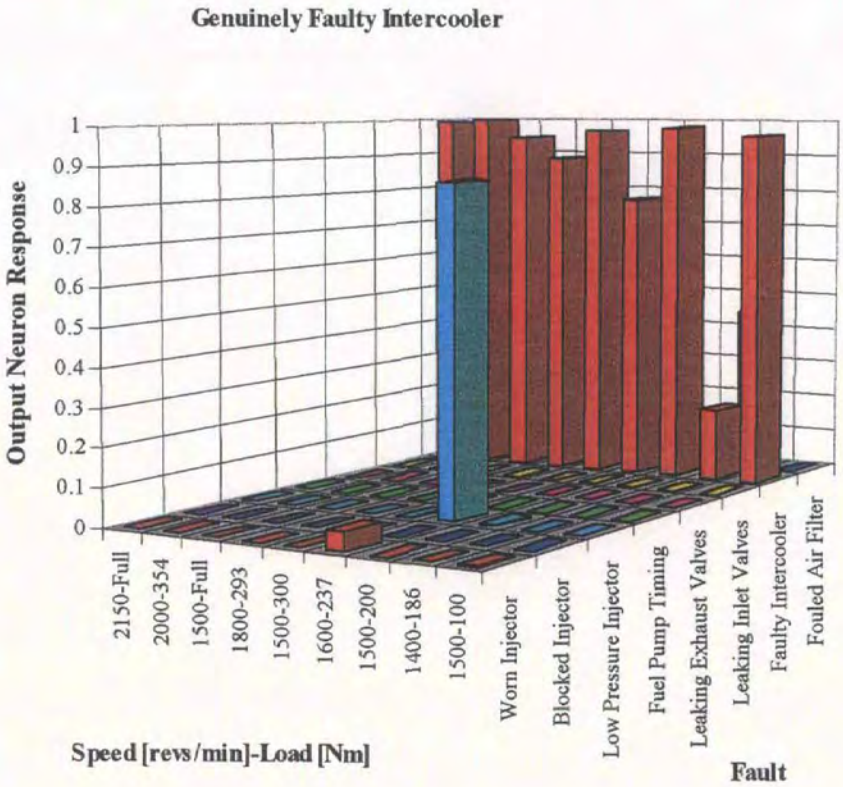

Figure 97 Ability Of Model 'B' To Diagnose Fouled Air Filter & Intercooler Faults When Tested With Previously Unseen Engine Data

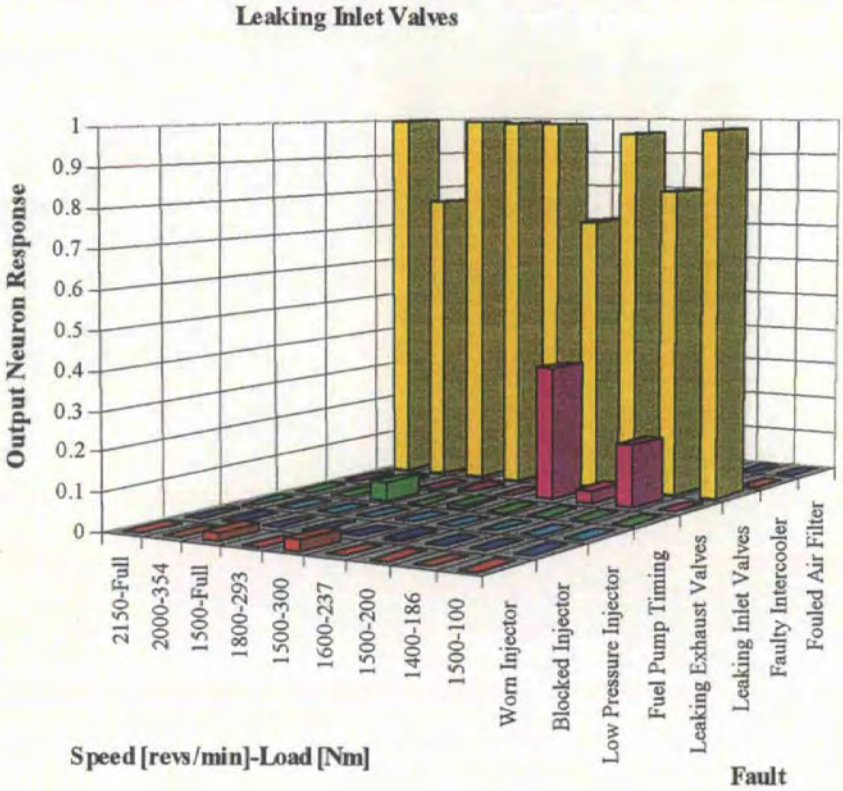

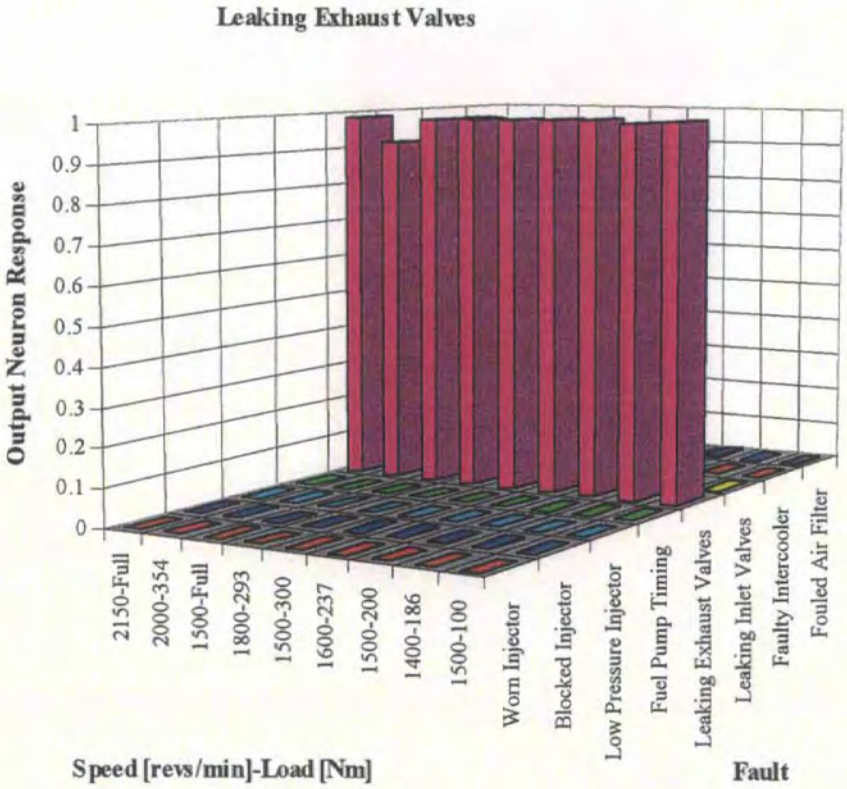

Figure 98 Ability Of Model 'B' To Diagnose Leaking Inlet and Exhaust Valves When Tested With Previously Unseen Engine Data

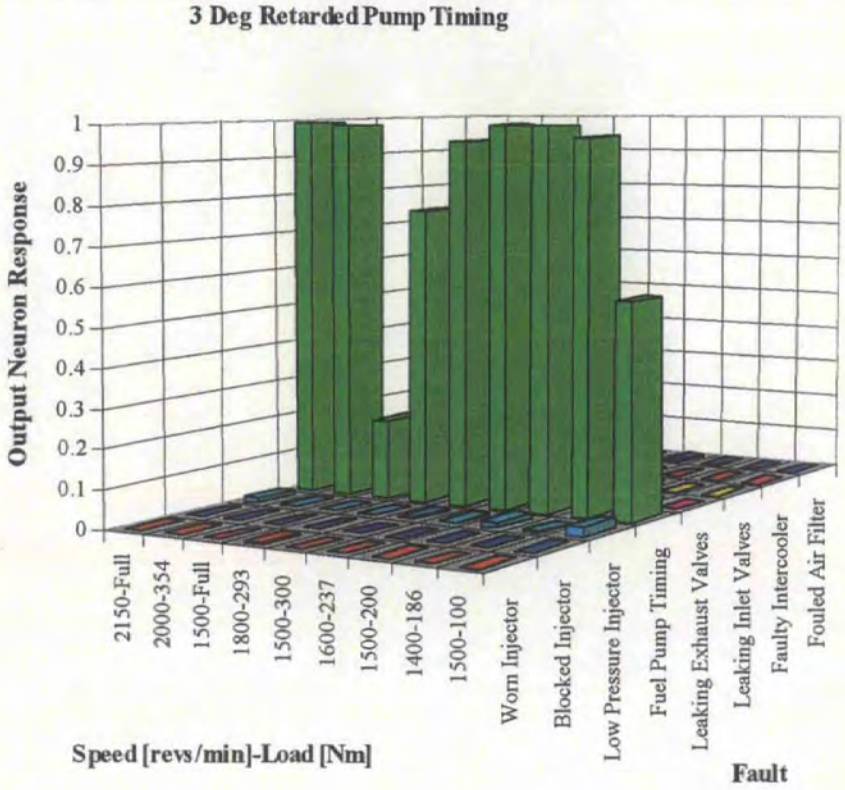

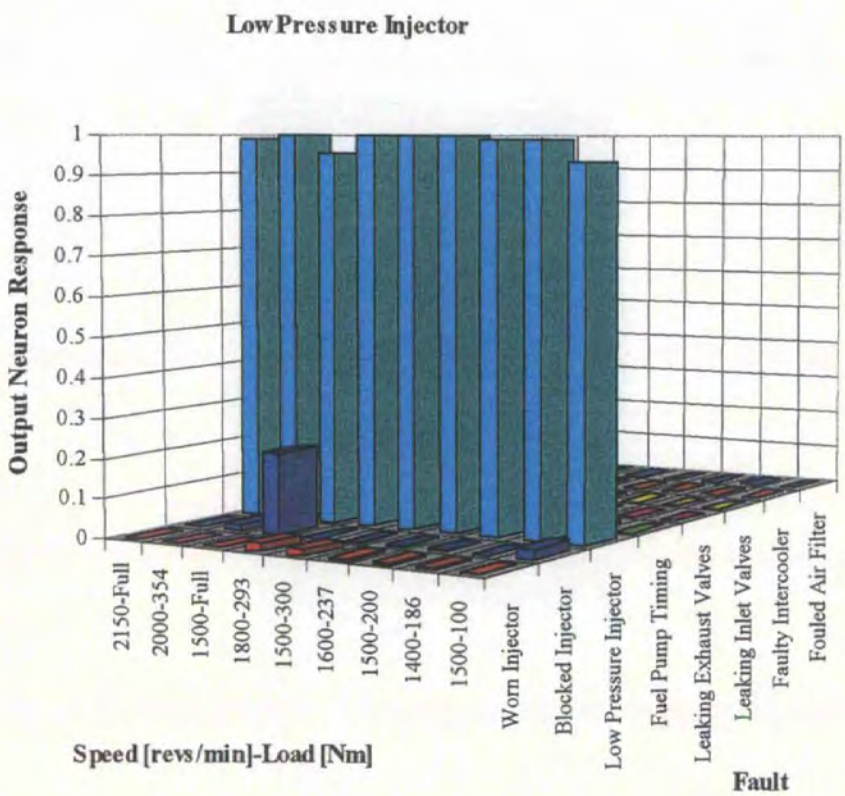

Figure 99 Ability Of Model 'B' To Diagnose Retarded Fuel Pump Timing & A Low Pressure Injector When Tested With Previously Unseen Engine Data

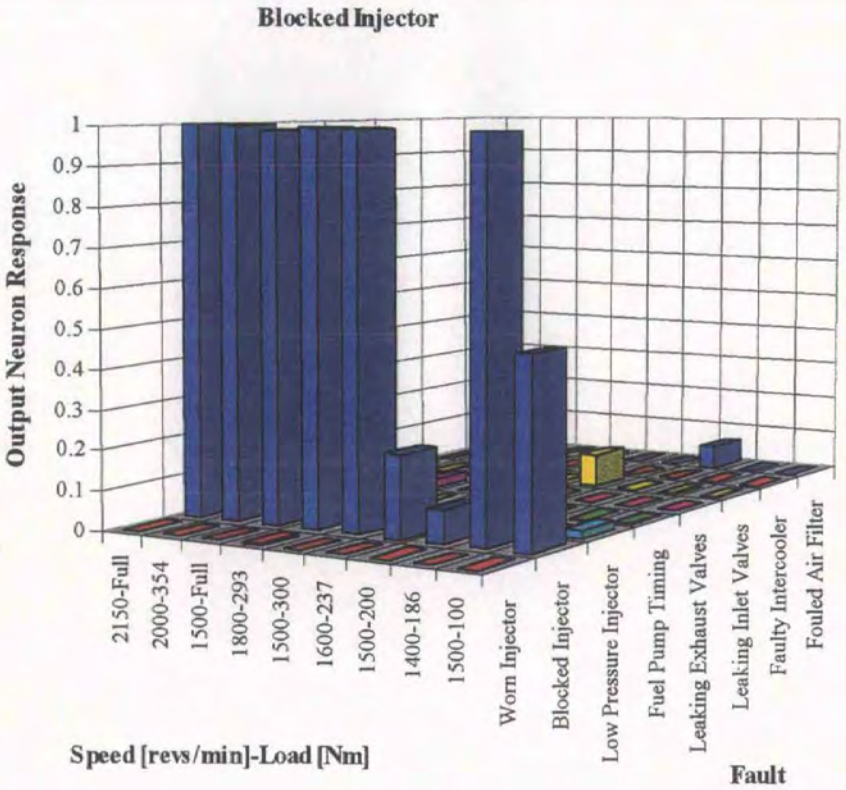

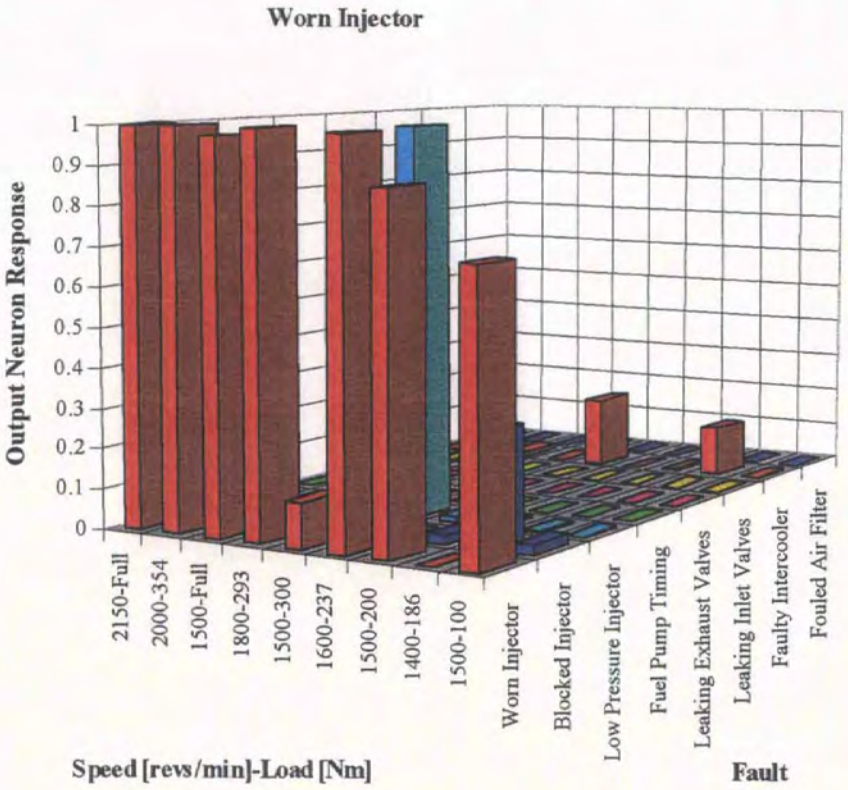

Figure 100 Ability Of Model 'B' To Diagnose A Blocked Injector & A Worn Injector When Tested With Previously Unseen Engine Data

Both models proved themselves to be competent diagnostic tools in the majority of cases. The following points summarise their performance.

- Both models correctly identified the healthy running condition of the engine in over 97% of instances. For example, if performance monitor performed 100 separate diagnosis's on a healthy engine it would incorrectly show the presence of a fault less than three times.
- Both models diagnosed an 80% blocked air filter with 100 % success and no mis-classifications.
- Model 'A' failed to diagnose a genuinely faulty intercooler at 1400 [revs/min] and 186 [Nm]. Similarly, Model 'B' gave a very poor diagnosis at this condition. At 1600 [revs/min] and 237 [Nm] both models mis-classified and gave outputs representing a low opening pressure injector. Model 'B', did however, simultaneously give an output representing a faulty charge cooler.
- Both models clearly diagnosed the presence of leaking inlet valves. Model 'A' also showed an output for leaking exhaust valves at 2150 [revs/min] and 372 [Nm].
- Exhaust valve leakage was 100 % diagnosed by both models with no mis-classifications.
- Model 'A' positively diagnosed 3° retarded injection at all torques and speeds except 1500 [revs/min] and 430 [Nm]. Model 'B's diagnosis was less positive throughout the speed and torque range and also suffered from poor diagnosis at 1500 [revs/min] and 430 [Nm]. Neither model mis-classified.
- Both models easily diagnosed a low opening pressure injector with no mis-classifications

- Model 'A's response to a blocked injector was good except at 1500 [revs/min] and 200 [Nm] where the output dropped to just above 0.5. Model 'B's performance was poor at three of the nine torques and speeds. Both models showed a very slight tendency to mis-classify.
- Diagnosis of a worn injector caused both models some problems. Model 'A' failed to diagnose at 3 speeds and torques and mis-classified the fault as either a low opening pressure injector or a blocked injector. Model 'B's performance was slightly better and only poorly diagnosed at 2 speeds and torques. As with Model 'A', Model 'B' also suffered mis-classification problems. Despite this mis-classification it was encouraging that both models identified that a fault was present, and that it was injector related.

9.3.2 Validation Of Neural Network Diagnostic Models 'A' & 'B' - Diagnosis Of Faults Of Lower Severity Than Those Trained On

The ability of the diagnostic models to identify the presence of a fault at its onset or before it becomes critical is a very valuable asset. If a diagnostic system has the ability to detect a fault in its infancy it allows the engineer to assess how the fault is developing, decide how long before corrective action is required and to correct the fault before it causes long term damage or catastrophic failure. To assess the models sensitivity to fault severity three faults were engine tested at two severities as follows;

- Engine testing of a fouled air filter was initially conducted at 80% fouling based on fault study and simulation results. Based on the engine test results obtained at 80% fouling further it was decided to undertake further engine testing at 30% fouling.

- The genuinely fouled and corroded intercooler obtained as a result of the fault study was subjected to engine test. Following this, engine test results were generated for a simulated faulty intercooler which created an intercooler fault of lower severity than the original genuinely faulty cooler tested.
- Simulation predicted that engine testing should start with 3° retarded fuel pump timing. After this, engine test was conducted with fuel pump timing set at 1.5^{o} retardation based on the engine test results obtained at 3°.

Neural Network Diagnostic Models 'A' & 'B' were trained and tested on the, 80% air filter fouling, genuinely faulty intercooler and 3° retarded injection engine test data as detailed in the above sections. The trained networks were then tested on engine data taken when the air filter was fouled by 30%, the intercooler had a simulated blockage less severe fault than the genuinely faulty intercooler and the fuel pump timing was retarded by 1.5^{o}. Full results can be seen in Appendix 'E'. The following comments summarise the performance of both models.

- Model 'A' detected and positively diagnosed the presence of a 30% fouled air filter at all speeds and torques except 1400 [revs/min] and 186 [Nm] and 2150 [revs/min] and 372 [Nm]. Although the response at these two test points was less than at other test points the neurons still registered an output. Generally the magnitude of output was less than experienced with the 80% filter fouling and no mis-classification occurred.

- Model 'A' successfully diagnosed the simulated faulty intercooler at the majority of torques and speeds. The poorest diagnosis occurring at 1400 [revs/min] and 186 [Nm]. Low neuron outputs were also experienced at 1500 [revs/min] and 430 [Nm] and 1800 [revs/min] and 293 [Nm].
- Model 'A' failed to diagnose 1.5^{o} retarded fuel pump timing at 1500 [revs/min] and 430 [Nm] and 1800 [revs/min] and 293 [Nm]. However, at all other torques and speeds this fault was positively diagnosed.
- The overall performance of Model 'B' was worse than model 'A'. All three faults were diagnosed with a generally lower level of confidence. Diagnosis of the 30% fouled air filter was not as positive as Model 'A', at three torque and speed conditions diagnosis was particularly poor.
- Model 'B's diagnosis of the simulated faulty intercooler was poor with 5 torques and speeds giving rise to neuron outputs of less than 0.5.
- Model 'B' failed to register an output for the 1.5^{o} retarded fuel pump timing at 2 speeds and torques. The neuron outputs at the other 7 speeds and torques were lower than Model 'A's.

9.3.3 Validation Of Neural Network Diagnostic Models 'A' & 'B' - Reaction To Completely Novel Faults

Models 'A' & 'B' were trained as described in Sections 9.2.1 and 9.2.2 but with a modified training set. All training data relating to leaking inlet valves and a worn injector was deleted from the training set. The network weights were completely randomised to destroy all former knowledge of these faults and then set to train. Both models converged to give a final maximum network error of less than 0.1. The models were then tested on leaking inlet valve and worn injector data sets. Both

responded well beyond expectations, full results of the diagnosis are contained in Appendix 'E'. The following comments summarise each models performance.

- When tested on the novel leaking inlet valve fault, Model 'A' gave outputs in excess of 0.9 at seven engine speeds and torques. More surprisingly it repeatably diagnosed the fault as leaking exhaust valves, which physically, is very similar to leaking inlet valves. At the remaining two speeds and torques where the diagnosis was not as positive the model gave smaller outputs, but still indicated that the fault was leaking exhaust valves.
- Model 'B' showed a similar response but only gave a positive diagnosis at six of the nine speeds and torques. Despite one output indicating a fuel pump timing fault, both models did not show any further evidence of mis-classification.
- Model 'A' gave a strong diagnosis when tested on the worn injector data, at 8 of the 9 speeds and torques. These high neuron outputs clearly diagnosed the fault as being a low pressure injector, which, in reality, is very similar to a worn injector .
- Model 'B' gave a similar response at 6 of the 9 speeds and torques on the worn injector data. With the exception of one output in both cases, the models did not indicate the presence of any other faults.
- The results of these tests proved that both models have the ability of making intelligent decisions when presented with completely novel data. Both models not only recognised that a fault was present but accurately made predictions on the nature of the fault.

9.3.4 Validation Of Neural Network Diagnostic Models 'A' & 'B' - Diagnostic Ability At Previously Unseen Speeds and Torques

The training data sets were edited and all engine test data relating to 1500 [revs/min] and 200 [Nm] was removed. The network weights were fully randomised to destroy any knowledge of the 1500 [revs/min] 200 [Nm] operating condition. Both networks were set to train until they converged to give a maximum network error of 0.1.

Both models were asked to perform a diagnosis when presented with data taken at 1500 [revs/min] and 200 [Nm] during both healthy and faulty modes of engine operation. The following points summarise the performance of both models, full results of the diagnosis can be found in Appendix 'E'.

- Model 'B' gave 4 significant outputs which indicated the presence of faults when presented with healthy engine test data. Model 'A's performance was significantly better giving only 1 output above 0.5 from the 32 sets of data presented to the model.
- Model 'A' correctly diagnosed the presence of an 80% fouled air filter, giving high outputs in 3 out of the 4 cases presented to the model. There was also some evidence of mis-classification. Model 'B's performance was particularly poor and failed to give a positive diagnosis of the 80% fouled filter. Further to this it had a tendency to mis-classify the fault as a faulty intercooler.
- Both models diagnosed the presence of a faulty intercooler 100% correctly with no mis-classifications.

- Leaking exhaust valves were positively diagnosed 100% correctly with no mis-classifications by both models.
- Both models positively diagnosed retarded fuel pump timing 100% correctly with no mis-classifications.
- The low opening pressure injector was clearly diagnosed in three out of four cases, by both models. Similarly, both mis-classified the low opening pressure injector as retarded fuel pump timing in the remaining case.
- Neither model performed particularly well on the blocked injector test data. Model 'B' only correctly diagnosed in one instance and managed to strongly mis-classify two other data sets. Model 'A's performance was slightly better since it also correctly diagnosed in one case, but only mis-classified once.

9.3.5 Validation Of Neural Network Diagnostic Models 'A' & 'B' - Diagnostic Performance On Noisy Sensor Data

Random variations of +/- 1% and +/- 2% were applied to each sensor reading in the validation data set, producing two more validation sets. These variations were set based on the magnitude of repeatabilities seen under test cell conditions and the performance repeatability of current production engines. The aim of this was to simulate poor sensor repeatability **above** that already experienced under test cell engine test conditions. It was thought that in practice data repeatability is worse than under test cell conditions. These two data sets were then presented to the inputs of both models. Both models were trained as described in Section 9.2. Full results can be found in Appendix 'E'. The following comments summarise each models performance.

- Model 'A' still effectively diagnosed the 80% fouled inlet air filter under both 1% and 2% simulated noisy data. Only the lowest speed and torque condition did not register a high neuron output. Model 'A' made 1 mis-classification on the 1% noisy data and 2 mis-classifications on the 2% noisy data. In comparison Model 'B's overall performance was similar. Model 'B' clearly diagnosed the 80% fouled air filter at 6 of the 9 speed and torque conditions and gave no mis-classifications on the 1% noisy data. When tested on the 2% noisy sensor data Model 'B' diagnosed the fouled air filter well at all speeds and torques except one and only gave one mis-classification.
- Diagnosis of the genuinely faulty intercooler was largely successful. Model 'A' diagnosed correctly at 7 of the 9 speeds and torques with no mis-classifications on the 1% noisy data. Model 'A's test on the 2% noisy data gave a good diagnosis of the faulty intercooler at 5 speeds and torques and one mis-classification. Model 'B' successfully diagnosed the genuinely faulty intercooler at 7 of the 9 speeds and torques and gave 2 mis-classifications when tested on the 1% noisy data. When tested on the 2% noisy data, Model 'B' correctly diagnosed at 6 speeds and torques and gave 1 mis-classification.
- Model 'A' diagnosed leaking inlet valves 100% correctly at all speeds and torques with no mis-classifications when tested on the 1% noisy data. Model 'A' also correctly diagnosed leaking inlet valves at 8 of the 9 speeds and torques and gave no mis-classifications on the 2% noisy data. Model 'B's performance on the 1% noisy data was comparable Model 'A's. Testing on the 2% noisy data, however, showed a poorer performance with positive diagnosis at only 7 speeds and torques and 1 mis-classification.

- Leaking exhaust valves were diagnosed well by both models based on the 1% noisy data. Model 'A' successfully diagnosed at 8 of the 9 speeds and torques and showed a tendency for mis-classification at one speed and torque. Model 'B' correctly diagnosed at all speeds and torques with one neuron output being slightly low and no evidence of mis-classifications. Testing on the 2% noisy data gave a similar response except Model 'B' gave one strong mis-classification.
- Model 'A' diagnosed retarded fuel pump timing at 8 and 7 of the 9 speeds and torques when tested on the 1% and 2% noisy data respectively. Model 'B's performance was poorer than Model 'A'. Model 'B's diagnosis on 1% noisy data gave low neuron outputs at 2 of the 9 speeds and torques. Testing on the 2 % noisy data gave low neuron outputs at 4 of the 9 speeds and torques and some evidence of mis-classifications.
- Diagnosis of the low opening pressure injector on 1% noisy data by both models was generally good, however both gave strong mis-classifications at one speed and torque. Testing on the 2% noisy data caused an increase in number of mis-classifications in both cases.
- Both models showed evidence of mis-classification when diagnosing a blocked injector. The number of misclassifications increased as the degree of noisiness of data increased. Despite this, neuron outputs indicating the presence of a blocked injector were high at the majority of speeds and torques for both models.
- The worn injector fault was poorly diagnosed by both models on 1% and 2% noisy data. Both models mis-classified on numerous occasions and gave low 'worn injector' neuron outputs at a number of speeds and torques.

9.3.6 Validation Of Neural Network Diagnostic Models 'A' & 'B' - Ability To Diagnose Selected Faults On Faulty Sensor Data

Both models were trained as described in Sections 9.2.1 and 9.2.2. Three faults were selected at random, namely, fouled inlet air filter, leaking inlet valves and retarded pump timing. For each of these faults two key diagnostic sensors were identified from the fault-symptom relationships developed in Chapter 8. Severe sensor failure often leads to the sensor giving either no reading at all or a full scale reading. To simulate sensor failure the validation data sets were modified. Data from both key sensors was changed to read either zero or full scale. Table 39 shows the key sensors chosen for each fault and the modified faulty sensor data which was substituted into the validation data sets for testing.

Test No.	Fault Description	Key Sensor 1 Reading	Key Sensor 2 Reading
1	Fouled Inlet Air Filter	0 [m^3/hr] inlet air flow	1200K 1 & 2 exhaust port temperature
2	Fouled Inlet Air Filter	700 [m^3/hr] inlet air flow	0 [K] 1 & 2 exhaust port temperature
3	Leaking Inlet Valves	0 [K] inlet manifold temperature	0 [K] turbine discharge temperature
4	Leaking Inlet Valves	1200 [K] inlet manifold temperature	1200 [K] turbine discharge temperature
5	Retarded Injection Timing	100000 [revs/min] turbocharger speed	0 [Kpa] inlet manifold temperature
6	Retarded Injection Timing	0 [revs/min] turbocharger speed	200 [Kpa] inlet manifold pressure

Table 39 Simulated Faulty Sensor Data Substituted Into The Validation Sets

The two models were tested on the simulated faulty sensor validation data sets. Full results can be seen in Appendix 'E'. The following comments summarise both models performance under faulty sensor data.

- Both models 100% correctly identified the fouled inlet filter under Test 1 conditions. Both models failed to diagnose the fouled inlet air filter on Test 2

validation data. Model 'A' mis-classified on a couple of occasions whilst Model 'B' mis-classified frequently.

- Model 'A' correctly diagnosed leaking inlet valves under Test 3 conditions. It also 100% diagnosed the fault as retarded injection timing simultaneously. Model 'B' correctly identified leaking inlet valves and gave no mis-classifications under Test 3 conditions. Both models diagnosed leaking inlet valves as a faulty intercooler under test 4 conditions. Further to this, Model 'B'' simultaneously diagnosed the fault as a worn injector.
- Both models diagnosed retarded injection timing as leaking inlet valves under Test 5 conditions. Model 'A' diagnosed retarded pump timing as a faulty intercooler, a worn injector and showed some evidence of low opening pressure injector neuron outputs under Test 6 conditions. Model 'B' clearly diagnosed the retarded injection timing as a faulty intercooler when tested on Test 6 data.

9.3.7 Summary Of Neural Network Diagnostic Models 'A' & 'B' Performance

Assuming that an output of greater than 0.5 on the correct neuron constitutes a correct diagnosis. The basic diagnostic performance of both models when tested on normal engine data representing conditions which the networks had been trained on was good. The following points compare and summarise the performance of both models.

- Model 'A's performance was marginally better than Model 'B's since it successfully diagnosed in 1% more cases when tested on the validation data set.
- Model 'A's performance on data representing varying fault severity was better than Model 'B's.

- Model 'A' proved to be more robust than Model 'B' on noisy sensor data. Model 'A' correctly diagnosed in 7% more cases on 1% noisy data and over 11% more cases on 2% noisy data when compared to Model 'B'.
- The diagnostic performance of both models was comparable when tested on data taken at a novel speed and torque or under novel fault conditions.
- Both model's performance on faulty sensor data was very poor.

9.4 Summary

This chapter has partially satisfied research objective 6, identified in Chapter 1, and has shown how a neural network can be developed to perform diesel engine fault diagnosis. Key diagnostic sensors have been identified and used as neural network inputs. Several training algorithms and were investigated to achieve optimum performance. The two most successful neural network models were validated against the practical success criteria defined in Section 9.0. The following points summarise.

- The sensors used for diagnosis were cheap, robust, relatively non-intrusive and easily installed.
- The Stochastic Back Propagation Algorithm offered the best method of neural network training.
- The degree of network training affected their diagnostic ability. Insufficient training led to 'fuzzy' results and a poor diagnosis. Too much training gave a good positive diagnosis. Unfortunately, it also led to an increased number of mis-classifications.

- The number of hidden layer neurons affected the neural networks diagnostic performances. In this research the number of both input and output neurons were fixed. Increasing the number of hidden layer neurons led to a 'fuzzy' diagnosis, too few neurons led to mis-classifications.
- The networks could diagnose the following faults at a genuine severity with varying levels of success.

  Fouled inlet air filter
  Genuinely fouled & corroded faulty intercooler
  Leaking inlet valves
  Leaking exhaust valves
  Retarded fuel pump timing
  Genuinely worn injector
  Genuinely blocked injector
  Genuine low pressure injector

- The networks could diagnose faults of lower severity than those found on engines currently in operation. This was demonstrated using the fouled air filter, intercooler and fuel injection timing faults.
- Diagnosis could be performed under noisy sensor data conditions however, the diagnostic accuracies of the neural network outputs were compromised. Previous research has also suggested this is true. It should, however, be noted that the noisier the data the worse the diagnosis.
- The diagnostic performance of the networks on novel faults on which they not had been trained was impressive. They clearly registered that a fault was present despite never being trained. More importantly, they had the ability to correctly draw similarities between novel faults which were physicaly similar to faults on which they had been trained.

- The neural networks could diagnose at a speed and torque at which they had not been trained but the diagnostic accuracies were slightly impaired.
- Despite previous research suggesting otherwise, the neural networks suffered a severe degradation in performance when given faulty data from key diagnostic sensors. It may be true to say that less important sensors could fail and not affect the diagnosis significantly. In this respect diagnosis would be much more robust if several parameters changed by a small amount as oppose one sensor giving huge deviations under fault conditions.

Based on the results of all the testing done Model 'A' was shown to be more competent diagnostic model than Model 'B'. Despite Model 'A' requiring a longer training time than Model 'B', it was thought that this disadvantage was out-weighed by the improved diagnostic performance. Although better than Model 'B', Model 'A' had the following weaknesses which needed to be addressed before it could be considered a practical diagnostic tool.

- The model gave 10 mis-classifications when tested on the validation data. This represents a mis-diagnosis rate of 1.2%
- The diagnostic ability of the model was degraded from 98% successful on the validation data to 79.8% on the 1% noisy data and, 71.7% on the 2% noisy data.
- The model failed to give neuron outputs greater than 0.5 in six instances of diagnosis based on normal validation data. Assuming that an output greater than 0.5 is required for a positive diagnosis. The model failed to diagnose that a fault was present in 8.3% of cases. For example, if the network was asked to perform

100 independent diagnoses on a faulty engine it would incorrectly identify that the engine was healthy 8.3 times.

- The model clearly fails to diagnose correctly when subjected to faulty sensor data.

The work has shown that even the best model developed was unsuitable for practical diesel engine fault diagnosis because of the deficiencies identified above. It was decided that further work was required to develop a practically viable neural network based diagnostic system. As a result, a significant amount of original work was completed to develop and validate two extra diagnostic modules. This work is discussed in Chapter 10.

CHAPTER 10

DEVELOPMENT & VALIDATION OF A NEURAL NETWORK BASED DIAGNOSTIC SYSTEM

10.0 Introduction

To address the weaknesses identified in Chapter 9 and satisfy the success criteria listed in Section 9.0 further work was required to create the final diagnostic system. The validation of the neural network showed that occasionally the network gave a weak output classifying the fault correctly, but not confidently. In other instances the model gave spurious mis-classifications. One of the objectives of the work discussed in this chapter was to develop and validate a technique which could take the raw neural network outputs and convert them into a data-set which would allow a correct, reliable and repeatable diagnosis to be made by the system despite the problems which existed with the raw neural network outputs under practical conditions.

As a result, original work has been conducted and a new technique for enhancing neural network generated data for diagnostic purposes has been developed and validated. Further to this, a method of recognising faulty sensor data has been developed which can be incorporated into the final diagnostic system.

This chapter also discusses how the individual elements of the performance monitoring package, neural network, neural network raw output processing and

faulty sensor data recognition modules can be combined together to create a practically viable, on-line diesel engine fault diagnosis system.

10.1 Development Of A Technique To Enhance Neural Network Diagnostic Ability

All of the validation work discussed so far has assumed that the ultimate diagnosis would be based on a single diagnosis from one data set. In reality, Performance Monitor could run continuously and generate many successive data sets. Considering this, and the knowledge that the neural network makes more correct diagnoses than incorrect, a new technique for dramatically improving the diagnostic performance of the neural network was developed. The whole principle is based on the fact that it is more probable the neural network will produce a comparatively larger output from the correct neuron than from an incorrect neuron for a given engine health condition. The neural network validation in Chapter 9.0 showed this to be true.

This new technique developed to enhance the diagnostic ability of a neural network uses the new approach of linking an on-line diagnostic database to the raw network outputs. The data actually used to perform the diagnosis comes from the diagnostic database. The database is fed successive raw neural network output vectors and re-computes it's output based on the current network output and the previous 'n' neural network output vectors. This worked by comparing a form of cumulative average of all previous network outputs held in the database, with the latest network outputs. If the latest diagnosis agreed with the database diagnosis then the maximum output of

the latest diagnosis was increased by a weighting factor. Similarly, lesser neuron outputs which disagreed with the database diagnosis were reduced even further to strengthen the diagnosis. The latest diagnosis result was then added to the database and further strengthened the databases diagnosis. By using a diagnostic database spurious mis-classifications could be eliminated and correct but small neuron outputs could be amplified since the database could enhance the latest diagnosis based on the results of many previous diagnoses.

To implement the on-line diagnostic database a Visual Basic For Applications, VBA, program was written which performed the following steps.

1. Select the key diagnostic sensor readings from the performance file.
2. Pass the sensor data to the neural network as the input stimulus.
3. Interrogated the neural network for the diagnosis.
4. Returned the neural network output layer results to an Excel worksheet.
5. Managed the data in the worksheet so that each successive diagnosis was added to a database.

A full copy of this program named DIAMAC.XLM can be found in Appendix 'E'. To perform the cumulative averaging and weighting of the neural network outputs in the database to give the improved diagnostic ability an algorithm was developed. As each successive diagnosis was added to the worksheet a series of calculations were performed as follows.

1. Calculate the cumulative average of each of the output neurons i.....j;

$$X_j^i = \frac{nd_j^i + (n+1)d_j^i .....Nd_j^i}{N} \qquad \text{Equation 21}$$

X = cumulative average, where *i* is the *ith* output neuron and *j* is the *jth* output neuron, *n* is the number of successive diagnosis's and *d* is the neuron output.

2. Calculate the cumulative product of output neurons *i.....j* after each diagnosis;

$$Z_j^i = nd_j^i * (n+1)d_j^i * .....Nd_j^i \qquad \text{Equation 22}$$

3. From the cumulative average and cumulative product calculate a confidence factor. The confidence factor was designed to increase the neuron output which had the most frequently occurring maximum output. Successively small outputs or occasional high outputs were heavily penalised. After '*n*' diagnoses the confidence factor was given by;

$$C_n = \left[\frac{Z_{j_n}^i}{Z_{j_n \max}^i} \right]^3 \qquad \text{Equation 23}$$

4. Calculate the database output after '*n*' diagnoses;

$$Y_{j_n}^i = X_{j_n}^i * C_n \qquad \text{Equation 24}$$

10.2 Validation Of The Diagnostic Database

Following the development of the on-line diagnostic database it was validated on previously unseen Performance Monitor files. The files were presented to the neural network in a completely random order and represented all of the following conditions.

- Normal experimental engine test data, previously unseen by the network, taken under healthy and all faulty modes of running at all test point speeds and torques.
- Experimental test data which had been subjected to random +/- 1 and +/- 2% variations above normal practical repeatability's on all sensor readings.
- Engine test data taken at speeds and torques on which the network had not been trained.
- Lower severity faults on which the network was not trained.

These conditions represented everything which the diagnostic system would be likely to see in a practical application with the exception of sensor failure. The outputs were monitored as the diagnostic database was tested on all of the above data sets. Figures 101 to 112 show a comparison between the raw neural network outputs and the diagnostic database outputs as successive diagnoses were made.

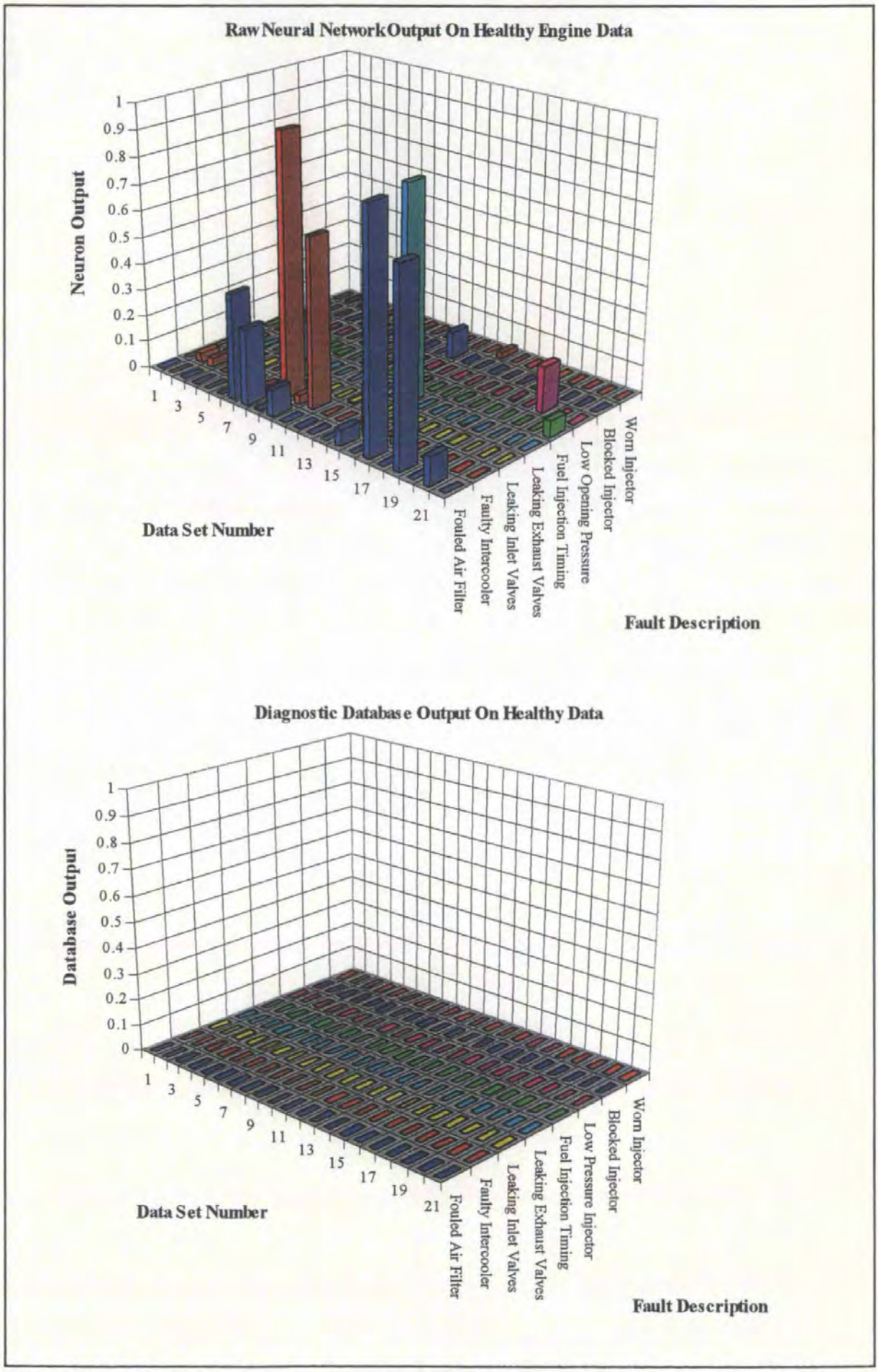

Figure 101 Neural Network & Diagnostic Database Results On Healthy Engine Data

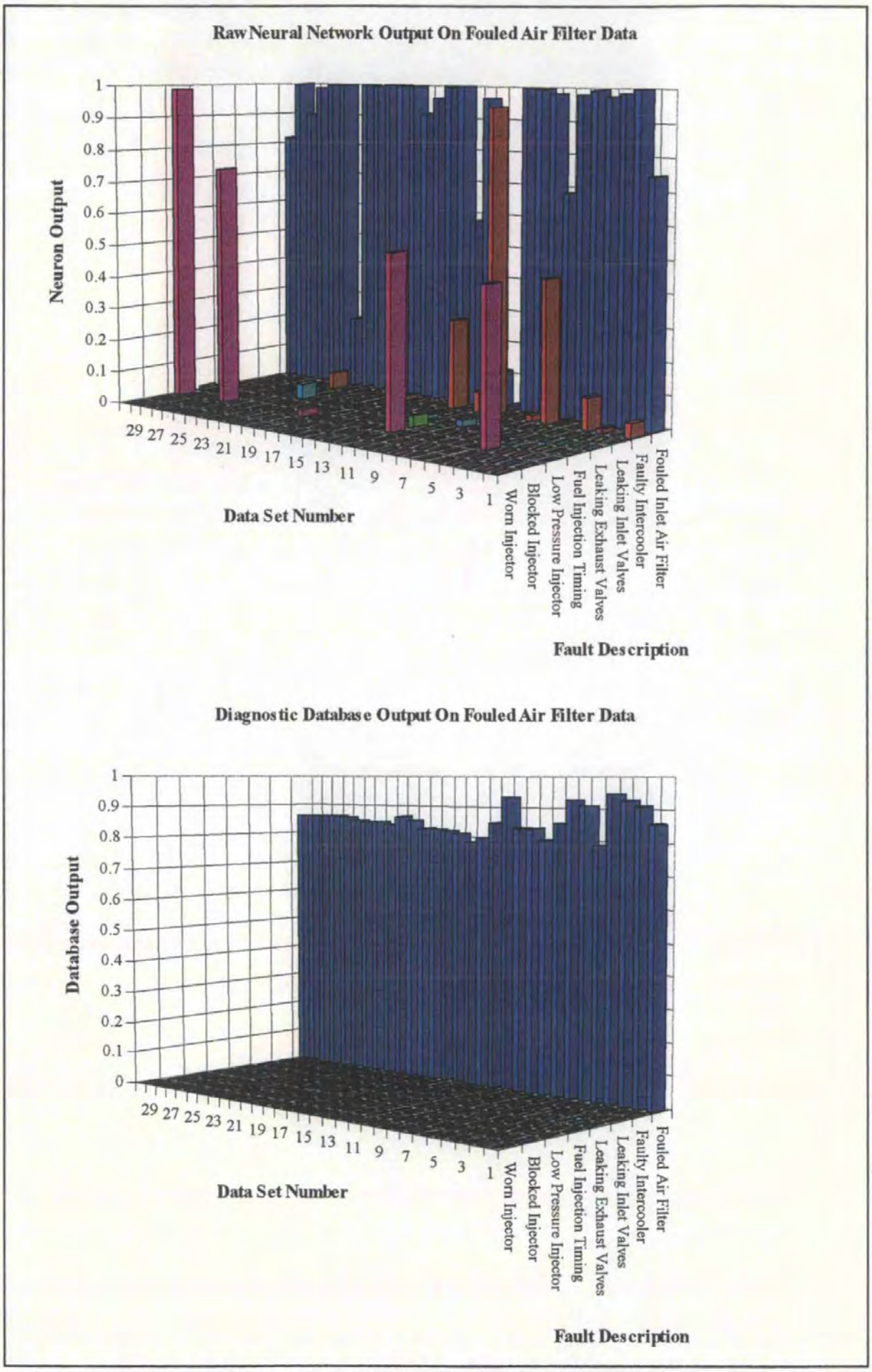

Figure 102 Neural Network & Diagnostic Database Results On Fouled Air Filter Engine Data

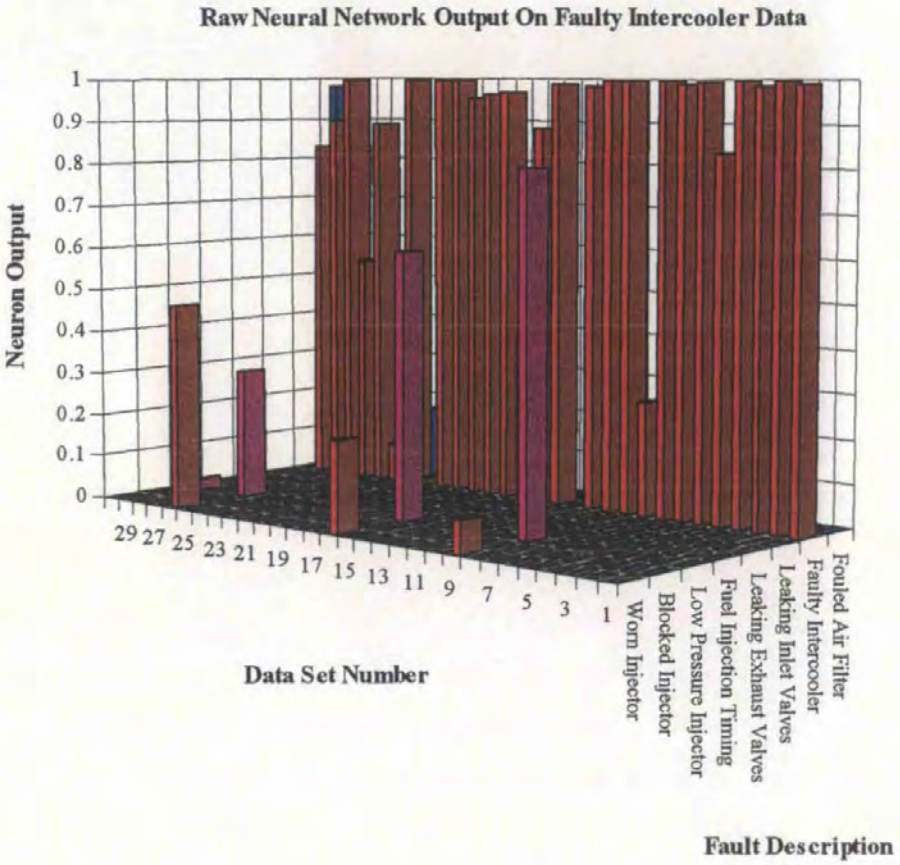

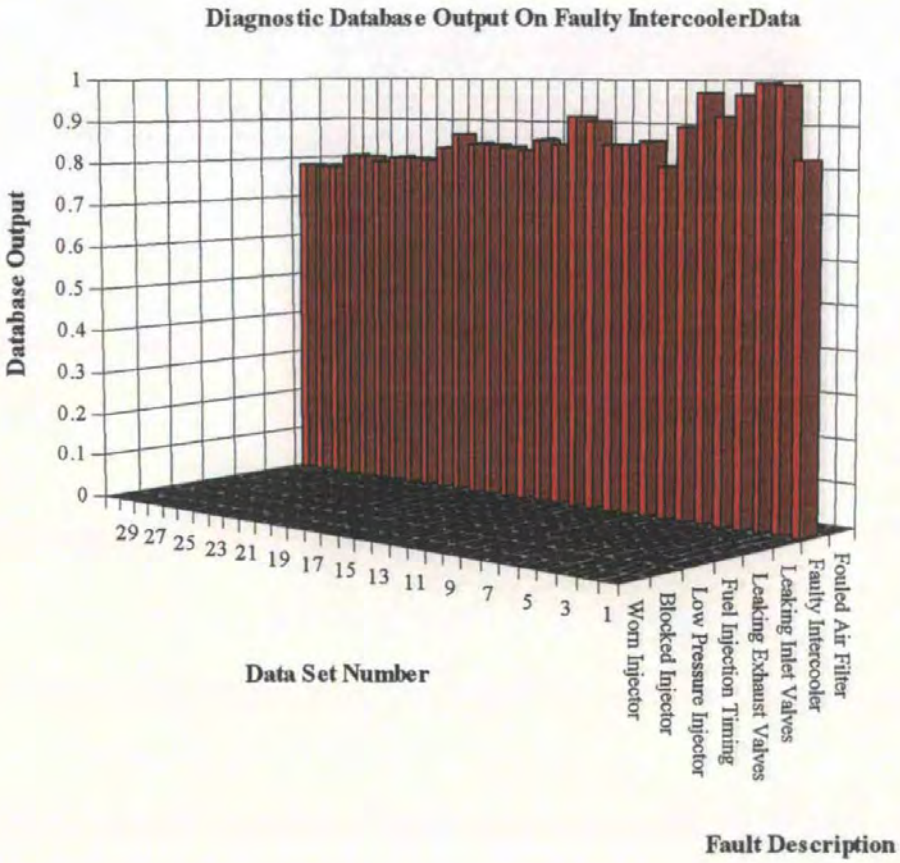

Figure 103 Neural Network & Diagnostic Database Results On Faulty Intercooler Engine Data

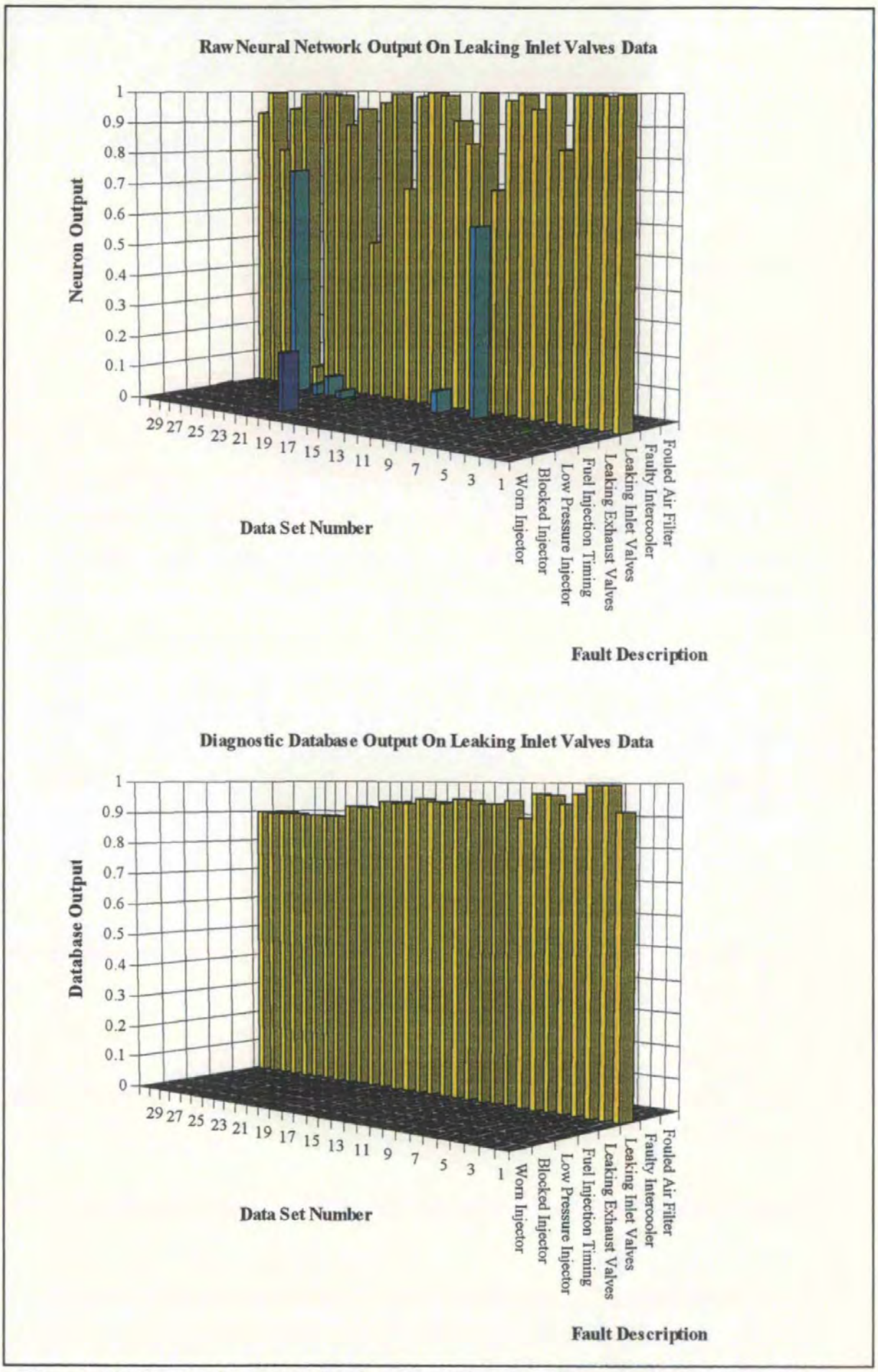

Figure 104 Neural Network & Diagnostic Database Results On Leaking Inlet Valves Engine Data

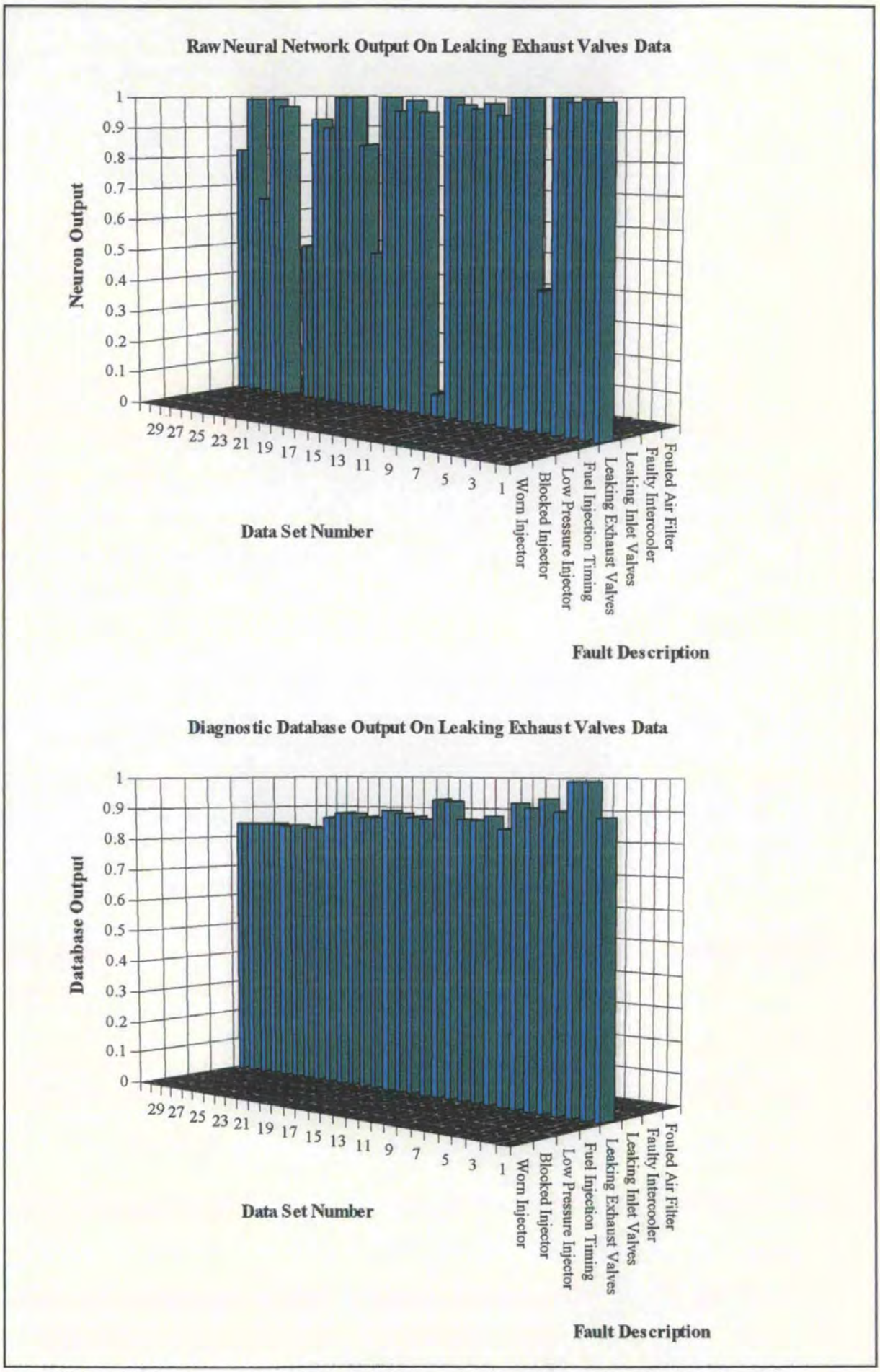

Figure 105 Neural Network & Diagnostic Database Results On Leaking Exhaust Valves Engine Data

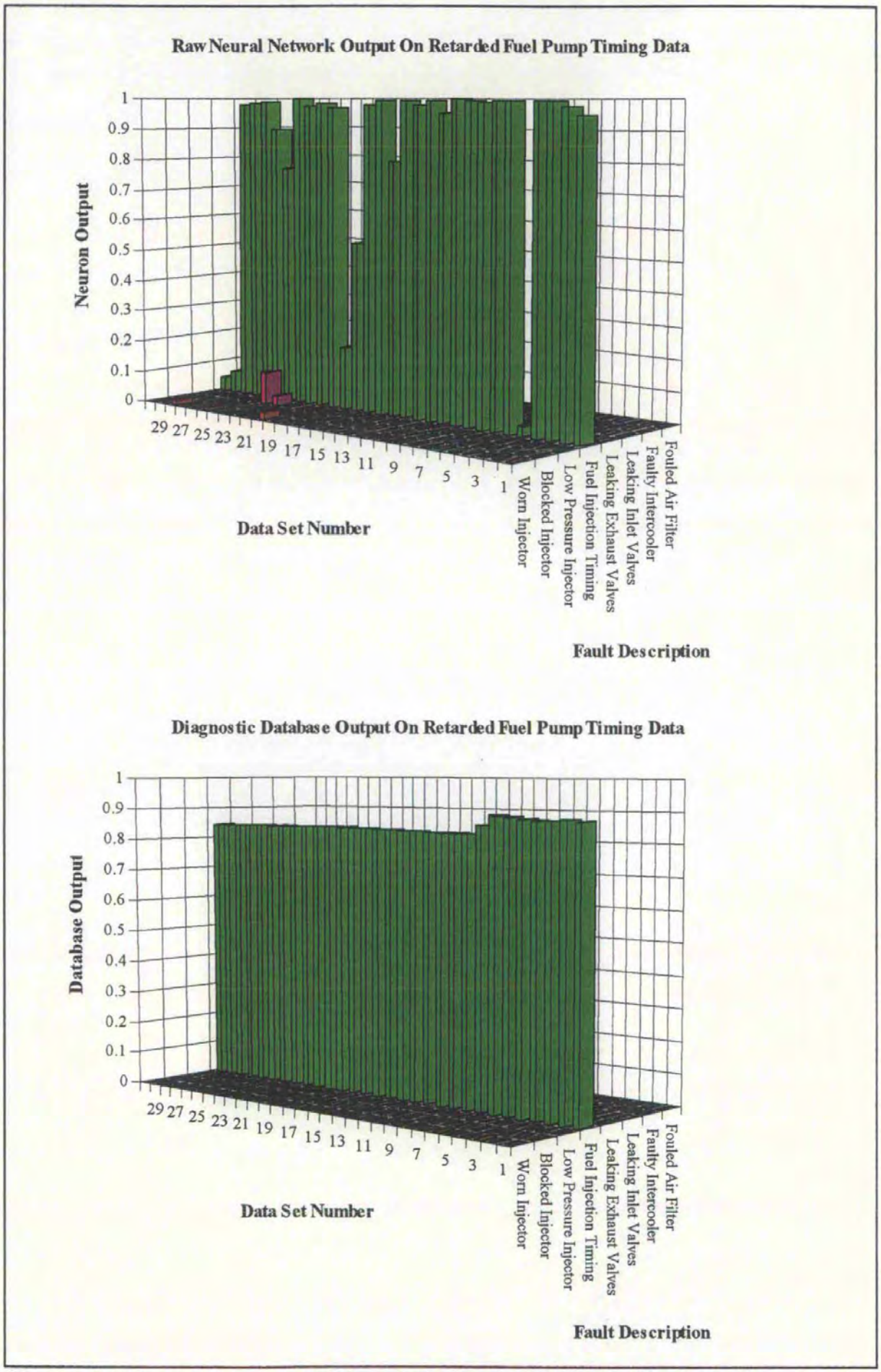

Figure 106 Neural Network & Diagnostic Database Results On 3 Deg Retarded Fuel Pump Engine Data

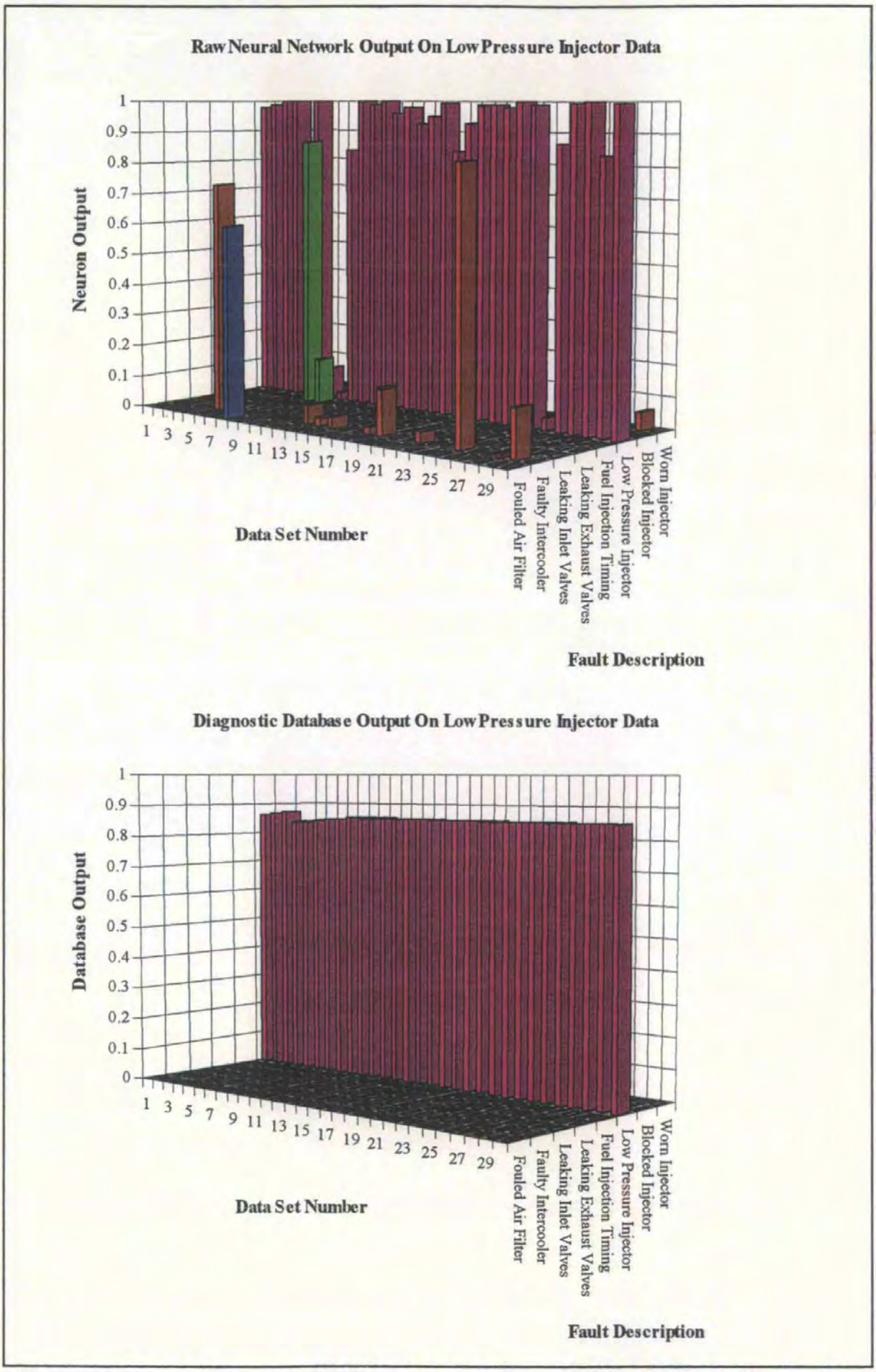

Figure 107 Neural Network & Diagnostic Database Results On Low Pressure Injector Engine Data

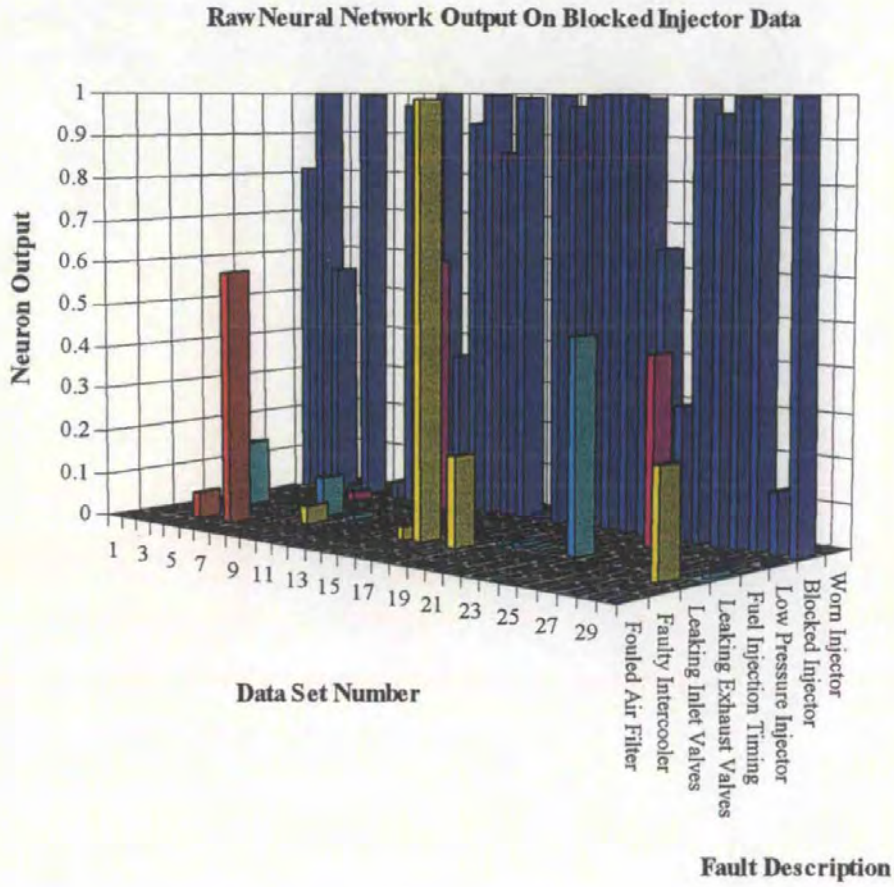

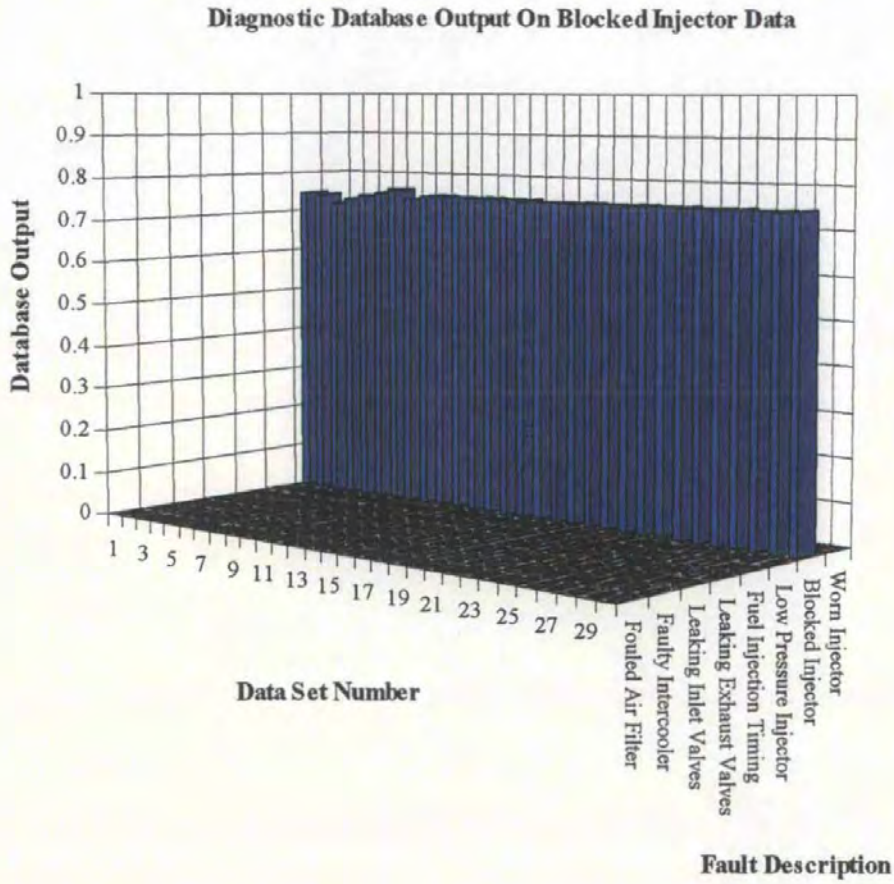

Figure 108 Neural Network & Diagnostic Database Results On Blocked Injector Engine Data

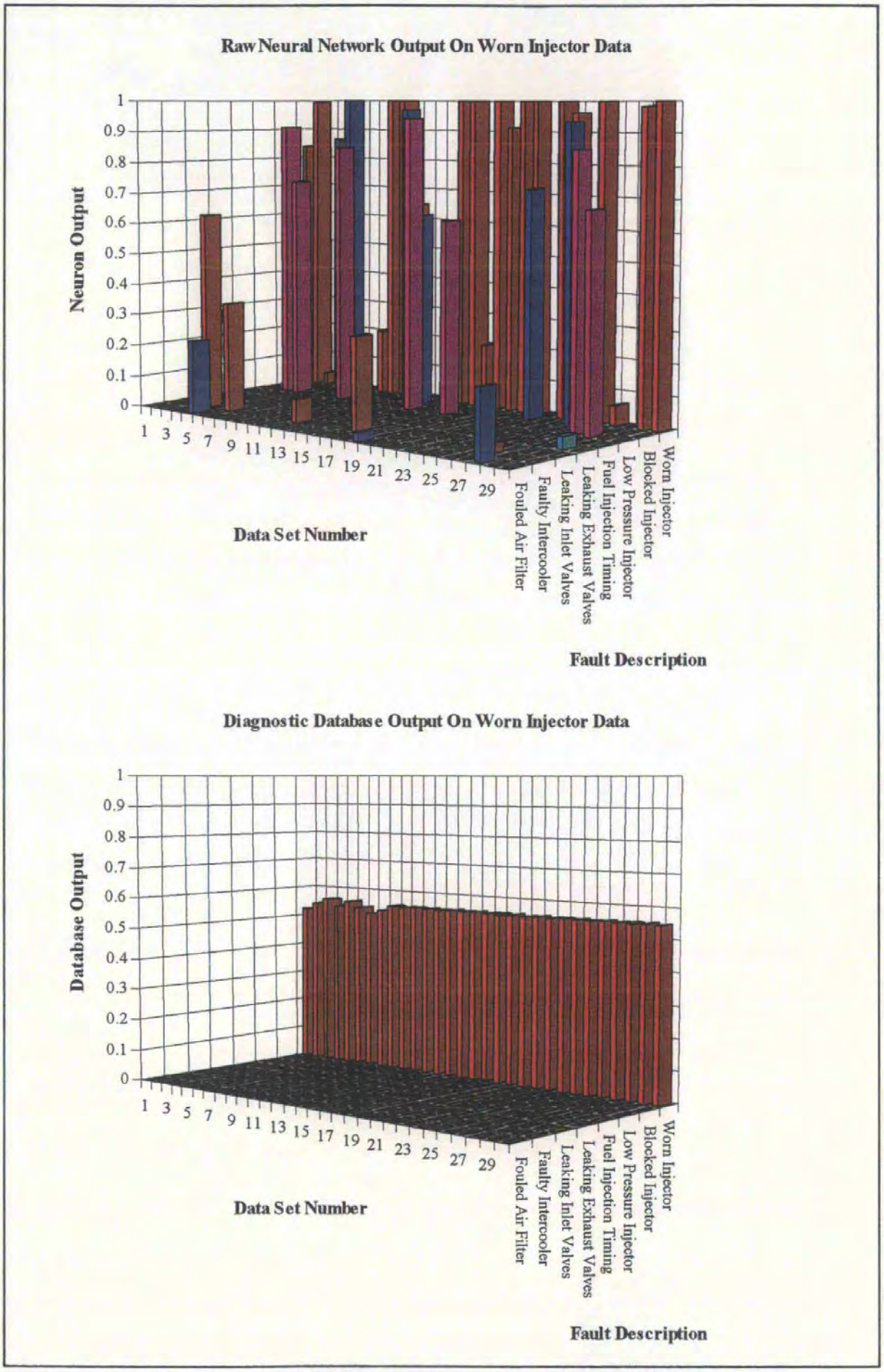

Figure 109 Neural Network & Diagnostic Database Results On Worn Injector Engine Data

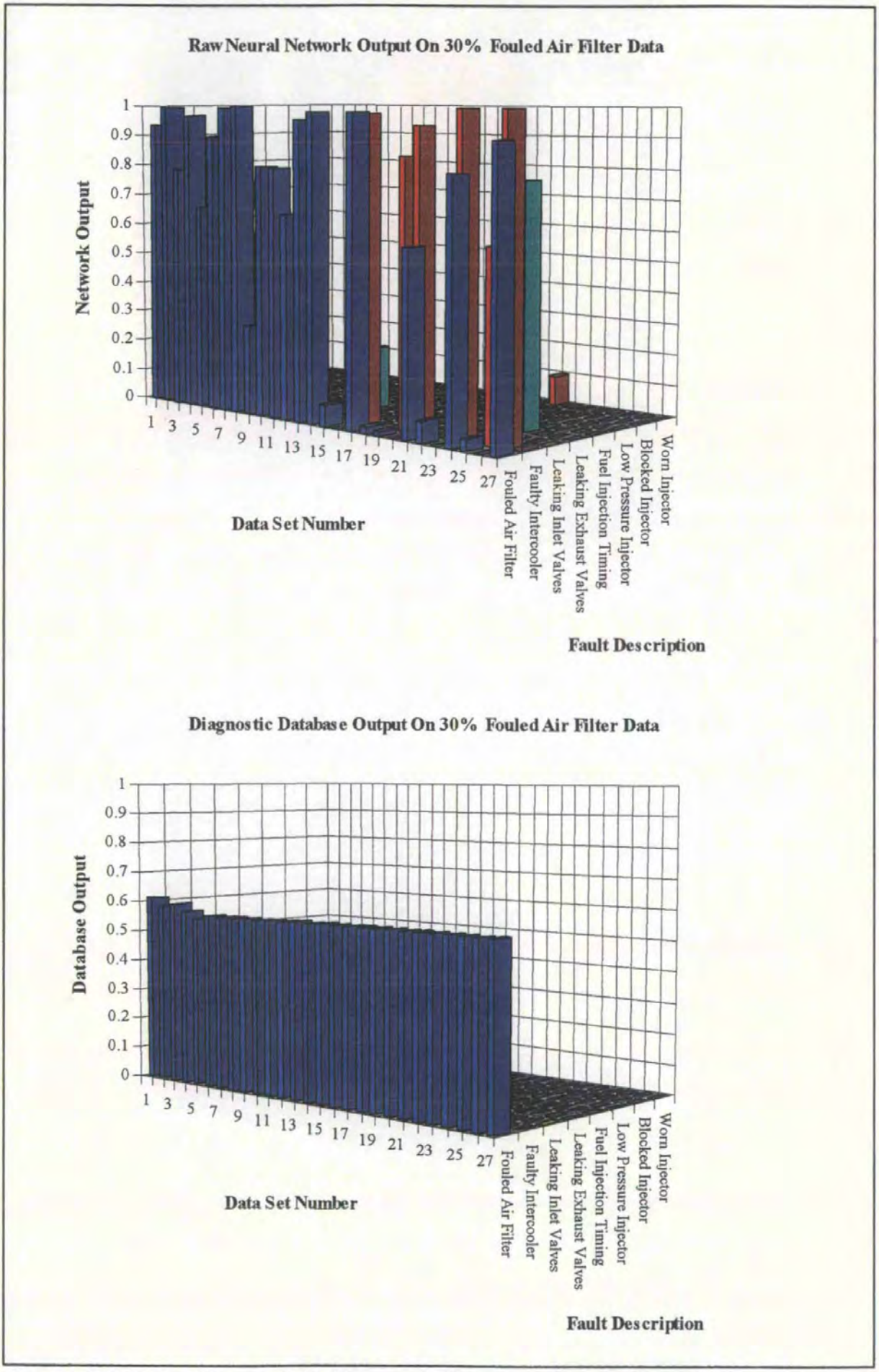

Figure 110 Neural Network & Diagnostic Database Results On 30% Fouled Air Filter Engine Data

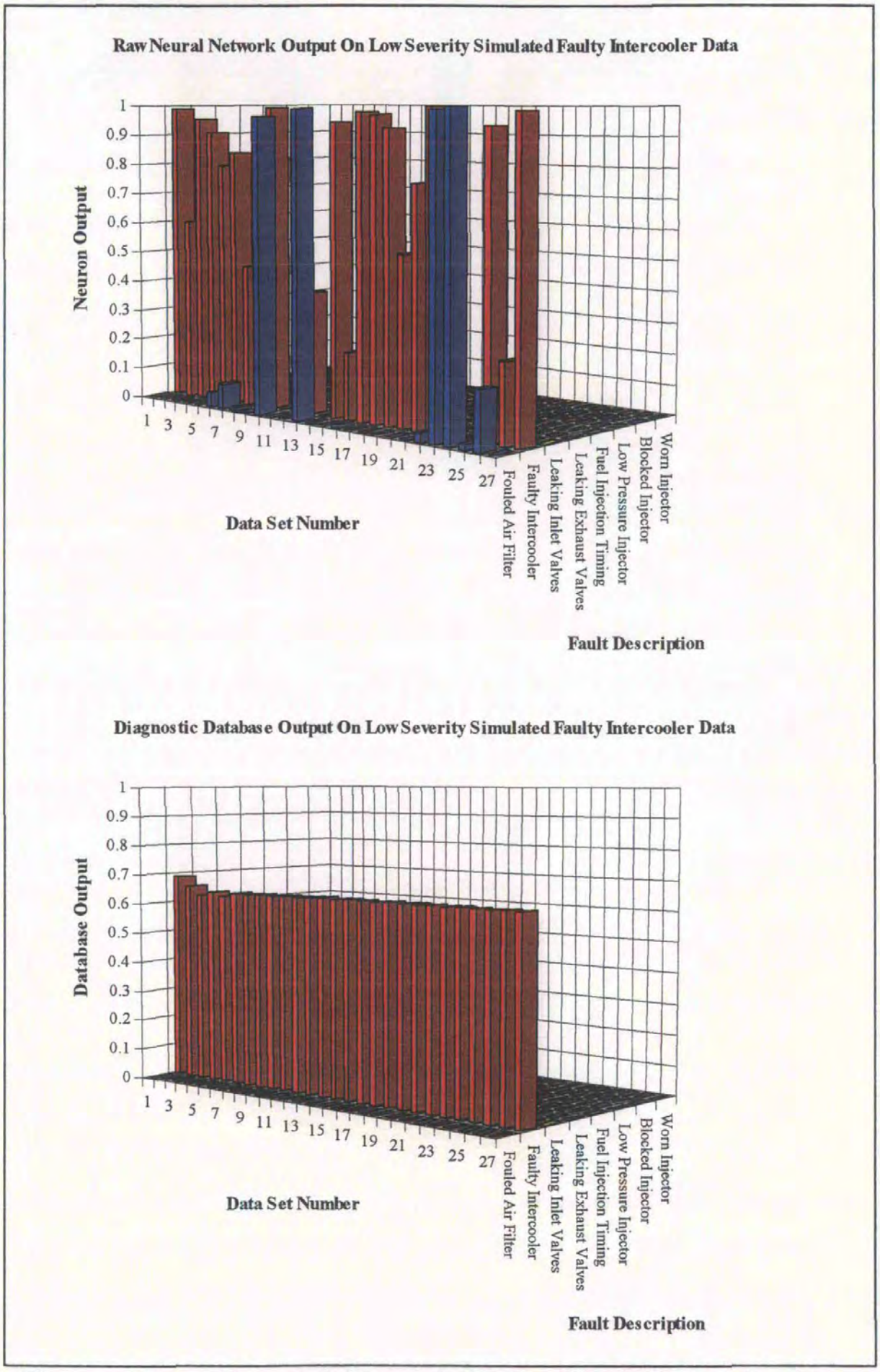

Figure 111 Neural Network & Diagnostic Database Results On Low Severity Simulated Faulty Intercooler Engine Data

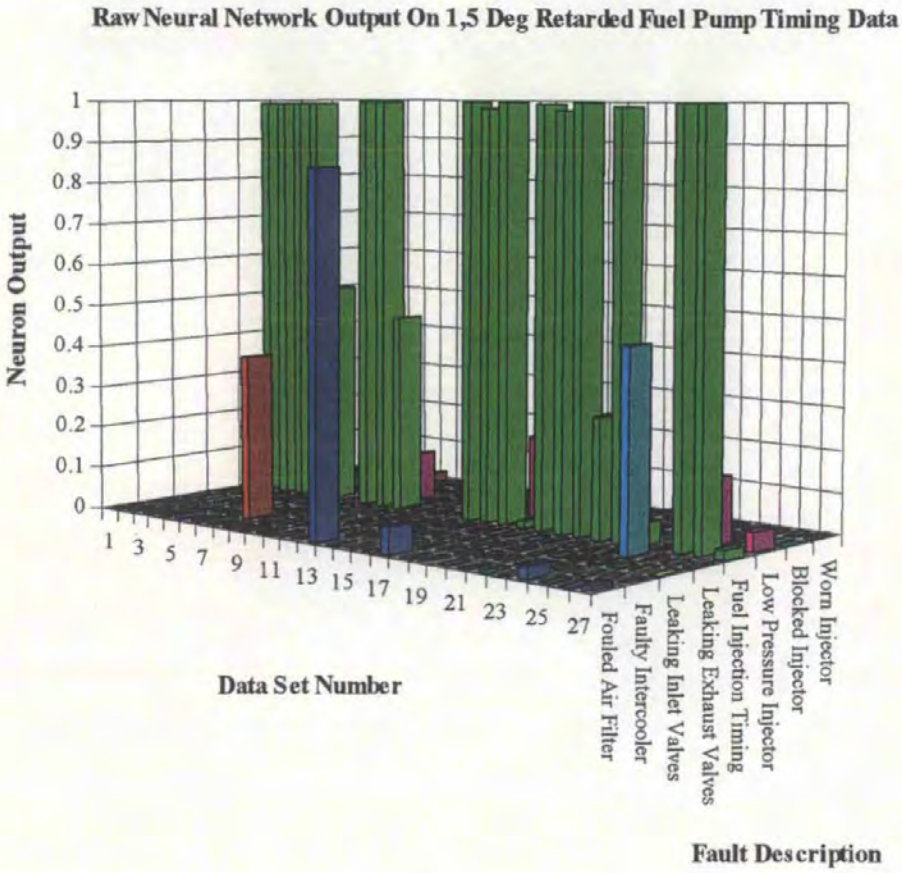

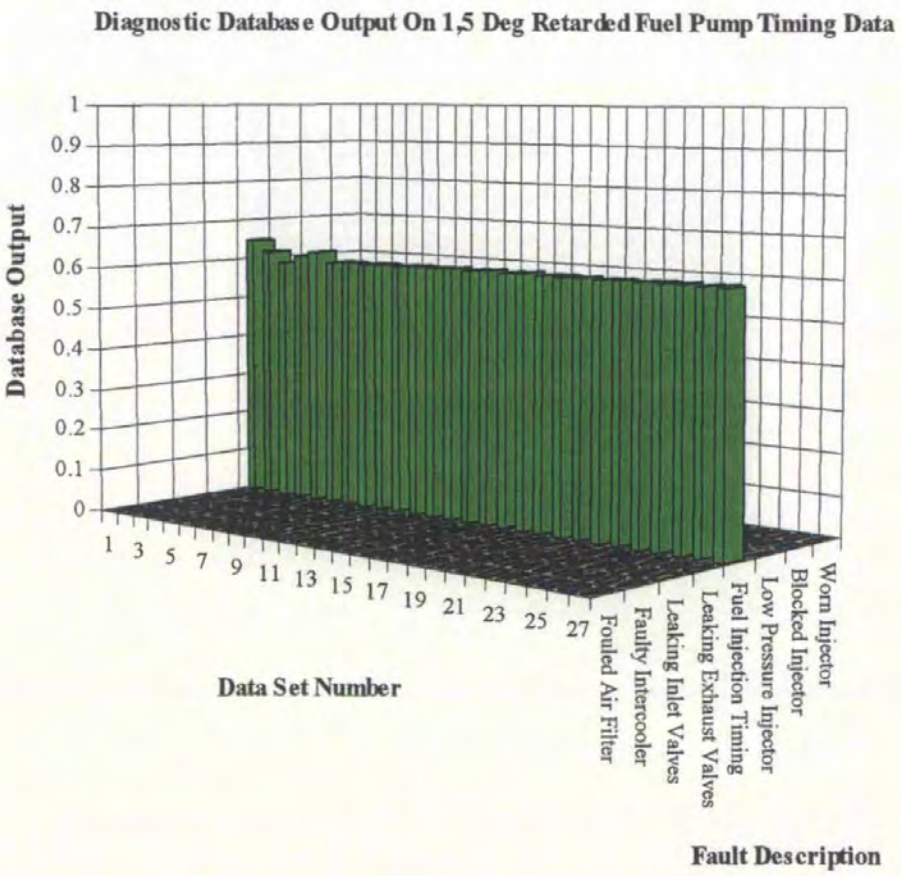

Figure 112 Neural Network & Diagnostic Database Results On 1.5 Deg Retarded Fuel Pump Timing

The results show that the novel approach of linking the neural network to an on-line diagnostic database **greatly improves** the diagnostic performance. The following comments discuss the diagnostic databases performance.

- Spurious mis-classifications were totally eliminated under all conditions including noisy sensor data and novel engine speeds and torques.
- Low neuron outputs which correctly identified the fault were enhanced by nature of the fact that the other seven neuron outputs were low and the low neuron output agreed with the current database output.
- The trend in successive database outputs can be used to monitor the development of the fault since the level of database output genuinely reflects the fault severity. The 80% fouled air filter gave a final database output of 0.86 on the correct neuron. The 30% fouled air filter gave a neuron output of 0.56. The genuinely faulty intercooler gave a final database output of 0.78 whereas the lower severity simulated faulty intercooler gave a database output of 0.64. The 3 degree retarded fuel pump timing gave a final database output of 0.84 as oppose to the 1.5 degree retarded fuel pump timing which gave a database output of 0.60. This is very important since the diagnostic system not only detects the low severity faults but can quantify the level of severity. This would allow minor faults develop and only implement corrective action when necessary.
- The diagnostic database accurately diagnoses 100% of the time under both healthy and faulty engine operation on all faults and under all conditions.
- The nature of the calculation in the database weights the successive diagnoses. This means that if the engine had been running healthily for an extended duration the database would be slow to respond to the occurrence of a fault. The rate of

detection would be proportional to the number of diagnoses made during healthy engine operation since any neuron output indicating a fault would be over-ruled by the database values. The number of successive database results should be limited to, say 10, and then the database be completely refreshed. The number of successive database results used is a function of desired diagnostic system response time and the diagnostic accuracy of the raw neural network inputs. For example a neural network with excellent diagnostic clarity would require fewer database values to provide a good basis for decision making.

- The confidence factor and weight adjusting algorithms discussed here work extremely well on single faults. Further work would be required to adapt this technique for the diagnosis of multiple faults.
- The database results allow very accurate and easy decision making by simple greater than/less than statements.

10.3 Safeguarding Against Incorrect Diagnosis Due To Sensor Failure

Section 9.3.6 showed that the model performed very badly when key diagnostic sensors failed. This often lead to very positive mis-classifications. The problem was addressed by developing a sensor filter network which was trained to recognise full scale or zero sensor outputs. The engine sensor data could be fed through the sensor filter before feeding into the engine diagnostic network. This would allow a sensor check to be performed before every diagnosis.

To demonstrate this principle a network was trained on three complete sets of engine data. The first set was the training set used for all network development in

this chapter. The second and third data sets had the air flow sensor readings modified to zero and full scale respectively. All three data sets included data which represented healthy and faulty modes of engine operation at all speeds and torques. The network trained very quickly using the Stochastic Back Propagation Algorithm and was tested on validation sets which were selected at random but represented healthy and faulty modes of engine operation and various speeds and torques. In all cases the sensor filter positively identified if the air flow sensor was healthy or faulty. Figure 113 shows the sensor filter's ability to diagnose the faulty air flow sensor.

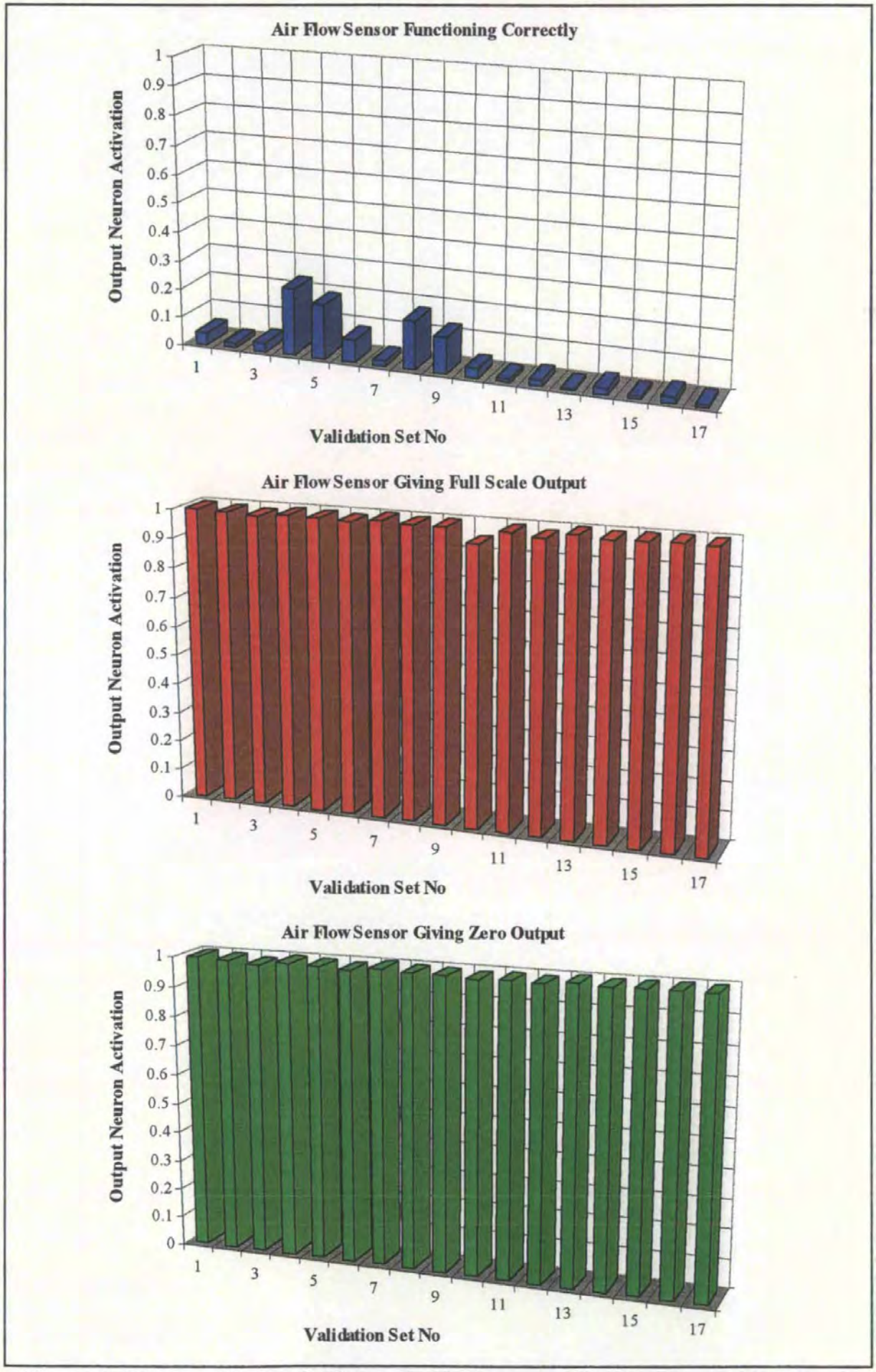

Figure 113 Sensor Diagnosis Networks Performance On Healthy And Faulty Air Flow Sensor Data

10.4 Integrating The Diagnostic System With Performance Monitor

The results screen shown in Figure 17 was modified to include options allowing the user to run the diagnostic system on the data contained within Performance Monitor files and see the on-line diagnostic database results. Further to this, the database and VBA program, DIAMAC.XLM, were modified to give decision making ability and automate the sensor check before the diagnosis. A copy of the program can be found in Appendix 'E'.

Decision making was achieved by looking at the last on-line diagnostic database output. If the maximum output was less than 0.2 the program returned the message "Engine Healthy" to the results screen. If the maximum output was greater than 0.2 the maximum output was located. Each output was assigned a message as shown in Table 38 which was returned to the results screen. The maximum output value was returned to the results screen to give the user a measure of diagnostic confidence. Further to this the diagnostic database results were presented in 3D graphical format to allow the analysis of diagnostic trends. Figure 114 shows the an overall schematic of the final performance monitoring and diagnostic package developed during this research. Figure 115 shows the performance monitoring & diagnostic package's final user screen.

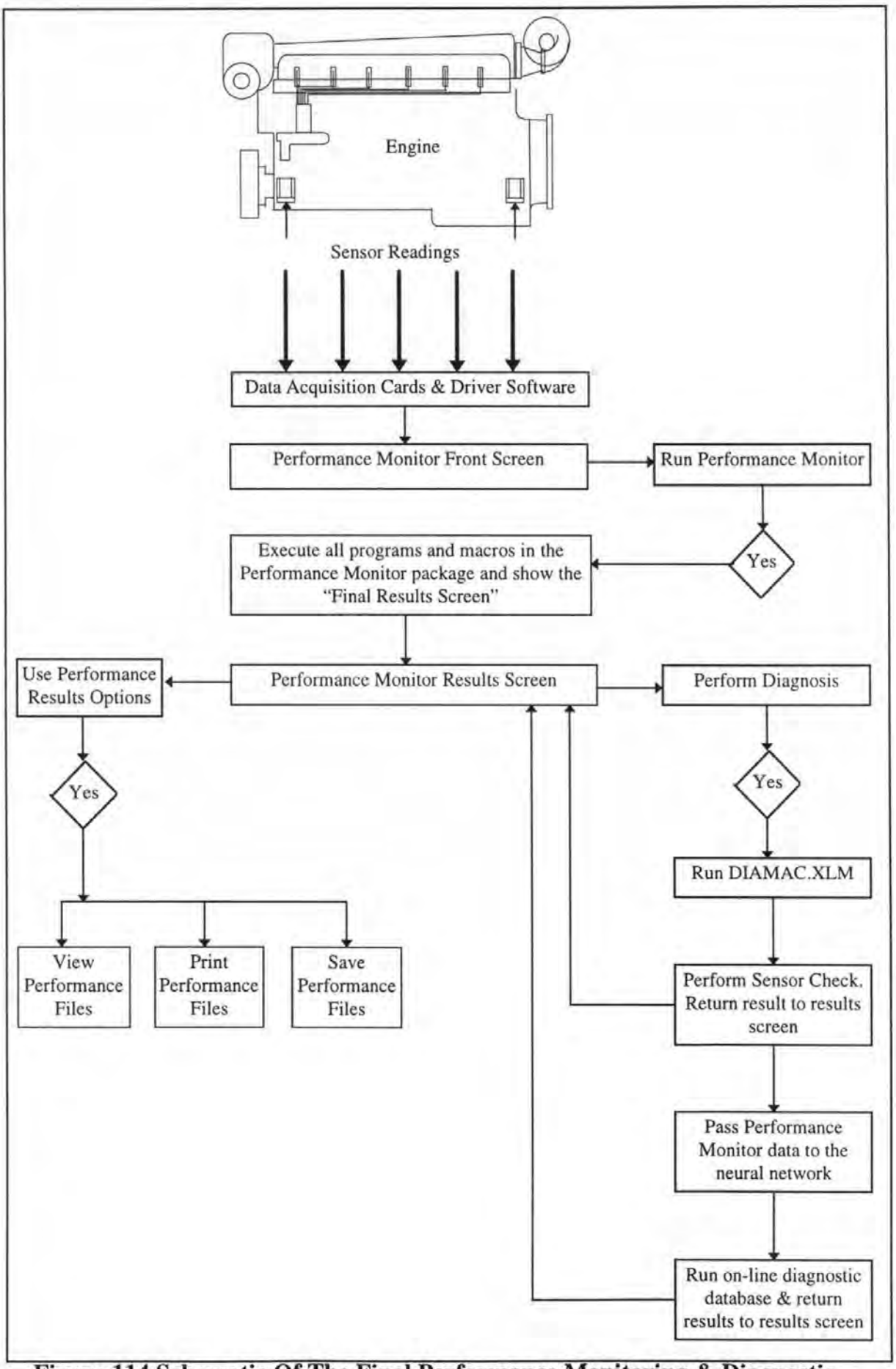

Figure 114 Schematic Of The Final Performance Monitoring & Diagnostic Package

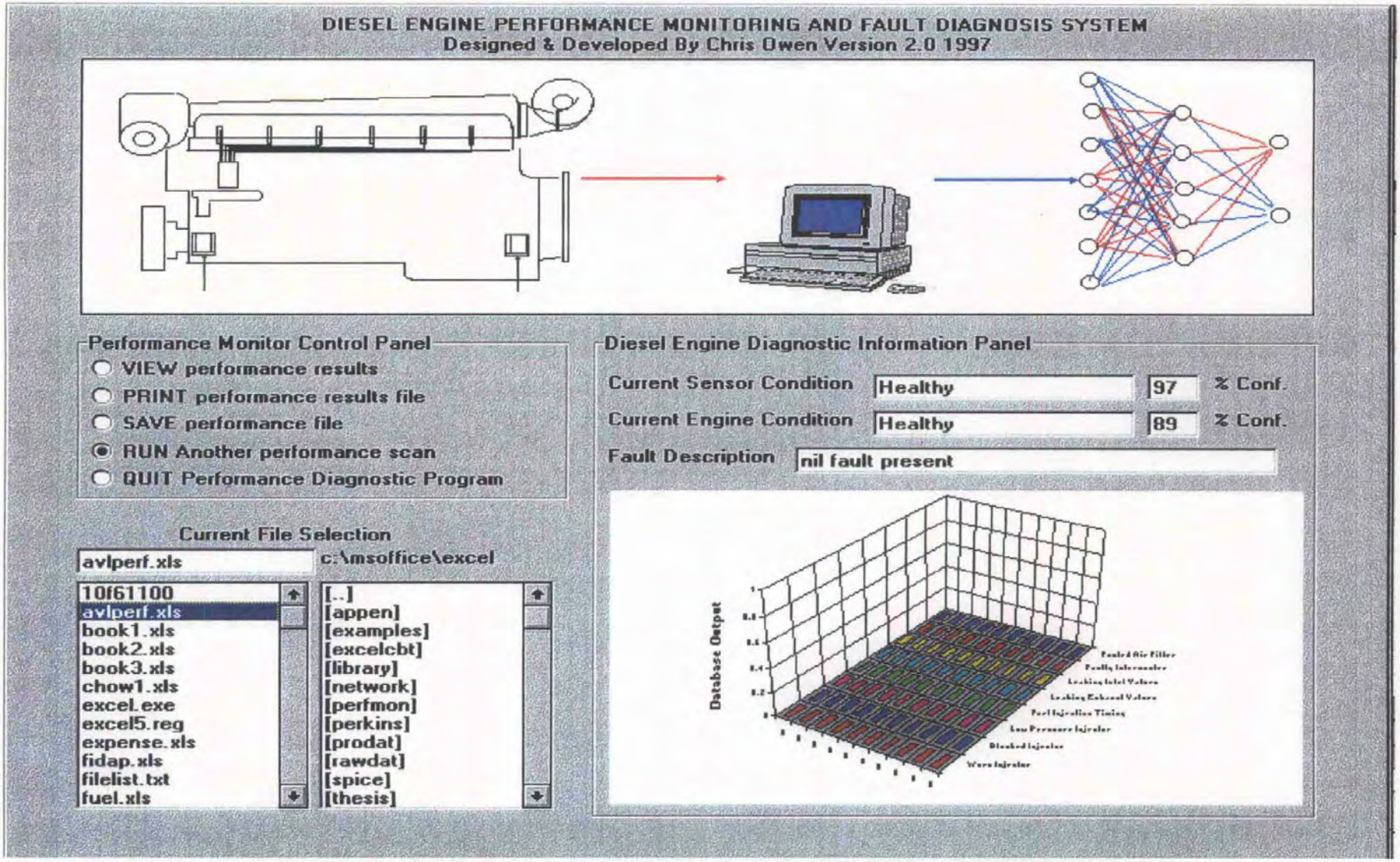

Figure 115 Performance Monitor & Diagnostic System Final User Results Screen

10.5 Summary

Combined with the work discussed in Chapter 9 this chapter has satisfied research objective 6, identified in Chapter 1, and shown how neural networks can be applied to diesel engine fault diagnosis. A totally new technique for improving the diagnostic ability of neural networks operating under practical conditions has been developed and validated. This utilised the novel combination of an on-line diagnostic database and a neural network and included the development of weight adjusting and 'confidence factor' algorithms. The diagnostic database approach has worked very well in this instance and it is conceivable that this approach could certainly be developed more widely for other kinds of decision making applications.

A diagnostic sensor filter was developed to demonstrate that sensor failures can also be detected by neural networks. The best neural network model was combined with the sensor filter and on-line diagnostic database to form a diagnostic system which satisfied the practical success criteria. The diagnostic system was integrated with Performance Monitor to give a complete on-line diesel engine condition monitoring and fault diagnosis system. The following points summarise;

- The system could diagnose the following faults at a genuine severity, 100% correctly on a repeatable basis;

  Fouled inlet air filter
  Genuinely fouled & corroded faulty intercooler
  Leaking inlet valves
  Leaking exhaust valves
  Retarded fuel pump timing
  Genuinely worn injector
  Genuinely blocked injector
  Genuine low pressure injector

- The system could diagnose faults of lower severity than those found on engines currently in operation. This was demonstrated using the fouled air filter, intercooler and fuel injection timing faults. Further to this the system gave a qualitative indication of fault severity.
- Diagnosis could be successfully performed under noisy sensor data conditions. The diagnostic accuracy of the raw neural network outputs were compromised. The use of the on-line diagnostic database addressed this and always ensured correct diagnosis. Previous research has also suggested this is true. It should, however, be noted that the noisier the data the worse the diagnosis.
- The neural network diagnostic performance on novel faults was impressive. It clearly registered that a fault was present despite never being trained. More importantly, the neural network had the ability to correctly draw similarities between novel faults and faults on which it had been trained.
- The neural network diagnostic system could diagnose at a speed and torque at which it had not been trained. The accuracy was slightly impaired but the on-line diagnostic database compensated for this deficiency.
- Despite previous research suggesting otherwise, the neural network suffered a severe degradation in performance when given faulty data from key diagnostic sensors. It may be true to say that less important sensors could fail and not affect the diagnosis significantly. In this respect diagnosis would be much more robust if several parameters changed by a small amount as oppose one sensor giving huge deviations under fault conditions. This work has, however, shown that neural networks can be trained to recognise and diagnose sensor failures prior to engine fault diagnosis.

CHAPTER 11

CONCLUSIONS & RECOMMENDATIONS

11.1 Conclusions

This research has designed, configured and validated a system which was capable of on-line condition monitoring and fault diagnosis of a marine diesel engine using a neural network based approach. The overall research aim was achieved through the satisfaction of all the research objectives identified in Chapter 1. Further to this, the research constitutes original work which has also satisfied recommendations made by previous research.

The work conducted in this research can be summarised as follows;

- An automated diesel engine performance monitoring system for a high speed marine diesel engine was designed, developed and fully validated.
- Prior to the main research testing programme a detailed study on diesel engine data sampling, repeatability and error analysis was undertaken.
- A detailed Perkins T6.354(M) diesel engine fault study was undertaken. The results determined the most commonly occurring faults. Causes and mechanisms for failure were also established through the application of findings from other research.
- Diesel engine computer simulation models and rig testing have been used to predict performance under both healthy and faulty modes of operation. The results from the simulations, rig testing and the fault study ensured that engine testing and results generated were credible.

- Performance Monitor could comfortably detect performance trends caused by leaking exhaust, inlet valves, 1.5° retarded fuel pump timing and a fouled inlet air filter. Computer simulation predicted that detection of these faults would be marginal. This demonstrates the distinct advantage of using real engine test data over un-validated simulation data to predict engine performance trends under faulty conditions, as has been the case in previous research[28] .
- During the course of this research a significant amount of engine testing was conducted under both healthy and faulty modes of engine operation. A detailed analysis was performed on the experimental data to explicitly define fault-symptom relationships.
- A neural network based system capable of diagnosing diesel engine faults has been developed and validated.

The following conclusions can be drawn from this research;

- Some of the most commonly occurring diesel engine faults are;

  Fouled air filter
  Faulty intercooler
  Leaking inlet valves
  Leaking exhaust valves
  Retarded fuel pump timing
  Worn injectors
  Blocked injectors
  Low pressure injectors

- These faults lead to degradations in the engines performance. The adverse trends in performance could be detected by an on-line performance monitoring system using the following measurements;

1. Engine torque
2. Engine speed
3. Compressor inlet pressure
4. Compressor inlet temperature
5. Cylinders 1 & 2 exhaust temperature
6. Cylinder 3 exhaust temperature
7. Cylinder 4 exhaust temperature
8. Cylinder 5 & 6 exhaust temperature
9. Fuel rack position
10. Intercooler cooling water discharge temperature
11. Inlet manifold pressure
12. Inlet manifold temperature
13. Turbine discharge temperature
14. Turbocharger rotational speed
15. Fuel mass flow rate
16. Charge air volume flow rate
17. Cooling water inlet temperature
18. Fuel line pressure (taken at 1° crank angle resolution)

- A neural network based diesel engine diagnostic model can;

  (a) Be substantially enhanced if used in conjunction with an on-line diagnostic database.

  (b) Intelligently diagnose completely novel faults and draw similarities between novel faults and faults on which it had been trained.

  (c) Diagnose faults in the presence of noisy sensor data and not suffer a severe degradation in performance.

  (d) Diagnose faults on data generated at speeds and torques at which it was not trained.

  (e) Detect and diagnose faults of a lower severity than those which it was trained on and give a quantitative indication of the level of severity.

  (f) Perform a correct diagnosis 100% of the time when linked to an on-line diagnostic database, even when faced with noisy sensor data or data taken at torques and speeds at which it had not been trained.

(g) Not perform an intelligent diagnosis when key diagnostic sensors fail, but could be trained to recognise and safeguard against faulty sensor data.

- Neural networks can be successfully be applied to practical diesel engine fault diagnosis and offer a realistic alternative to current techniques.

11.2 Worth Of This Research

This work has shown that a wide range of diesel engine faults can be successfully diagnosed using a limited number of sensors. Much effort has been directed towards the selection of key diagnostic sensors. As a result, the sensors chosen allow this system to be practically viable. The PC based strategy combined with these sensors would allow a similar system to be used as either a fixed or portable diagnostic tool. The application of such a system could give the following practical benefits.

- Only equipment which requires attention is dismantled for assessment. This minimises wastage of labour, replacement consumables such as gaskets and seals and engine operating time.
- Only components or assemblies which are defective are replaced.
- Effective prediction and planning of maintenance operations.
- The rate of development of a fault can be monitored and informed decisions can be made as to when corrective action should take place. This increases reliability, minimises unplanned down-time and allows a fault to develop until maintenance is forced by safety considerations, catastrophic failure or long term engine damage.

- Improved decision making ability when selecting optimum engine operating conditions.
- More effective negotiations with manufacturers or sub-contracted engineers, backed up by systematic measurements of engine condition.
- Measurements of the engine parameters from new, at the end of the guarantee/warranty period and after overhaul gives useful comparative data.

This work has made a significant contribution to knowledge in the following areas.

- The approach of developing and configuring a comprehensive, fully automated, PC based system to monitor engine performance using largely 'off the shelf' software and hardware.
- A detailed analysis of high speed diesel engine instrumentation repeatability and the effects of data sampling and averaging.
- A comprehensive study of commonly occurring high speed diesel engine faults, reasons for their occurrence and quantification of fault severities experienced on real in-service engines.
- As a result of **engine testing genuine faults of realistic severity**, explicit fault-symptom relationships were developed and key diagnostic sensors for a high speed diesel engine were identified.
- The **training and testing** of a neural network based diagnostic system on real engine data including fuel injection system faults.
- An assessment of several neural network training algorithms and architectures to give optimum diagnostic performance when applied to a diesel engine.

- The approach of combining an on-line engine diagnostic database with a neural network was developed. This included the development of weight adjusting and 'confidence factor' algorithms.
- A diagnostic sensor filter was developed to demonstrate that sensor failures can also be detected by neural networks.
- Neural network testing on new engine faults and torques and speeds which the network had not been trained on. And an assessment of neural network performance on noisy and faulty engine test data.

11.3 Recommendations

Finally, as a result of this research the following recommendations can be made;

1. This research has shown that a neural network based system can successfully be trained to diagnose genuine diesel engine faults on real engine test data generated from one engine. Further validation work is required to test this diagnostic system on many engines of a similar type and rating to establish whether the neural network developed in this research is generic.

2. Variations in barometric pressure, air inlet temperature, cooling water temperature and relative humidity were all restricted to ranges found in the UK over approximately one calendar year. If this system were to be installed in an application it could possibly see huge variations in climatic conditions. Further engine test work and neural network validation are required to

establish the diagnostic ability of the system under various extremes of climatic conditions.

3. The key diagnostic sensors chosen for the inputs to the neural network would not currently be installed onto a production engine of this type. However, the drive for increased engine efficiencies and lower gaseous and particulate emissions has led to the development of electronic fuel injection and engine management systems. It is predicted that within the next few years production engines will be fitted with more sophisticated instrumentation which will include the majority on the sensors used in the development of the diagnostic system in this research. It is suggested that the implementation of a diagnostic system could 'piggy-back' on the changes which are already occurring in diesel engine development today. Engines will be controlled using an Engine Control Unit, ECU, which would accept conditioned signals from various sensors. Since neural networks can be embedded onto a chip, the network could simply be an addition to the existing ECU.

4. The fuel line pressure instrumentation used in this research allowed the diagnosis of all of the fuel injection equipment faults. This instrument was cheap, non-intrusive, robust and gave repeatable results. For these reasons it is ideally suited to fault diagnosis and condition monitoring type applications. Based on the results obtained in this research it is thought that the combination of this sensor and a neural network warrants much further investigation.

5. This research has concentrated on the diagnosis of single faults. Further work is required to establish the performance of a neural network based system on multiple diesel engine faults.

6. Work by Kirkman et.al.[29] has shown how accurate cylinder pressure data can be obtained using a cylinder head bolt mounted strain gauge linked to a neural network. It is suggested that the results from the research presented in this thesis should be used to investigate inferred sensor readings for cylinder pressure, injector needle lift, fuel flow rate and inlet air flow rate using neural networks.

APPENDIX 'A'

Perkins T6.354(M) Engine Specification

Figure 116 Holset 3LD Mk I Compressor Map

Figure 117 Holset 3LD Mk I Turbine Map

Perkins T6.354(M) Engine Specification

Type:	4 stroke, compression ignition	
No. of cylinders:	6	
Nominal bore:	98.4 [mm]	
Stroke:	127 [mm]	
Connecting rod length	219.07 [mm]	
Surface area of piston	10326.5 [mm^2]	
Nominal compression ratio:	16:1	
Firing order:	1-5-3-6-2-4	
Manifold groupings	Induction -	single
	Exhaust -	twin (1,2,3 ; & 4,5,6)
Valve timings:	Inlet -	opens 19° BBDC closes 49° ABDC
	Exhaust -	opens 52° BBDC closes 16° ATDC
Valve lift (both valves):	10.29mm	
Inlet manifold dimensions:	Length:	1100[mm]
	Effective Diam:	49.88[mm]
Exhaust (1,2 & 3)manifold dimensions:	Length:	700[mm]
	Effective Diam:	43.7[mm]
Exhaust (4,5 & 6) manifold dimensions:	Length:	450[mm]
	Effective Diam:	49.88 [mm]
Fuel injection pump:	Lucas CAV, DPA type	
Nominal performance at continuous rating:	90 [kW] at 2250 [revs/min]	
Turbocharger:	Holset 3LD Mk I	

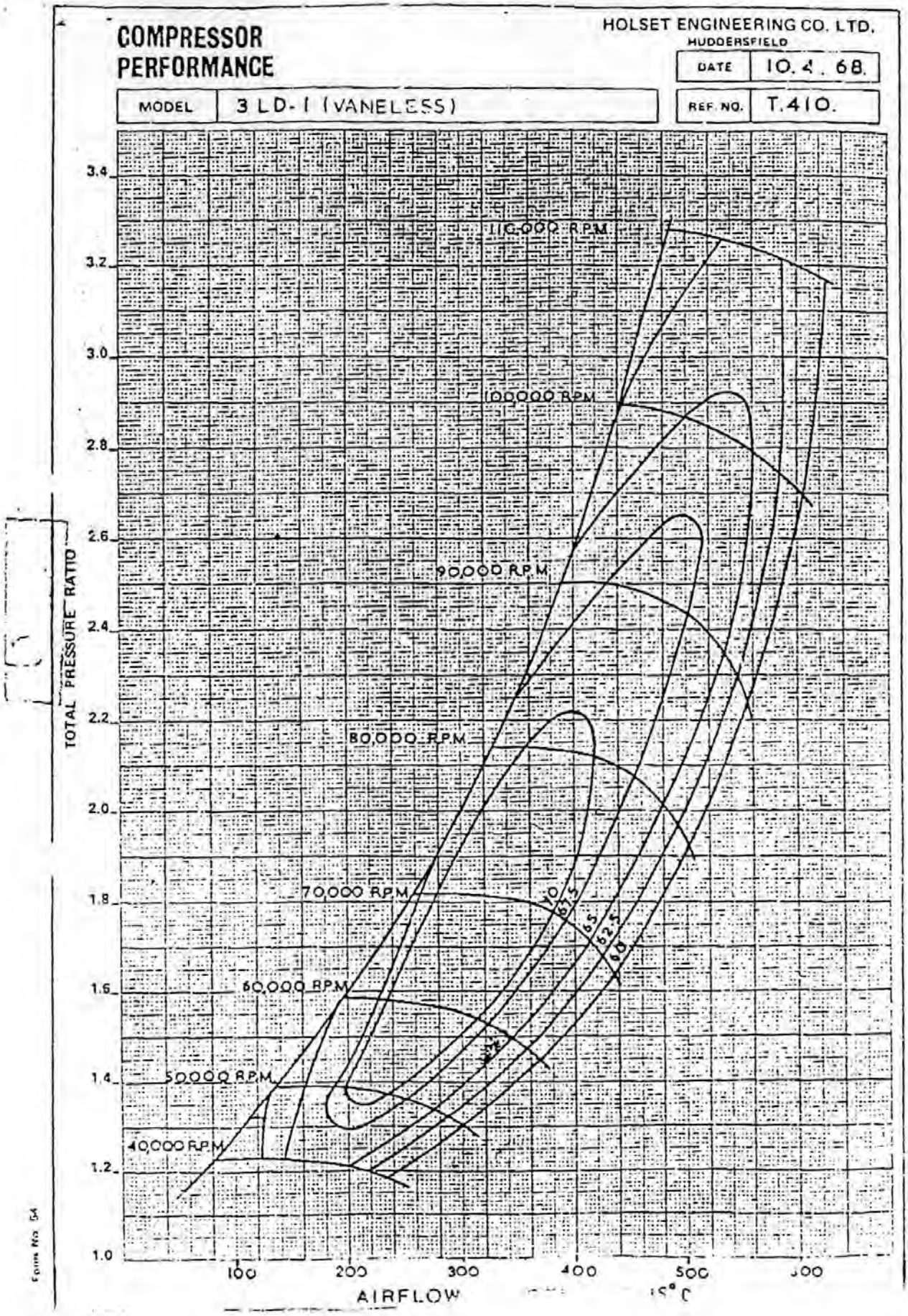

Figure 116 Holset 3LD MkI Compressor map

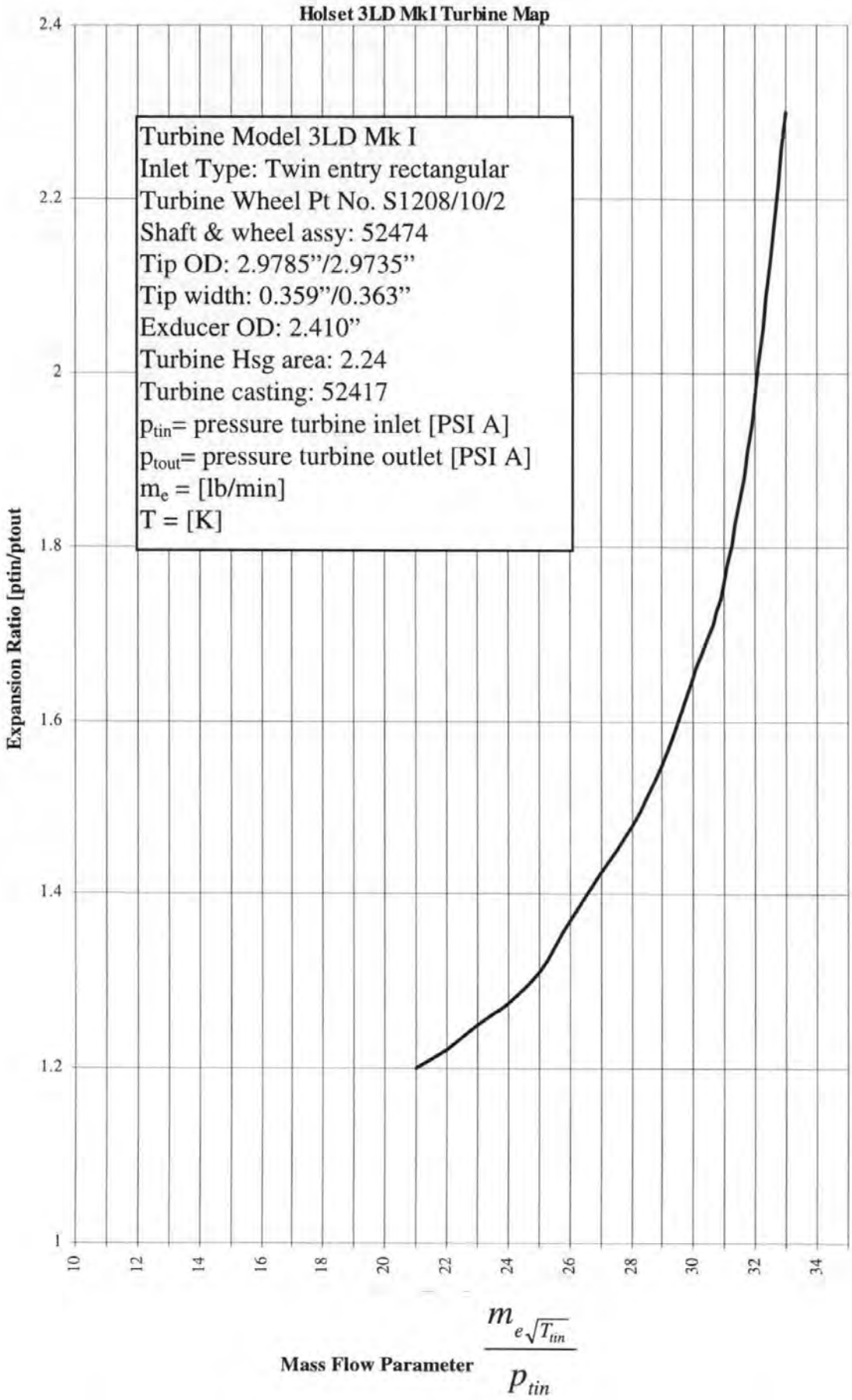

Figure 117 Holset 3LD MkI Turbine Map

APPENDIX 'B'

Performance Monitor Central Command Macro [DAC.XLM]

Performance Monitor Cylinder Pressure Macro [CYLINDER.XLM]

Performance Monitor Needle lift Macro [NEEDLE.XLM]

Performance Monitor Fuel Line Pressure Macro [FUEL.XLM]

Performance Monitor Turbo C High Speed Data Averaging Program

Performance Monitor Formulae

Performance Monitor Central Command Macro

ACQUISITION & DATA PROCESSING

```
=ECHO(FALSE)
=OPEN("c:\msoffice\excel\intro.xlm")
=DIALOG.BOX('D:\INTRO.XLM'!intro)
=IF(B7=FALSE,GOTO(C5))
=CLOSE()
=EXEC("c:\windsped\streamer.exe")
=APP.ACTIVATE("windspeed streamer")
=SEND.KEYS("~")
=SEND.KEYS("%f",TRUE)
=SEND.KEYS("h",TRUE)
=SEND.KEYS("t6354h.ims",TRUE)
=SEND.KEYS("~",TRUE)
=WAIT(NOW()+"00:00:02")
=SEND.KEYS("%c",TRUE)
=SEND.KEYS("c:\windsped\1.imx",TRUE)
=WAIT(NOW()+"00:00:02")
=SEND.KEYS("~",TRUE)
=SEND.KEYS("y",TRUE)
=WAIT(NOW()+"00:00:05")
=SEND.KEYS("%S",TRUE)
=WAIT(NOW()+"00:00:20")
=SEND.KEYS("~",TRUE)
=SEND.KEYS("%f",TRUE)
=SEND.KEYS("x",TRUE)
=WAIT(NOW()+"00:00:01")
=EXEC("c:\windsped\imxtoxl")
=SEND.KEYS("~",TRUE)
=SEND.KEYS("%s",TRUE)
=SEND.KEYS("c:\windsped\1.imx",TRUE)
=SEND.KEYS("%d",TRUE)
=SEND.KEYS("c:\tc\in.dat",TRUE)
=SEND.KEYS("%C",TRUE)
=WAIT(NOW()+"00:03:40")
=SEND.KEYS("%f",TRUE)
=SEND.KEYS("x",TRUE)
=WAIT(NOW()+"00:00:02")
=DIRECTORY("c:\tc")
=EXEC("stoaty.exe")
=WAIT(NOW()+"00:00:40")
=DIRECTORY("C:\TC")
=OPEN("C:\TC\FUEL.DAT",2)
=SELECT("R2C1:R1441C1")
=COPY()
=OPEN("C:\msoffice\excel\fuel.xlm")
=SELECT("R1C9:R1440C9")
=PASTE()
=CLOSE(TRUE)
=CANCEL.COPY()
=CLOSE(TRUE)

=OPEN("C:\TC\NEEDLE.DAT",2)
=SELECT("R2C1:R1441C1")
=COPY()
=OPEN("C:\msoffice\excel\needle.xlm")
=SELECT("R1C9:R1440C9")
```

```
=PASTE()
=CLOSE(TRUE)
=CANCEL.COPY()
=CLOSE(TRUE)
=OPEN("C:\TC\CYL.DAT",2)
=SELECT("r2c1:r1441c1")
=COPY()
=OPEN("C:\msoffice\excel\cylinder.xlm")
=SELECT("R1C1:R1440C1")
=PASTE()
=RUN('D:\CYLINDER.XLM'!cylinder)
=CLOSE(TRUE)
=CANCEL.COPY()
=CLOSE(TRUE)
```

START LOGGING SLOW SPEED DATA

```
=DIRECTORY("c:\windmill")
=EXEC("logger.exe")
=SEND.KEYS("~",TRUE)
=SEND.KEYS("%F",TRUE)
=SEND.KEYS("r",TRUE)
=SEND.KEYS("2lab.wlg",TRUE)
=SEND.KEYS("~",TRUE)
=WAIT(NOW()+"00:00:01")
=SEND.KEYS("%s",TRUE)
=SEND.KEYS("o",TRUE)
=WAIT(NOW()+"00:02:55")
=SEND.KEYS("%t",TRUE)
=SEND.KEYS("%f",TRUE)
=SEND.KEYS("x",TRUE)
=OPEN("c:\windmill\1.wl")
=SELECT("r6c2:r180c28")
=COPY()
=OPEN("c:\msoffice\excel\logger.xls")
=PASTE()
=OPEN("c:\msoffice\excel\perform.xls",3)
=CLOSE(TRUE)
=CLOSE(FALSE)
=CANCEL.COPY()
=CLOSE(FALSE)
=BEEP()
=OPEN("c:\msoffice\excel\results.xlm")
=DIALOG.BOX('D:\RESULTS.XLM'!results)
=CLOSE(TRUE)
=IF(('D:\[RESULTS.XLM]RESULTS'!G5)=1,GOTO(D2))
=IF(('D:\[RESULTS.XLM]RESULTS'!G5)=2,GOTO(E2))
=IF(('D:\[RESULTS.XLM]RESULTS'!G5)=3,GOTO(F2))
=IF(('D:\[RESULTS.XLM]RESULTS'!G5)=4,GOTO(G3))
=IF(('D:\[RESULTS.XLM]RESULTS'!G5)=5,GOTO(H1))
=RETURN()
```

Performance Monitor Cylinder Pressure Macro

```
=IF(A1>5,GOTO(D1))
=IF(A1<5,GOTO(E1))
=RETURN()
```

```
=COPY(A1:A720,B721:B1440)
=CANCEL.COPY()
=COPY(A721:A1440,B1:B720)
=CANCEL.COPY()
=OPEN("c:\msoffice\excel\fuel.xlm")
=RUN("c:\msoffice\excel\fuel.xlm!r1c2")
=CLOSE(TRUE)
=OPEN("c:\msoffice\excel\needle.xlm")
=RUN("c:\msoffice\excel\needle.xlm")
=CLOSE(TRUE)
=RETURN()
```

```
=COPY(A1:A1440,B1:B1440)
=CANCEL.COPY()
=OPEN("c:\msoffice\excel\fuel.xlm")
=RUN("c:\msoffice\excel\fuel.xlm!r1c3")
=CLOSE(TRUE)
=OPEN("c:\msoffice\excel\needle.xlm")
=RUN("c:\msoffice\excel\needle.xlm!r1c3")
=CLOSE(TRUE)
=RETURN()
```

Performance Monitor Needle Lift Macro

A

```
=IF('D:\[CYLINDER.XLM]CYLINDER'!A1>10,GOTO(B1))
=IF('D:\[CYLINDER.XLM]CYLINDER'!A1<10,GOTO(C1))
=RETURN()
```

B

```
=COPY(I1:I720,J721:J1440)
=CANCEL.COPY()
=COPY(I721:I1440,J1:J720)
=CANCEL.COPY()
=GOTO(D1)
=RETURN()
```

C

```
=COPY(I1:I1440,J1:J1440)
=CANCEL.COPY()
=GOTO(D1)
=RETURN()
```

D

```
=FORMULA(MAX(J1:J1443),H1)
=FORMULA(AVERAGE(J1:J300),H2)
=FORMULA((H1-H2),H3)
=FORMULA((H3*0.1),H4)
=FORMULA((H2+H4),H5)
=FOR.CELL("instant",J1:J1443,FALSE)
=IF(instant>H5,GOTO(E1))
=NEXT()
=FOR.CELL("lift",K1:K1443,FALSE)
=IF(lift>0,GOTO(F1))
=NEXT()
=FOR.CELL("seat",lift:K1443,FALSE)
=IF(seat=0,GOTO(G1))
=NEXT()
=SELECT(K1:K1443)
=CLEAR(3)
=RETURN()
```

E

```
=SELECT("instant")
=COPY()
=SELECT(,"rc[1]")
=PASTE()
=CANCEL.COPY()
=GOTO(D8)
```

F

```
=SELECT("lift")
=FORMULA(GET.CELL(2),H6)
=FORMULA(((((H6)-1)/2)-360),H7)
=BREAK()
=GOTO(D11)
=RETURN()
```

G

```
=SELECT("seat")
=FORMULA(GET.CELL(2),H8)
=FORMULA(((((H8)-1)/2)-360),H9)
=BREAK()
=GOTO(D14)
=RETURN()
```

Performance Monitor Fuel Line Pressure Macro

A

```
=IF('D:\[CYLINDER.XLM]CYLINDER'!A1>10,GOTO(B1))
=IF('D:\[CYLINDER.XLM]CYLINDER'!A1<10,GOTO(C1))
=RETURN()
```

B

```
=COPY(I1:I720,J721:J1440)
=CANCEL.COPY()
=COPY(I721:I1440,J1:J720)
=CANCEL.COPY()
=GOTO(D1)
=RETURN()
```

C

```
=COPY(I1:I1440,J1:J1440)
=CANCEL.COPY()
=GOTO(D1)
=RETURN()
```

D

```
=FORMULA(MAX(J1:J1443),H1)
=FORMULA(AVERAGE(J1:J300),H2)
=FORMULA((H1-H2),H3)
=FORMULA((H3*0.1),H4)
=FORMULA((H2+H4),H5)
=FOR.CELL("instant",J1:J1443,FALSE)
=IF(instant>H5,GOTO(E1))
=NEXT()
=FOR.CELL("rise",K1:K1443,FALSE)
=IF(rise>0,GOTO(F1))
=NEXT()
=FOR.CELL("fall",rise:K1443,FALSE)
=IF(fall=0,GOTO(G1))
=NEXT()
=SELECT(K1:K1443)
=CLEAR(3)
=RETURN()
```

E

```
=SELECT("instant")
=COPY()
=SELECT(,"rc[1]")
=PASTE()
=CANCEL.COPY()
=GOTO(D8)
```

F

```
=SELECT("rise")
=FORMULA(GET.CELL(2),H6)
=FORMULA(((((H6)-1)/2)-360),H7)
=BREAK()
=GOTO(D11)
=RETURN()
```

G

```
=SELECT("fall")
=FORMULA(GET.CELL(2),H8)
=FORMULA(((((H8)-1)/2)-360),H9)
=BREAK()
=GOTO(D14)
=RETURN()
```

Performance Monitor High Speed Data Averaging Turbo C

```
#include <stdio.h>
main(){
        #define sample 1440 /*no of samples per wave */
        FILE *fopen(),*fp[4];
        int i,j,k;
        char c[8];
        double num,val[3][sample],atof();
        void fgetword();

        /* Open files */
        if((fp[0]=fopen("c:\in.dat","r"))==NULL){
          printf("Cannot open input file \n");
          exit(1);
        }
        if((fp[2]=fopen("fuel.dat","w"))==NULL){
                printf("Error file out1");
                exit(1);
        }
        if((fp[1]=fopen("cyl.dat","w"))==NULL){
                printf("Error file cyl");
                exit(1);
        }
        if((fp[3]=fopen("needle.dat","w"))==NULL){
                printf("Error file needle");
                exit(1);
        }

        /* Read in no. of wave cycles to be averaged */
        printf("\nPLEASE WAIT PROCESSING HIGH SPEED DATA");


        /* Strip header from input file */
        for(i=0;i<4;i++)fgetword(fp[0],c);

        /* Initialise variables */
        i=0;
        num=0.0;
        for(i=0;i<3;i++)
                for(j=0;j<sample;j++)
                        val[i][j]=0.0;
        for(i=0;i<8;i++)c[i]=' ';

        /* total wave arrays */
        for(j=0;j<50;j++)
                for(i=0;i<sample;i++){
                        fgetword(fp[0],c);        /* disregard time value */
                        for(k=0;k<3;k++){
                                fgetword(fp[0],c);
                                num=atof(c);


                                        val[k][i]=val[k][i]+num;
                        }
                }
```

```
        /* Find average */
        for(i=0;i<sample;i++)
                for(j=0;j<3;j++){
                        val[j][i]=val[j][i]/50;
                        fprintf(fp[j+1],"\n %4.4f",val[j][i]);
                }

        for(i=0;i<4;i++)
                fclose(fp[i]);
}

/* read a number from input file and return */
void fgetword (fp,w)
FILE *fp;
char w[];
{
        int i;
        char c;

        i=0;
        c=w[i]=getc(fp);
        while((c!=EOF) && (c!='\r') && (c!=' ') && (c!='\t') && (c!='\n')){
                ++i;
                c=w[i]=getc(fp);
        }
}

/* convert character string to double precision floating point number */
double atof(s)
char s[];
{
        double val,power=1.0;
        int i,sign;

        for (i=0;s[i]==' ' || s[i]=='\n' || s[i]=='\t';i++);
        sign=1;
        if(s[i]=='+' || s[i]=='-')
                sign=(s[i++]=='+')?1:-1;
        for (val=0;s[i]>='0' && s[i]<='9';i++)
                val=10*val+s[i]-'0';
        if(s[i]=='.')i++;
        for (power=1;s[i]>='0' && s[i]<='9';i++){
                val=10*val+s[i]-'0';
                power*=10;
        }
        return(sign*val/power);
}
```

Performance Monitor Formulae

Brake Power [kW]

$$Brake\ Power\ [kW] = \frac{2 * \pi * n * T_b}{1000}$$

Brake Mean Effective Pressure: BMEP [Bar]

$$BMEP\ [Bar] = \frac{BrakePower[kW]}{L * A_p * N_c * n * 100}$$

Indicated Power [kW]

$$Indicated\ Power\ [kW] = IMEP[Bar] * L * A_p * N_c * n * 100$$

Friction Mean Effective Pressure; FMEP [Bar]

$$FMEP = IMEP - BMEP$$

Brake Specific Fuel Consumption; BSFC [kg/kW/hr]

$$BSFC = \frac{m_f * 3600}{P_b}$$

Indicated Specific Fuel Consumption; ISFC [kg/kW/hr]

$$ISFC = \frac{m_f * 3600}{P_i}$$

Brake Thermal Efficiency

$$\eta_{btherm} = \frac{P_b}{Q_c * m_f}$$

Indicated Thermal Efficiency

$$\eta_{itherm} = \frac{P_i}{Q_c * m_f}$$

Mechanical Efficiency

$$\eta_{mech} = \frac{P_b}{P_i}$$

Compressor Mass Flow Parameter

$$CompressorMassFlowParameter = \frac{m_a * \sqrt{T_{cin}}}{p_{cin}}$$

Compressor Pressure Ratio [non - dimensional]

$$Compressor\,\mathrm{Pr}essureRatio = \frac{p_{cout}}{p_{cin}}$$

Compressor Speed Parameter

$$CompressorSpeedParameter = \frac{N_{ct}}{\sqrt{T_{cin}}}$$

Compressor Isentropic Efficiency

$$\eta_{ct} = \frac{\left(\frac{p_{cout}}{p_{cin}}\right)^{\frac{(\gamma-1)}{\gamma}} - 1}{\left(T_{cout} - T_{cin}\right) - 1}$$

Intercooler Effectiveness

$$\eta_{ic} = \frac{\left(T_{a0} - T_{a1}\right)}{\left(T_{a0} - T_{w0}\right)}$$

Volumetric Efficiency

$$\eta_{vol} = \frac{2Q_a}{V_{sw} * n}$$

Exhaust Gas Mass Flow Rate [kg/s]

$$m_e = m_a + m_f$$

Turbine Mass FlowRate Parameter

$$TurbineMassFlowParameter = \frac{m_e * \sqrt{T_{tin}}}{p_{tin}}$$

Turbine Expansion Ratio [non - dimensional]

$$TurbineExpansionRatio = \frac{p_{tin}}{p_{tout}}$$

Turbine Speed Parameter

$$TurbineSpeedParameter = \frac{N_t}{\sqrt{T_{tin}}}$$

Turbine Isentropic Efficiency

$$\eta_{tt} = \frac{1 - \left(\frac{T_{tout}}{T_{tin}}\right)}{1 - \left(\frac{p_{tout}}{p_{tin}}\right)^{\frac{\gamma - 1}{\gamma}}}$$

Overall Air Fuel Ratio

$$A / FRatio = \frac{m_a}{m_f}$$

APPENDIX 'C'

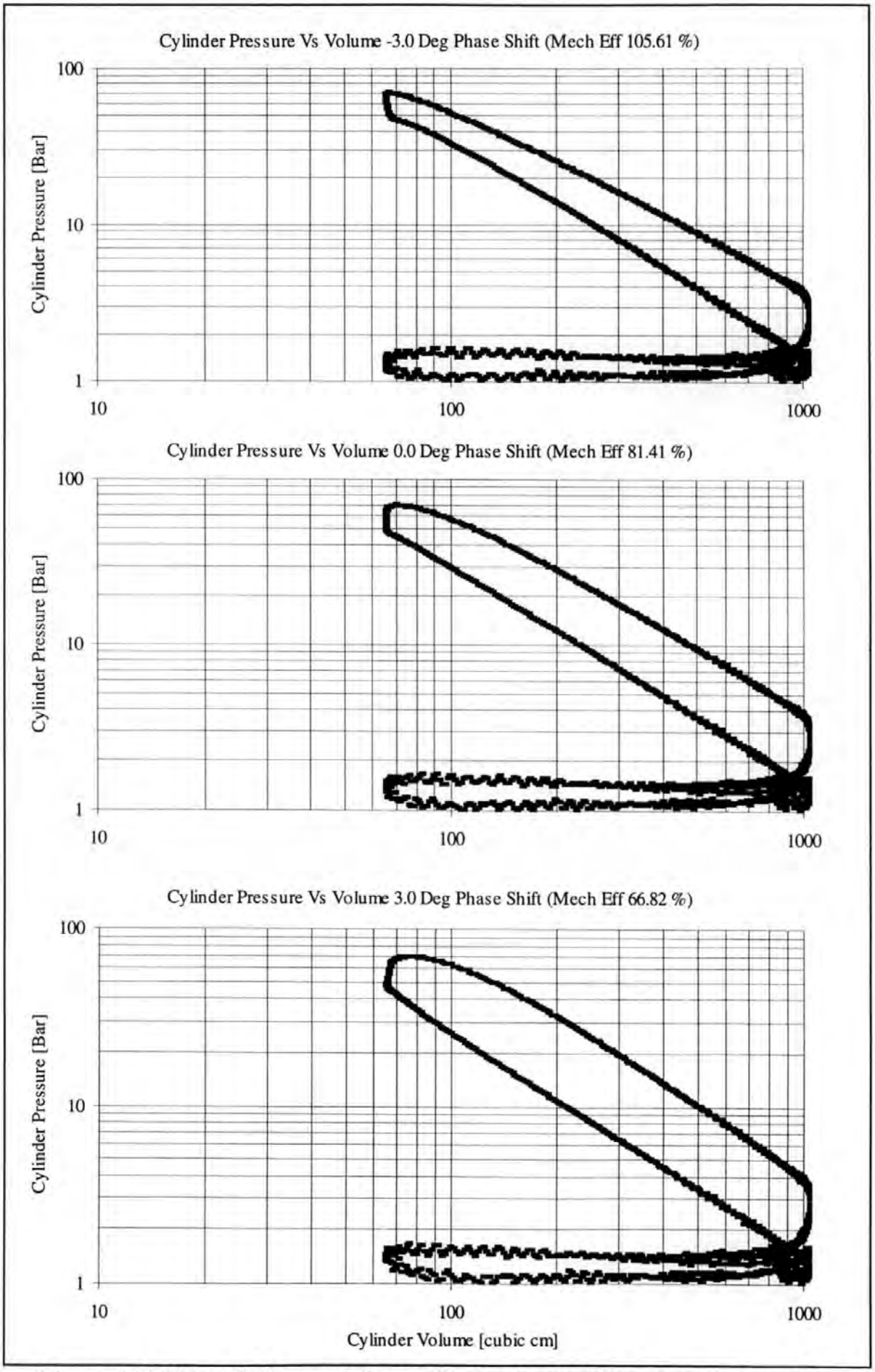

Figure 118 Effect Of Dynamic Data Phasing On P-V Plot. [expansion and compression lines should be parrallel and rounded at TDC for correct phasing]

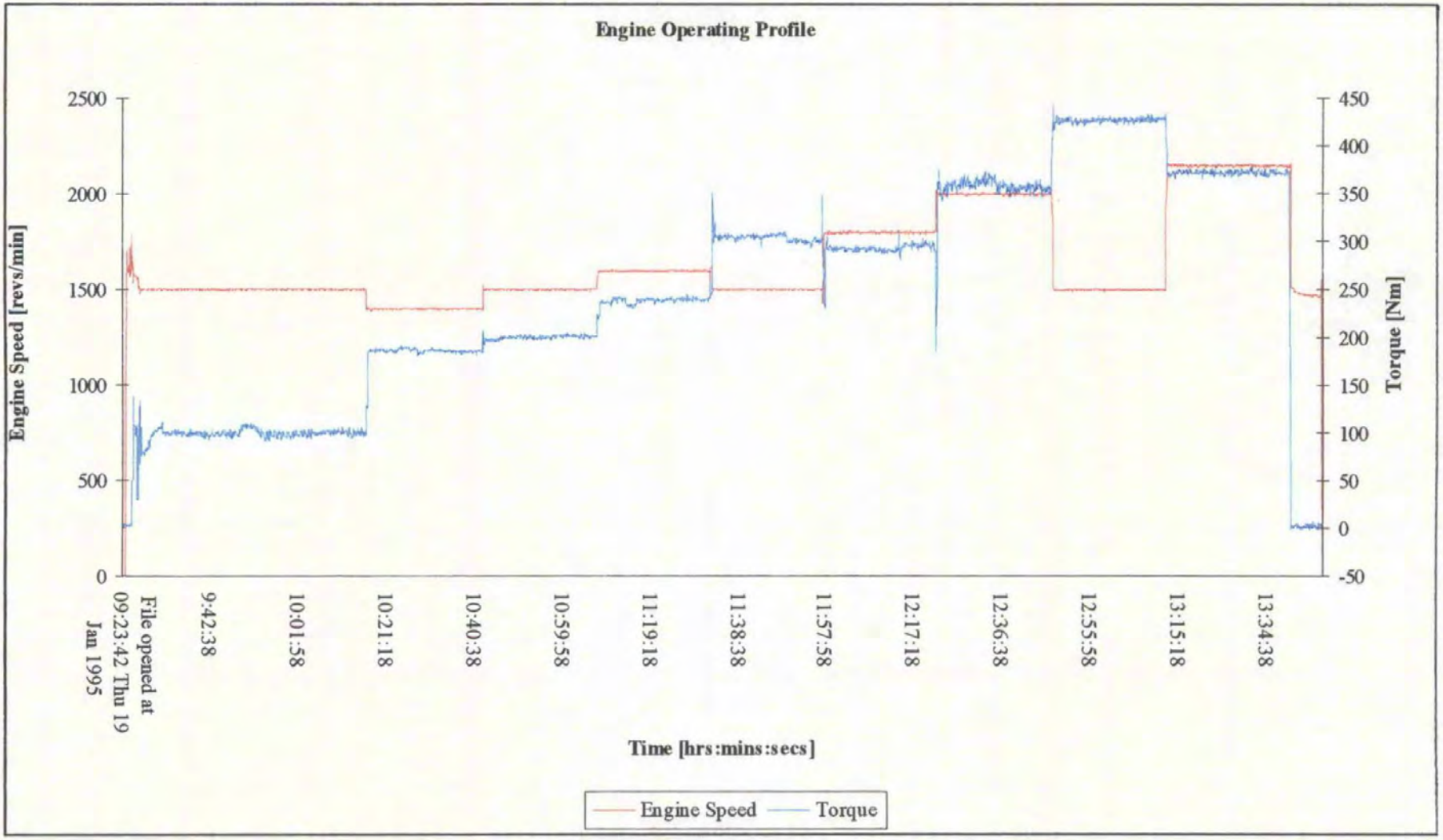

Figure 119 Engine Warm-up Trial Torque And Speed Settings

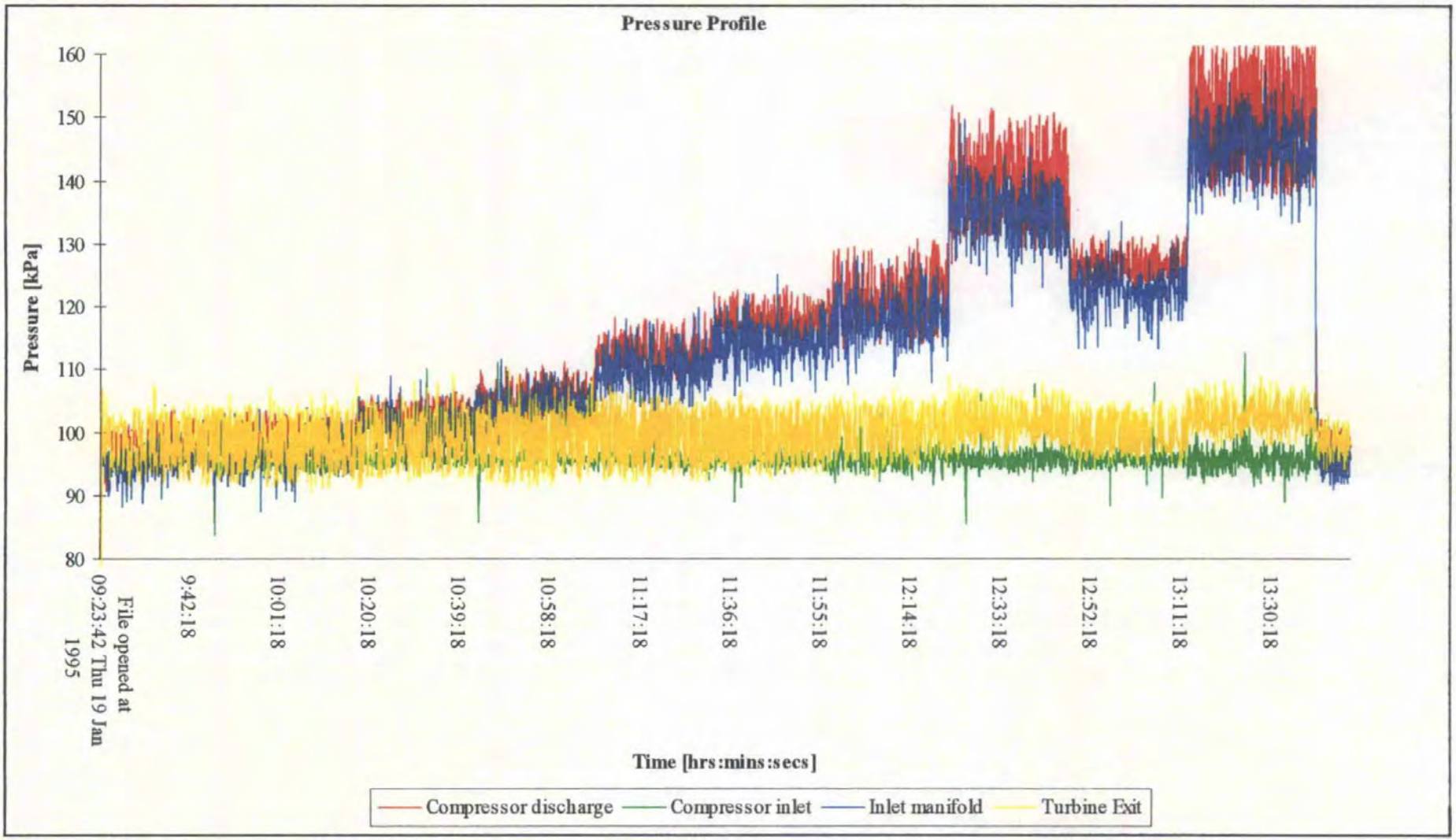

Figure 120 Engine Warm-up Trial; Pressure Profiles

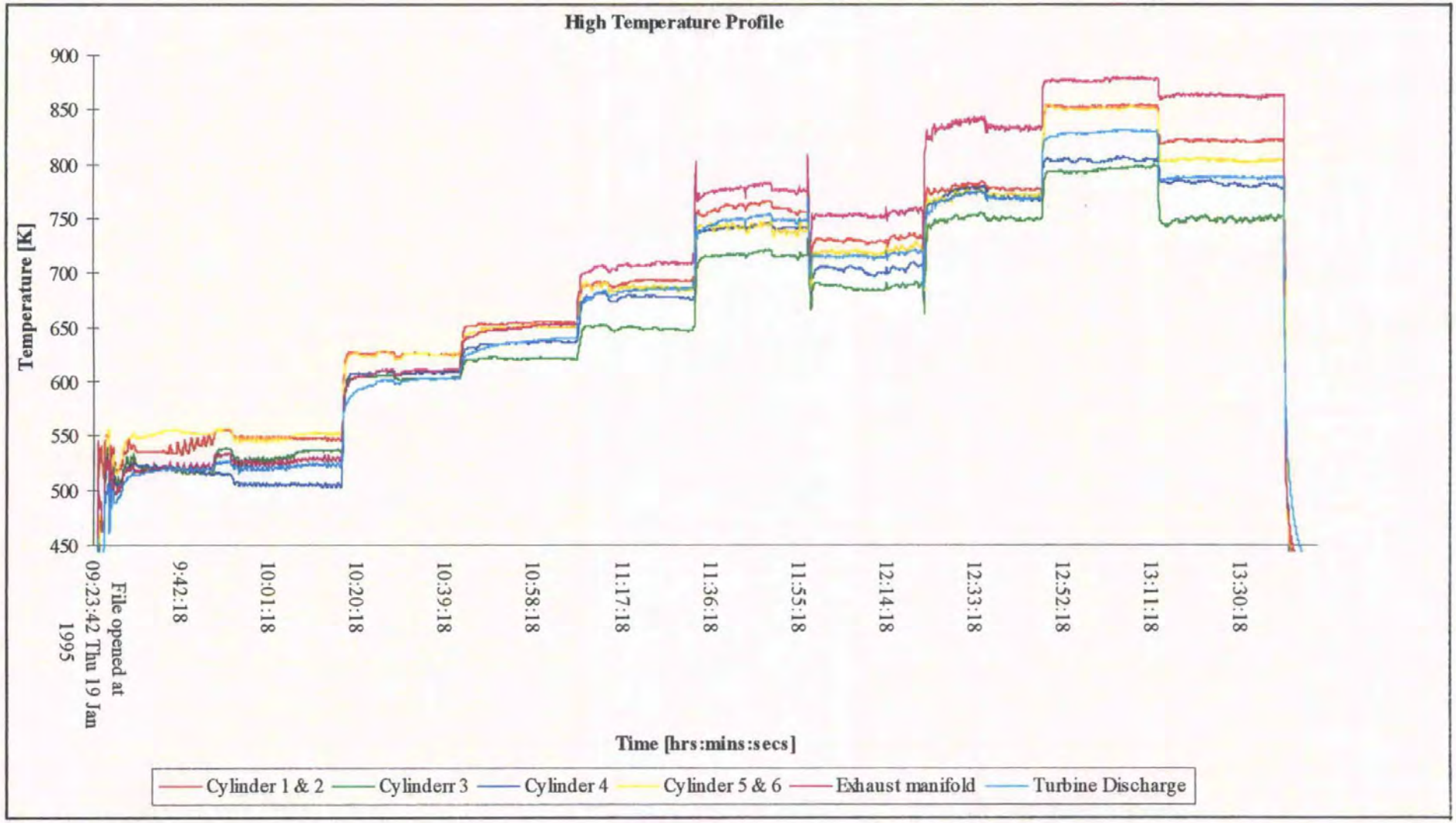

Figure 121 Engine Warm-up Trial; High Temperature Profiles

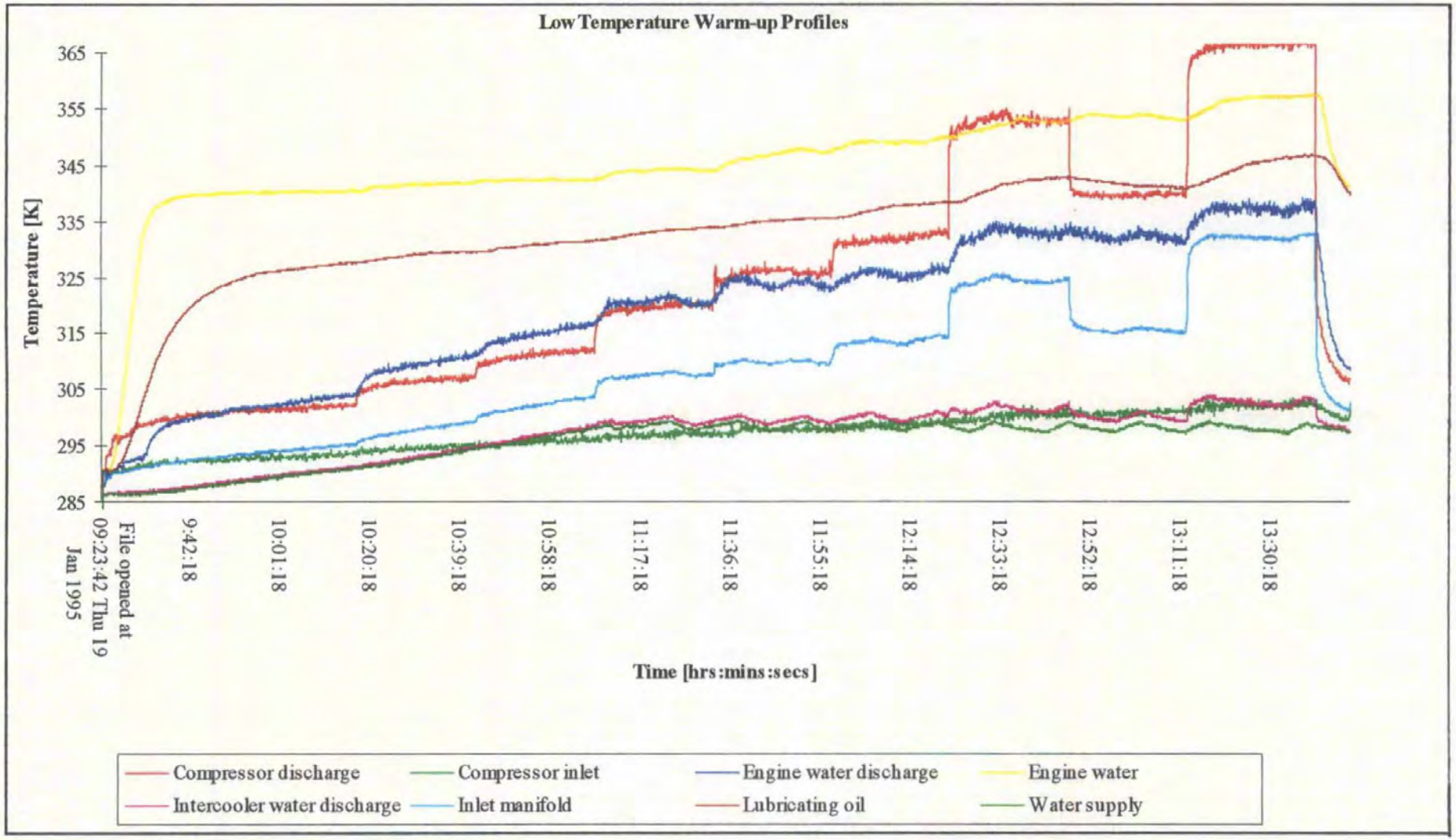

Figure 122 Engine Warm-up Trial; Low Temperature Profiles

APPENDIX 'D'

***SPICE II PERKINS 6 CYLINDER T 6.354(M) SINGLE STAGE TURBOCHARGED DIESEL ENGINE**

```
*CONTROL & SYSTEM DATA
1                                   * mode 1
1                                   * reference cylinder
c ncyc step nv nj ns nhr nhrf ng nht nval
  20   2  9 14 2 1   0 4  1   2
* PRINT & PLOT CONTROLS
20 20                               * plot data for cycles i to j
1 1 0 4 4 1
1 7 8 9
1 2 13 14
2
* CONTROL VOLUME DATA
0 1 1 1 1  360  4 1  11  1 2        * cylinder 1
0 1 1 1 1  600  4 1  11  1 2        * cylinder 2
0 1 1 1 1  120  4 1  11  1 2        * cylinder 3
0 1 1 1 1  480  4 1  11  1 2        * cylinder 4
0 1 1 1 1  240  4 1  11  1 2        * cylinder 5
0 1 1 1 1    0  4 1  11  1 2        * cylinder 6
1 2 0 0 1    0  0 0  0  0 0         * intake manifold
1 3 0 0 1    0  0 0  0  0 0         * exhaust manifold
1 4 0 0 1    0  0 0  0  0 0         * exhaust manifold
* FLOW JUNCTION DATA
1  1 0 7 0 0 0 1 1                  * intake valve cylinder 1
1  2 0 1 0 0 0 8 1                  * exhaust valve cylinder 1
1  1 0 7 0 0 0 2 2                  * intake valve cylinder 2
1  2 0 2 0 0 0 8 2                  * exhaust valve cylinder 2
1  1 0 7 0 0 0 3 3                  * intake valve cylinder 3
1  2 0 3 0 0 0 8 3                  * exhaust valve cylinder 3
1  1 0 7 0 0 0 4 4                  * intake valve cylinder 4
1  2 0 4 0 0 0 9 4                  * exhaust valve cylinder 4
1  1 0 7 0 0 0 5 5                  * intake valve cylinder 5
1  2 0 5 0 0 0 9 5                  * exhaust valve cylinder 5
1  1 0 7 0 0 0 6 6                  * intake valve cylinder 6
1  2 0 6 0 0 0 9 6                  * exhaust valve cylinder 6
2  0 0 0 0 0 0 7 2                  * compressor
3  0 2 8 9 0 0 0 2                  * turbine
* SHAFT DATA
1  0.0    0.00                      * crankshaft
2  0.5E-3  0.80                     * T/C Rotor
* HEAT RELEASE DATA SETS
0 709 150 42.5e6 5.50e-5 0 0 0 0
* GEOMETRIC DATA SETS
0.0984 .127 14.0 .219  1.0          * cylinder geometry
2.14E-3  0 0 0 0                    * intake manifold geometry
1.38E-3  0 0 0 0                    * exhaust manifold geometry
1.20E-3  0 0 0 0                    * exhaust manifold
```

```
* HEAT TRANSFER DATA
3                          * no. of surface areas
0    0.0126   0.0158       * areas
573.0  673.0    773.0      * respective temeratures
* VALVE DATA SETS

24 0 1 1                   *intake valve
350 360 370 380 390 400 410 420 430 440 450 460 470 480 490 500 510 520 530 540
550 560 570 580
 0.0 3.44e-5 1.34e-4 2.67e-4 3.74e-4 5.02e-4 6.57e-4 6.94e-4 7.07e-4 7.41e-4
 7.42e-4 7.43e-4 7.42e-4 7.44e-4 7.44e-4 7.1e-4 6.95e-4 6.61e-4 5.25e-4 3.73e-4
 2.87e-4 1.36e-4 3.44e-5 0.0

26 0 1 1                   * exhaust valve
125 135 145 155 165 175 185 195 205 215 225 235 245 255 265 275 285 295 305 315
325 335 345 355 365 375
 0.0 9.11e-6 5.3e-5 1.37e-4 2.53e-4 4.05e-4 5.35e-4 5.96e-4 6.42e-4 6.69e-4
 6.64e-4 6.66e-4 6.7e-4 6.7e-4 6.6e-4 6.61e-4 6.55e-4 6.53e-4 6.25e-4 5.63e-4
 4.57e-4 3.11e-4 1.8e-4 7.7e-5 2.15e-5 0.0

* ENTRY AND EXIT CONDITIONS
100.5E+3 303.4 100.5E+3 794

* INITIAL SHAFT SPEEDS
 2150.0000
 63378
* INITIAL PRESSURE/TEMPERATURE/FUEL-AIR RATIO
 179864.29  820.1090   4.2025646e-02
 256147.71  461.4268   1.2475206e-03
 708221.1  1265.3490   4.4623716E-02
 189895.90  416.6010   1.5031702E-03
 173277.24  881.4562   4.4690090E-02
 11677172.  1655.4655   1.4050251E-02
 150280.60   332.53050  3.7844169E-10
 155285.88   871.9995  4.4870996E-04
 155213.07  871.3113  4.4820266E-04
```

*** SPICE II PERKINS T6354(M) TURBOCHARGER TURBINE DATA FILE**

```
* CONTROL DATA...No.SPEED CURVES    ROTOR DIAM   SCALING:RP  N  EFF  M
7 0.075 1.5 1.2 0.80 1.2e-5
* TABULATED TURBINE MAP: P-RATIO   M FLOW PAR    EFFICIENCY
920
1.10 1.60 0.40
1.11 2.10 0.55
1.20 2.60 0.60
1.38 3.00 0.65
1.66 3.16 0.65
2.00 3.20 0.60
*
1290
1.18 1.60 0.40
1.21 2.20 0.48
1.32 2.70 0.56
1.50 3.00 0.67
1.80 3.13 0.60
2.00 3.15 0.50
*
1550
1.22 1.60 0.35
1.28 2.30 0.45
1.40 2.70 0.67
1.55 2.95 0.75
1.80 3.05 0.65
2.00 3.10 0.50
*
1875
1.25 1.60 0.30
1.31 2.20 0.45
1.43 2.60 0.66
1.60 2.90 0.75
1.90 3.00 0.60
2.00 3.05 0.55
*
2078
1.28 1.60 0.30
1.33 2.10 0.45
1.43 2.50 0.62
1.60 2.80 0.78
1.90 2.95 0.82
2.00 3.00 0.65
*
```

2281
1.33 1.60 0.30
1.36 2.00 0.43
1.47 2.45 0.66
1.65 2.74 0.70
1.90 2.85 0.75
2.00 2.90 0.63
*
3531
1.36 1.60 0.30
1.39 1.90 0.35
1.52 2.42 0.66
1.72 2.72 0.73
1.90 2.83 0.65
2.00 2.87 0.60
*

*** SPICE II PERKINS T6.354(M) TURBOCHARGER COMPRESSOR FILE**

```
* CONTROL DATA:No. OF SPEED CURVES,SCALING FATORS,RP,N,E,M
8 0.83 1 1 1e-5
* INTERCOOLER DATA
1320 298.4 0.521
* TABULATED MAP
1000
1.01 0.10 0.55
1.01 0.40 0.60
1.00 1.14 0.60
1.00 1.40 0.62
1.00 1.55 0.55
1.00 1.44 0.50
*
1375
1.08 0.10 0.60
1.07 0.50 0.65
1.07 1.20 0.67
1.06 1.50 0.70
1.05 1.75 0.65
1.04 2.00 0.60
*
2171
1.19 0.40 0.57
1.17 0.80 0.62
1.17 1.30 0.66
1.15 1.80 0.70
1.13 2.10 0.65
1.12 2.30 0.60
*
2357
1.23 0.80 0.60
1.22 1.10 0.62
1.22 1.30 0.68
1.20 1.90 0.70
1.18 2.20 0.68
1.17 2.40 0.57
*
2946
1.39 1.30 0.63
1.39 1.50 0.65
1.38 1.80 0.67
1.37 1.95 0.70
1.35 2.50 0.65
1.30 2.80 0.62
*
```

3536
1.580 1.90 0.62
1.575 2.20 0.70
1.560 2.80 0.75
1.505 3.20 0.67
1.460 3.50 0.62
1.440 3.60 0.60
*
4125
1.820 2.60 0.67
1.820 2.80 0.72
1.800 3.50 0.72
1.740 3.90 0.67
1.680 4.10 0.62
1.600 4.20 0.57
*
4714
2.140 3.20 0.67
2.140 3.50 0.70
2.100 4.30 0.68
2.060 4.50 0.67
2.000 4.70 0.65
1.920 4.80 0.60
*

***SPICE II PERKINS 6 CYLINDER T 6.354(M) SINGLE STAGE TURBOCHARGED DIESEL ENGINE WITH FOULED AIR INLET FILTER**

```
*CONTROL & SYSTEM DATA
1                                   * mode 1
1                                   * reference cylinder
c ncyc step nv nj ns nhr nhrf ng nht nval
  20   2 10 15 2 1  0 6  1   2
* PRINT & PLOT CONTROLS
20 20                               * plot data for cycles i to j
1 1 0 4 4 1
1 7 8 9
1 2 13 14
2
* CONTROL VOLUME DATA
0 1 1 1 1  360  4 1  11  1 2        * cylinder 1
0 1 1 1 1  600  4 1  11  1 2        * cylinder 2
0 1 1 1 1  120  4 1  11  1 2        * cylinder 3
0 1 1 1 1  480  4 1  11  1 2        * cylinder 4
0 1 1 1 1  240  4 1  11  1 2        * cylinder 5
0 1 1 1 1    0  4 1  11  1 2        * cylinder 6
1 2 0 0 1    0  0 0  0  0 0         * intake manifold
1 3 0 0 1    0  0 0  0  0 0         * exhaust manifold
1 4 0 0 1    0  0 0  0  0 0         * exhaust manifold
1 5 0 0 1    0  0 0  0  0 0         * filter volume
* FLOW JUNCTION DATA
1  1 0 7 0 0 0 1 1                  * intake valve cylinder 1
1  2 0 1 0 0 0 8 1                  * exhaust valve cylinder 1
1  1 0 7 0 0 0 2 2                  * intake valve cylinder 2
1  2 0 2 0 0 0 8 2                  * exhaust valve cylinder 2
1  1 0 7 0 0 0 3 3                  * intake valve cylinder 3
1  2 0 3 0 0 0 8 3                  * exhaust valve cylinder 3
1  1 0 7 0 0 0 4 4                  * intake valve cylinder 4
1  2 0 4 0 0 0 9 4                  * exhaust valve cylinder 4
1  1 0 7 0 0 0 5 5                  * intake valve cylinder 5
1  2 0 5 0 0 0 9 5                  * exhaust valve cylinder 5
1  1 0 7 0 0 0 6 6                  * intake valve cylinder 6
1  2 0 6 0 0 0 9 6                  * exhaust valve cylinder 6
2  0 0 1 0 0 0 0 7 2                * compressor
3  0 2 8 9 0 0 0 2                  * turbine
0  6 0 0 0 0 0 1 0 0                * filter orfice
* SHAFT DATA
1  0.0    0.00                      * crankshaft
2  0.5E-3  0.80                     * T/C Rotor
* HEAT RELEASE DATA SETS
0 719.4 100 42.5e6 2.92e-5 0 0 0 0
```

```
* GEOMETRIC DATA SETS
0.0984 .127 14.0 .219  1.0          * cylinder geometry
2.14E-3  0 0 0 0                    * intake manifold geometry
1.38E-3  0 0 0 0                    * exhaust manifold geometry
1.20E-3  0 0 0 0                    * exhaust manifold
1.42e-3  0 0 0 0                    * inlet duct vol
2.21e-3  0 0 0 0                    * filter EFA
* HEAT TRANSFER DATA
3                                   * no. of surface areas
0    0.0126   0.0158                * areas
573.0  673.0    773.0               * respective temeratures
* VALVE DATA SETS

24 0 1 1                            *intake valve
350 360 370 380 390 400 410 420 430 440 450 460 470 480 490 500 510 520 530 540
550 560 570 580
 0.0 3.44e-5 1.34e-4 2.67e-4 3.74e-4 5.02e-4 6.57e-4 6.94e-4 7.07e-4 7.41e-4
 7.42e-4 7.43e-4 7.42e-4 7.44e-4 7.44e-4 7.1e-4 6.95e-4 6.61e-4 5.25e-4 3.73e-4
 2.87e-4 1.36e-4 3.44e-5 0.0

26 0 1 1                            * exhaust valve
125 135 145 155 165 175 185 195 205 215 225 235 245 255 265 275 285 295 305 315
325 335 345 355 365 375
 0.0 9.11e-6 5.3e-5 1.37e-4 2.53e-4 4.05e-4 5.35e-4 5.96e-4 6.42e-4 6.69e-4
 6.64e-4 6.66e-4 6.7e-4 6.7e-4 6.6e-4 6.61e-4 6.55e-4 6.53e-4 6.25e-4 5.63e-4
 4.57e-4 3.11e-4 1.8e-4 7.7e-5 2.15e-5 0.0

* ENTRY AND EXIT CONDITIONS
101.6E+3 297.5 101.4E+3 647

* INITIAL SHAFT SPEEDS
 1500.0000
 31135
* INITIAL PRESSURE/TEMPERATURE/FUEL-AIR RATIO
 179864.29   820.1090   4.2025646e-02
 256147.71   461.4268   1.2475206e-03
 708221.1   1265.3490   4.4623716E-02
 189895.90   416.6010   1.5031702E-03
 173277.24   881.4562   4.4690090E-02
 11677172.   1655.4655   1.4050251E-02
 110380.60   305.53050   3.7844169E-10
 117685.88   665.9995   4.4870996E-04
 117613.07   665.3113   4.4820266E-04
 100900.00   297.3      4.48e-10
```

***SPICE II PERKINS 6 CYLINDER T 6.354(M) SINGLE STAGE TURBOCHARGED DIESEL ENGINE WITH EXHAUST VALVE LEAK**

```
*CONTROL & SYSTEM DATA
1                                   * mode 1
1                                   * reference cylinder
c ncyc step nv nj ns nhr nhrf ng nht nval
  20   2  9 20 2 1   0 5  1   2
* PRINT & PLOT CONTROLS
20 20                               * plot data for cycles i to j
1 1 0 4 4 1
1 7 8 9
1 2 13 14
2
* CONTROL VOLUME DATA
0 1 1 1 1  360  4 1  11  1 2        * cylinder 1
0 1 1 1 1  600  4 1  11  1 2        * cylinder 2
0 1 1 1 1  120  4 1  11  1 2        * cylinder 3
0 1 1 1 1  480  4 1  11  1 2        * cylinder 4
0 1 1 1 1  240  4 1  11  1 2        * cylinder 5
0 1 1 1 1    0  4 1  11  1 2        * cylinder 6
1 2 0 0 1    0  0 0 0  0 0          * intake manifold
1 3 0 0 1    0  0 0 0  0 0          * exhaust manifold
1 4 0 0 1    0  0 0 0  0 0          * exhaust manifold
* FLOW JUNCTION DATA
1  1 0 7 0 0 0 1 1                  * intake valve cylinder 1
1  2 0 1 0 0 0 8 1                  * exhaust valve cylinder 1
1  1 0 7 0 0 0 2 2                  * intake valve cylinder 2
1  2 0 2 0 0 0 8 2                  * exhaust valve cylinder 2
1  1 0 7 0 0 0 3 3                  * intake valve cylinder 3
1  2 0 3 0 0 0 8 3                  * exhaust valve cylinder 3
1  1 0 7 0 0 0 4 4                  * intake valve cylinder 4
1  2 0 4 0 0 0 9 4                  * exhaust valve cylinder 4
1  1 0 7 0 0 0 5 5                  * intake valve cylinder 5
1  2 0 5 0 0 0 9 5                  * exhaust valve cylinder 5
1  1 0 7 0 0 0 6 6                  * intake valve cylinder 6
1  2 0 6 0 0 0 9 6                  * exhaust valve cylinder 6
2  0 0 0 0 0 0 7 2                  * compressor
3  0 2 8 9 0 0 0 2                  * turbine
0  5 0 1 0 0 0 8 0                  * valve leak 1 cyl
0  5 0 2 0 0 0 8 0                  * valve leak 2 cyl
0  5 0 3 0 0 0 8 0                  * valve leak 3 cyl
0  5 0 4 0 0 0 9 0                  * valve leak 4 cyl
0  5 0 5 0 0 0 9 0                  * valve leak 5 cyl
0  5 0 6 0 0 0 9 0                  * valve leak 6 cyl
* SHAFT DATA
1  0.0    0.00                      * crankshaft
2  0.5E-3  0.80                     * T/C Rotor
```

```
* HEAT RELEASE DATA SETS
0 713 100 42.5e6 6.07e-5 0 0 0 0
* GEOMETRIC DATA SETS
0.0984 .127 16.0 .219  1.0          * cylinder geometry
4.88E-2  0 0 0 0                    * intake manifold geometry
1.38E-2  0 0 0 0                    * exhaust manifold geometry
1.20E-2  0 0 0 0                    * exhaust manifold
0.000000372  0 0 0 0                * leakage EFA
* HEAT TRANSFER DATA
3                                   * no. of surface areas
0     0.0126   0.0158               * areas
573.0  673.0    773.0               * respective temeratures

* VALVE DATA SETS

24 0 1 1                            *intake valve
350 360 370 380 390 400 410 420 430 440 450 460 470 480 490 500 510 520 530 540
550 560 570 580
 0.0 3.44e-5 1.34e-4 2.67e-4 3.74e-4 5.02e-4 6.57e-4 6.94e-4 7.07e-4 7.41e-4
 7.42e-4 7.43e-4 7.42e-4 7.44e-4 7.44e-4 7.1e-4 6.95e-4 6.61e-4 5.25e-4 3.73e-4
 2.87e-4 1.36e-4 3.44e-5 0.0

26 0 1 1                            * exhaust valve
125 135 145 155 165 175 185 195 205 215 225 235 245 255 265 275 285 295 305 315
325 335 345 355 365 375
 0.0 9.11e-6 5.3e-5 1.37e-4 2.53e-4 4.05e-4 5.35e-4 5.96e-4 6.42e-4 6.69e-4
 6.64e-4 6.66e-4 6.7e-4 6.7e-4 6.6e-4 6.61e-4 6.55e-4 6.53e-4 6.25e-4 5.63e-4
 4.57e-4 3.11e-4 1.8e-4 7.7e-5 2.15e-5 0.0

* ENTRY AND EXIT CONDITIONS
98E+3 294 100E+3 298

* INITIAL SHAFT SPEEDS
  1500.0000
  76525.55
* INITIAL PRESSURE/TEMPERATURE/FUEL-AIR RATIO
  179864.29   820.1090   4.2025646e-02
  256147.71   461.4268   1.2475206e-03
  708221.1   1265.3490   4.4623716E-02
  189895.90   416.6010   1.5031702E-03
  173277.24   881.4562   4.4690090E-02
  11677172.   1655.4655   1.4050251E-02
  192664.60    381.3050   3.7844169E-05
  150385.88    960.9995   4.4870996E-02
  171113.07   1004.3113   4.4820266E-02
```

***SPICE II PERKINS 6 CYLINDER T 6.354(M) SINGLE STAGE TURBOCHARGED DIESEL ENGINE WITH INLET VALVE LEAK**

```
*CONTROL & SYSTEM DATA
1                                   * mode 1
1                                   * reference cylinder
c ncyc step nv nj ns nhr nhrf ng nht nval
  20   2  9 20 2 1   0 5  1   2
* PRINT & PLOT CONTROLS
20 20                               * plot data for cycles i to j
1 1 0 4 4 1
1 7 8 9
1 2 13 14
2
* CONTROL VOLUME DATA
0 1 1 1 1  360  4 1  11  1 2        * cylinder 1
0 1 1 1 1  600  4 1  11  1 2        * cylinder 2
0 1 1 1 1  120  4 1  11  1 2        * cylinder 3
0 1 1 1 1  480  4 1  11  1 2        * cylinder 4
0 1 1 1 1  240  4 1  11  1 2        * cylinder 5
0 1 1 1 1    0  4 1  11  1 2        * cylinder 6
1 2 0 0 1    0  0 0  0  0 0         * intake manifold
1 3 0 0 1    0  0 0  0  0 0         * exhaust manifold
1 4 0 0 1    0  0 0  0  0 0         * exhaust manifold
* FLOW JUNCTION DATA
1  1 0 7 0 0 0 1 1                  * intake valve cylinder 1
1  2 0 1 0 0 0 8 1                  * exhaust valve cylinder 1
1  1 0 7 0 0 0 2 2                  * intake valve cylinder 2
1  2 0 2 0 0 0 8 2                  * exhaust valve cylinder 2
1  1 0 7 0 0 0 3 3                  * intake valve cylinder 3
1  2 0 3 0 0 0 8 3                  * exhaust valve cylinder 3
1  1 0 7 0 0 0 4 4                  * intake valve cylinder 4
1  2 0 4 0 0 0 9 4                  * exhaust valve cylinder 4
1  1 0 7 0 0 0 5 5                  * intake valve cylinder 5
1  2 0 5 0 0 0 9 5                  * exhaust valve cylinder 5
1  1 0 7 0 0 0 6 6                  * intake valve cylinder 6
1  2 0 6 0 0 0 9 6                  * exhaust valve cylinder 6
2  0 0 0 0 0 0 7 2                  * compressor
3  0 2 8 9 0 0 0 2                  * turbine
0  5 0 1 0 0 0 7 0                  * valve leak 1 cyl
0  5 0 2 0 0 0 7 0                  * valve leak 2 cyl
0  5 0 3 0 0 0 7 0                  * valve leak 3 cyl
0  5 0 4 0 0 0 7 0                  * valve leak 4 cyl
0  5 0 5 0 0 0 7 0                  * valve leak 5 cyl
0  5 0 6 0 0 0 7 0                  * valve leak 6 cyl
* SHAFT DATA
1  0.0    0.00                      * crankshaft
2  0.5E-3  0.80                     * T/C Rotor
```

```
* HEAT RELEASE DATA SETS
0 713 100 42.5e6 6.07e-5 0 0 0 0
* GEOMETRIC DATA SETS
0.0984 .127 16.0 .219  1.0          * cylinder geometry
4.88E-2  0 0 0 0                    * intake manifold geometry
1.38E-2  0 0 0 0                    * exhaust manifold geometry
1.20E-2  0 0 0 0                    * exhaust manifold
0.0000002488  0 0 0 0               * leakage EFA
* HEAT TRANSFER DATA
3                                   * no. of surface areas
0    0.0126   0.0158                * areas
573.0  673.0    773.0               * respective temeratures

* VALVE DATA SETS

24 0 1 1                            *intake valve
350 360 370 380 390 400 410 420 430 440 450 460 470 480 490 500 510 520 530 540
550 560 570 580
 0.0 3.44e-5 1.34e-4 2.67e-4 3.74e-4 5.02e-4 6.57e-4 6.94e-4 7.07e-4 7.41e-4
 7.42e-4 7.43e-4 7.42e-4 7.44e-4 7.44e-4 7.1e-4 6.95e-4 6.61e-4 5.25e-4 3.73e-4
 2.87e-4 1.36e-4 3.44e-5 0.0

26 0 1 1                            * exhaust valve
125 135 145 155 165 175 185 195 205 215 225 235 245 255 265 275 285 295 305 315
325 335 345 355 365 375
 0.0 9.11e-6 5.3e-5 1.37e-4 2.53e-4 4.05e-4 5.35e-4 5.96e-4 6.42e-4 6.69e-4
 6.64e-4 6.66e-4 6.7e-4 6.7e-4 6.6e-4 6.61e-4 6.55e-4 6.53e-4 6.25e-4 5.63e-4
 4.57e-4 3.11e-4 1.8e-4 7.7e-5 2.15e-5 0.0

* ENTRY AND EXIT CONDITIONS
98E+3 294 100E+3 298

* INITIAL SHAFT SPEEDS
 1500.0000
 76525.55
* INITIAL PRESSURE/TEMPERATURE/FUEL-AIR RATIO
 179864.29   820.1090   4.2025646e-02
 256147.71   461.4268   1.2475206e-03
 708221.1   1265.3490   4.4623716E-02
 189895.90   416.6010   1.5031702E-03
 173277.24   881.4562   4.4690090E-02
 11677172.   1655.4655   1.4050251E-02
 192664.60    381.3050   3.7844169E-05
 150385.88    960.9995   4.4870996E-02
 171113.07   1004.3113   4.4820266E-02
```

Speed [revs/min] - T [Nm]	1500-100		1400-186		1500-200		1600-237		1500-300		1800-293		1500-427		2000-354		2150-372	
Data Source	Engine	Sim	Engine	Sim	Engine	Sim	Engine	Sim	Engine	Sim	Engine	Sim	Engine	Sim	Engine	Sim	Engine	Sim
POI [Deg CA]	-5.3	-1.3	-3.6	-1	-4	-0.6	-5	-2	-5	-3	-12	-13	-12.9	-12	-12	-12	-12.2	-11
Mass FPS [kg]	1.98E-05	1.28E-05	2.98E-05	2.73E-05	3.19E-05	2.97E-05	3.72E-05	3.56E-05	4.68E-05	4.30E-05	4.30E-05	4.27E-05	6.16E-05	5.80E-05	5.24E-05	5.20E-05	5.61E-05	5.50E-05
Inlet man P [kPa]	102.6	104.3	107.6	107.5	110.3	111.8	116.3	117	121.5	120.4	124.2	123.4	129.4	129.6	140.2	139.7	150.9	152
Inlet man T [K]	299	302	302.6	304	305	306	308.5	308	336	311	314	314	315.5	316	324.5	322	332	329
Inlet air mass flow [kg/s]	0.0699	0.0719	0.06735	0.692	0.07419	0.0767	0.08307	0.0858	0.08045	0.0827	0.09849	0.1001	0.08286	0.0878	0.12242	0.1245	0.136418	0.1437
Exhaust mass flow [kg/s]	0.0714	0.0728	0.06944	0.705	0.07658	0.0784	0.08604	0.0884	0.084	0.0852	0.1024	0.1038	0.087483	0.0921	0.1277	0.1297	0.14244	0.149
Exhaust man P [kPa]	111	116	114.6	118	117	122	121	1.26	123.6	127	129.2	136	128	135	143	151	155.5	163
Exhaust man T [K]	536	655	628	747	665	759	717	796	791	898	757	871	876	966	838	927	871	935
Max cylinder P [Bar]	42.66	43	46.9	48	48.8	49	52.8	53	55.24	54	67.3	68	74.8	74	75.1	75	79.4	78
Deg CA P max [Deg CA]	11.7	10	12.2	10	11.6	10	10.4	12	9.2	10	6.9	6	8.5	8	9.2	8	8.7	8
Torque [Nm]	99	94	185.4	179	200	190	237	232	301.7	297	292.7	286	427	406	355	357	369	373
BSFC [kg/kW/hr]	0.3511	0.338	0.2774	0.266	0.2742	0.268	0.2699	0.256	0.27	0.249	0.253	0.256	0.2481	0.244	0.2529	0.251	0.2651	0.253
Comp P ratio	1.01	1.05	1.057	1.07	1.089	1.12	1.15	1.18	1.21	1.203	1.23	1.23	1.284	1.29	1.4	1.4	1.508	1.53
Comp mass flow	1.204	1.23	1.204	1.18	1.278	1.31	1.434	1.47	1.392	1.41	1.708	1.72	1.437	1.51	2.13	2.15	2.38	2.49
Comp Eff	9	59	9	59	42.6	61	50.6	63	55.5	63	53.7	66	57	65	57.2	69.8	58.7	71
Turbo speed [revs/min]	23686	31654	27557	35900	31135	38740	37420	40883	41464	42418	45302	45031	47949	49354	57126	56686	63378	64372
Turb expansion ratio	1.096	1.15	1.147	1.18	1.16	1.22	1.21	1.26	1.24	1.29	1.264	1.34	1.272	1.38	1.42	1.52	1.508	1.62
Turbine mass flow	1.508	1.59	1.521	1.6	1.707	1.73	1.917	1.92	1.917	1.93	2.214	2.19	2.029	2.03	2.56	2.54	2.705	2.72
Turbine eff	51	36	47.55	36	75.3	36	79	37	68.63	39	80.8	41	79.9	40	83	44	79.6	47
Mech eff	58	59.5	79.6	74	80.62	74	81.62	77	88.3	82	83.4	78	95.6	85.1	84.6	80	83.5	80
IMEP [Bar]	3.623	3.42	5.06	5.25	5.39	5.53	6.3	6.52	7.41	7.87	7.61	7.91	9.69	10.35	9.09	9.63	9.59	10.08
Brake therm eff	23.922	25.07	30.27	31.8	30.63	32	31.12	33.1	31.1	34	33.2	33	33.8	34.7	33.2	33.7	32.11	33.4
Volumetric eff	83.4	80.8	82.8	81	83.4	82	83.8	83.5	83.2	84	84.2	84	81.8	85	85.3	85.2	84.3	85.9

Table 40 Comparison Of Healthy SPICE Model & Experimental Results

Speed [revs/min] - T [Nm]	1500-300		1800 - 293		1500 - 427		200 - 354		2150 - 372	
Data Source	Faulty	Healthy	Faulty	Healthy	Faulty	Healthy	Faulty	Healthy	Faulty	Healthy
POI [Deg CA]	-3	-3	-13	-13	-12	-12	-12	-12	-11	-11
Mass FPS [kg]	0.000043	0.000043	0.000042	0.000042	0.000058	0.000058	0.000052	0.000052	0.000055	0.000055
Inlet man P [kPa]	121.3	121.3	121.4	122.6	128.3	129	137.9	139.5	150.3	149.6
Inlet man T [K]	310	311	313	313	316	316	322	322	329	328
Inlet air mass flow [kg/s]	0.0813	0.08279	0.0986	0.09968	0.0867	0.0875	0.1226	0.1243	0.142	0.1474
Exhaust mass flow [kg/s]	0.0859	0.0859	0.102	0.1035	0.0912	0.0918	0.127	0.1295	0.148	0.1474
Exhaust man P [kPa]	128	128.2	135.6	136.1	134	134.3	150	150.9	159.8	162.7
Exhaust man T [K]	895	894	876	871	972	967	936	930	945	944
Max cylinder P [Bar]	55	55	67	67.5	74	74	74	75	77	77
Deg CA P max [Deg CA]	9	10	6	6	8	8	8	8	10	10
Torque [Nm]	297	296.2	284.9	285.9	404.8	405.8	355.3	356.8	375	373.5
BSFC [kg/kw/hr]	0.248	0.2496	0.258	0.2573	0.244	0.244	0.252	0.2512	0.251	0.2528
Comp P ratio	1.21	1.212	1.22	1.224	1.28	1.289	1.38	1.397	1.502	1.502
Comp mass flow	1.4	1.42	1.7	1.72	1.5	1.51	2.14	2.15	2.49	2.49
Comp Eff	67	67	68	69	65	65	69	69	71	71
Turbo speed [revs/min]	43.13	43.052	44.469	44.538	48.751	48.738	56.552	56.567	64.338	63.017
Turb expansion ratio	1.29	1.297	1.33	1.334	1.37	1.375	1.51	1.518	1.598	1.61
Turbine mass flow	1.94	1.94	2.17	2.19	2.03	2.03	2.53	2.54	2.77	2.71
Turbine eff	38	38	38	38	38	38	43	43	48	48
Mech eff	85.5	81.7	83.6	78.39	84.7	85.14	85.6	80.4	86.2	80.24
IMEP [Bar]	7.89	7.86	7.88	7.92	10.31	10.34	9.58	9.62	10.14	10.09
Brake therm eff	34	33.9	33	32.91	34.6	34.7	33.6	33.7	33.6	33.5

Table 41 Faulty Intercooler SPICE Results

Speed [revs/min] - T [Nm]	**1500 - 300**		**1800 - 293**		**1500 - 427**		**2000 - 354**		**2150 - 372**	
Data source	Faulty	Healthy	Faulty	Healthy	Faulty	Healthy	Faulty	Healthy	Faulty	Healthy
POI [Deg CA]	-3	-3	-13	-13	-12	-12	-12	-12	-11	-11
Mass FPS [kg]	0.000043	0.000043	0.000042	0.000042	0.000058	0.000058	0.000052	0.000052	0.000055	0.00005.
Inlet man P [kPa]	121	121.3	121.7	122.6	128.5	129	138.4	139.5	149.3	149.6
Inlet man T [K]	311	316	313	319	316	323	322	332	340	328
Inlet air mass flow [kg/s]	0.08279	0.0815	0.09968	0.09753	0.0875	0.0856	0.1243	0.1204	0.1373	0.1474
Exhaust mass flow [kg/s]	0.0847	0.0859	0.1013	0.1035	0.0899	0.0918	0.1256	0.1295	0.1431	0.1474
Exhaust man P [kPa]	127.8	128.2	135.5	136.1	133.7	134.3	149.8	150.9	161.5	162.7
Exhaust man T [K]	904	894	883	871	983	967	947	930	966	944
Max cylinder P [Bar]	54	55	67	67.5	73	74	74	75	75.3	77
Deg CA P max [Deg CA]	10	10	6	6	9	8	8	8	10	10
Torque [Nm]	296.2	296.2	283.4	285.9	403.4	405.8	353	356.8	370	373.5
BSFC [kg/kw/hr]	0.2493	0.2496	0.2595	0.2573	0.246	0.244	0.2539	0.2512	0.2555	0.2528
Comp P ratio	1.211	1.212	1.223	1.224	1.29	1.289	1.394	1.397	1.499	1.502
Comp mass flow	1.4	1.42	1.68	1.72	1.47	1.51	2.08	2.15	2.38	2.45
Comp Eff	67	67	69	69	65	65	69	69	71	71
Turbo speed [revs/min]	43	43.052	44.439	44.538	48.678	48.738	56.273	56.567	62.799	63.017
Turb expansion ratio	1.293	1.297	1.372	1.334	1.369	1.375	1.504	1.518	1.598	1.61
Turbine mass flow	1.93	1.94	2.16	2.19	2.02	2.03	2.51	2.54	2.68	2.71
Turbine eff	38	38	38	38	38	38	43	43	48	48
Mech eff	81.7	81.7	78.29	78.39	85.1	85.14	80.33	80.4	80.14	80.24
IMEP [Bar]	7.86	7.86	7.85	7.92	10.29	10.34	9.54	9.62	10.01	10.09
Brake therm eff	33.9	33.9	32.64	32.91	34.4	34.7	33.3	33.7	33.1	33.5
Volumetric Eff	84.6	83.95	83.9	83.65	84.8	85.2	85.7	85.2	86.4	85.8

Table 42 80% Fouled Air Filter SPICE Results

Speed - revs/min] - T [Nm]	1500-300		1800-293		1500-427		2000-354		2150-372	
Data Source	Faulty	Healthy	Faulty	Healthy	Faulty	Healthy	Faulty	Healthy	Faulty	Healthy
POI	-3	-3	-13	-13	-12	-12	-12	-12	-11	-11
Mass FPS	0.000043	0.000043	0.000042	4.3E-05	0.000058	0.000058	0.000052	5.2E-05	0.000055	5.5E-05
Inlet man P	121.1	121.3	122.8	122.6	128.9	129	139.9	139.5	149.4	149.6
Inlet man T	311	311	317	313	322	316	326	322	331	328
Inlet air mass flow	0.0813	0.0826	0.0984	0.09968	0.0861	0.0875	0.123	0.1243	0.1397	0.1474
Exhaust mass flow	0.0859	0.0854	0.1022	0.1035	0.0901	0.0918	0.1281	0.1295	0.1455	0.1474
Exhaust man P	128	127.9	135.75	136.1	134.2	134.3	150.5	150.9	161.8	162.7
Exhaust man T	896.5	894	879	871	981	967	937	930	952	944
Max cylinder P	54.8	55	67	67.5	73	74	72	75	76	77
Deg CA P max	10	10	6	6	8	8	8	8	10	10
Torque	296	296.2	284.9	285.9	402.8	405.8	352.2	356.8	371	373.5
BSFC	0.25	0.2496	0.2581	0.2573	0.2464	0.244	0.2532	0.2512	0.2542	0.2528
Comp P ratio	1.21	1.212	1.224	1.224	1.287	1.289	1.398	1.397	1.5	1.502
Comp mass flow	1.42	1.42	1.69	1.72	1.48	1.51	2.13	2.15	2.42	2.49
Comp Eff	67	67	68	69	65	65	69	69	71	71
Turbo speed	42.971	43.052	44.5	44.538	48.581	48.738	56.608	56.567	62.874	63.017
Turb expansion ratio	1.294	1.297	1.33	1.334	1.366	1.375	1.515	1.518	1.605	1.61
Turbine mass flow	1.93	1.94	2.17	2.19	2.01	2.03	2.53	2.54	2.7	2.71
Turbine eff	38	38	38	38	38	38	43	43	48	48
Mech eff	81.69	81.7	78.34	78.39	85.06	85.14	80.33	80.4	80.18	80.24
IMEP	7.86	7.86	7.89	7.92	10.27	10.34	9.51	9.62	10.05	10.09
Brake therm eff	33.94	33.9	32.83	32.91	34.3	34.7	33.44	33.7	33.32	33.5
Volumetric Eff	84.1	83.95	83.9	83.65	84.1	85.2	85.5	85.2	85.9	85.8

Table 43 Leaking Inlet Valves SPICE Simulation Results

Speed - revs/min] - T [Nm]	1500-300		1800-293		1500-427		2000-354		2150-372	
Data Source	Faulty	Healthy	Faulty	Healthy	Faulty	Healthy	Faulty	Healthy	Faulty	Healthy
POI [Deg CA]	-3	-3	-13	-13	-12	-12	-12	-12	-11	-11
Mass FPS [kg]	0.000043	0.000043	0.000042	0.000042	0.000058	0.000058	0.000052	0.000052	0.000055	0.00005.
Inlet man P [kPa]	121.1	121.3	122.7	122.6	128.9	129	140.2	139.5	149.7	149.6
Inlet man T [K]	311	311	313	313	316	316	322	322	328	328
Inlet air mass flow [kg/s]	0.08261	0.0826	0.09975	0.09968	0.08738	0.0875	0.1248	0.1243	0.1416	0.1474
Exhaust mass flow [kg/s]	0.08545	0.0854	0.1035	0.1035	0.09166	0.0918	0.12998	0.1295	0.1474	0.1474
Exhaust man P [kPa]	127.9	127.9	136.15	136.1	134.65	134.3	151.4	150.9	162.8	162.7
Exhaust man T [K]	896	894	874	871	973	967	933	930	948	944
Max cylinder P [Bar]	54.66	55	67	67.5	74	74	73	75	76	77
Deg CA P max [Deg CA]	10	10	6	6	8	8	8	8	10	10
Torque [Nm]	296	296.2	284.4	285.9	403.6	405.8	353.4	356.8	372	373.5
BSFC [kg/kw/hr]	0.25	0.2495	0.2587	0.2573	0.2454	0.244	0.2523	0.2512	0.2536	0.2528
Comp P ratio	1.21	1.212	1.224	1.224	1.287	1.289	1.402	1.397	1.503	1.502
Comp mass flow	1.42	1.42	1.72	1.72	1.5	1.51	2.16	2.15	2.45	2.49
Comp Eff	67	67	68	69	65	65	69	69	71	71
Turbo speed [revs/min]	42.925	43.052	44.539	44.538	48.59	48.738	56.843	56.567	63.07	63.017
Turb expansion ratio	1.294	1.297	1.333	1.334	1.37	1.375	1.521	1.518	1.612	1.61
Turbine mass flow	1.93	1.94	2.19	2.19	2.03	2.03	2.55	2.54	2.71	2.71
Turbine eff	38	38	38	38	38	38	43	43	48	48
Mech eff	81.68	81.7	78.31	78.39	85.09	85.14	80.36	80.4	80.19	80.24
IMEP [Bar]	7.85	7.86	7.876	7.92	10.287	10.34	9.535	9.62	10.06	10.09
Brake therm eff	33.94	33.9	32.74	32.91	34.52	34.7	33.58	33.7	33.39	33.5
Volumetric Eff	84.05	83.95	83.9	83.65	84.1	85.2	85.2	85.2	85.7	85.8

Table 44 Leaking Exhaust Valves SPICE Simulaton Results

Speed - revs/min] - T [Nm]	1500-300		1800-293		1500-427		2000-354		2150-372	
Data Source	Faulty	Healthy	Faulty	Healthy	Faulty	Healthy	Faulty	Healthy	Faulty	Healthy
POI [Deg CA]	-3	-3	-13	-13	-12	-12	-12	-12	-11	-11
Mass FPS [kg]	0.000043	4E-05	0.0000427	4E-05	0.000058	6E-05	0.000052	5E-05	0.000055	6E-05
Inlet man P [kPa]	122.3	121.3	123.7	122.6	130.4	129	141.2	139.5	151.2	149.6
Inlet man T [K]	312	311	314	313	316	316	323	322	328	328
Inlet air mass flow [kg/s]	0.08336	0.0826	0.10056	0.0997	0.0884	0.0875	0.1256	0.1243	0.149	0.1416
Exhaust mass flow [kg/s]	0.866	0.0854	0.10436	0.1035	0.09267	0.0918	0.1308	0.1295	0.1483	0.1487
Exhaust man P [kPa]	129	127.9	137.1	136.1	135.4	134.3	152.4	150.9	164.1	162.7
Exhaust man T [K]	912	894	886	871	985	967	940	930	955	944
Max cylinder P [Bar]	51	55	64	67.5	69	74	70	75	71	77
Deg CA P max [Deg CA]	10	10	8	6	10	8	10	8	10	10
Torque [Nm]	293.8	296.2	290	285.9	408.6	405.8	355.6	356.8	369	373.5
BSFC [kg/kw/hr]	0.252	0.2495	0.254	0.2573	0.2435	0.244	0.2518	0.2512	0.2545	0.2528
Comp P ratio	1.221	1.212	1.234	1.224	1.302	1.289	1.414	1.397	1.517	1.502
Comp mass flow	1.43	1.42	1.73	1.72	1.52	1.51	2.17	2.15	2.48	2.45
Comp Eff	67	67	68	69	65	65	69	69	71	71
Turbo speed [revs/min]	43.762	43.052	45.277	44.538	49.7	48.738	57.59	56.567	63.78	63.017
Turb expansion ratio	1.308	1.297	1.346	1.334	1.389	1.375	1.533	1.518	1.628	1.61
Turbine mass flow	1.95	1.94	2.2	2.19	2.05	2.03	2.55	2.54	2.73	2.71
Turbine eff	38	38	38	38	38	38	43	43	48	48
Mech eff	81.77	81.7	78.8	78.39	85.44	85.14	80.585	80.4	80.31	80.24
IMEP [Bar]	7.79	7.86	7.98	7.92	10.37	10.34	9.57	9.62	9.99	10.09
Brake therm eff	33.61	33.9	33.35	32.91	34.77	34.7	33.63	33.7	33.29	33.5
Volumetric Eff	84.2	83.95	83.7	83.65	84.9	85.2	85.4	85.2	85.9	85.8

Table 45 3° Crank Angle Retarded Pump Timing SPICE Simulation Results

APPENDIX 'E'

The Back Propogation Algorithm

Model 'A' & 'B's Diagnostic Performance On Faults Of A Lower Severity Than Those Trained On

Model 'A' & 'B's Diagnostic Performance On Novel Faults

Model 'A' & 'B's Diagnostic Ability At A Speed and Torque Not Trained At

Model 'A' & 'B's Diagnostic Ability On +/- 1% Randomly Noisy Data

Model 'A' & 'B's Diagnostic Ability On +/- 2% Randomly Noisy Data

Model 'A' & 'B's Diagnostic Ability On Faulty Sensor Data

Automated Sensor Check Program

Semi Intelligent On -Line Diagnostic Database Program, DIAMAC.XLM

The Back Propagation Algorithm

The back propagation algorithm has been successfully applied to many diagnostic problems as discussed in Chapter 1. It works by progressively moving down the networks error surface. The rate at which it moves down the error surface is inversely proportional to the gradient of the error surface. If the walls are steep the networks take large steps during each iteration. As the gradient of the error surface decreases it takes progressively smaller steps to reach convergence. The error surface represents the entire network error for all combinations of weights and therefore any movement on the error surface will require the network weights to be adjusted. Rummelhart [60] detailed how the algorithm makes these weight adjustments for Standard Back Propagation. This is shown below;

1. The output of the *i*th neuron in layer *m*, V_i^m is given by the sigmoid function;

$$V_i^m = \frac{1}{1+e^{\left(\sum W_{ij}^m V_j^{m-1} + \varphi_i\right)}}$$

2. Set all weights to small random values.

3. Present a training vector I and an output vector O. Apply I to the input layer neurons (m=0) so that $V^o = I$.

4. For other layers, m = 1.....M, perform the forward pass computation ;

$$V_i^m = f\left(\sum_j W_{ij}^m V_j^{m-1}\right)$$

where W_{ij}^m is the connection weight from V_j^{m-1} to V_i^m

5. Compute the errors in the output layer;

$$\delta_i^M = V_i^M\left(1 - V_i^M\right)\left(O_i - V_i^M\right)$$

6. Compute the back propagation errors for the preceding layers M-1,...,1;

$$\delta_i^{m-1} = V_i^{m-1}\left(1 - V_i^{m-1}\right)\sum_j W_{ji}^m \delta_j^m$$

7. Adjust the weights;

$$W_{ij}^m(t+1) = W_{ij}^m(t) + \alpha \delta_i^m V_j^{m-1}$$

where α is the gain parameter. Thresholds are adjusted in a similar way to weights.

8. Iterate by going to step 3.

The algorithm continues until the overall error, which is the mean square difference between the desired and actual outputs for all training patterns is reduced to the criteria set in Neuraldesk. The Stochastic Back Propagation algorithm deviates from this slightly because the weights are adjusted at a different point in the learning process. Stochastic Back Propagation adjusts the weights after each input vector is applied to the input neurons.

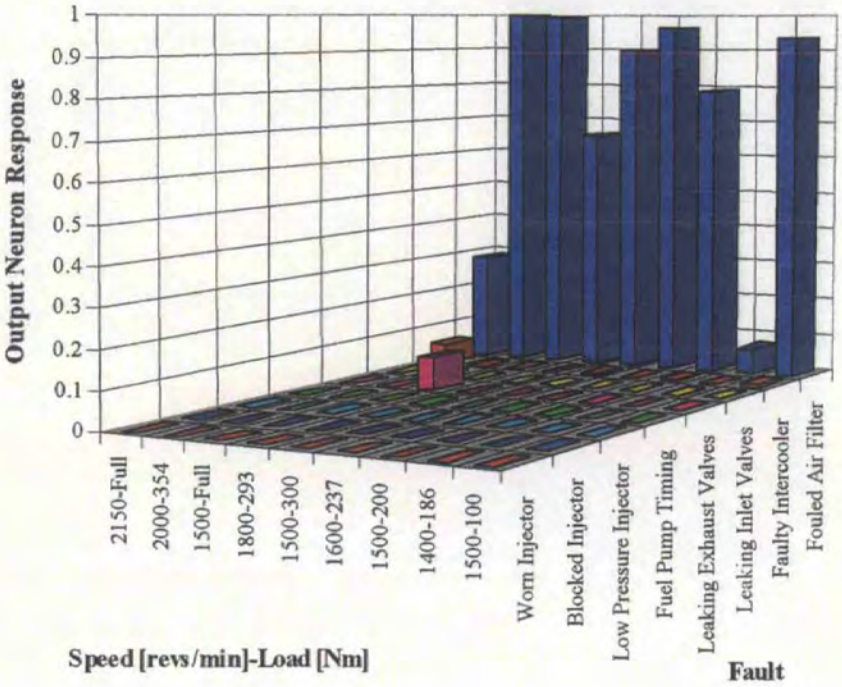

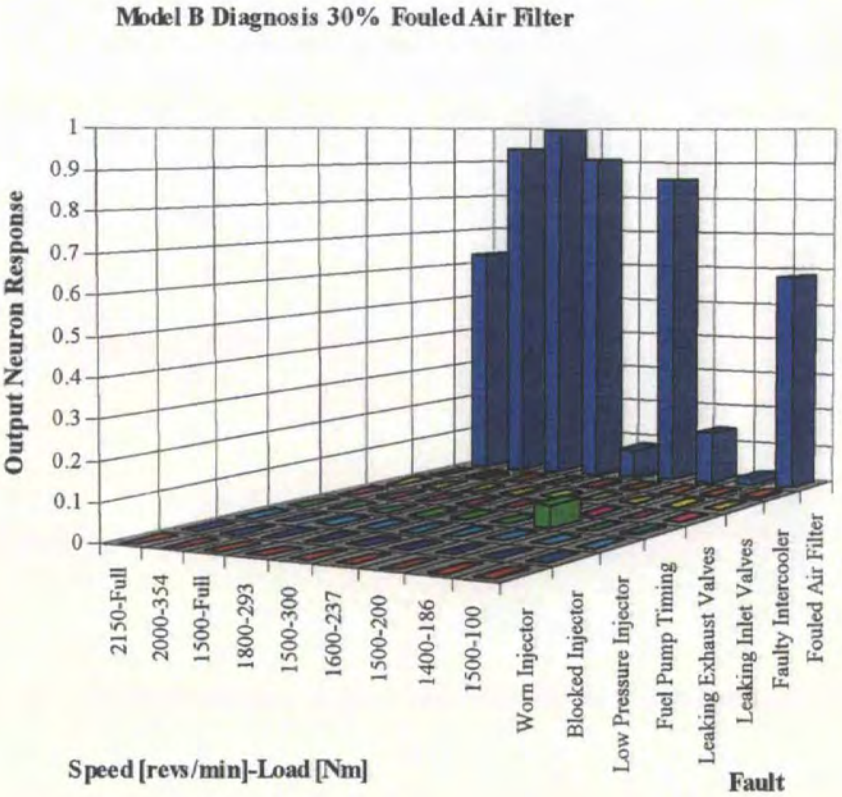

Figure 123 Model 'A' & 'B's Diagnostic Performance On 30% Fouled Air Filter Data

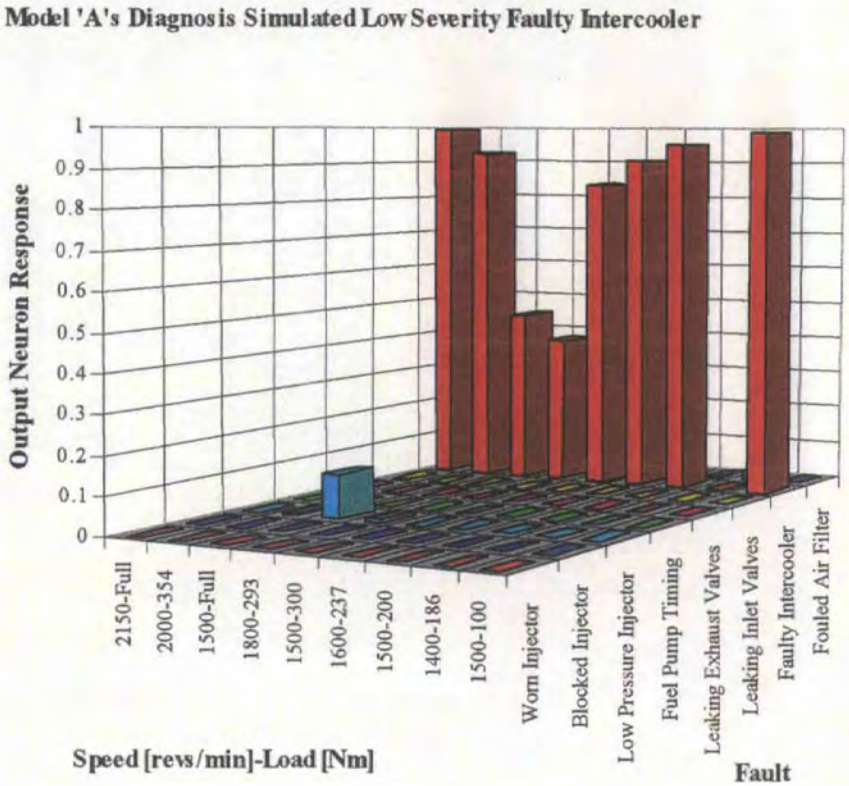

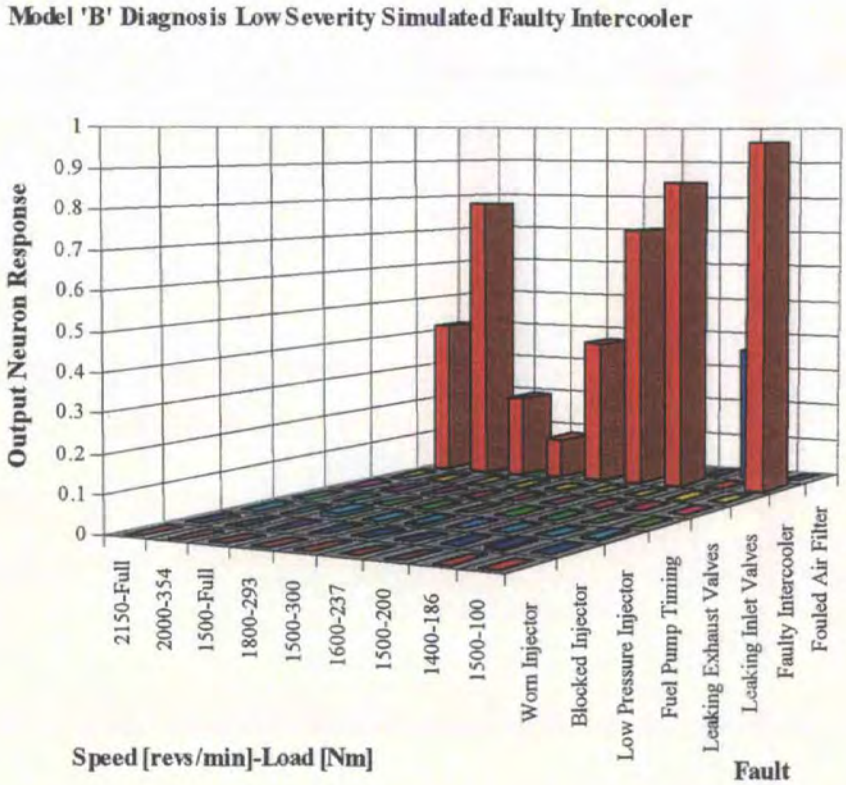

Figure 124 Model 'A' & 'B's Diagnostic Performance On Low Severity Simulated Faulty Intercooler Data

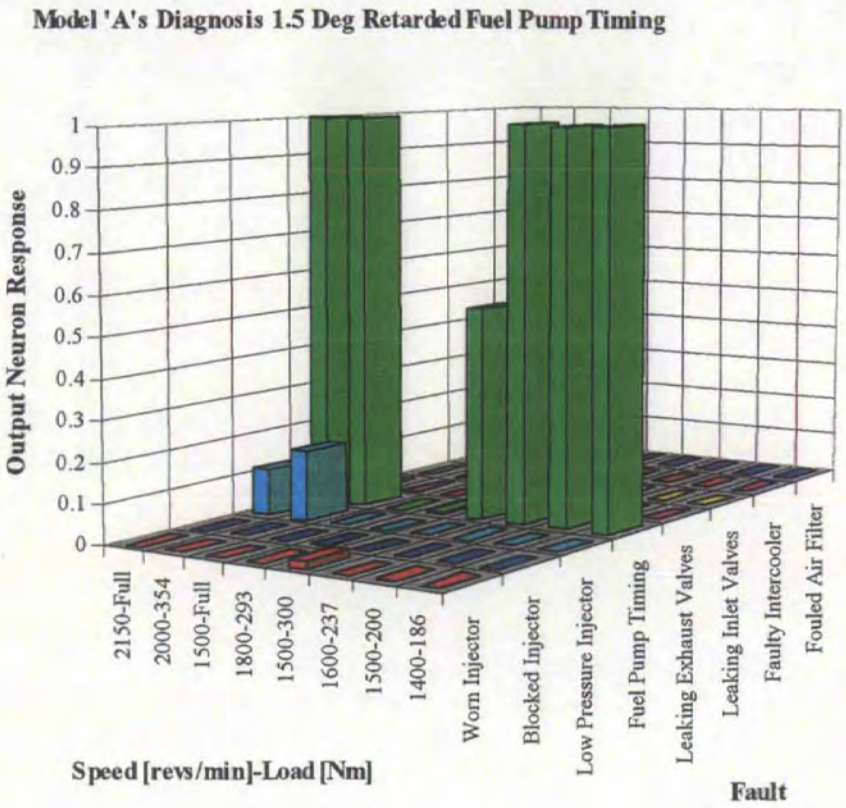

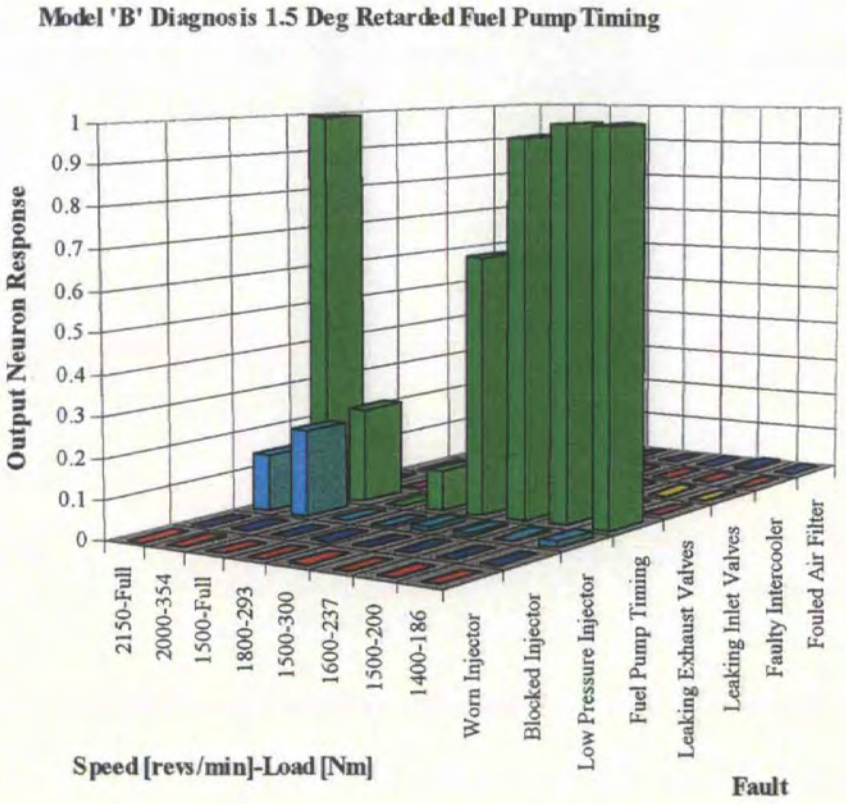

Figure 125 Model 'A' & 'B's Diagnostic Performance On 1.5 Deg Retarded Fuel Pump Timing Data

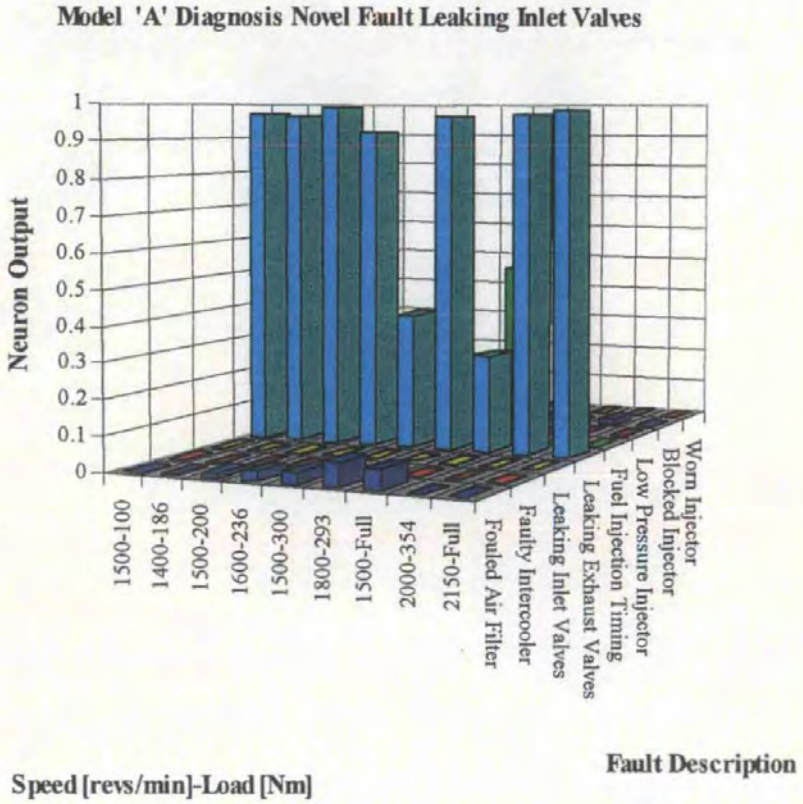

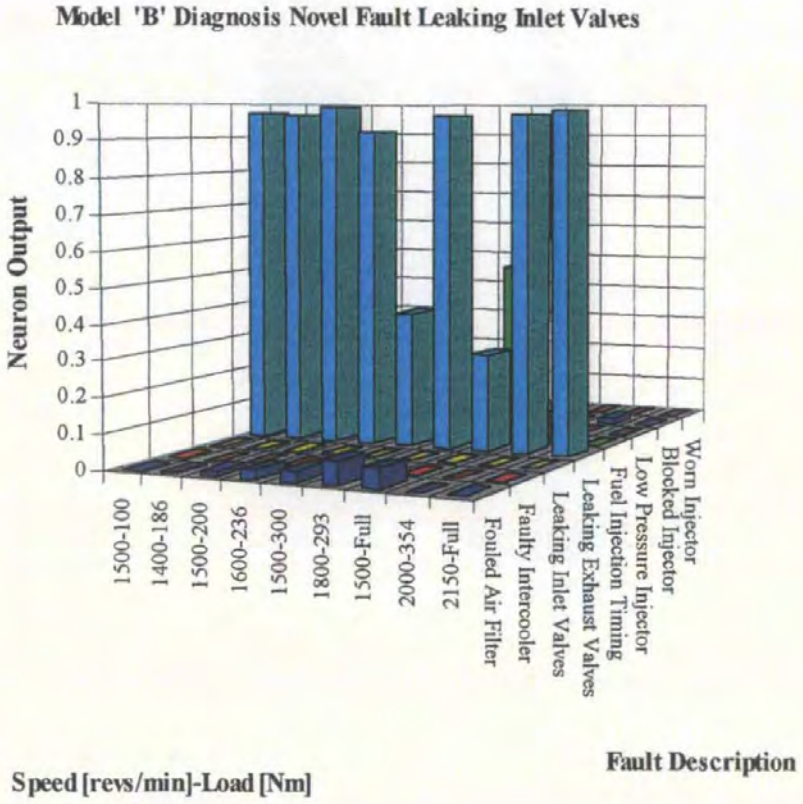

Figure 126 Model 'A' & 'B's Diagnostic Performance On A Novel Fault - Leaking Inlet Valves

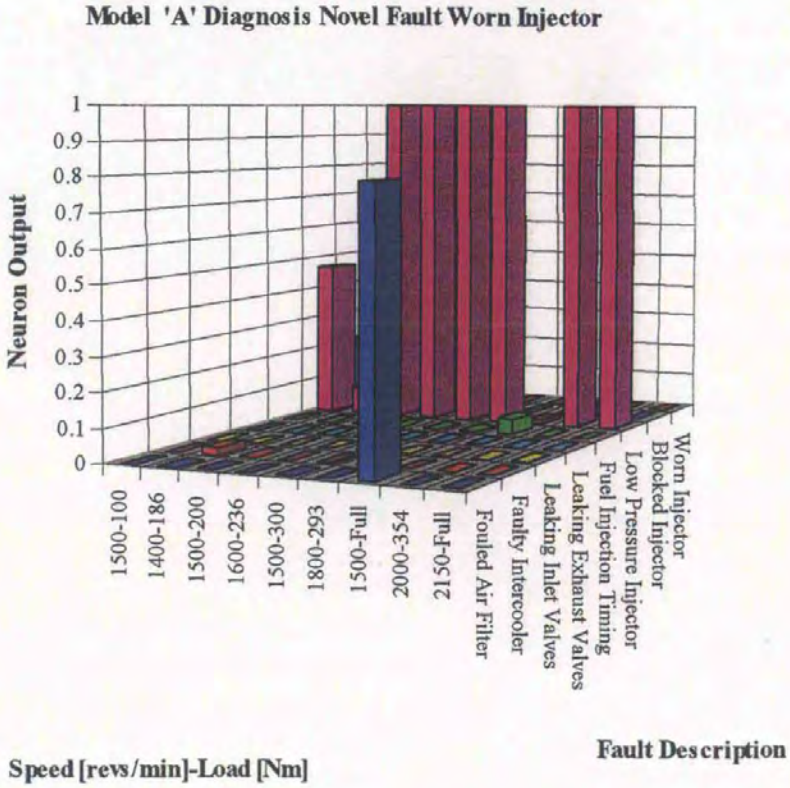

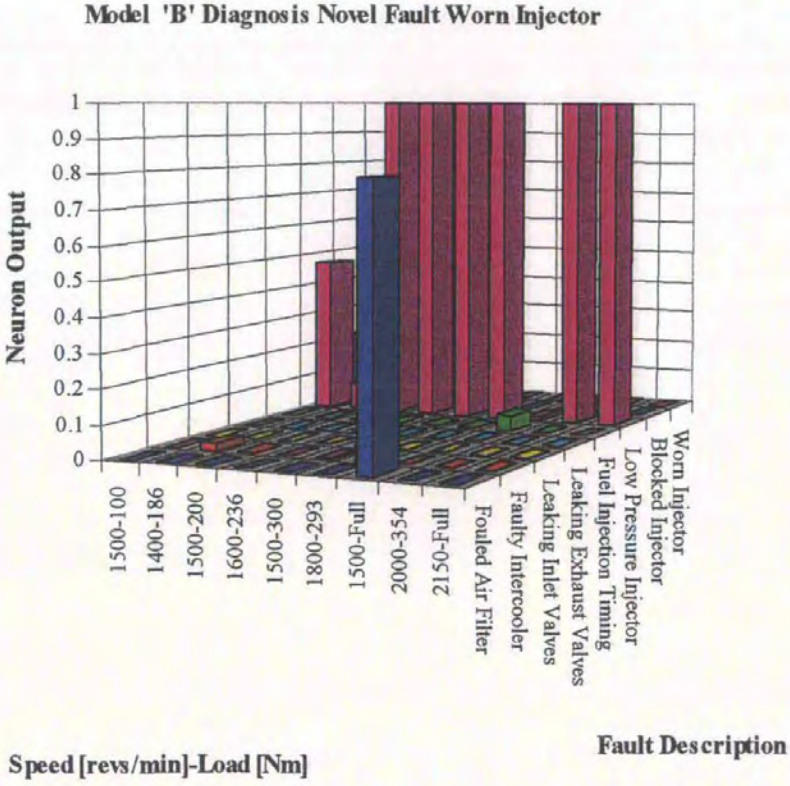

Figure 127 Model 'A' & 'B's Diagnostic Performance On A Novel Fault - Worn Injector

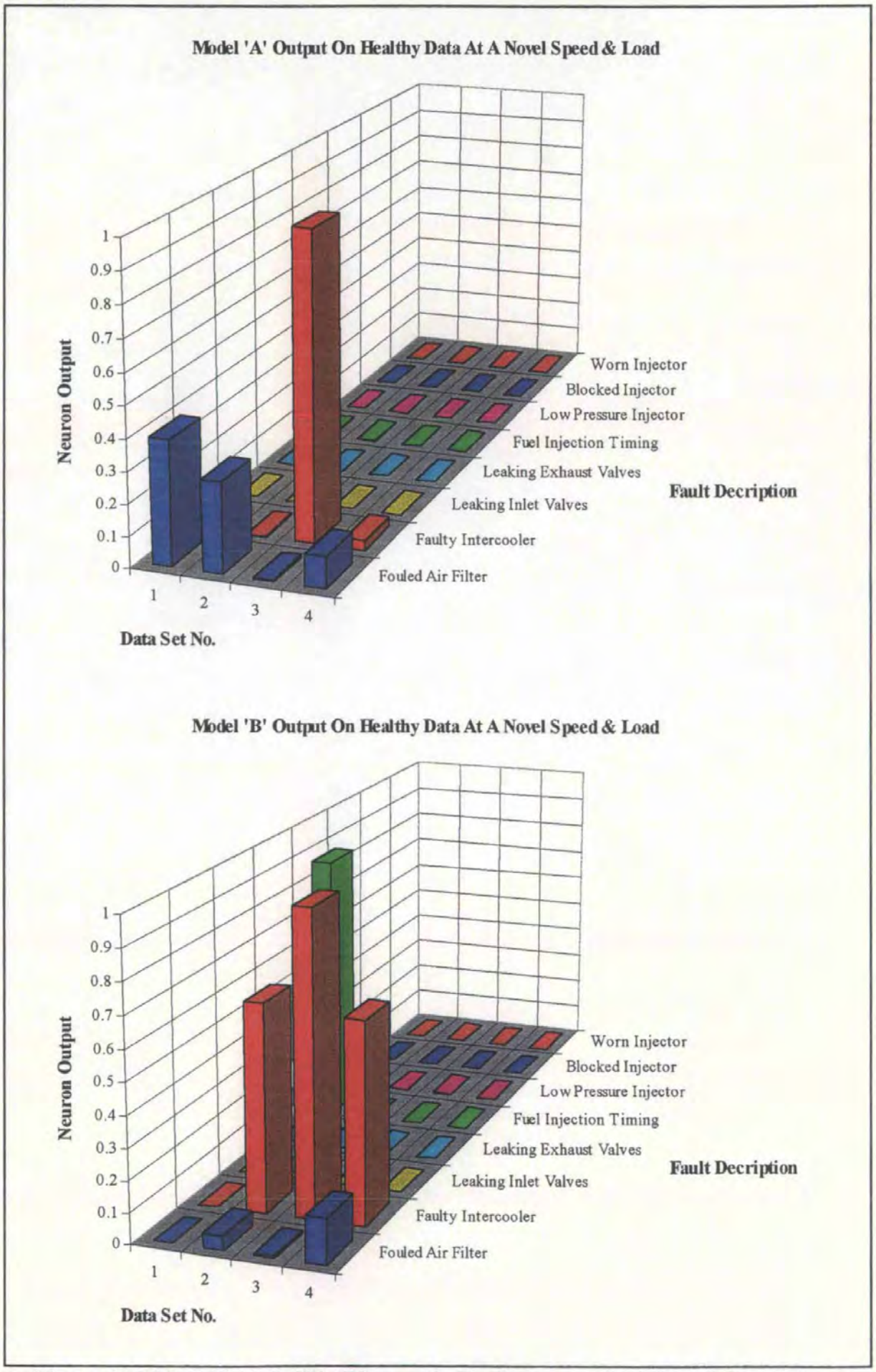

Figure 128 Model 'A' & 'B's Diagnostic Performance At A Novel Speed & Torque On Healthy Data

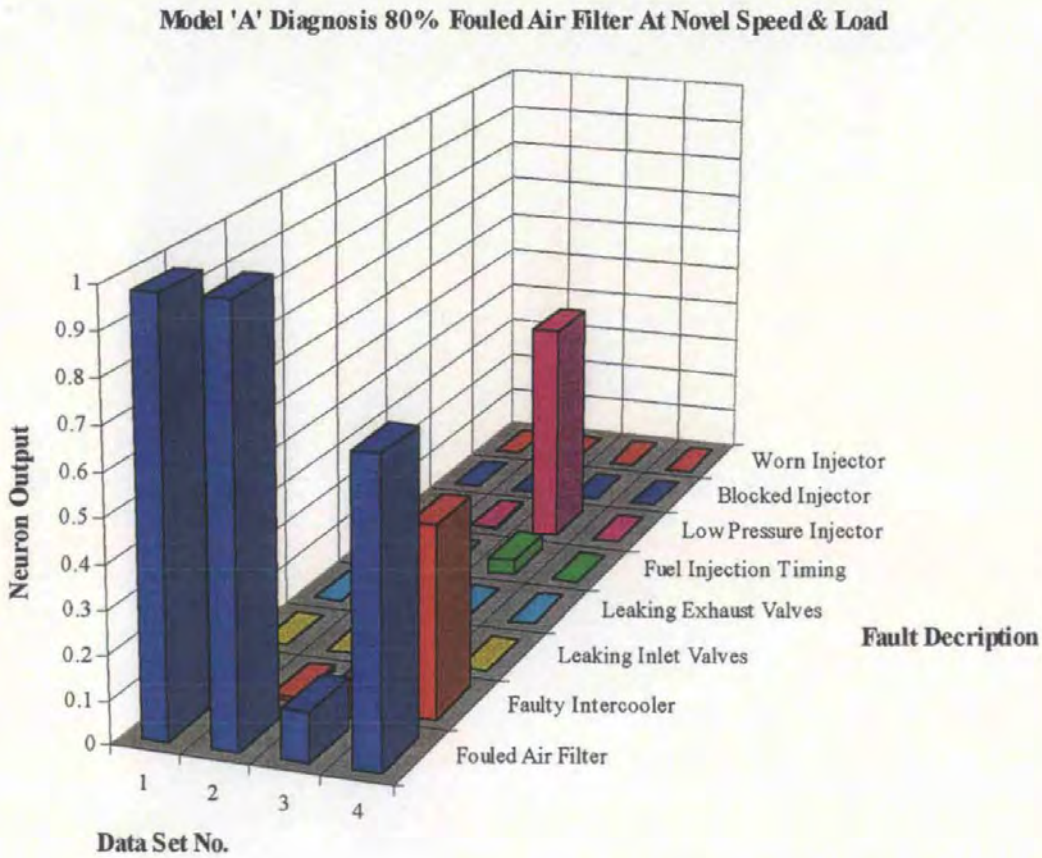

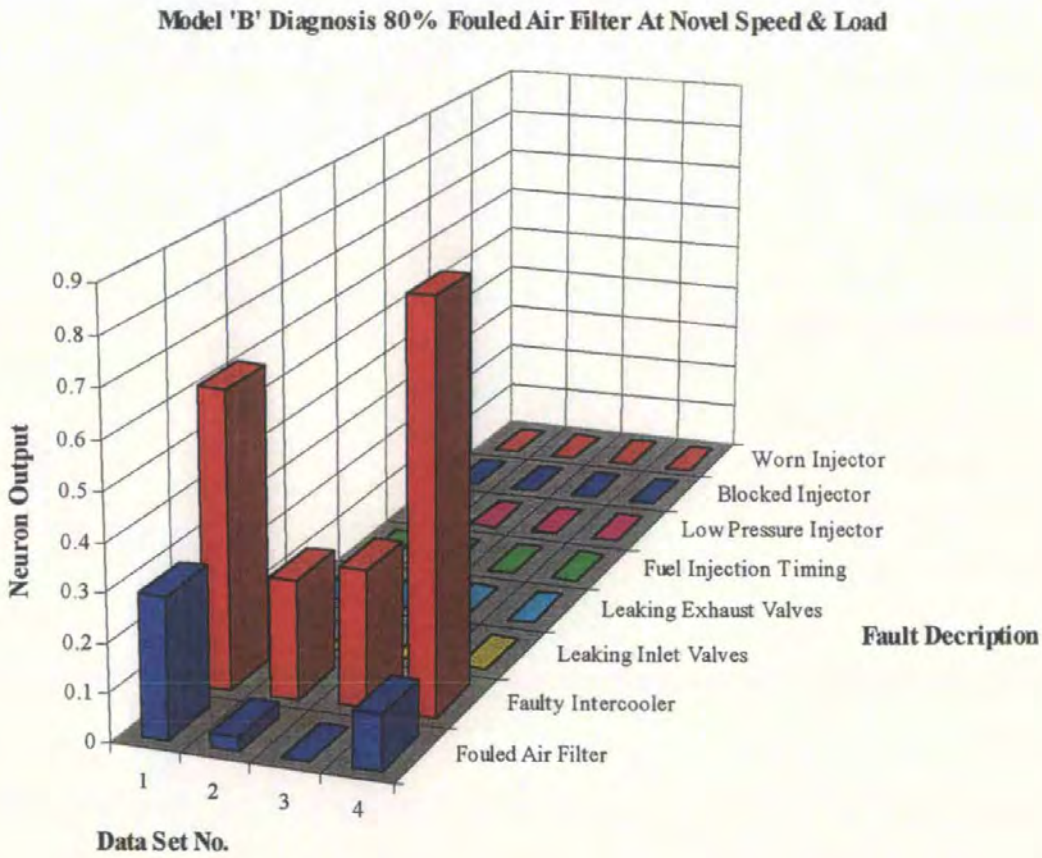

Figure 129 Model 'A' & 'B's Diagnostic Performance At A Novel Speed & Torque On 80% Fouled Air Filter Data

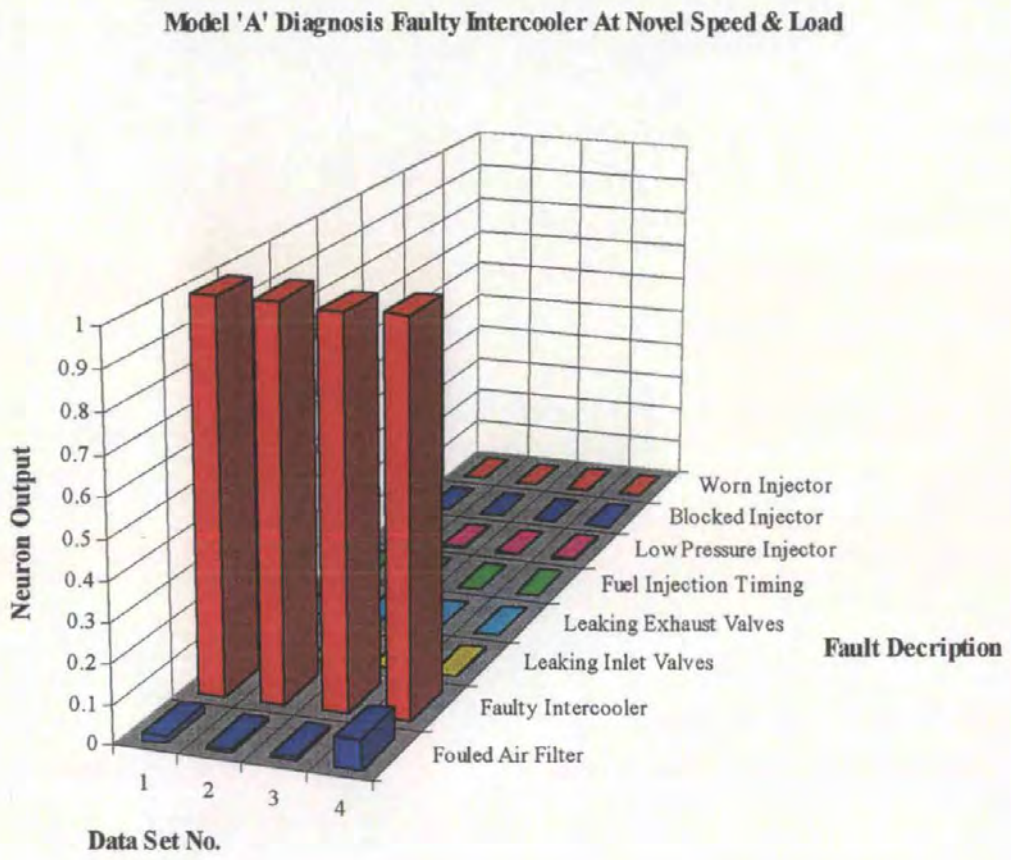

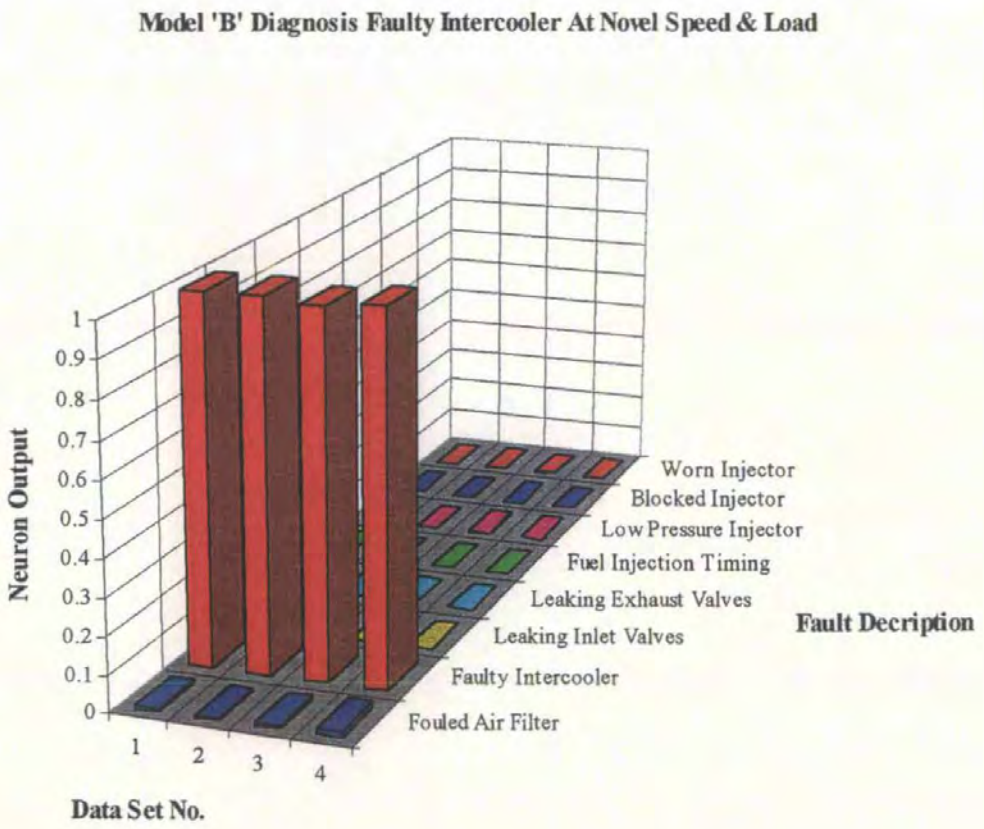

Figure 130 Model 'A' & 'B's Diagnostic Performance At A Novel Speed & Torque On Faulty Intercooler Data

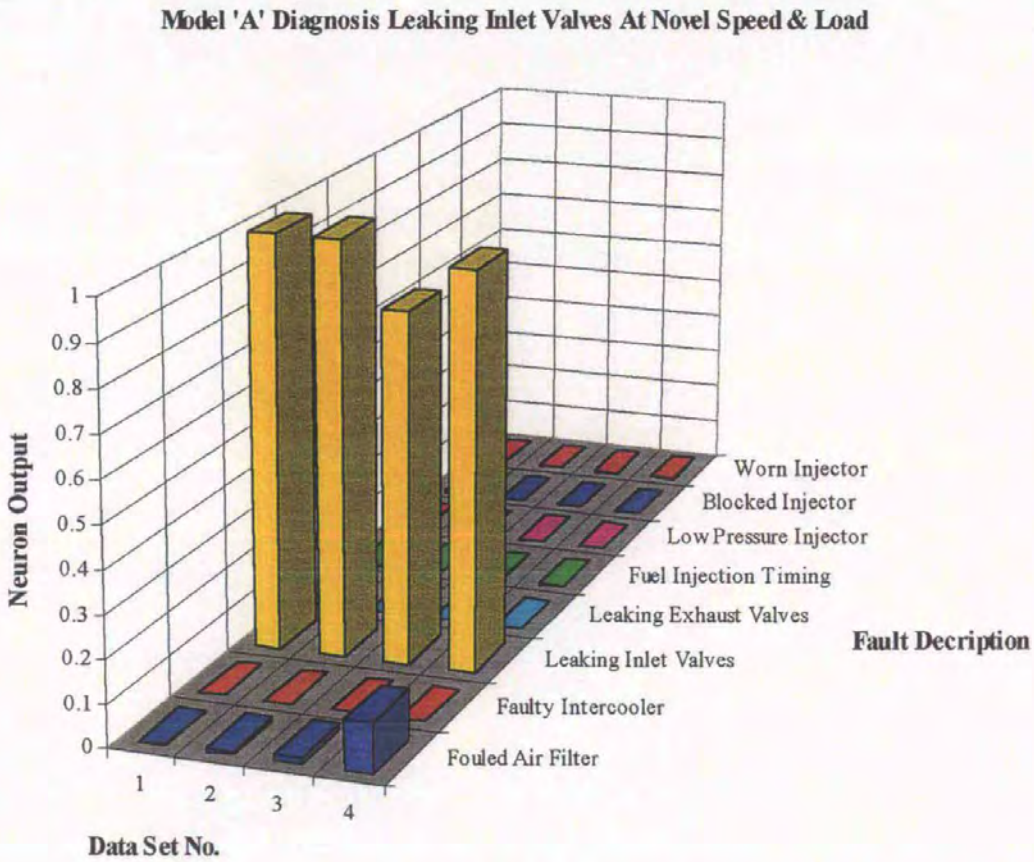

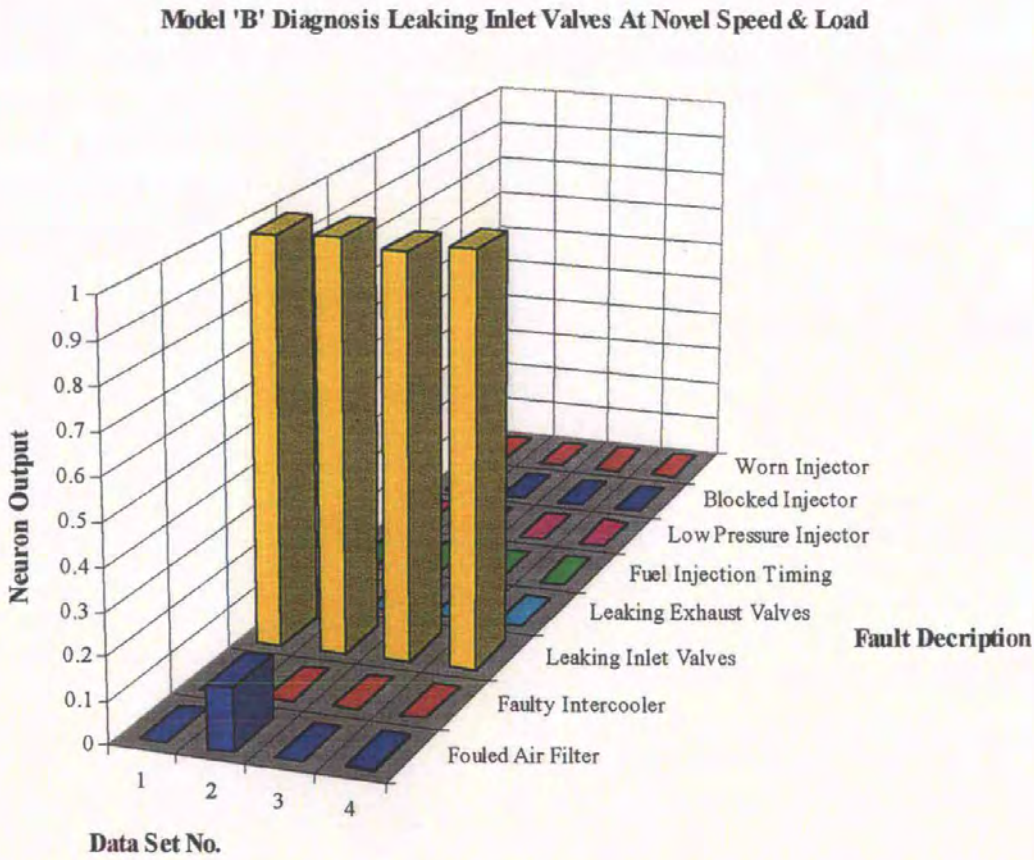

Figure 131 Model 'A' & 'B's Diagnostic Performance At A Novel Speed & Torque On Leaking Inlet Valves Data

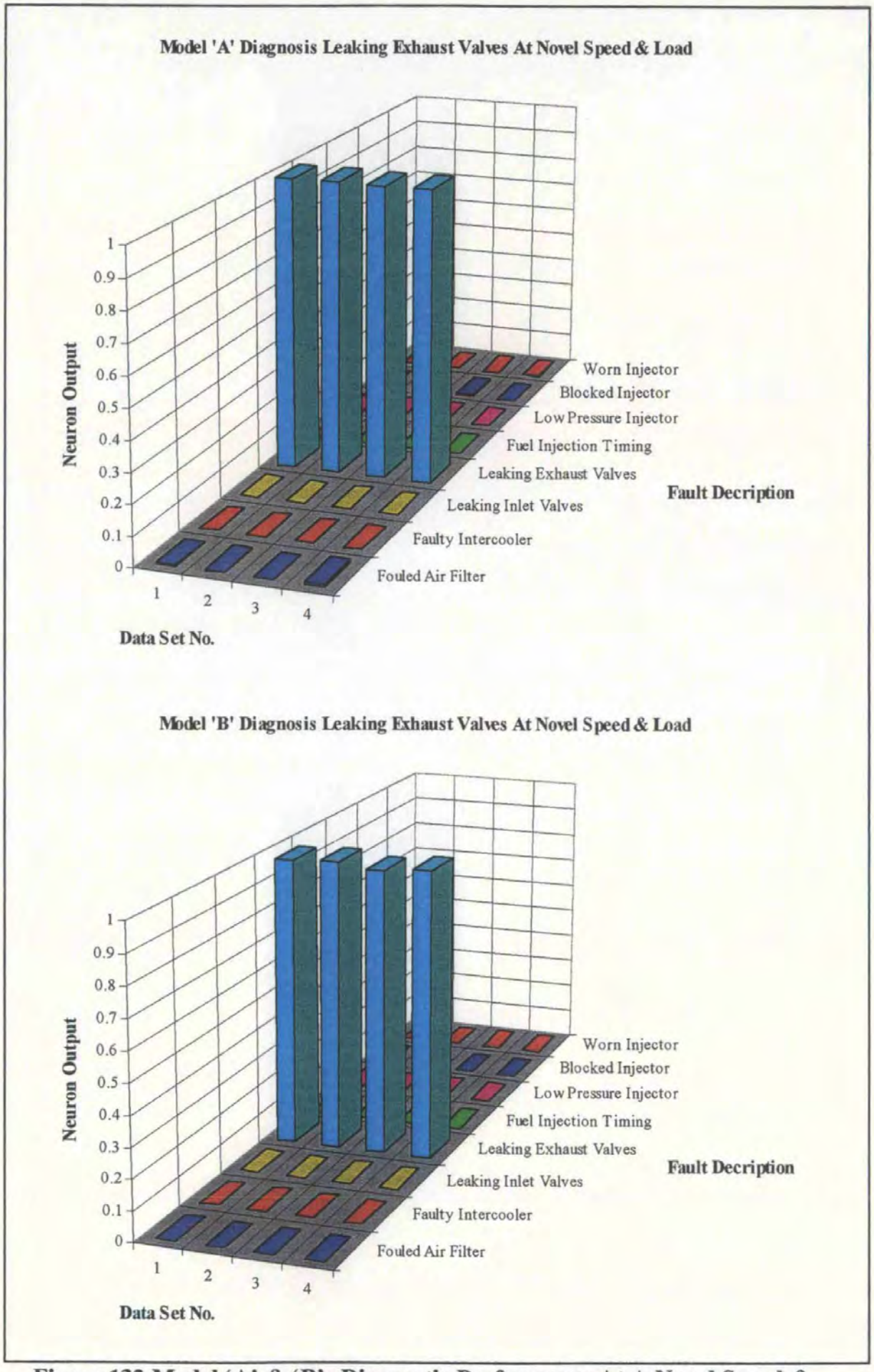

Figure 132 Model 'A' & 'B's Diagnostic Performance At A Novel Speed & Torque On Leaking Exhaust Valves Data

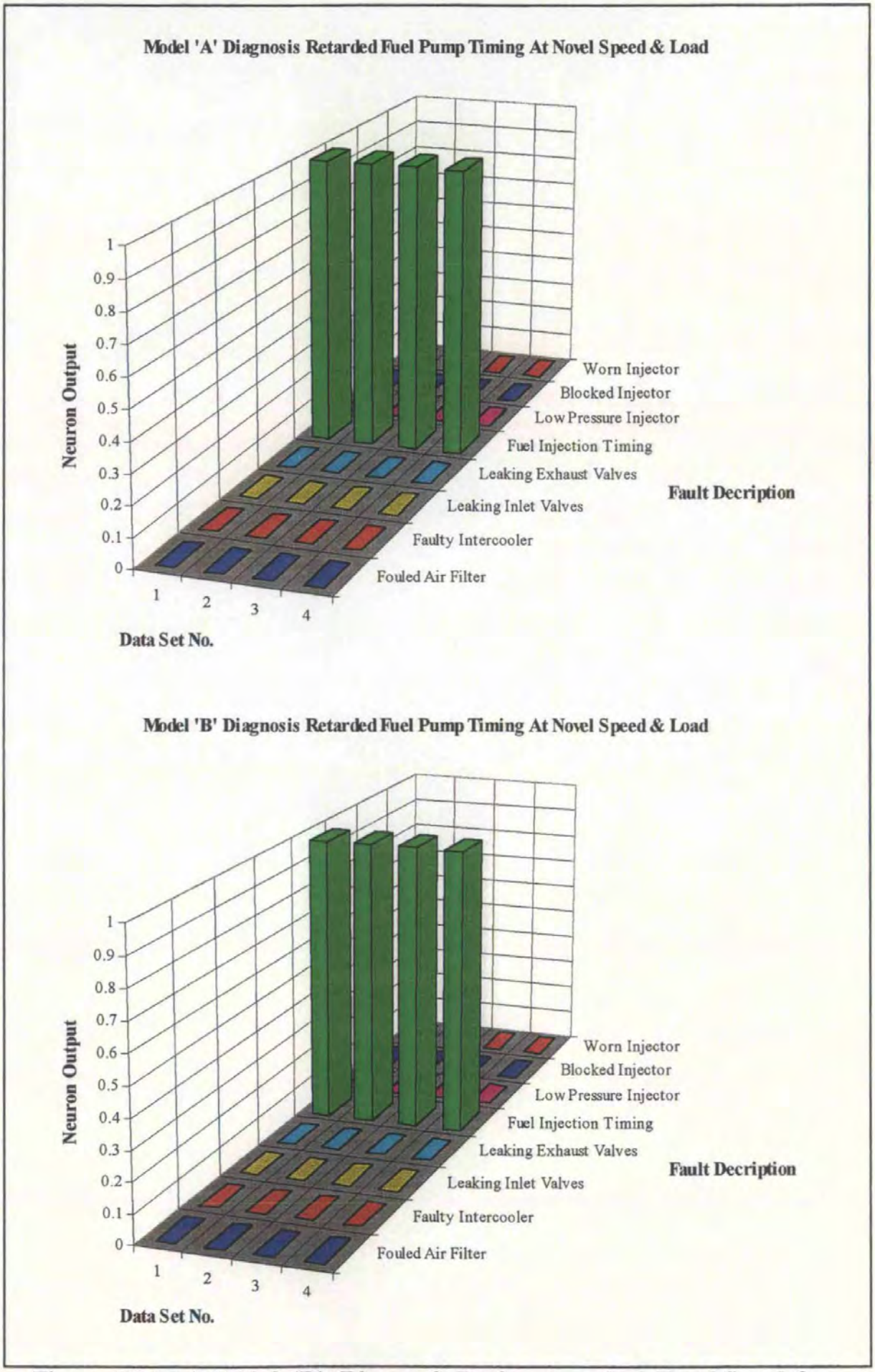

Figure 133 Model 'A' & 'B's Diagnostic Performance At A Novel Speed & Torque On Retarded Fuel Pump Timing Data

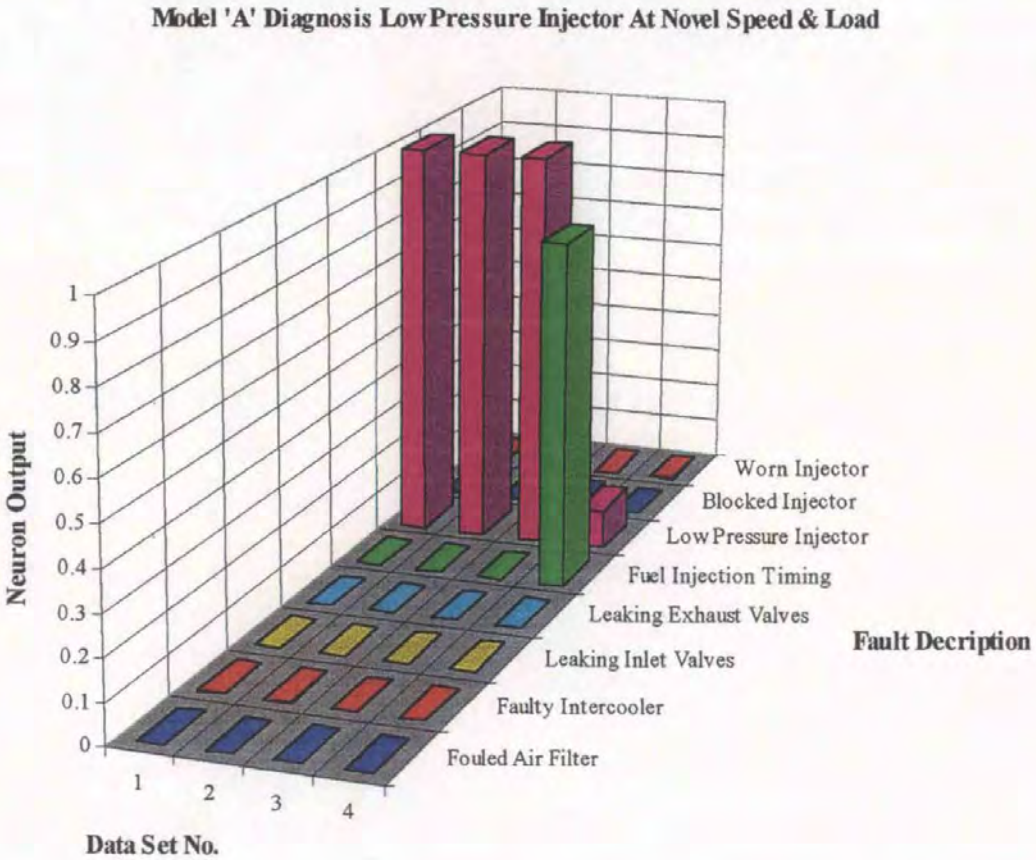

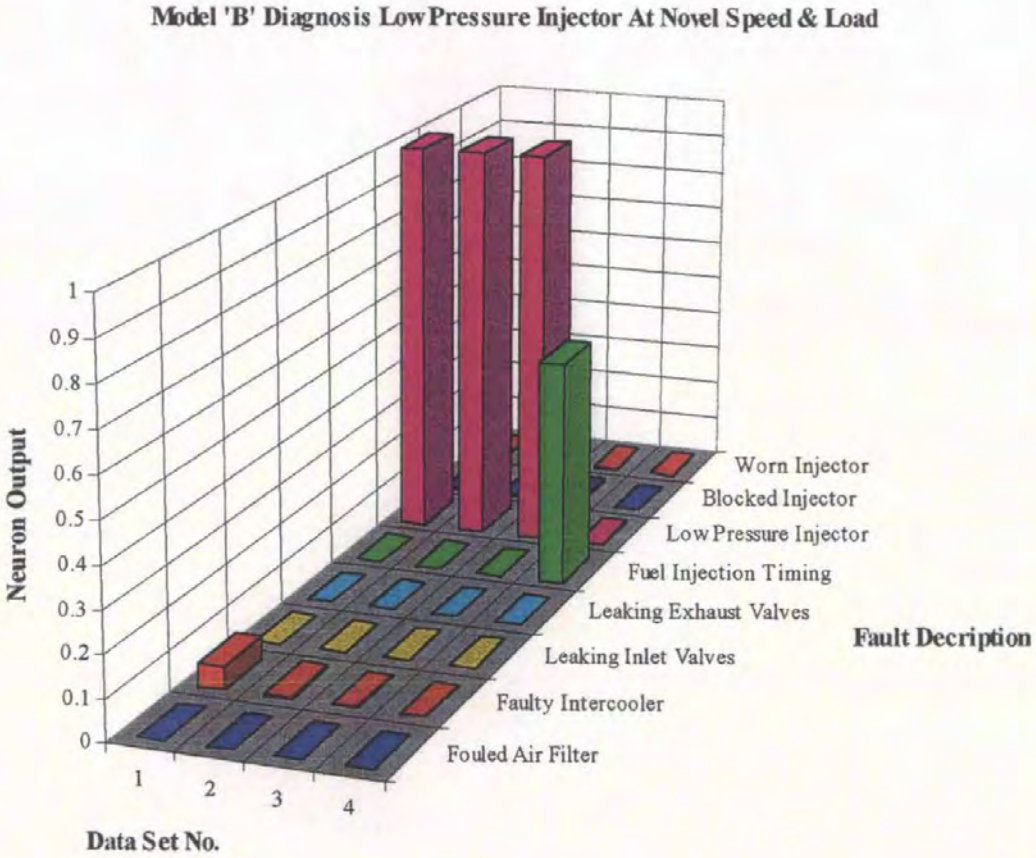

Figure 134 Model 'A' & 'B's Diagnostic Performance At A Novel Speed & Torque On Low Pressure Injector Data

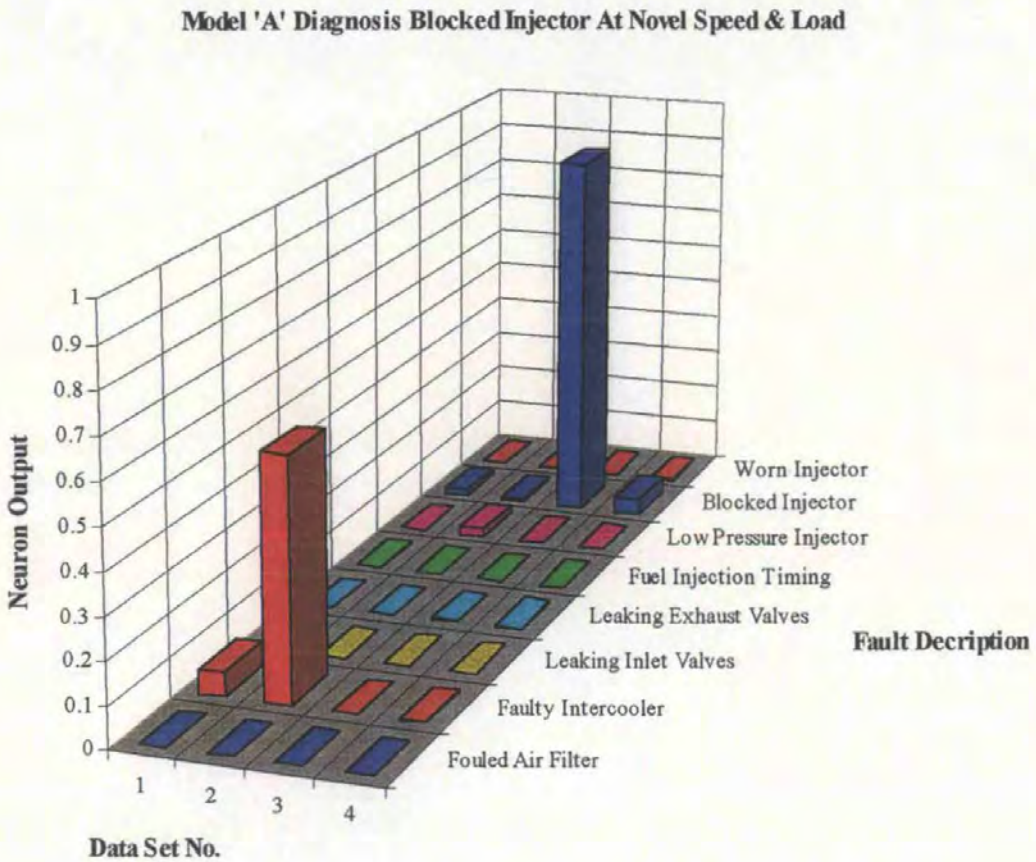

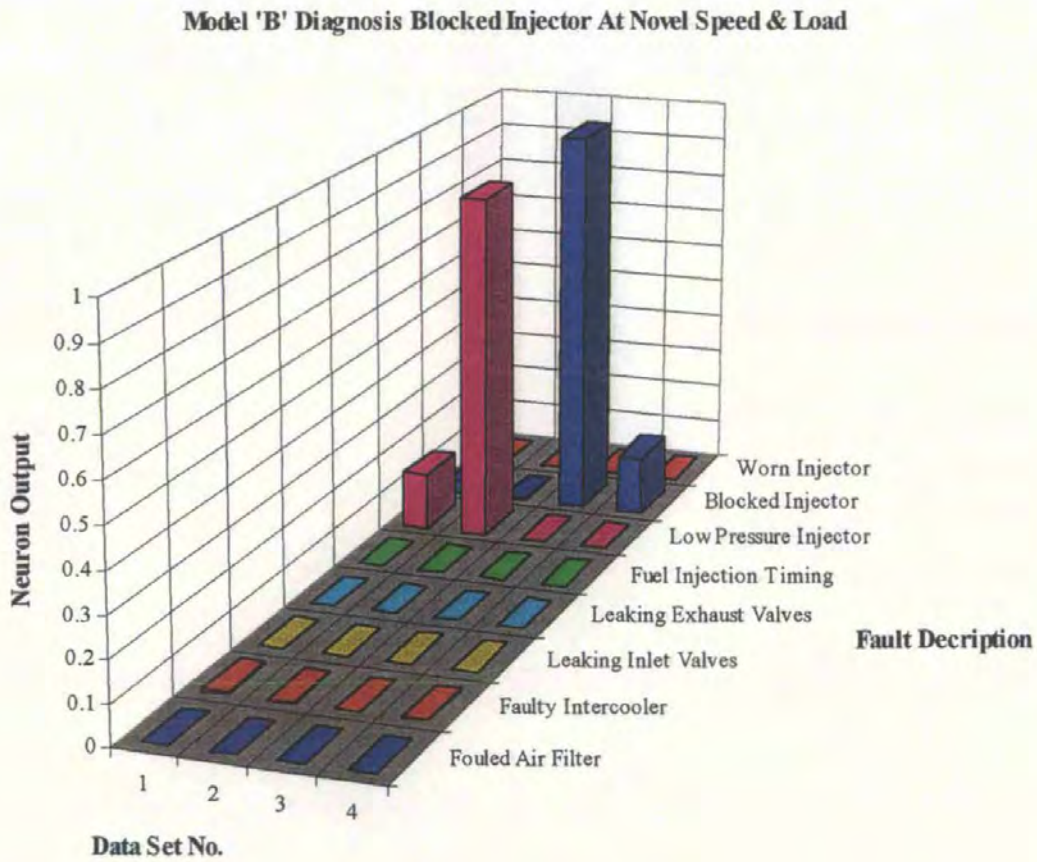

Figure 135 Model 'A' & 'B's Diagnostic Performance At A Novel Speed & Torque On Blocked Injector Data

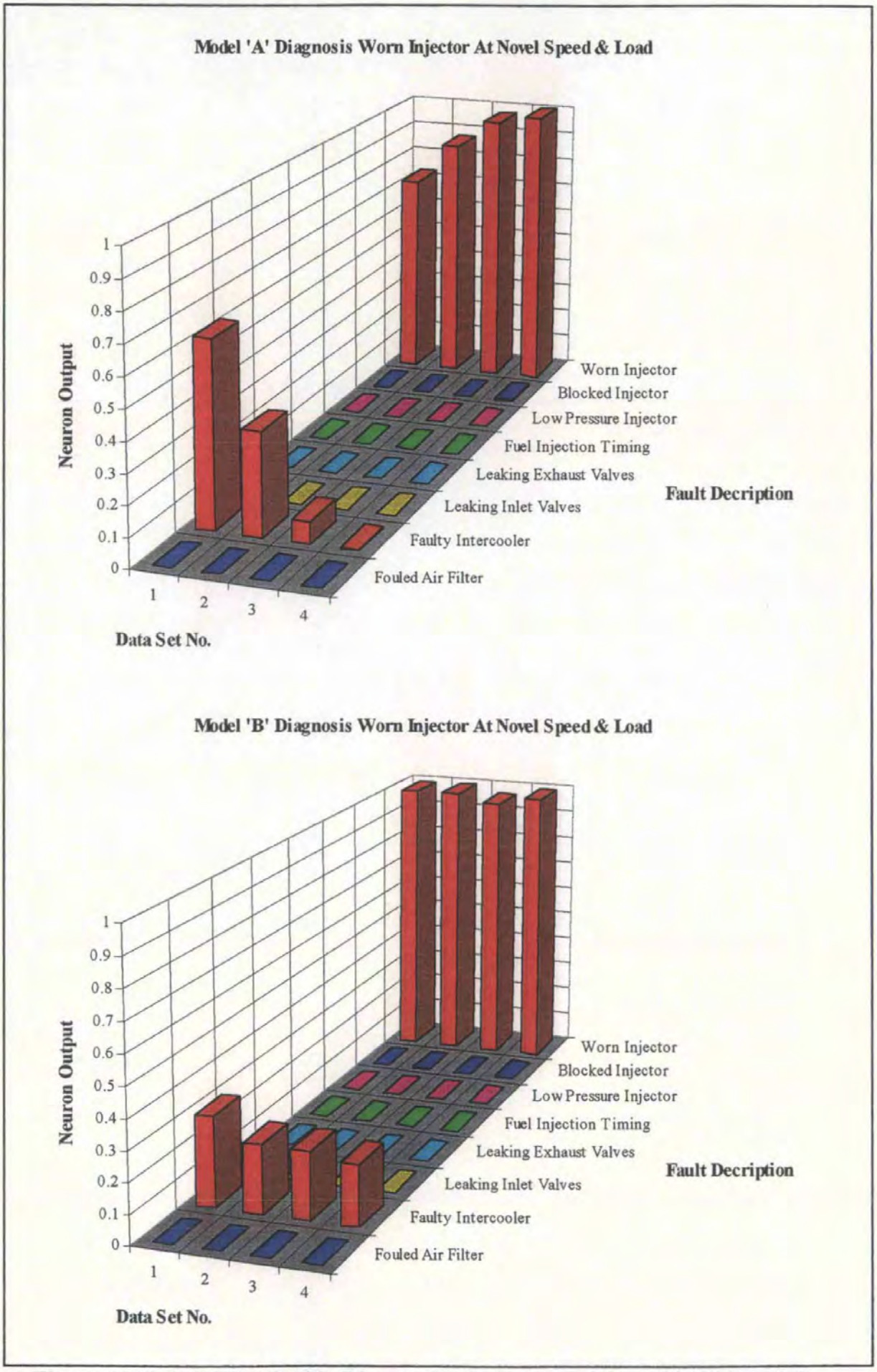

Figure 136 Model 'A' & 'B's Diagnostic Performance At A Novel Speed & Torque On Worn Injector Data

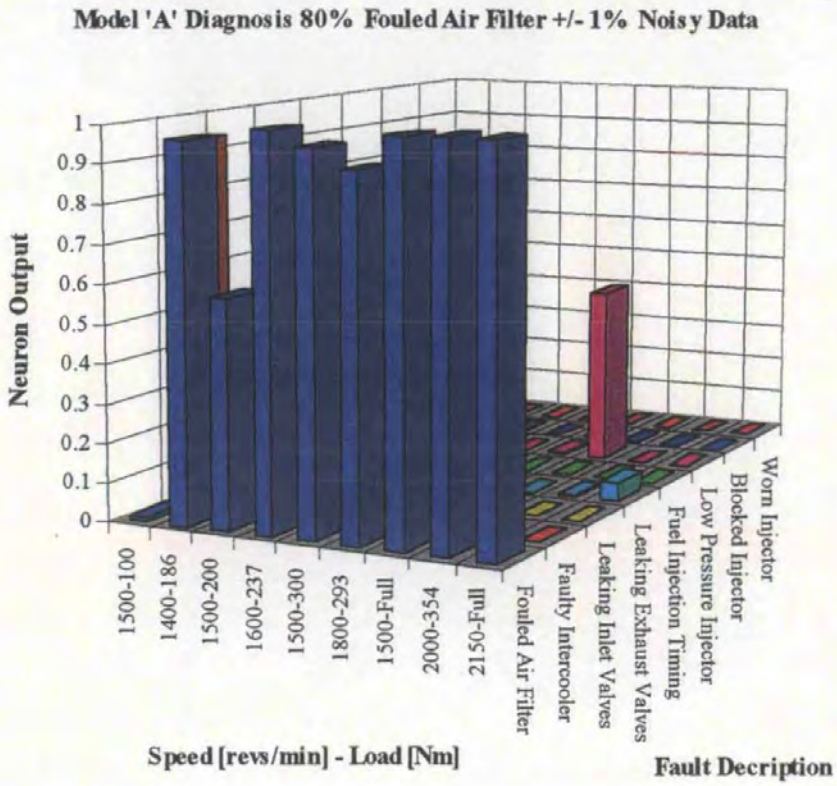

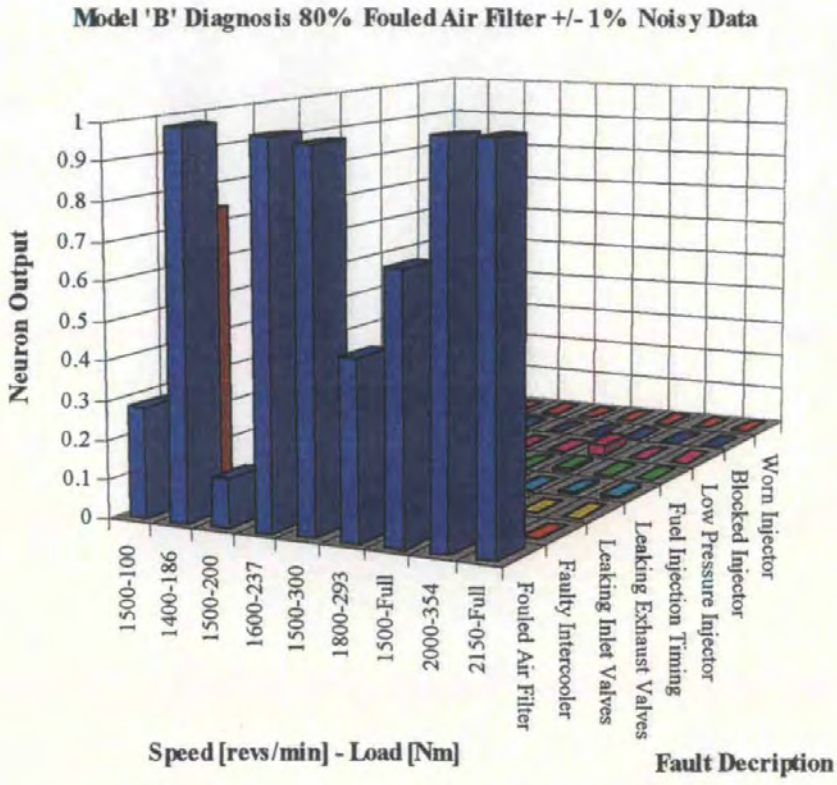

Figure 137 Model 'A' & 'B's Diagnostic Performance on +/- 1% Noisy Fouled Air Filter Data

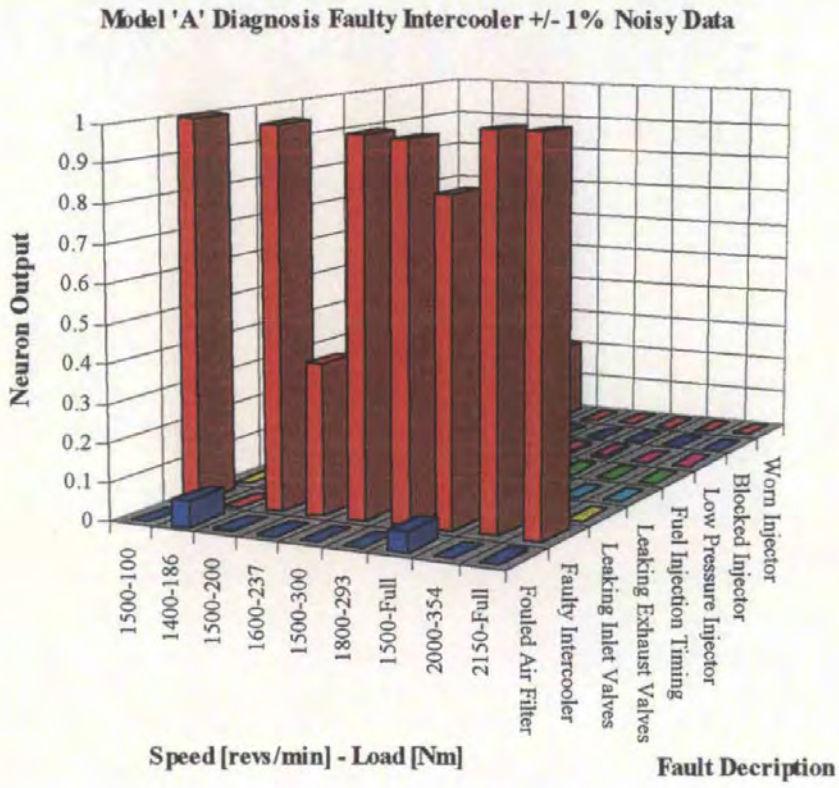

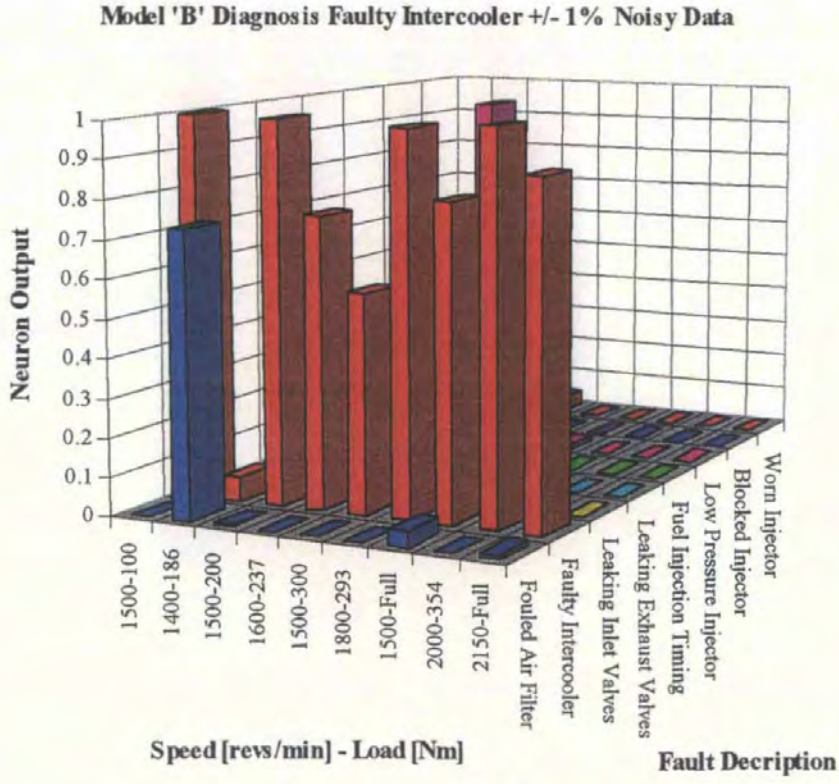

Figure 138 Model 'A' & 'B's Diagnostic Performance on +/- 1% Noisy Faulty Intercooler Data

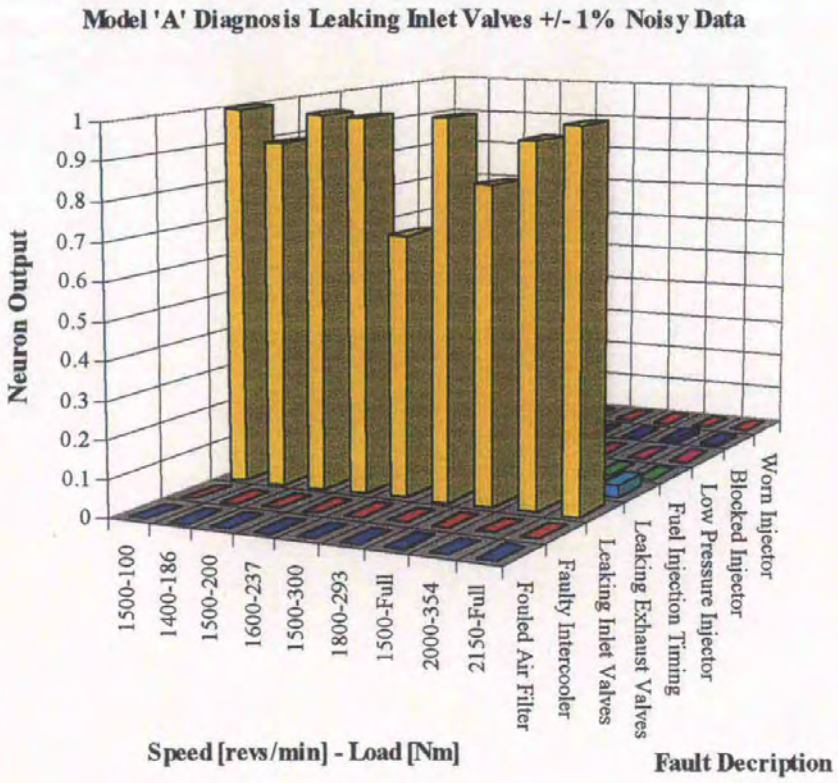

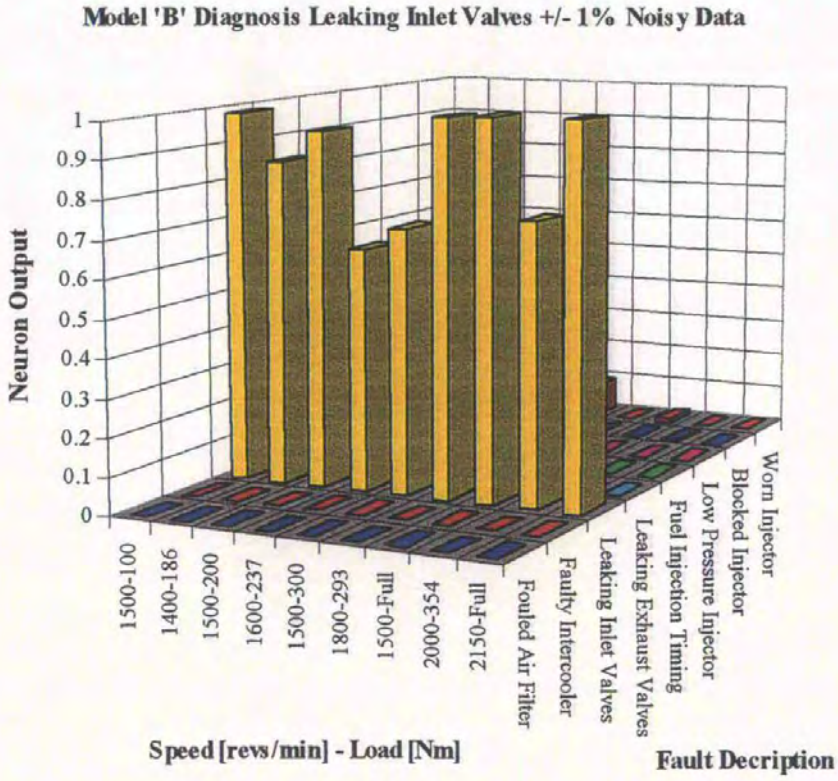

Figure 139 Model 'A' & 'B's Diagnostic Performance on +/- 1% Noisy Leaking Inlet Valves Data

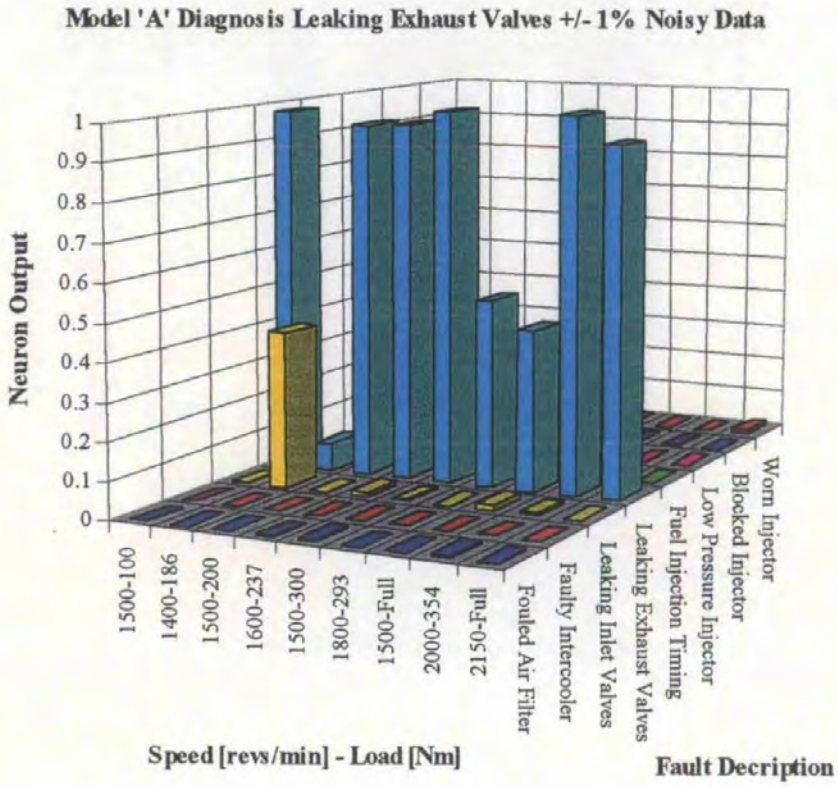

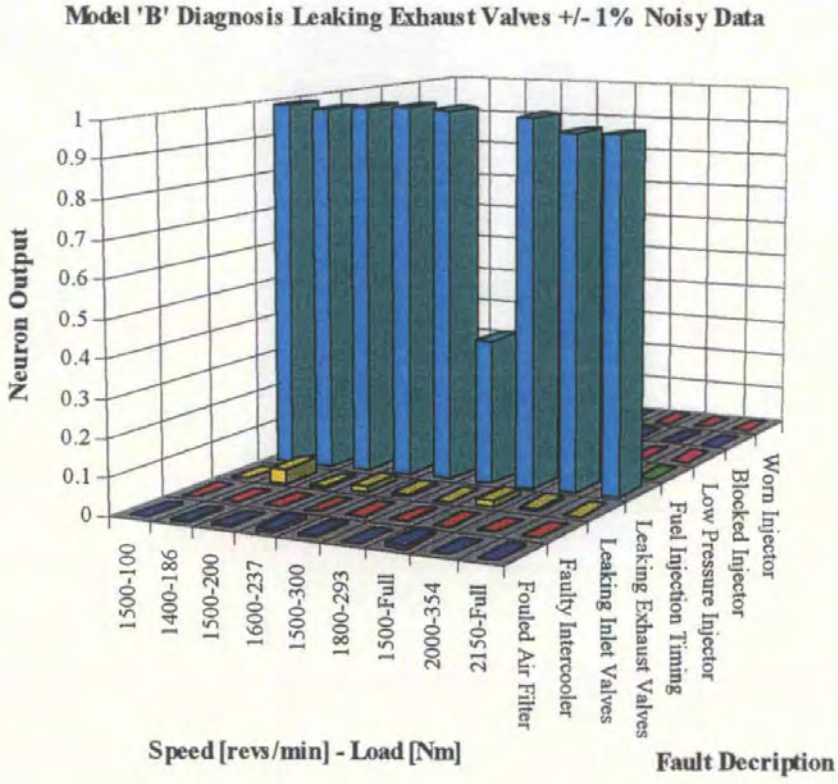

Figure 140 Model 'A' & 'B's Diagnostic Performance on +/- 1% Noisy Leaking Exhaust Valves Data

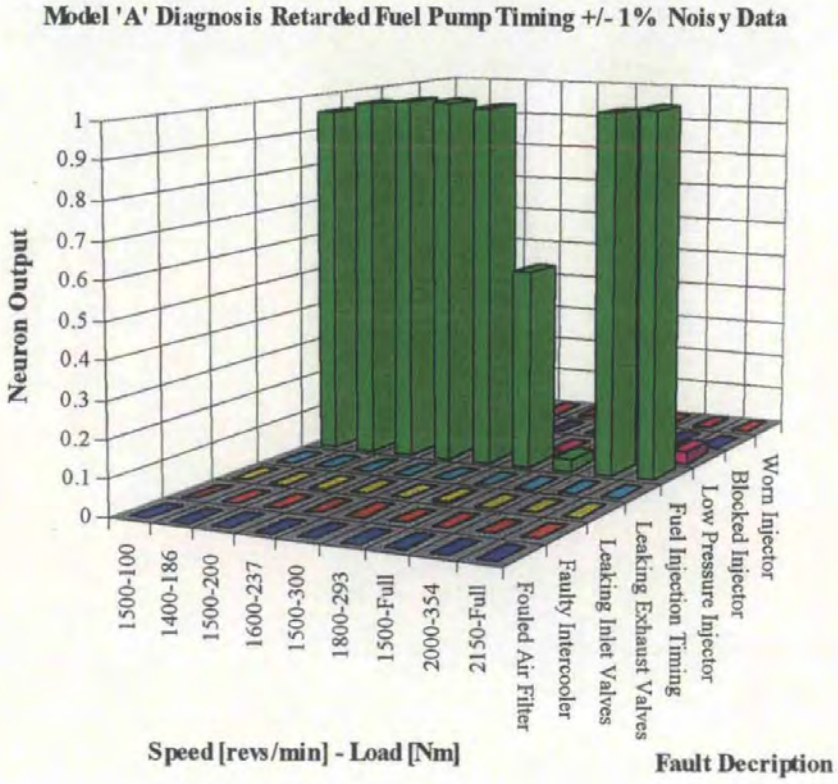

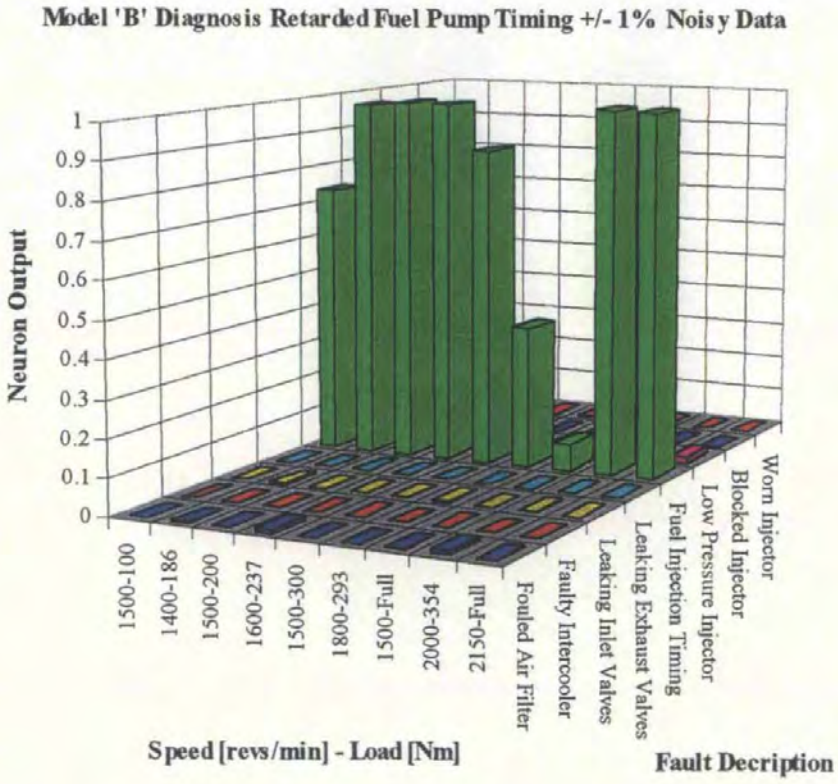

Figure 141 Model 'A' & 'B's Diagnostic Performance on +/- 1% Noisy Retarded Fuel Pump Timing Data

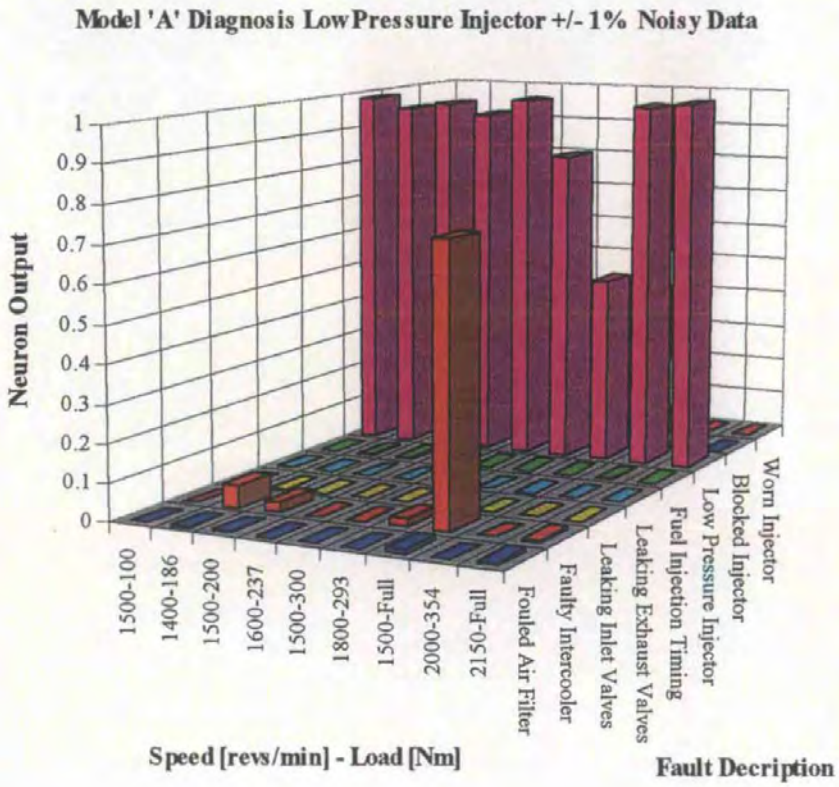

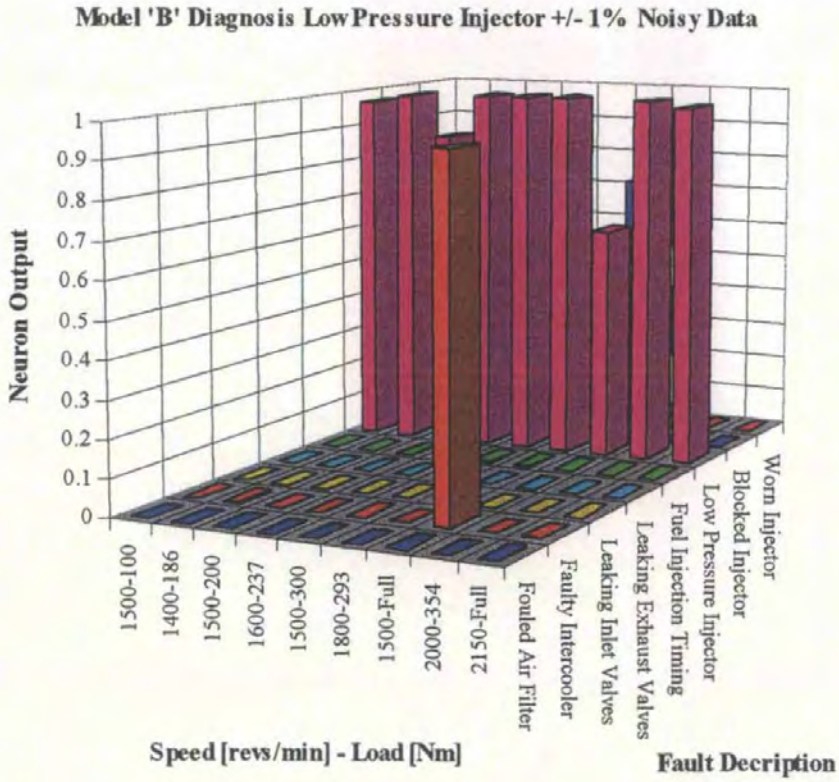

Figure 142 Model 'A' & 'B's Diagnostic Performance on +/- 1% Noisy Low Pressure Injector Data

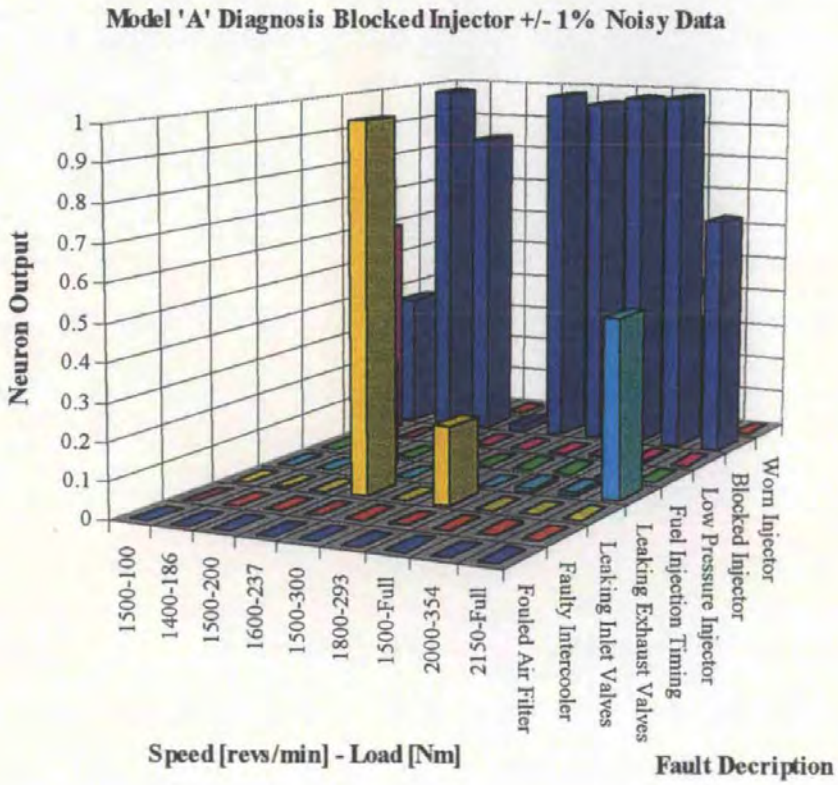

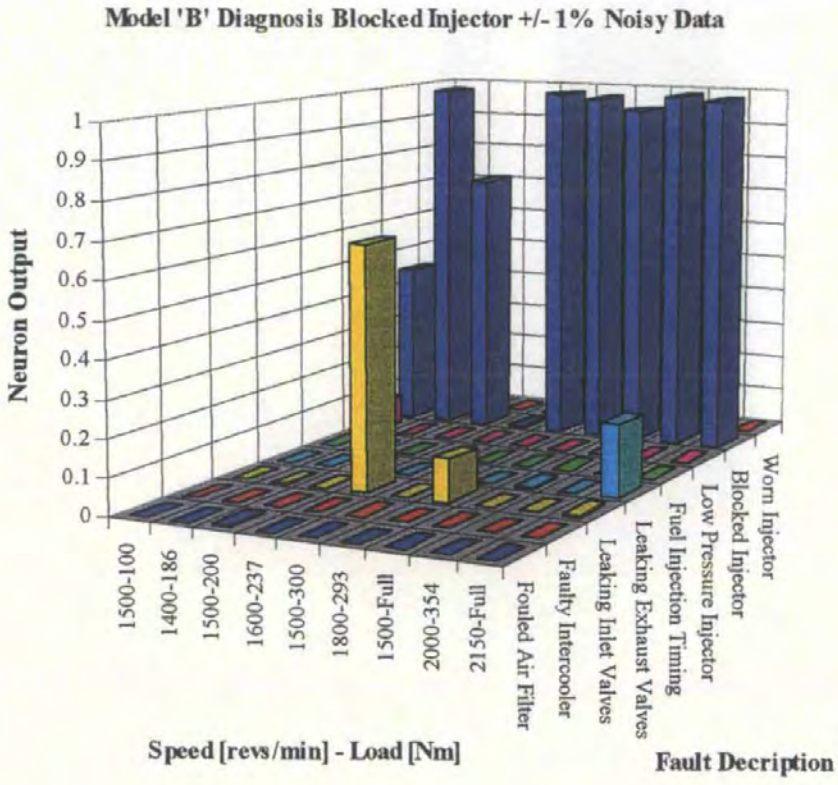

Figure 143 Model 'A' & 'B's Diagnostic Performance on +/- 1% Noisy Blocked Injector Data

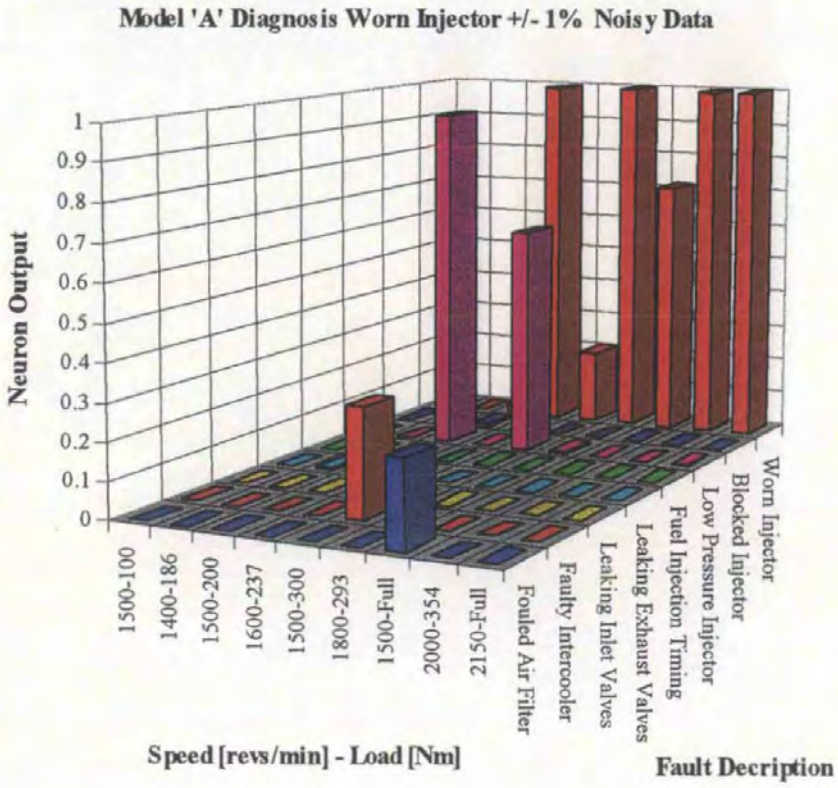

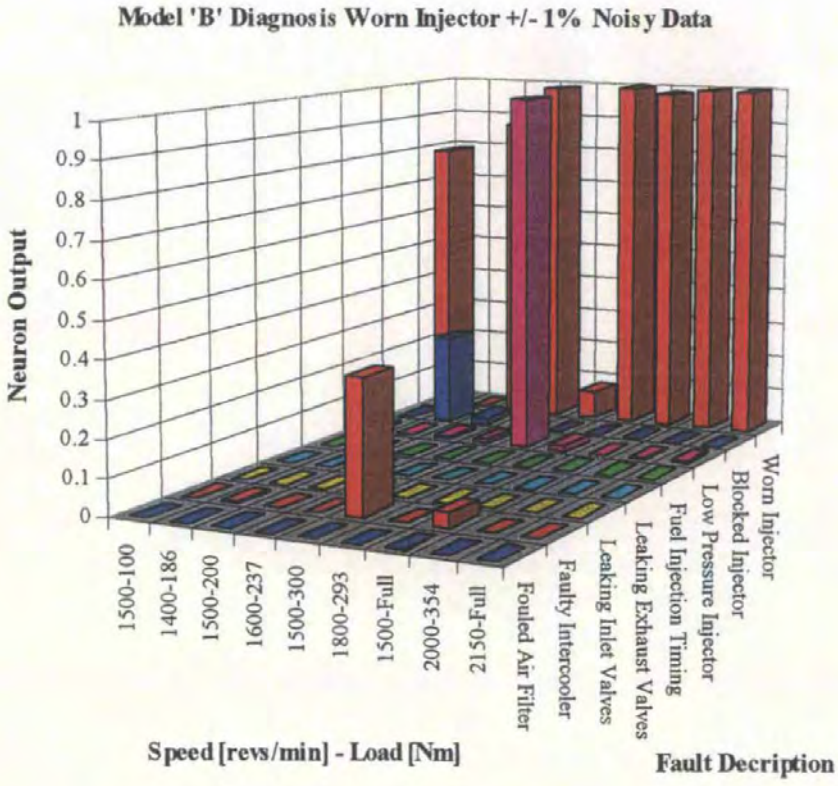

Figure 144 Model 'A' & 'B's Diagnostic Performance on +/- 1% Noisy Worn Injector Data

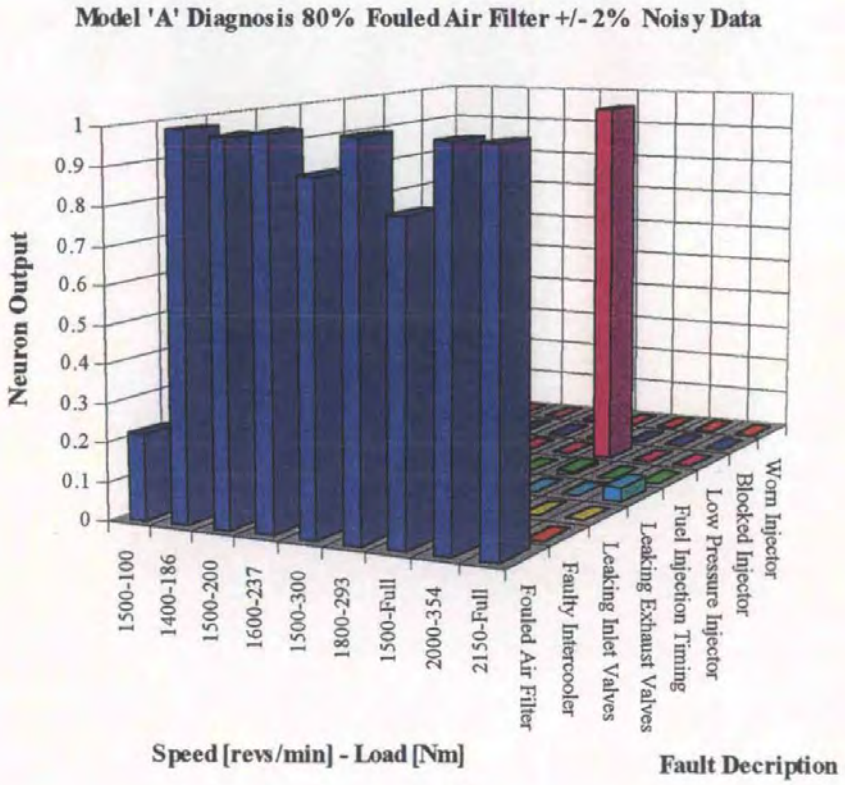

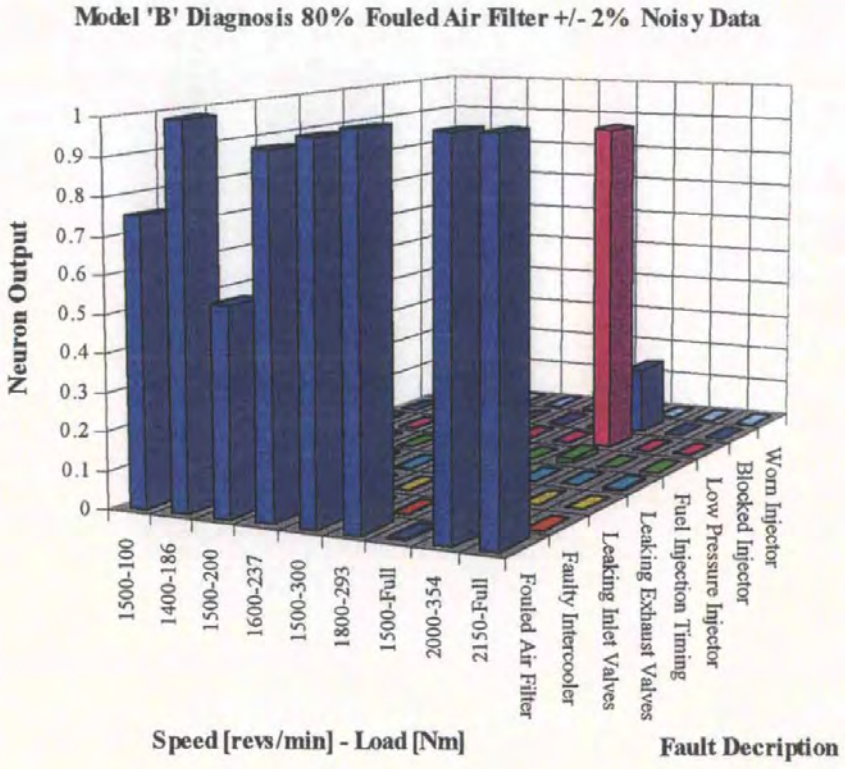

Figure 145 Model 'A' & 'B's Diagnostic Performance on +/- 2% Noisy Fouled Air Filter Data

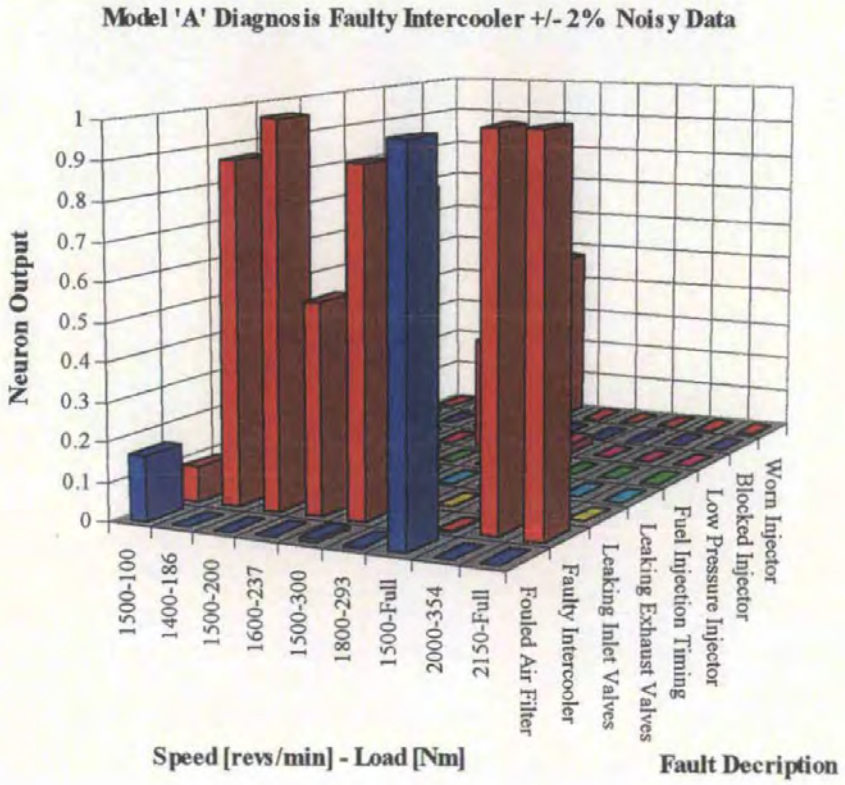

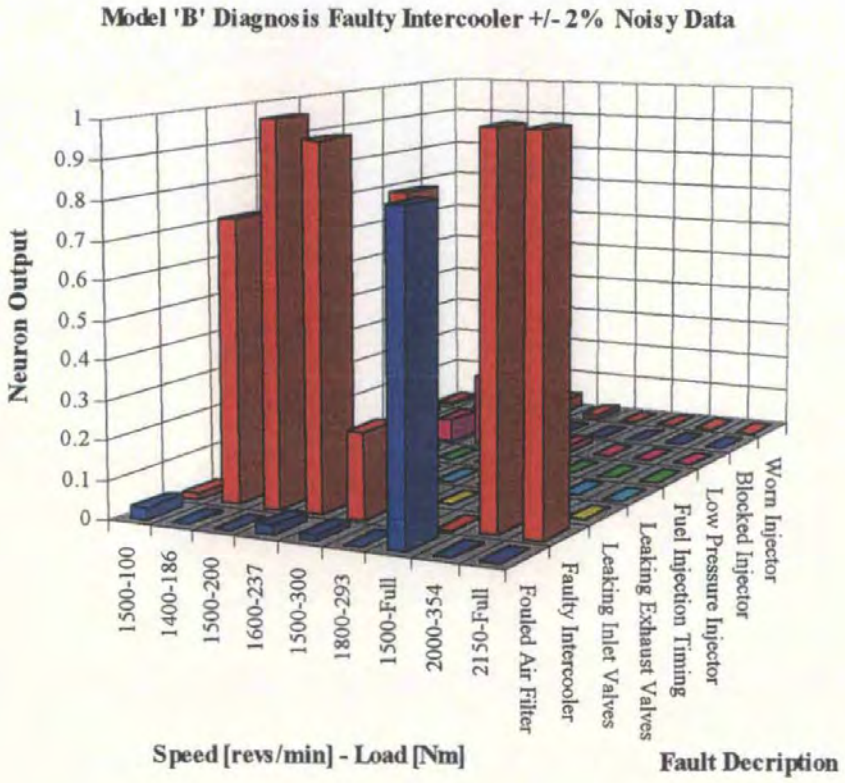

Figure 146 Model 'A' & 'B's Diagnostic Performance on +/- 2% Noisy Faulty Intercooler Data

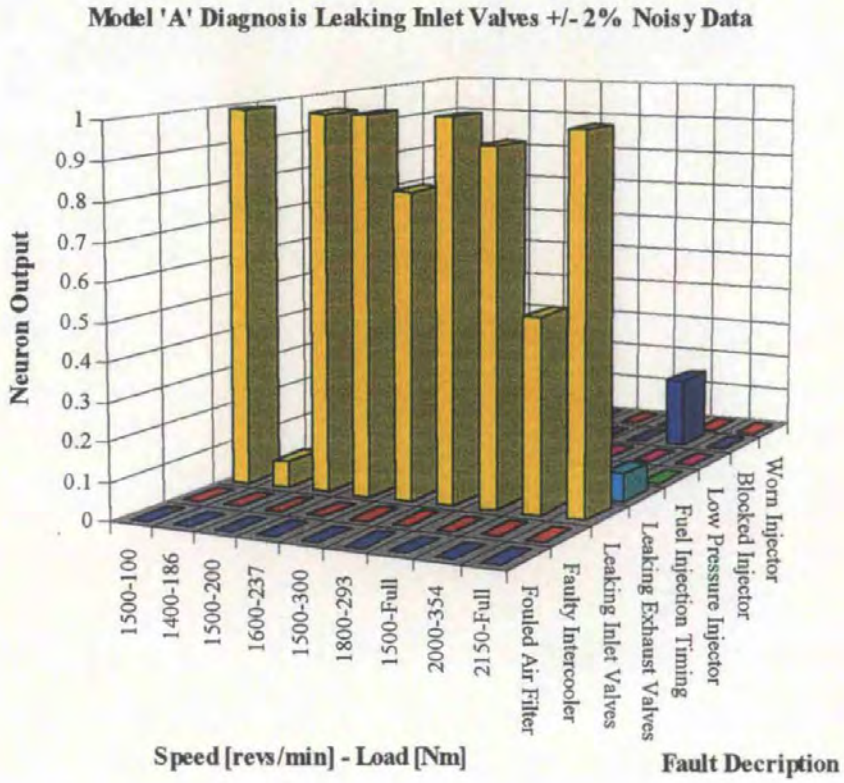

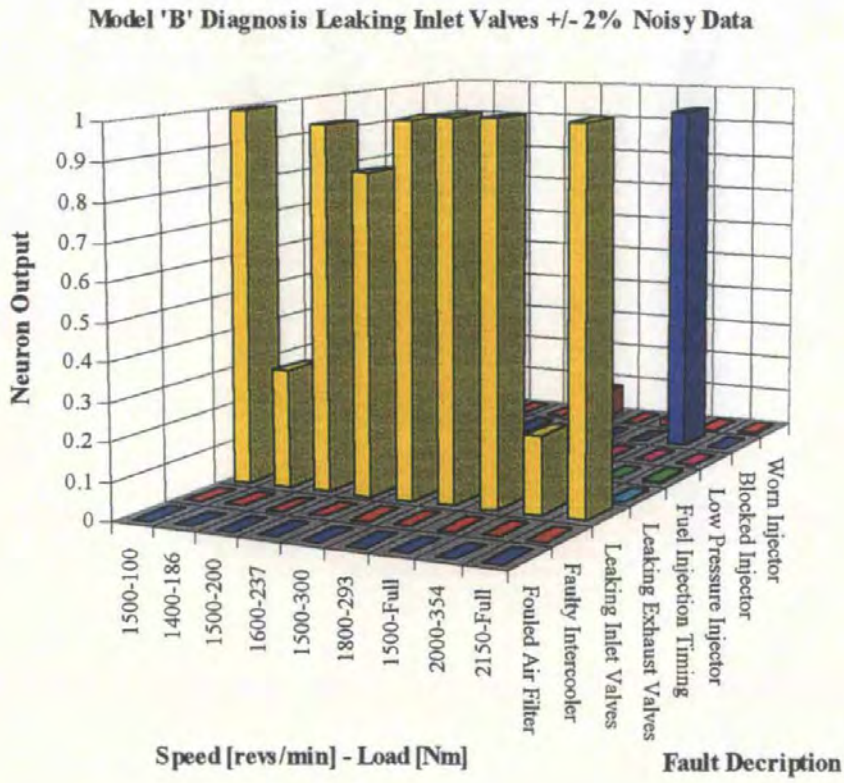

Figure 147 Model 'A' & 'B's Diagnostic Performance on +/- 2% Noisy Leaking Inlet Valves Data

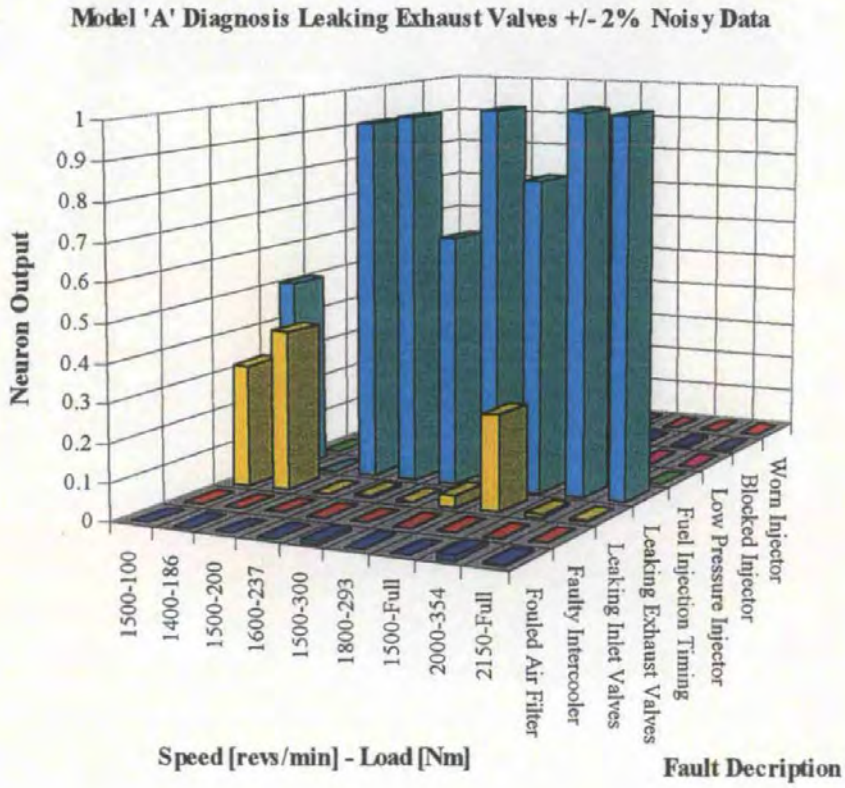

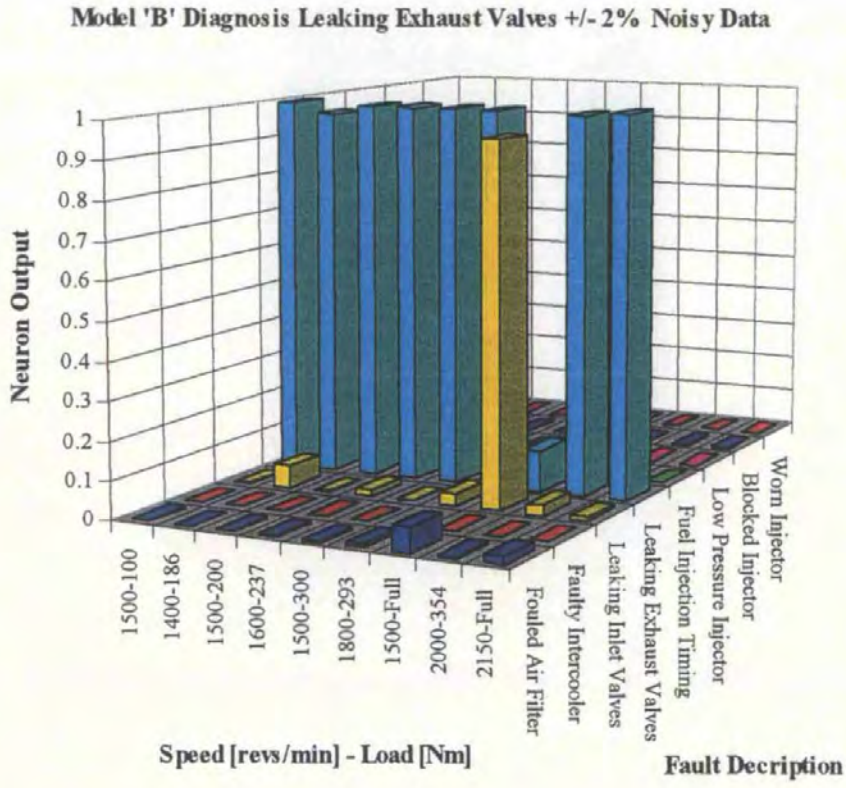

Figure 148 Model 'A' & 'B's Diagnostic Performance on +/- 2% Noisy Leaking Exhaust Valves Data

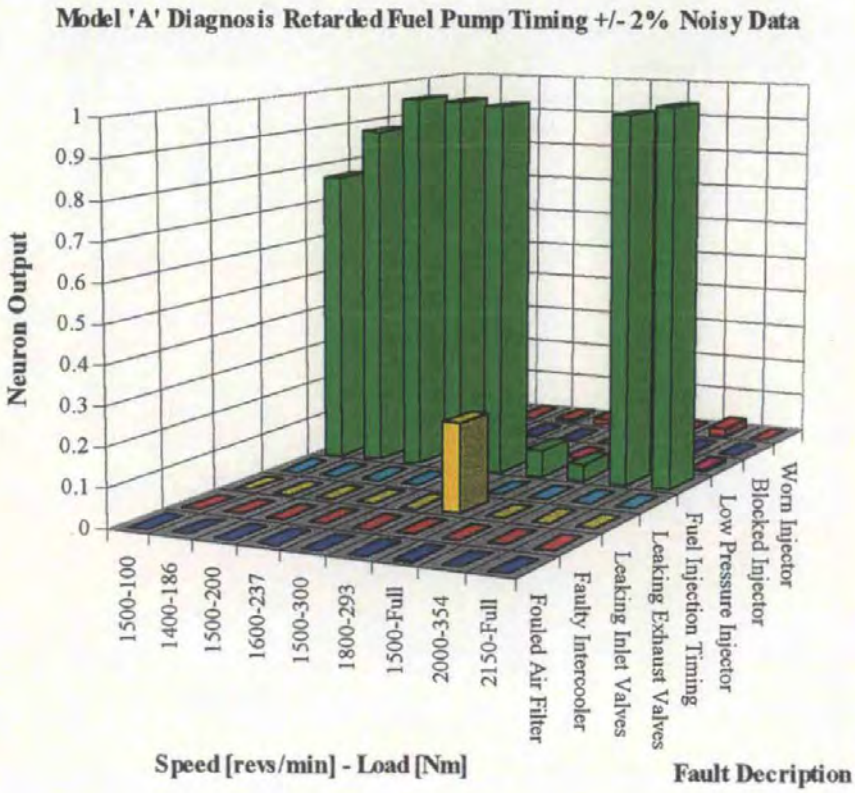

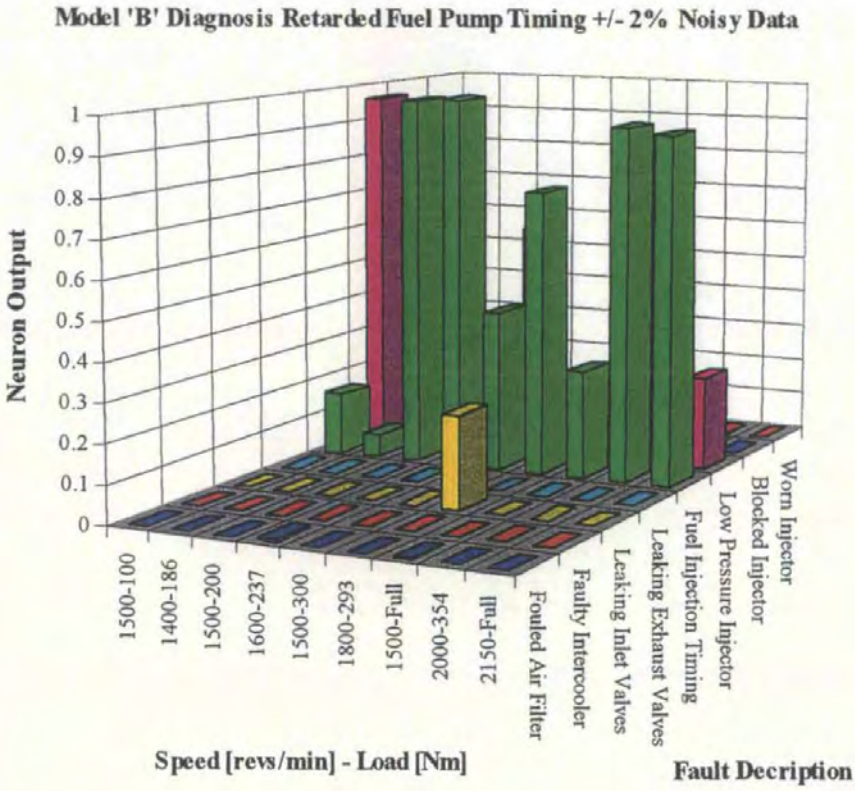

Figure 149 Model 'A' & 'B's Diagnostic Performance on +/- 2% Noisy Retarded Fuel Pump Timing Data

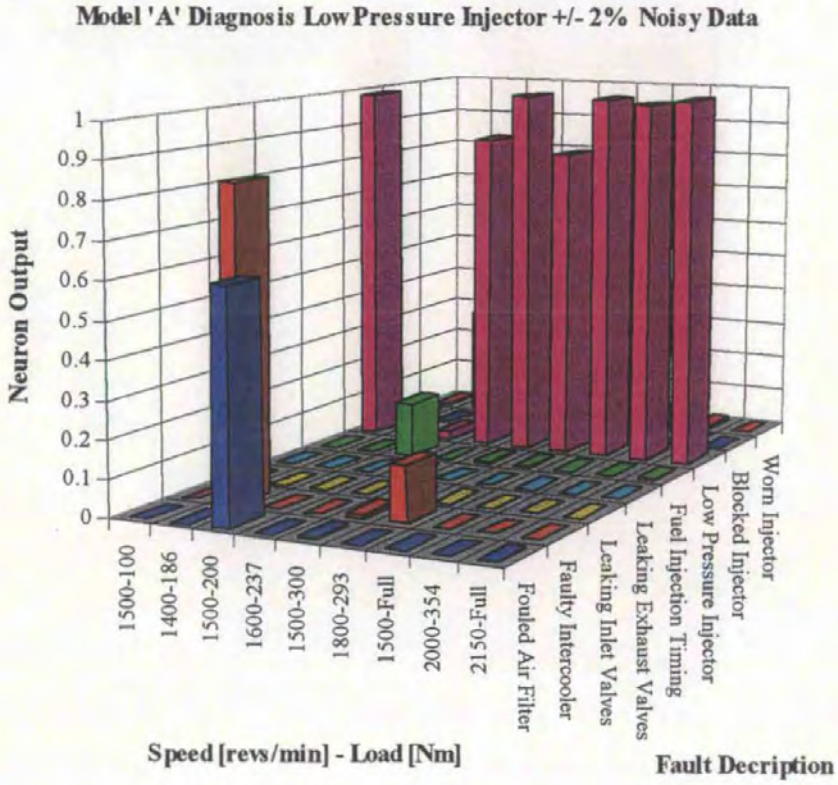

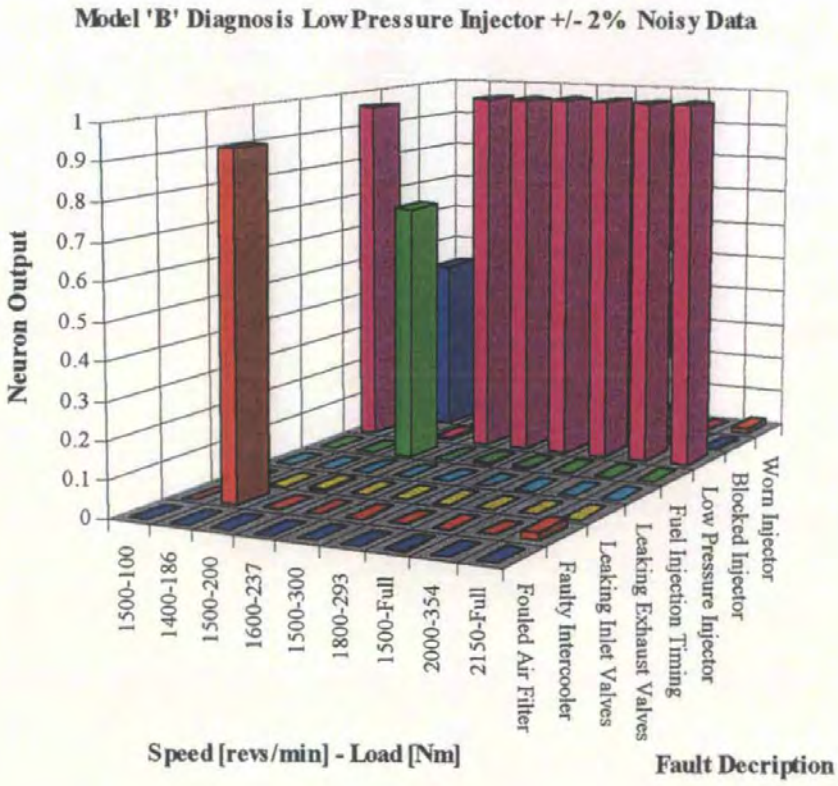

Figure 150 Model 'A' & 'B's Diagnostic Performance on +/- 2% Noisy Low Pressure Injector Data

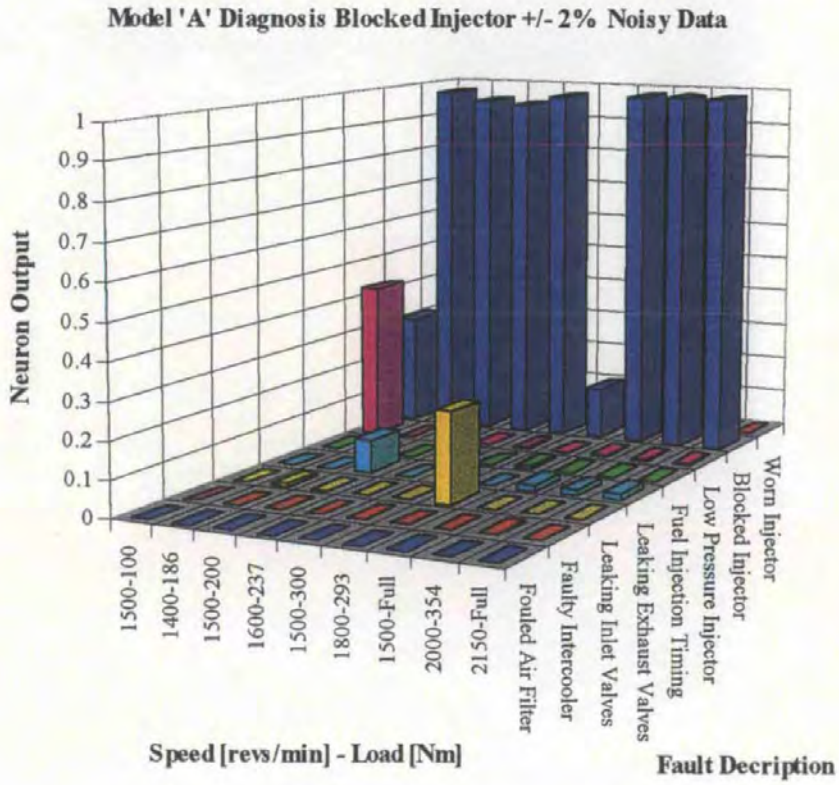

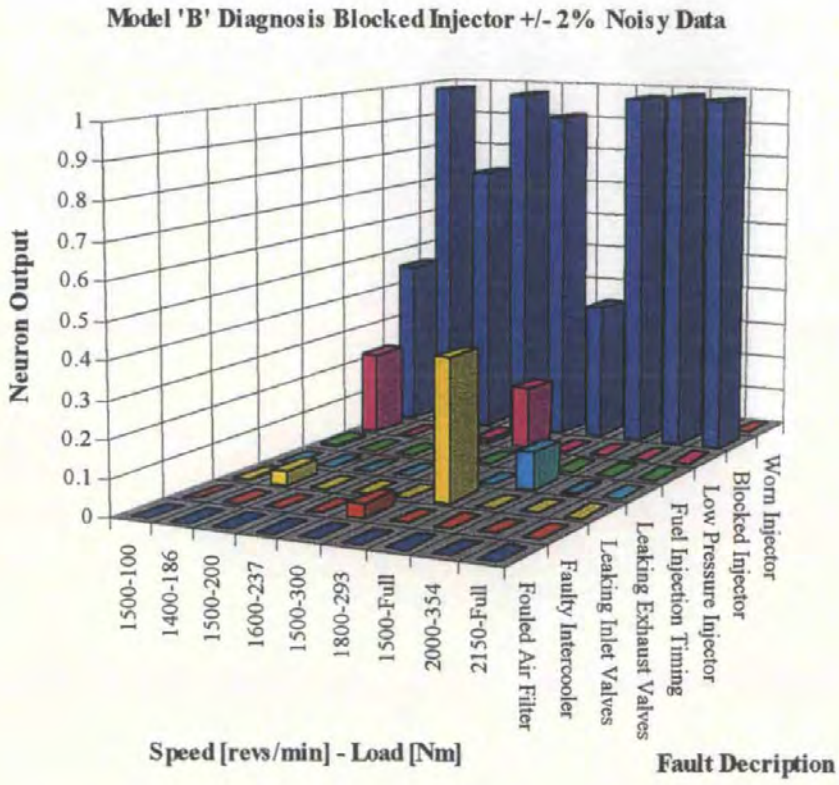

Figure 151 Model 'A' & 'B's Diagnostic Performance on +/- 2% Noisy Blocked Injector Data

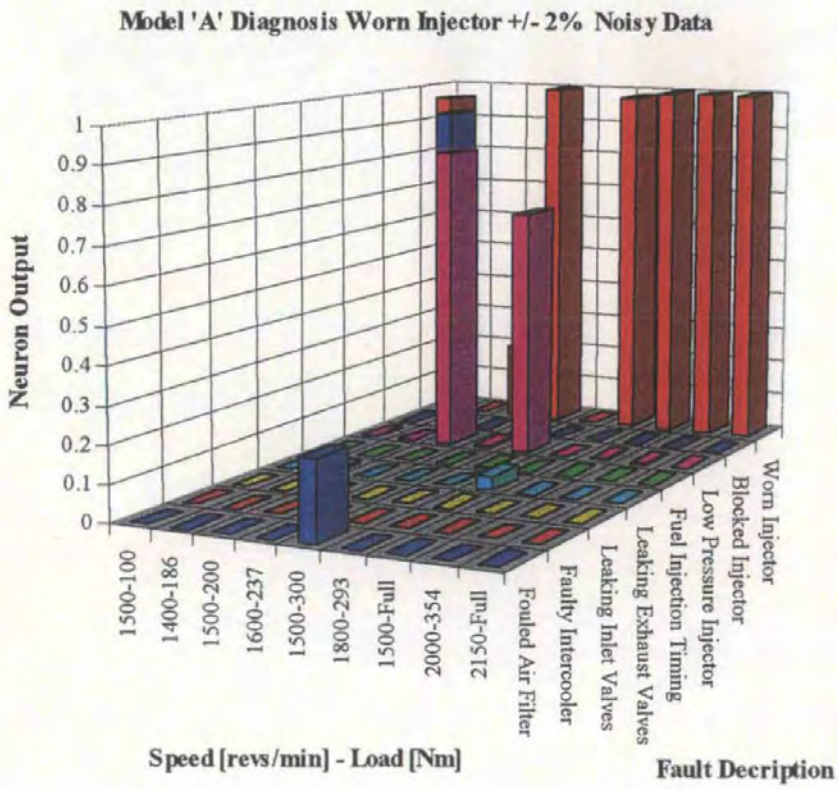

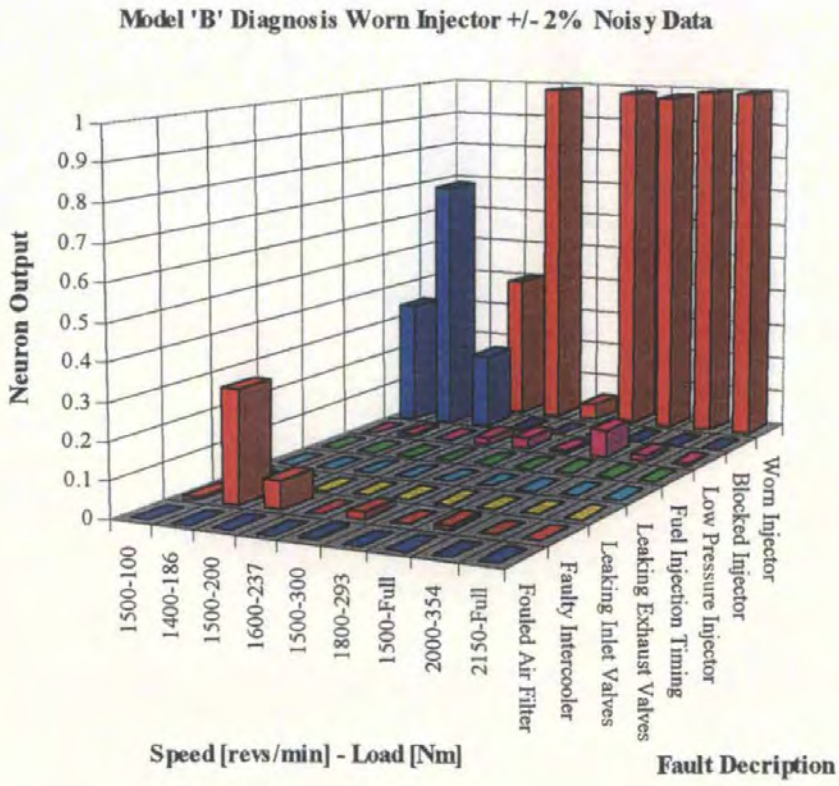

Figure 152 Model 'A' & 'B's Diagnostic Performance on +/- 2% Noisy Worn Injector Data

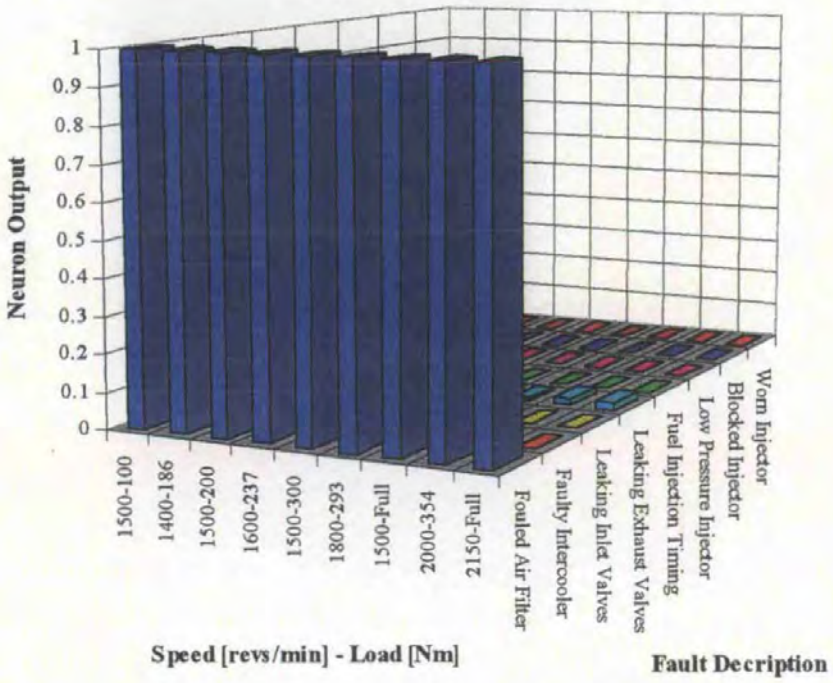

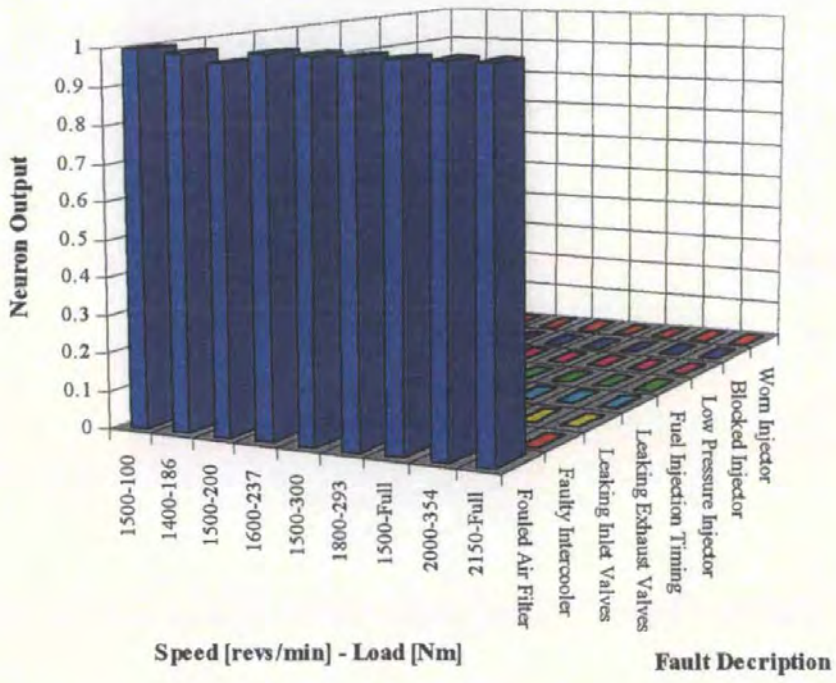

Figure 153 Model 'A' & 'B's Diagnostic Performance on 80% Fouled Air Filter Data With Zero Air Flow Sensor Output & Full Scale 1 & 2 Cylinder Port Temperatures

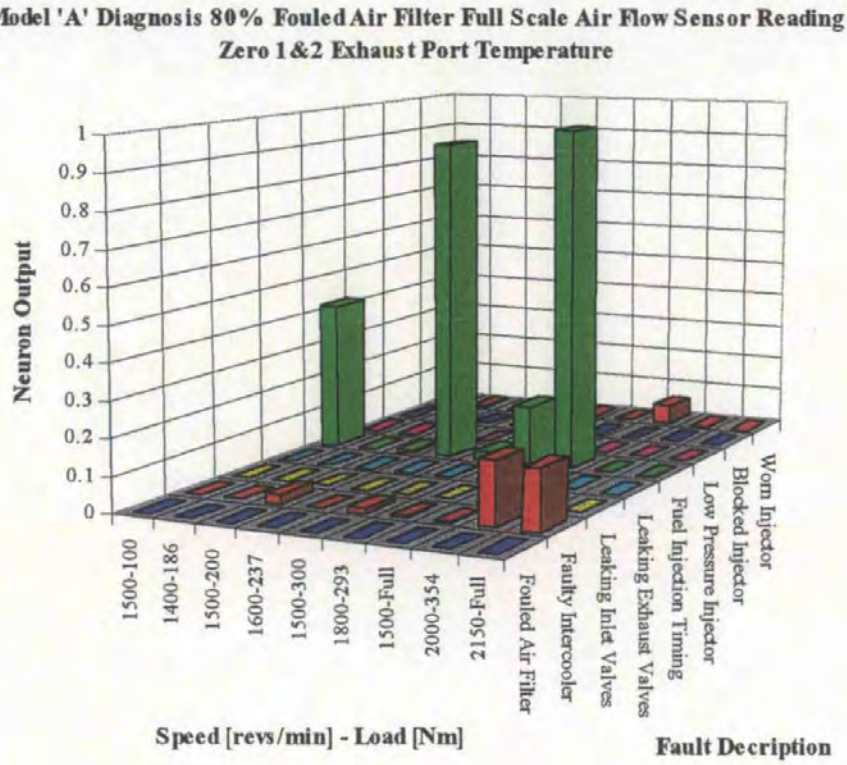

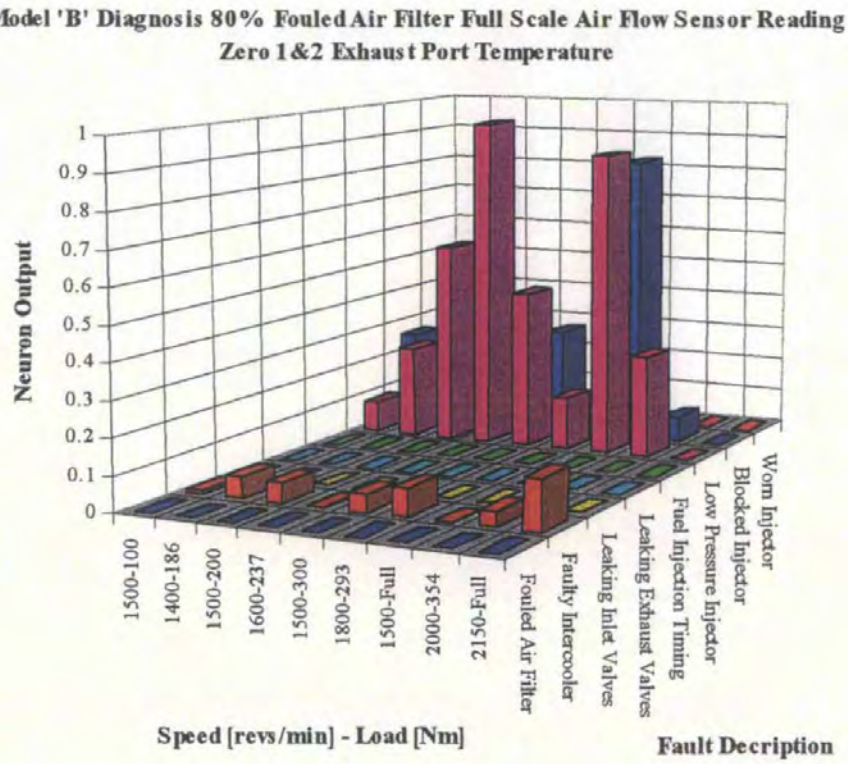

Figure 154 Model 'A' & 'B's Diagnostic Performance on 80% Fouled Air Filter Data With Full Scale Air Flow Sensor Output & Zero 1 & 2 Cylinder Port Temperatures

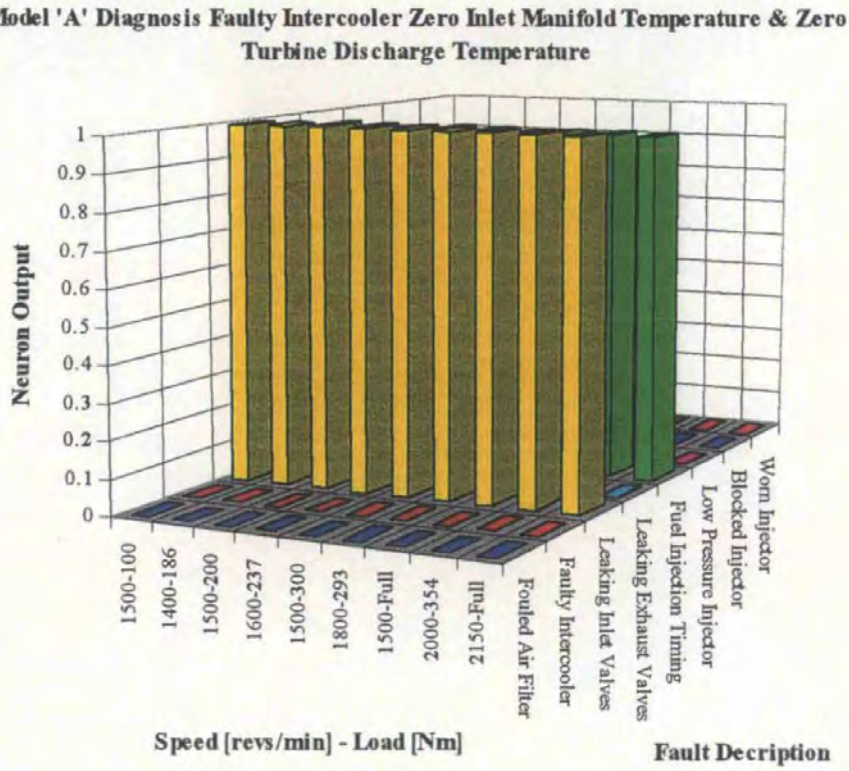

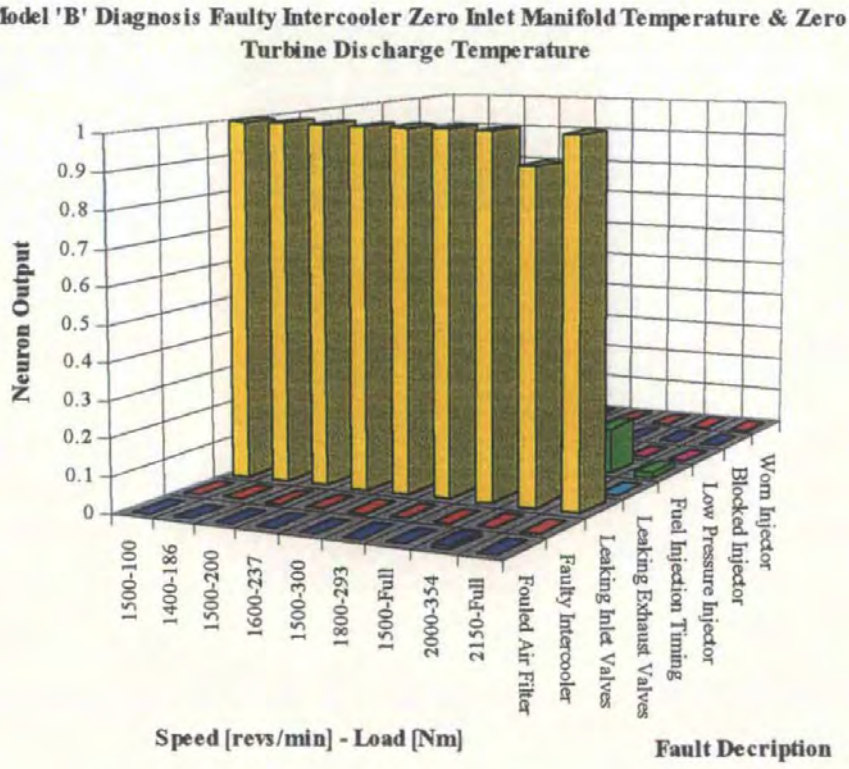

Figure 155 Model 'A' & 'B's Diagnostic Performance on Faulty Intercooler Data With Zero Inlet Manifold Temperature & Zero Turbine Discharge Temperature

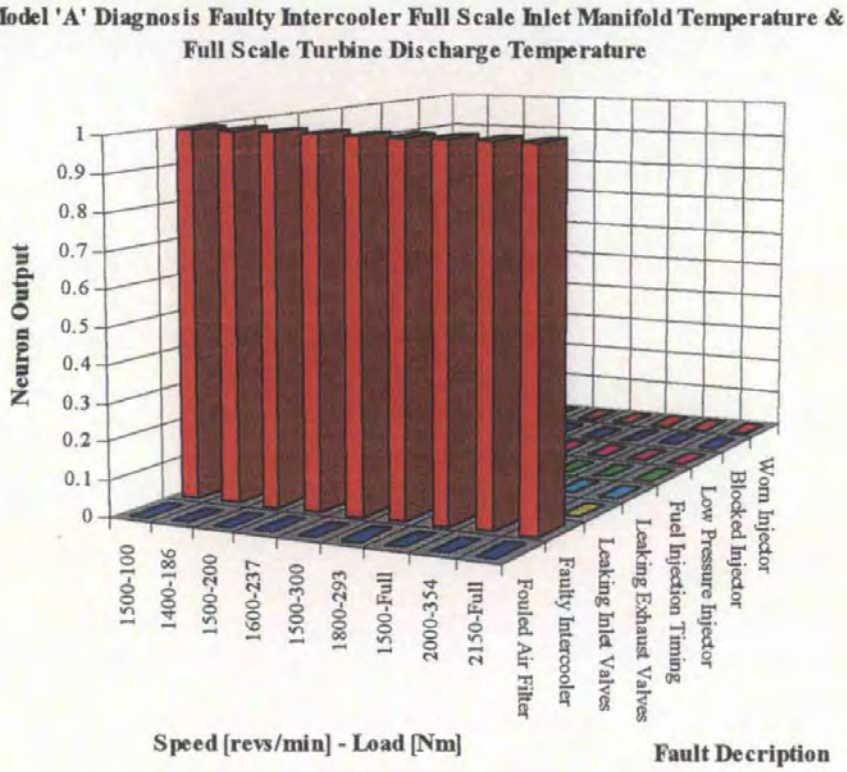

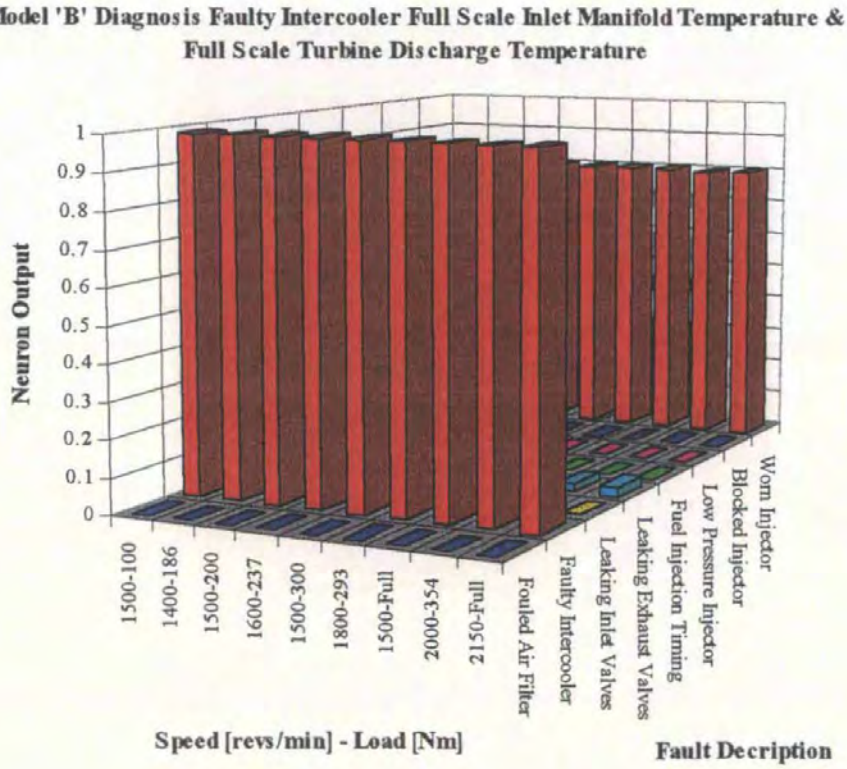

Figure 156 Model 'A' & 'B's Diagnostic Performance on Faulty Intercooler Data With Full Scale Inlet Manifold Temperature & Full Scale Turbine Discharge Temperature

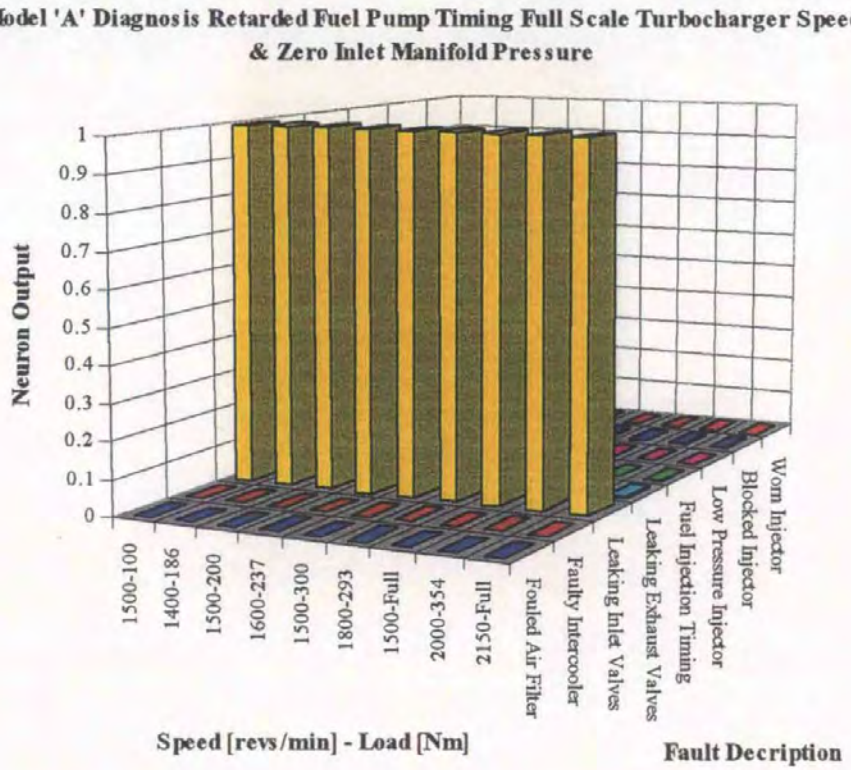

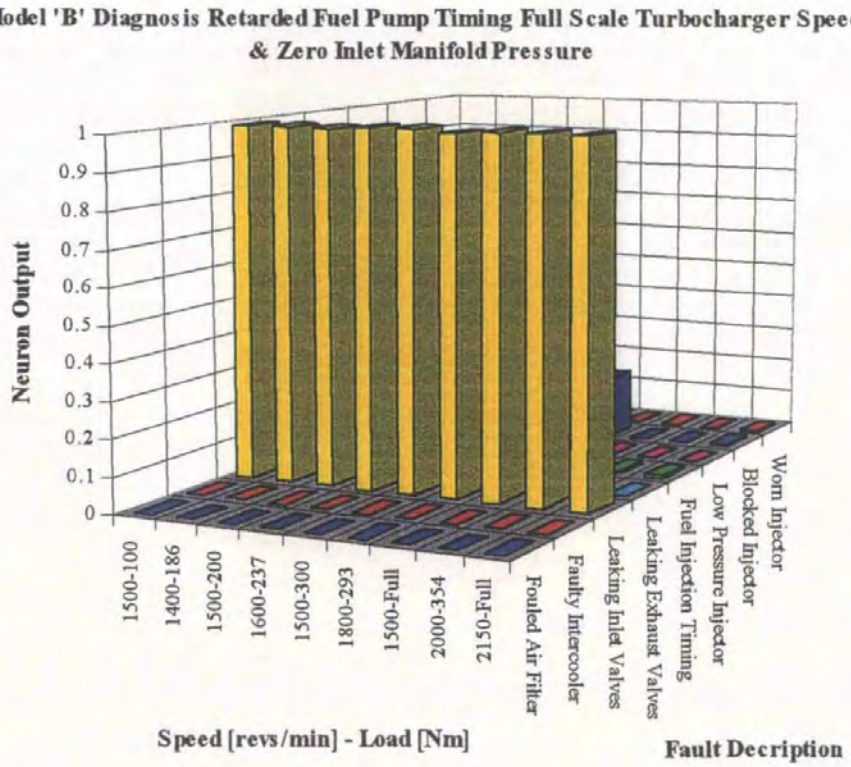

Figure 157 Model 'A' & 'B's Diagnostic Performance on Retarded Fuel Pump Timing Data With Full Scale Turbocharger Speed & Zero Inlet Manifold Pressure

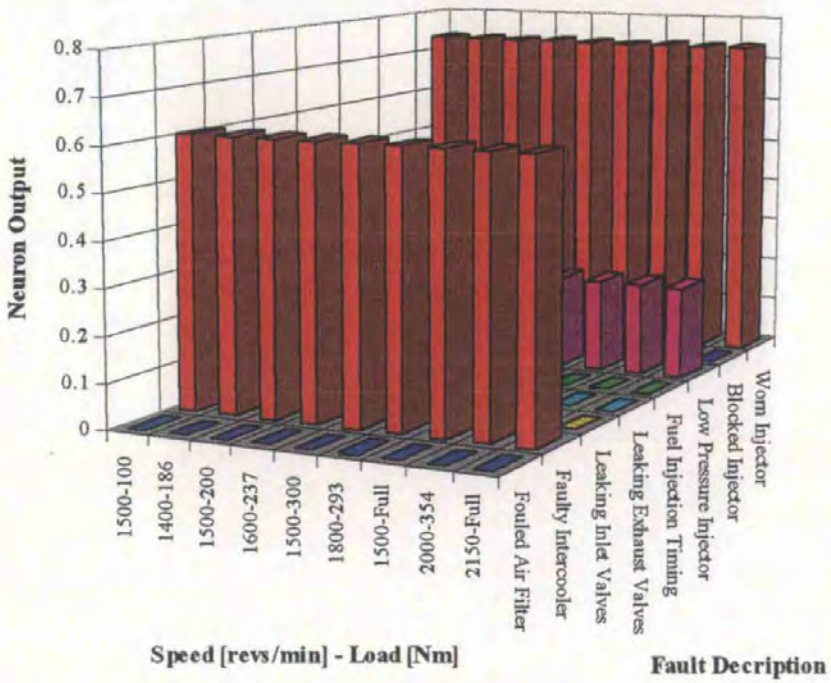

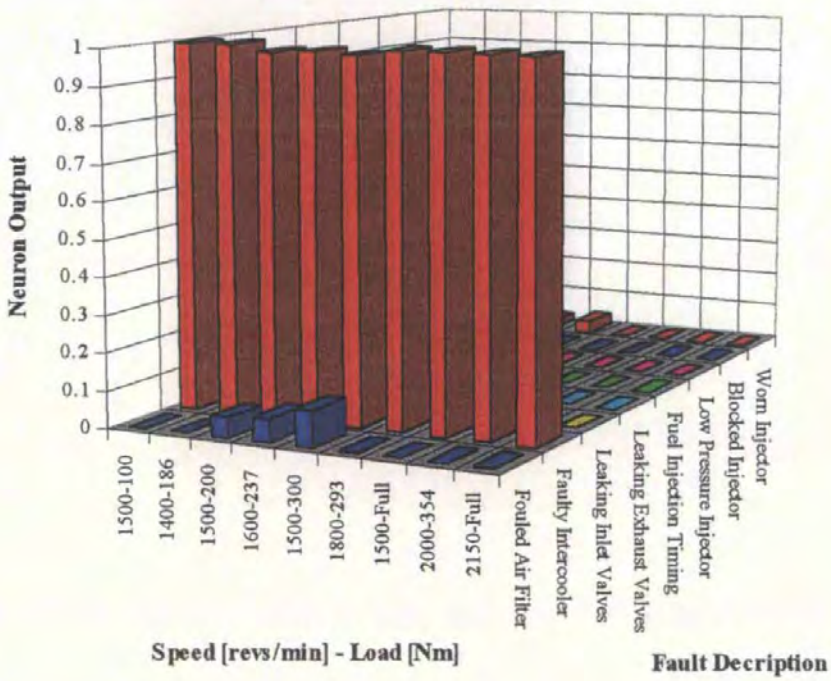

Figure 158 Model 'A' & 'B's Diagnostic Performance on Retarded Fuel Pump Timing Data With Zero Turbocharger Speed & Full Scale Inlet Manifold Pressure

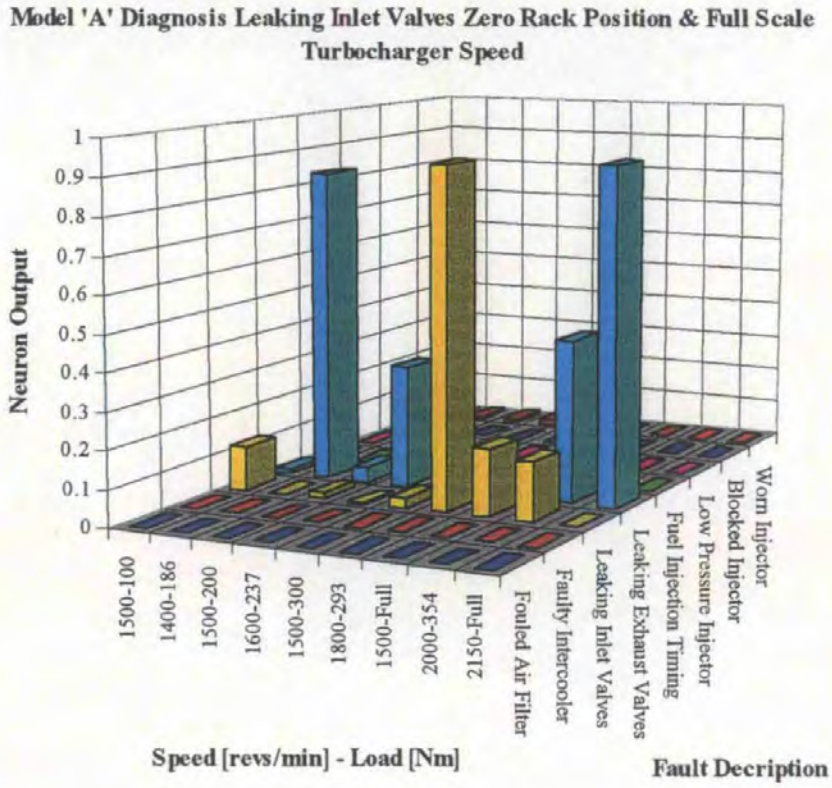

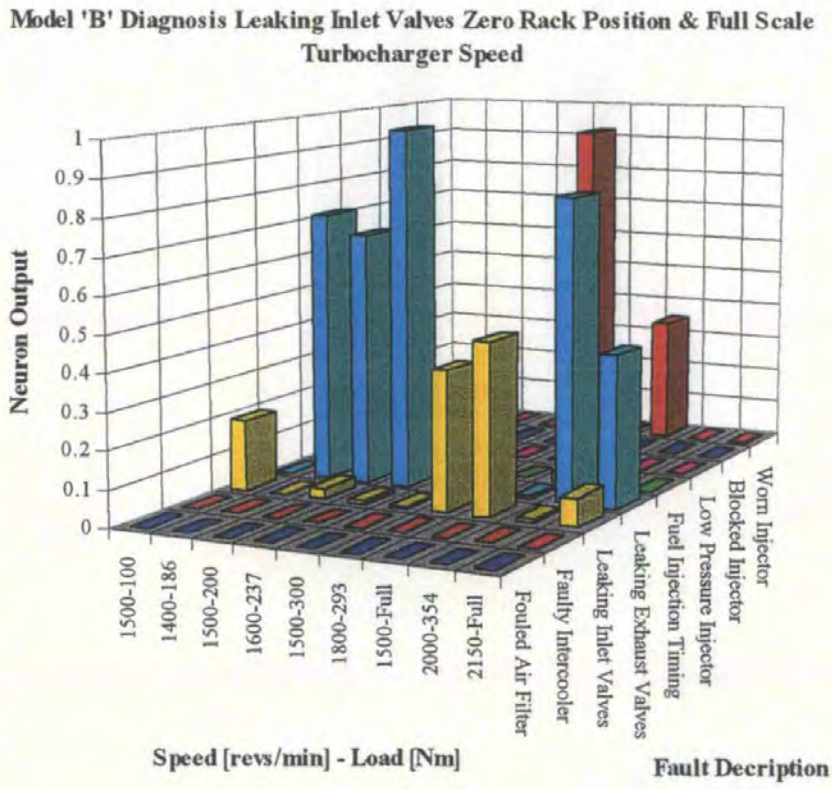

Figure 159 Model 'A' & 'B's Diagnostic Performance on Leaking Inlet Valves Data With Zero Rack Position & Full Scale Turbocharger Speed

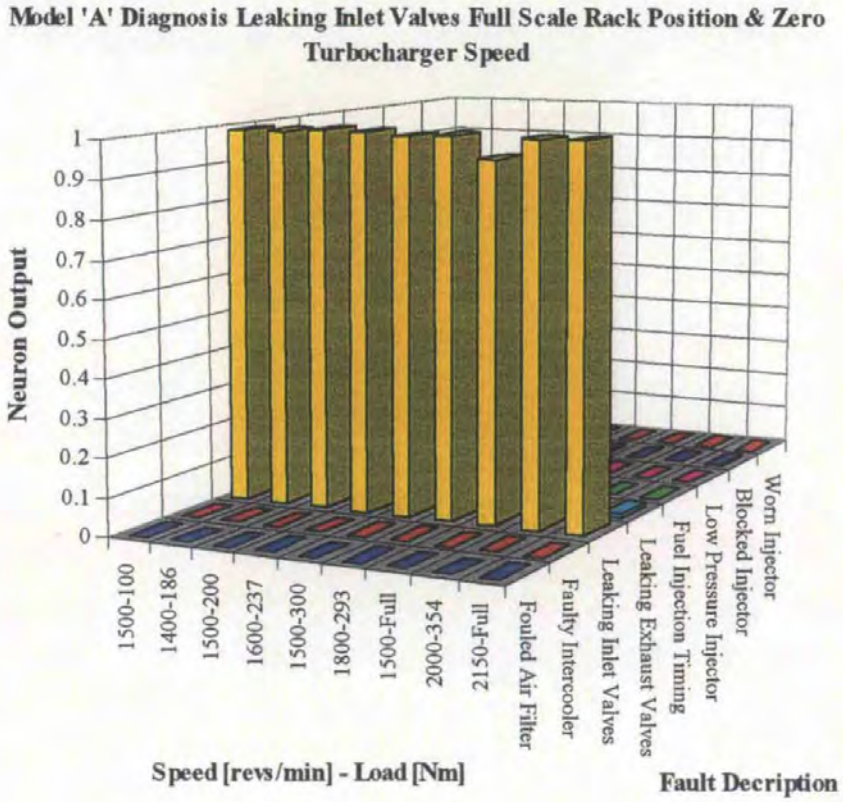

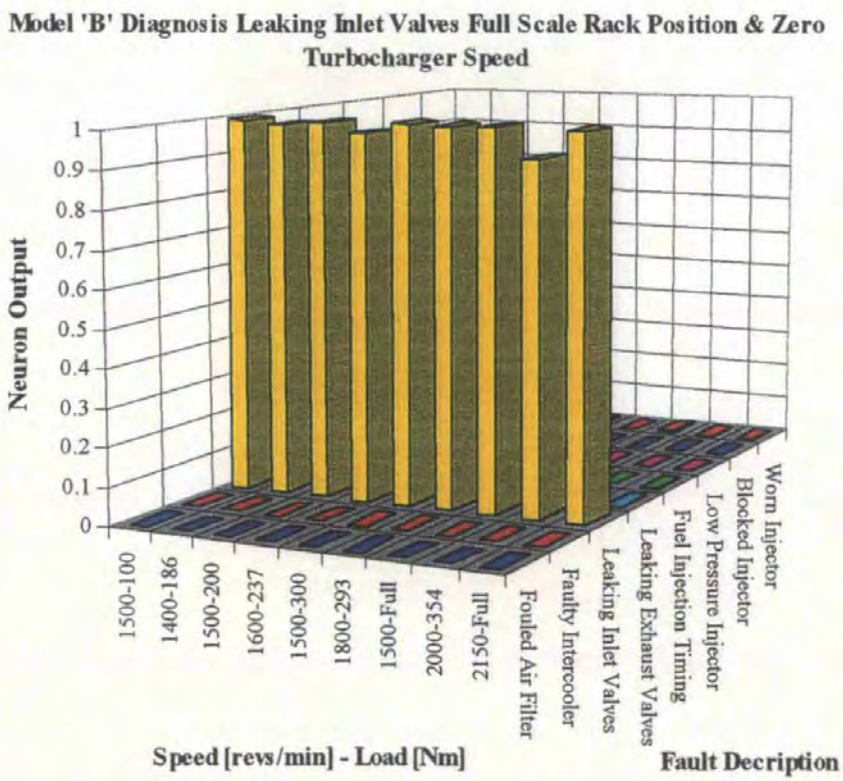

Figure 160 Model 'A' & 'B's Diagnostic Performance on Leaking Inlet Valves Data With Full Scale Rack Position & Zero Turbocharger Speed

Automated Sensor Check Program

A1

```
=EXEC("c:\ncs\neurun c:\ncs\sensor.ncs")
=INITIATE("neurun","sensor.ncs")
=OPEN("c:\msoffice\excel\perfmon\diagnose.xls",0)
=SELECT("r78c7:r78c125")
=POKE(A3,"InterrogStimulus",SELECTION())
=EXECUTE(A3,"[Process(Relate)]")
=SET.NAME("Result",REQUEST(A3,"InterrogResponse"))
=SELECT('C:\MSOFFICE\EXCEL\PERFMON\[DIAGNOSE.XLS
]Sheet1'!$O$1:$V$1)
=SELECT('C:\MSOFFICE\EXCEL\PERFMON\[DIAGNOSE.XLS
]Sheet1'!$O$1:$V$1)
=FORMULA.ARRAY("=DIAMAC.XLM!Result")
=EXECUTE(A3,"[Process(QUIT)]")
=TERMINATE(A3)
=FOR.CELL("Max",O1:V1,FALSE)
=IF(max>A23,GOTO(B2))
=NEXT()
=GOTO(B9)
=GOTO('C:\MSOFFICE\EXCEL\PERFMON\[DIAGNOSE.XLM]
DIAGNOSE'!A1)
=RUN()
=RETURN()
```

A22

0 .5

A25

AIR FLOW SENSOR FAILURE PLEASE CHECK
PERFORMANCE FILE RESULTS

A27

SENSORS ALL FUNCTIONING OK

B1

```
=COPY(A26)
=OPEN("c:\msoffice\excel\perfmon\results.xlm"
=FILE.CLOSE(TRUE)
=GOTO(A18)
=RETURN()
```

B8

```
=COPY(A28)
=OPEN("c:\msoffice\excel\perfmon\results.xlm"
=FILE.CLOSE(TRUE)
=GOTO(A18)
=RETURN()
```

DIAMAC.XLM On-line Database Program

```
A1
=EXEC("c:\ncs\neurun c:\ncs\net4sto2.ncs")
=INITIATE("neurun","net4sto2.ncs")
=OPEN("c:\msoffice\excel\perfmon\diagnose.xls",0)
=SELECT("r78c7:r78c125")
=POKE(A3,"InterrogStimulus",SELECTION())
=EXECUTE(A3,"[Process(Relate)]")
=SET.NAME("Result",REQUEST(A3,"InterrogResponse"))
=SELECT('C:\MSOFFICE\EXCEL\PERFMON\[DIAGNOSE.XLS]Sheet1'!$G$1:$N$1)
=SELECT('C:\MSOFFICE\EXCEL\PERFMON\[DIAGNOSE.XLS]Sheet1'!$G$1:$N$1)
=FORMULA.ARRAY("=DIAMAC.XLM!Result")
=EXECUTE($A$3,"[Process(QUIT)]")
=TERMINATE(A3)
=RUN("DIAMAC.XLM!r1c2")
=RETURN()

C2
=FORMULA((C1+1),C1)
=IF($C$1<10,GOTO($A$24))
=GOTO($A$30)
=RETURN()

A23
=SELECT('C:\MSOFFICE\EXCEL\PERFMON\[DIAGNOSE.XLS]Sheet1'!$G$1:$N$1)
=COPY()
=SELECT(OFFSET(SELECTION(),2,($C$1),8,1))
=PASTE.SPECIAL(3,1,FALSE,TRUE)
=RETURN()
A29
=SELECT("r10c7:r17c16")
=CUT()
=SELECT(OFFSET(SELECTION(),0,-1))
=PASTE()
=SELECT("r10c6:r17c6")
=CLEAR()
=SELECT('C:\MSOFFICE\EXCEL\PERFMON\[DIAGNOSE.XLS]Sheet1'!$G$2:$N2)
=COPY()
=SELECT("r10c16:r17c16")
=PASTE.SPECIAL(3,1,FALSE,TRUE)
=RETURN()
```

REFERENCES

1. Fox T.B., '*Operating Experience With A Vehicle Fault Diagnosis System*', Proceedings I Mech E, C44/85, (1985)

2. Speed. S, et al, '*Condition Monitoring And Maintenance - Four Years Fleet Experience*', BP Tanker Company Ltd, Appendix 'C', pp 21-39. (1975)

3. Riley R.J., '*Health Monitoring Of Machinery And Its Effects On Minimum Manning Levels*', Transactions I Mar E, Vol 99, Paper 3, pp 1-4

4. Rudston S.G., '*Lubricant & Wear Debris Analysis For Machine Condition Monitoring Offshore*', I Mech. E Tribology Group Seminar (May 10th 1984)

5. Anon., '*DEEDS Condition Monitoring Project Being Finalised*', MER, (April 1991)

6. Shamsolmaali S., Banisoleiman K., '*Real Time Diagnostic Techniques And Condition Monitoring Application*', Transactions I Mar E, Vol. 103, pp 357-363 (1990)

7. Ahlqvist I., '*Development Of A Fault Avoidance Knowledge System*', Maritime Communications & Control, Paper 3, (21-23rd November 1990)

8. Anon, '*A Diagnostic Approach To Engine Health*', The Motor Ship, Vol. 70, pp 62-65, (September 1989)

9. Richards R.A., '*Expert Systems For Condition Monitoring Of Diesel Engines*', Proceedings Of I Mar E, (1988)

10. Kincaid C.E., '*Computerised Diagnostics For Cummins Engines*', IEEE Proceedings - International Congress on Transportation Electronics, Convergence 84, pp 49 -54, (October 1984)

11. *Asea Brown Boveri Commercial Literature*

12. O'Connor L (ed), '*Diagnosing Diesel Engines*', Mechanical Engineering, pp 44-50 (March 1992)

13. Autar R.K., '*An Automated Diagnostic Expert System For Diagnosing Diesel Engines*', ICE Vol. 22, Heavy Duty Engines, A Look At The Future, pp 325-333, (1994)

14. Kouremenos D.A., et al, '*Development And Validation Of A Diagnosis Method For Diesel Engines,* Proceedings of the ASME, Advanced Energy Systems Division, AES Vol 36, pp 527-539 (ASME 1996)

15. Lipmann R.P., *'Pattern Classification Using Neural Networks'*, IEEE Communications Magazine, pp 47-64, (November 1989)

16. Venkatasubramanian V., Chan K., *'A Neural Network Methodology For Process Fault Diagnosis'*, American Institute Of Chemical Engineers Journal, Vol 35, No. 12, pp 1993-2002, (December 1989)

17. Hoskins J.C., et al, *'Fault Diagnosis In Complex Chemical Plants Using Artificial Neural Networks'*, American Institute Of Chemical Engineers Journal, Vol 37, No. 1, pp 137-141, (January 1991)

18. Watanabe K., et al, *'Incipient Fault Diagnosis Of Chemical Processes Via Neural Networks'*, American Institute Of Chemical Engineers Journal, Vol. 35, No. 11, pp 1803-1812, (November 1989)

19. Venkatasubramanian V, et al, *'Process Fault Detection & Diagnosis Using Neural Networks: Steady State Processes'*, Computers In Chemical Engineering, Vol. 14, No. 7, (1990)

20. Tanaka T., Endo H., *'Trouble Forecasting System By Multi Neural Network On Continuous Casting Process Of Steel Production'*, Artificial Neural Networks, pp 835-840, (1991)

21. Kavuri S.N., Venkatasubramanian V, *'Combining Pattern Classification And Assumption Based Techniques For Process Fault Diagnosis'*, Computers And Chemical Engineering, Vol. 16, pp 299-312, (April 1992)

22. Shepherd C., *'Neural Networks - Theory & Practice'*, EDS Scicon Product Literature, pp 205-215.

23. Banisolieman K., et al, *'A Review Of Techniques For Diesel Engine Fault Diagnosis By Performance Monitoring'*, The Institute Of Diesel And Gas Turbine Engineers Conference, INPOWER 91, pp 1- 13, (1991)

24. Hobday J. S., et al, *'The Role Of Expert Systems And Neural Networks In The Marine Industry'*, Technical Investigation Report, Lloyds Register.

25. Ray A.K., *'Equipment Fault Diagnosis - A Neural Network Approach'*, Computers In Industry, Vol. 16, pp 169-177, (1991)

26. Healy A.J., et al, *'Failure Diagnosis For Underwater Vehicles: A Neural Network Approach'*, Manoeuvring & Control Of Marine Craft, P.A. Wilson (Ed) Computational Mechanics Publications, pp 293-305

27. Chow M., Yee S., *'Methodology For On Line Incipient Fault Detection In Single Phase Squirrel Cage Induction Motors Using Artificial Neural Networks'*, Institute Of Electrical & Electronic Engineers Transactions On Energy Conversion, Vol. 6, No. 3, pp 536-545, (September 1991)

28. Dietz W.E. et al, *'Pattern Based Fault Diagnosis Using Neural Networks'*, 1st Conference Of Industrial And Engineering Applications Of Artificially Intelligent And Expert Systems, pp 13-23, (1988)

29. Kirkman E.F.T, Elliot C., *'Condition Monitoring Of Marine Engineering Equipment Using Neural Computing'*, Presented at I Mar E, 8 pages, (15 March 1995)

30. Gu F., et al, *'A RBF Neural Network Model For Cylinder Pressure Reconstruction In Internal Combustion Engines'*, IEEE Colloquium, No. 260, Paper 4, 11 pages, (September 1996)

31. Leonhardt S, et al., *'Real Time Supervision Of Fuel Injection With RBF-Based Neural Networks'*, Proceedings Of The American Control Conference, Seattle, Washington. pp 2128-2132, (June 1995)

32. Leonhardt S., et al., *'Real-Time Supervision For Diesel Engine Injection'*, Control Engineering Practice, Vol. 3, No 7, pp 1003 - 1010, Permagon Press, (1995)

33. Ludwig C., et al, *'Measurement & Monitoring Of Pressure Curves In Diesel Engines'*. Proceedings Of The American Control Conference, San Francisco, California, pp 1796 - 1800, (June 1993)

34. Scaife M.W., et al., *'A Neural Network For Fault Recognition'*, International Congress & Exposition, Detroit, Michigan, SAE Technical Paper 930861, 8 pages, (March 1993)

35. Ayoubi M, *'Nonlinear Dynamic Systems Identification With Dynamic Neural Networks For Fault Diagnosis In Technical Processes'*, Proceedings Of The 1994 IEEE Conference On Systems, Man & Cybernetics, Part 3, IEEE 0-7803-2129-4/94, pp 2120-2125, (October 1994)

36. Ludwig C., Ayoubi M., *'Fault Detection Schemes For A Diesel Engine Turbocharger'*. Proceedings Of The American Control Conference Part 3 1995, Seattle, Washington, pp 2118 - 2122, (June 1995)

37. National Physics Laboratory Standard On Temperature Measurement.

38. British Standard BS1042/BS848, *Measurement of Fluid Flows In Enclosed Ductings.*

39. Heywood J.B., *'Internal Combustion Engine Fundamentals'*, McGraw-Hill Publishing, pp 130-131, ISBN 0-07-028637-X, (1988)

40. Lancaster D. R., et al,' *Measurement & Analysis Of Engine Pressure Data'*, SAE Transactions, Vol. 84, Paper No. 750036, (1975)

41. *Diesel & Gas Turbine Engineers Working Costs & Annual Report*, Analysis Of Stoppages, (1983 - 1993).

42. Isaias L., '*Performance Simulation Of A Medium Speed Diesel Engine Under Optimum And Fault Conditions*', PhD Thesis, University Of Newcastle, (1989)

43. Kern J., Wallner R., '*Water Cooled Charge Air Coolers For Heavy Diesel Engines*', Third International Conference On Turbocharging & Turbochargers, I Mech. E, Paper C116/86, pp 261-268, (1986)

44. Dyberg A., '*How Congested Air Coolers Affect Diesel Performance*', MER April 1987, pp 27-28. (1987)

45. Newcastle University Condition & Performance Monitoring Project, Short Term Sensitivity Test Report.

46. Taborek J., et al, '*Fouling: The Unresolved Problem In Heat Transfer*', Chemical Engineering Progress, Vol. 68, No 2, pp 59-67, (February 1972)

47. Colwell A. T., '*The Problem Of Valve Stem & Valve Head Deposits*', SAE Journal (Transactions), Vol. 47, No. 3, pp 358-366, (September 1940)

48. Kingston-Jones M. G., et al, '*Review Of Operating Experience With Current Valve Materials*', Diesel Engine Combustion Chamber Materials For Heavy Fuel Operation, Paper 2, pp 15-28, (1990)

49. Umland F., Ritzkopf M., '*Valve Corrosion In Diesel Engines*', MTZ , Vol. 36, No. 7/8, pp 191-195.

50. Takaishi T., et al, '*The Problems Associated With Burning Heavy Fuels In Diesel Engines: A Study Of Blowby Through Exhaust Valve Seats As A Result Of Burning Heavy Fuels In Diesel Engines*' Diesel Engine Combustion Chamber Materials For Heavy Fuel Operation, Paper 8, pp 83-89, (1990)

51. Leugner Lloyd, *Problem Diagnosis In Diesel Engines*, Canadian Mining Journal, October 1986, pp 54-61, (1986)

52. Gerwiner W.J., *Principles Of Fuel Injection Equipment Selection*, Technical Paper Of American Bosch Division, Springfield, Massachusetts.

53. Liegh-Jones C., '*Prediction Of Diesel Engine Fault Conditions By Monitoring Crank Case Environment Parameters*', MPhil. Thesis, Newcastle University, (1989).

54. Charlton S.J., '*Simulation Program For Internal Combustion Engines User Manual*', Release 2, (May 1990)

55. Watson N., et al,' *A Combustion Correlation For Diesel Engine Simulation'*, SAE 800029, (1980)

56. Woschni G., '*A Universally Applicable Equation For The Instantaneous Heat Transfer Coefficient In The IC Engine'*, SAE 670931, (1967)

57. Chen S.K., Flynn P.F., '*Development Of A Single Cylinder Compression Ignition Research Engine'*, SAE 650733, (1965)

58. Annand W.J.D., Roe J.E., '*Gas Flow In The Internal Combustion Engine'*, Haesner Publishing, Newfoundland, NJ, (1974)

59. Jones A.D, Charlton S.J., '*Multi-Processor Simulation Of Diesel Engines For Condition Monitoring Applications'*, American Society Of Mechanical Engineers, Energy Sources & Technology Conference, (Jan 1988)

60. Rummelhart D.E., et. al. '*Parallel Distributed Programming'*, MIT Press, Cambridge, Mass., (1986)

Copyright Statement

Signed.....

Christopher Lloyd Owen, May 1998